RÉPUBLIQUE FRANÇAISE
Liberté
Égalité
Fraternité

Université de Toulouse

Doctorat de l'Université de Toulouse

préparé à l'Université Toulouse III - Paul Sabatier

Catalyse commutable utilisant des complexes à transition de spin

Thèse présentée et soutenue, le 17 décembre 2024 par

Yongjian LAI

École doctorale
SDM - SCIENCES DE LA MATIERE - Toulouse

Spécialité
Chimie Organométallique et de Coordination

Unité de recherche
LCC - Laboratoire de Chimie de Coordination

Thèse dirigée par
Azzedine BOUSSEKSOU et Lucie ROUTABOUL

Composition du jury
M. Fabien DELPECH, Président, Université Toulouse III - Paul Sabatier
M. Bohuslav DRAHO, Rapporteur, Palacký University Olomouc
Mme Raluca MALACEA KABBARA, Rapporteure, CNRS Centre Est
M. Azzedine BOUSSEKSOU, Directeur de thèse, CNRS Occitanie Ouest

Membres invités
Mme Lucie ROUTABOUL, Université Toulouse III - Paul Sabatier

Table of contents

Acknowledgements ... 1

List of abbreviation ... 2

General introduction ... 3

Chapter 1 Bibliographic overview of the spin crossover phenomenon and of the influence of spin states on chemical reactivity ... 5

1.1 Spin crossover phenomenon ... 5

1.1.1 General presentation of the spin crossover phenomenon ... 5

1.1.2 How the spin crossover phenomenon is induced by the application of the stimulus? ... 7

1.1.2.1 Temperature-induced spin crossover phenomenon ... 7

1.1.2.2 Light-induced spin crossover phenomenon ... 9

1.1.2.3 Pressure-induced spin crossover phenomenon ... 9

1.1.3 Application of Spin Crossover Materials ... 10

1.1.3.1 Application of spin crossover materials in photonic devices ... 10

1.1.3.2 Application of spin crossover materials in electronic devices ... 10

1.1.3.3 Spin crossover materials as mechanical actuators ... 11

1.2 Spin state effect on chemical reactivity ... 12

1.2.1 General presentation of the spin state effect on chemical reactivity ... 12

1.2.1.1 Spin state effect on activation energies of reactions ... 12

1.2.1.2 Spin state effect on reaction pathway ... 13

1.2.1.3 Spin state effect on the selectivity of reactions ... 14

1.2.2 Importance of the spin state effect in different chemical fields ... 15

1.2.2.1 Importance of the spin state effect in biochemistry ... 15

1.2.2.2 Importance of the spin state effect in organometallic chemistry ... 15

1.2.2.2.1 Influence of metal spin state on ligand coordination ... 15

1.2.2.2.2 Influence of metal spin state on the reaction mechanism ... 16

1.2.2.2.3 Influence of metal spin state on rate of reaction ... 17

1.2.2.3 Importance of the spin state effect in catalysis ... 17

1.2.2.3.1 Alkene isomerization ... 18

1.2.2.3.2 C-H Activation ... 18

1.2.2.3.3 Cycloaddition ... 20

1.2.2.3.4 Polymerizations ... 21

1.2.2.3.5 Electrocatalysis ... 23

1.3 Spin crossover in catalysis ... 24

1.3.1 Spin crossover during the catalytic reaction ... 24

1.3.1.1 Spin crossover during electrocatalytic reaction ... 24

1.3.1.2 Spin crossover during C-H bond silylation reaction..... 26
1.3.2 Direct use of spin crossover complexes as catalysts 27
1.4 References 30
Chapter 2 Spin state effect on the efficiency of a post-synthetic modification reaction on a spin-crossover complex 37
2.1 Introduction 37
2.2 The objective of this chapter 42
2.3 The effect of thermal activation, structural effect and spin state on the PSM method.. 43
2.3.1 Comparison of the temperature effect on the PSM reaction/imine ligand synthesis 44
2.3.2 Study of the efficiency of the PSM reaction as a function of the temperature 45
2.3.3 Study of the influence of the spin state of complex 1 on the yield of the PSM reaction 47
2.4 Study of the reproducibility of results 49
2.4.1 Accuracy and precision of the method 49
2.4.2 Batch 2 with a reaction time of 4h at 55°C..... 51
2.4.3 Batch 2 with a reaction time of 3.5, 4h, 4.5 and 5.5h at 55 ℃ 52
2.4.4 Batch 3 with a reaction time of 4h (sonication and ethanol 98%)..... 54
2.4.5 Batch 4 with a reaction time of 4h (HS and HS2) 55
2.4.6 Batch 5 with a reaction time of 4h (normal conditions), 4 and 5h (sonicated in ethanol 98%) 56
2.4.7 Batch 5 with a reaction time of 4, 4.5, 5.5, 6 and 6.5h 58
2.5 Statistical study..... 59
2.5.1 The ratio of the imine percentage of the HS complex to the percentage obtained for the complex in the LS2 state (Ratio 1). 60
2.5.2 The ratio of the difference in imine percentage between the two spin states of the complex to the imine percentage obtained for the complex in the HS state. (ratio 2)..... 61
2.5.3 Standard deviation of all values (yields of HS, LS2, and Δ (HS-LS2)). 62
2.6 Comparison of the properties of complex 2 obtained at 35°C and 90°C 65
2.7 Conclusion..... 66
2.8 Experiment section 66
2.8.1 Methodology for the Post-synthetic modification 66
2.8.1.1 General procedure 66
2.8.1.2 PSM reaction using ethanol 98% and sonication (batch 3 and 5) 67
2.8.1.3 PSM reaction at HS2 (Batch 4) 67
2.8.2 Methodology used for the digestion and quantification of the PSM reaction 68
2.8.2.1 Digestion of the sample 68
2.8.2.2 Integration of the NMR spectra 68
2.8.2.3 Quantification of the digested solution..... 69

2.8.2.4 Selected NMR spectra of the digested samples 70
2.9 References 73
Chapter 3 Study of the catalytic activity of the SCO coordination polymer $[Fe(NH_2trz)_3](NO_3)_2$ for imine formation from 4-amino-1,2,4-triazole 75
3.1 Introduction 75
3.2 Study of catalytic reaction 78
3.3 Study of the effect of solvent on reaction rate 80
3.3.1 Effect of the nature of the catalyst on reaction rate. 81
3.3.1.1 Influence of complex particle size and complex particle agglomerate size on reaction rate 81
3.3.1.2 Influence of the counterion of the complex on reaction rate 82
3.3.1.3 Influence of the oxidation state of iron on reaction rate 83
3.4 Kinetic monitoring of catalysis reactions and study of post-catalysis complexes 83
3.4.1 Study of the effect of catalyst pre-treatment on catalysis reaction kinetics 83
3.4.2 IR spectroscopy analysis of post-catalysis complexes 84
3.4.3 Result of digestion of post-catalysis complexes 85
3.4.4 Study of the crystal structure and morphology of complex particles recovered after catalysis 85
3.4.5 Variable temperature reflectivity measurement 88
3.4.6 Study of the reproducibility of results obtained from complexes recovered after catalysis 89
3.4.7 Study of the complex recovered after the reaction between p-anisaldehyde b and aminotriazole a catalyzed by imine complex 2 90
3.4.8 Study of the complex recovered after the reaction between *p*-anisaldehyde b and aminotriazole a catalyzed by imine complex 3 93
3.5 Investigation of the mechanism of the PSM reaction leading to the amine 1 complex from the imine complex 2 94
3.6 Mechanism study of the catalytic reaction 98
3.6.1 Investigation of catalytic reactions when the substituent in the imine complex differs from that of the aldehyde that serves as the catalytic substrate. 98
3.6.1.1 Study of the reaction between aminotriazole a and vanillin d catalysed by the imine complex 2. 98
3.6.1.2 Study of the presence of a catalytic amount of imine complex 4 in the reaction between aminotriazole a and p-anisaldehyde b 100
3.6.2 Competitive reaction using aminotriazole, imine complex and aldehyde 101
3.6.2.1 Competitive reaction using aminotriazole a, imine complex 2 and vanillin d101
3.6.2.2 Competitive reaction using aminotriazole a, imine complex 2 and p-anisaldehyde b 103
3.7 Conclusion 103
3.8 Experiment section 105

3.8.1 Materials synthesis 105
3.8.1.1 Synthesis of $[Fe(NH_2trz)_3](NO_3)_2$, complex 1 105
3.8.1.2 Synthesis of nanoparticles of complex 1 105
3.8.1.3 Synthesis of [Fe(NH2-trz)3](SO4), complex 1b 105
3.8.1.4 Synthesis of imine complex 2 from complex 1 106
3.8.1.5 Synthesis of Iron III complex (complex 3) 106
3.8.1.6 Synthesis of imine complex 4 from complex 1 106
3.8.1.7 Synthesis of $[^{15}N_4]$ 4-amino-1,2,4- triazole 106
3.8.1.8 Test for ligand exchange reaction with ^{15}N-aminotriazole 106
3.8.2 The general procedure of the catalytic reaction 107
3.8.3 Calculation of yield of catalytic reaction 108
3.8.4 The methodology used for the digestion and quantification of the percentage of imine functionality on the complex 109
3.8.5 Calculation of conversion and yield (for competitive reaction) 109
3.8.6 Selected NMR spectra 110
3.8.6.1 Selected NMR spectra of the catalytic reaction 110
3.8.6.2 Selected NMR spectra of the digested samples 112
3.9 References 116
Chapter 4 Spin state effect on the catalytic activation of acetalization reaction 118
4.1 Introduction 118
4.2 Presentation of our scientific approach 118
4.2.1 Criteria we considered when selecting the catalyst 118
4.2.2 Criteria we considered when choosing the catalytic reaction 119
4.3 Study of the effect of spin state on the catalytic activity of the $[Fe(NH_2trz)_3](NO_3)_2$ 120
4.4 Study of the reproducibility of results 124
4.5 Optimization of experimental conditions 125
4.5.1 Study of the effect of using 96% EtOH instead of absolute EtOH 125
4.5.1.1 Study of the use of 96% EtOH as a solvent in catalytic reactions. 125
4.5.1.2 Study of the SCO transition of $[Fe(NH_2trz)_3](NO_3)_2$ suspended in absolute EtOH or 96% EtOH 127
4.5.1.3 Study of the reproducibility of the effect of 96% EtOH in the reaction medium on the catalytic activity of $[Fe(NH_2trz)_3](NO_3)_2$ 131
4.5.1.4 Comparative study of the kinetics of the catalytic reaction in the presence and absence of 96% EtOH 132
4.5.1.5 Study of the effect of washing the complex with 96% EtOH on its catalytic activity 134
4.5.2 Effect of the ratio (catalyst/aldehyde) 135
4.6 Mechanistic study of the catalysis reaction 138

4.6.1 Mechanism involving PSM reactions 138
4.6.2 Mechanism involving hydrogen bonds 139
4.6.3 Mechanism involving the presence of a Lewis acid 140
4.7 Investigation of the origin of the spin state effect on the catalytic activity of $[Fe(NH_2trz)_3](NO_3)_2$ 141
4.8 Study of the catalytic efficiency of the $[Fe(NH_2trz)_3](NO_3)_2$ in other acetalisation reactions 144
4.8.1 Study of the acetalization of *p*-anisaldehyde in the presence of trimethyl orthoformate 144
4.8.2 Acetalization reaction from other aldehydes 146
4.9 Conclusion 148
4.10 Experiment section 149
4.10.1 Acetalization reaction 149
4.10.2 Calculation of yield of the acetalisation reaction 150
4.10.3 NMR spectra of the product 152
4.11 References 159
Chapter 5 Spin Crossover Composite Films as Catalysts for Acetalization Reactions 161
5.1 Introduction 161
5.2 Our selections for spin crossover complex-based composite films used in catalysis.. 165
5.2.1 Our selection of catalytic reaction 165
5.2.2 Our selection of spin crossover complexes 165
5.2.3 Our selection of Polymer 166
5.3 Fabrication and characterization of the SCO complexes@TPU films 166
5.3.1 Monolayer film 167
5.3.2 Bilayer film 171
5.4 Three-layer film 173
5.5 Study of the movement of bilayer film in EtOH 173
5.6 Reaction of acetalization with SCO complexes@TPU films as the catalyst 178
5.6.1 Use of the monolayer film as a catalyst 178
5.6.1.1 Catalytic reaction under batch conditions 178
5.6.1.2 Catalytic reaction under continuous flow conditions 182
5.6.1.2.1 Presentation of our system inspired by continuous flow chemistry 182
5.6.1.2.2 Catalytic performance under flow condition 183
5.6.1.2.3 Study of the effect of the spin state on the catalytic activation of complex 1. 184
5.6.2 Use of the bilayer films as a catalyst 185
5.6.2.1 Catalytic reaction under batch conditions 185
5.6.2.2 Acetalisation using an H tube system in flow condition 187

5.6.2.3 Study of the spin state effect on catalytic activation. 189
5.6.2.4 Design and fabrication of microreactor 192
5.6.2.4.1 Acetalisation reaction using microreactor in flow condition 192
5.6.3 Use of the three layers film as a catalyst 196
5.7 Mechanism study of $[Fe(NH_2trz)_3](NO_3)_2$@TPU films as the catalyst 197
5.7.1 Characterisation of SCO composite film after use in catalytic reaction 198
5.7.1.1 Results of composite film from experiment A after 7 test cycles 198
5.7.1.2 Results of composite film from experiment B after 14 test cycles 200
5.7.1.3 Results of composite film from experiment C after 21 test cycles 202
5.7.1.4 Results of composite film from experiment D after 28 test cycles 203
5.7.2 The effect of solvent/reagent on SCO composite film 205
5.7.3 Study of a possible formation of imine complex in composite materials 207
5.7.4 Study of the effect of the solvent and the aldehyde on the morphology of complex 1 particles 209
5.7.5 Hydrolysis reaction of triethyl orthoformate 211
5.8 Conclusion 216
5.9 Experiment section 216
5.9.1 The general procedure of testing the composite film in the batch condition 216
5.9.2 The general procedure of testing the composite film in the H tube system 217
5.10 References 218
General conclusions and perspectives 221
Abstracts in English and French 225
Résumé de la thèse en français 227

Acknowledgements

I would like to express my sincere appreciation to all the members of my jury: Dr Azzedine Bousseksou, Dr Lucie Routaboul, Dr Bohuslav Drahoš, Dr Raluca Malacea Kabbara, and Dr Fabien Delpech. Thank you for dedicating your time and energy to reviewing my manuscript and attending the defence of this thesis. Your insightful feedback and constructive criticism have been invaluable in shaping my research and improving the quality of my work.

I am especially grateful to my supervisors, Lucie and Azzedine, for their unwavering guidance, support and patience throughout my Ph.D. journey. In particular, I would like to thank Lucie for her unwavering support over the past three years, which has been crucial to the successful completion of this thesis. She has profound knowledge, innovative thinking, excellent analytical skills for experiments and professional guidance for my work.

I would also like to thank all the members of the Switchable Molecular Materials team (Team P) at the LCC-CNRS for their support, the welcoming atmosphere and their kindness to me. Special thanks also go to my friends in Slovakia (Adam and Jana) and the Czech Republic (Petr). Your kindness has meant a lot to me and it is a great pleasure to meet all of you.

I am also deeply thankful to Vincent Colliere and Antoine Bonnet for their technical support and assistance.

None of this would have been possible without the unwavering support of my family and friends. Their encouragement and belief in me gave me the strength I needed to keep going.

Finally, I would like to express my gratitude to the China Scholarship Council for their financial support.

List of abbreviation

SCO = spin crossover

HS = high spin

LS = low spin

PSM = post-synthetic modification

aminotriazole = 4-amino-4H-1,2,4-triazole

EtOH = ethanol

MeOH = methanol

TEOF = Triethyl orthoformiate

TMB = 1,3,5-trimethylbenzene

THF = tetrahydrofuran

MEK = butanone

DMSO-d6 = deuterated dimethyl sulfoxide

BCG = bromocresol green

FTIR = fourier-transform infrared spectroscopy

NMR = nuclear magnetic resonance

TGA = thermogravimetric analysis

XRD = X-ray diffraction

SEM = scanning electron microscopy

Ea = activation energy

Arr = Arrhenius factor

TPU = thermoplastic polyurethane

P(VDF-TrFE) = poly (vinylidene difluoride-co-trifluoroethylene)

General introduction

Molecular spin crossover (SCO) complexes exhibit reversible switching between low-spin (LS) and high-spin (HS) states. This switching can be triggered by various external factors, including temperature, pressure, light, intense magnetic fields, or the presence of solvent or guest molecules. During spin state transitions, SCO compounds undergo significant changes in their physical properties, such as magnetism, dielectric behaviour, optical characteristics, and mechanical properties. The ability of SCO materials to switch between spin states in response to external stimuli makes them highly promising for a wide range of applications, such as photonic devices, electronics, and mechanical actuators. Furthermore, the impact of spin-state on chemical reactivity plays a crucial role in inorganic and organometallic chemistry, especially in reactions involving transition metal complexes. The spin states of transition metals depend on the arrangement of electrons within their d-orbitals and the surrounding coordination environment, which in turn affects reaction pathways, activation energies, and selectivities. Paradoxically, very few results in the literature concern the study of the spin state on the chemical reactivity of complexes developed for their spin crossover properties. We strongly believe that exploring the reactivity of these SCO complexes would enable us to develop a new class of switchable catalysts by taking advantage of the spin crossover phenomenon. In this context, this thesis focuses on the 1D polymeric iron(II)-triazole complex, $Fe(NH_2trz)_3(NO_3)_2$ (Complex **1**), which possesses excellent spin transition properties. Although this complex has already demonstrated numerous applications, we now want to use it as a model to explore the effect of the spin state on its organic reactivity and catalytic efficiency.

A bibliographical overview of the spin crossover phenomenon and the uses of spin crossover complexes is given in Chapter 1 of this thesis. The current understanding of how spin states affect chemical reactivity, notably in biochemistry, organometallic chemistry, and catalysis, is then reviewed. The final topics covered are the impact of spin states on catalytic reactions and the application of spin crossover complexes as catalysts.

The research work reported in Chapter 2 started with the finding that a temperature increase could very dramatically accelerate a post-synthetic modification (PSM) reaction on complex **1**. Our interest in this observation arose from our hope that this improvement in reaction efficiency was caused, at least in part, by the iron's spin state. Therefore, chapter 2 outlines the scientific approach we used to address the challenge of isolating the impact of iron's spin state from the other factors that might account for an increase in reaction efficiency. An indisputable advantage in accomplishing this goal was the outstanding spin crossover characteristics of complex **1**. So, Chapter 2 presents a comprehensive study of the effect of spin state on the efficiency of the PSM reaction on complex **1**. The statistical analysis made feasible by the huge number of experiments highlighted how the drastic effect of the iron atom's spin state on the PSM reaction yield is both general and reproducible. To the best of our knowledge, this work is the first to demonstrate that the spin state affects organic reactivity of a functional group in a metal complex.

Chapter 3 reveals how we serendipitously moved from the mechanistic study of the PSM reaction on complex **1** to the use of this complex in catalysis. We demonstrated that, under appropriate conditions, complex **1** can be used as a catalyst for the formation of imines. Although this is only the second reported example of a 1D spin crossover triazole polymer complex exhibiting catalytic activity, it is the first example where the catalytically active species is the SCO complex. In Chapter 3, we also highlight the extent to which PSM reactions may be involved in the catalytic activity of complex **1**. The fact that we regularly recovered and analysed the complexes after the catalysis reactions gave us an insight into how these reactions proceeded. This work illustrates that even if a catalytic mechanism is well established in the

literature, it is necessary to consider the reaction studied as a whole, as the mechanism can be highly dependent on the catalyst and/or the catalytic substrates.

The main aim of the research in Chapter 4 was to demonstrate that the iron atom's spin state can efficiently control the catalytic activity of a spin-crossover complex. We start this chapter by describing our reasoning for selecting complex **1** as a prime candidate for this investigation and the requirements we believed the catalytic reaction needed to meet. After this, chapter 4 details each stage of the investigation that was conducted, allowing us to clearly demonstrate how the spin state greatly affected the catalytic ability of complex **1** in an acetalization reaction. We also conducted tests to learn more about the catalytic mechanism of complex **1** in acetalization reactions. This chapter also contains the investigation we conducted to identify the origin of the spin state effect on the catalytic activity of compound **1**. The findings of this research work reveal that the catalytic activity of the SCO coordination polymer can be profoundly influenced by the spin state of iron. The initial step in using SCO complexes in switchable catalysis is also validated by this outcome.

Chapter 5 presents a detailed study of spin crossover polymer composite films used as catalysts in acetalisation reactions. Incorporating complex **1** into a polymer matrix was important to us for two reasons: 1) to make recycling the catalyst easier and more effective, and 2) to investigate a possible synergy between complex **1** and another SCO complex that might increase the difference in catalytic activity between two spin states of complex **1**. It was our hope that the second spin transition of the SCO complex would cause the composite material to change its shape and porosity. These two occurrences have the potential to alter access of substrates to the catalytic site, which could impact catalytic efficiency of complex **1**. Following an explanation of our goals and the approach we have taken, this chapter will go over these composite materials, from their production to the investigation of their post-catalysis recyclability, including their characterization and an examination of how the spin state affects their catalytic capacity. Notably, this chapter will also cover the formation of a reactor, the use of a continuous flow chemistry-inspired system, and the investigation of a second reaction that complex **1** catalyzes, which may facilitate the purification of acetal.

The thesis ends with some general conclusions and perspectives.

Chapter 1 Bibliographic overview of the spin crossover phenomenon and of the influence of spin states on chemical reactivity

This introduction had to address the spin crossover phenomenon since my thesis is about the application of a spin crossover complex in catalysis. Since the effect of the spin state on the chemical reactivity of the spin crossover complex is the subject of two of my thesis chapters, it seemed appropriate to address this notion as well. The discussion of the few findings on the application of spin crossover complex in catalysis that have been documented in the literature marks the conclusion of the bibliographic overview.

1.1 Spin crossover phenomenon

1.1.1 General presentation of the spin crossover phenomenon

The spin crossover (SCO) phenomenon refers to a reversible transition between high spin (HS) and low spin (LS) states in certain transition metal complexes, triggered by external stimuli such as temperature[1], pressure[2], light[3] and magnetic field[4]. The SCO phenomenon is typically observed in octahedral complexes of transition metals with d^4-d^7 electron configurations. The change in spin state can significantly alter the properties of the material, making SCO complexes valuable in applications such as sensors, electronic devices and mechanical actuators.[5-7]

According to crystal field theory, the interaction between the central ion of a coordination compound and its ligands can be considered as a purely electrostatic force.[8] The positively charged central ion is situated within a crystal field created by the negatively charged ligands. When a transition metal ion is exposed to the electrostatic influence of these ligands, the degenerate d-orbitals of the metal ion split into different energy levels. In octahedral complexes (Fig.1-1), the five d-orbitals are divided into two energy levels: the e_g orbitals (d_{z^2} and $d_{x^2-y^2}$) and the t_{2g} orbitals (d_{xy}, d_{xz}, and d_{yz}), with the e_g orbitals being higher in energy than the t_{2g} orbitals. The energy difference between these split d-orbitals called the crystal field splitting energy (Δ).

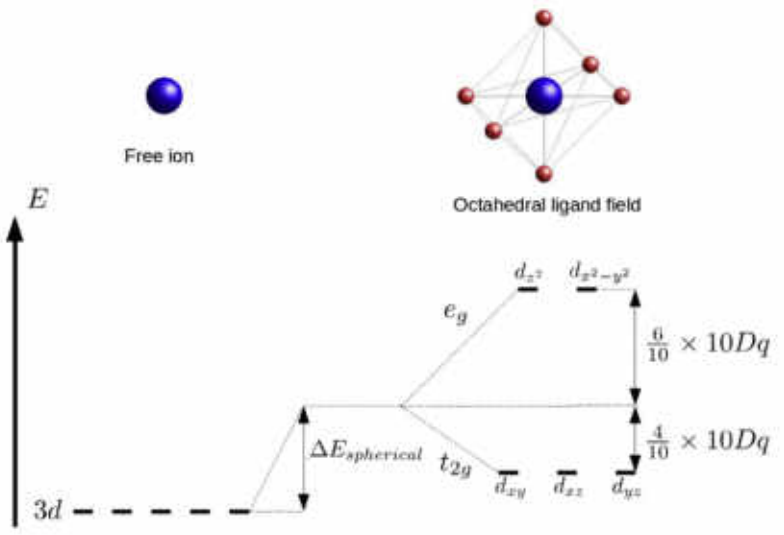


Fig.1-1 Schematic representation of the partial degeneracy splitting of 3d orbitals due to the presence of the octahedral ligand field.[8]

As depicted in Fig.1-2, the distribution of electrons within these d-orbitals adheres to the principles of minimum energy and Hund's rule. When the crystal field splitting energy (Δ) exceeds the electron pairing energy (P), electrons preferentially pair in the lower-energy t_{2g} orbitals before occupying the higher-energy e_g orbitals, thereby resulting in a low-spin state for the central ion. In contrast, if Δ is less than P, electrons will occupy the maximum number of orbitals in accordance with Hund's rule, leading to a high-spin state in the central ion.[9, 10]

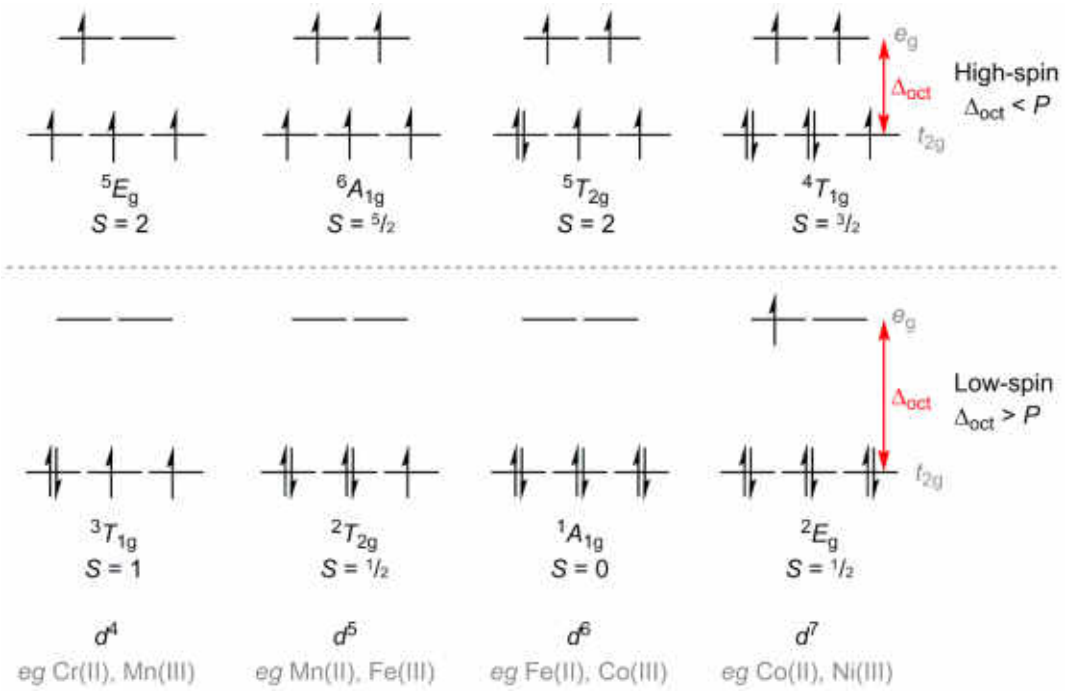


Fig.1-2 In an octahedral ligand field, d^4–d^7 transition metal ions can exhibit either high-spin or low-spin electron configurations, depending on the strength of the crystal field splitting energy relative to the pairing energy of the electrons.[9, 10]

When the splitting energy (Δ) is comparable to the electron pairing energy (P), and the energy difference between the high-spin and low-spin ground states is on the same order of magnitude as kT (where k is the Boltzmann constant and T is the temperature), the spin states can be interconverted by external factors such as temperature, light, or pressure. This phenomenon is known as spin crossover (SCO).

In recent years, Fe(II) [11], Fe(III)[12], Mn(III)[13], Co(III)[14], Co(II)[15], and Ni(II)[16]has been the extensively studied metal ions in the field of spin crossover. Among these transition metal ions, Fe (II) (d^6) is the most extensively studied metal ion in the spin crossover field, particularly when coordinated with six nitrogen donors. Under external stimuli, it could exhibit a significant change in magnetic response that transitions from a diamagnetic low-spin state to a high-spin state with four unpaired electrons. For example, in Fe(II) SCO complexes, the originally degenerate five d-orbitals split into two groups with different energy levels (t_{2g} and, e_g.) under the influence of an octahedral crystal field (Fig.1-3). When the pairing energy P is less than the splitting energy Δ, the electron configuration is ${t_{2g}}^6{e_g}^0$, resulting in a stable low-spin state with a spin quantum number S = 0, which corresponds to diamagnetism. Conversely, when the pairing energy P is greater than the splitting energy Δ, the electron configuration becomes ${t_{2g}}^4{e_g}^2$, leading to a stable high-spin state with a spin quantum number S = 2, exhibiting in paramagnetism.[8]

In addition to this pronounced spin state transition, several other significant changes occur in

Fe(II) SCO complexes, including 1) The LS state is typically more intensely coloured (e.g., purple or dark red), whereas the HS state is usually paler (e.g., white or yellow). This change in colour of the complexes can be observed using optical reflectivity measurements and UV-vis spectroscopy[17]. 2) In the LS state, the Fe-N bond lengths (approximately 1.8-2.0 Å) are about 10% shorter than in the HS state (approximately 2.0-2.2 Å) due to the absence of electrons in the antibonding e_g orbitals. This difference can be measured by X-ray crystallography[18]. 3)The electron density at the nucleus varies between the LS and HS states, resulting in distinct isomer shifts and quadrupole splitting, which can be observed in Mössbauer spectra.[8] 4) Heat is released during the transition from the HS to the LS state and absorbed when returning to the HS state. This thermal change can be detected by Differential Scanning Calorimetry (DSC), which also facilitates the determination of the enthalpy (ΔH) and entropy (ΔS) associated with the SCO process[19].

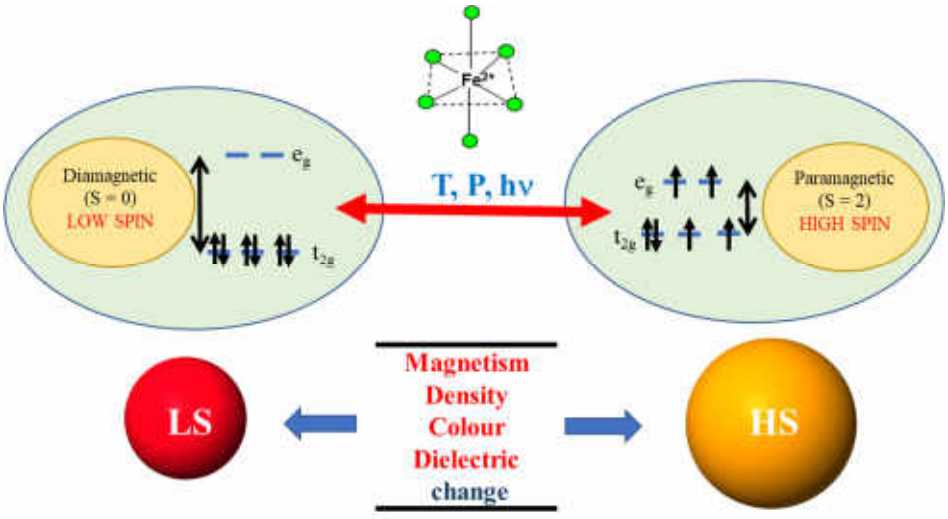


Fig.1-3 Overview of the Iron(II) SCO phenomenon.

1.1.2 How the spin crossover phenomenon is induced by the application of the stimulus?

As we just discussed, the spin crossover complex has the ability to change its spin state when a stimulus is applied. This raises the question of how the spin crossover phenomenon is influenced by the stimuli. What kind of stimuli is used determines the answer. As an example, I will describe how temperature, light, and pressure influence the spin crossover process.

1.1.2.1 Temperature-induced spin crossover phenomenon

Temperature is the most common external stimulus for inducing spin crossover. As the temperature increases or decreases, the population distribution between the high-spin and low-spin states changes. The magnetic behaviour associated with the spin crossover phenomenon can be represented using temperature-dependent magnetic susceptibility (γ HS vs T) curves, where γ HS is the mole fraction of high-spin state molecules within the total fraction [nHS(T) + nLS(T)], and T is the temperature. As shown in Fig.1-4, the γ HS = f(T) curve illustrates that spin crossover behaviour can be classified into five types[8]: (a) Gradual transition: The spin transition occurs slowly and smoothly over a wide temperature range. (b) Abrupt transition: The spin transition happens quickly within a narrow temperature range. (c) Abrupt transition with thermal hysteresis: The transition is abrupt, but there is a difference in the transition

temperature when heating versus cooling. The difference between these two temperatures is called the hysteresis width. (d) Two-step transition: The spin transition occurs in two distinct steps, with an intermediate state between the high-spin and low-spin states. (e) Incomplete transition: The transition does not proceed fully from one spin state to another, resulting in a mixture of high-spin and low-spin states at the end of the transition.

A gradual transition occurs when the change from the low-spin state to the high-spin state (or vice versa) happens slowly over a broad temperature range. In a gradual transition, the interactions between the molecules or ions within the solid are relatively weak. This means that the spin state of one molecule does not strongly influence the spin state of its neighbours, leading to a more individualistic and gradual response to changes in temperature. In contrast, abrupt spin transition complexes have a narrow transition temperature range, and there is a strong elastic interaction (high cooperativity) in this type of complex; the stronger the synergy, the faster the spin change occurs. Importantly, when the synergy is strong at a certain level, a hysteresis loop will appear.

The hysteresis loop refers to a delay in the magnetic response during temperature changes, leading to a loop in the magnetic susceptibility versus temperature plot for the complex. This occurs because the transition temperature on the cooling cycle differs from that on the warming cycle. Within this loop, the spin crossover compound exhibits bistability, with its spin state determined by its recent thermal history. For example, when the compound enters the loop region from a low temperature, it remains in the LS state, whereas entering the loop from a high temperature preserves the HS state. These two states can be seen as a molecular analogue of a memory component. It is important to note the distinction between a compound that undergoes SCO with thermal hysteresis (memory) and one that merely undergoes SCO. The latter functions only as a switch, as it cannot exist in two distinct spin states at the same temperature and, therefore, lacks a "memory". Hysteretic behaviour associated with this memory effect is considered for molecular memory applications.[20, 21] Meanwhile, abrupt transitions are relevant for thermal sensors,[22, 23] and gradual conversions could be applied in fields such as microthermometry.[24]

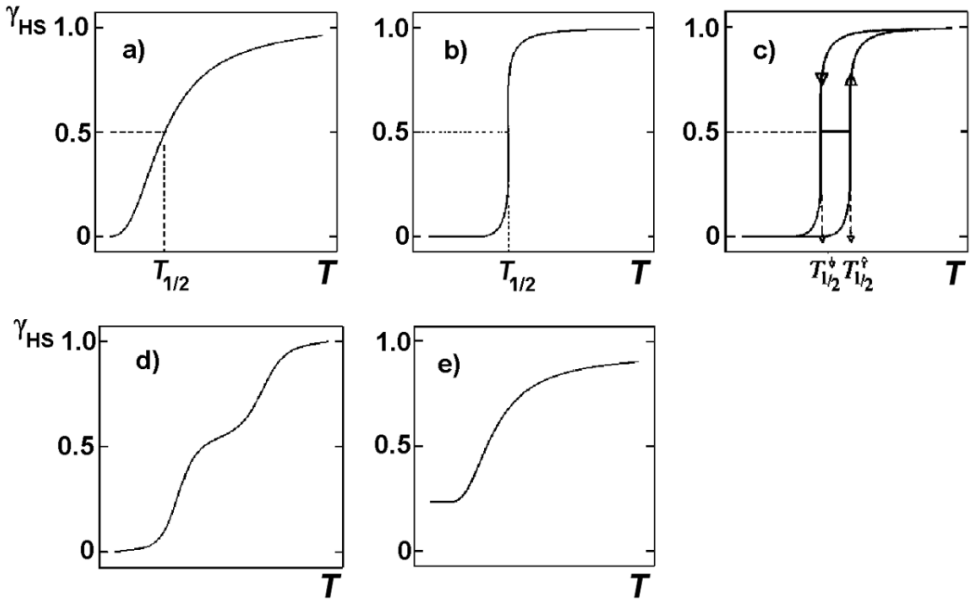


Fig.1-4 Schematic representation of five types spin transition curves. (a) gradual (b) abrupt (c) abrupt with thermal hysteresis (d) two step and incomplete.[8]

1.1.2.2 Light-induced spin crossover phenomenon

Light-induced spin crossover, including the Light-Induced Excited Spin State Trapping (LIESST) effect and the Ligand-Driven Light-Induced Spin Crossover (LD-LISC) effect, are of significant interest in the study of spin-crossover complexes. The LIESST effect is a direct influence on the metal ion, typically occurring at low temperatures. In this process, the molecule is photoexcited from its LS state via either a metal-centered d-d transition or a metal-to-ligand charge transfer transition, subsequently relaxing into a metastable HS state (Fig.1-5).[25, 26]

In contrast, the LD-LISC effect involves an indirect mechanism, mediated through a photoisomerizable coordinated ligand, and can occur at relatively higher temperatures (compared to LIESST). This phenomenon is observed in some complexes containing photosensitive ligands. Upon light irradiation, a photochemical reaction induces a conformational change in the ligand, which in turn modifies the crystal field strength at the metal centre, thereby inducing a spin-state transition in the metal ion.[26]

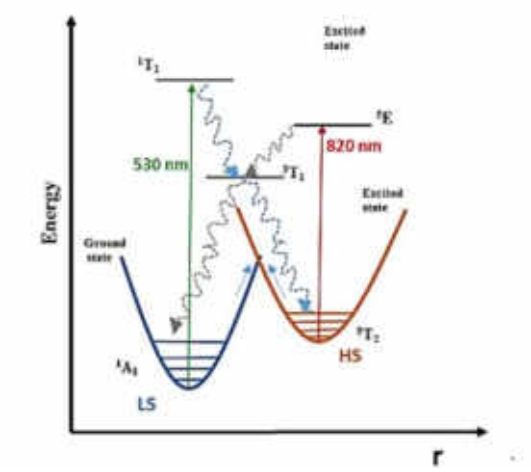


Fig.1-5 Scheme of LIESST effects of SCO complex induce by light.[26]

1.1.2.3 Pressure-induced spin crossover phenomenon

Spin crossover can also be induced by applying external pressure. Increasing pressure generally favours the LS state due to its smaller ionic radius, as the more compact LS state allows the material to occupy less volume under high pressure. Conversely, decreasing pressure tends to favour the HS state. As an example shown in Fig.1-6, the spin crossover curves become increasingly gradual, and the width of the hysteresis loop tends to decrease.[27]

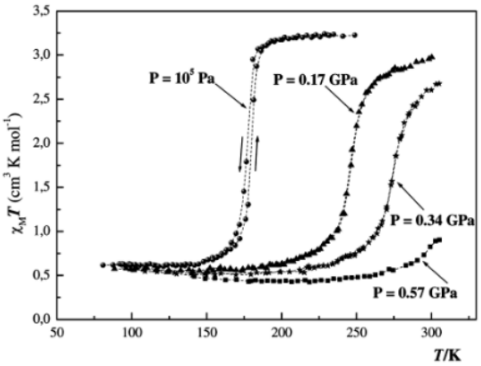


Fig.1-6 The magnetic properties of a SCO complex under different pressure.[27]

1.1.3 Application of Spin Crossover Materials

Spin crossover materials are versatile and hold significant promise across broad applications due to their unique ability to switch between different spin states in response to external stimuli. This tunability in properties such as magnetism, color, and conductivity makes them highly suitable for advanced technological applications in photonic devices, electronic devices, and mechanical actuators.[5, 6]

1.1.3.1 Application of spin crossover materials in photonic devices

The optical properties of spin crossover compounds, which can change in response to various external stimuli, make them ideal for use in photonic sensor devices that monitor changes in the physical and chemical parameters of the external environment.[28] Furthermore, the reversible transition between high-spin and low-spin states, triggered by altering external conditions, enables these compounds to function as a reversible switch between "optical OFF" and "optical ON" states in photonic switch devices.[29] For example, Gentili et al.[28] presented a study on the multi-modal sensing capabilities of the neutral spin crossover (SCO) compound with the molecular formula $[Fe(L)_2]$ (where L is 2-(pyrazol-1-yl)-6-(1H-tetrazol-5-yl)pyridine) (Fig.1-7). This SCO compound was used to fabricate a selective sensor for methanol and ethanol. Its unique properties were further exploited by integrating the neutral, room-temperature switchable compound into a micrometric TAG sensitive to colour and birefringence. This study demonstrated that the sensing capabilities of the SCO compound arise from the incorporation of alcohol molecules into its crystalline structure, which subsequently modulates the transition temperature and the associated physical properties.

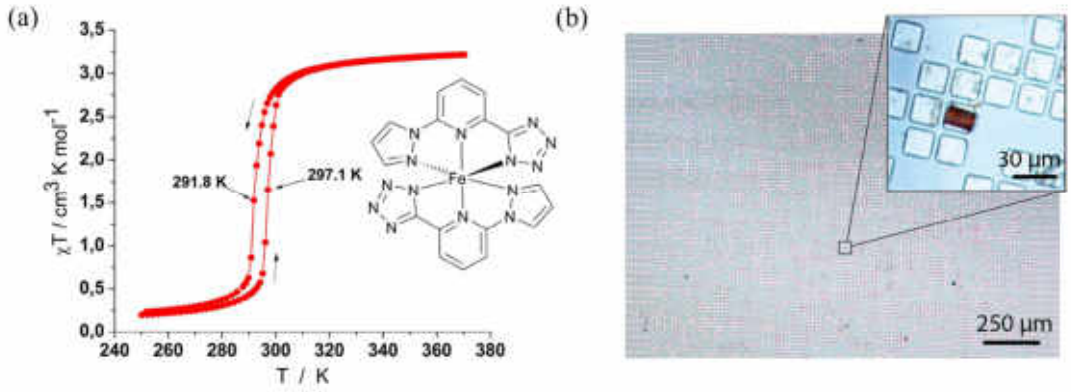


Fig.1-7 (a) Magnetic characterisation. (b) Optical image of addressable crystallites printed on a micrometric TAG.[28]

1.1.3.2 Application of spin crossover materials in electronic devices

The integration of spin crossover complexes into electronic devices has emerged as an exciting area of research in molecular electronics. SCO complexes, which exhibit reversible switching between the low-spin and high-spin electronic configurations in response to external stimuli, offer a unique opportunity to design molecular devices with tunable electronic and magnetic properties.

In 2011, Prins et al.[30] successfully fabricated a molecular device that exhibited switching behaviour near room temperature by depositing nanoparticles of the Fe(II) coordination polymer $Fe(trz)_3(BF_4)$ (trz = triazole) with a core-shell structure between two nanometer-spaced electrodes (see Fig.1-8). A temperature-dependent conductance investigation of this device

revealed that current could be transmitted through the particles, demonstrating bistability in conductance as a function of temperature. As illustrated in Fig.1-8 (a), the observed hysteretic behaviour in the temperature-dependent conductance characteristics closely resembles the spin crossover curve of the particles. Two year later, Rotaru et al.[31] successfully deposited $Fe(trz)_3(BF_4)$ (trz = triazole) nanorods between electrodes with a 4 μm gap using an ethanol solution. Fig.1-8 (b) presents the thermal variation of the electrical conductivity and current-voltage characteristics of the resulting device. By applying an AC voltage, the electric field gradient facilitated the preferential alignment of the spin crossover nanorods within the gaps between the electrodes. A clear indication of the spin transition was observed in the temperature-dependent current (I-T) measurements. As the temperature increased (from LS to HS), a decrease in current intensity was observed. Conversely, as the temperature decreased, an increase in current intensity was observed.

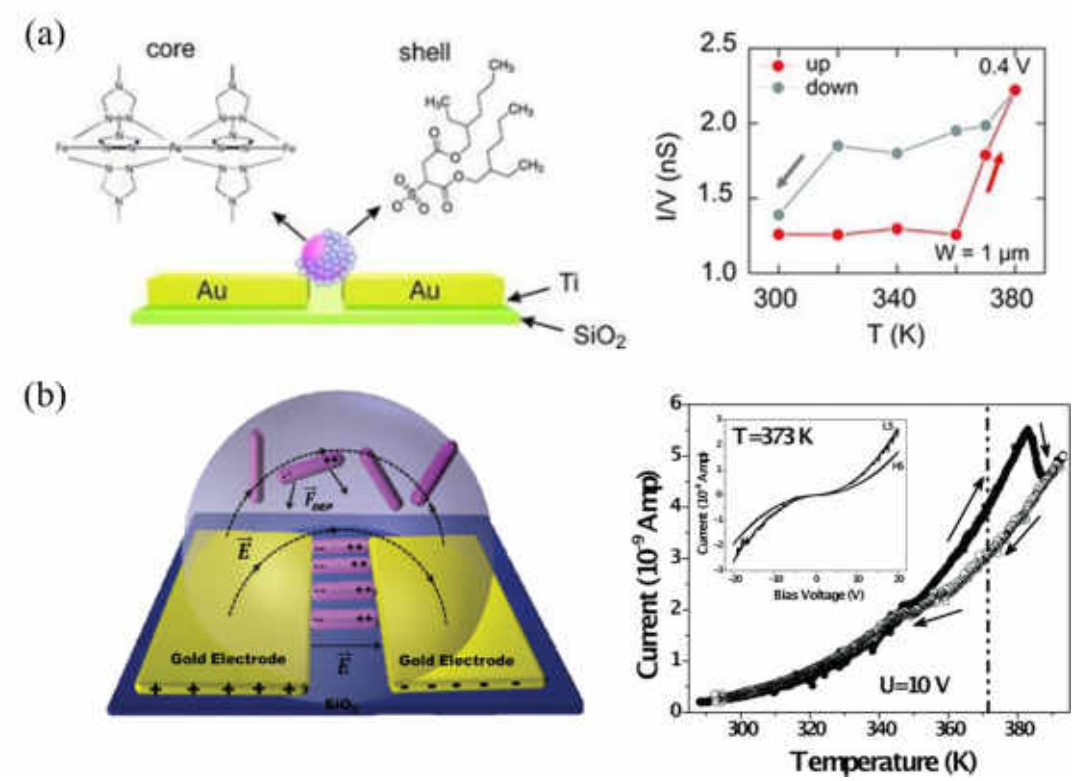


Fig.1-8 (a) Electronic devices fabricated by placing $[Fe(Htrz)_2(trz)](BF_4)$ nanoparticles with core-shell in the electrode gap: schematic and IV characteristics.[30] (b) Schematic diagram of the arrangement of $[Fe(Htrz)_2(trz)](BF_4)$ microrods in the plane electrode gap and the result temperature dependence of the current measurement during heating and cooling cycles with a bias voltage of 10 V.[31]

1.1.3.3 Spin crossover materials as mechanical actuators

In some spin-crossover materials, the transition from the LS to the HS state is accompanied by a significant lattice expansion, leading to volume increases of up to 22% and an 11% increase in the uniaxial direction. This substantial change in lattice dimensions imparts notable mechanical properties, making spin-crossover materials excellent candidates for mechanical actuator development.[32, 33]

The first attempt to create molecular actuators in cantilever form was made by Shepherd et al in 2013.[34] They successfully fabricated a bilayer actuator using highly anisotropic crystals of $Fe(3\text{-}CNpy)[Au(CN)_2]_2 \cdot H_2O$, which were coated with aluminium. The movement of the

cantilever tip was attributed to the differential thermal expansion between the two layers. Additionally, uniaxial negative thermal expansion (NTE) and a sharp spin crossover property of the crystal produced the opposite effect. More recently, soft bilayer SCO@polymer actuators were developed by Piedrahita-Bello et al using a blade casting method, which integrated a series of SCO nanoparticles within a P(VDF-TrFE) matrix[35, 36]. Incorporating silver flakes in the second layer facilitated electrothermal actuation via Joule heating. These composite materials effectively combined the natural compliance and damping properties of the polymer matrix with the high work density of the spin crossover filler. Consequently, the bilayer spin crossover (SCO)@polymer nanocomposites demonstrated robust and controllable actuation cycles in response to electrical stimuli (Fig.1-9).

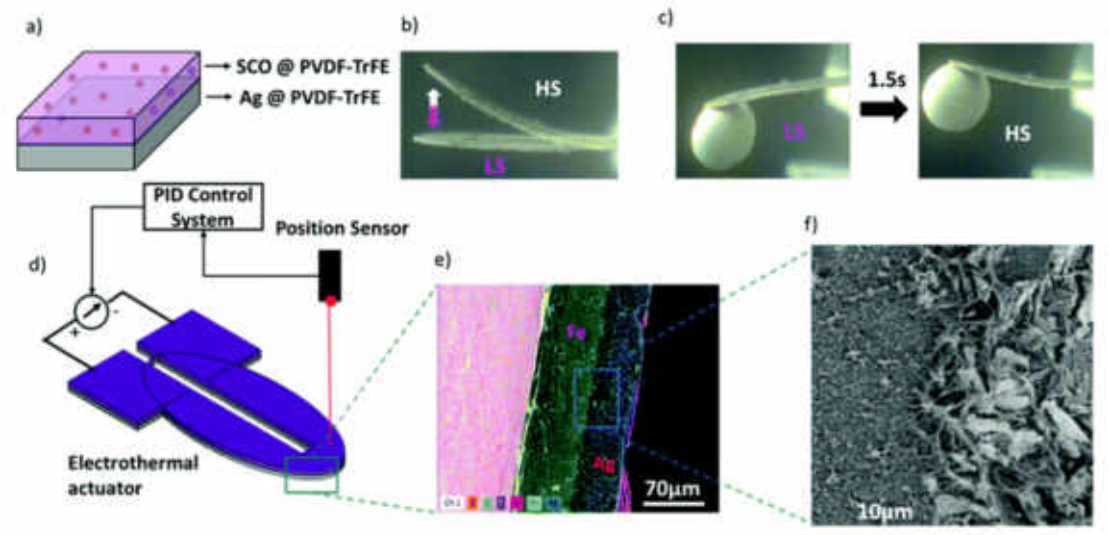


Fig.1-9 (a) Schematic illustration of the two-layer SCO composite. The two-layer device is reversibly driven (b) without load and (c) with load between HS and LS states. (d) Schematic diagram of actuator test bench. (e) EDX mapping image of a bilayer cross-section showing the distribution of Fe (green) and Ag (blue) atoms. (f) SEM image of the bilayer SCO composite interface.[36]

1.2 Spin state effect on chemical reactivity

1.2.1 General presentation of the spin state effect on chemical reactivity

The impact of spin-state effects on chemical reactivity is a fundamental concept in inorganic and organometallic chemistry, especially in reactions involving transition metal complexes. Transition metals can exhibit various spin states, which are determined by the specific arrangement of electrons within their d-orbitals and the surrounding coordination environment. The spin states significantly influence activation energies of reactions, reaction pathways and selectivity.[37-39]

1.2.1.1 Spin state effect on activation energies of reactions

Transitions between spin states, such as from high-spin to low-spin configurations, may involve substantial energy changes that directly affect the activation energies of reactions. Reactions may proceed more efficiently when accompanied by favourable spin-state changes. For example, in 2018, Macaulay et al.[40] investigated the reactivity of structurally analogous (N-phosphinoamidinate)metal ($N(SiMe_3)_2$) pre-catalysts ((PN)M; where M = Mn^{2+}, Fe^{2+}, Co^{2+}, and

Ni^{2+}; d^5–d^8) in the isomerization–hydroboration of 1-octene, cis-4-octene, and trans-4-octene with HBPin (Fig.1-10). Their study revealed divergent catalytic reactivity and selectivity across the (PN)M series complexes: while (PN)Mn and (PN)Ni exhibited poor hydroboration yields, (PN)Fe and (PN)Co achieved high conversion rates and selectivity for the final borylation product. The Density Functional Theory calculations further elucidated that the reactivity differences among these pre-catalysts are closely related to their spin-state energy gaps. In the reaction involving (PN)MnH and trans-4-octene, the lack of a viable spin crossover mechanism resulted in slow migratory insertion and, consequently, low reaction yields. In contrast, (PN)FeH accessed lower reaction barriers through spin crossover, and (PN)CoH demonstrated a very low migratory insertion barrier in its low-spin state. This study enhances the understanding of both the mechanistic pathways and the relative catalytic performances of the (PN)M pre-catalyst series, highlighting the crucial role of the spin state in accelerating catalytic reactions.

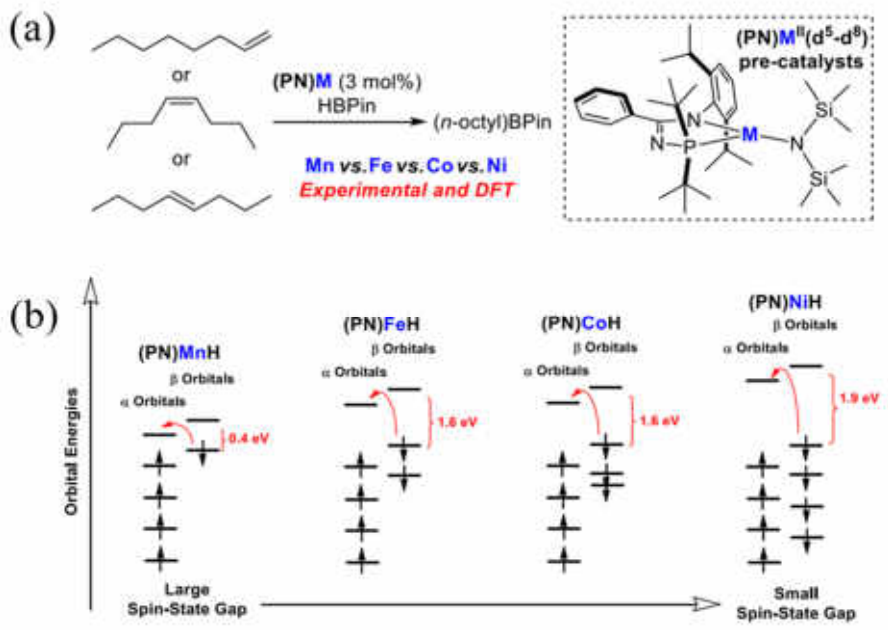


Fig.1-10 (a) Alkene isomerization-hydroboration catalyzed by Mn, Fe, Co and Ni N-Phosphinoamidinate Complexes. (b) Idealised d-orbital occupation changes from lower to higher spin states. [40]

1.2.1.2 Spin state effect on reaction pathway

The spin state of a complex can significantly influence its preferred reaction pathway. For example, in 2017, Andris et al.[41] demonstrated that the photodissociation of the octahedral iron(III) azide complex $[(MePy_2TACN)Fe(N_3)]^{2+}$ ($MePy_2TACN$ = Nmethyl-N,N-bis(2-picolyl)-1,4,7-triazacyclononane) is strongly governed by its spin states. The spin-state population of this iron(III) azide complex can be modulated by temperature, with the sextet state population decreasing as the temperature lowers. Below 200 K, the doublet state becomes dominant and is exclusively populated at very low temperatures (around 3 K). Photodissociation of the doublet state, which exhibits absorption at λ max=530nm, predominantly leads to photooxidation, resulting in the formation of an iron(V) nitride complex. In contrast, photodissociation of the sextet state, with an absorption maximum at λ max=455 nm, mainly results in photoreduction, characterized by the loss of an N_3* radical (Fig.1-11). This study underscores how different spin states can drive the complex along distinct reaction pathways.

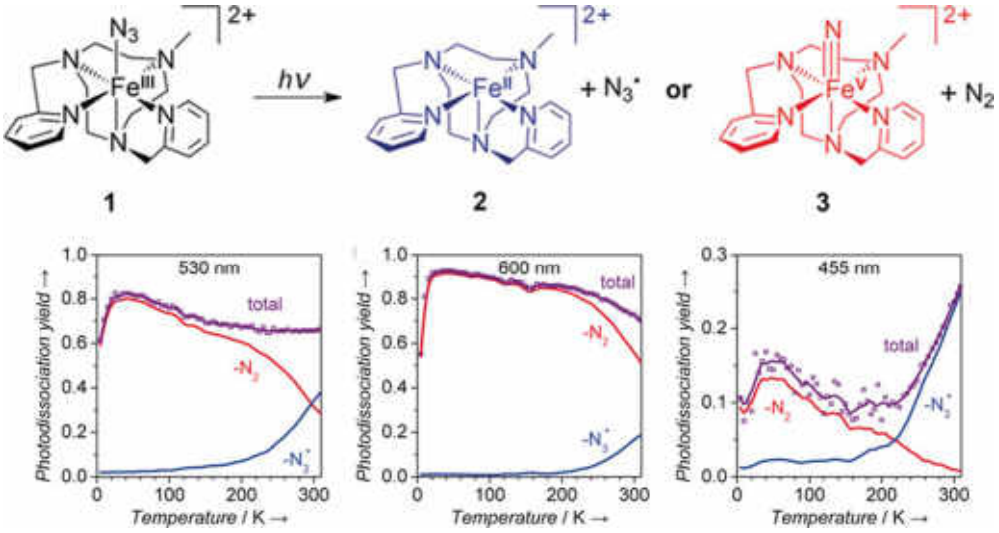


Fig.1-11 (a) Photodissociation of the iron azide complex $[(MePy_2TACN)Fe(N_3)]^{2+}$ **1** leads to two possible outcomes: it can either undergo photoreduction to form $[(MePy_2TACN)Fe]^{2+}$ **2** or photooxidation to produce the iron nitride complex $[(MePy_2TACN)FeN]^{2+}$ **3**. (b) Result of temperature-dependent photofragmentation.[41]

1.2.1.3 Spin state effect on the selectivity of reactions

The spin state of a molecule can significantly influence the selectivity of a reaction. For example, in 2019, Zima et al.[42] investigated the activity and selectivity of S=1/2 and S=3/2 oxide (V) intermediates in comparison to the related oxide (IV) species. They utilized a bioinspired catalyst system based on a chiral non-heme iron complex with PDP type N4-donor ligands (PDP = N,N'-bis(pyridin-2-ylmethyl)-2,2'-bipyrrolidine), with substituents on the pyridine rings, 4-NMe_2 in complex **7** and 3,5-Me_2-4-OMe in complex **6** (Fig.1-12 (a)). These complexes efficiently catalyzed the enantioselective epoxidation of alkenes using H_2O_2 and peracetic acid in the presence of a carboxylic acid additive. Catalyst systems based on complex **7**, which features a high-spin perferryl intermediate (S=3/2), exhibited higher enantioselectivity compared to those based on complex **6**, which has a low-spin perferryl intermediate (S=1/2). The high-spin (S=3/2) perferryl intermediate, stabilized by strongly electron-donating NMe_2 groups, ensures greater enantioselectivity in olefin epoxidations with H_2O_2 than analogous systems involving low-spin (S=1/2) perferryl intermediates. The study highlighted how variations in the spin state of intermediates can lead to significant differences in catalytic efficiency and selectivity (Fig.1-12 (b)).

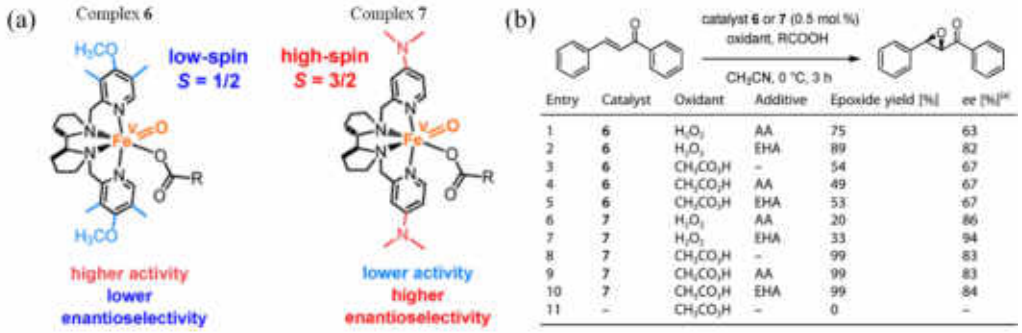


Fig.1-12 (a) chiral non-heme iron complex with PDP type N4-donor ligands. (b) result of catalytic reaction.[42]

1.2.2 Importance of the spin state effect in different chemical fields

Currently, the effect of spin state is a topic of significant interest across various scientific disciplines. The following section will discuss the impact of spin-state effects on chemical reactivity in different fields, including biochemistry, organometallic, and catalysis.

1.2.2.1 Importance of the spin state effect in biochemistry

Heme-containing proteins are integral to various biological processes, including electron transfer, oxygen transport and catalysis.[43] Cytochrome P450, a prototypical and extensively studied example, illustrates a fascinating catalytic cycle involving multiple spin state transitions (Fig.1-13).[44] In its resting state, the enzyme exists as a low-spin state (doublet) with water molecules coordinated at the active site. Upon substrate binding, the spin state transitions to a high-spin (sextet) configuration. This transition facilitates the first electron reduction, converting the enzyme to a high-spin state (quintet). At this stage, dioxygen can enter the active site, triggering a second spin flip to a low-spin f (singlet) state. Following this, the enzyme undergoes double protonation of the distal oxygen and a second electron reduction, likely resulting in the formation of FeIV=O iron-oxo species. The distal oxygen is subsequently released as a water molecule. FeIV=O iron-oxo species then hydroxylates the substrate.[45, 46]

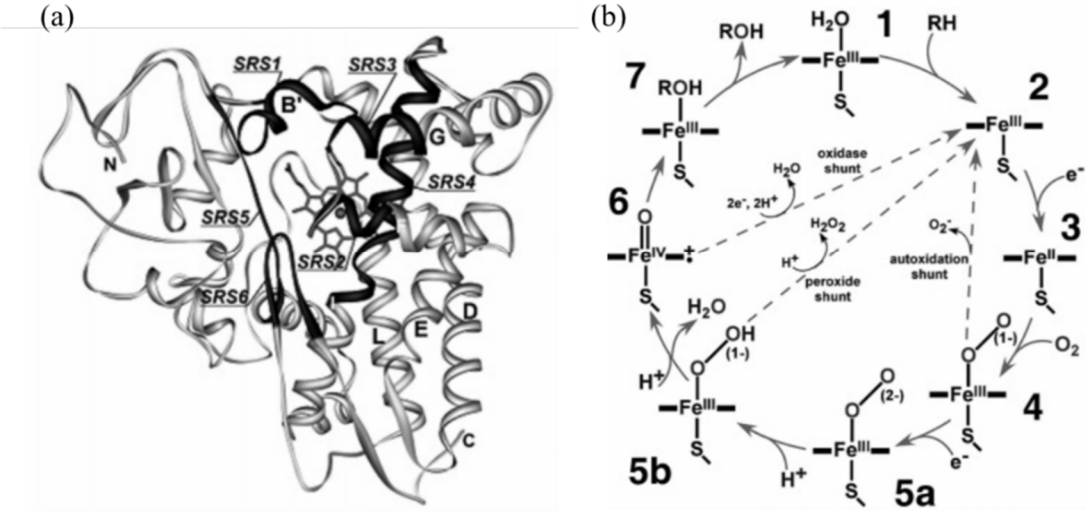


Fig.1-13 (a) The fold of cytochrome P450s is highly conserved and shown in a ribbon representation. (b)P450 catalytic cycle.[45]

1.2.2.2 Importance of the spin state effect in organometallic chemistry

The spin state in organometallic complexes plays a pivotal role in determining their electronic structure, bonding, reactivity, stability, geometry, and magnetic properties. A thorough understanding and precise control of the spin state are essential for designing complexes with specific reactivity and desired properties.[47] Through three examples, we'll show that the metal spin state will influence the ligand coordination mode, the reaction mechanism and the reaction rate.

1.2.2.2.1 Influence of metal spin state on ligand coordination

In 2015, Afyouni et al.[48] investigated a cobalt(I) system exhibiting hemilability and on the cusp of a spin-state change, allowing for rapid interconversion between different spin states and structures, known as "spin isomers." The cobalt(I) monocarbonyl complex LtBuCo(CO) was

identified as a singlet in the solid state, characterized by a diketiminate binding mode where one of the C=C double bonds of an aromatic ring completes a pseudo-square-planar coordination. Upon dissolution, a significant population of the triplet state emerged, attributed to strong spin-orbit coupling with a low-lying excited state (Fig.1-14). This interconversion between spin isomers was found to be rapid, even at low temperatures. They demonstrated that instead of dissociation, the cobalt atom was observed to slide along the aromatic system, balancing strain energy with cobalt–ligand bonding. These results introduce new strategies for the development of reactive low-coordinate sites for catalysis and for the implementation of magnetic switching in molecular materials.

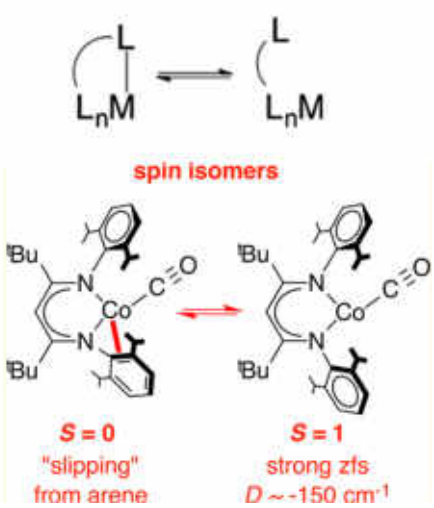


Fig.1-14 Hemilabile ligands can reversibly dissociate one donor atom from the metal centre.[48]

1.2.2.2.2 Influence of metal spin state on the reaction mechanism

In 2013, Liu et al. [49] investigated and compared the geometric and electronic structures as well as the reactivity of mononuclear nonheme S = 5/2 (HS) (TMC)FeIII-OOH complexes (TMC = 1,4,8,11-tetramethyl-1,4,8,11-tetraazacyclotetradecane) and S = 1/2 (LS) (N_4Py)FeIII-OOH complexes (N_4Py=N,N-bis(2-pyridylmethyl)-N-bis(2-pyridyl)methylamine) using density functional theory calculations. The study aimed to elucidate the similarities and differences in the mechanisms of O-O bond homolysis and electrophilic hydrogen atom abstraction reactions.

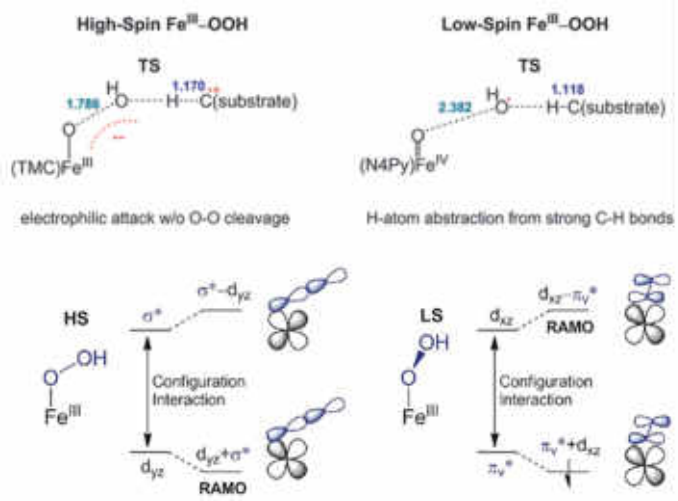


Fig.1-15 The transition states of the HS and LS FeIII−OOH complexes during the H-atom abstraction reaction (top), and the configuration interactions of these two complexes (bottom).[49]

Their findings revealed that both the HS and LS FeIII-OOH complexes are capable of performing direct hydrogen atom abstraction, albeit through distinct reaction coordinates. For the LS FeIII-OOH complex, the transition state is characterised as late along the O-O coordinate and early along the C-H coordinate. Conversely, the HS FeIII-OOH complex exhibits an early transition state along the O-O coordinate and a more advanced transition state along the C-H coordinate. Additionally, significant electron transfer from the substrate to the HS FeIII-OOH complex occurs at the transition state, a phenomenon not observed in the LS transition state. Consequently, the H-atom abstraction reactivity of the HS FeIII−OOH complex is highly dependent on both the ionization potential and the C-H bond strength of the substrate, in contrast to the LS complex. The LS FeIII-OOH complex is more effective at abstracting hydrogen atoms from substrates with strong C-H bonds, whereas the higher reduction potential of the HS FeIII-OOH complex enables it to engage in electrophilic reactions without O-O bond cleavage.

1.2.2.2.3 Influence of metal spin state on rate of reaction

In the same year, Bellows et al.[50] conducted a study on the pathways for β-hydride elimination (βHE) in alkyl complexes of iron(II) and cobalt(II) coordinated with β-diketiminate ligands, using density functional theory. Their research revealed that rapid βHE can occur in certain high-spin iron(II) and cobalt(II) alkyl complexes, even without the typically necessary empty d orbitals (Fig.1-16). Notably, they found that only the spin-crossover pathway aligned with the experimentally observed reaction rates. In this pathway, the lower-spin transition state adopts a square-planar geometry, which is particularly favorable for depopulating an in-plane d orbital, allowing it to accept electrons from the β-hydrogen. This finding underscores the crucial role of spin crossover in the βHE reactions of high-spin alkyl complexes, enabling a spin-accelerated mechanism in which the transition state has a lower-spin electronic configuration than both the reactants and products.

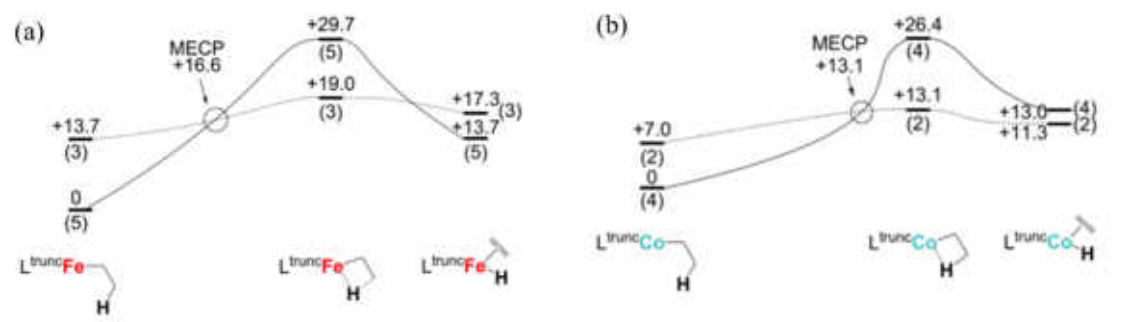


Fig.1-16 The potential energy diagram for βHE of L^{trunc}FeEt and L^{trunc}CoEt is presented, displaying the Gibbs free energies in kcal/mol for both the doublet and quartet spin states. The energy of the minimum energy crossing point (MECP) has not been adjusted for spin-hopping probability. The respective spin states are indicated in parentheses.[50]

1.2.2.3 Importance of the spin state effect in catalysis

Pérez et al. considered that the spin state is so important that it constitutes a field of catalysis in itself, which he called spin-catalysis.[51] In this section, I will show that the spin state influences a wide range of catalytic reactions.

1.2.2.3.1 Alkene isomerization

Alkene isomerization refers to the chemical reaction in which one alkene, a molecule containing at least one carbon-carbon double bond, is converted into another alkene with a different structure but the same molecular formula. This process can involve shifts in the position of the double bond, rearrangements of the carbon chain, or changes in the configuration around the double bond (cis-trans isomerization). Many examples in the literature have shown that the spin state of the catalyst complex can significantly influence both the mechanism and the outcome of alkene isomerization, due to variations in electronic configuration and energy associated with different spin states.[52-55] For example, in 2020, Lutz et al.[55] investigated the mechanism of alkene isomerization catalyzed by the iron complex [K(2.2.2-cryptand)][$Ph_2B(tBuIm)_2FeCH_2$ $tBu(N_2)$], where the reaction proceeds via the allyl pathway (Fig.1-17). By combining experimental and computational results, they demonstrated that alkene binding occurs on the S = 3/2 surface, while the transition states leading to alkene isomerization are situated on the S = 1/2 surface. The high-spin configuration results in weak binding of σ-bases on the S = 3/2 surface, providing substantial resistance to typical catalyst poisons.

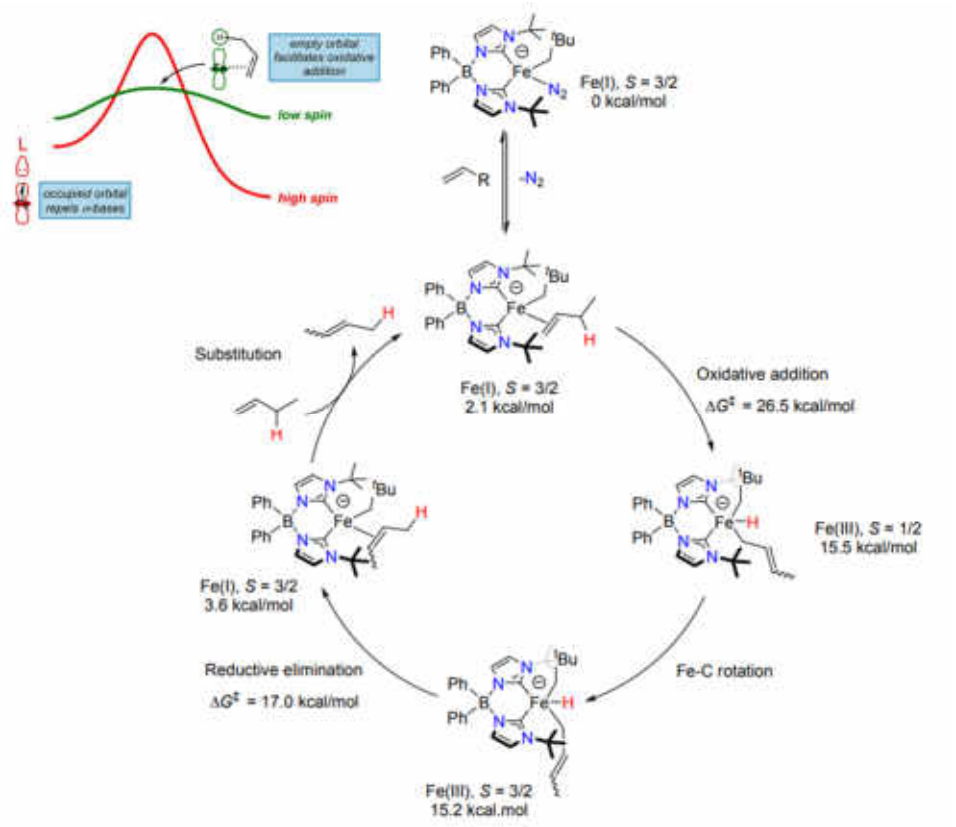


Fig.1-17 Catalytic cycle of alkene isomerization catalysed by iron complex [K(2.2.2-cryptand)][$Ph_2B(tBuIm)_2FeCH_2$ $tBu(N_2)$].[55]

1.2.2.3.2 C-H Activation

C-H activation is a chemical reaction in which a carbon-hydrogen (C-H) bond, typically considered relatively inert and unreactive, is cleaved and replaced by a bond to another atom or group. This transformation is highly valuable in organic synthesis, as it enables the direct functionalization of hydrocarbons, eliminating the need for pre-functionalized starting materials. In recent years, the spin state of the transition metal catalyst has been recognized as a critical factor in this process, significantly influencing the reaction mechanism, activation energy, and overall efficiency.[56-64]

In 2016, Sun et al. [56] investigated the mechanism of C-H arylation reactions catalyzed by low-valent iron complexes. Their findings demonstrated that the low-spin Fe(II) singlet state, which is initially an excited state, crosses over the high-spin ground state, thereby facilitating C-H bond cleavage (Fig.1-18). Subsequently, aryl transmetalation occurs, accompanied by the oxidation of Fe(II) to Fe(III) via a single-electron transfer process, with dichloroalkane serving as the oxidant. This oxidation step promotes the final C-C coupling, thereby completing the C--H functionalization. The regeneration of the Fe(II) catalyst for subsequent cycles of C-H activation involves the single-electron oxidation of the Fe(I) species formed after C-C bond coupling. This study offers a novel strategy for the development of C-H activation reactions.

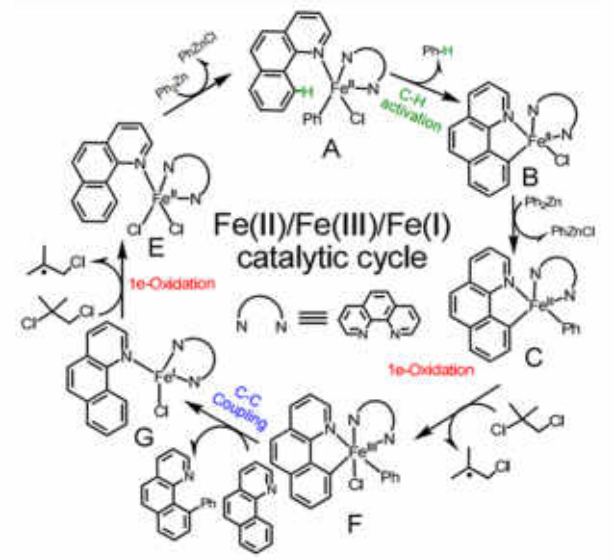


Fig.1-18 The proposed catalytic cycles for the low-valent iron-catalyzed arylation reaction include the crucial C-H activation and C-C coupling steps.[56]

The following year, Hickey et al.[64] demonstrated that the C-H insertion reaction of a low-valent, low-coordinate iron complex involves two-state reactivity, as revealed through a combination of experimental and computational methods. The coordinatively unsaturated iron(0) species undergoes a triplet-to-singlet spin-state transition prior to the C-H insertion, which occurs on the singlet surface (Fig.1-19).

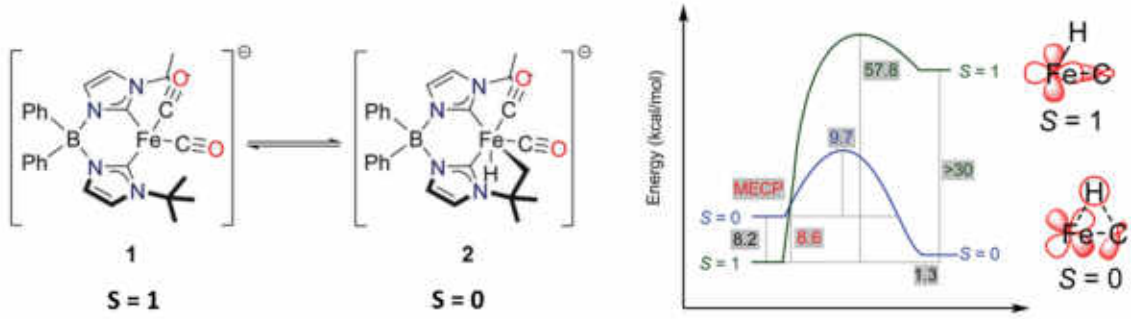


Fig.1-19 The equilibrium between species 1 and 2 involves a reversible C-H insertion reaction and the reaction coordinate for this reversible C-H insertion reaction was calculated using Density Functional Theory. [64]

More recently, Liu et al.[63] reported the isolation of an iron(IV) complex, [(IPr)Fe(NC(CF_3)$_2$Ph)$_2$], with an S=1 ground spin state, capable of undergoing intramolecular

C-H bond activation. Theoretical investigations suggest that this transformation proceeds via a hydrogen atom abstracti on mechanism. The electron-withdrawing trifluoromethyl group plays a crucial role by making the imido ligands in both the iron(IV) complex and the transition state of the abstraction step structurally similar, contributing to a low activation barrier pathway for the observed C-H bond activation (Fig.1-20).

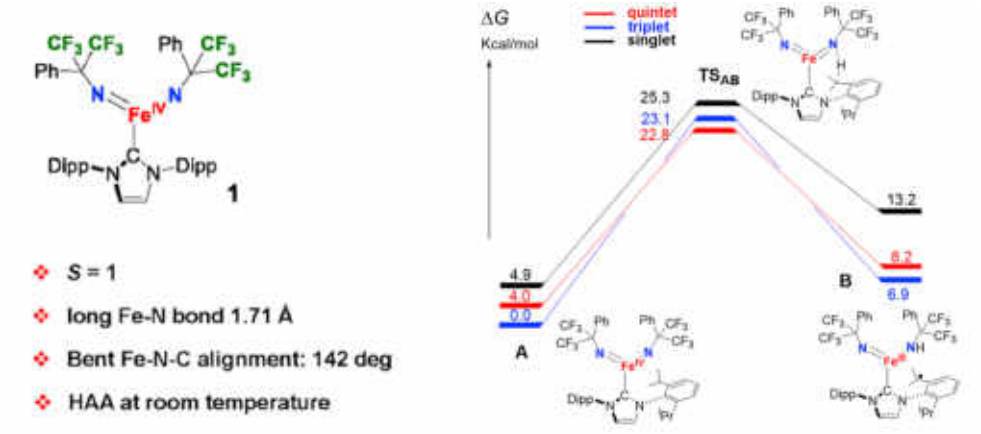


Fig.1-20 Scheme of an iron(IV) complex and the reaction profile of the hydrogen-atom-abstraction (HAA) reaction at different energy surfaces. [63]

1.2.2.3.3 Cycloaddition

Cycloaddition is a chemical reaction in which two or more unsaturated molecules, or different parts of a single molecule, combine to form a cyclic compound. This reaction is a fundamental transformation in organic chemistry, playing a critical role in the synthesis of various ring structures, including those present in natural products and pharmaceuticals.[65, 66] Over the past decade, researchers have discovered that the spin state is crucial in cycloaddition reactions, as it dictates the electronic configuration of the reactants, thereby influencing both the feasibility and the pathway of the reaction.[67-70]

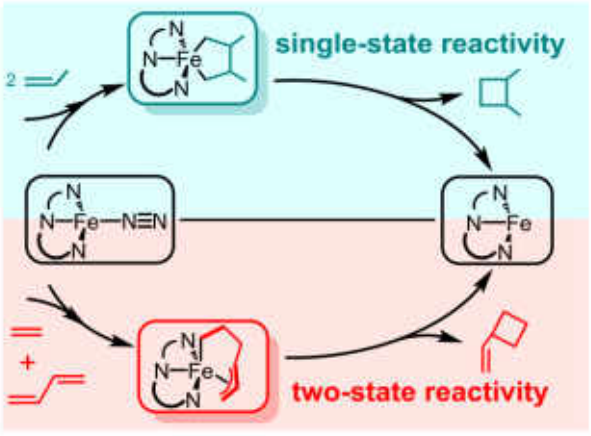


Fig.1-21 Substrate-dependent in Iron-Catalyzed [2+2] Alkene Cycloaddition Reactions. The cross cycloaddition between a mono olefin and a diene exhibits two-state reactivity, while the cycloaddition of unactivated mono olefins involves only single-state reactivity.[71]

In 2017, Hu et al.[71] utilised density functional theory to explore the fundamental mechanisms of iron-catalyzed [2+2] alkene cycloaddition reactions on two representative substrates: the

cycloaddition of unactivated mono olefins and the cross cycloaddition between a mono olefin and a 1,3-diene (Fig.1-21). Their study revealed that the reaction mechanism in [2+2] cycloaddition is intriguingly substrate-dependent. Specifically, the cross cycloaddition between a mono olefin and a diene exhibits two-state reactivity, while the cycloaddition of unactivated mono olefins involves only single-state reactivity. Based on the DFT results, they suggested that enhancing the efficiency of spin-state transitions between singlet and triplet states could serve as an alternative strategy to boost C-C coupling reactivity in cross [2+2] cycloaddition reactions between mono olefins and dienes.

More recently, Zhang et al.[72] investigated iron diimine-catalyzed hydroxylation and discovered that the low-spin state plays a crucial role in both oxidative coupling and β-hydride transfer steps (Fig.1-22). The demonstrate that the triplet state is more effective at stabilizing intermediates and imposes fewer geometric constraints, allowing the substrate greater flexibility in adjusting its conformation. In contrast, the singlet state, with an additional available metal d orbital, enhances interaction with the ligand, facilitating oxidative coupling of the diene with an incoming alkene, β-hydride transfer, and ligand substitution. Their findings represent a significant advancement in understanding first-row transition-metal catalysis and could inform the future design of spin-based catalytic systems.

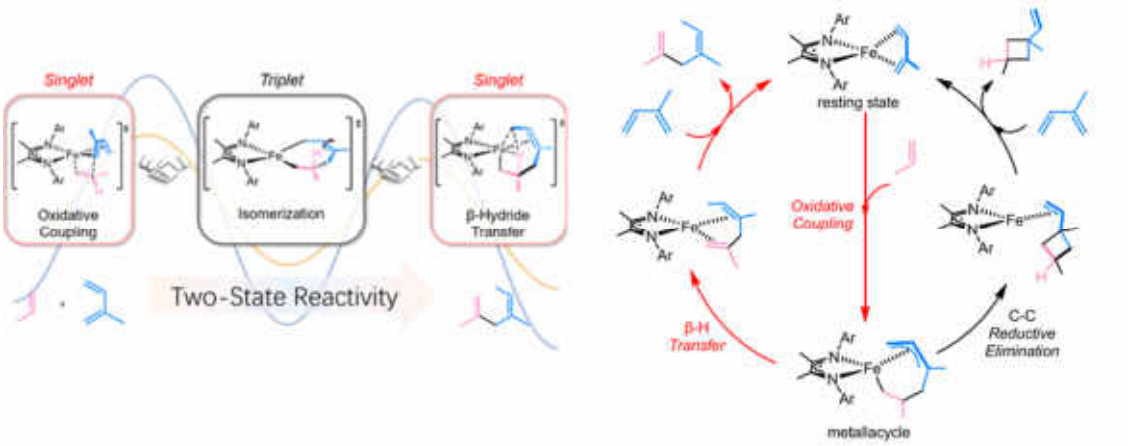


Fig.1-22 Scheme of 1,4-selective hydrovinylation catalyzed by an iron diamine catalyst and preliminary reaction mechanism.[72]

1.2.2.3.4 Polymerizations

Polymerization is a chemical process in which small molecules, known as monomers, combine to form larger macromolecules called polymers. This process can occur through various mechanisms, including chain-growth (addition) polymerization, step-growth (condensation) polymerization, and more specialized types such as ring-opening polymerization. Over the past decade, numerous studies in the literature have demonstrated that the spin state plays a significant role in determining the reactivity of certain intermediates in polymerization processes, particularly within radical and coordination polymerization mechanisms.[73-78]

In 2006, Gibson and colleagues[79] reported a polymerization reaction utilizing α-diimine-FeII complexes, revealing a correlation between the spin state of the catalyst and its catalytic reactivity (Fig.1-23). Their study demonstrated that different spin states led to distinct reaction pathways. The spin state of the complex depends on the ligands R1 and R2. For complexes with high spin states (S = 5/2, R1 = cyclohexyl or tert-butyl; R2 = H), the reaction proceeded via the atom-transfer radical polymerisation (ATRP) pathway. Conversely, complexes with other

ligands (S = 3/2, R1 = 2,6-isopropyl2-phenyl; R2 = H) exhibited an intermediate spin state and followed the catalytic chain transfer (CCT) pathway. Their work demonstrated that the metal spin state of the iron species can be controlled through careful selection of α-diimine ligand substituents and subsequently lead to different reaction pathways, underscoring the potential for rational catalyst design based on the metal spin state.

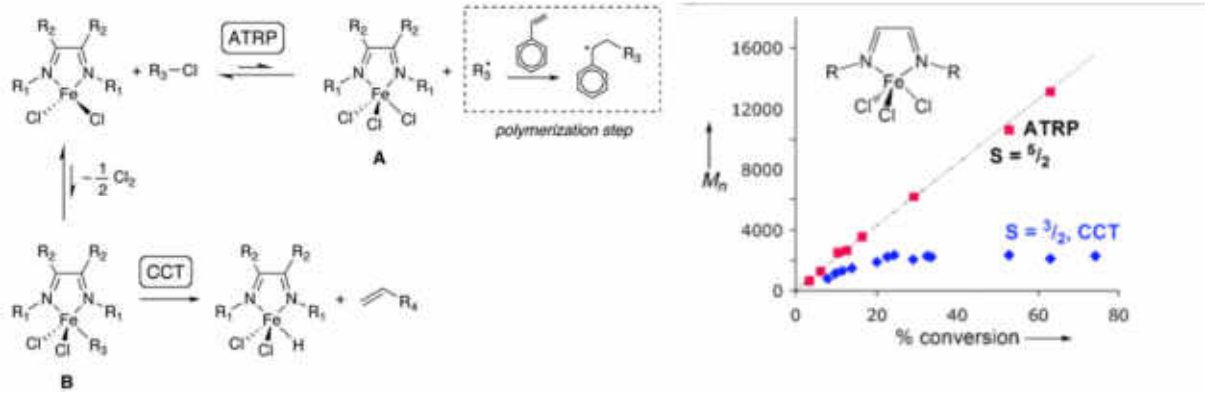


Fig.1-23 Equilibria involved in atom-transfer radical polymerization (ATRP) versus catalytic chain transfer (CCT) polymerization and a plot of molecular weight (M_n) versus conversion for the polymerization of styrene.[79]

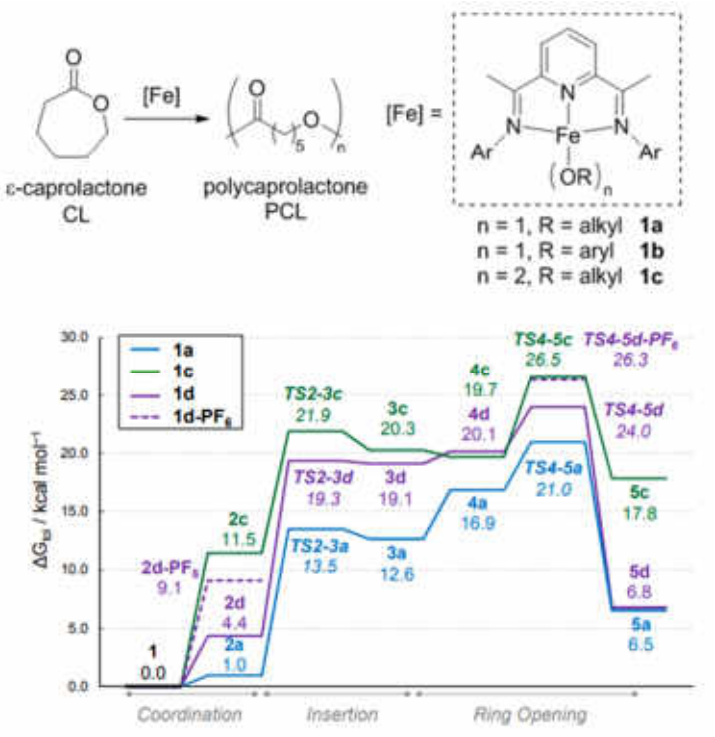


Fig.1-24 Scheme of Iron-catalyzed ring-opening polymerization of ε-caprolactone and the reaction coordinates for the initiation step.[78]

In 2016, Ortuno et al.[78] investigated the electronic structures of a series of iron-based catalysts with bis(imino)pyridine ligands and their corresponding reaction mechanisms for the ring-opening polymerization of ε-caprolactone (Fig.1-24). Their findings demonstrated that high-spin species exhibit greater Lewis acidity compared to low-spin intermediates. The diminished

Lewis acidity of the doublet state, relative to the quartet state, results in a preference for the high-spin state among all intermediates along the reaction coordinate. The low-spin (doublet) state is insufficiently Lewis acidic to bind species effectively and facilitate polymerization. This study provides valuable mechanistic insights that enhance the understanding of the spin sate effect in ring-opening polymerization processes.

1.2.2.3.5 Electrocatalysis

Electrocatalysis involves the enhancement of an electrochemical reaction at an electrode surface through the use of a catalyst. In fuel cells, this process is essential for reactions such as the oxygen reduction reaction (ORR) at the cathode and the hydrogen oxidation reaction (HOR) at the anode. Pyrolyzed Fe-N-C materials represent a promising class of electrocatalysts, particularly for the ORR in proton-exchange membrane fuel cells. The spin state of the iron centres in these pyrolyzed Fe-N-C electrocatalysts plays a critical role in determining their performance in electrocatalytic processes, such as the ORR.[80-85]

In 2019, Mineva et al.[82] conducted a combined theoretical and experimental study on the structure of Pyrolyzed Fe-N-C materials. Their findings revealed that the primary FeN_x moieties present are $Fe(III)N_4C_{12}$ porphyrinic moieties in high-spin states and $Fe(II)N_4C_{10}$ pyridinic moieties in low-spin states (Fig.1-25). Additionally, a minor fraction of FeN_x moieties was identified as existing in the intermediate-spin state (Fe(II) S=1).

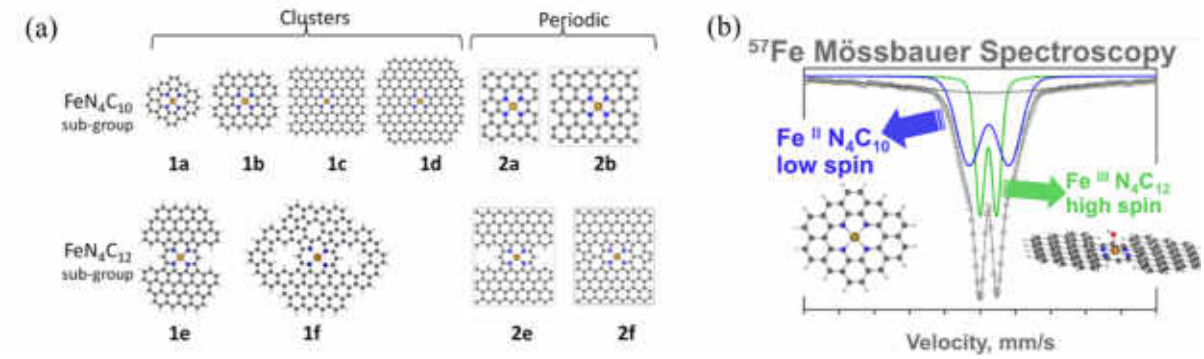


Fig.1-25 (a) Clustered and periodic models of FeN_4C_y and (b) ^{57}Fe Mössbauer spectra. [82]

In 2022, Sun et al.[86] systematically investigated the effect of spin state on the demetalation durability and oxygen reduction reaction (ORR) activity of two types of Fe-N-C electrocatalyst: pyridinic-type FeN_4C_{10} (S=0 or 1) and pyrrolic-type FeN_4C_{12} (S=5/2) (Fig.1-26). They discovered that the low-spin pyridinic-type FeN_4 with OH modification [$OH\text{-}Fe(II)N_4C_{10}$ (S = 0)] and the medium-spin pyridinic-type FeN_4 with O_2 modification [$O_2\text{-}Fe(II)N_4C_{10}$ (S = 1)] exhibit excellent acid durability and high ORR activity. In contrast, the high-spin pyrrolic-type $OH\text{-}Fe(III)N_4C_{12}$ (S = 5/2) demonstrates impressive $4e^-$ ORR activity but suffers from poor stability in acidic environments. Their findings highlighted that the catalytic activity and adsorption strength of oxygenated intermediates are strongly correlated with the intrinsic charges and spin state of the catalytic center.[86]

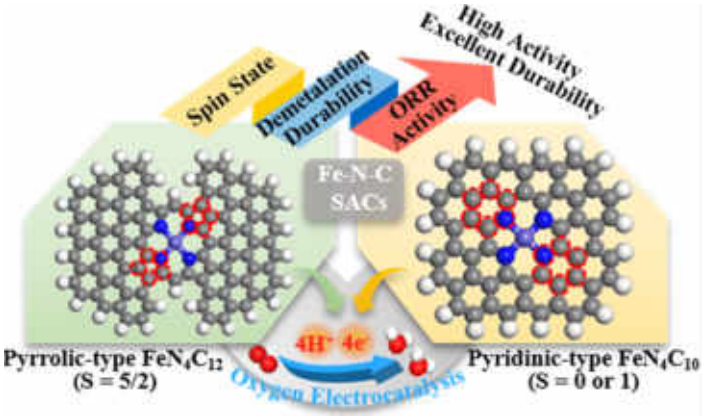


Fig.1-26 Scheme of spin state participation in demetalation durability and activity of Pyrolyzed Fe-N-C materials.[86]

1.3 Spin crossover in catalysis.

In catalytic systems, spin crossover can significantly influence reactivity and process efficiency. Changes in the spin state of the metal centre in spin-crossover materials can impact the ligand environment, alter activation energies, and modify reaction pathways. This phenomenon can be observed in various catalytic systems, where the transition between high-spin and low-spin states plays a crucial role in determining the catalytic activity and selectivity. Understanding spin crossover dynamics is essential for optimizing catalyst performance and designing more effective catalytic processes.[87-89]

In addition, the direct employment of spin crossover complexes as catalysts may present a promising approach to enhance catalytic processes. SCO complexes, characterized by their ability to undergo reversible spin state transitions, can exhibit significant changes in their catalytic properties depending on the spin state. By exploiting these transitions, it is possible to modulate the electronic environment of the metal center, potentially leading to improved catalytic activity and selectivity. The application of SCO complexes as catalysts facilitates dynamic control over reaction conditions and opens the door for developing novel catalytic systems with tunable properties.[90-94]

1.3.1 Spin crossover during the catalytic reaction

1.3.1.1 Spin crossover during electrocatalytic reaction

In 2020, Li et al.[87] developed a novel electrochemical system employing single-Fe-atom catalysts with precisely controlled site density and a well-defined N-coordination environment. Their study revealed that the active single-Fe-atom moieties directly capture the $*O^{2-}$ and $*OH^{-}$ intermediates under oxygen reduction reaction (ORR) conditions. It was observed that the Fe-N bond length shortens as the central Fe atom in the N-FeN_4C_{10} moves into the N_4-plane, which is accompanied by the transition of the Fe^{2+} electronic state from high-spin to low-spin upon the formation of the O^{2-}-FeN_5 intermediate near the ORR onset potential (0.9 V vs. RHE). Conversely, the Fe-N bond length increases as the central Fe atom in FeN_4C_{12} shifts out of the N4-plane, accompanied by the transition of the Fe^{2+} electronic state from low-spin to high-spin upon the formation of the O^{2-}-FeN_4 intermediate at higher biases (0.7 and 0.5 V vs. RHE) (Fig.1-27). This work provides both experimental and theoretical evidence for the involvement

of spin crossover in the ORR mechanism.

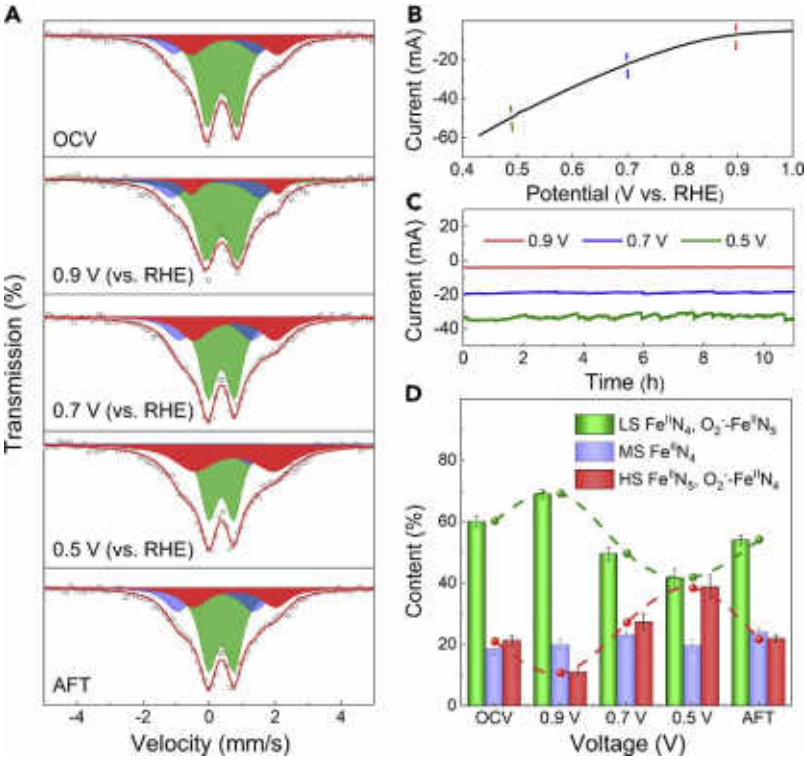


Fig.1-27 Result of Operando ^{57}Fe Mössbauer Measurements.[87]

More recently, to investigate the role of spin multiplicity in electrocatalysis, Yu et al. studied the structural evolution of high-spin (HS) and intermediate-spin (IS) FeN_4 sites during the OER and ORR processes.[88][86] Their findings revealed that spontaneous oxidation occurs from Fe(II)N_4 (IS) to Fe(III)N4 (HS) at a potential of 0.4 V. Additionally, the results showed that FeN_4 (IS) undergoes sequential adsorption of *OH and *OOH as the potential increases, leading to a spin state transition from IS to HS state. Geometry and orbital analyses indicated that the Fe-N bond length and the coordination number of the Fe centre significantly impact d-orbital splitting energy, thereby influencing the stability change between HS and IS states in OER/ORR intermediates. This study underscores the critical importance of spin crossover in electrocatalysis.

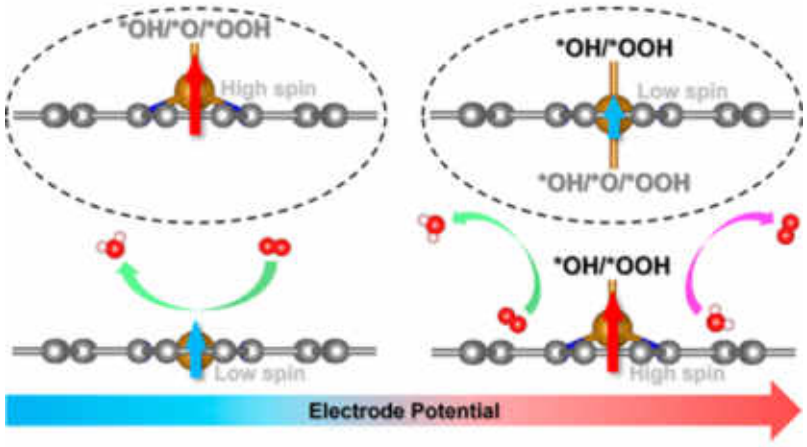


Fig.1-28 Scheme of spin state evolution in OER/ORR Catalyzed by Pyrolyzed Fe–N–C materials.[88]

1.3.1.2 Spin crossover during C-H bond silylation reaction

In 2024, He et al.[89] investigated the mechanism of using open-shell catalysts, specifically 1,10-phenanthroline/iron complexes, in allylic C(sp^3)-H silylation and hydrosilylation reactions of 1,3-enynes. Through a combination of experimental observations and density functional theory calculations, they revealed that spin crossover allows a single intermediate to participate in different reactions by accessing various spin-state potential energy surfaces, thereby leading to distinct products. This finding suggests that spin crossover introduces a novel and promising approach to regulating chemoselectivity. As illustrated in Fig.1-29, spin crossover leads the transformation of **3int3** into **5int3**, followed by a reductive elimination step that produced the hydrosilylation product **b12**. In contrast, when spin crossover did not occur, C-H activation led to the formation of the C-H silylation product **a12**.

Furthermore, spin crossover can either enhance or inhibit specific steps within a catalytic reaction. After hydrogen transfer occurs at **3ts3**, the intermediate **3int5** is generated at 31.4 kcal/mol (Fig.1-29). At this stage, a reductive elimination step with an energy barrier of 19.6 kcal/mol is required to produce product **a12**. However, rapid spin crossover can partially convert **3int5** into the more thermodynamically stable intermediate **5int5** at 37.2 kcal/mol, where the subsequent reductive elimination step faces an increased energy barrier of 24.3 kcal/mol. This result indicates that spin crossover in this step is unfavourable for this particular reductive elimination process. These findings underscore the significant impact of spin crossover in iron-catalyzed chemical transformations.

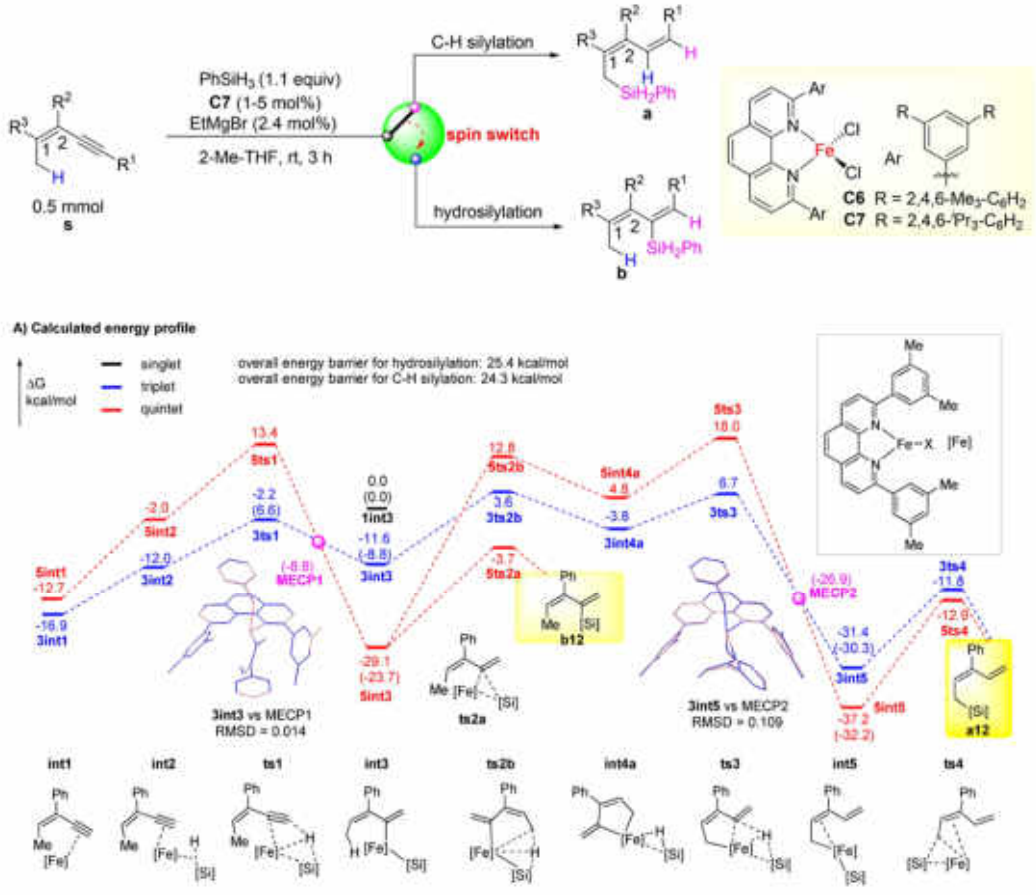


Fig.1-29 Scheme of Iron-catalyzed C-H silylation and hydrosilylation of 1,3-enynes, and Calculated energy profile. Numbers in parentheses indicate electronic energies.[89]

1.3.2 Direct use of spin crossover complexes as catalysts

In 2013, Prat et al.[91] synthesized and investigated a family of iron complexes with the general formula [FeII(R,R'Pytacn)$(X)_2]^{n+}$, where R,R'Pytacn refers to the tetradentate ligand 1-[(4-R'-6-R-2-pyridyl)methyl]-4,7-dimethyl-1,4,7-triazacyclononane. In this formula, R denotes the group at the α-position of the pyridine, R' represents the group at the γ-position, and X refers to either CH_3CN or CF_3SO_3 (Fig.1-30). The study revealed that introducing different substituents into the pyridine ring can change the geometric parameters of the complexes, as well as the electronic properties of the iron centre. Specifically, substituents at the γ-position of the pyridine (class I compounds) significantly impact the electronic properties of the iron centre, while steric constraints introduced by substituents at the α-position (class II compounds) favour the high-spin configuration over the low-spin configuration. In addition, the entire family of complexes was evaluated as catalysts in C-H and C=C oxidation reactions using H_2O_2, demonstrating excellent efficiency in the stereospecific hydroxylation of alkanes and olefin oxidation. Notably, R'-substituents had a weak effect on the efficiency and chemoselectivity of the catalytic activity, while selectivity toward olefin cis-dihydroxylation was enhanced in complexes with R = Me, F, or Cl. Moreover, the R-substituents group also played a crucial role in determining the origin of the oxygen atom transferred during the epoxidation reaction. Overall, this work highlights the potential of Fe^{II}(Pytacn) spin-crossover (SCO) complexes as catalysts in C-H and C=C oxidation reactions, demonstrating that substituents can influence both the SCO properties and the catalytic reactivity of these complexes.

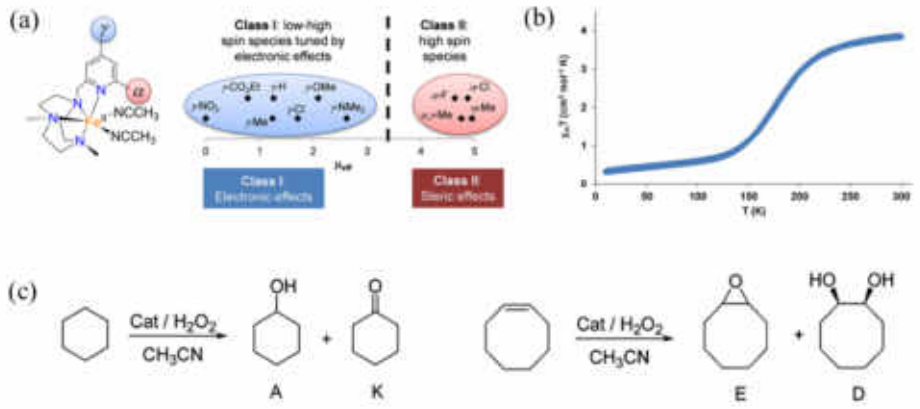


Fig.1-30 (a) family of Fe^{II}(Pytacn) complexes. (b) represent magnetic properties of this type of complex. (c) Oxidation of Cyclohexane and *cis*-Cyclooctene with H_2O_2.[91]

In 2017, Gural'skiy et al.[92] first reported the use of one-dimensional triazole polymeric spin-crossover complexes, specifically $[Fe(NH_2trz)_3]Br_2$ (where NH_2trz = 4-amino-1,2,4-triazole), in the oxidation of 3,4,5,6-tetrachlorocatechol (TCC) to its corresponding quinone in the presence of 3-chloroperbenzoic acid (CPBA). Their findings revealed that the low-spin (LS) species exhibited higher reaction rates and lower activation energies compared to their high-spin (HS) analogues. In addition, their study also demonstrated that the active species in this catalytic process is the oxidized SCO complex, which is formed through oxidation with CPBA. Once oxidized, this complex is subsequently reduced by TCC, thereby regenerating the initial SCO complex. Thus, the true active catalyst in this system is not the Fe(II) complex itself, but its oxidized form. The higher catalytic activity observed for the LS species was attributed to the fact that the rate-determining step (the oxidation of the SCO complex) occurs more readily in the LS state than in the HS state.

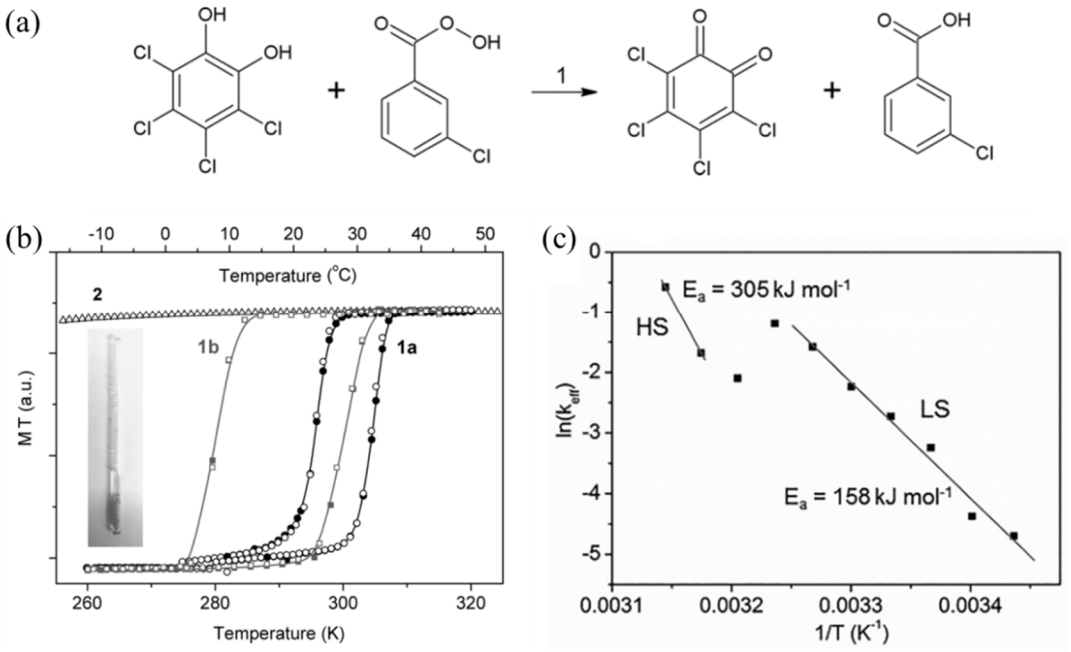


Fig.1-31 (a) Oxidation of 3,4,5,6-tetrachlorocatechol to its corresponding quinone in the presence of 3-chloroperbenzoic acid. (b) Magnetic properties of $[Fe(NH_2trz)_3]Br_2$. (c) Arrhenius plot illustrating the presence of two kinetic regimes corresponding to HS and LS.[92]

On year later, Bell-Taylor et al[90] reported two CoII complexes, one is with SCO, CoII(bsbpc)$(MeCN)_2](ClO_4)_2$, (bsbpc = N-benzenesulfonyl- N,N'-bis(2-pyridylmethyl)-1,2-cyclohexanediamine). Another is entirely high-spin complex, CoII(bbpc)$(MeCN)_2](ClO_4)_2$, (N,N'-dibenzyl-N,N'-bis(2-pyridylmethyl)-1,2-cyclohexanediamine). The reactivity of these two complexes was compared, revealing that both are capable of catalyzing the oxidation of benzylic and allylic C-H bonds using iodosobenzene (PhIO) and meta-chloroperbenzoic acid (MCPBA) (Fig.1-32). However, the spin-crossover [Co^{II}(bsbpc)] complex cannot be oxidized to a Co(III) species, whereas the entirely high-spin [Co^{II}(bbpc)] complex can be oxidized and is capable of reacting with aldehydes. This study highlights the differences in reactivity between a spin-crossover Co(II) complex and an entirely high-spin Co(II) complex.

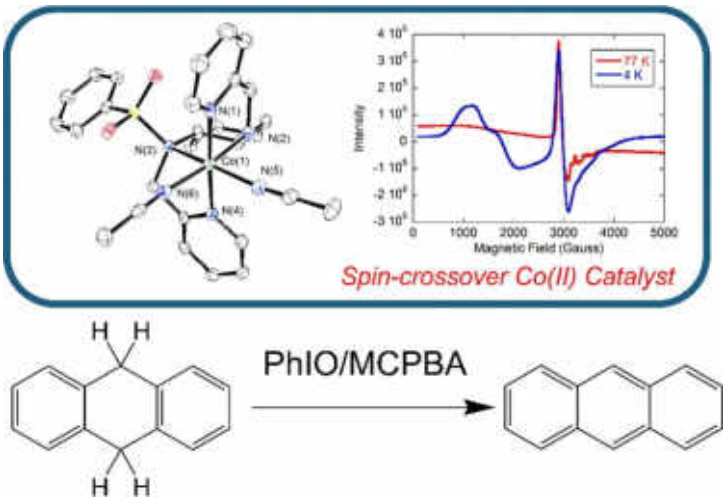


Fig.1-32 A spin-crossover Co(II) complex can be use as catalyst for the oxidation of weak C–H bonds using the two-electron oxidants iodosobenzene and meta-chloroperbenzoic acid.[90]

The study conducted by Isegawa et al.[93] in 2022 investigated the mechanisms underlying CO_2 reduction and hydrogen (H_2) production using a copper (Cu) complex as a photosensitizer, and an FeII spin-crossover complex, [FeII(dmp)$_2$(NCS)$_2$] (dmp = dimethyl-1,10-phenanthroline), as a catalyst. The Fe(dmp)$_2$(NCS)$_2$ complex is in high-spin state at room temperature and low-spin state at approximately 40 K. Density functional theory calculations revealed that the photocatalytic process begins with electronic excitation induced by light irradiation, leading to charge transfer from the metal d-orbital to the ligand orbital in the Cu photosensitizer. This is followed by electron transfer from the one-electron-reduced Cu photosensitizer to the Fe(dmp)$_2$(NCS)$_2$ complex, thereby driving CO_2 reduction (Fig.1-33). Free energy profile calculations of the catalytic cycle suggest that the rate-limiting step in CO_2 reduction is the binding of CO_2 to the iron centre, while the rate-limiting step in H_2 production involves proton transfer from the Brønsted acid ($TEOAH^+$) to the Fe centre. In fact, the spin state of the iron centre changed when the CO_2 bound to the iron centre, and the low-spin state was not involved in either reaction; only the intermediate and high-spin states played active roles.

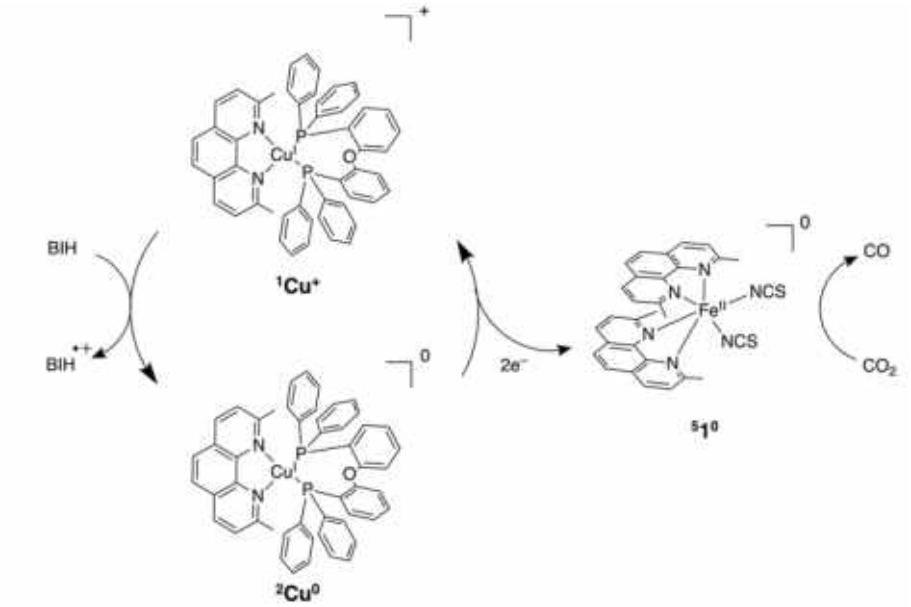


Fig.1-33 Proposed catalytic cycle of photo-induced CO_2 reduction by the Fe(dmp)$_2$(NCS)$_2$ complex.[93]

Recently, Huang et al.[94] introduced an innovative catalyst system based on spin-crossover Hofmann clathrates, specifically Fe(Pz)-[PtII(CN)$_4$]·$_2$H$_2$O, for the photocatalytic production of H_2O_2. The spin-state transition of the metal centres in this system can be chemically modulated through iodine treatment (Fig.1-34). Their findings revealed that when the Fe(II) centres in the Fe-Pt polymer are in the high-spin state, only the photocatalytic oxygen reduction reaction (ORR) occurs, preventing the photosynthesis of H_2O_2 in pure water. In contrast, by inducing the iodide coordination, adjusting the spin state of Fe(II) to the low-spin state enables both ORR and the water oxidation reaction (WOR), facilitating the photosynthesis of H_2O_2 from O_2 and H_2O. Theoretical calculations combined with in situ measurements demonstrated that the increased charge transfer between the Fe(II) and Pt(IV) sites in the low-spin state clathrate enhances light-harvesting capabilities and carrier transport efficiency, resulting in improved photocatalytic activity. This work highlights the potential for developing innovative catalyst systems based on spin crossover complexes.

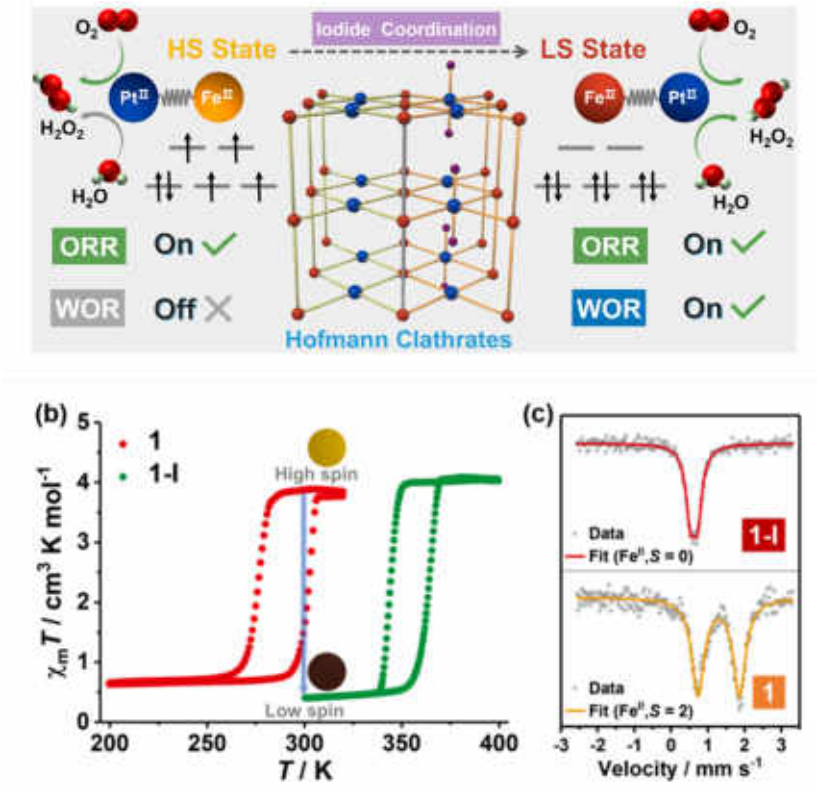


Fig.1-34 Schematic illustration of catalyst system based on spin-crossover Hofmann clathrates for the photocatalytic production of H_2O_2. The spin-state transition of the metal centres in this system can be chemically modulated through iodine treatment.[94]

1.4 References

[1] A. Bousseksou, G. Molnár, G. Matouzenko, Switching of molecular spin states in inorganic complexes by temperature, pressure, magnetic field and light: towards molecular devices, *Eur. J. Inorg. Chem.* **2004**, 2004, 4353-4369.

[2] D. Paliwoda, L. Vendier, W. Nicolazzi, G. Molnár, A. Bousseksou, Pressure tuning of coupled structural and spin state transitions in the molecular complex [Fe (H2B (pz) 2) 2 (phen)], *Inorg. Chem.* **2022**, 61, 15991-16002.

[3] L. Zhang, K. Ridier, O.Y. Horniichuk, S. Calvez, L. Salmon, G. Molnár, A. Bousseksou, Reversible switching of strong light–matter coupling using spin-crossover molecular materials, *The Journal of Physical Chemistry Letters* **2023**, 14, 6840-6849.

[4] A. Bousseksou, K. Boukheddaden, M. Goiran, C. Consejo, M. Boillot, J.-P. Tuchagues, Dynamic response of the spin-crossover solid C o (H 2 (fsa) 2 e n)(py) 2 to a pulsed magnetic field, *Physical Review B* **2002**, 65, 172412.

[5] A. Bousseksou, G. Molnár, L. Salmon, W. Nicolazzi, Molecular spin crossover phenomenon: recent achievements and prospects, *Chem. Soc. Rev.* **2011**, 40, 3313-3335.

[6] G. Molnár, S. Rat, L. Salmon, W. Nicolazzi, A. Bousseksou, Spin crossover nanomaterials: from fundamental concepts to devices, *Adv. Mater.* **2018**, 30, 1703862.

[7] A. Enriquez-Cabrera, A. Rapakousiou, M.P. Bello, G. Molnár, L. Salmon, A. Bousseksou, Spin crossover polymer composites, polymers and related soft materials, *Coord. Chem. Rev.* **2020**, 419, 213396.

[8] W. Nicolazzi, A. Bousseksou, Thermodynamical aspects of the spin crossover phenomenon, *C. R. Chim.* **2018**, 21, 1060-1074.

[9] C.J. O'Connor, Magnetochemistry—advances in theory and experimentation, *Prog. Inorg. Chem.* **1982**, 203-283.

[10] M.A. Halcrow, The effect of ligand design on metal ion spin state—lessons from spin crossover complexes, *Crystals* **2016**, 6, 58.
[11] A. Römer, L. Hasecke, P. Blöchl, R.A. Mata, A review of density functional models for the description of Fe (II) spin-crossover complexes, *Molecules* **2020**, 25, 5176.
[12] B. Dey, V. Chandrasekhar, Fe II spin crossover complexes containing N 4 O 2 donor ligands, *Dalton Trans.* **2022**, 51, 13995-14021.
[13] S. Amabilino, R.J. Deeth, DFT analysis of spin crossover in Mn (III) complexes: is a two-electron S= 2 to S= 0 spin transition feasible?, *Inorg. Chem.* **2017**, 56, 2602-2613.
[14] E.R. King, G.T. Sazama, T.A. Betley, Co (III) imidos exhibiting spin crossover and C–H bond activation, *J. Am. Chem. Soc.* **2012**, 134, 17858-17861.
[15] S. Hayami, Y. Komatsu, T. Shimizu, H. Kamihata, Y.H. Lee, Spin-crossover in cobalt (II) compounds containing terpyridine and its derivatives, *Coord. Chem. Rev.* **2011**, 255, 1981-1990.
[16] H. Ma, J.L. Petersen, V.G. Young Jr, G.T. Yee, M.P. Jensen, Solid-state spin crossover of Ni (II) in a bioinspired N3S2 ligand field, *J. Am. Chem. Soc.* **2011**, 133, 5644-5647.
[17] C. Gandolfi, C. Moitzi, P. Schurtenberger, G.G. Morgan, M. Albrecht, Improved cooperativity of spin-labile iron (III) centers by self-assembly in solution, *J. Am. Chem. Soc.* **2008**, 130, 14434-14435.
[18] H.L. Feltham, C. Johnson, A.B. Elliott, K.C. Gordon, M. Albrecht, S. Brooker, "Tail" tuning of iron (II) spin crossover temperature by 100 K, *Inorg. Chem.* **2015**, 54, 2902-2909.
[19] R. Kulmaczewski, J. Olguín, J.A. Kitchen, H.L. Feltham, G.N. Jameson, J.L. Tallon, S. Brooker, Remarkable scan rate dependence for a highly constrained dinuclear iron (II) spin crossover complex with a wide thermal hysteresis loop, *J. Am. Chem. Soc.* **2014**, 136, 878-881.
[20] A. Bousseksou, G. Molnár, P. Demont, J. Menegotto, Observation of a thermal hysteresis loop in the dielectric constant of spin crossover complexes: towards molecular memory devices, *J. Mater. Chem.* **2003**, 13, 2069-2071.
[21] D. Tanaka, N. Aketa, H. Tanaka, S. Horike, M. Fukumori, T. Tamaki, T. Inose, T. Akai, H. Toyama, O. Sakata, Facile preparation of hybrid thin films composed of spin-crossover nanoparticles and carbon nanotubes for electrical memory devices, *Dalton Trans.* **2019**, 48, 7074-7079.
[22] L. Salmon, G. Molnár, D. Zitouni, C. Quintero, C. Bergaud, J.-C. Micheau, A. Bousseksou, A novel approach for fluorescent thermometry and thermal imaging purposes using spin crossover nanoparticles, *J. Mater. Chem.* **2010**, 20, 5499-5503.
[23] C. Bartual-Murgui, A. Akou, C. Thibault, G. Molnár, C. Vieu, L. Salmon, A. Bousseksou, Spin-crossover metal–organic frameworks: promising materials for designing gas sensors, *Journal of Materials Chemistry C* **2015**, 3, 1277-1285.
[24] G. Molnár, L. Salmon, W. Nicolazzi, C. Quintero, A. Akou, K. Abdul-kader, G. Félix, T. Mahfoud, C. Bergaud, C. Bartual-Murgui, Bistable photonic nanostructures based on molecular spin crossover complexes, Photonic Crystal Materials and Devices X, SPIE, 2012, pp. 206-213.
[25] C.-C. Wu, J. Jung, P.K. Gantzel, P. Gütlich, D.N. Hendrickson, LIESST effect studies of Iron (II) spin-crossover complexes with phosphine ligands: Relaxation kinetics and effects of solvent molecules, *Inorg. Chem.* **1997**, 36, 5339-5347.
[26] P. Gütlich, H. Goodwin, M.-L. Boillot, J. Zarembowitch, A. Sour, Ligand-driven light-induced spin change (LD-LISC): a promising photomagnetic effect, *Spin crossover in transition metal compounds II* **2004**, 261-276.
[27] V. Ksenofontov, A. Gaspar, G. Levchenko, B. Fitzsimmons, P. Gütlich, Pressure effect on spin crossover in [Fe (phen) 2 (NCS) 2] and [CrI2 (depe) 2], *The Journal of Physical Chemistry B* **2004**, 108, 7723-7727.
[28] D. Gentili, N. Demitri, B. Schäfer, F. Liscio, I. Bergenti, G. Ruani, M. Ruben, M. Cavallini, Multi-modal sensing in spin crossover compounds, *Journal of Materials Chemistry C* **2015**, 3, 7836-7844.
[29] K. Abdul-Kader, M. Lopes, C. Bartual-Murgui, O. Kraieva, E.M. Hernández, L. Salmon, W. Nicolazzi, F. Carcenac, C. Thibault, G. Molnár, Synergistic switching of plasmonic resonances and molecular spin states, *Nanoscale* **2013**, 5, 5288-5293.

[30] F. Prins, M. Monrabal‐Capilla, E.A. Osorio, E. Coronado, H.S. van der Zant, Room‐temperature electrical addressing of a bistable spin‐crossover molecular system, *Adv. Mater.* **2011**, 23, 1545-1549.
[31] A. Rotaru, J. Dugay, R.P. Tan, I.A. Guralskiy, L. Salmon, P. Demont, J. Carrey, G. Molnár, M. Respaud, A. Bousseksou, Nano-electromanipulation of Spin Crossover Nanorods: Towards Switchable Nanoelectronic Devices, *Adv. Mater.* **2013**, 25, 1745-1749.
[32] J.E. Angulo-Cervera, M. Piedrahita-Bello, B. Martin, S.E. Alavi, W. Nicolazzi, L. Salmon, G. Molnár, A. Bousseksou, Thermal hysteresis of stress and strain in spin-crossover@ polymer composites: Towards a rational design of actuator devices, *Materials Advances* **2022**, 3, 5131-5137.
[33] M. Grzywa, R. Röß-Ohlenroth, C. Muschielok, H. Oberhofer, A. Błachowski, J. Żukrowski, D. Vieweg, H.-A.K. Von Nidda, D. Volkmer, Cooperative large-hysteresis spin-crossover transition in the iron (II) triazolate [Fe (ta) 2] metal–organic framework, *Inorg. Chem.* **2020**, 59, 10501-10511.
[34] H.J. Shepherd, I.y.A. Gural'skiy, C.M. Quintero, S. Tricard, L. Salmon, G. Molnár, A. Bousseksou, Molecular actuators driven by cooperative spin-state switching, *Nat. Commun.* **2013**, 4, 2607.
[35] M. Piedrahita-Bello, Y. Zan, A. Enriquez-Cabrera, G. Molnár, B. Tondu, L. Salmon, A. Bousseksou, Effect of the spin crossover filler concentration on the performance of composite bilayer actuators, *Chem. Phys. Lett.* **2022**, 793, 139438.
[36] M. Piedrahita-Bello, J.E. Angulo-Cervera, A. Enriquez-Cabrera, G. Molnár, B. Tondu, L. Salmon, A. Bousseksou, Colossal expansion and fast motion in spin-crossover@ polymer actuators, *Materials Horizons* **2021**, 8, 3055-3062.
[37] J.N. Harvey, R. Poli, K.M. Smith, Understanding the reactivity of transition metal complexes involving multiple spin states, *Coord. Chem. Rev.* **2003**, 238, 347-361.
[38] D. Schröder, S. Shaik, H. Schwarz, Two-state reactivity as a new concept in organometallic chemistry §, *Acc. Chem. Res.* **2000**, 33, 139-145.
[39] J.P. Lomont, S.C. Nguyen, C.B. Harris, Ultrafast infrared studies of the role of spin states in organometallic reaction dynamics, *Acc. Chem. Res.* **2014**, 47, 1634-1642.
[40] C.M. Macaulay, S.J. Gustafson, J.T. Fuller III, D.-H. Kwon, T. Ogawa, M.J. Ferguson, R. McDonald, M.D. Lumsden, S.M. Bischof, O.L. Sydora, Alkene isomerization–hydroboration catalyzed by first-row transition-metal (Mn, Fe, Co, and Ni) N-phosphinoamidinate complexes: origin of reactivity and selectivity, *ACS Catalysis* **2018**, 8, 9907-9925.
[41] M. Faraji, M. Yousefi, S. Yousefzadeh, M. Zirak, N. Naseri, T.H. Jeon, W. Choi, A.Z. Moshfegh, Two-dimensional materials in semiconductor photoelectrocatalytic systems for water splitting, *Energy & Environmental Science* **2019**, 12, 59-95.
[42] A.M. Zima, O.Y. Lyakin, K.P. Bryliakov, E.P. Talsi, High‐Spin and Low‐Spin Perferryl Intermediates in Fe (PDP)‐Catalyzed Epoxidations, *ChemCatChem* **2019**, 11, 5345-5352.
[43] S.E. Bowman, K.L. Bren, The chemistry and biochemistry of heme c: functional bases for covalent attachment, *Nat. Prod. Rep.* **2008**, 25, 1118-1130.
[44] G.H. Loew, D.L. Harris, Role of the heme active site and protein environment in structure, spectra, and function of the cytochrome P450s, *Chem. Rev.* **2000**, 100, 407-420.
[45] S. Shaik, D. Kumar, S.P. de Visser, A. Altun, W. Thiel, Theoretical perspective on the structure and mechanism of cytochrome P450 enzymes, *Chem. Rev.* **2005**, 105, 2279-2328.
[46] I.G. Denisov, T.M. Makris, S.G. Sligar, I. Schlichting, Structure and chemistry of cytochrome P450, *Chem. Rev.* **2005**, 105, 2253-2278.
[47] M.L. Merlini, G.J. Britovsek, M. Swart, P. Belanzoni, Understanding the catalase-like activity of a bioinspired manganese (II) complex with a pentadentate NSNSN ligand framework. A computational insight into the mechanism, *ACS Catalysis* **2018**, 8, 2944-2958.
[48] M.H. Al-Afyouni, E. Suturina, S. Pathak, M. Atanasov, E. Bill, D.E. DeRosha, W.W. Brennessel, F. Neese, P.L. Holland, Spin Isomers and Ligand Isomerization in a Three-Coordinate Cobalt (I) Carbonyl Complex, *J. Am. Chem. Soc.* **2015**, 137, 10689-10699.
[49] L.V. Liu, S. Hong, J. Cho, W. Nam, E.I. Solomon, Comparison of high-spin and low-spin nonheme FeIII–OOH complexes in O–O bond homolysis and H-atom abstraction reactivities,

J. Am. Chem. Soc. **2013**, 135, 3286-3299.
[50] S.M. Bellows, T.R. Cundari, P.L. Holland, Spin crossover during β-hydride elimination in high-spin iron (II)–and cobalt (II)–alkyl complexes, *Organometallics* **2013**, 32, 4741-4751.
[51] P. Pérez, J. Andrés, V. Safont, O. Tapia, R. Contreras, Spin-philicity and spin-donicity as auxiliary concepts to quantify spin-catalysis phenomena, *The Journal of Physical Chemistry A* **2002**, 106, 5353-5357.
[52] C. Chen, T.R. Dugan, W.W. Brennessel, D.J. Weix, P.L. Holland, Z-selective alkene isomerization by high-spin cobalt (II) complexes, *J. Am. Chem. Soc.* **2014**, 136, 945-955.
[53] E.A. Glascoe, K.R. Sawyer, J.E. Shanoski, C.B. Harris, The influence of the metal spin state in the iron-catalyzed alkene isomerization reaction studied with ultrafast infrared spectroscopy, *The Journal of Physical Chemistry C* **2007**, 111, 8789-8795.
[54] K.R. Sawyer, E.A. Glascoe, J.F. Cahoon, J.P. Schlegel, C.B. Harris, Mechanism for Iron-Catalyzed Alkene Isomerization in Solution, *Organometallics* **2008**, 27, 4370-4379.
[55] S.A. Lutz, A.K. Hickey, Y. Gao, C.-H. Chen, J.M. Smith, Two-state reactivity in iron-catalyzed alkene isomerization confers σ-base resistance, *J. Am. Chem. Soc.* **2020**, 142, 15527-15535.
[56] Y. Sun, H. Tang, K. Chen, L. Hu, J. Yao, S. Shaik, H. Chen, Two-state reactivity in low-valent iron-mediated C–H activation and the implications for other first-row transition metals, *J. Am. Chem. Soc.* **2016**, 138, 3715-3730.
[57] B.K. Mai, Y. Kim, The Kinetic Isotope Effect as a Probe of Spin Crossover in the C H Activation of Methane by the FeO+ Cation, *Angew. Chem.* **2015**, 127, 4018-4023.
[58] Z.-C. Wang, S. Yin, E.R. Bernstein, Double C–H bond activation of hydrocarbons by a gas phase neutral oxide cluster: the importance of spin state, *The Journal of Physical Chemistry A* **2013**, 117, 2294-2301.
[59] D. Balcells, E. Clot, O. Eisenstein, C H Bond Activation in Transition Metal Species from a Computational Perspective, *Chem. Rev.* **2010**, 110, 749-823.
[60] S.E. Kalman, A. Petit, T.B. Gunnoe, D.H. Ess, T.R. Cundari, M. Sabat, Facile and regioselective C–H bond activation of aromatic substrates by an Fe (ii) complex involving a spin-forbidden pathway, *Organometallics* **2013**, 32, 1797-1806.
[61] G. Parthasarathy, M. Thomas, Z. Daniel, C. Gianpiero, W. Svenja, A. Lutz, 3d Transition Metals for C–H Activation, *Chem. Rev.* **2018**, 119, 2192-2452.
[62] E.R. King, E.T. Hennessy, T.A. Betley, Catalytic C− H bond amination from high-spin iron imido complexes, *J. Am. Chem. Soc.* **2011**, 133, 4917-4923.
[63] Q. Liu, L. Long, P. Ma, Y. Ma, X. Leng, J. Xiao, H. Chen, L. Deng, Synthesis, structure, and C–H bond activation reaction of an iron (IV) terminal imido complex bearing trifluoromethyl groups, *Cell Reports Physical Science* **2021**, 2.
[64] A.K. Hickey, S.A. Lutz, C.-H. Chen, J.M. Smith, Two-state reactivity in C–H activation by a four-coordinate iron (0) complex, *Chem. Commun.* **2017**, 53, 1245-1248.
[65] S. Poplata, A. Tröster, Y.-Q. Zou, T. Bach, Recent advances in the synthesis of cyclobutanes by olefin [2+ 2] photocycloaddition reactions, *Chem. Rev.* **2016**, 116, 9748-9815.
[66] G. Domínguez, J. Pérez-Castells, Recent advances in [2+ 2+ 2] cycloaddition reactions, *Chem. Soc. Rev.* **2011**, 40, 3430-3444.
[67] O. El Bakouri, M. Garcia-Borras, R.M. Girón, S. Filippone, N. Martín, M. Sola, On the regioselectivity of the Diels–Alder cycloaddition to C 60 in high spin states, *Phys. Chem. Chem. Phys.* **2018**, 20, 11577-11585.
[68] P. Pérez, J. Andres, V. Safont, R. Contreras, O. Tapia, Exploring two-state reactivity pathways in the cycloaddition reactions of triplet methylene, *The Journal of Physical Chemistry A* **2005**, 109, 4178-4184.
[69] J. Sun, Y. Wang, How Does Spin Play with the Cycloaddition to Paramagnetic Endohedral Metallofullerenes? The Curious Case of TiSc2N@ C80, *Inorg. Chem.* **2022**, 61, 19183-19192.
[70] A. Roglans, A. Pla-Quintana, M. Sola, Mechanistic studies of transition-metal-catalyzed [2+ 2+ 2] cycloaddition reactions, *Chem. Rev.* **2020**, 121, 1894-1979.
[71] L. Hu, H. Chen, Substrate-dependent two-state reactivity in iron-catalyzed alkene [2+ 2] cycloaddition reactions, *J. Am. Chem. Soc.* **2017**, 139, 15564-15567.
[72] Z. Zhang, J.-X. Zhang, F.K. Sheong, Z. Lin, 1, 4-Selective hydrovinylation of diene catalyzed

by an Iron diimine catalyst: A computational case study on two-state reactivity, *ACS Catalysis* **2020**, 10, 12454-12465.
[73] S. Liu, S. Srinivasan, J. Tao, M.C. Grady, M. Soroush, A.M. Rappe, Modeling spin-forbidden monomer self-initiation reactions in spontaneous free-radical polymerization of acrylates and methacrylates, *The Journal of Physical Chemistry A* **2014**, 118, 9310-9318.
[74] I.V. Khudyakov, N. Arsu, S. Jockusch, N.J. Turro, Magnetic and spin effects in the photoinitiation of polymerization, *Des. Monomers Polym.* **2003**, 6, 91-101.
[75] B. Minaev, A. Baryshnikova, W.-H. Sun, Spin-dependent effects in ethylene polymerization with bis (imino) pyridine iron (II) complexes, *J. Organomet. Chem.* **2016**, 811, 48-65.
[76] I. Rintoul, Kinetic control of aqueous polymerization using radicals generated in different spin states, *Processes* **2017**, 5, 15.
[77] L.E. Allan, M.P. Shaver, A.J. White, V.C. Gibson, Correlation of metal spin-state in α-diimine iron catalysts with polymerization mechanism, *Inorg. Chem.* **2007**, 46, 8963-8970.
[78] M.A. Ortuno, B. Dereli, K.R.D. Chiaie, A.B. Biernesser, M. Qi, J.A. Byers, C.J. Cramer, The role of alkoxide initiator, spin state, and oxidation state in ring-opening polymerization of ε-caprolactone catalyzed by iron bis (imino) pyridine complexes, *Inorg. Chem.* **2018**, 57, 2064-2071.
[79] M.P. Shaver, L.E. Allan, H.S. Rzepa, V.C. Gibson, Correlation of metal spin state with catalytic reactivity: polymerizations mediated by alpha-diimine-iron complexes, *Angewandte Chemie International Edition* **2006**, 45, 1241-1244.
[80] K. Muñoz-Becerra, R. Venegas, L. Duque, J.H. Zagal, F.J. Recio, Recent advances of Fe–N–C pyrolyzed catalysts for the oxygen reduction reaction, *Current Opinion in Electrochemistry* **2020**, 23, 154-161.
[81] D. Xue, P. Yuan, S. Jiang, Y. Wei, Y. Zhou, C.-L. Dong, W. Yan, S. Mu, J.-N. Zhang, Altering the spin state of Fe-NC through ligand field modulation of single-atom sites boosts the oxygen reduction reaction, *Nano Energy* **2023**, 105, 108020.
[82] T. Mineva, I. Matanovic, P. Atanassov, M.-T. Sougrati, L. Stievano, M. Clémancey, A. Kochem, J.-M. Latour, F. Jaouen, Understanding active sites in pyrolyzed Fe–N–C catalysts for fuel cell cathodes by bridging density functional theory calculations and 57Fe Mossbauer spectroscopy, *Acs Catalysis* **2019**, 9, 9359-9371.
[83] G. Yang, J. Zhu, P. Yuan, Y. Hu, G. Qu, B.-A. Lu, X. Xue, H. Yin, W. Cheng, J. Cheng, Regulating Fe-spin state by atomically dispersed Mn-N in Fe-NC catalysts with high oxygen reduction activity, *Nat. Commun.* **2021**, 12, 1734.
[84] C. Chen, Y. Wu, X. Li, Y. Ye, Z. Li, Y. Zhou, J. Chen, M. Yang, F. Xie, Y. Jin, Modulating Fe spin state in FeNC catalysts by adjacent Fe atomic clusters to facilitate oxygen reduction reaction in proton exchange membrane fuel cell, *Applied Catalysis B: Environmental* **2024**, 342, 123407.
[85] M. Ren, X. Zhu, Q. Luo, X. Li, J. Yang, Proposal of spin crossover as a reversible switch of catalytic activity for the oxygen evolution reaction in two dimensional metal–organic frameworks, *Nanoscale* **2023**, 15, 10661-10666.
[86] F. Sun, F. Li, Q. Tang, Spin state as a participator for demetalation durability and activity of Fe–N–C electrocatalysts, *The Journal of Physical Chemistry C* **2022**, 126, 13168-13181.
[87] X. Li, C.-S. Cao, S.-F. Hung, Y.-R. Lu, W. Cai, A.I. Rykov, S. Miao, S. Xi, H. Yang, Z. Hu, Identification of the electronic and structural dynamics of catalytic centers in single-Fe-atom material, *Chem* **2020**, 6, 3440-3454.
[88] M. Yu, A. Li, E. Kan, C. Zhan, Substantial Impact of Spin State Evolution in OER/ORR Catalyzed by Fe–N–C, *ACS Catalysis* **2024**, 14, 6816-6826.
[89] P. He, M.H. Guan, M.Y. Hu, Y.J. Zhou, M.Y. Huang, S.F. Zhu, Iron-Catalyzed Allylic C (sp3)−H Silylation: Spin-Crossover-Efficiency-Determined Chemoselectivity, *Angewandte Chemie International Edition* **2024**, 63, e202402044.
[90] A. Bell-Taylor, J.D. Gorden, E.E. Hardy, C.R. Goldsmith, A spin-crossover Co (II) complex catalyzes the activation of sp3 C–H bonds by two-electron oxidants, *Inorg. Chim. Acta* **2018**, 482, 206-212.
[91] I. Prat, A. Company, T. Corona, T. Parella, X. Ribas, M. Costas, Assessing the impact of

electronic and steric tuning of the ligand in the spin state and catalytic oxidation ability of the FeII (Pytacn) family of complexes, *Inorg. Chem.* **2013**, 52, 9229-9244.
[92] I.y.A. Gural'skiy, S.I. Shylin, V. Ksenofontov, W. Tremel, Spin-State-Dependent Redox-Catalytic Activity of a Switchable Iron (II) Complex, *Eur. J. Inorg. Chem.* **2017**, 2017, 3125-3131.
[93] M. Isegawa, Mechanism of Photocatalytic CO2 Reduction by Iron Spin-Crossover Complex with Copper Photosensitizer, *Organometallics* **2022**, 41, 3568-3580.
[94] G.-Z. Huang, Y.-S. Xia, F. Yang, W.-J. Long, J.-J. Liu, J.-P. Liao, M. Zhang, J. Liu, Y.-Q. Lan, On–off switching of a photocatalytic overall reaction through dynamic spin-state transition in a Hofmann clathrate system, *J. Am. Chem. Soc.* **2023**, 145, 26863-26870.
[95] E. Coronado, Molecular magnetism: from chemical design to spin control in molecules, materials and devices, *Nature Reviews Materials* **2020**, 5, 87-104.
[96] O. Roubeau, Triazole-based one-dimensional spin-crossover coordination polymers, *Chemistry–A European Journal* **2012**, 18, 15230-15244.
[97] A. Sugahara, H. Kamebuchi, A. Okazawa, M. Enomoto, N. Kojima, Control of spin-crossover phenomena in one-dimensional triazole-coordinated iron (II) complexes by means of functional counter ions, *Inorganics* **2017**, 5, 50.
[98] A. Enríquez-Cabrera, L. Routaboul, L. Salmon, A. Bousseksou, Complete post-synthetic modification of a spin crossover complex, *Dalton Trans.* **2019**, 48, 16853-16856.
[99] L. Sun, A. Rotaru, Y. Garcia, A non-porous Fe (II) complex for the colorimetric detection of hazardous gases and the monitoring of meat freshness, *J. Hazard. Mater.* **2022**, 437, 129364.
[100] K. Ridier, A.-C. Bas, Y. Zhang, L. Routaboul, L. Salmon, G. Molnár, C. Bergaud, A. Bousseksou, Unprecedented switching endurance affords for high-resolution surface temperature mapping using a spin-crossover film, *Nat. Commun.* **2020**, 11, 3611.
[101] R. Torres-Cavanillas, M. Gavara-Edo, E. Coronado, Bistable Spin-Crossover Nanoparticles for Molecular Electronics, *Adv. Mater.* **2024**, 36, 2307718.
[102] Y. Zan, M. Piedrahita-Bello, S.E. Alavi, G. Molnár, B. Tondu, L. Salmon, A. Bousseksou, Soft Actuators Based on Spin-Crossover Particles Embedded in Thermoplastic Polyurethane, *Advanced Intelligent Systems* **2023**, 5, 2200432.
[103] B. Tondu, M. Piedrahita-Bello, L. Salmon, G. Molnár, A. Bousseksou, Robust linear control of a bending molecular artificial muscle based on spin crossover molecules, *Sensors and Actuators A: Physical* **2022**, 335, 113359.
[104] M. Piedrahita-Bello, X. Yang, S.E. Alavi, G. Molnár, L. Salmon, A. Bousseksou, Anisotropic spin-crossover composite actuators displaying pre-programmed movements, *Sensors and Actuators B: Chemical* **2023**, 393, 134147.
[105] S. Mandal, S. Natarajan, P. Mani, A. Pankajakshan, Post-synthetic modification of metal–organic frameworks toward applications, *Adv. Funct. Mater.* **2021**, 31, 2006291.
[106] J.L. Segura, S. Royuela, M.M. Ramos, Post-synthetic modification of covalent organic frameworks, *Chem. Soc. Rev.* **2019**, 48, 3903-3945.
[107] C.F. Wang, R.F. Li, X.Y. Chen, R.J. Wei, L.S. Zheng, J. Tao, Synergetic Spin Crossover and Fluorescence in One-Dimensional Hybrid Complexes, *Angew. Chem.* **2015**, 127, 1594-1597.
[108] A.D. Burrows, C.G. Frost, M.F. Mahon, C. Richardson, Post-Synthetic Modification of Tagged Metal–Organic Frameworks, *Angew. Chem.* **2008**, 120, 8610-8614.
[109] V. Valtchev, G. Majano, S. Mintova, J. Pérez-Ramírez, Tailored crystalline microporous materials by post-synthesis modification, *Chem. Soc. Rev.* **2013**, 42, 263-290.
[110] Y. Goto, H. Sato, S. Shinkai, K. Sada, "Clickable" metal− organic framework, *J. Am. Chem. Soc.* **2008**, 130, 14354-14355.
[111] U. Fluch, B.D. McCarthy, S. Ott, Post synthetic exchange enables orthogonal click chemistry in a metal organic framework, *Dalton Trans.* **2019**, 48, 45-49.
[112] S. Yuan, W. Lu, Y.-P. Chen, Q. Zhang, T.-F. Liu, D. Feng, X. Wang, J. Qin, H.-C. Zhou, Sequential linker installation: precise placement of functional groups in multivariate metal–organic frameworks, *J. Am. Chem. Soc.* **2015**, 137, 3177-3180.
[113] J.E. Clements, J.R. Price, S.M. Neville, C.J. Kepert, Perturbation of Spin Crossover Behavior

by Covalent Post-Synthetic Modification of a Porous Metal–Organic Framework, *Angewandte Chemie International Edition* **2014**, 53, 10164-10168.
[114] L.-F. Wang, W.-M. Zhuang, G.-Z. Huang, Y.-C. Chen, J.-Z. Qiu, Z.-P. Ni, M.-L. Tong, Spin-crossover modulation via single-crystal to single-crystal photochemical [2+ 2] reaction in Hofmann-type frameworks, *Chemical Science* **2019**, 10, 7496-7502.
[115] H. Flötotto, T. Secker, P. Kögerler, C. Besson, Amine - Functionalized Spin Crossover Building Blocks, *Eur. J. Inorg. Chem.* **2019**, 2019, 4621-4624.
[116] D.L. Reger, J.R. Gardinier, W.R. Gemmill, M.D. Smith, A.M. Shahin, G.J. Long, L. Rebbouh, F. Grandjean, Formation of third generation Poly (pyrazolyl) borate ligands from alkyne coupling reactions of Fe [(p-IC6H4) B (3-Rpz) 3] 2 (R= H, Me; pz= Pyrazolyl): Pathways toward controlling an Iron (II) electronic spin-state crossover, *J. Am. Chem. Soc.* **2005**, 127, 2303-2316.
[117] J.H. Askew, H.J. Shepherd, Post-synthetic anion exchange in iron (II) 1, 2, 4-triazole based spin crossover materials via mechanochemistry, *Dalton Trans.* **2020**, 49, 2966-2971.
[118] X. Yang, A. Enriquez-Cabrera, D. Toha, Y. Coppel, L. Salmon, A. Bousseksou, Spin crossover in mixed-anion Fe (NH 2 trz) 3 (BF 4)(SiF 6) 0.5 crystalline rod-shaped particles: the strength of the solid–liquid post synthetic modification, *Dalton Trans.* **2023**, 52, 10828-10834.
[119] C.F. Wang, G.Y. Yang, Z.S. Yao, J. Tao, Monitoring the Spin States of Ferrous Ions by Fluorescence Spectroscopy in Spin - Crossover–Fluorescent Hybrid Materials, *Chemistry–A European Journal* **2018**, 24, 3218-3224.
[120] E. Resines-Urien, L. Piñeiro-López, E. Fernandez-Bartolome, A. Gamonal, M. Garcia-Hernandez, J.S. Costa, Covalent post-synthetic modification of switchable iron-based coordination polymers by volatile organic compounds: a versatile strategy for selective sensor development, *Dalton Trans.* **2020**, 49, 7315-7318.
[121] A. Enríquez - Cabrera, K. Ridier, L. Salmon, L. Routaboul, A. Bousseksou, Complete and versatile post - synthetic modification on iron - triazole spin crossover complexes: a relevant material elaboration method, *Eur. J. Inorg. Chem.* **2021**, 2021, 2000-2016.
[122] A. Enriquez-Cabrera, L. Getzner, L. Salmon, L. Routaboul, A. Bousseksou, Post-synthetic modification mechanism for 1D spin crossover coordination polymers, *New J. Chem.* **2022**, 46, 22004-22012.
[123] A. Grosjean, P. Négrier, P. Bordet, C. Etrillard, D. Mondieig, S. Pechev, E. Lebraud, J.F. Létard, P. Guionneau, Crystal structures and spin crossover in the polymeric material [Fe (htrz) 2 (trz)](BF4) including coherent - domain size reduction effects, *Eur. J. Inorg. Chem.* **2013**, 2013, 796-802.
[124] A. Grosjean, N. Daro, S. Pechev, C. Etrillard, G. Chastanet, P. Guionneau, Crystallinity and microstructural versatility in the spin - crossover polymeric material [Fe (Htrz) 2 (trz)](BF4), *Eur. J. Inorg. Chem.* **2018**, 2018, 429-434.
[125] A. Grosjean, N. Daro, S. Pechev, L. Moulet, C. Etrillard, G. Chastanet, P. Guionneau, The spin - crossover phenomenon at the coherent - domains scale in 1D polymeric powders: evidence for structural fatigability, *Eur. J. Inorg. Chem.* **2016**, 2016, 1961-1966.
[126] A. Grosjean, Matériaux polymériques 1D à transition de spin: investigations structurales multi-échelles, Université de Bordeaux 1, 2013.
[127] X. Yang, A. Enriquez-Cabrera, K. Jacob, Y. Coppel, L. Salmon, A. Bousseksou, Room temperature spin crossover properties in a series of mixed-anion Fe (NH 2 trz) 3 (BF 4) 2− x (SiF 6) x/2 complexes, *Dalton Trans.* **2024**, 53, 6830-6838.
[128] D. Paliwoda, L. Vendier, L. Getzner, F. Alabarse, D. Comboni, B. Martin, S.E. Alavi, M.P. Bello, L. Salmon, W. Nicolazzi, Elastic Properties of the Iron (II)–Triazole Spin Crossover Complexes [Fe (Htrz) 2trz] BF4 and [Fe (NH2trz) 3] SO4, *Cryst. Growth Des.* **2023**, 23, 1903-1914.

Chapter 2 Spin state effect on the efficiency of a post-synthetic modification reaction on a spin-crossover complex

2.1 Introduction

Spin-crossover (SCO) complexes are a fascinating material that exhibits a reversible transition between different spin states in response to external stimuli such as temperature, pressure, and light. Among these complexes, iron(II)-triazole complexes are noteworthy for their well-defined and adjustable SCO properties.[1, 2] These complexes typically follow the general formula $[Fe(NH_2trz)_3]Anion \cdot xH_2O$, where Anion represents mono- or divalent counterions (Fig. 2-1). They consist of iron(II) coordinated to triazole ligands, forming a 1D coordination polymer chain that displays an abrupt transition with a large hysteresis loop above room temperature.[3-5] The impressive SCO properties of iron-triazole complexes make them highly suitable for various technological applications, including sensors,[6, 7] electronic devices[8] and artificial muscle.[9-11]

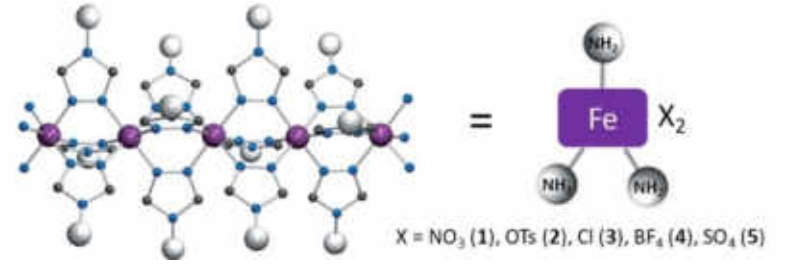


Fig. 2-1 Molecular structure of 1D coordination polymer chains of $[Fe(NH_2trz)_3]Anion \cdot xH_2O$ [1]

From an application perspective, the synthesis of various iron-triazole SCO complexes is of significant interest. Post-synthetic modification (PSM) reactions are an attractive method for producing a wide range of these complexes.[12] This approach is commonly used in the fields of metal-organic frameworks (MOFs) and covalent organic frameworks (COFs).[13-15] As illustrated in Fig. 2-2, the PSM method begins with the synthesis of the materials. Functional groups present in these materials are then modified by chemical reactions, resulting in the desired compounds. The same materials can also be obtained through the traditional direct synthesis (DS) method, which involves first modifying the ligand and then coordinating it with the metal ion.

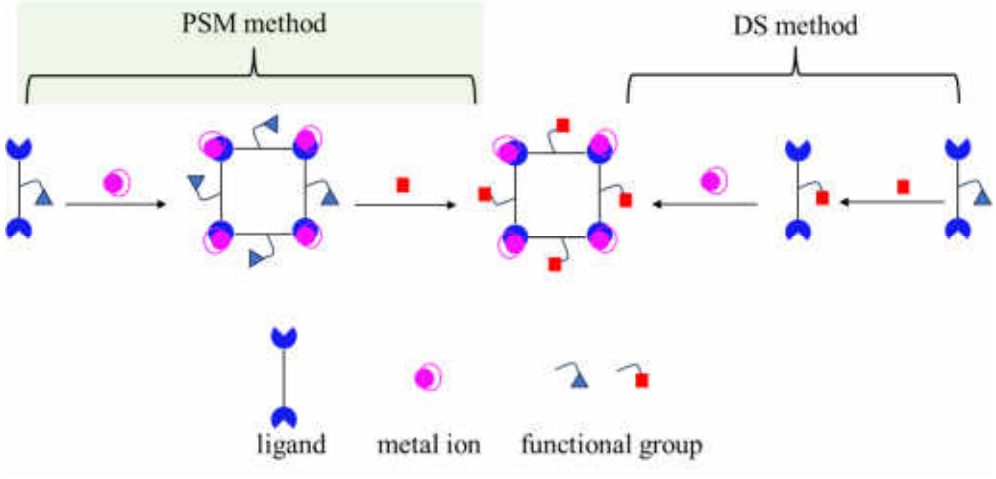


Fig. 2-2 Schematic representation of post-synthetic modification and direct synthesis methods.

Using the PSM method offers several advantages over traditional direct synthesis methods:

1) The PSM method provides access to a wide range of compounds from a single parent molecule (Fig. 2-3). Numerous examples in the literature show that authors have obtained a series of MOFs from the same parent material.[16-17]

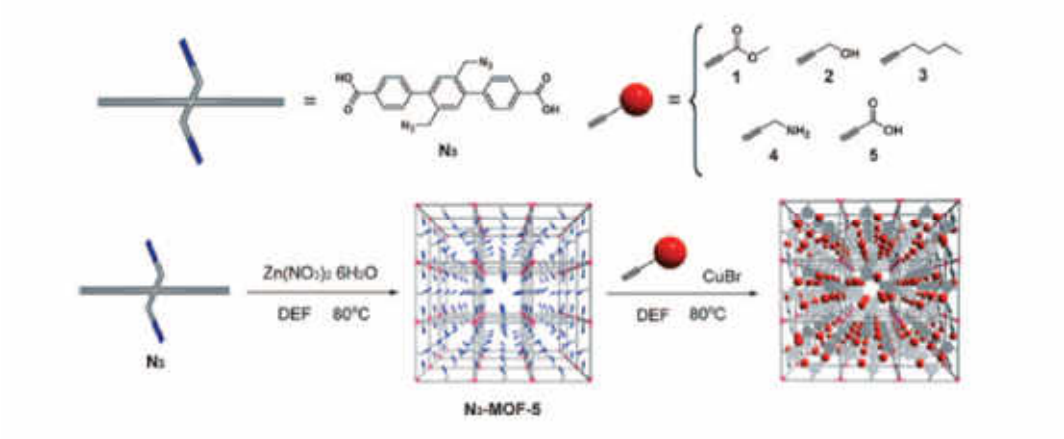


Fig. 2-3 Example of synthesis of a series of MOFs by PSM reaction and from the same parent material.[17]

2) In some cases, the PSM method provides access to complexes that are difficult or impossible to synthesize using other synthetic methods. For example, Ott et al. have successfully synthesized a series of MOFs with 1,2,3 -triazole functions. Their strategy was to start with the MOF UiO-67, then by post-synthetic exchange, connectors from this MOF were exchanged for connectors possessing either an azide or an alkyne group. Substituted 1,2,3-triazoles were then formed by click chemistry. The sequential realization of the two 1,3-dipolar cyclizations enabled them to create a whole library of MOFs. Note that this family of MOFs cannot be synthesized by a direct method, as the triazole moiety is not stable under the conditions used to form the MOF.[18]

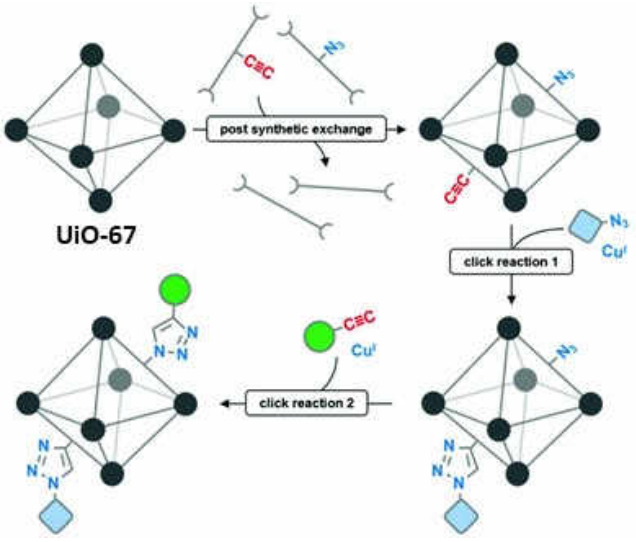


Fig. 2-4 Example of access, thanks to the PSM method, to a MOF that cannot be synthesized by a direct synthesis method.[18]

3) The PSM method can offer better control over the chemical structure of the material. For example, Zhou et al have synthesized MOFs with different linkers. Their strategy for accessing the desired MOFs was based on the PSM method and involved sequential installation of the linkers. This really was a key step, as using the direct method does not allow such fine control

over the position of the linkers in the molecular edifice.[19]

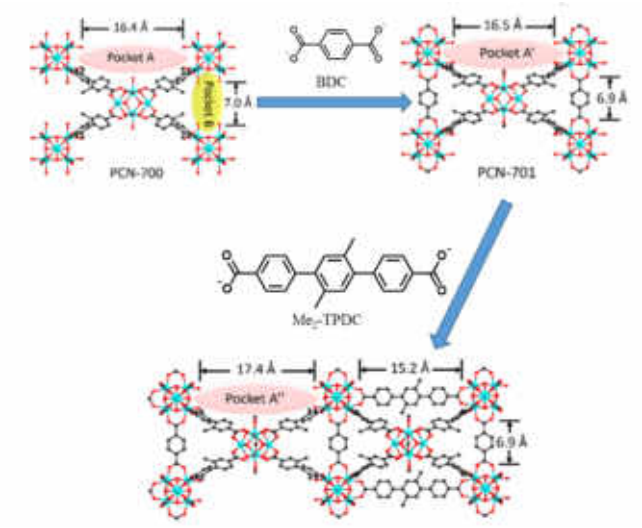


Fig. 2-5 Example of control of the linker positioning in the molecular edifice using the PSM method.[19]

Over the past decades, there has been increasing interest in synthesizing new spin crossover compounds via the PSM method. While examples in the literature are described on the application of the PSM method to MOFs[20, 21], or molecular systems[22, 23], this chapter focuses on the use of this method to the iron coordination polymer of formula: $[Fe(NH_2trz)_3]$Anion. Two main approaches have been identified for synthesising new SCO compounds through the PSM method: the modification of the counter anion and the modification of the cation (organic part).

Modification of the counter anion

Shepherd et al.[24] described a facile method for the post-synthesis exchange of anions in iron(II) spin-crossover materials using mechanochemistry (Fig. 2-6). By dry grinding the $[Fe(NH_2trz)_3]Cl_2$ complex with an excess sodium halide salt, they achieved complete anion exchange, leading to the formation of $[Fe(NH_2trz)_3]Br_2$ and $[Fe(NH_2trz)_3]I_2$. Recently, Salmon et al [118]. presented a solid-liquid post-synthetic modification approach to obtain a pure mixed-anion $[Fe(NH_2trz)_3](BF_4)(SiF_6)_{0.5}$ SCO complex from the parent complex $[Fe(NH_2trz)_3](BF_4)_2$. The anion SiF_6^{2-} is formed by a reaction between the tetrafluoroborate anion and TEOS (tetraethyl orthosilicate). The resulting SCO complex exhibited highly crystalline properties with homogeneous micrometric rod-shaped particles. It also presented an abrupt spin transition with a narrow hysteresis loop centred just above room temperature, making it highly promising for integration into various applications.

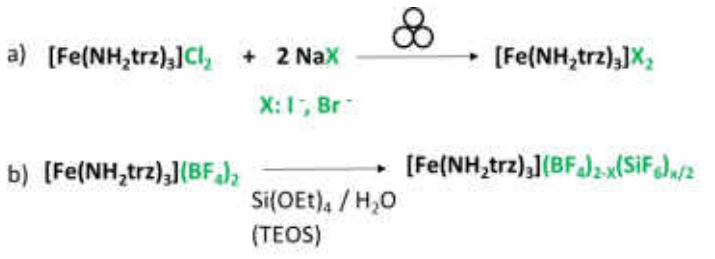


Fig. 2-6 Modification of the complex anion by PSM reaction. a) PSM reaction by mechanochemistry; b) PSM reaction between iron complex and TEOS. [24]

Modification of the cation (organic part).

Tao et al. were the first to transform NH_2 groups on the iron 1D coordination polymer using the PSM reaction. [14,26] It should be noted that in their case, the percentage substitution of NH_2 groups is at most 15%. The formation of imine functions by PSM reaction enabled them to connect a fluorophore group, such as pyrene, to the iron complex. The authors observe a correlation between the SCO transition temperature and the temperature at which fluorescent intensity reverses (Fig. 2-7). This research demonstrates the synergistic effect of spin transition and luminescence.

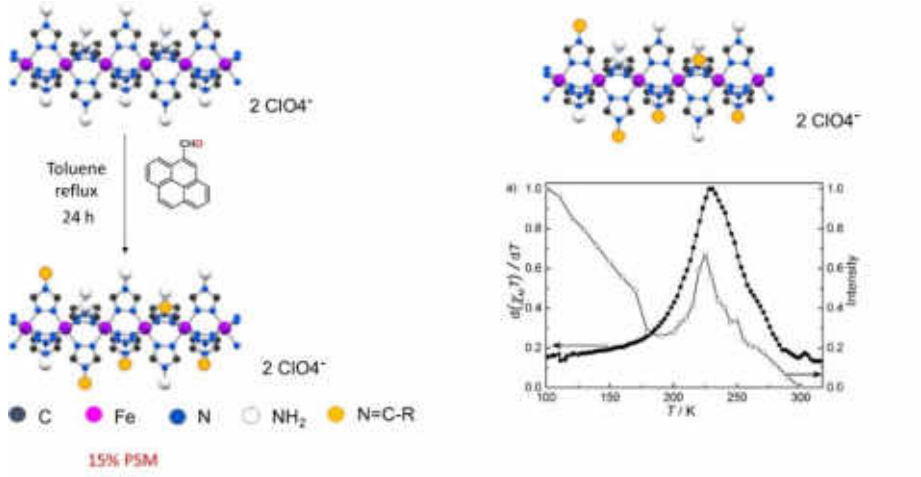


Fig. 2-7 Synthesis by PSM reaction and synergy between luminescence and SCO properties of a 1D iron coordination polymer with fluorophore groups.[26]

In 2019, our research team investigated the post-synthetic reaction between *p*-anisaldehyde and the SCO complex $[Fe(NH_2trz)_3](NO_3)_2$. The reaction was carried out at 35°C and, by adjusting the reaction time, different transformation percentages were obtained, ranging from 23% to total conversion. This research, in contrast to the results of Tao et al., highlights the possibility of quantitative post-chemical transformation. Another remarkable result of this article is that the spin-transition properties of the material also depend strongly on the synthesis method used to synthesise the iron complex (Fig. 2-8). The difference in SCO properties has been attributed to the different crystallinity of the materials. Indeed, the PSM material has crystalline characteristics, while the DS material is fully amorphous.[5]

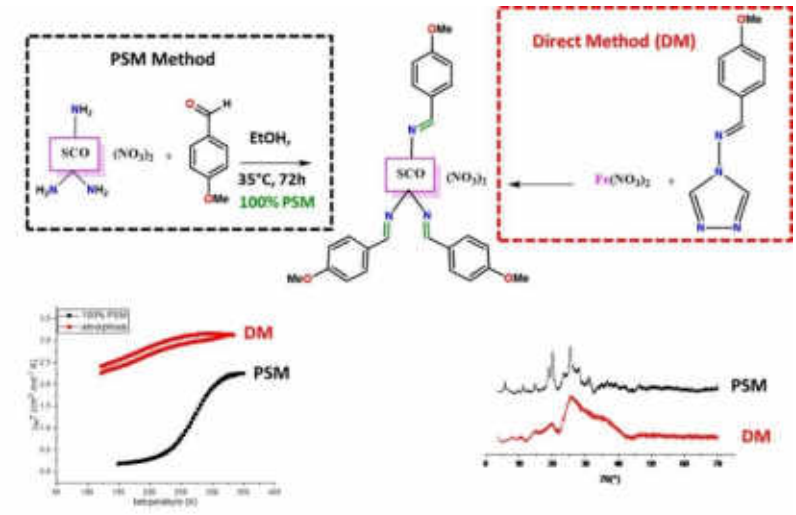


Fig. 2-8 Influence of the complex synthesis method on the crystallinity and SCO properties of the material.[5]

A year later, Costa et al. described quantitative PSM reactions from the complex $[Fe(NH_2trz)_3](OTs)_2$. The reactions are carried out between the complex in the solid state and the reagent (formaldehyde, benzaldehyde or acetone) in the vapour state (Fig. 2-9). Each of these organic compounds can react with the NH_2 group of the SCO complex, thereby modifying the magnetic properties of the material. The authors have thus demonstrated that the parent material can act as a selective chemosensor for volatile organic compounds, particularly formaldehyde. [27].

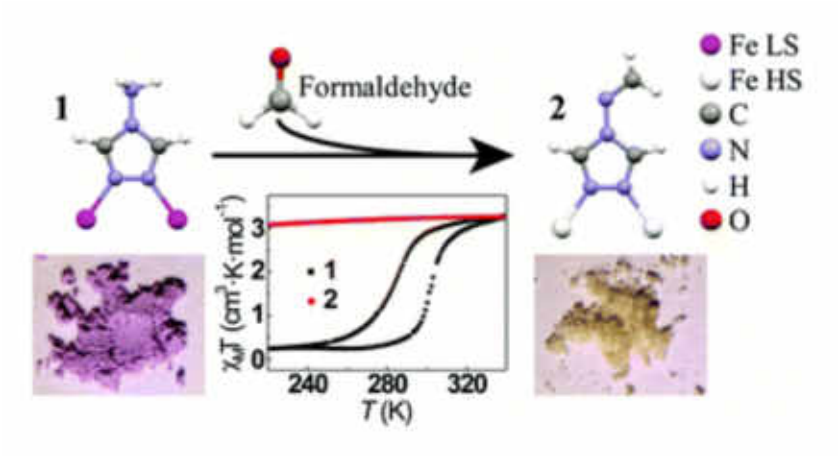


Fig. 2-9 Effect on the SCO properties of the material of the PSM reaction on the complex $[Fe(NH_2trz)_3](OTs)_2$ with formaldehyde vapours. [27]

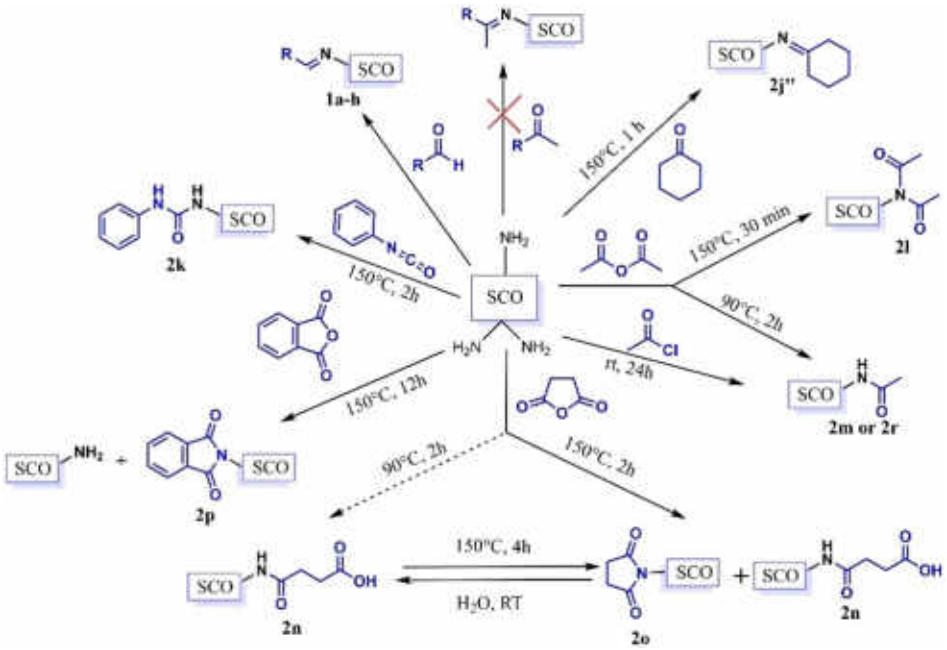


Fig. 2-10 Examples of complexes that can be obtained by applying the PSM method to the coordination polymer $[Fe(NH_2trz)_3](OTs)_2$.[28]

In the same year, our research team demonstrated that the application of the PSM method to the complex $[Fe(NH_2trz)_3](OTs)_2$ is not limited to the formation of Schiff bases.[28] This article illustrates the advantages of the PSM method for SCO compounds. Firstly, a large library of compounds could be synthesized from the same parent complex (Fig. 2-10). This result shows that the parent complex is stable under different experimental conditions. Moreover, as all the

complexes synthesized are insoluble, they can be easily separated from the reaction medium. Sometimes, the PSM method gives us greater control over the chemical structure. For example, by adjusting the experimental conditions, it is possible to form either the diamide or the monoamide. Finally, compound **2o** (Fig. 2-10) can only be obtained by the PSM method. In this article, we have also demonstrated that the efficiency of the PSM reaction is highly dependent on the nature of the anion in the complex, as well as on the conditions used to carry out the PSM reaction.

In 2022, our research team investigated the mechanism of the PSM reaction between p-anisaldehyde and the $[Fe(NH_2trz)_3](NO_3)_2$ complex. [29] It is important to note that obtaining quantitative yields from an insoluble complex possessing a very compact molecular arrangement was intriguing. While the team claimed that the transformation of the material was due to a PSM reaction between the reagent in solution and the complex in the solid state, others thought that imine formation took place in solution. We therefore considered the formation of the imine complex in solution, but as we had expected, the experiments we carried out demonstrated that this type of reaction pathway is highly unlikely. We were also convinced that the solvent plays a key role in the efficiency of the PSM reaction. Indeed, for the PSM reaction to take place, there must be effective contact between the NH_2 functions of the complex and the aldehyde (Fig. 2-11). To achieve this, the solvent must allow the separation of both the complex particles and the polymeric chains of the complex.

As expected, we have demonstrated that the use of appropriate solvents, such as ethanol or methanol, is crucial for performing a quantitative PSM reaction. Conversely, the use of unsuitable solvents leads either to no reaction at all or to a product that is not the desired compound (formation of the iron(III) imine complex). The team has also demonstrated that the PSM reaction significantly modifies the size and shape of complex nanoparticles. Beyond the field of spin transition, this work illustrates that solvents can influence the molecular arrangements of insoluble solid compounds and that PSM reactions are not limited to porous solids.

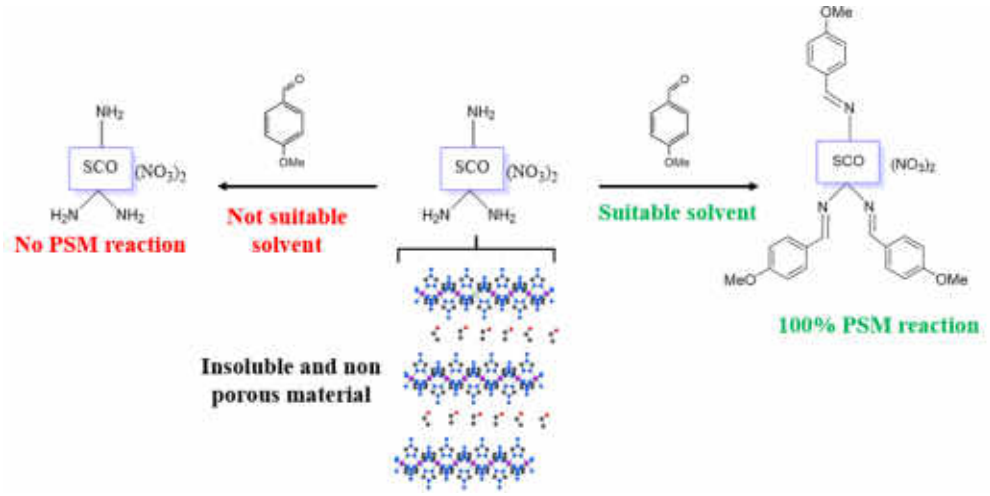


Fig. 2-11 Influence of the solvent on the PSM on the $[Fe(NH_2trz)_3](NO_3)_2$ spin crossover (SCO) complex[29].

2.2 The objective of this chapter

Previous studies carried out by our team have confirmed the feasibility of carrying out quantitative PSM reactions from the parent complex $[Fe(NH_2trz)_3](NO_3)_2$. In particular, they

demonstrated that the same imine complex could be obtained quantitatively either by performing the PSM reaction at 35°C for 72h or at 90°C for 10 minutes (Fig. 2-12).



Fig. 2-12 An imine complex was synthesised through a post-synthetic reaction, with one reaction being carried out at a low and high temperature.[5,28]

Thus, the efficiency of the PSM method also strongly depends on the reaction temperature. The team, therefore, wondered whether this difference in PSM efficiency could be induced by the spin state of the complex. Isolating the effect of the spin state from other possibilities that could explain a difference in reactivity is a real challenge. The difference in PSM reaction efficiency may be due to a single cause, or to a combination of factors. We have identified three different factors: thermal activation, structural effect, and spin state effect.

This chapter presents the scientific approach used by the team to study the effect of spin state on the efficiency of the PSM method. In particular, we will see that the large hysteresis cycle of the parent complex was a real asset for this study. I'd also like to mention that I was involved in the study of the reproducibility of the results (Sections 2.4 and 2.5).

2.3 The effect of thermal activation, structural effect and spin state on the PSM method

As already mentioned, the effect of temperature on the efficiency of the PSM reaction could be attributed to three different factors:

1) **Thermal activation**: Indeed, higher temperatures can provide the energy needed to overcome activation barriers for functionality formation, thus facilitating product synthesis. As a general rule, higher temperatures lead to higher yields, and when a desired product is not obtained or reaction rates are low, higher temperatures are often attempted as a solution.

2) **Structural effect**: An increase in temperature can facilitate interactions between the reactants, as well as between the reactants and the solvent. This is an important parameter, as the speed of a reaction in which one of the reactants is in the solid state is highly dependent on the contact between the reactants. Indeed, a change in molecular interactions will result in a change in the molecular arrangement of the solid compound, leading to different access to functional groups. This parameter should not be overlooked, as the team has previously demonstrated that ethanol enables better separation of the polymer chains of complex **1**, leading to a quantitative PSM reaction.[29]

3) **Spin state effect**: Complex **1** is in the LS state at a low temperature (35 °C) but in the HS state at a high temperature (90 °C). Since the reactivity of the iron complex also depends

on the spin state of its metal, it is then conceivable that the spin state has an influence on the efficiency of the PSM reaction.

2.3.1 Comparison of the temperature effect on the PSM reaction/imine ligand synthesis

To investigate whether the increase in efficiency is due to surpassing the activation energy barrier, it is crucial to understand the effect of temperature on the formation of imine functionality. Several experiments were conducted to compare the temperature effect on the PSM reaction (*p*-anisaldehyde with complex **1**) and imine ligand synthesis (*p*-anisaldehyde with 4-amino-1,2,4-triazole). Despite the solubility difference between the ligand amino-triazole and the insoluble SCO complex, this model provides a straightforward and relevant way to determine if a similar effect is observed on the free ligand. The team decided to carry out this study first, as it would allow them to assess the value of investigating, in greater detail, this difference in the efficiency of the PSM reaction. The team decided to continue this study only if the increase in temperature from 35°C to 90°C had a very different effect on the PSM reaction from complex **1** than on the reaction in solution from aminotriazole (Fig. 2-13). Indeed, if both systems reacted in the same way, this would indicate that the yield increase was not related to the spin state of the complex, and so there would be no benefit for us to continue this study.

Before discussing the results, it is important to note that yields were measured using ^{1}H NMR with an internal standard for the ligand and post-digestion for the complex (see Experiment section 2.8.2). In the imine ligand synthesis, yields after 2 hours of reaction were 11% at 90 °C and 14% at 35 °C, indicating that temperature increase did not impact the yields of imine ligand formation (Fig. 2-13). Therefore, the significant temperature dependency observed in the reaction efficiency appears to be specific to the PSM reaction on complex **1** and may not solely be explained by a thermal activation energy barrier.

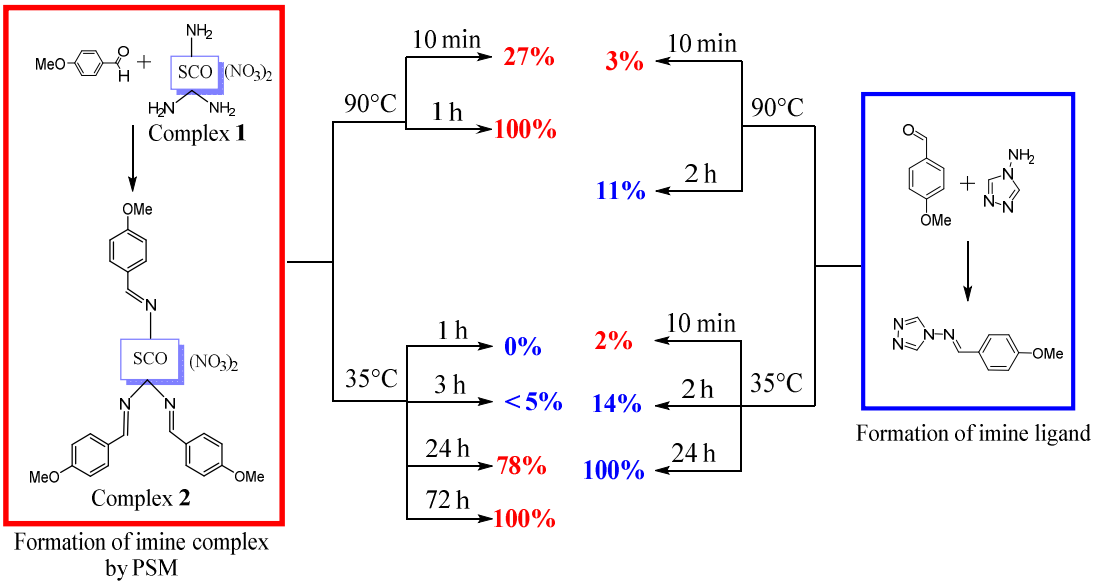


Fig. 2-13 Experimental conditions and yields for the synthesis of corresponding complex **2** (left) and the imine ligand (right)

2.3.2 Study of the efficiency of the PSM reaction as a function of the temperature

Having shown that the significant effect of increasing temperature on the reaction yield was specific to complex **1**, we set out to determine whether the yield increased linearly with temperature, or whether, on the contrary, a significant change in reaction rate was observed at certain temperatures. If the spin state influences the efficiency of the PSM reaction, then a change in reaction rate should be observed at the spin crossover temperature of complex **1**.

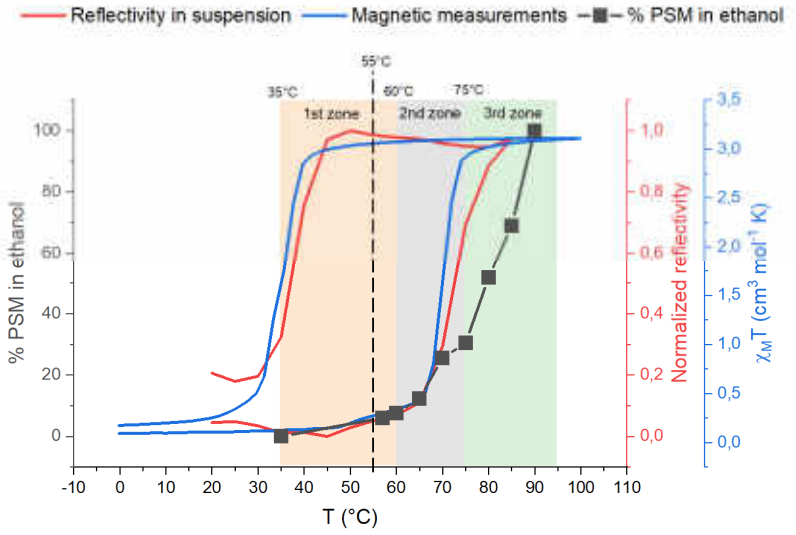


Fig. 2-14 (a) Variable temperature magnetic measurements (blue curve); variable temperature reflectivity measurements of complex **1** in ethanol suspension (red curve); (b)Yields of PSM in the function of the reaction temperature (black curve).

Fig. 2-14 shows three different curves as a function of temperature: 1) the black curve shows the yield of the PSM reaction; 2) the blue curve shows the magnetic properties of pure and solid-state complex **1**; 3) the red curve shows the spin transition properties of complex **1** suspended in ethanol.

The SCO properties of $[Fe(NH_2\text{-}trz)_3](NO_3)_2$ (complex **1**) were determined by analysing the variable magnetic susceptibility (courbe blue). The transition temperatures from LS to HS state and HS to LS were found to be 70 °C and 36 °C, respectively, with a hysteresis cycle width of 34 °C, consistent with previous studies[98, 121, 122]. The initial thermal cycle in this iron triazole complex often differs from subsequent cycles, possibly due to factors like solvent loss or stress relaxation. Optical reflectivity measurements, based on the color change of the complex in different spin states, are commonly used to follow the spin transition, usually in the solid state. It is important to note that magnetic susceptibility measurements were conducted on the pure solid complex **1**, while the PSM reaction occurs in the presence of EtOH. Although complex **1** is insoluble in EtOH, the presence of solvent can alter the molecular arrangement and thus affect its SCO properties. Therefore, reflectivity measurements were also performed with complex **1** suspended in EtOH, as shown in the red curve in Fig. 2-14. The experimental results indicate that the transition temperatures in suspension are close to those of the solid complex **1** for the initial cycle ($T_{1/2\uparrow}$ = 72.5°C, $T_{1/2\downarrow}$ = 37.5, ΔT= 35 °C). Unlike in the solid state, subsequent thermal cycles in suspension are not fully the same as the first cycle, likely due to trapped solvent molecules. Notably, the abrupt spin transition and hysteresis cycle are maintained even when the complex **1** is suspended in EtOH.

The PSM reaction was carried out for 1 h at temperatures ranging from 35°C to 90°C. We selected one hour since we know that the PSM reaction is quantitative in 1 hour at 90°C. So, in order to compare all temperature reactions, the reaction time should not exceed more than 1 hour. The results showing the yields as a function of reaction temperature after 1 h of PSM reaction are depicted in Fig. 2-14 (black curve) and Table 2-1. Note that PSM yields were determined by elemental analysis of the complexes recovered after reaction (Table 2-2).

Table 2-1 Yields of PSM reaction after 1 h of reaction at different temperatures

T (°C)	% PSM in 1 h
35	0
57	6
60	7
65	12
70	25
75	30
80	52
85	69
90	100

Table 2-2 Elemental analysis for 1h reaction at different temperatures

Temperature (°C)	Chemical formula	% amine	% imine	Anal Calcd.			Found		
				C	H	N	C	H	N
57	$[Fe(Atrz)_{2.82}(Itrz)_{0.18}](NO_3)_2(H_2O)_{0.73}$	94.0	6.0	19.1	3.1	42.0	18.8	2.5	41.4
60	$[Fe(Atrz)_{2.77}(Itrz)_{0.23}](NO_3)_2(H_2O)_{0.80}$	92.5	7.5	19.8	3.1	41.4	19.4	2.8	41.0
65	$[Fe(Atrz)_{2.63}(Itrz)_{0.37}](NO_3)_2(H_2O)_{0.83}$	87.8	12.2	21.8	3.2	39.9	21.4	2.7	39.8
70	$[Fe(Atrz)_{2.23}(Itrz)_{0.77}](NO_3)_2(H_2O)_{1.48}$	74.4	25.6	26.5	3.5	35.6	26.2	3.1	35.2
75	$[Fe(Atrz)_{2.09}(Itrz)_{0.91}](NO_3)_2(H_2O)_{1.30}$	69.6	30.4	28.3	3.5	34.8	28.3	3.3	34.5
80	$[Fe(Atrz)_{1.44}(Itrz)_{1.56}](NO_3)_2(H_2O)_{1.25}$	48.2	51.8	34.7	3.7	30.7	34.2	3.2	30.2
85	$[Fe(Atrz)_{0.93}(Itrz)_{2.07}](NO_3)_2(H_2O)_{3.10}$	31.0	69.0	37.0	4.2	26.7	36.6	3.7	26.3
90	$[Fe(Itrz)_3](NO_3)_2(H_2O)_{3.22}$	0	100	42.6	4.3	23.2	42.1	3.9	23.0

Atrz = $C_2H_4N_4$; Itrz = $C_{10}H_{10}N_4O$

The yield of the PSM reaction does not increase linearly with temperature, and the black curve seems to highlight three distinct zones. Firstly, between 35 and 60°C, very few imine formations occur within 1 hour (Orange area in Fig. 2-14). In the second zone, yields increase more significantly, from around 7% at 60°C to 30% at 75°C (Grey area in Fig. 2-14). Finally, in the third zone, the increase is more pronounced, rising from 30% at 75°C to 100% at 90°C. (Green area in Fig. 2-14). It is noteworthy that the reaction takes place in a hermetically sealed pressure tube, enabling heating up to 90°C, surpassing the boiling temperature of EtOH. The comparison of yields between the PSM reaction (black curve) and reflectivity measurement (red curve) in Fig. 2-14 shows that the first zone corresponds to the complex in the LS state, the second zone aligns with the ascending spin transition branch, and the third zone correlates with the complex in the HS state.

While this study is very much in line with expectations and gives us grounds for optimism, it is not proof of the influence of the spin state on the efficiency of the PSM reaction. Indeed, the increased efficiency of the PSM reaction at higher temperatures could be due to a change in the spin state of the material and/or to more favourable interactions between EtOH and the polymer chains (solvothermal effect).

2.3.3 Study of the influence of the spin state of complex 1 on the yield of the PSM reaction

If we want to separate the spin state effect from the solvatothermal effect, we need to perform the PSM reaction at the same temperature for both spin states of the complex. Although it is often impossible to test both spin states of the complex under identical experimental conditions, in our case it is absolutely feasible. Indeed, the red curve in Fig. 2-14 shows that complex **1** suspended in ethanol retains its thermal hysteresis loop. Thus, within the temperature range of this hysteresis loop, both spin states of complex **1** are stable. We chose to carry out the study at 55°C, as this temperature lies in the middle of the hysteresis loop (temperature 55°C is indicated by a dotted line in Fig. 2-14). To stabilize the complex in the LS state, the compound was suspended in ethanol and then placed in a preheated oil bath maintained at 55°C (Fig. 2-15). The HS complex was obtained by heating the suspension of complex **1** in ethanol at 90°C for 2 minutes, then immediately placing the suspension in the oil bath at 55°C (Fig. 2-15). Note that the colour of the solids enables us to check that the complex is in the desired spin state (pink for the low-spin state and white for the HS state). It is important to note that the heating process to 90°C to stabilise the HS state may potentially affect the molecular arrangement within the polymer chains. To address this, a comparative sample (referred to as LS2) was prepared by subjecting complex **1** to the same treatment as for the HS state, then cooling it to room temperature for 5 minutes to revert it to the LS state before placing it in the oil bath at 55°C (Fig. 2-15). Importantly, the aldehyde was not introduced during the stabilisation processes for LS, HS, and LS2, ensuring consistent conditions for the reaction between the aldehyde and the iron complex across all spin states. Following maintenance of all three samples at 55°C for 10 minutes, pre-heated aldehyde solution was added to each suspension to initiate the reaction. (for more details, see the Experiment section 2.8.1).

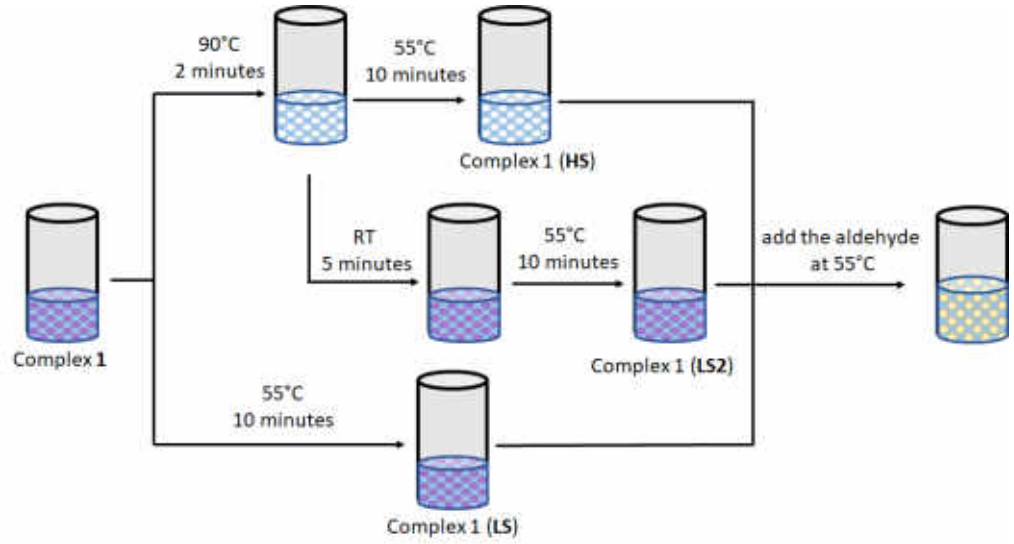


Fig. 2-15 Schematic representation of the preparation of complex **1** in the HS, LS and LS2 states.

Table 2-3 groups together the yields of the PSM reaction after different reaction times. Firstly, whatever the spin state of the complex, a much greater increase in yield is observed between 3 and 4 hours of reaction, which is consistent with the results of previous research carried out by our team.[5] Indeed, we have previously demonstrated a significant increase in the rate of the PSM reaction when the yield reaches 30-40%. This result can be easily explained if we consider

that the formation of imine groups leads to a better separation of the polymeric chains of the complex, and thus facilitates the PSM reaction. Most impressively, PSM yields when complex **1** is in the HS state are consistently and significantly higher than those obtained under the same conditions from the complex in the LS state. We were very pleased to see that the difference in yield could be as much as 21%. These results indicate that the HS complex is more reactive toward aldehyde than the LS complex. Thus, this study demonstrates that the spin state of complex **1** does influence the efficiency of the PSM reaction. This result highlights for the first time that the spin state of the metal influences the organic reactivity of the ligand. It has also been shown that the effect of the spin state of the metal is far from being restricted to the group coordinated directly to the metal.

Table 2-3 PSM reaction yields as a function of reaction time and spin state of the complex **1** (batch 1).

	PSM as function of the spin state(%)			difference in the efficiency of the PSM (%)		
time (hour)	LS	HS	LS2	Δ_{HS-LS2}	Δ_{HS-LS}	Δ_{LS2-LS}
1	6	8	/	/	2	/
3	29	41	33	8	12	4
4	50	72	51	21	22	1

The higher reactivity of the PSM reaction of complex **1** in the HS state may be due to a combination of electronic and steric influences. The spin state of the iron complex affects the electron density at the NH_2 function, leading to more nucleophilic nitrogen that accelerates the reaction with the aldehyde. Furthermore, the rate of reactions involving solid-state complexes is highly dependent on the efficiency with which the reactants are brought into contact. It is noteworthy that the transition from LS to HS state results in an expansion of the molecular volume of the SCO complex. In the family of 1D-coordination iron triazole SCO polymers, research conducted by Grosjean et al.[123-126] indicates that the distance between iron atoms in adjacent polymeric chains is greater in the HS state compared to the LS state. This increased distance could potentially facilitate the reaction between amino and aldehyde functionalities. However, complex **1** exhibits unique characteristics as it does not display the significant volumetric expansion typically observed in this class of SCO complexes. For complex **1**, the transition from LS to HS state results in an elongation along the polymer chain axis, accompanied by a contraction in other directions, leading to an overall volumetric expansion of only about 1%. This contrasts with other compounds in this category that have shown larger volume changes (6% for $[Fe(NH_2trz)_3](BF_4)(SiF_6)_{0.5}$[34], 10% for $[Fe(Htrz)_2(trz)](BF_4)$[30], and 5% for $[Fe(NH_2trz)_3](SO_4)$[35]). We believe that this low volumetric expansion does not explain the difference in the efficiency of the PSM reaction. In our previous study,[28] it was observed that conducting the PSM reaction in toluene rather than ethanol did not yield any reaction, even when the complex was in the HS state. While the effect of volumetric expansion due to the spin transition cannot be completely excluded, the experiments clearly demonstrate that ethanol is a key element of this PSM reaction. The strength and quantity of interactions between the polymeric chains and ethanol may vary depending on the spin state of the iron complex. Thus, stronger interactions between the complex and ethanol can lead to increased separation of polymeric chains and a faster PSM reaction. Furthermore, the yields of the PSM reaction from the LS2 complex were slightly higher than those from the LS complexes, potentially due to a unique molecular arrangement in the LS2 complex. It is expected that heating the suspension of the complex in ethanol to 90°C will enhance interactions between the solvent and the polymeric chains, resulting in a novel molecular arrangement of the material.

2.4 Study of the reproducibility of results

We have now proved that the spin state does influence the efficiency of the PSM reaction. This is an excellent result, but we still need to check its reproducibility. To achieve this, four additional batches (Batches 2-5) of complex **1** were examined, resulting in a total of 44 sets of experiments. Each set of experiments entailed reactions with the complex in both the HS and LS2 states, all performed under strictly identical experimental conditions. These experiments were performed in the same oil bath at 55°C, with consistent reaction time, quantities, solvent, and reagents (using the same bottle of ethanol or *p*-Anisaldehyde). Following the PSM reaction, the resulting complex underwent several washes, drying, grinding, and so on (for detailed information, see the experiment section). Subsequently, 2 samples (Sample 1 and 2) for each spin state experiment were taken and independently analysed using the digestion method. In the following figures, Series 1 encompasses the results of sample 1 of the experiments, while Series 2 comprises the results from sample 2 of the experiments.

2.4.1 Accuracy and precision of the method

Firstly, we wanted to assess the accuracy of the digestion method used to determine the amount of imine and amine functionality present in the recovered complex. To this end, eight different mixtures were prepared from known quantities of pure imine and amine complexes. After grinding, two samples (samples 1 and 2) were taken from each mixture (Fig. 2-16). Each sample was then subjected independently to the digestion method. Comparison of the quantities of imine and amine obtained with those expected enables us to assess the accuracy of the digestion method.

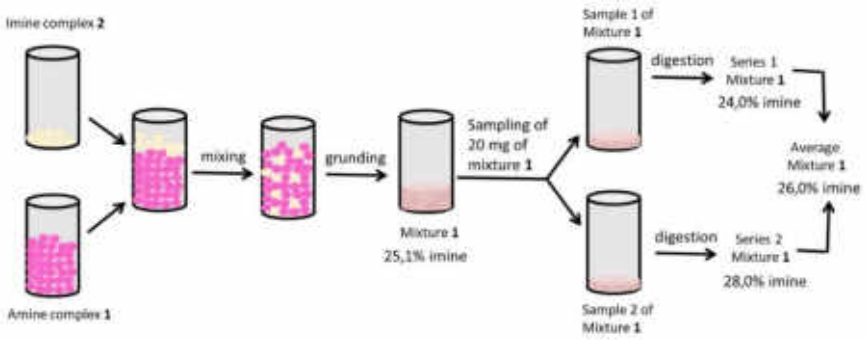


Fig. 2-16 Schematic representation of the preparation of the mixtures used to study the accuracy of the digestion method

Fig. 2-17 and Table 2-4 summarize the results obtained (Series 1, Series 2, the average of the two Series) and the expected values for the 8 mixtures. We chose to produce mixtures with 3 different types of imine molar percentages: a mixture containing a low imine content (25%), an equimolar mixture and a mixture containing a majority of imine (75%). Furthermore, as the large majority of results obtained by digestion of the complexes recovered after the PSM reaction were between 25% and 75% imine, these three types of mixtures enabled us to verify the validity of the digestion method for all our results. Taken as a whole, this study is very reassuring, as it shows that the digestion method gives us results close to what we expected to find, and that it is valid for all three types of mixtures studied. Apart from one case (7.3%), all the values obtained are within 4% of the expected value. The high percentage of error (7.3%) for series 2 of mixture 3 can be explained by an error in the aqueous phase sampling (slightly

more solution was taken, but this excess could not be precisely determined). Overall, the results of the two series are in agreement. Then, this study demonstrated the accuracy, precision, and reproducibility of the digestion method developed to quantify the percentage of imine in the complex. There are two advantages to analysing the mixture twice independently: on the one hand, it enables us to check that the imine value obtained is not an outlier; on the other hand, it generally enables us to get even closer to the expected value. In general, the mean values calculated from the results obtained for Series 1 and 2 correspond to the expected percentage of imine, with a margin of error generally not exceeding ±2%. Hence, an error bar of ± 2% has been utilised in all subsequent figures.

Finally, we systematically measured a mixture before starting to analyse the digestion of the complexes recovered after PSM. This measurement enabled us to check that there were no problems with the standards prepared for the day of measurement (between 20 and 40 complex digestions were carried out on the same day).

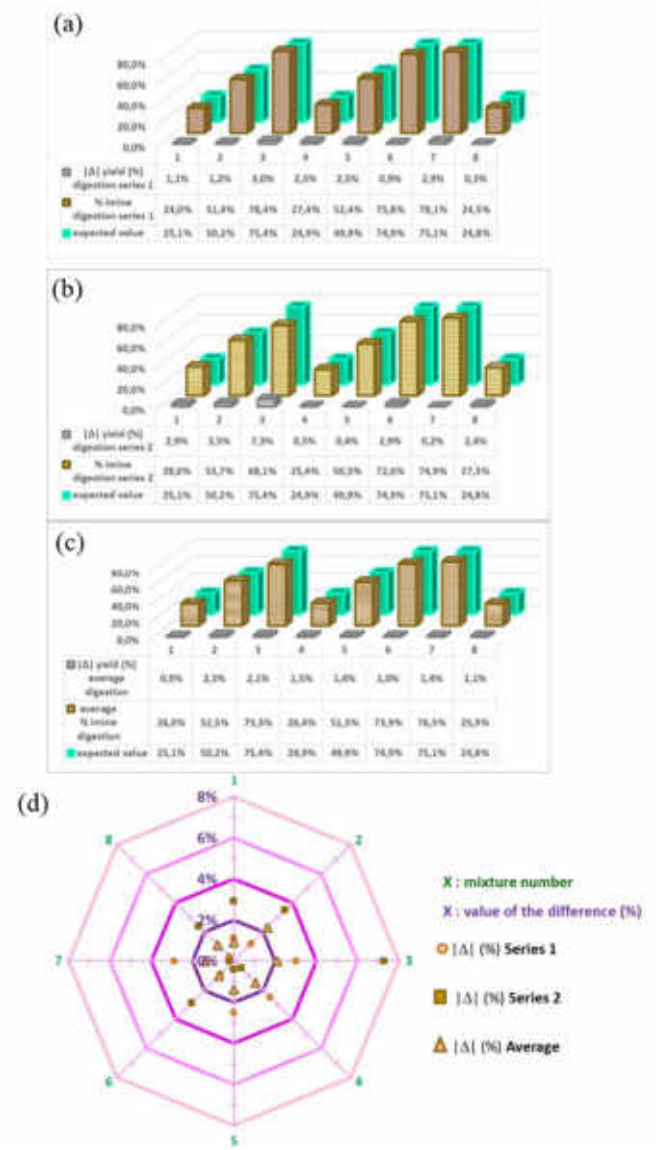


Fig. 2-17 Comparison of the difference between the results obtained by digestion and their expected value (method error) (a) Series 1, (b) Series 2, (c) average of Series 1 and Series 2. (d) Other representation of the difference between the values obtained and the expected values (target center) for each of the mixture

Table 2-4 Quantification of different physical mixtures of imine and amine

name exp	% imine digestion series 1	% imine digestion series 2	expected value	Δ yield (%) digestion series 1	|Δ| yield (%) digestion series 1	Δ yield (%) digestion series 2	|Δ| yield (%) digestion series 2	average % imine digestion	Δ yield (%) average digestion	|Δ| yield (%) average digestion
Mixt 1	24,0%	28,0%	25,1%	1,1%	1,1%	-2,9%	2,9%	26,0%	-0,9%	0,9%
Mixt 2	51,4%	53,7%	50,2%	-1,2%	1,20%	-3,5%	3,5%	52,5%	-2,3%	2,3%
Mixt 3	78,4%	68,1%	75,4%	-3,0%	3,0%	7,3%	7,3%	73,3%	2,1%	2,1%
Mixt 4	27,4%	25,4%	24,9%	-2,5%	2,5%	-0,5%	0,5%	26,4%	-1,5%	1,5%
Mixt 5	52,4%	50,3%	49,9%	-2,5%	2,5%	-0,4%	0,4%	51,3%	-1,4%	1,4%
Mixt 6	75,8%	72,0%	74,9%	-0,9%	0,9%	2,9%	2,9%	73,9%	1,0%	1,0%
Mixt 7	78,1%	74,9%	75,1%	-2,9%	2,9%	0,2%	0,2%	76,5%	-1,4%	1,4%
Mixt 8	24,5%	27,3%	24,8%	0,3%	0,3%	-2,4%	2,4%	25,9%	-1,1%	1,1%

2.4.2 Batch 2 with a reaction time of 4h at 55°C

We began our reproducibility study by performing the same reaction 6 times on batch 2 of complex **1** with a reaction time of 4h at 55°C. We made this choice because, starting from batch 1 of complex **1**, these experimental conditions enabled us to obtain 21% more imine when the PSM reaction was carried out using complex **1** in the HS state. By carrying out the same reaction six times, we wanted to verify that under the same experimental conditions and using the same batch of complex, similar results were obtained. As observed for batch 1 and whatever the experiment, a higher percentage of imine formation is observed when the complex is in the HS state compared with the LS2 state. (Fig. 2-18). By performing the same reaction a large number of times, we were able to point out that the results of experiment 2 are outliers. With the exception of experiment 2, similar results are obtained, and the results of the two series are comparable. This is very comforting, as it is a first element in favour of the reproducibility of the results. On average, when the complex was in the HS state, 33% imine was formed, whereas in the LS2 state, only 25% imine was produced.

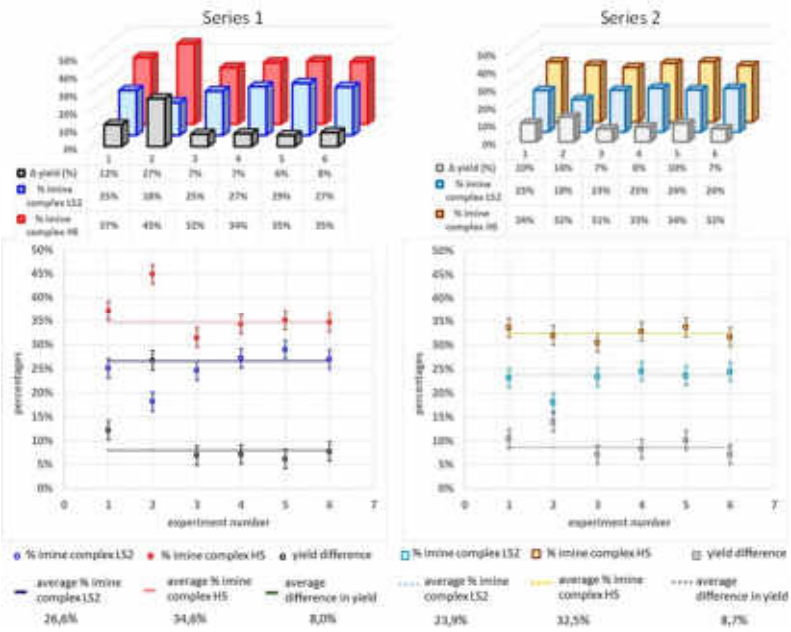


Fig. 2-18 Yields of imine obtained after 4h of PSM reaction for batch 2 at 55°C (Series 1 and 2), and the difference between HS and LS2 states.

It should be noted that the results of experiment 2 were not used for the calculation of averages (Fig. 2-18 and Fig. 2-19). This 8% difference in PSM is sufficient to differentiate the experiments using the complex in the HS state from those in the LS2 state. These experimental findings were more in line with those from batch 1, with a reaction time of 3 hours, rather than with those obtained after 4 hours of reaction (Table 2-3). In conclusion, these initial results from batch 2 confirm that complex **1** in the HS state appears to be more reactive towards aldehyde than the complex in the low-spin state. In comparison with batch 2, much lower yields were obtained, highlighting the need to study the experimental conditions for each batch of complex **1** in order to obtain the desired imine percentage.

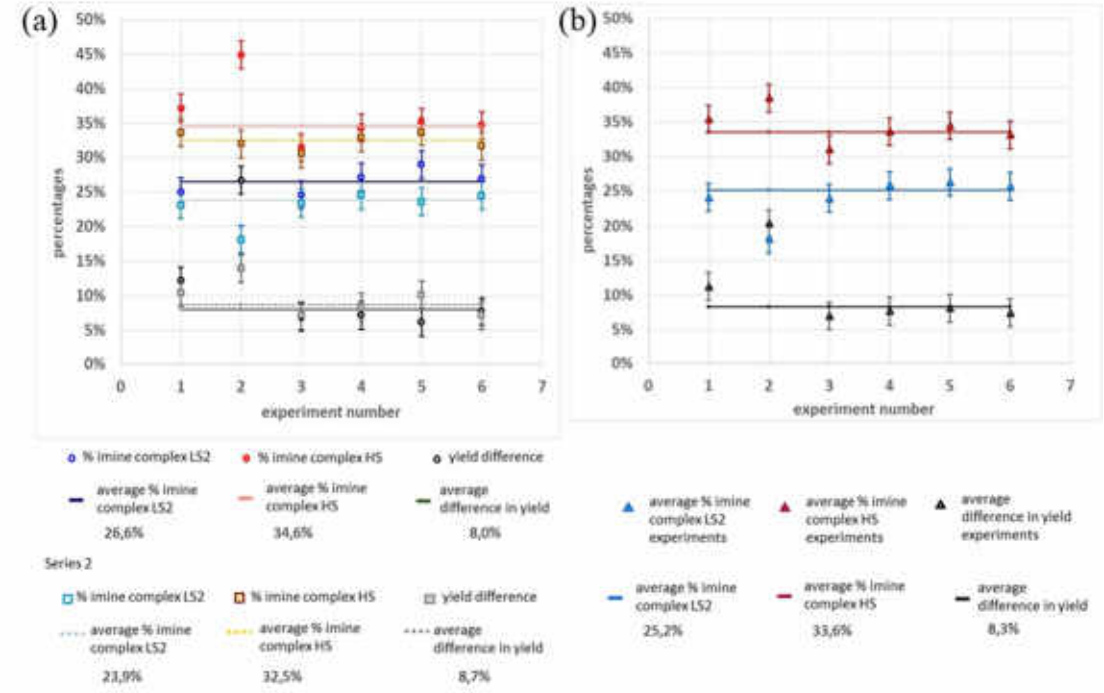


Fig. 2-19 Comparison of the results of the digestion method for Batch 2 with a reaction time of 4h at 55°C (a)Series 1 and 2; (b)average

2.4.3 Batch 2 with a reaction time of 3.5, 4h, 4.5 and 5.5h at 55 °C

As it is very likely that to obtain higher yields from batch 2, the reaction time needs to be increased, we took the opportunity to carry out a kinetic study of imine formation. (Fig. 2-20 and Fig. 2-21). This kinetic study confirms what we had observed when studying the mechanism of the PSM reaction[122], namely that the PSM reaction requires an initiation phase (after 3 hours of reaction between 20-30% imine is obtained), then when the imine percentage reaches around 40%, the reaction rate accelerates considerably (20% more imine is formed in 1 hour). As expected, prolonging the reaction time resulted in higher imine percentages. Experiments with 5.5 hours of reaction time indicated imine percentages of 60-70% for the HS state and around 50% for the LS2 state. Under these experimental conditions, we observed an average difference in yield (between the two spin states) of around 13%. It would have been interesting to carry out more experiments to confirm this average, but this was not possible as too few of the batch remained. Results show that in batch 2, a difference of approximately 8% exists between imine percentages of the HS and LS2 states when the HS complex ranges from 28 to 43%. In conclusion, although imine percentages are similar between batches 1 and 2, batch 2 requires a longer reaction time. This difference may be due to water content in the

complex or ethanol, as well as variations in complex particle size. For example, a comparison between experiments using 98% ethanol versus absolute ethanol showed a 5% increase in imine, suggesting water presence accelerates the PSM reaction, and this result is also consistent with our previous study.[29]

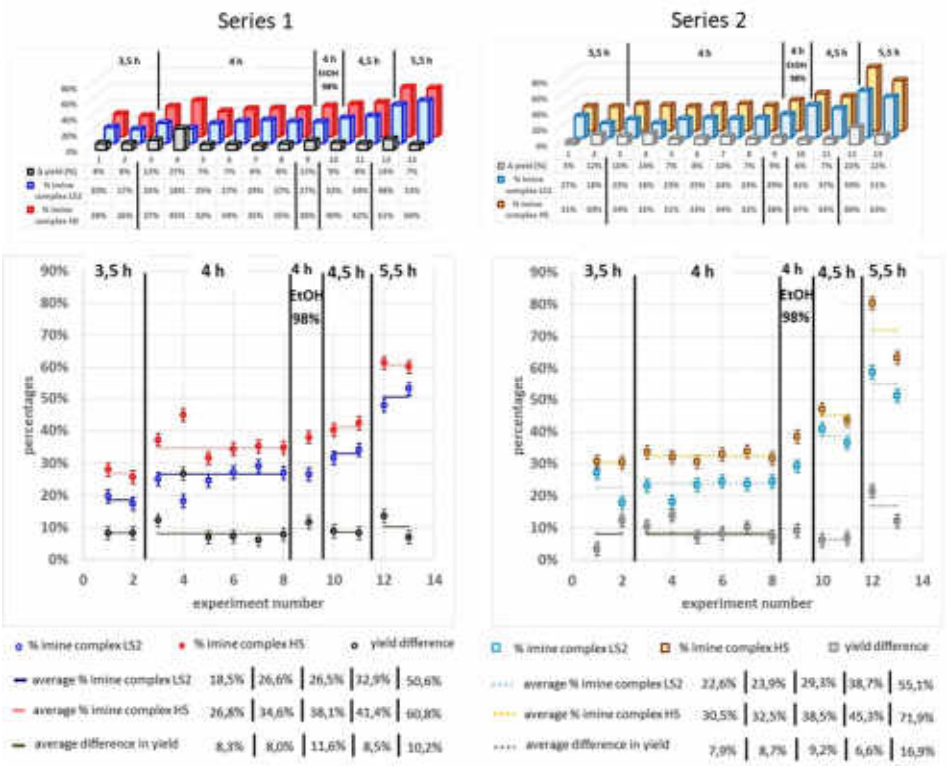


Fig. 2-20 Comparison of the results of the digestion method for the Batch 2 (3.5, 4h, 4.5 and 5.5h, Series 1 and 2)

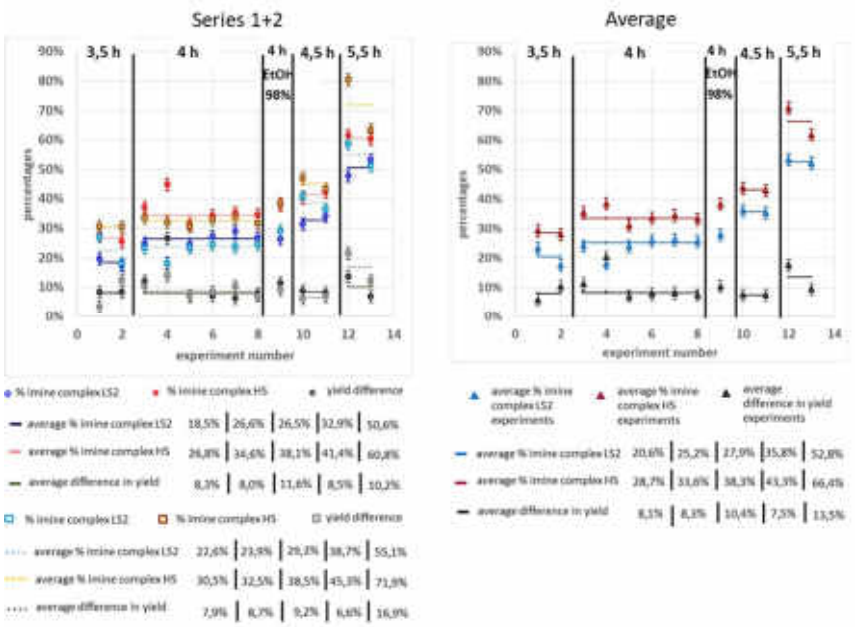


Fig. 2-21 Comparison of the results of the digestion method for the Batch 2 (3.5, 4h, 4.5 and 5.5h, Series 1+2; average)

2.4.4 Batch 3 with a reaction time of 4h (sonication and ethanol 98%)

We have just seen that in order to obtain high imine percentages from batch 2, we had to substantially increase the reaction time. We believe that there were two other parameters that could be used to increase the imine percentage without having to lengthen the reaction time. These were the reduction in particle agglomerate size and the presence of a small amount of water in the medium.

1) **the reduction in particle agglomerate size**: The PSM reaction takes place between the solid-state complex and the aldehyde in solution, meaning that the size of the complex particles and agglomerates significantly influences the reaction time. In general, smaller particles have a larger contact surface area, leading to shorter reaction times. This is why, before stabilizing the complex in the desired spin state (see experiment section, Fig. 2-38), we want to place the suspension of complex **1** in ethanol in an ultrasonic bath. The use of an ultrasonic bath will limit the size of the agglomerates of particles and ensure better dispersion of complex **1** in ethanol.

2) **the presence of a small amount of water in the medium**: We believe that the interaction with ethanol helps separate the polymeric chains of complex **1**. Water is even more effective than ethanol in separating these polymeric chains. Indeed, Guillaume Chastanet et al. have shown that water creates hydrogen bonds with the NH_2 functions of the complex, enabling the formation of channels between polymeric chains.[33] The formation of these channels is of great interest to us, as it would enable better contact between the NH_2 functions of the complex and the aldehyde, and thus lead to an increase in the efficiency of the PSM reaction. Note that this small amount of water must be added at 55°C, and after the complex suspension, in the desired spin state, has been thermalized at this temperature for 10 minutes.

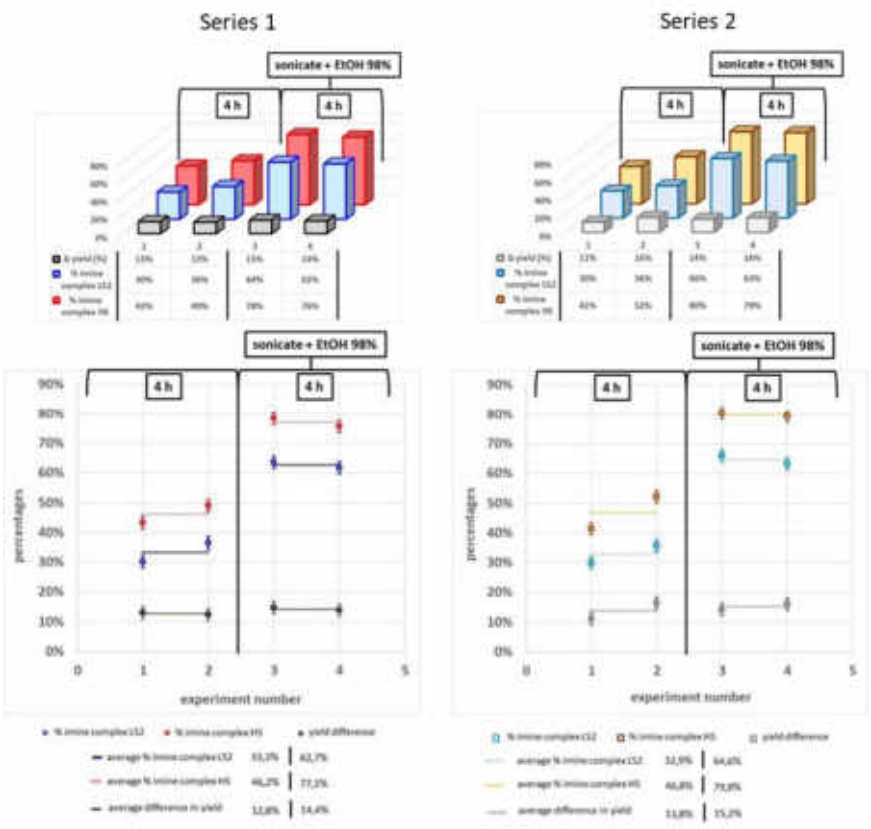


Fig. 2-22 Comparison of the results of the digestion method for Batch 3 (4h, normal conditions and with sonication and ethanol 98%, Series 1 and 2).

To determine whether these two parameters significantly increase the imine yield from batch 3, we also carried out two experiments under standard conditions using the same batch of complex **1** (for more details, see the experiment section 2.8.1). The results, depicted in Fig. 2-22 and Fig. 2-23, again confirm that more imine is obtained from complex **1** in the HS state than when it was in the LS state. As expected, the application of both reaction parameters (sonication of the complex suspension and the presence of traces of water in the medium) resulted in a 30% increase in imine percentages for both spin states. Specifically, the LS2 sample saw an increase from 33.1% to 63.6%, while the HS sample increased from 46.5% to 78.4% on average, with a 14.8% difference between the HS and LS2 samples. These results suggest that the presence of small amounts of water and sonication of the complex suspension do indeed increase the efficiency of the PSM reaction. Perhaps applying these two parameters could limit the differences in reactivity between batches of complex **1**.

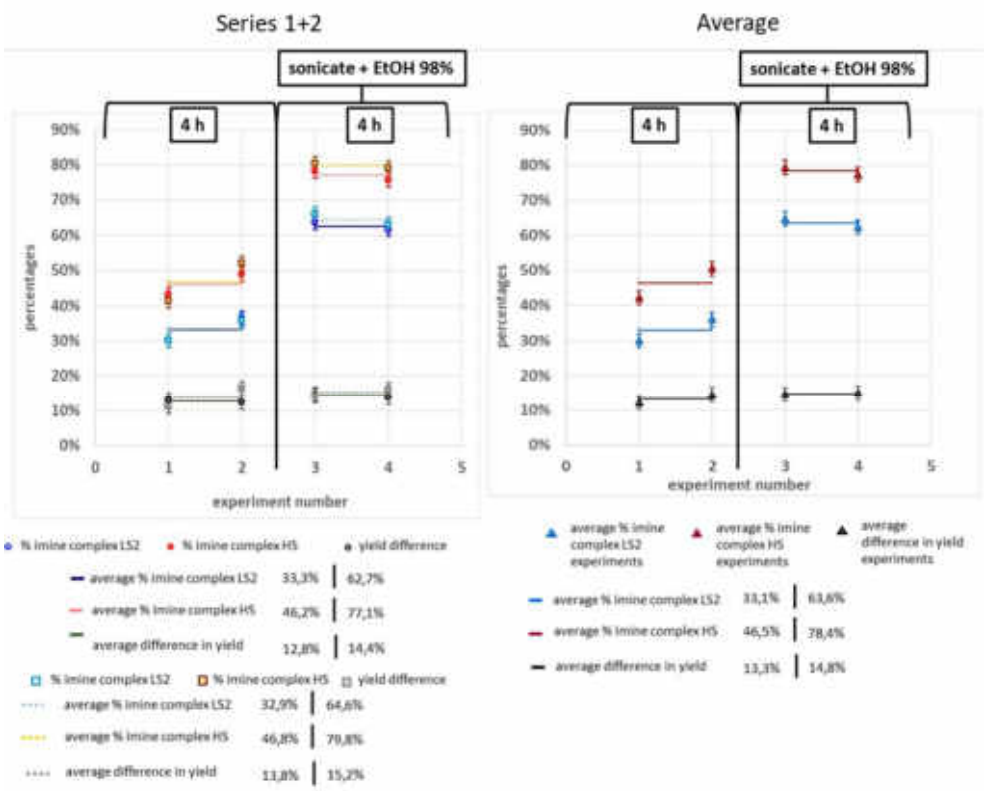


Fig. 2-23 Comparison of the results of the digestion method for Batch 3 (4h, normal conditions and with sonication and ethanol 98%, Series 1 + 2; average)

2.4.5 Batch 4 with a reaction time of 4h (HS and HS2)

In Batch 4, this study aimed to investigate the potential enhancement of the PSM reaction efficiency by subjecting the HS complex to a second heating (HS2 sample). The detailed experimental process is described in the experiment section 2.8.1. The results from experiments, presented in Table 2-5 and 0, indicated that the average yield of imine for the HS sample was 39.3%, while for the HS2 sample, it was 42.6%. This shows a slight increase of 3% in the yield for the HS2 sample compared to the HS sample, a difference slightly larger than the error margin of the digestion method. These results suggest that the second heating leads to only a minor enhancement in the efficiency of the PSM reaction, which is in the error range. Therefore, further investigation into the impact of the second heating on the efficiency of the PSM reaction is unnecessary.

Table 2-5 Results of the digestion method for the Batch 4

Entry	Name of the experiment	Experiment	% of imine		
			Series 1	Series 2	average
1	X1	HS	38.8%	39.8%	39.3%
2	X2	HS2	42.3%	42.9%	42.6%
3	Y1	LS	28.4%	28.4%	28.4%
4	Y2	LS2	32.3%	33.3%	32.8%

Table 2-6 Results of the digestion method for the Batch 4

Entry	% Δ(HS2-HS)	% Δ(HS-LS2)	% Δ(LS2-LS)
Series 1	3.6%	6.4%	4.0%
Series 2	3.1%	6.5%	4.9%
average	3.3%	6.5%	4.4%

2.4.6 Batch 5 with a reaction time of 4h (normal conditions), 4 and 5h (sonicated in ethanol 98%)

The previous section showed the effect of spin state on PSM efficiency. It was observed that under certain conditions, the difference in PSM efficiency could exceed 20%, which is a significant finding. In the upcoming section, our focus will be on studying the best conditions (e.g. reaction time of 5.5h, sonication in 98% ethanol and reaction of 4h) where a substantial difference in PSM efficiency was observed between the HS and LS2 samples. This study aims to validate the reproducibility of this noteworthy and crucial result.

In the initial six experiments of batch 5, the complex was sonicated in suspension in absolute ethanol, followed by the addition of 96% ethanol and a reaction time of 4h at 55°C (See experiment section 2.8.1). Similar to batch 3, with a 4h reaction, the imine percentages for the HS sample averaged 70.2%, and for the LS2 sample averaged 53.6%, with a yield difference of approximately 16.5% between the two spin states (Fig. 2-24 and Fig. 2-25). The sonication of the suspension and the presence of a small amount of water significantly enhanced the imine yields by approximately 30%. Subsequently, to investigate if the yield difference in PSM efficiency between HS and LS2 samples could be larger if the yield for the HS sample reaches a higher value (e.g. 90%), two additional sets of experiments were conducted with a reaction time of 5h at 55°C. This resulted in an increase in imine percentage to 88.6% for the HS sample and 70.2% for the LS2 sample on average, with a yield difference of approximately 17.3% in PSM efficiency. The yield difference between HS and LS2 samples remained around 17% even when the reaction was prolonged, and the yield for the HS sample reached approximately 90%.

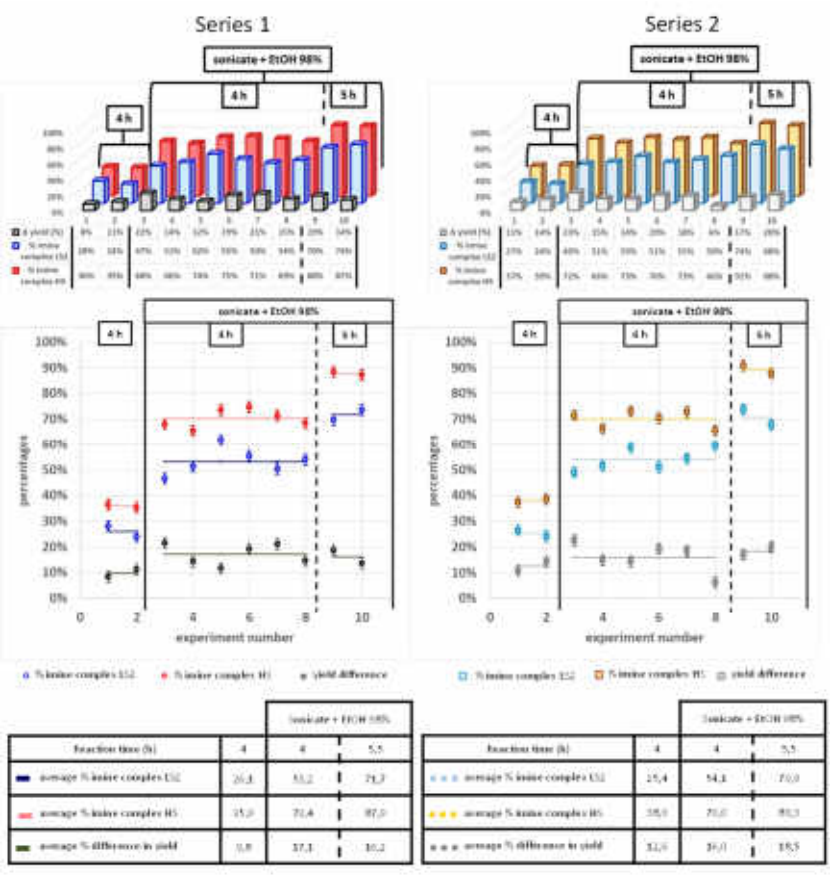


Fig. 2-24 Yields of PSM reaction obtained for batch 5 (Series 1 in the left and Series 2 in the right) after 4h of reaction (normal conditions), 4 and 5h (sonicated in ethanol 98%) of reaction, for the HS and LS2 and the difference between the two spin states.

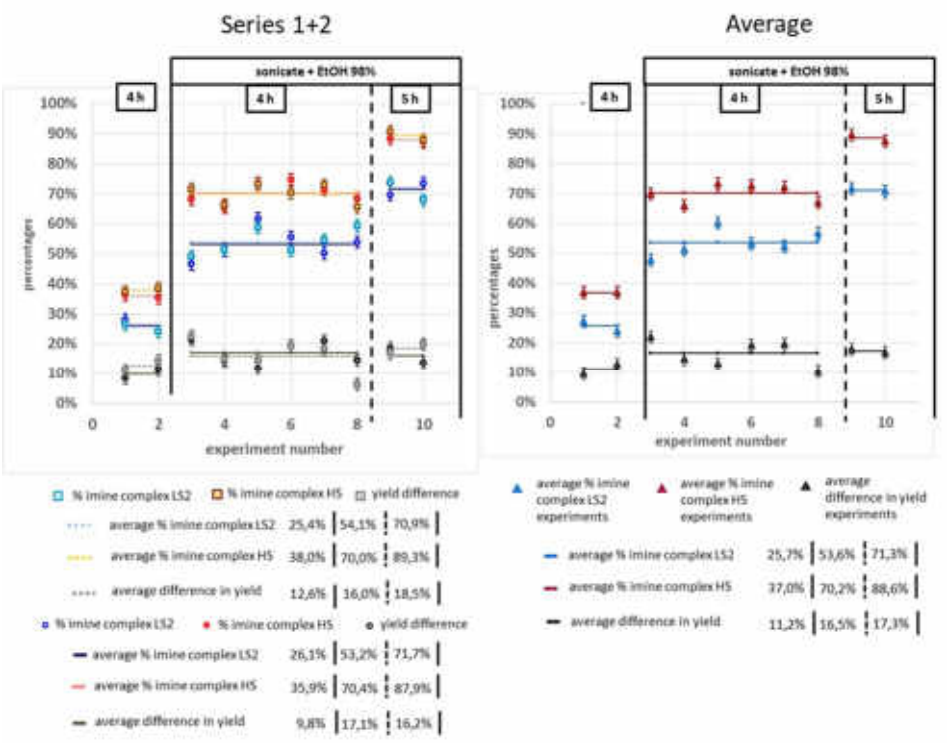


Fig. 2-25 Comparison of the results of the digestion method for Batch 5 (4h; 4h, sonicate and ethanol 98%; 5h, sonicate and ethanol 98%, Series 1 + 2; average)

2.4.7 Batch 5 with a reaction time of 4, 4.5, 5.5, 6 and 6.5h

The subsequent 10 experiments involved subjecting the samples to a temperature of 55°C for 5.5 hours without sonication and using 96% ethanol. The results, illustrated in Fig. 2-26 and Fig. 2-27, showed that the HS sample achieved an average imine percentage close to 73%, while the LS2 sample reached 51%, resulting in a difference in PSM efficiency of approximately 22% between the two spin states. In another experiment depicted in Fig. 2-26 and Fig. 2-27, the PSM reaction was conducted under varying reaction times to investigate the difference in PSM efficiency between HS and LS2 states. The results showed that for batch 5, when the imine percentage in the HS state ranged from 40 to 50%, a difference of about 10% with LS2 was observed. Conversely, when the imine percentage in the HS state was between 70 to 90%, a difference of over 20% was recorded.

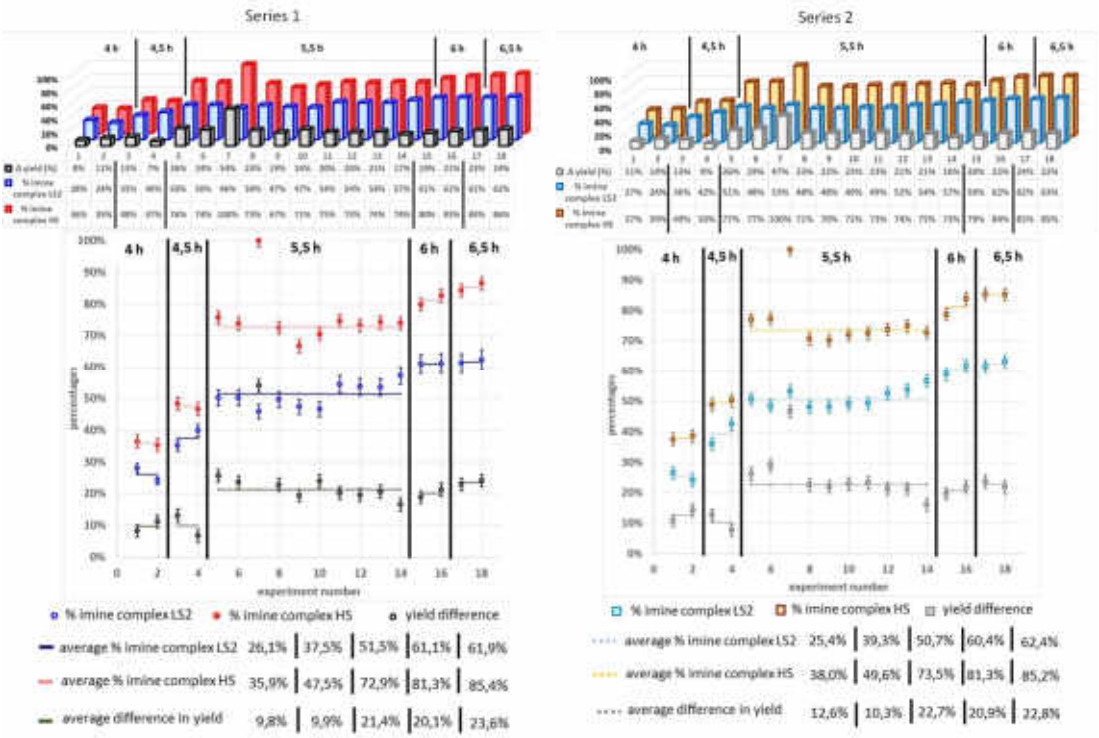


Fig. 2-26 Yields of imine obtained for batch 5 (series 1 and 2) after 4, 4.5, 5.5, 6 and 6.5h of reaction (normal conditions), for the HS and LS2 and the difference in between the two spin states.

In conclusion, this reproducibility study is based on 44 sets of experiments. We are very pleased to note that the percentage of imine is systematically and significantly higher when the reaction is carried out using complex **1** in the HS state. It is therefore reasonable to conclude that complex **1** in the HS state is more reactive towards aldehyde than when in the LS state. This difference in the reactivity of the two spin states of complex **1** was observed for PSM yields, from complex **1** in the HS state, ranging from 30% to 90%. This study also shows that if the PSM yield for complex **1** in the HS state is between 30 and 50%, a difference in activity between the two spin states of around 10% will be obtained, whereas a yield between 60 and 90% will lead to a difference in reactivity of around twenty percent. The same trend can be seen with 5 different batches of complex **1**. Carrying out the same experiment up to 10 times, and independently analyzing each experiment twice, gives us even greater confidence in the validity of these results. Finally, this study also shows that to obtain the desired percentage of imine, it is necessary to optimize the experimental conditions for each batch of complex **1**. To increase the imine percentage, we can either leave the reaction running longer or sonicate the suspension

of complex **1** in ethanol and add traces of water to the reaction medium.

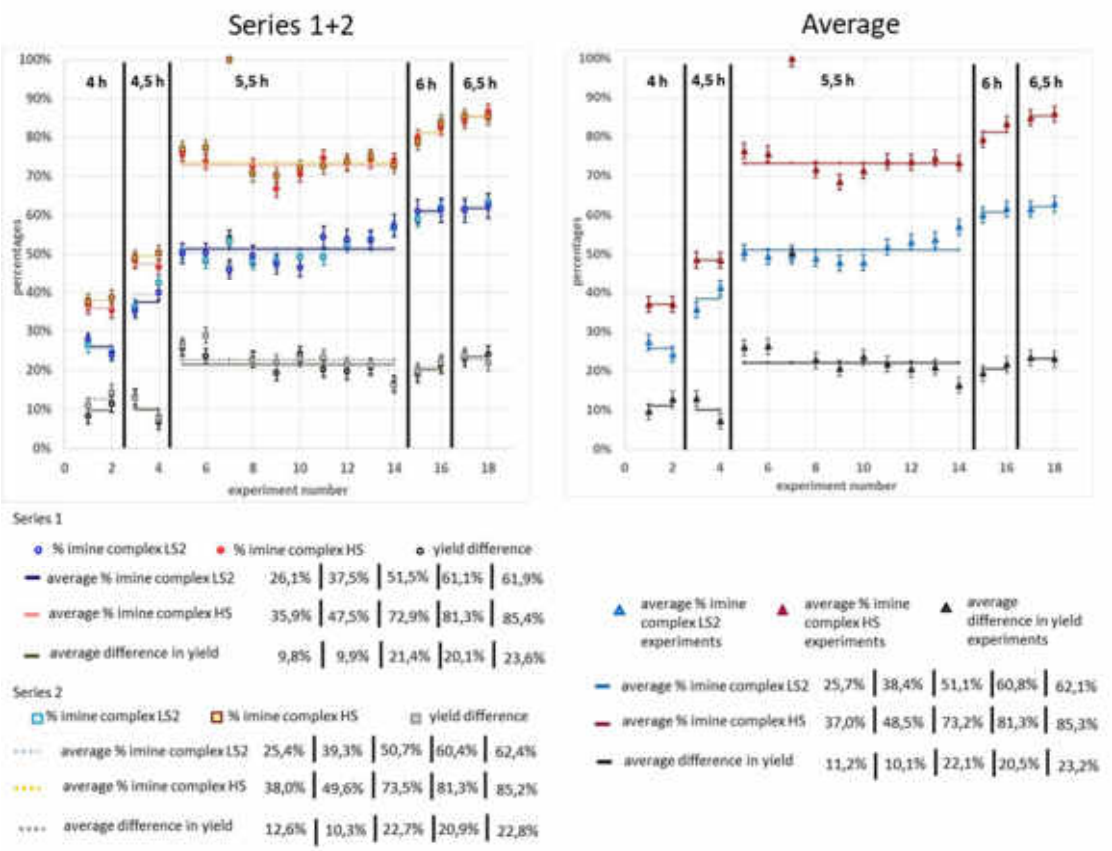


Fig. 2-27 Comparison of the results of the digestion method for the Batch 5 (4h, 4.5, 5.5, 6 and 6.5h, Series 1 + 2; average).

2.5 Statistical study

The fact that we have carried out a study containing 44 series of experiments constitutes a sufficiently large database for a statistical study to make sense. This study would enable us to estimate how consistent the results obtained are. Across the 44 experiments, calculations were performed on: 1) the Ratio of the yield between HS and LS2 samples (Eq 2-1); 2) the Ratio of the difference in yields between the two spin states divided by the percentage obtained for the HS sample (Eq 2-2); and 3) the standard deviation of all values (yields of HS, LS2, and $\Delta_{(HS-LS2)}$).

$$Ratio\ \mathbf{1} = \frac{the\ yield\ of\ PSM\ reaction\ for\ HS\ sample}{the\ yield\ of\ PSM\ reaction\ for\ LS2\ sample} \qquad \text{(Eq 2-1)}$$

$$Ratio\ \mathbf{2} = \frac{the\ yield\ difference\ between\ two\ spin\ states}{the\ yield\ of\ PSM\ reaction\ for\ HS\ sample} \times 100\% \qquad \text{(Eq 2-2)}$$

2.5.1 The ratio of the imine percentage of the HS complex to the percentage obtained for the complex in the LS2 state (Ratio 1).

Calculation of the ratio of %HS/%LS2 (Ratio **1**) allows for estimating the difference in PSM efficiency between the two spin states. A higher ratio indicates a more distinct reactivity difference between the spin states of the complex. Initially, the histogram and the Gaussian curve (in orange) depicted in Fig. 2-28(a) and encompassing all ratios, were computed from 44 sets of experiments. The average ratio **1** from these 44 sets is 1.376, with a standard deviation (σ) of 0.18. Excluding two outlier experiments (B2/A2 (set 2) and N3/M3 (set 25)), a new figure (Fig. 2-28(b)) was generated with 42 sets of experiments. Removing the two outliers led to a slight decrease in the ratio **1** value (from 1.376 to 1.343) but a significant reduction in standard deviation (from 0.18 to 0.11). On average, the %HS/%LS ratio is 1.34, with a standard deviation of approximately 0.1. A lower standard deviation implies more consistent and reproducible outcomes from the experiments. It's reasonable to conclude that the results are particularly consistent. Indeed, for 42 sets of experiments, only 5 values of ratio are observed, and they are all between 1.2 and 1.6. Furthermore, these results indicate that, on average, 1.34 times more imine is formed when complex **1** is in the HS state than in the LS state. This value for the difference in reactivity between the two spin states of complex **1** is very significant indeed.

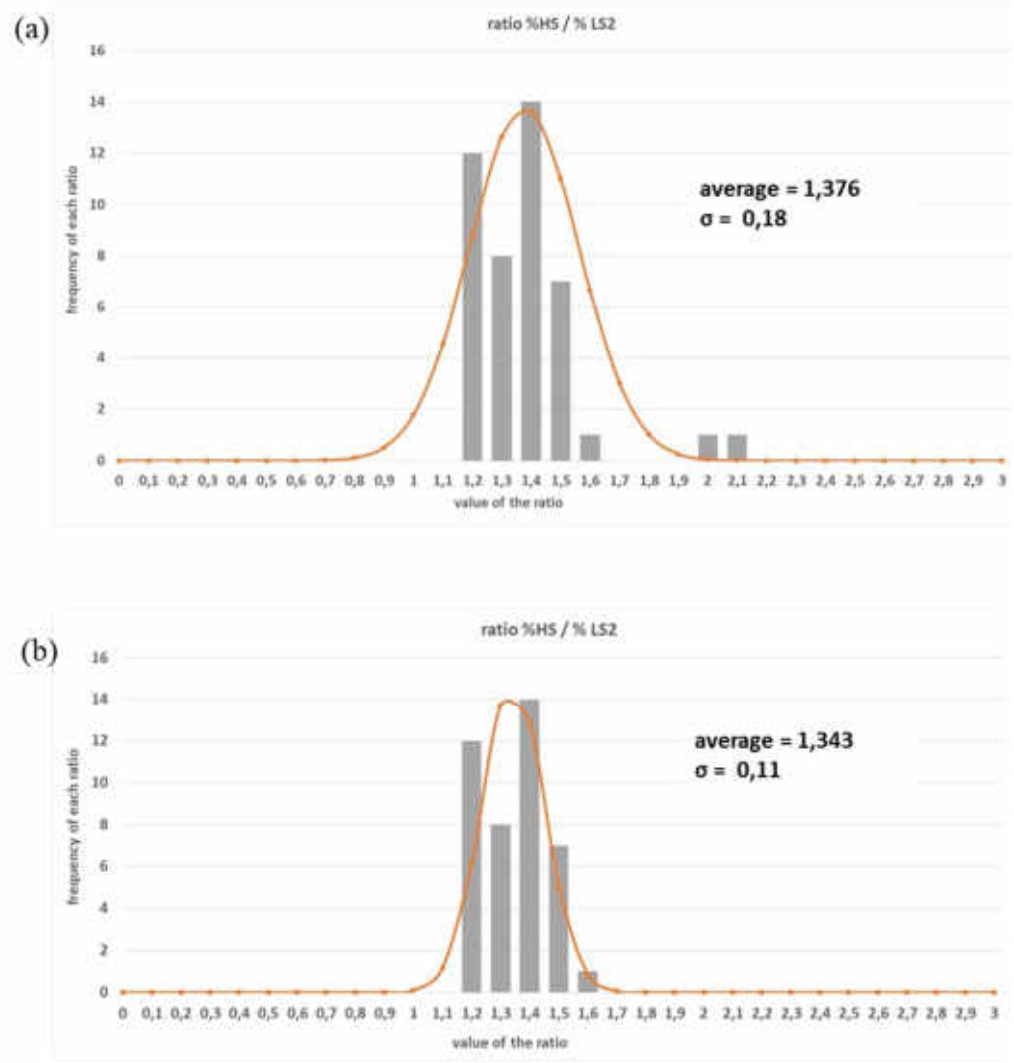


Fig. 2-28 Frequency of ratio %HS/%LS2 value, (a) average of Series 1 and Series 2, 44 sets of experiments. (b) average of Series 1 and Series 2, 42 sets of experiments.

2.5.2 The ratio of the difference in imine percentage between the two spin states of the complex to the imine percentage obtained for the complex in the HS state. (ratio 2)

This ratio **2** (yield difference in PSM reaction between the two spin states compared to the HS sample) is another way of highlighting the difference in reactivity of the complex between its two spin states. The higher the ratio, the greater the difference in reactivity between the two spin states. Initially, the histogram and the Gaussian curve (in orange) depicted in Fig. 2-29 (a) and encompassing all ratios were computed from 44 sets of experiments. The average ratio **2** from these 44 sets is 26%, with a standard deviation (σ) of 8%. Excluding two outlier experiments (B2/A2 (set 2) and N3/M3 (set 25)), a new figure (Fig. 2-29 (b)) was generated with 42 sets of experiments. Removing the outliers led to a slight decrease in the ratio **2** value (from 26% to 25%) and standard deviation (from 8% to 6%). On average, the ratio is around 25%, with a standard deviation of approximately 6%. This lower standard deviation implies more consistent and reproducible outcomes from the experiments. The same conclusions apply as in the previous section. In other words, it is reasonable to conclude that the results are particularly consistent. Indeed, for 42 sets of experiments, only 5 ratio values are observed, and they all lie between 15 and 35%. Furthermore, these results indicate that the difference in yields between the two spin states corresponds to 25% of the yield obtained for complex **1** in the HS state. This value is highly significant.

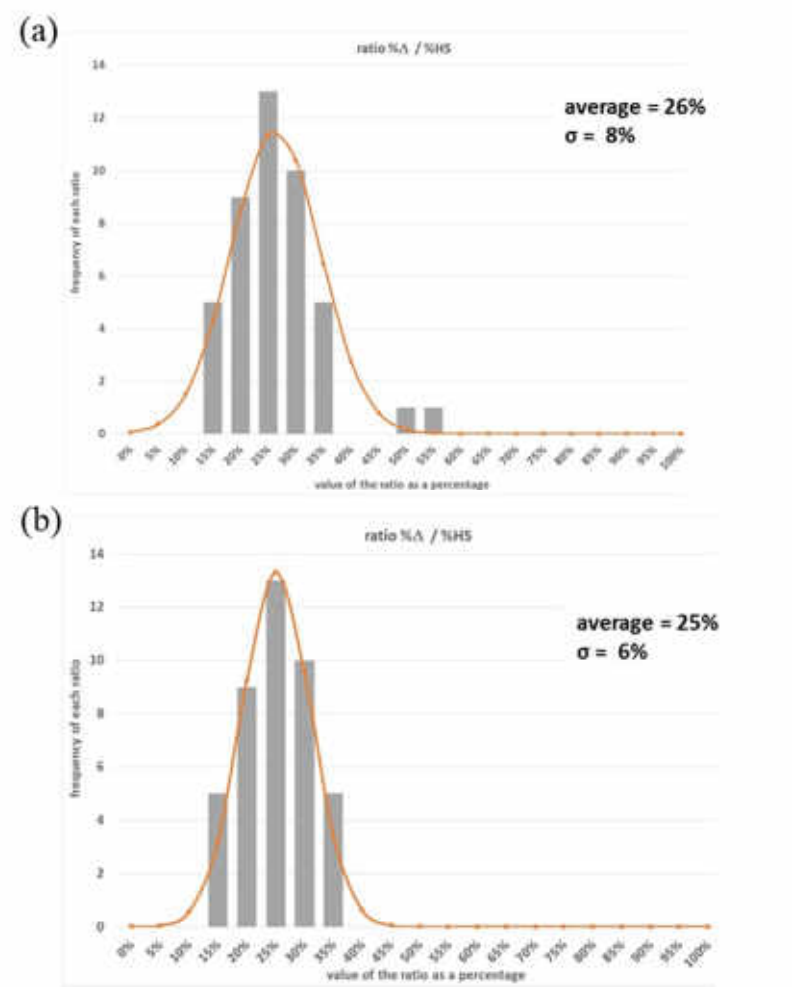


Fig. 2-29 Frequency of ratio %Δ / %HS value for each experiment. (a) average of Series 1 and Series 2, 44 sets of experiments. (b) average of Series 1 and Series 2, 42 sets of experiments.

2.5.3 Standard deviation of all values (yields of HS, LS2, and Δ (HS-LS2)).

For the study of standard deviation, the aim is on the difference between the obtained results and the mean value calculated from experiments conducted under identical conditions (from the same batch of complex, under the same experimental conditions and at the same spin state). Note that this type of study is often carried out for analytical methods, and that the values obtained are generally compared with those expected. In our case, we can't do it this way, as we don't know the expected value. The histogram provides an overview of the distribution of difference values in all 44 sets of experiments, while the target diagram illustrates the differences between the obtained values and the mean value for each set of experiments (Fig. 2-30). On average, one value is 2.26% away from the mean value, and the standard deviation(σ) is 3.66%.

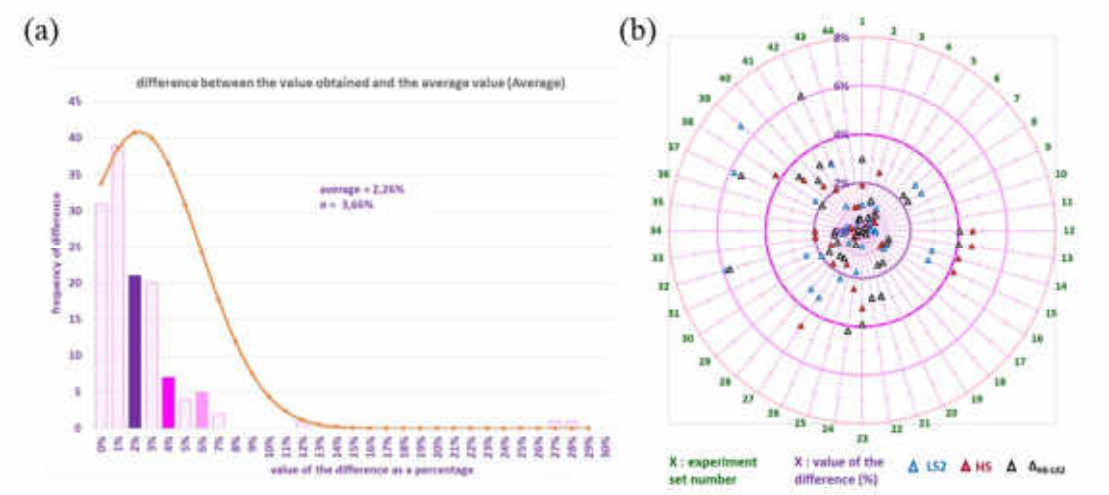


Fig. 2-30 (a) Standard deviation and (b) target diagram of all values average of Series 1 and Series 2, 44 sets of experiments.

Fig. 2-31 shows the results for 40 sets of experiments, excluding two sets with unusually high imine percentages for the HS complex (sets 2 and 25) and two sets where experiments were only conducted once under identical conditions (sets 9 and 18). The exclusion of these 4 sets resulted in lower mean difference values (from 2.26% to 1.81%) and a significant decrease in standard deviation (from 3.66% to 1.57%). The reduction in standard deviation is evident in the Gaussian curve depicted in orange in the Fig. 2-31 (a), indicating a tighter distribution. Note that 40 sets of experiments represent 120 values, since for each set of experiments there is a yield value for the complex in the HS state, a value for the complex in the LS state and a value for the difference in yields between the two spin states. Overall, a majority of values (62% to 70%) fell within a 0-2% difference from the mean calculated value, with most values within 0-4% in the target diagram. These findings suggest that, despite occasional outliers, the results are generally highly consistent.

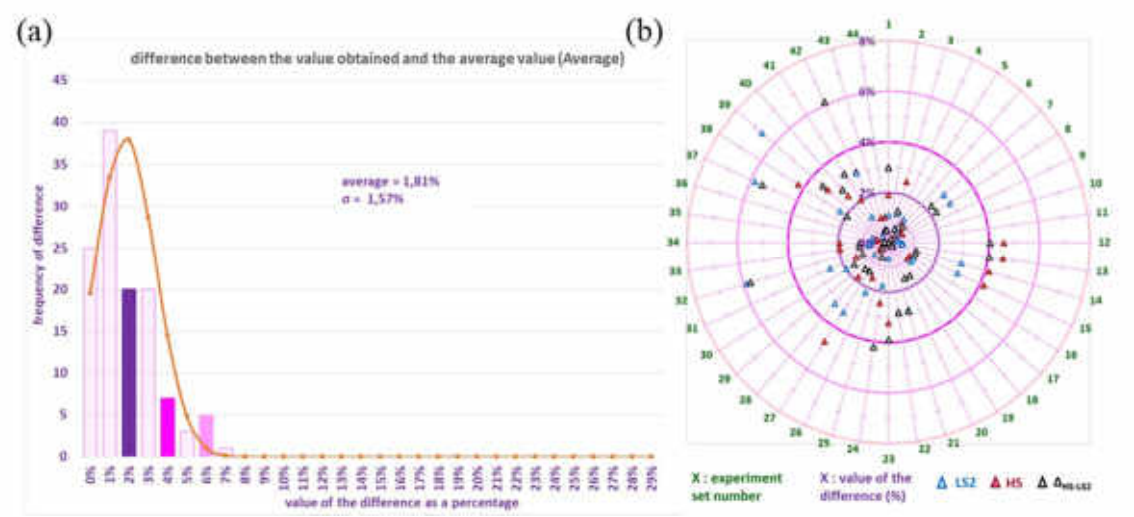


Fig. 2-31 (a) Standard deviation and (b) target diagram of all values average of Series 1 and Series 2, 40 sets of experiments.

The focus of this study is to demonstrate the reactivity difference of complex **1** between two spin states. For this reason, we were particularly interested in carrying out a deviation study on the values of the imine percentage difference between the complex in the HS and LS2 states (Δ HS-LS2). As mentioned above, in all sets of experiments, two sets with unusually high imine percentages for the HS sample (sets 2 and 25) and two sets (9 and 18) where experiments were conducted only once under identical conditions were excluded. Fig. 2-33, Fig. 2-33, Fig. 2-34 and Fig. 2-35 concern series 1, series 2, series 1+series 2, and the average of series 1 and 2 respectively. Fig. 2-35, which concerns series 1+series 2, shows the 40 yield difference values between the two spin states obtained for series 1 as well as the 40 yield difference values obtained for series 2. It can be seen that the values for series 1 are more grouped than those for series 2. Indeed, 95% of values in series 1 have a difference between 0 and 4%, while 80% of values in series 2 are between 0 and 4%. This difference between the two series is due to the distribution of values after 2%, as the two series are very comparable in the first two percentages of difference (68% for series 1 and 70% for series 2). As expected, the mean value of the deviation between a value and the mean value for series 1+series 2 corresponds to the mean of the mean values of the deviations obtained for series 1 and 2. Similarly, the standard deviation of Series 1+Series 2 is identical to the average of the standard deviations obtained for Series 1 and Series 2. It is interesting to note that the values (deviation and standard deviation) obtained for the averages of series 1 and 2 are lower than those for series 1+series 2. Thus, performing the analysis of the same experiment twice and considering the mean of the values obtained further improves the consistency of the values. If we consider the average of the two series, 67,5% of values fall within a 0-2% difference from the mean, with 92,5% of values within a 0-4% difference. Despite occasional outliers, the results exhibit a high level of consistency.

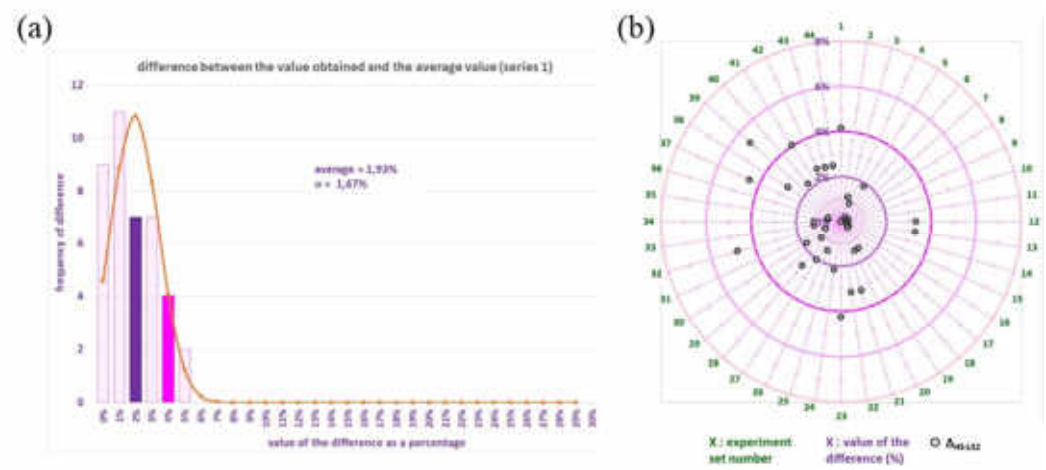


Fig. 2-32 (a) Standard deviation and (b) target diagram of Δ HS-LS2 (Series 1, 40 sets of experiments).

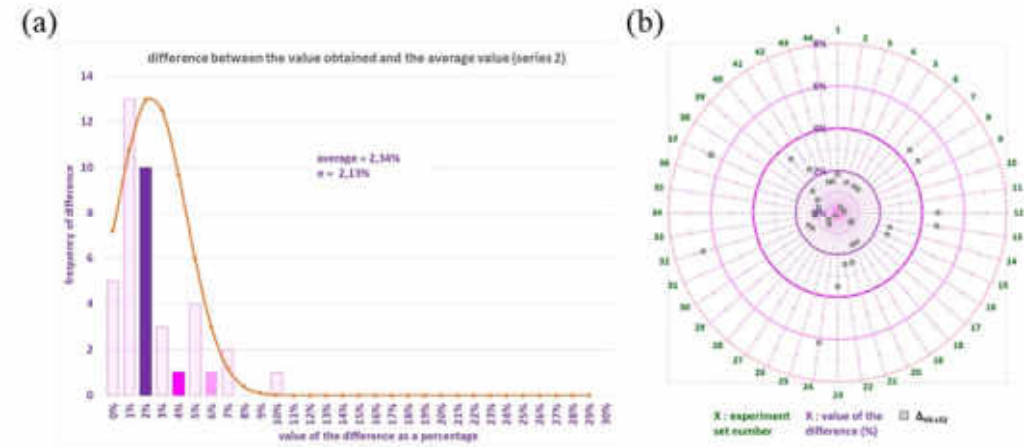


Fig. 2-33 (a) Standard deviation and (b) target diagram of Δ HS-LS2 (Series 2, 40 sets of experiments).

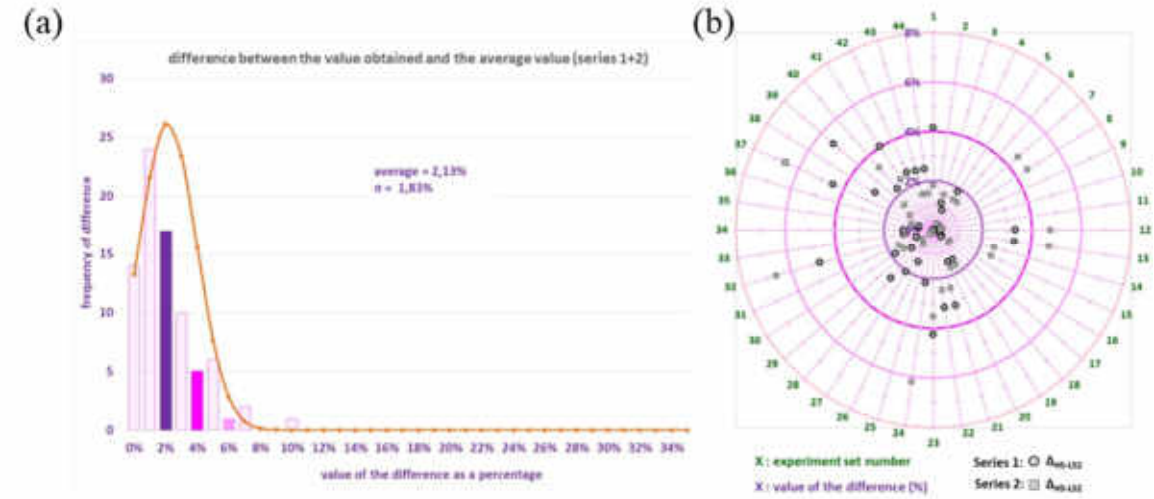


Fig. 2-34 (a) Standard deviation and (b) target diagram of $\Delta_{HS\text{-}LS2}$ (Series 1+2, 40 sets of experiments).

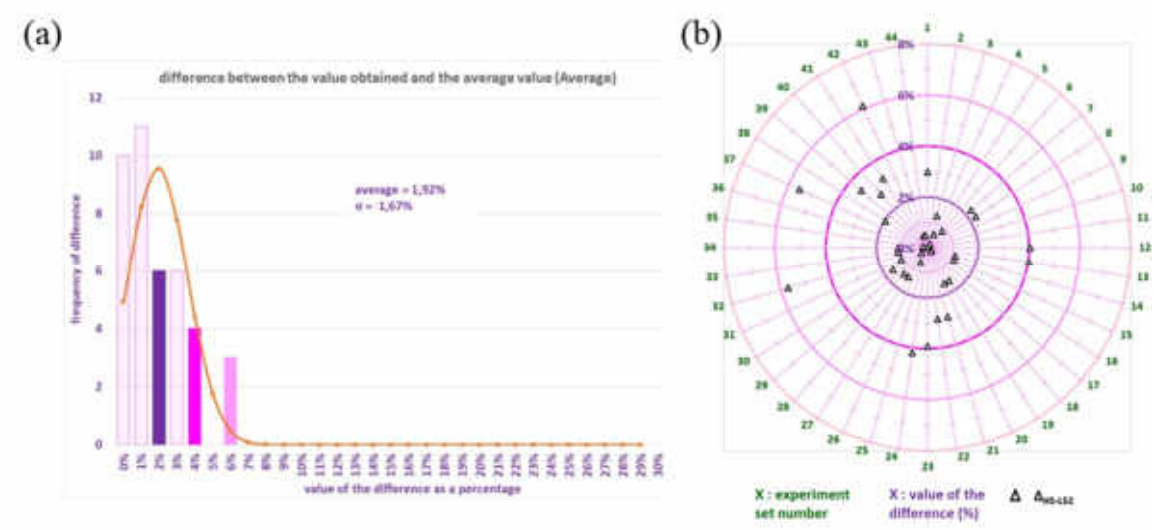


Fig. 2-35 (a) Standard deviation and (b) target diagram of $\Delta_{HS\text{-}LS2}$ (average, 40 sets of experiments).

2.6 Comparison of the properties of complex 2 obtained at 35°C and 90°C

The previous study has shown that the kinetics of the PSM method are influenced by the spin state of complex **1**. However, it is unclear whether the properties of the synthesised materials are also affected by the spin state of the parent material. Complex **2**, which underwent a full transformation of amine into imine functional groups in ethanol at varying temperatures (1 hour at 90°C and 72 hours at 35°C), was analysed using powder X-ray diffraction and variable temperature magnetic measurements. Regardless of the temperature used to synthesise complex 2, similar crystalline features were observed, as depicted in Fig. 2-36, and almost identical SCO properties were observed in both cases. The magnetic behaviour exhibited a gradual conversion with a $T_{1/2}$ value close to room temperature, as previously described in the literature.[28, 29, 36] This suggests that the final complex **2** remains consistent irrespective of the reaction temperature.

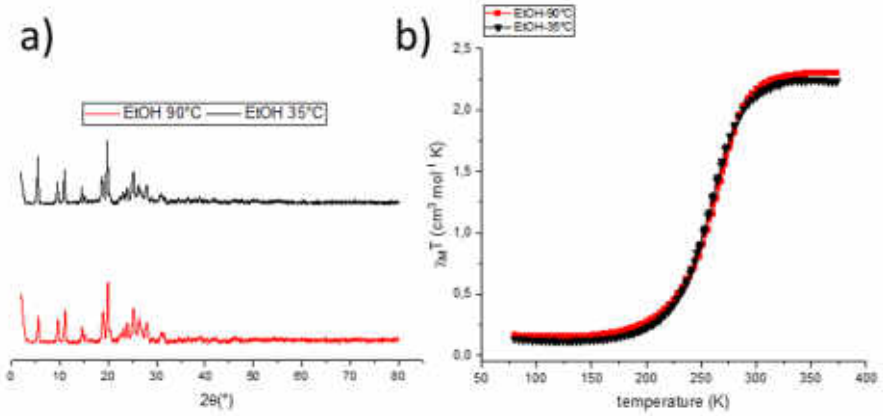


Fig. 2-36 (a) Diffractogram of PXRD measurement at room temperature and (b) Variable temperature magnetic measurements of complex **2** obtained in ethanol at 35°C (black) and 90°C (red).

2.7 Conclusion

In this chapter, we have discussed the increase in PSM efficiency with temperature can be due to these three reasons: 1) overcoming the energy activation barrier; 2) thermal solvent effects between complex **1** and the reaction solvent; 3) spin state effect. Eventually, experimental results suggest that the spin state plays the most significant role. Across 44 sets of experiments conducted on 5 different batches of complex **1**, it was consistently noted that the percentage of imine for the HS sample exceeded the LS2 sample. A notable 22% improvement in PSM efficiency was observed when complex **1** was under HS state compared to LS state. The multitude of experiments and error estimation of the digestion method (± 2%) substantiate the significant reactivity difference between the two spin states, even with an 8% PSM variation. On average, 1.37 times more imine is formed when complex 1 is in the HS state than in the LS2 state. This study presents the first example of the spin state effect on post-synthetic modification in a 1D SCO coordination polymer. Notably, it is the first observation of the spin state effect on the organic reactivity of a functional group within a metal complex. This finding underscores that spin state influence extends beyond the first coordination sphere of metal. Remarkably, the spin state appears only to affect the kinetics of desired product formation, as complex **2** obtained at 35°C exhibits identical structural characteristics and SCO properties to that obtained at 90°C.

2.8 Experiment section

2.8.1 Methodology for the Post-synthetic modification

2.8.1.1 General procedure

In a vial, 50 mg of the SCO complex **1** was suspended in 2 mL of absolute ethanol. For the LS sample, the vial was immersed in an oil bath at 55°C; for the HS sample, the vial was first immersed at 90°C for 2 minutes, then transferred to the same oil bath at 55°C. As for the LS2 sample, the vial was initially heated at 90°C for 2 minutes, allowed to cool at room temperature for 5 minutes, and finally placed in the 55°C oil bath. Once all three samples were in the oil bath, they were left to equilibrate at 55°C for 10 minutes. In a separate vial, p-anisaldehyde was pre-heated at 55°C. 300 µL of p-anisaldehyde pre-heated at 55°C was carefully added to each sample to maintain the spin state, and then the vial was sealed and stirred for a specific duration. After the reaction, the tube was promptly transferred to an ice bath to halt the reaction. Following a 1 minute interval, 0.5 mL of ethanol and 10 mL of diethyl ether were introduced to the mixture. The mixture underwent centrifugation, followed by two washes with 10 mL of diethyl ether, and was subsequently air-dried overnight.

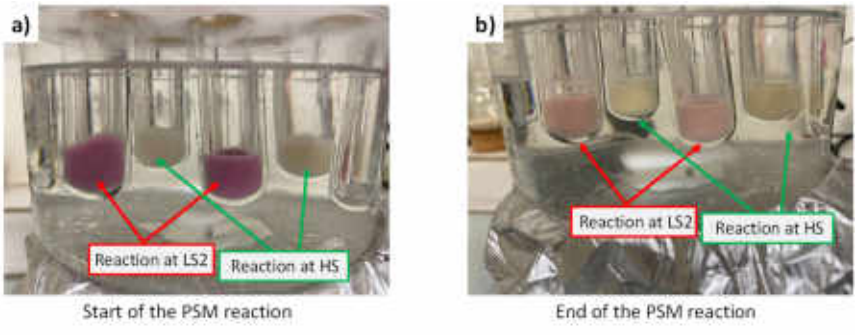


Fig. 2-37 Oil bath where the PSM reactions at HS and LS2 are done at the same time, under the same conditions.

2.8.1.2 PSM reaction using ethanol 98% and sonication (batch 3 and 5)

50 mg of the SCO complex **1** were suspended in 1 mL of absolute ethanol in a vial and sonicated for 10 min. For the HS sample, the vial was first immersed at 90 °C in a oil bath for 2 min, then transferred to an oil bath at 55 °C. As for the LS2 sample, the vial underwent the same initial heating at 90 °C for 2 min, followed by cooling at room temperature for 5 min, and then immersion in the 55 °C oil bath. After allowing both samples to equilibrate at 55 °C for 10 min, 1 mL of pre-heated ethanol 96% was added, and the mixtures were stirred at 55 °C for an additional 10 min. Simultaneously, p-anisaldehyde was heated at 55 °C in a separate vial. Subsequently, 300 mL of the pre-heated p-anisaldehyde was carefully added to each sample to maintain the spin state, followed by closing the vial and stirring for a specified time period. It is important to note that if the ethanol 96% is added before heating the complex at 90 °C, the thermal hysteresis of complex **1** is reduced, resulting in both samples remaining in the HS state at 55 °C. The final steps of the reaction were conducted as previously described in the general process.

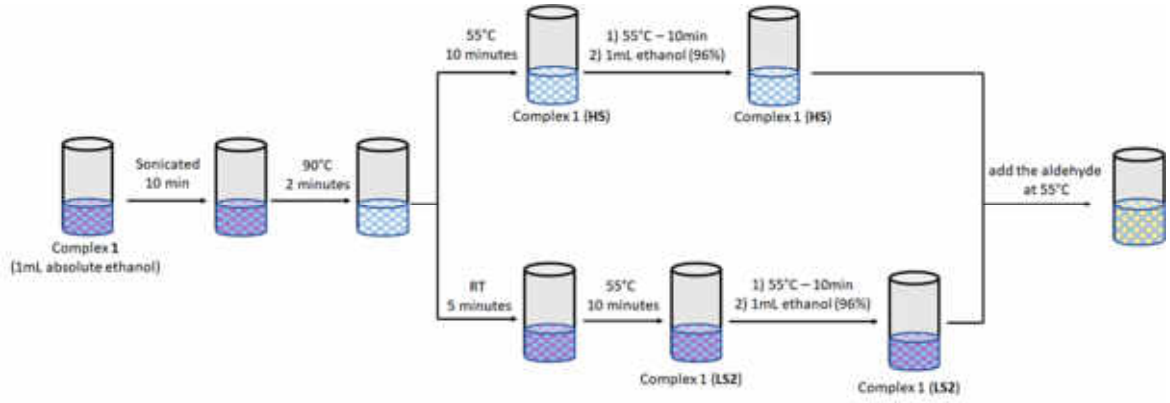


Fig. 2-38 Scheme with the procedure to prepare the complex **1** in **HS** and **LS2** with ethanol 98%.

2.8.1.3 PSM reaction at HS2 (Batch 4)

In a vial, 50 mg of the SCO complex **1** was suspended in 2 mL of absolute ethanol. The vial was heated at a 90 °C pre-heated oil bath for 2 minutes, followed by cooling at room temperature for 5 minutes. Subsequently, it was reheated in the oil bath at 90 °C for another 2 minutes before being transferred to a 55 °C oil bath. The remaining steps were carried out as previously described.

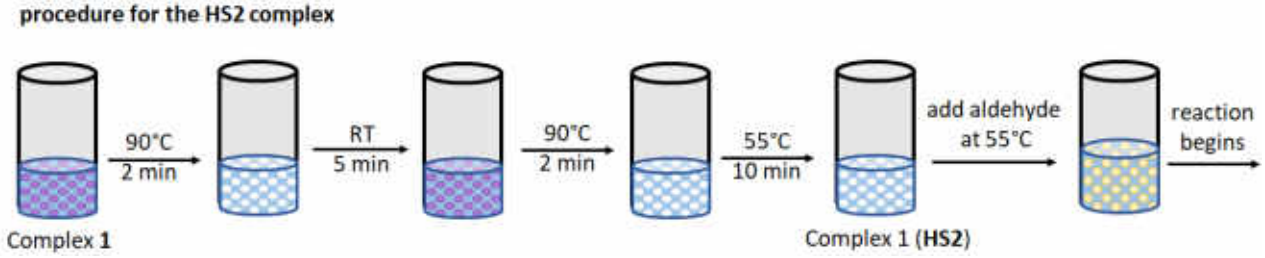


Fig. 2-39 Scheme with the procedure to prepare the complex **1** in **HS2**

2.8.2 Methodology used for the digestion and quantification of the PSM reaction

2.8.2.1 Digestion of the sample

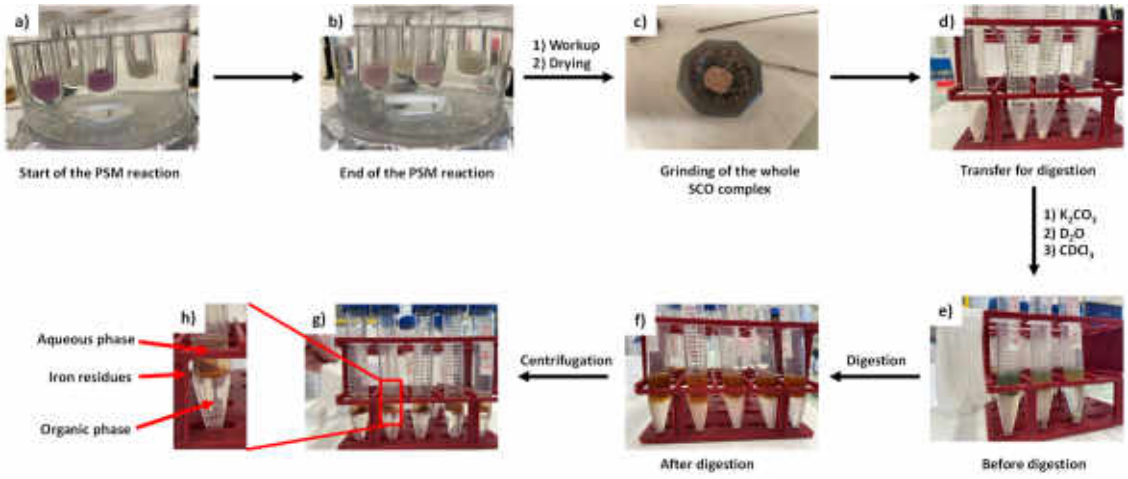


Fig. 2-40 The step-by-step procedure from the PSM reaction to the digestion involves (a) initiating the PSM reaction, (b) completing the PSM reaction, (c) grinding the resulting PSM complex post-reaction workup, (d) transferring the SCO complex to a 15 mL Falcon conical centrifuge tube, (e) observing the SCO complex pre-digestion, following the addition of D_2O, $CDCl_3$, and K_2CO_3, (f) the SCO complex after vigorous stirring in the Falcon tube, (g) centrifuging the Falcon tubes, and (h) separating the aqueous and organic phases with an interlayer of iron residues.

The digestion process was carried out following the established methodology[5, 28]. Standard solutions of 1,3,5-trimethylbenzene (TMB) in $CDCl_3$ and 2,2-dimethyl-1,3-propanediol (NPG) in D_2O were prepared and used on the same day to prevent solvent evaporation. Approximately 20 mg of the standard was weighed and added to a 10 mL volumetric flask. The PSM complex was ground to ensure sample homogeneity. Subsequently, around 20 mg of the PSM complex was accurately weighed into a falcon tube, along with 2 mL of D_2O, 2 mL of $CDCl_3$, and 276 mg of K_2CO_3. The tube was sealed, vigorously stirred, and sonicated for 5 to 10 minutes until a yellow-orange suspension devoid of SCO powder residues appeared. After centrifugation to separate the organic and aqueous phases, as well as iron residues, the complex was disintegrated, and the uncoordinated ligands (amino-triazole in the aqueous phase and imine in the organic phase) were quantified. Subsequently, 0.4 mL of the digested $CDCl_3$ or D_2O solution was transferred to an NMR tube, followed by the addition of 0.2 mL of the respective standard solution for subsequent ^{1}H-NMR analysis.

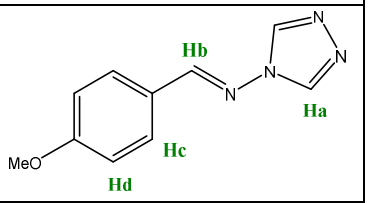
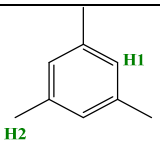
2.8.2.2 Integration of the NMR spectra

The software Mestrenova was utilised for processing the spectra. Following acquisition of the $_1$H-NMR data, an exponential apodisation of 0.1 Hz was consistently applied to spectra obtained using $CDCl_3$ as the solvent for the organic phase, and 1.0 Hz for D_2O in the aqueous phase. Additionally, adjustments were made to the phase and/or baseline as needed, ensuring a signal-to-noise ratio (SNR) of at least 250:1. Integration limits for each signal were determined based on Table 2-7, with these limits remaining consistent across all spectra for the organic phase. These specific regions were selected because there is no signal overlap except for the

imine and triazole signals.

In the case of the aqueous phase, the integration was chosen as 50 times the full width at half maximum (FWHM) of each peak.

Table 2-7 Integration limits for the organic phase

Signal	signal[a]	+/- limit[a,b]	
Ha + Hb	8.57	0.19	
Hc	7.815	0.12	
Hd	7.035	0.10	
OMe	3.92	0.15	
H1	6.821	0.08	
H2	2.30	0.12	

[a]: in ppm; [b]: in both directions of the signal

2.8.2.3 Quantification of the digested solution

To calculate the concentration of imine in the NMR tube, Eq. 2-3 was used

$$C_{imine\ in\ NMR\ tube} = \left(\frac{\#H_{TMB}}{I_{TMB}}\right) \times \left(\frac{I_{imine}}{\#H_{imine}}\right) \times C_{TMB\ in\ NMR\ tube} \quad \text{(Eq. 2-3)}$$

Where I_{TMB}, I_{imine} corresponds to the integration of a specific peak, $\#H_{TMB}, \#H_{imine}$ to the number of hydrogens that corresponds to the integrated peak, and C_{TMB} to the concentration of the TMB in the NMR tube.

To calculate the concentration of imine in the falcon tube, Eq. 2-4 was used

$$C_{imine\ in\ the\ centrifuge\ tube} = \frac{C_{imine\ in\ NMR\ tube} \times V_{NMR\ tube}}{V_{imine\ in\ the\ centrifuge\ tube}} \text{ (Eq. 2-4)}$$

The same procedure was done for the quantification of the amine, replacing TMB with NPG and imine with amine. Once the number of moles of imine and amine is known, the percentage of imine in the sample was calculated using Eq. 2-5

$$\%imine = \frac{mol_{imine}}{mol_{imine} + mol_{amine}} \times 100 \quad \text{(Eq. 2-5)}$$

2.8.2.4 Selected NMR spectra of the digested samples

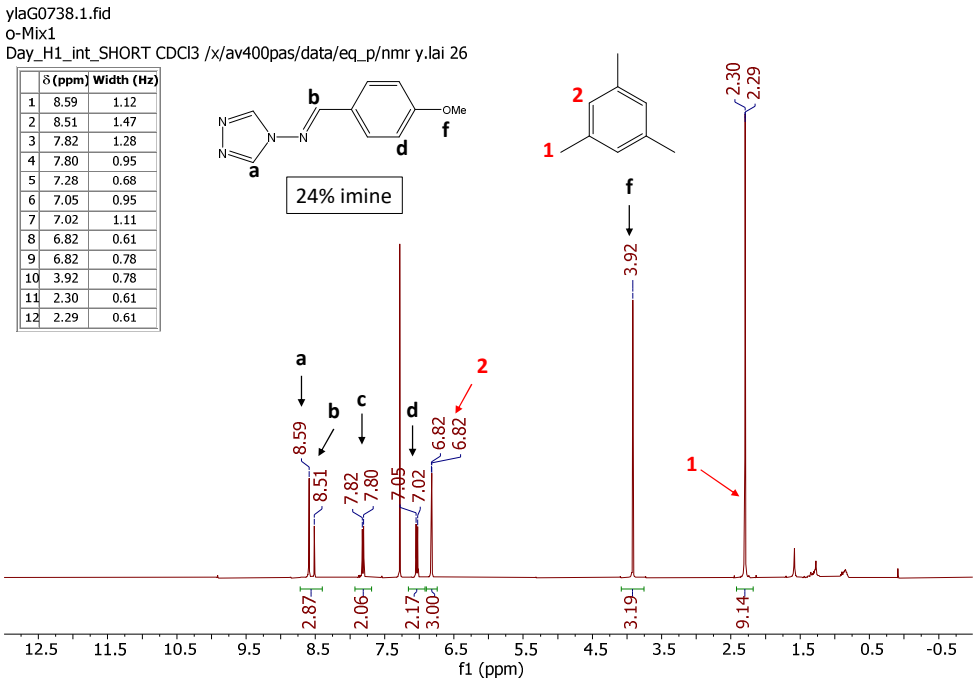


Fig. 2-41 ^{1}H-NMR ($CDCl_3$) of the digestion of the experiment Mixt 1

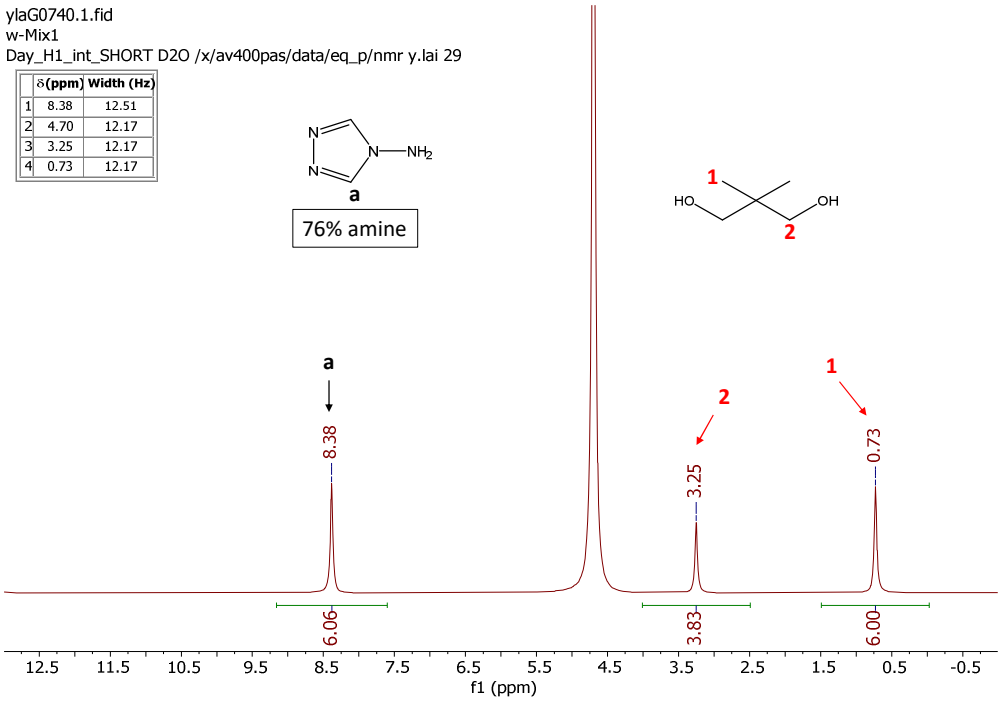
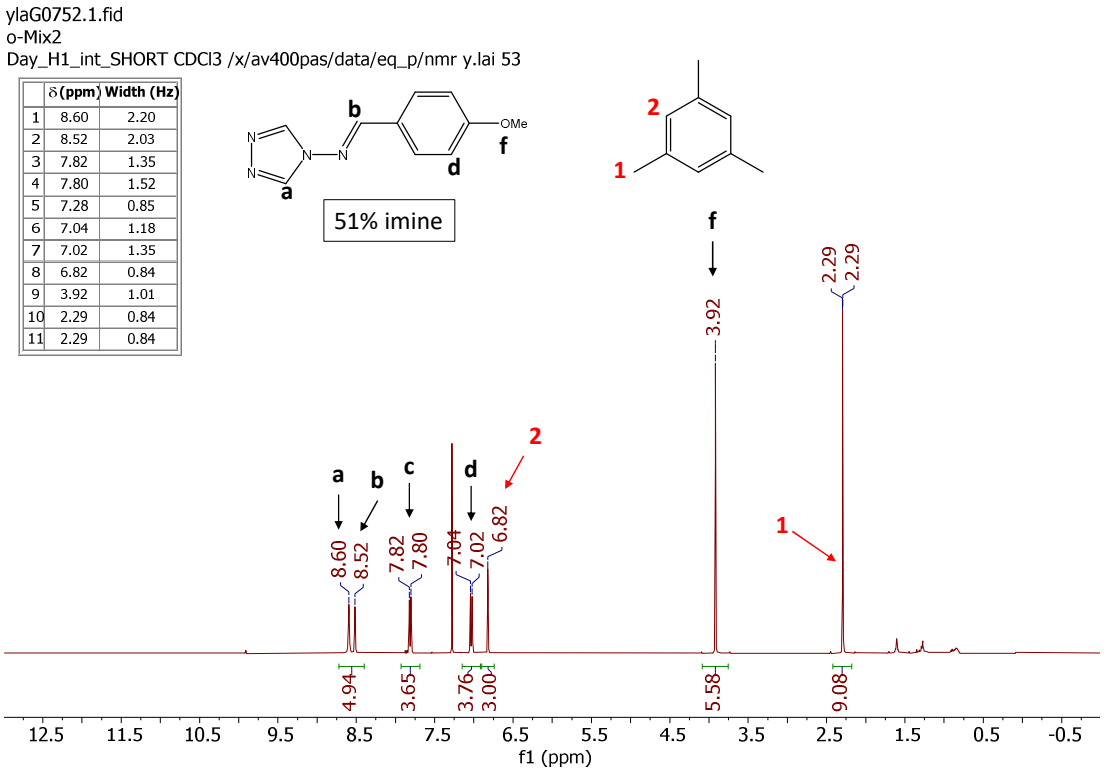
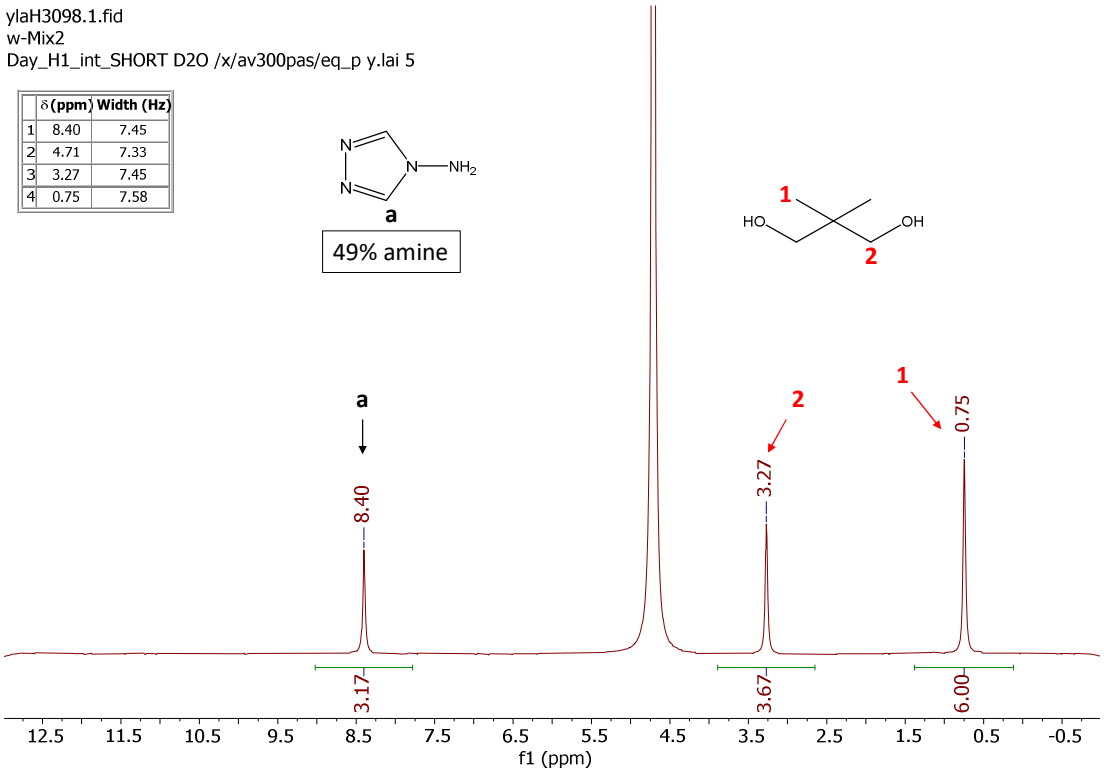


Fig. 2-42 ^{1}H NMR (D_2O) of the digestion of the experiment Mixt 1



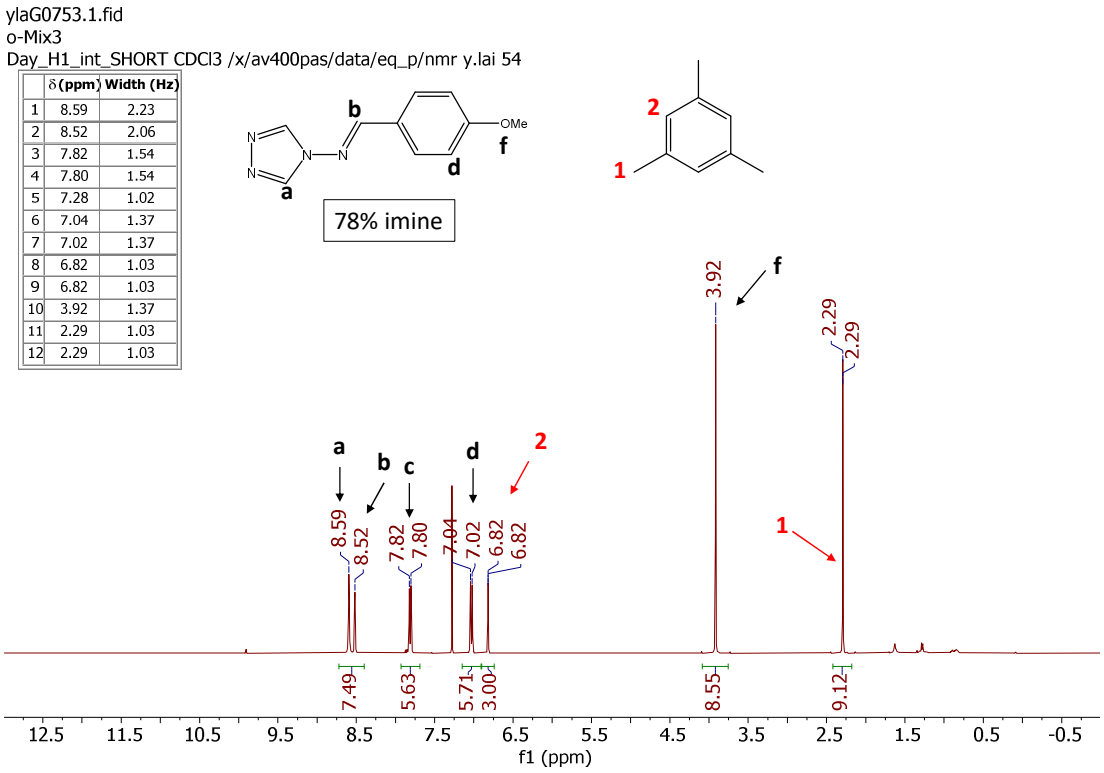
	δ (ppm)	Width (Hz)
1	8.60	2.20
2	8.52	2.03
3	7.82	1.35
4	7.80	1.52
5	7.28	0.85
6	7.04	1.18
7	7.02	1.35
8	6.82	0.84
9	3.92	1.01
10	2.29	0.84
11	2.29	0.84

Fig. 2-43 ^{1}H-NMR ($CDCl_3$) of the digestion of the experiment Mixt 2



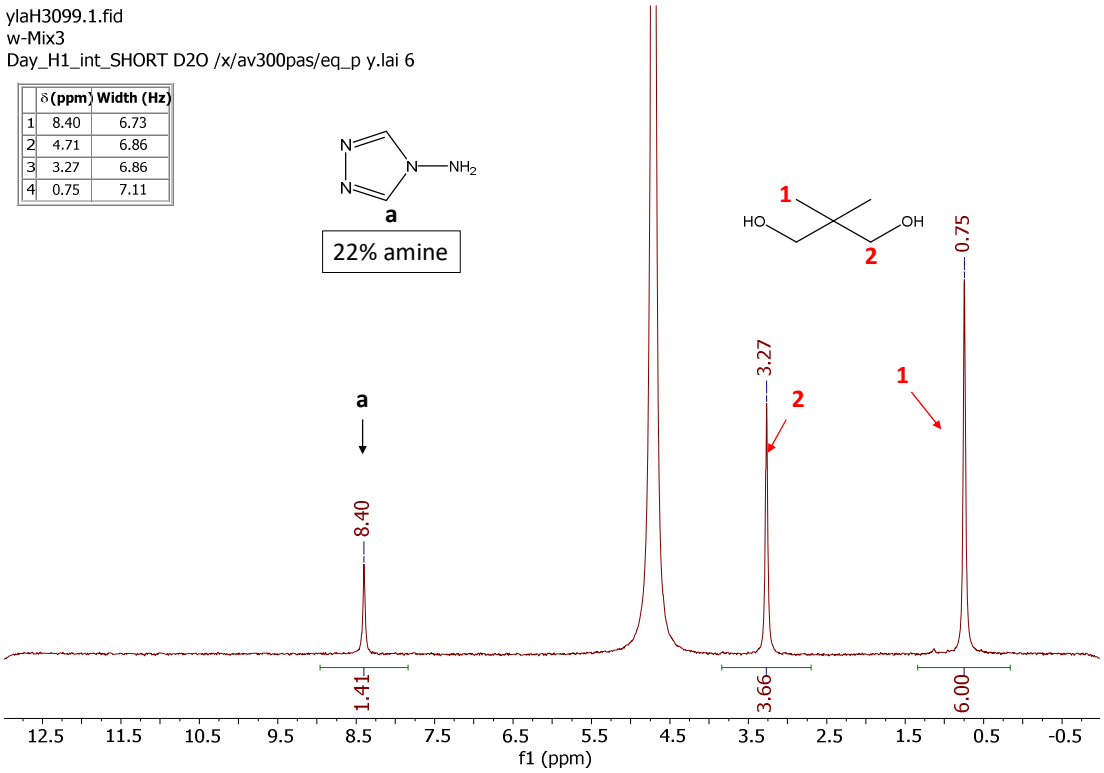
	δ (ppm)	Width (Hz)
1	8.40	7.45
2	4.71	7.33
3	3.27	7.45
4	0.75	7.58

Fig. 2-44 ^{1}H NMR (D_2O) of the digestion of the experiment Mixt 2



	δ (ppm)	Width (Hz)
1	8.59	2.23
2	8.52	2.06
3	7.82	1.54
4	7.80	1.54
5	7.28	1.02
6	7.04	1.37
7	7.02	1.37
8	6.82	1.03
9	6.82	1.03
10	3.92	1.37
11	2.29	1.03
12	2.29	1.03

Fig. 2-45 ^{1}H-NMR ($CDCl_3$) of the digestion of the experiment Mixt 3



	δ (ppm)	Width (Hz)
1	8.40	6.73
2	4.71	6.86
3	3.27	6.86
4	0.75	7.11

Fig. 2-46 ^{1}H NMR (D_2O) of the digestion of the experiment Mixt 3

2.9 References

[1] E. Coronado, Molecular magnetism: from chemical design to spin control in molecules, materials and devices, *Nature Reviews Materials* **2020**, 5, 87-104.

[2] G. Molnár, S. Rat, L. Salmon, W. Nicolazzi, A. Bousseksou, Spin crossover nanomaterials: from fundamental concepts to devices, *Adv Mater* **2018**, 30, 1703862.

[3] O. Roubeau, Triazole - based one - dimensional spin - crossover coordination polymers, *Chemistry–A European Journal* **2012**, 18, 15230-15244.

[4] A. Sugahara, H. Kamebuchi, A. Okazawa, M. Enomoto, N. Kojima, Control of spin-crossover phenomena in one-dimensional triazole-coordinated iron (II) complexes by means of functional counter ions, *Inorganics* **2017**, 5, 50.

[5] A. Enríquez-Cabrera, L. Routaboul, L. Salmon, A. Bousseksou, Complete post-synthetic modification of a spin crossover complex, *Dalton Trans* **2019**, 48, 16853-16856.

[6] L. Sun, A. Rotaru, Y. Garcia, A non-porous Fe (II) complex for the colorimetric detection of hazardous gases and the monitoring of meat freshness, *J Hazard Mater* **2022**, 437, 129364.

[7] K. Ridier, A.-C. Bas, Y. Zhang, L. Routaboul, L. Salmon, G. Molnár, C. Bergaud, A. Bousseksou, Unprecedented switching endurance affords for high-resolution surface temperature mapping using a spin-crossover film, *Nat Commun* **2020**, 11, 3611.

[8] R. Torres-Cavanillas, M. Gavara-Edo, E. Coronado, Bistable Spin-Crossover Nanoparticles for Molecular Electronics, *Adv Mater* **2024**, 36, 2307718.

[9] Y. Zan, M. Piedrahita-Bello, S.E. Alavi, G. Molnár, B. Tondu, L. Salmon, A. Bousseksou, Soft Actuators Based on Spin - Crossover Particles Embedded in Thermoplastic Polyurethane, *Advanced Intelligent Systems* **2023**, 5, 2200432.

[10] B. Tondu, M. Piedrahita-Bello, L. Salmon, G. Molnár, A. Bousseksou, Robust linear control of a bending molecular artificial muscle based on spin crossover molecules, *Sensors and Actuators A: Physical* **2022**, 335, 113359.

[11] M. Piedrahita-Bello, X. Yang, S.E. Alavi, G. Molnár, L. Salmon, A. Bousseksou, Anisotropic spin-crossover composite actuators displaying pre-programmed movements, *Sensors and Actuators B: Chemical* **2023**, 393, 134147.

[12] S. Mandal, S. Natarajan, P. Mani, A. Pankajakshan, Post-synthetic modification of metal–organic frameworks toward applications, *Adv Funct Mater* **2021**, 31, 2006291.

[13] J.L. Segura, S. Royuela, M.M. Ramos, Post-synthetic modification of covalent organic frameworks, *Chem Soc Rev* **2019**, 48, 3903-3945.

[14] C.F. Wang, R.F. Li, X.Y. Chen, R.J. Wei, L.S. Zheng, J. Tao, Synergetic Spin Crossover and Fluorescence in One-Dimensional Hybrid Complexes, *Angew Chem* **2015**, 127, 1594-1597.

[15] A.D. Burrows, C.G. Frost, M.F. Mahon, C. Richardson, Post-Synthetic Modification of Tagged Metal–Organic Frameworks, *Angew Chem* **2008**, 120, 8610-8614.

[16] V. Valtchev, G. Majano, S. Mintova, J. Pérez-Ramírez, Tailored crystalline microporous materials by post-synthesis modification, *Chem Soc Rev* **2013**, 42, 263-290.

[17] Y. Goto, H. Sato, S. Shinkai, K. Sada, "Clickable" metal− organic framework, *J Am Chem Soc* **2008**, 130, 14354-14355.

[18] U. Fluch, B.D. McCarthy, S. Ott, Post synthetic exchange enables orthogonal click chemistry in a metal organic framework, *Dalton Trans* **2019**, 48, 45-49.

[19] S. Yuan, W. Lu, Y.-P. Chen, Q. Zhang, T.-F. Liu, D. Feng, X. Wang, J. Qin, H.-C. Zhou, Sequential linker installation: precise placement of functional groups in multivariate metal–organic frameworks, *J Am Chem Soc* **2015**, 137, 3177-3180.

[20] J.E. Clements, J.R. Price, S.M. Neville, C.J. Kepert, Perturbation of Spin Crossover Behavior by Covalent Post-Synthetic Modification of a Porous Metal–Organic Framework, *Angewandte Chemie International Edition* **2014**, 53, 10164-10168.

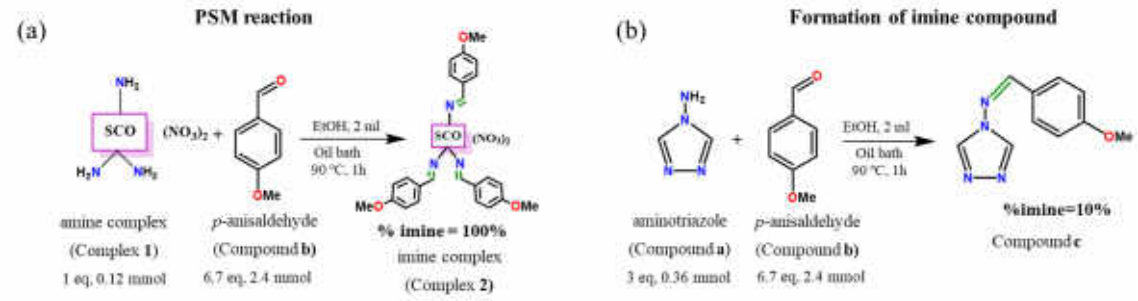
[21] L.-F. Wang, W.-M. Zhuang, G.-Z. Huang, Y.-C. Chen, J.-Z. Qiu, Z.-P. Ni, M.-L. Tong, Spin-crossover modulation via single-crystal to single-crystal photochemical [2+ 2] reaction in Hofmann-type frameworks, *Chemical Science* **2019**, 10, 7496-7502.

[22] H. Flötotto, T. Secker, P. Kögerler, C. Besson, Amine-Functionalized Spin Crossover Building Blocks, *Eur J Inorg Chem* **2019**, 2019, 4621-4624.
[23] D.L. Reger, J.R. Gardinier, W.R. Gemmill, M.D. Smith, A.M. Shahin, G.J. Long, L. Rebbouh, F. Grandjean, Formation of third generation Poly (pyrazolyl) borate ligands from alkyne coupling reactions of Fe [(p-IC6H4) B (3-Rpz) 3] 2 (R= H, Me; pz= Pyrazolyl): Pathways toward controlling an Iron (II) electronic spin-state crossover, *J Am Chem Soc* **2005**, 127, 2303-2316.
[24] J.H. Askew, H.J. Shepherd, Post-synthetic anion exchange in iron (II) 1, 2, 4-triazole based spin crossover materials via mechanochemistry, *Dalton Trans* **2020**, 49, 2966-2971.
[25] X. Yang, A. Enriquez-Cabrera, D. Toha, Y. Coppel, L. Salmon, A. Bousseksou, Spin crossover in mixed-anion Fe (NH 2 trz) 3 (BF 4)(SiF 6) 0.5 crystalline rod-shaped particles: the strength of the solid–liquid post synthetic modification, *Dalton Trans* **2023**, 52, 10828-10834.
[26] C.F. Wang, G.Y. Yang, Z.S. Yao, J. Tao, Monitoring the Spin States of Ferrous Ions by Fluorescence Spectroscopy in Spin-Crossover–Fluorescent Hybrid Materials, *Chemistry–A European Journal* **2018**, 24, 3218-3224.
[27] E. Resines-Urien, L. Piñeiro-López, E. Fernandez-Bartolome, A. Gamonal, M. Garcia-Hernandez, J.S. Costa, Covalent post-synthetic modification of switchable iron-based coordination polymers by volatile organic compounds: a versatile strategy for selective sensor development, *Dalton Trans* **2020**, 49, 7315-7318.
[28] A. Enríquez-Cabrera, K. Ridier, L. Salmon, L. Routaboul, A. Bousseksou, Complete and versatile post-synthetic modification on iron-triazole spin crossover complexes: a relevant material elaboration method, *Eur J Inorg Chem* **2021**, 2021, 2000-2016.
[29] A. Enriquez-Cabrera, L. Getzner, L. Salmon, L. Routaboul, A. Bousseksou, Post-synthetic modification mechanism for 1D spin crossover coordination polymers, *New J Chem* **2022**, 46, 22004-22012.
[30] A. Grosjean, P. Négrier, P. Bordet, C. Etrillard, D. Mondieig, S. Pechev, E. Lebraud, J.F. Létard, P. Guionneau, Crystal structures and spin crossover in the polymeric material [Fe (htrz) 2 (trz)](BF4) including coherent-domain size reduction effects, *Eur J Inorg Chem* **2013**, 2013, 796-802.
[31] A. Grosjean, N. Daro, S. Pechev, C. Etrillard, G. Chastanet, P. Guionneau, Crystallinity and microstructural versatility in the spin-crossover polymeric material [Fe (Htrz) 2 (trz)](BF4), *Eur J Inorg Chem* **2018**, 2018, 429-434.
[32] A. Grosjean, N. Daro, S. Pechev, L. Moulet, C. Etrillard, G. Chastanet, P. Guionneau, The spin-crossover phenomenon at the coherent-domains scale in 1D polymeric powders: evidence for structural fatigability, *Eur J Inorg Chem* **2016**, 2016, 1961-1966.
[33] A. Grosjean, Matériaux polymériques 1D à transition de spin: investigations structurales multi-échelles, Université de Bordeaux 1, 2013.
[34] X. Yang, A. Enriquez-Cabrera, K. Jacob, Y. Coppel, L. Salmon, A. Bousseksou, Room temperature spin crossover properties in a series of mixed-anion Fe (NH 2 trz) 3 (BF 4) 2− x (SiF 6) x/2 complexes, *Dalton Trans* **2024**, 53, 6830-6838.
[35] D. Paliwoda, L. Vendier, L. Getzner, F. Alabarse, D. Comboni, B. Martin, S.E. Alavi, M.P. Bello, L. Salmon, W. Nicolazzi, Elastic Properties of the Iron (II)–Triazole Spin Crossover Complexes [Fe (Htrz) 2trz] BF4 and [Fe (NH2trz) 3] SO4, *Cryst Growth Des* **2023**, 23, 1903-1914.
[36] A. Enriquez-Cabrera, A. Rapakousiou, M.P. Bello, G. Molnár, L. Salmon, A. Bousseksou, Spin crossover polymer composites, polymers and related soft materials, *Coord Chem Rev* **2020**, 419, 213396.

Chapter 3 Study of the catalytic activity of the SCO coordination polymer $[Fe(NH_2trz)_3](NO_3)_2$ for imine formation from 4-amino-1,2,4-triazole

3.1 Introduction

In this introduction, I'll be presenting in particular how we went from studying the PSM method on the complex **1** ($[Fe(NH_2trz)_3](NO_3)_2$) to evaluating its catalytic activity in the formation of imine from 4-amino-1,2,4-triazole. During the study to prove the influence of the spin state of iron on the PSM method (chapter 2 of my thesis), we observed that at 90°C in 1h of the PSM reaction with *p*-anisaldehyde (**b**) is quantitative (Scheme 3-1). In contrast, the same reaction time at 90°C only leads to the formation of around 10% of (4-methoxybenzylidene)-4H-1,2,4-triazol-4-amine (from now on it is called imine compound **c**) from 4-amino-1,2,4-triazole **a** (referred to as aminotriazole in this chapter).



Scheme 3-1 Reactions carried out under oil bath at 90°C for 1h. (a) PSM reaction on complex **1** with aldehyde **b**. (b) Formation of imine compound **c** between aminotriazole **a** and aldehyde **b**.

The work detailed in chapter 3 began with the results displayed in Scheme 3-1. Since this would provide us with more evidence that the production of the imine complex **2** was the consequence of a PSM reaction on the amine complex **1**, we chose to continue comparing the two types of reactions at 90°C. As was specifically stated in the Chapter 1 introduction, complex **1**, which has a compact molecular arrangement without apparent holes, is insoluble in ethanol. For these reasons, some researchers expected the transformation of NH_2 groups on complex **1** to occur in solution rather than via a solid PSM reaction (Fig. 3-1). A reaction path in solution should proceed through these three distinct steps: (1) Step A: decoordination of the ligand, leading to the release of aminotriazole ***a*** into the solution; (2) Step B: the formation of the imine ***c*** from the amine ***a*** in solution; and (3) Step C: the subsequent formation of complex **2**. The research team has already demonstrated that this pathway is highly unlikely, as steps A and C are unfavourable.[1]

Based on the results in Scheme 3-1, the additional argument in favour of the transformation of NH_2 groups on the complex by PSM is the significant difference in yields observed between the PSM reaction (100%) on SCO complex **1** and the imine formation reaction (10%) between aminotriazole **a** and *p*-anisaldehyde **b** in solution. For quantitative imine formation on complex **1**, the formation of imine **c** in solution (step B, Fig. 3-1) should proceed at a rapid rate. However, as shown in Scheme 3-1, this is not the case, as imine formation on the complex occurs much more rapidly than in the solution of the free ligand.

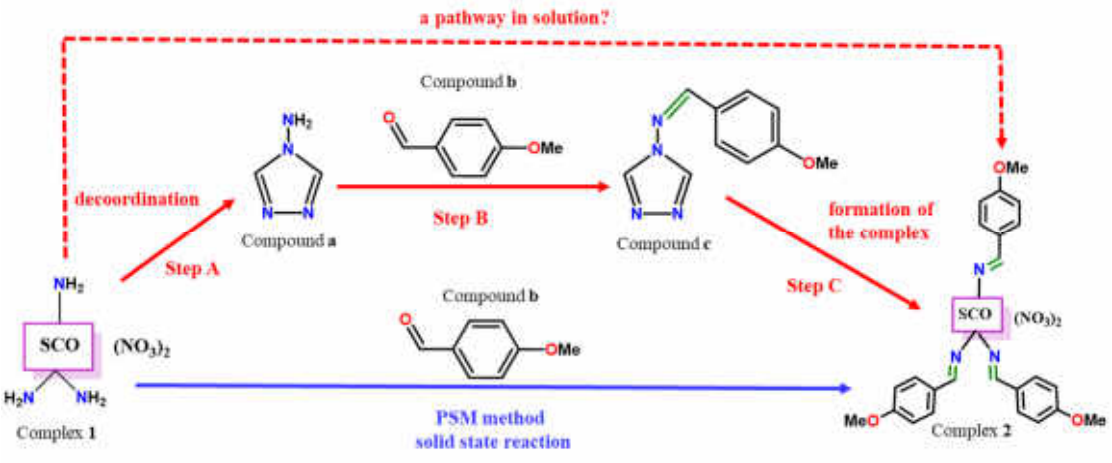


Fig. 3-1 Proposed reaction pathways for the transformation of complex **1** to complex **2.**[1]

To pursue this study, we first decided to switch from thermal heating in an oil bath to microwave irradiation (MWI). In particular, MWI enables faster, more uniform heating of the reaction medium. The use of this activation method can lead to an increase in reaction rates. As shown in Fig. 3-2(a) and (b), the PSM reaction under microwave irradiation was completed in 10 minutes, which is comparable to the results obtained after 1 hour in an oil bath maintained at 90°C. However, the reaction between aminotriazole **a** and *p*-anisaldehyde **b** yielded only around 10% of imine compound **c**.

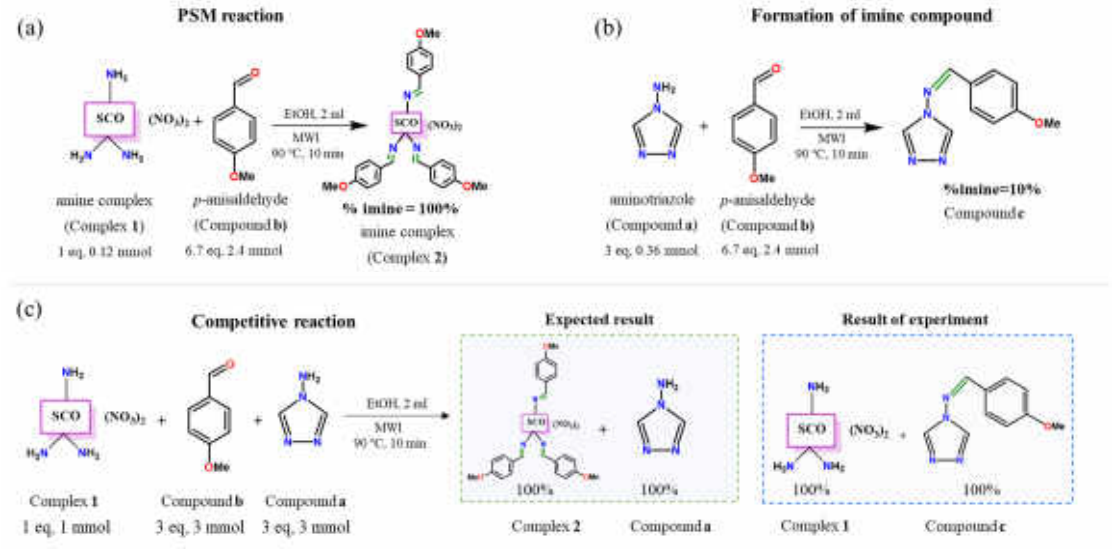


Fig. 3-2 Reactions carried out under microwave irradiation at 90°C for 10 minutes. (a) PSM reaction on complex **1** with aldehyde **b**. (b) Formation of imine compound between aminotriazole **a** and aldehyde **b**. (c) Competitive reaction in the presence of complex **1**, amine a, and aldehyde **b**.

On the one hand, these results suggest that a reaction involving an insoluble reagent, such as complex **1**, is not necessarily slower than one where all reagents are in solution. On the other

hand, this result illustrates that coordination on a metal can significantly alter the organic reactivity of the ligand. Therefore, combining the PSM method with a reaction such as complex digestion, which decoordinates the ligand from iron, presents a promising approach for synthesizing new triazole-based organic molecules. This is particularly significant given the numerous applications of triazole derivatives in both the medical[2-4] and materials[5, 6] fields. On the other hand, these results confirm that the rate of reaction in step B is far too slow to enable complex **2** to be formed quantitatively in 10 minutes by a reaction pathway in solution. In order to demonstrate that the amine complex **1** is more reactive toward aldehyde **b** than aminotriazole **a**, a competitive reaction, as depicted in Fig. 3-2 (c), was carried out to verify this point. Based on the results of the individual imine formation reactions (Fig. 3-2 (a) and (b)), it was expected that the imine complex (complex **2**) would form quantitatively, with only aminotriazole **a** remaining in the solution. However, the experimental outcomes were contrary to expectations: 100% of the NH_2 groups of the free ligand were transformed, and the recovered complex corresponded to the amine complex **1**. As each experiment, individual and competitive, was repeated three times with consistent results, we can consider these results reproducible, ruling out the possibility that the difference in behaviour observed between the individual reactions and the competitive reaction was due to experimental error. Although the competitive reaction does not provide additional support for the transformation of NH_2 groups in complex **1** via the PSM method, it does suggest that the iron spin-crossover complex **1** catalyses the formation of imine **c**.

This finding is particularly intriguing and noteworthy because, to the best of our knowledge, it represents only the second example described in the literature of this family of complexes being utilized in catalysis[7]. In that study, the authors utilized this type of SCO complex in the oxidation of 3,4,5,6-tetrachlorocatechol (TCC) to the corresponding quinone in the presence of 3-chloroperbenzoic acid (CPBA). Their findings indicated that the active species was the oxidized SCO complex, formed through a reaction with CPBA. Once oxidized, this species was subsequently reduced by TCC, regenerating the original SCO complex. In this case, the active catalyst was not the Fe(II) complex but the oxidized species. Although higher catalytic activity was observed for the LS state, this was attributed to the rate-determining step being the oxidation of the SCO complex, a process that occurs more readily in the LS state than in the HS state. Even more generally, very few synthesized spin-crossover complexes have been explored for catalytic applications.[8-11] Generally, the design of spin crossover complexes fundamentally differs from that of complexes commonly used in catalysis. For SCO complexes, it is crucial that ligands remain coordinated to the metal under varying conditions to preserve the desired transition properties. In contrast, catalytic complexes often rely on hemilabile or easily substitutable ligands, which facilitate the coordination of catalytic substrates to the metal centre. However, it would be more beneficial to go beyond these preliminary views, as iron complexes have recently garnered significant attention in catalysis due to their catalytic efficiency, availability, and environmental sustainability. Furthermore, certain imines synthesized from aminotriazole show potential for medical applications[12, 13], and these imines also serve as effective ligands for various metals,[14-16] the resulting metal complexes could exhibit interesting properties or find use in medical[17, 18] or environmental[19, 20] applications. Up to now, there is no example can be found in literature for the iron-catalyzed reaction between aminotriazole **a** and aldehyde **b**, with the closest example being the reaction between aminotriazole **a** and 9H-xanthen-9-ol, catalyzed by ferric hydrogenosulfat.[21]

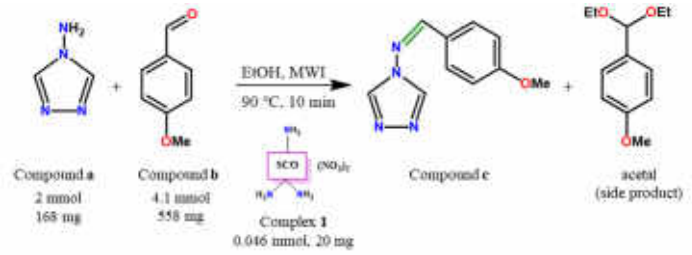
So, we show that by adding aminotriazole to the reaction, it is possible to go from a quantitative PSM reaction on the $Fe(NH_2trz)_3(NO_3)_2$ complex with an aldehyde to the efficient utilization of this complex as a catalyst for imine production under the right circumstances. While this is the second example of a cross-spin 1D triazole polymer complex demonstrating catalytic

activity, we will specifically demonstrate in the remaining sections of this chapter that it is the first instance where the active species is unmistakably identified as the SCO complex. To further clarify the catalytic mechanism of this SCO iron complex, tests have been conducted.

3.2 Study of catalytic reaction

We hypothesize that complex **1** may serve as a catalyst in the formation of imine **c** from aminotriazole **a** and aldehyde **b.** In order to verify the proposed hypothesis, the formation of imine ligand **c** (Table 3-1) was investigated in the presence of a catalytic amount of complex **1** (2.3 mol% in relation to aminotriazole **a**).

Table 3-1 Formation of the imine **c** catalyzed by the iron complex **1**.



Entry	Catalyst[a]	Conditions				Yield (imine)	Yield (acetal)
		Sonicate[b]	Heating[c]	Prep-treatment[d]	Reaction		
1	Complex **1**	-	-	-	10 min	40%	2%
2	-	-	-	-		10%	2%
3	Complex **1**	10 min	-	-		54%	2%
4	Complex **1**	10 min	10 min	-		58%	2%
5	Complex **1**	10 min	-	10 min		>98%	1%

[a] 20 mg of the complex was suspended in 0.5 mL of ethanol, two different solutions with a concentration of 4.1 mM of aldehyde (mixture 1) and 2 mM of aminotriazole (mixture 2) were prepared. [b] Sonicating only the suspension of the complex at room temperature. [c] Heating only the suspension of the complex at 90°C under MWI. [d] 1 mL of mixture 1 was added to the complex in suspension, and it was heated at 90 °C under MWI.

First, the formation of trace amounts of acetal (approximately 2%) was observed as a side product, resulting from the acetalization of aldehyde **b** in the presence of ethanol. Additionally, the presence of complex **1** in catalytic quantities significantly increased the imine yield, from 10% without the catalyst to 40% with the catalyst (Entries 1 and 2, Table 3-1). Sonication of complex **1** in an ethanol suspension for 5 minutes before the catalytic reaction further improved the yield to 54% (Entry 3, Table 3-1). This increase in yield can be attributed to better access to the catalytic site, as complex **1** is insoluble in ethanol, and it is well-known that increasing the contact surface area of a heterogeneous catalyst enhances its catalytic activity.[1] Although the sonication conditions used for the suspension of complex **1** in ethanol do not reduce the particle size of complex **1**, they are sufficient to reduce the size of agglomerates. The yield could be slightly further increased by applying microwave irradiation at 90°C for 10 minutes to the previously sonicated suspension of complex **1** in ethanol (Entry 4, Table 3-1). This heating likely facilitates the interaction between ethanol and complex **1**, allowing greater diffusion of the solvent into the solid and leading to better separation of the polymeric chains in complex **1**. As observed in our previous study of the PSM method, this improved separation

of the polymeric chains can result in higher yields.[15] Finally, imine **c** was obtained quantitatively when complex **1** was pre-treated (Entry 4, Table 3-1). This pre-treatment of the complex led to a clear increase in yield. Complex **1** and aldehyde **b**'s reaction mixture in ethanol was heated using microwaves for ten minutes at 90°C as part of the pre-treatment (Fig. 3-3).

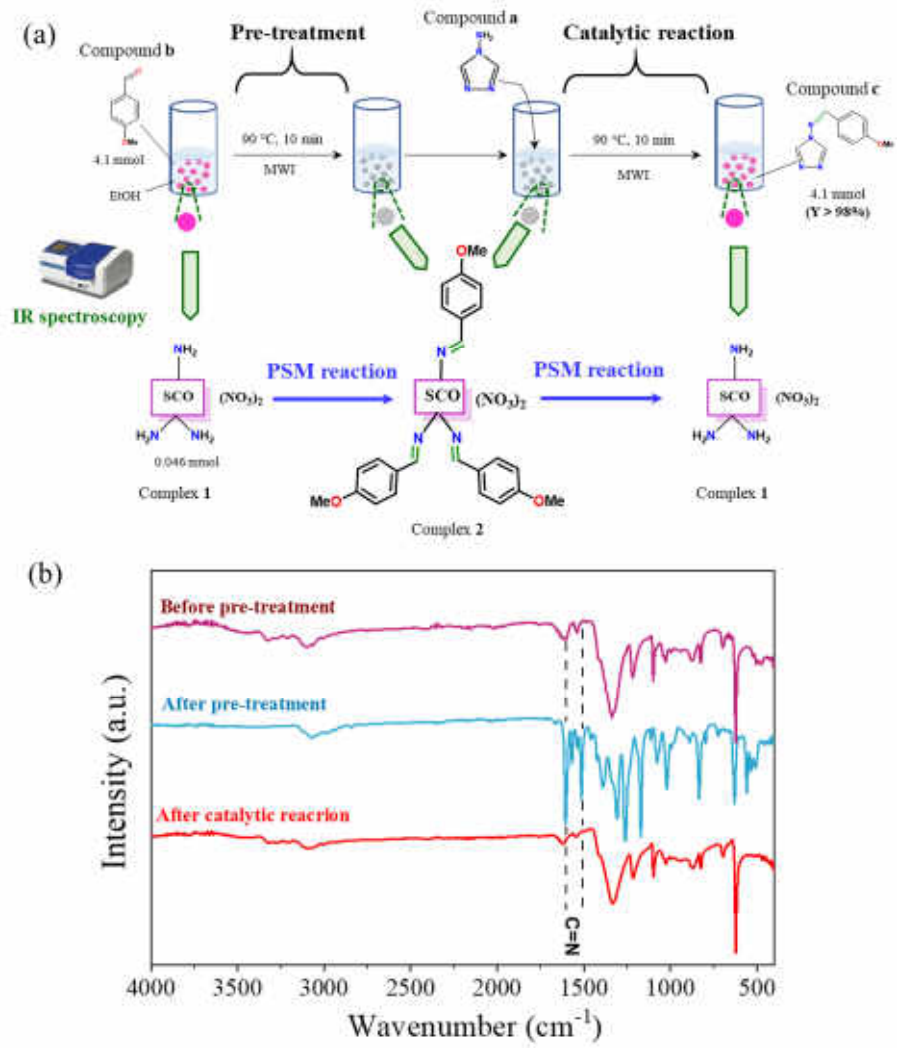


Fig. 3-3 Pre-treatment of complex **1** prior to its use in catalysis. a) Schematic representation of the procedure followed. b) IR spectra of the complex obtained after pre-treatment.

But what happens to complex **1** during pre-treatment and the catalytic reaction? As shown in Fig. 3-3, the amine complex suspended in ethanol is pink at room temperature. However, after microwave irradiation in the presence of the aldehyde **b** and subsequent cooling to room temperature, the colour of the complex changes to white, suggesting a change in its chemical structure. To understand what happens to the complex during pre-treatment, we recovered the complex and analyzed it using IR spectroscopy. As shown in Fig. 3-3 (b), the IR spectra of the recovered complex after pre-treatment revealed the appearance of bands characteristic of the C=N bond, confirming that complex **1** was transformed into complex **2** during the pre-treatment. After the catalytic reaction and subsequent cooling to room temperature, the recovered complex returns to its pink colour. The IR analysis confirms that the recovered complex after catalysis no longer shows the characteristic bands of the C=N functionality; instead, it corresponds to

that of the amine complex **1**. Thus, the amine complex **1** undergoes two PSM reactions during the pre-treatment and catalytic reactions. The first PSM reaction occurs when the amine complex **1** reacts with the aldehyde **b**, resulting in the formation of the corresponding imine complex **2**. A second PSM reaction takes place only if aminotriazole **a** is present in the solution, where it reacts with the imine complex **2** to regenerate the starting complex **1**, leaving the imine compound **c** in the solution.

3.3 Study of the effect of solvent on reaction rate

In our previous work, we demonstrated that the nature of the solvent significantly influences the efficiency of the PSM method.[22] In this study, we intend to investigate the influence of the solvent on the catalytic activity of the iron coordination polymer. (Table 3-2 and Table 3-3). Before discussing the various results obtained, it is important to note that a solution of aminotriazole **a** in ethanol was systematically added to the iron complex suspension. This approach was chosen because aminotriazole **a** is slightly soluble in toluene, and the presence of ethanol ensures that both reagents (aminotriazole and aldehyde) remain in the solution.

Table 3-2 Comparison of EtOH and 96% EtOH used in suspension and in the Mixture

Entry	Solvent			Catalyst[a]	Conditions				Yield
	Suspension of complex	aldehyde	aminotriazole		Sonicate[b]	Heating[c]	Pre-treatment[d]	Reaction	
1	96% EtOH	EtOH	EtOH	complex **1**	-	-	-	10 min	40%
2				complex **1**	10 min	-	-		49%
3				complex **1**	10 min	10 min	-		53%
4				complex **1**	10 min	-	10 min		100%
5				-	-	-	-		10%
6	EtOH	EtOH	EtOH	complex **1**	-	-	-	10 min	38%
7				complex **1**	10 min	-	-		48%
8				complex **1**	10 min	10 min	-		48%
9				complex **1**	10 min	-	10 min		71%
10				-	-	-	-		11%
11	96% EtOH	96% EtOH	96% EtOH	complex **1**	-	-	-	10 min	45%
12				complex **1**	10 min	-	-		53%
13				complex **1**	10 min	10 min	-		63%
14				complex **1**	10 min	-	10 min		91%
15				-	-	-	-		10%

[a] 20 mg of the complex was suspended in 0.5 mL of solvent, two different solutions with a concentration of 4.1 mM of aldehyde (mixture 1) and 2 mM of aminotriazole (mixture 2) were prepared. [b] Sonicating only the suspension of the complex at room temperature. [c] Heating only the suspension of the complex at 90°C under MWI. [d] 1 mL of mixture 1 was added to the complex in suspension, and it was heated at 90 °C under MWI.

Table 3-3 Effect of solvent on catalytic reaction efficiency

Entry	Solvent			Catalyst[a]	Conditions				Yield
	Suspension of complex	aldehyde	Sonicate[b]		Sonicate[b]	Heating[c]	Pre-treatment[d]	Reaction	
1	96% EtOH	EtOH	EtOH	Complex **1**	-	-	-	10 min	40%
2				Complex **1**	10 min	-	-		54%
3				Complex **1**	10 min	10 min	-		58%
4				Complex **1**	10 min	-	10 min		100%
5				-	-	-	-		10%
6	MeOH	MeOH	EtOH	Complex **1**	-	-	-	10 min	45%
7				Complex **1**	10 min	-	-		58%
8				Complex **1**	10 min	10 min	-		74%
9				Complex **1**	10 min	-	10 min		100%
10				-	-	-	-		11%
11	Toluene	Toluene	EtOH	Complex **1**	-	-	-	10 min	33%
12				Complex **1**	10 min	-	-		38%
13				Complex **1**	10 min	10 min	-		39%
14				Complex **1**	10 min	-	10 min		41%
15				-	-	-	-		12%

[a] 20 mg of the complex was suspended in 0.5 mL of solvent, two different solutions with a concentration of 4.1 mM of aldehyde (mixture 1) and 2 mM of aminotriazole (mixture 2) were prepared. [b] Sonicating only the suspension of the complex at room temperature. [c] Heating only the suspension of the complex at 90°C under MWI. [d] 1 mL of mixture 1 was added to the complex in suspension, and it was heated at 90 °C under MWI.

First of all, the amount of water present in the ethanol is crucial. The best results were achieved when the amino complex **1** was suspended in 96% ethanol, and the reagents (aldehyde **b** and aminotriazole **a**) were dissolved in absolute ethanol (Table 3-2, entries 1-5). This can be explained by our previous result, which showed that the presence of a small amount of water in ethanol facilitates faster formation of the imine complex **2**.[1] The fact that there is no discernible difference between experiments conducted with a water-ethanol mixture and those conducted with 100% ethanol when imine complex **2** is utilized lends credence to this hypothesis (Table 3-4, entries 10-11). A slightly improved yield was obtained when methanol was used as the solvent (Table 3-3, entries 6-10). This result was expected, given that methanol is more polar than ethanol and interacts even more strongly with the amine complex. However, when toluene was used as the solvent for suspending the complex and for dissolving the aldehyde, poorer results were observed compared to those obtained with methanol or ethanol (Table 3-3, entries 11-15). The presence of toluene could modify the interactions between the coordination polymer and the solvent, as well as the agglomeration of complex particles. In the presence of toluene, pre-treatment had a very limited effect on the yield of the catalytic reaction, in contrast to the significant improvement observed with ethanol or methanol. This outcome is expected. The IR result of the complex recovered after processing in toluene is shown in Fig. 3-4. In line with the earlier finding, no production of imine complex **2** was seen.[22] The employment of imine complex **2** in an ethanol-toluene mixture, at last, produced a 74% imine yield in 10 minutes of reaction (Table 3-4, entry 12). Compared to when the reaction is conducted in ethanol, this yield is noticeably lower. Indeed, imine **c** was quantitatively produced in ethanol under the latter circumstances, leading to a reduced reaction time (Table 3-4, entry 10). This yield discrepancy may be explained by a slower PSM reaction or less advantageous interaction between the aminotriazole and imine complex as a result of increased particle agglomeration in the ethanol-toluene combination.

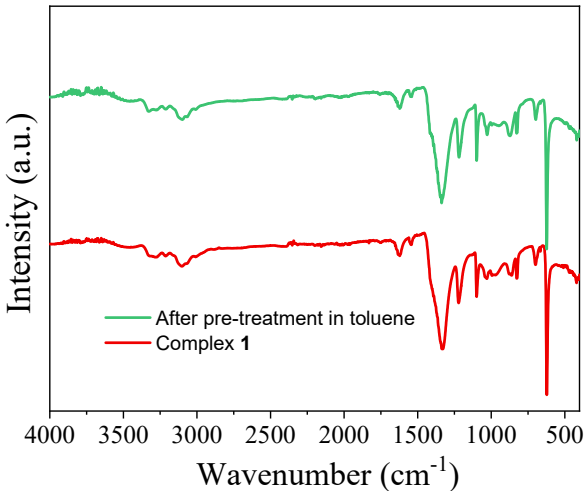


Fig. 3-4 The IR spectra of complex **1** (red curve) and the correspond recovered complex (green curve) after the pre-treatment in toluene.

3.3.1 Effect of the nature of the catalyst on reaction rate.

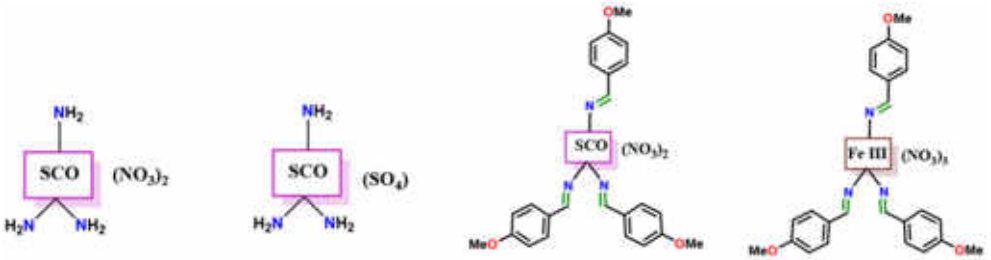
3.3.1.1 Influence of complex particle size and complex particle agglomerate size on reaction rate

In general, catalyst particle size can significantly influence performance. Smaller catalyst

particles often lead to faster reactions due to their higher contact surface and better interaction with the reactants. Consequently, it was expected that the use of complex **1** nanoparticles would show greater efficiency. This expectation was confirmed by experimental results, which demonstrated higher yields when 50 nm nanoparticles were used under similar conditions. (Table 3-4, entries 1-3).

Table 3-4 Effect of catalyst nature on catalytic reaction efficiency

Entry	Solvent			Catalyst[a]	Conditions				Yield
	Suspension of complex	aldehyde	aminotriazole		Sonicate[b]	Heating[c]	Pre-treatment[d]	Reaction	
1	96% EtOH	EtOH	EtOH	nanoparticles of complex **1**	-	-	-	10 min	76%
2	96% EtOH	EtOH	EtOH		10 min	-	-	10 min	81%
3	96% EtOH	EtOH	EtOH		10 min	-	10 min	10 min	100%
4	96% EtOH	EtOH	EtOH	complex **1b**	10 min	-	-	10 min	20%
5	96% EtOH	EtOH	EtOH		10 min	-	10 min	10 min	22%
6	96% EtOH	EtOH	EtOH	complex **3**	10 min	-	-	2 min	69%
7	96% EtOH	EtOH	EtOH		10 min	-	-	5 min	80%
8	96% EtOH	EtOH	EtOH		10 min	-	-	7min	100%
9	96% EtOH	EtOH	EtOH	complex **2**	10 min	-	-	5 min	100%
10	96% EtOH	EtOH	EtOH		10 min	-	-	10 min	100%
11	EtOH	EtOH	EtOH		10 min	-	-	10 min	100%
12	Toluene	Toluene	EtOH		10 min			10 min	74%



[a] 20 mg of the complex was suspended in 0.5 mL of solvent, two different solutions with a concentration of 4.1 mM of aldehyde (mixture 1) and 2 mM of aminotriazole (mixture 2) were prepared. [b] Sonicating only the suspension of the complex at room temperature. [c] Heating only the suspension of the complex at 90°C under MWI. [d] 1 mL of mixture 1 was added to the complex in suspension, and it was heated at 90 °C under MWI..

3.3.1.2 Influence of the counterion of the complex on reaction rate

We then investigated the effect of the counterion on the catalytic efficiency of the complex **1**. Specifically, we tested the catalytic activity of the iron aminotriazole complex **1b** with a sulfate ion as the counterion ($[Fe(NH_2trz)_3]SO_4$). When this complex **1b** was used, significantly lower yields (20%) were observed compared to complex **1** with a nitrate counterion (Table 3-4, entries 4-5). Furthermore, in the experiment with pre-treatment, the yield was nearly identical to that obtained without pre-treatment (22% vs 20%), indicating that pre-treatment did not enhance the catalytic reaction. This is likely due to the absence of imine complex formation. As shown by the IR spectra (Fig. 3-5), the recovered complex after pre-treatment was identical to the starting complex **1b**, suggesting that the amine complex **1b** did not transform into the imine complex under these conditions when the counterion was sulfate. This result aligns with our

previous study, which demonstrated that imine formation in iron triazole complexes is highly dependent on the counterion.[22]

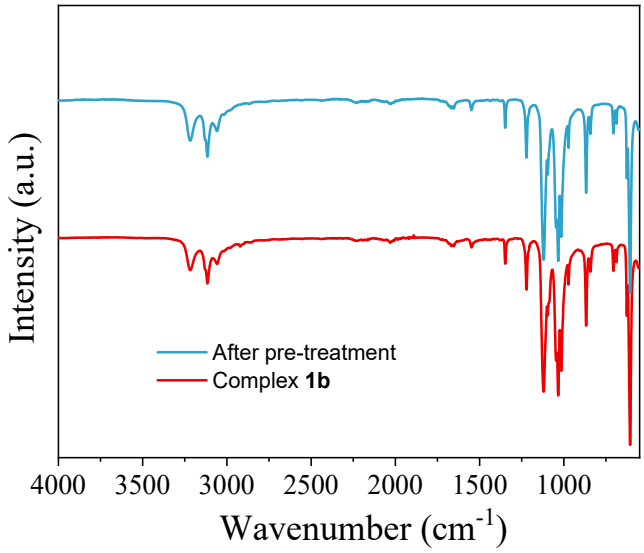


Fig. 3-5 The IR spectra of complex **1b** (red curve) and the corresponding recovered complex (blue curve) after pre-treatment.

3.3.1.3 Influence of the oxidation state of iron on reaction rate

We also tested the catalytic activity of the iron(III) imine complex **3** (Table 3-4, entries 6-8). When catalysis was performed with the iron(III) complex **3**, quantitative yields were obtained within 7 minutes. If we consider that iron(III) complexes are stronger Lewis acids than iron(II) complexes,[23] we would expect the iron(III) imine complex to be more efficient catalysts. However, experimental results indicate that the catalytic efficiency of the iron(III) complex is comparable to that of the iron(II) complex (Table 3-4, entries 6-8). One possible explanation for this outcome is that the iron II complex undergoes quick oxidation to iron III under catalytic experimental conditions, followed by reduction to iron II during or at the end of the reaction. We wanted to confirm or refute this hypothesis. According to section 3.3.8, the iron complex is still mostly iron II even though a tiny amount of the complex may oxidize. Therefore, we can conclude that the complex's catalytic activity in both oxidation states is of the same magnitude. Given that iron III complexes typically exhibit more catalytic activity than iron II complexes, this finding raises the possibility that the catalytic mechanism of the iron II complex may not be of the Lewis acid type.

3.4 Kinetic monitoring of catalysis reactions and study of post-catalysis complexes

3.4.1 Study of the effect of catalyst pre-treatment on catalysis reaction kinetics

Before going into the findings, it should be noted that every point in the kinetic studies

correlates to an experiment. That is to say, we performed experiments with the intended reaction time in order to carry out this kinetic investigation, rather than sampling the reaction medium at the desired time. A kinetic study of the reaction catalyzed by complex **1** without pre-treatment was carried out. For this study, the suspension of complex **1** in EtOH was placed in an ultrasound bath for 10 minutes prior to the catalytic reaction, the result of which is shown in Fig. 3-6a (red curve). The catalytic reaction was quantitative within 50 minutes. The transformation of the NH_2 function of aminotriazole appears to be linear over time, with a change in rate after 20 minutes (yield around 67%). Regardless of the reaction time, the yields were significantly higher than those obtained in the absence of the complex (blue curve, Fig. 3-6a), confirming that complex **1** effectively catalyzes the reaction. Furthermore, these experiments demonstrate that when the complex is pre-treated (microwave irradiation at 90°C for 10 minutes with a mixture of aldehyde **b** and complex **1** suspended in ethanol), the reaction is complete within 10 minutes (black curve, Fig. 3-6a). Even after 20 minutes, the yield remains quantitative, indicating that the imine **c** does not undergo hydrolysis under these experimental conditions. At the end of these experiments, the complexes were recovered and analyzed using serval techniques, including IR spectroscopy, powder X-ray diffraction, scanning electron microscopy, and temperature-dependent reflectivity measurements.

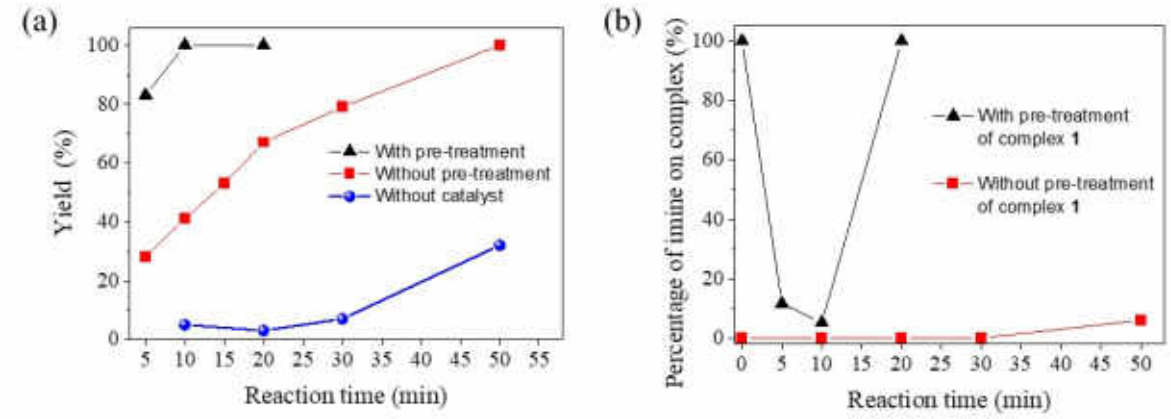


Fig. 3-6 Kinetic study of the catalysis reaction. a) yield of imine **c** as a function of reaction time; b) percentage of imine functionality, on the complex recovered after catalysis, as a function of reaction time.

3.4.2 IR spectroscopy analysis of post-catalysis complexes

IR spectroscopy provided a quick and straightforward method for determining whether the recovered complex more closely resembled the amine complex **1** or the imine complex **2**. When the suspension of complex **1** was only sonicated prior to use in the catalytic reaction, the recovered complex, regardless of the reaction time, corresponded more closely to the amine complex **1** (Fig. 3-7a). However, when catalytic reactions were preceded by catalyst pre-treatment, the type of recovered complex varied depending on the reaction time (Fig. 3-7b). For reaction times of 5 and 10 minutes, the recovered complexes were predominantly the amine complex **1**, while at 20 minutes, the recovered complex was the imine complex 2 (Fig. 3-7b).

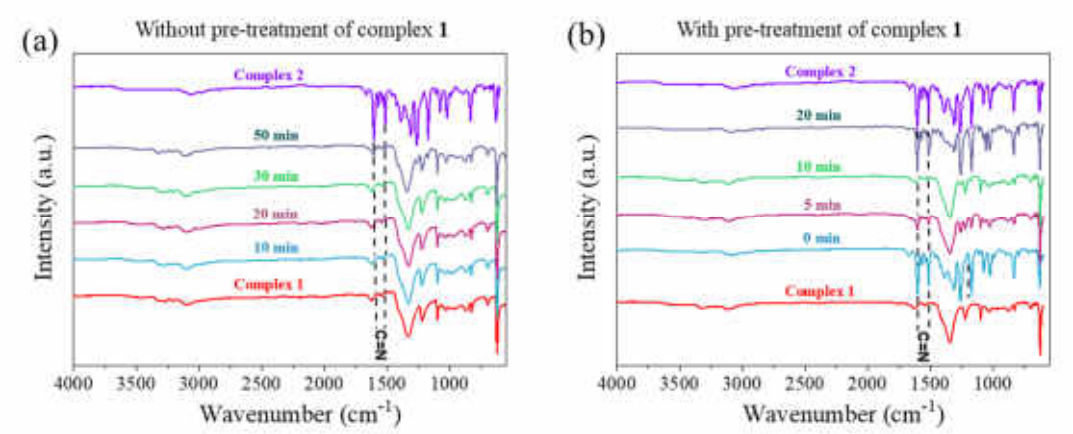


Fig. 3-7 IR spectra of the complex recovered after experiments. (a) without pre-treatment. (b) with pre-treatment.

3.4.3 Result of digestion of post-catalysis complexes

Fig. 3-6b illustrates the percentage of imine functions present in the complexes recovered after different catalytic times. The percentages of imine on the complex were determined by digesting the complex in an aqueous basic medium and analyzing the aqueous and organic phases via proton NMR (for detailed information, see experiment section 3.8.4). The result of digestion of the recovered complex are consistent with the IR spectroscopy results. Notably, Fig. 3-6b (black curve) shows that although all of the amine complex **1** was transformed into the imine complex **2** during pre-treatment, after 5 minutes of reaction, 12% of imine formation was observed on the recovered complex. Additionally, the results after pre-treatment and a reaction time of 20 minutes indicate that imine complex **2** can be synthesized under these conditions, once aminotriazole a is no longer present in the medium. When complex **1** was used as a catalyst without pre-treatment, only traces of imine functions were observed on the complex after 10 minutes of reaction, with the imine functions estimated at 6% after 50 minutes (Fig. 3-6b, red curve).

3.4.4 Study of the crystal structure and morphology of complex particles recovered after catalysis

The recovered complexes were also analyzed using X-ray powder diffraction (XRD, Fig. 3-8) and scanning electron microscopy (SEM, Fig. 3-9). The XRD measurement provided insight into the molecular arrangements while SEM characterization offered a view of the particle morphology. Before discussing the recovered complexes, we first analyze complexes **1** and **2**, which were synthesized according to previously published procedures.[1, 22] The XRD pattern of the amine complex **1** is consistent with the diffraction patterns typically observed for this type of complex (Fig. 3-8).[22] SEM images show that the particles of complex **1** are approximately 10 µm in size and generally spherical in shape (Fig. 3-9). At higher magnification, it becomes evident that these particles are actually composed of compact stacks of platelets. In some particles, distinct layers of these compact platelet stacks can also be observed.

XRD analysis of the powder and SEM images of the imine complex **2** aligns with the previously published results (Fig. 3-8 and Fig. 3-9).[22] Imine complex particles typically appear as rods

that can reach several micrometres in length, with smaller particles occasionally observed around these rods. After pre-treatment, the resulting complex is confirmed as imine complex **2**. However, SEM images of the pre-treated complex reveal significant differences in both size and shape compared to the original particles. The particle size appears to range from tens to hundreds of nanometers, and their shape, though difficult to ascertain, is clearly not rod-like. Additionally, the resulting complex exhibits little to no crystallinity.

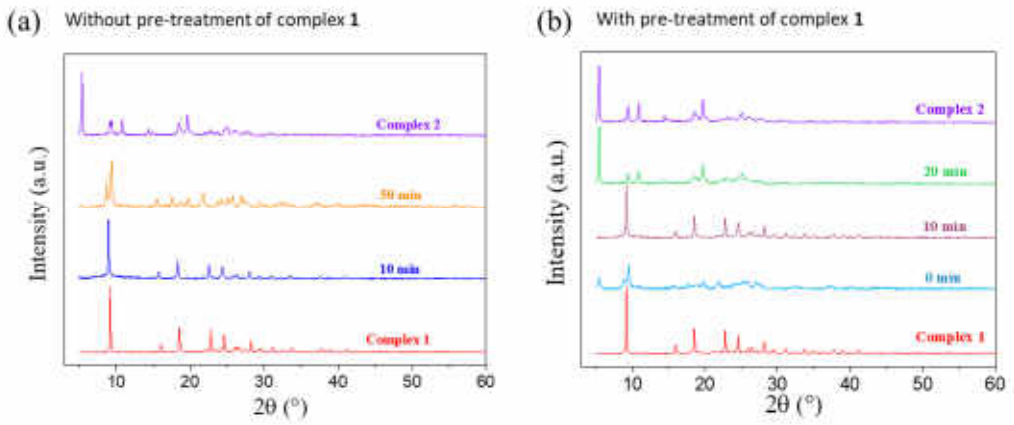


Fig. 3-8 XRD pattern of the complex recovered after experiments. (a) without pre-treatment of complex **1**; b) with pre-treatment of complex **1**. The XRD pattern of complex **1** and **2** were added to compare

Interestingly, the XRD pattern of the complex recovered after 10 minutes of catalytic reaction (with pre-treatment) matches that of the amine complex **1** (Fig. 3-8(b)). SEM images show that the primary difference between the recovered complex and amine complex **1** is the absence of spherical particles (Fig. 3-9), while the platelet stacks and distinct platelet stacking layers remain intact. After 20 minutes of catalysis, the XRD pattern of the recovered complex matches that of the imine complex **2**, yet the particles are still not rod-shaped. Instead, the particles appear as agglomerates of fairly uniform, hexahedral shapes.

It is important to note that 89 equivalents of aldehyde were added to the amine complex during pre-treatment, compared to the 33 equivalents used in the PSM reaction. This significant difference in experimental conditions, particularly the higher aldehyde concentration during pre-treatment (five times greater), could potentially induce π-stacking interactions between the aldehyde and the imine complex **2**. This suggests that the large excess of aldehyde might act as a co-solvent, improving the dispersion of the imine complex particles. After 20 minutes of catalysis, the imine functions on the complex are fully formed, and approximately 100 equivalents of imine ligands are present in the solution. In previous studies, it was hypothesized that the rod-like structures observed were formed by the association of multiple imine complex particles.[1] This association was thought to be favoured due to the minimal decoordination of the imine. However, in this case, the presence of such a large excess of ligand makes it less likely that the particles of complex **2** will associate.

It is also notable to observe the differences between the initial amine complex and those obtained after the two types of PSM reactions (Fig. 3-9). The transformation of the NH_2 group in the complex results in the disappearance of spherical particles and the emergence of platelet-shaped particles. In heterogeneous catalysis, smaller particles often offer significant advantages. Therefore, performing a PSM reaction with aldehyde, followed by a PSM reaction with aminotriazole on amine complex **1**, allows for modification of the particle morphology without

affecting its SCO properties (Fig. 3-11). This finding is relevant not only for heterogeneous catalysis, where particle size and shape influence catalytic activity, but also for applications requiring deposition of the compound in various devices.

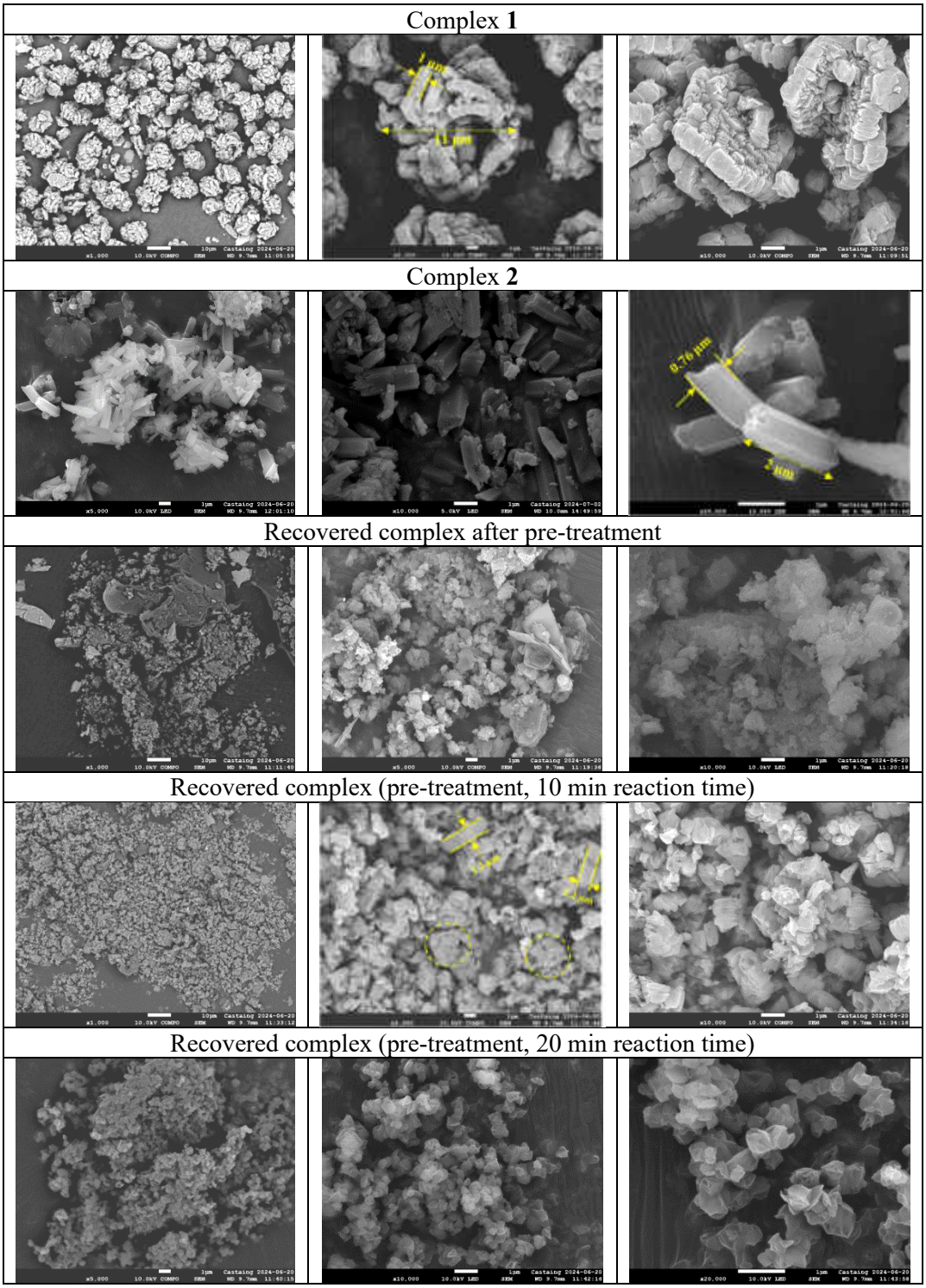


Fig. 3-9 SEM images of complex**1**, **2** and the recovered complexes after catalysis (with pre-treatment)

Further analysis of the complexes recovered after catalysis from the without pre-treated amine complex **1** showed less significant structural changes compared to those observed after the PSM

reactions. After 50 minutes of reaction, the number of spherical particles was notably reduced compared to the initial complex or after a 10-minute reaction, while compact stacking of platelets was still present (Fig. 3-10).

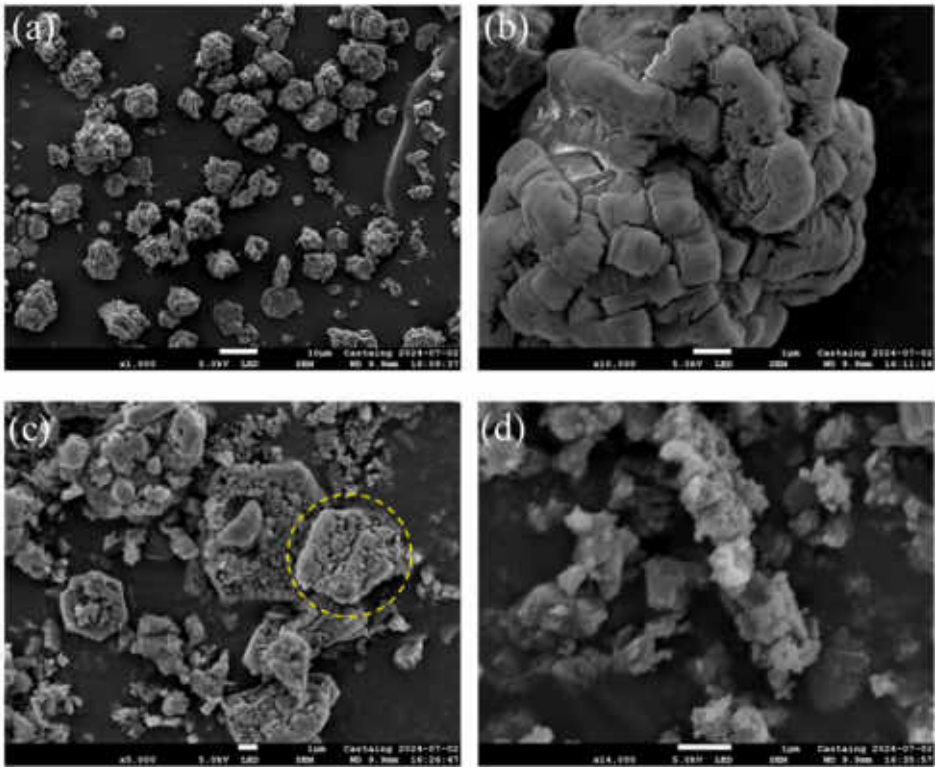


Fig. 3-10 SEM images of recovered complexes after reaction without pre-treatment. (a)-(b) 10 min of reaction. (c)-(d) 50 min of reaction.

3.4.5 Variable temperature reflectivity measurement

Subsequently, variable temperature reflectivity measurements were conducted on the amine complexes recovered post-catalysis (Fig. 3-11). The results reveal that these complexes exhibit spin-crossover properties closely resembling those of the initial complex. Specifically, they demonstrate sharp transitions at temperatures nearly identical to those of the original material, along with a broad thermal hysteresis cycle. This indicates that performing a PSM reaction with aldehyde, followed by another PSM reaction with aminotriazole on the amine complex **1**, enables the alteration of particle morphology without compromising the SCO property. This finding holds significant implications not only for heterogeneous catalysis, where particle size and shape are critical to catalytic performance, but also for applications that require a reduction in complex size, such as the deposition of this compound in various devices.

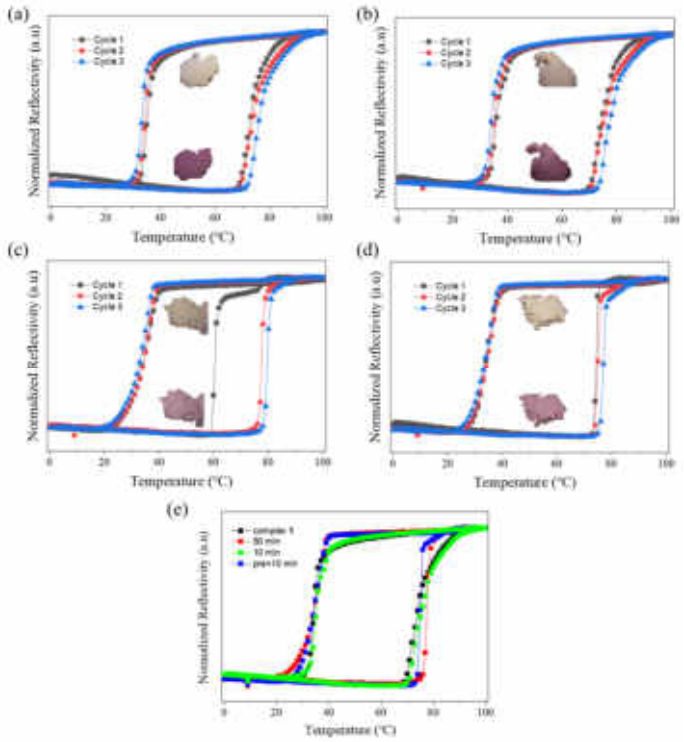


Fig. 3-11 Variable temperature optical reflectivity measurement. (a) complex **1**. (b) recovered complex after 10 min of reaction (without pre-treatment). (c) recovered complex after 50 min of reaction (without pre-treatment). (d) recovered complex after 10 min of reaction (with pre-treatment). (e) In a comparison of the above four complexes, the second cycles were selected to compare.

3.4.6 Study of the reproducibility of results obtained from complexes recovered after catalysis

To ensure the reproducibility of the experiment, new batches of complex **1** and complex **2** were synthesized. The pre-treatment experiments were then repeated using the newly synthesized batch of complex **1**. The reaction, following pre-treatment, proceeded quantitatively within 10 minutes, consistent with the results obtained from the initial batch. The complexes recovered after pre-treatment, using both batch **1** and batch 2 of complex **1**, were analyzed. Additionally, the new batches of complexes **1** and **2** were subjected to XRD and SEM analyses. These analyses confirmed the consistency and reproducibility of the experimental outcomes across different batches.

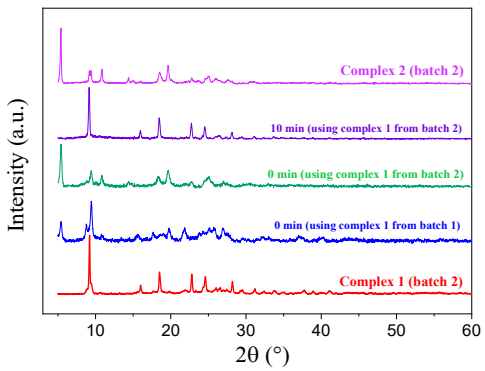


Fig. 3-12 Reproducible result of XRD pattern of the complex recovered after the pre-treatment and with a reaction time of 10 min. The XRD pattern of complex **1** and **2** were added to compare

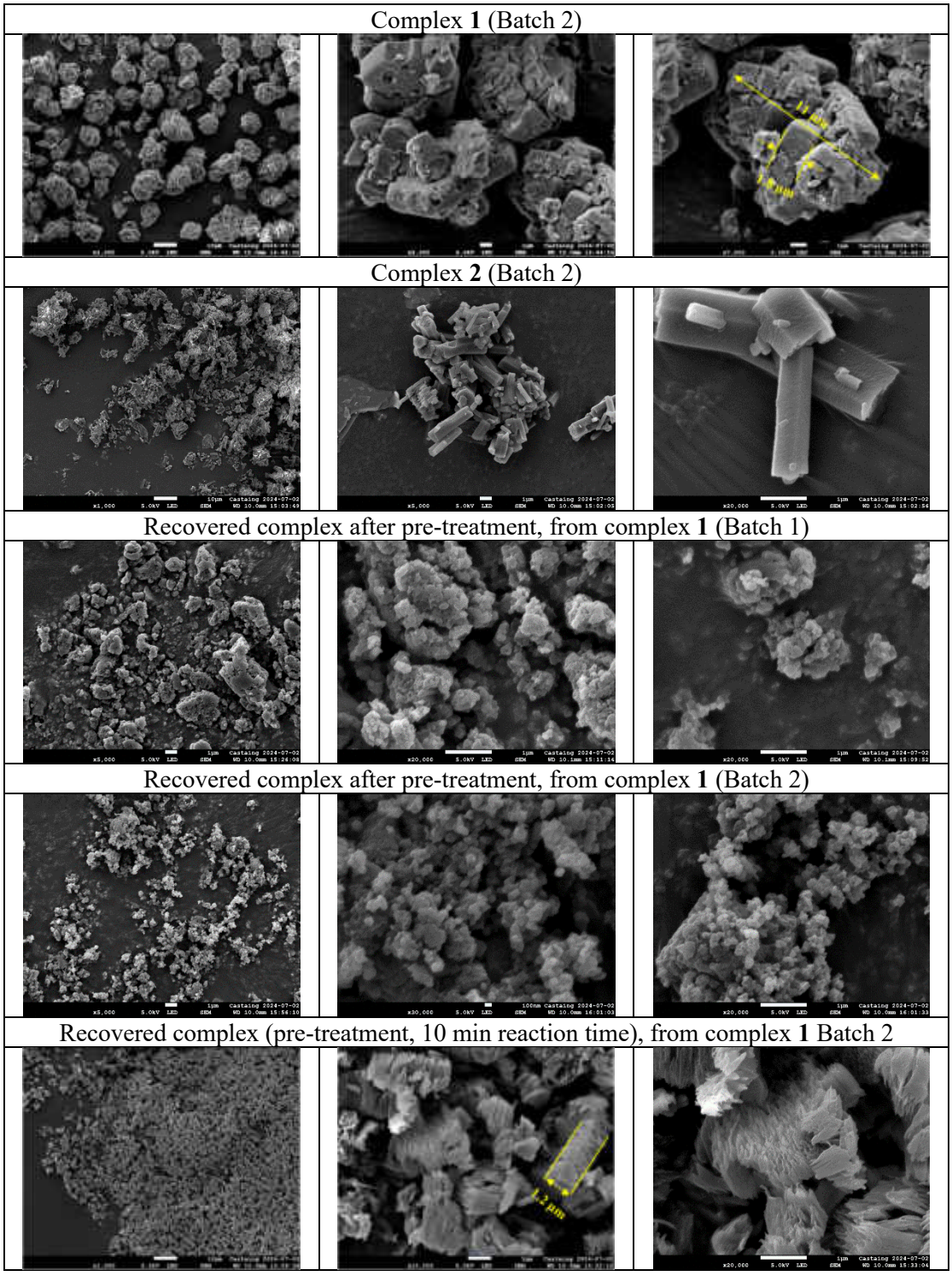


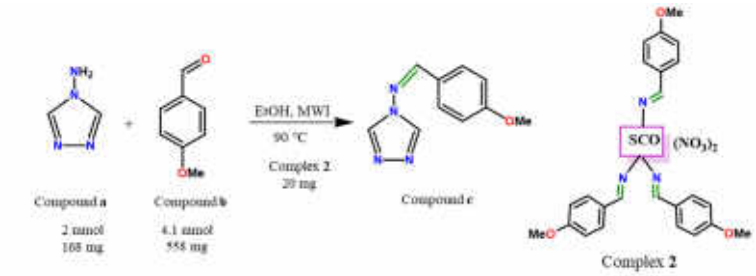
Fig. 3-13 Reproducible result of SEM images of complex**1**, **2** and the recovered complexes after pre-treatment and catalysis

3.4.7 Study of the complex recovered after the reaction between p-anisaldehyde b and aminotriazole a catalyzed by imine complex 2

We wanted to know what morphology the particles of the amine complex recovered after catalysis would have if we used the imine complex **2** as a catalyst. In particular, we wondered whether the particles of the amine complex recovered after catalysis would retain the rod-like

structure observed for the imine complex **2**. We began with a kinetic study of the reaction catalyzed by the imine complex **2**.

Table 3-5 Kinetic study of the reaction of *p*-anisaldehyde and aminotriazole using complex **2** as catalyst



Entry	Solvent			Catalyst[a]	Conditions				Yield
	Suspension of complex	aldehyde	aminotriazole		Sonicate[b]	Heating[c]	Pre-treatment[d]	Reaction	
1	96% EtOH	EtOH	EtOH	complex **2**	10 min	-	-	1 min	72%
2	96% EtOH	EtOH	EtOH	complex **2**	10 min	-	-	2 min	85%
3	96% EtOH	EtOH	EtOH	complex **2**	10 min	-	-	3 min	96%
4	96% EtOH	EtOH	EtOH	complex**2**	10 min	-	-	5 min	100%

[a] 20 mg of the complex was suspended in 0.5 mL of solvent, two different solutions with a concentration of 4.1 mM of aldehyde (mixture 1) and 2 mM of aminotriazole (mixture 2) were prepared. [b] Sonicating only the suspension of the complex at room temperature. [c] Heating only the suspension of the complex at 90°C under MWI. [d] 1 mL of mixture 1 was added to the complex in suspension, and it was heated at 90 °C under MWI.

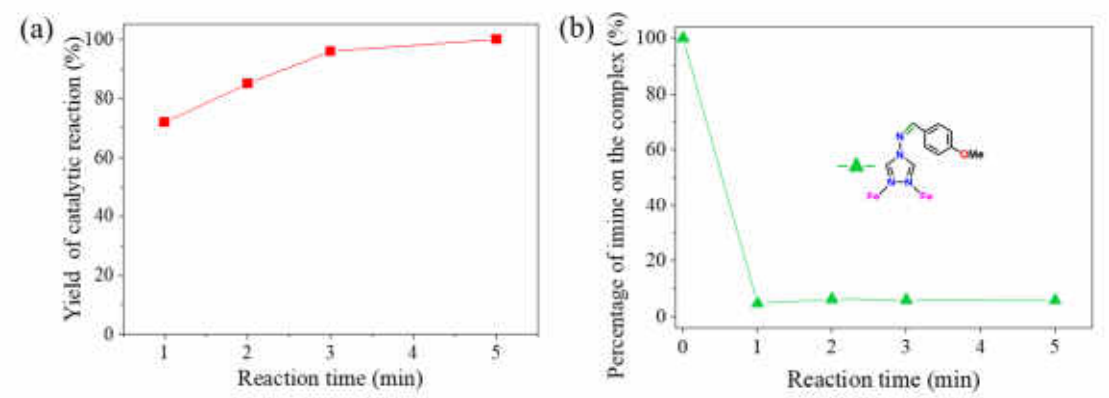


Fig. 3-14 (a) The yield of after 1, 2, 3 and 5 min of reaction. (b) The result of digestion of the complex recovered from the reaction. (c) The XRD pattern of the complex recovered after 5 min of reaction

As shown in Table 3-5 and Fig. 3-14a, the reaction is quantitative within 5 minutes. According to the digestion result (Fig. 3-14b), from the first minute up to 5 minutes, the complex recovered after the catalytic reaction corresponds to amino complex **1**. SEM images of the complex recovered after 5 minutes of reaction (Fig. 3-15) revealed numerous rods in the micrometer range, as well as some compact stack of platelets. Compared to imine complex **2** (Fig. 3-9), the particles of the recovered amine complex are more agglomerated, with only large agglomerates observed. This agglomeration can be attributed to the stronger interactions between the particles of the amine complex **1** compared to those of the imine complex **2**. The result of XRD measurement (Fig. 3-16) indicates that the diffractogram of the recovered amine complex is similar to that of amine complex **1**.

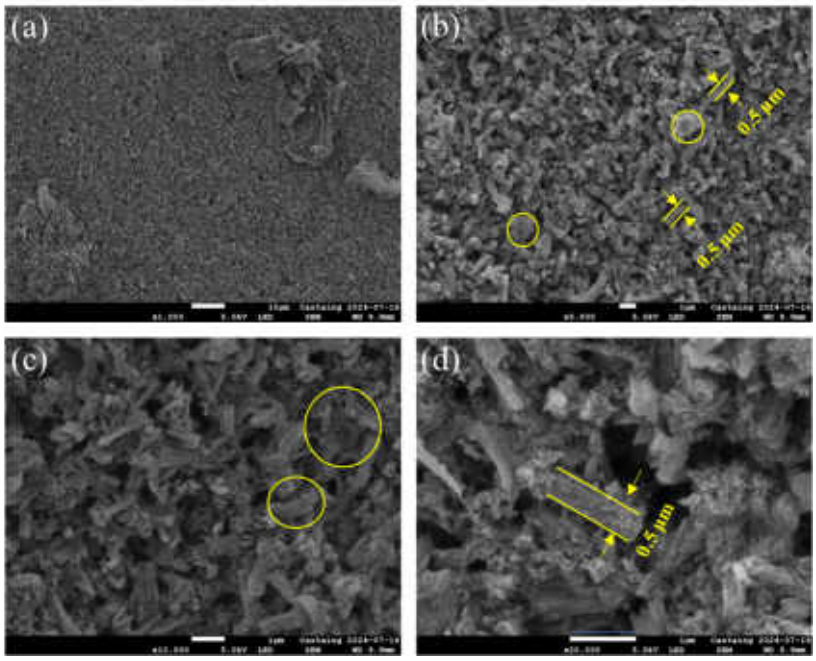


Fig. 3-15 SEM images of recovered complex (complex **2** as catalyst, after 5 min of catalytic reaction)

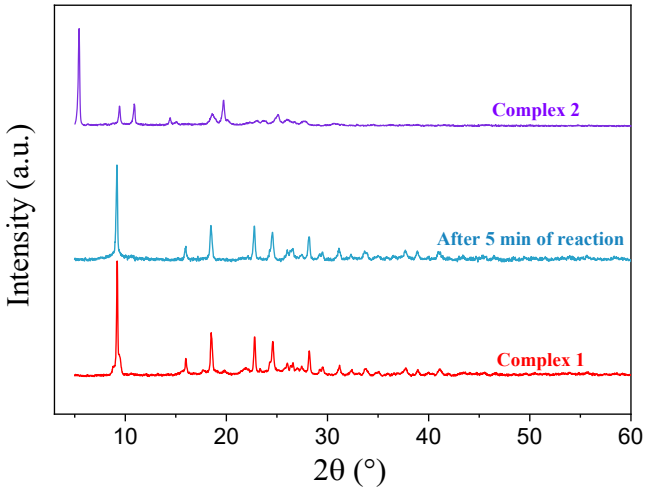


Fig. 3-16 The XRD pattern of the complex recovered after 5 min of reaction

Additionally, temperature-dependent reflectivity measurements of the amine complex recovered after catalysis ((Fig. 3-17) demonstrate spin crossover (SCO) properties similar to those of the synthesized amine complex **1**. These measurements reveal abrupt transitions at temperatures close to those of complex **1**, along with a broad thermal hysteresis cycle. Notably, when starting with imine complex **2** as a catalyst, the recovered complex exhibits an identical XRD pattern and SCO properties to complex **1** (Fig. 3-16 and Fig. 3-17), with the morphology retaining its 1D rod-like structure (Fig. 3-15). These results are significant for the synthesis of complex **1** with a 1D structure. Moreover, the similarity in colour and SCO properties between the recovered complex and complex **1** indicates that the majority of the recovered complex remains in the iron(II) state after the catalytic reaction.

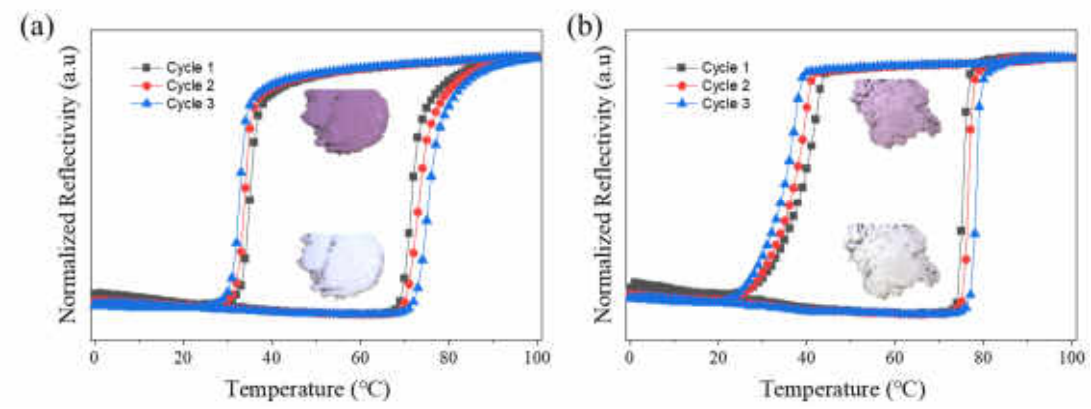


Fig. 3-17 Variable temperature reflectivity measurement. (a) complex **1**. (b) the complex recovered after 5 min of reaction.

3.4.8 Study of the complex recovered after the reaction between *p*-anisaldehyde b and aminotriazole a catalyzed by imine complex 3

As shown in the previous section, we also tested the catalytic activity of the iron(III) imine complex **3** (Table 3-4, entries 6-8). When catalysis was performed with the iron(III) complex **3**, quantitative yields were obtained within 7 minutes. If we consider that iron(III) complexes are stronger Lewis acids than iron(II) complexes,[23] we would expect the iron(III) imine complex to be more efficient catalysts. However, experimental results indicate that the catalytic efficiency of the iron(III) complex is comparable to that of the iron(II) complex (Table 3-4, entries 6-8). To explain this result, one hypothesis is that under the catalytic conditions, the iron(II) complex is rapidly oxidized to iron(III), and then, during or at the end of the reaction, it is reduced back to iron II.

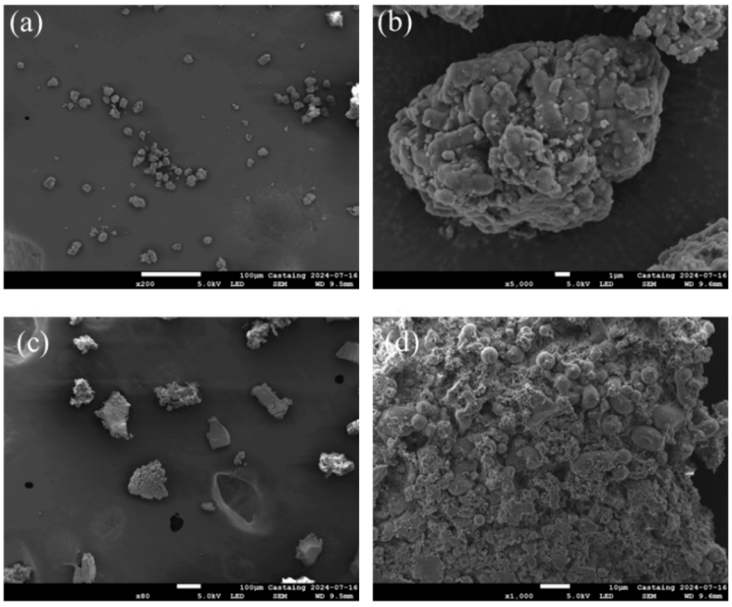


Fig. 3-18 SEM images of (a)-(b) complex **3**, (c)-(d) recovered complex (complex **3** as catalyst, after 7 min of catalytic reaction)

When comparing the iron(II) complex **1** after pre-treatment with the imine complex **3** to the iron(III) complex, significant differences in morphology and properties are observed. The SEM

characterization reveals that the iron(III) complex consists of small spherical particles (Fig. 3-18(a)-(b)), which are distinctly different from the iron(II) complex (Fig. 3-9). Additionally, the color of the two complexes varies significantly: the iron(III) complex exhibits a very dark orange-brown hue, whereas the iron(II) complex, recovered after pre-treatment, is beige, similar to imine **2**. Further SEM images of the iron(III) complex after catalysis show agglomerates of small, spherical particles (Fig. 3-18 (c)-(d)), closely resembling the initial iron(III) complex rather than the iron(II) complex. This result suggests that if the iron complex were oxidized to iron(III) during pre-treatment, then, under catalytic conditions, the iron(III) would need to be reduced back to iron(II), which is highly improbable. To test this hypothesis, the iron(III) complex recovered after a 7-minute reaction was analyzed by XRD measurement (Fig. 3-19), revealing a diffractogram that does not correspond to either complex **1** or complex **2**.

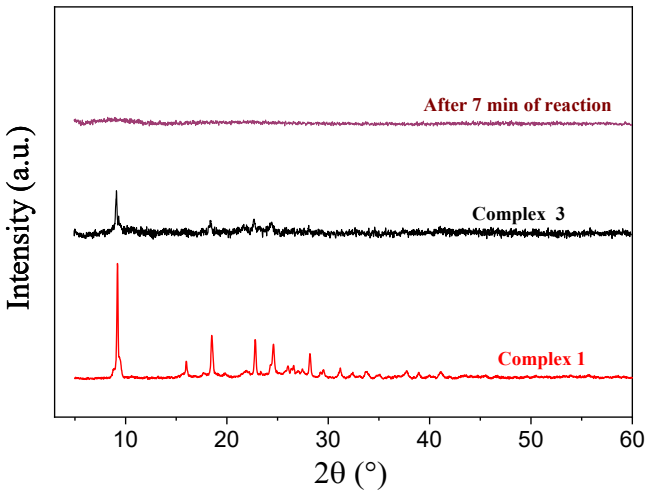


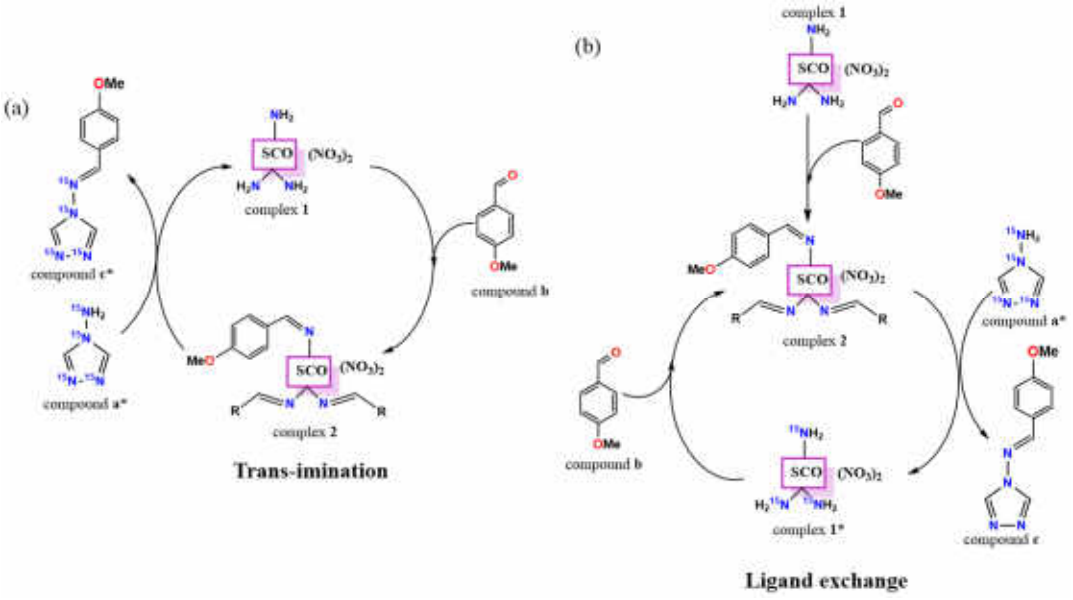
Fig. 3-19 The XRD pattern of the complex recovered after 7 min of reaction and complex **3**

Finally, temperature-dependent reflectivity measurements were conducted on the complex recovered after the reaction was catalyzed by complex **3**. Unlike the amine complexes recovered following catalysis by complex **1**, the complex recovered after catalysis by complex **3** did not exhibit spin crossover properties. In conclusion, this result suggests that, although the presence of trace amounts of iron(III) cannot be entirely excluded, the majority of the complex remains in the iron(II) state during the catalytic process if it begins with the iron (II) complex in the reaction. The catalytic mechanism of the iron II complex may not be of the Lewis acid type, as it is usually observed that iron(III) complexes have a higher catalytical activity than iron(II) complexes.

3.5 Investigation of the mechanism of the PSM reaction leading to the amine 1 complex from the imine complex 2

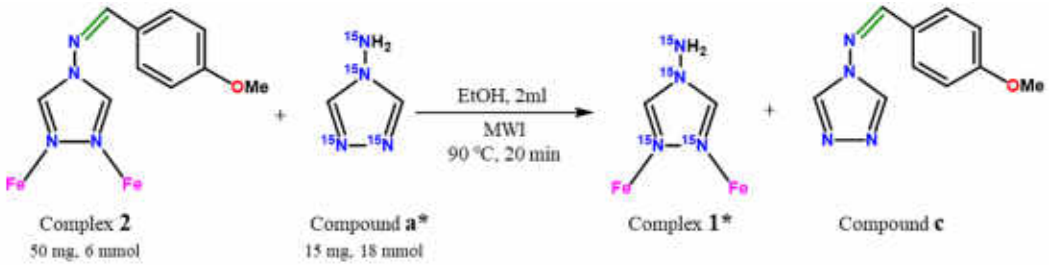
The two mechanisms by which we have envisioned this transformation taking place are ligand

exchange and trans-imination (Scheme 3-2).



Scheme 3-2 Mechanisms envisaged for the formation of complex **1** from complex **2**

In the case of trans-imagination, amine complex **1** is formed by the nucleophilic attack of the NH_2 group of aminotriazole **a** on the imine functionality of complex **2**. *according to the ligand exchange mechanism, amine complex **1** is generated through the decoordination of imine **c** and the subsequent coordination of aminotriazole **a** to the iron centre. The differentiation between these two mechanisms can be achieved by performing a PSM reaction using aminotriazole **a*** that is fully enriched with the isotope ^{15}N (Scheme 3-3). Indeed, the presence of ^{15}N in the recovered complex after the reaction would support the ligand-exchange mechanism. Conversely, if imine **c*** (labeled with ^{15}N) is found in large quantities in the solution, the mechanism would be indicative of trans-imination (Scheme 3-2).



Scheme 3-3 PSM reaction on complex **2** with aminotriazole **a***

Solid-state ^{15}N NMR analysis of the recovered complex reveals a peak at 67.8 ppm in the ^{15}N Hahn echo MAS NMR spectra (Fig. 3-20). This peak is attributed to the presence of ^{15}N in the complex, which enhances the signal intensity by up to 270 times due to the low natural abundance of ^{15}N (0.37%) and its inherently low sensitivity, making it nearly impossible to observe otherwise.[24, 25] Additionally, NMR analysis of the solution indicates that the PSM reaction is incomplete, as some ^{15}N aminotriazole **a*** remains in solution (Fig. 3-21).

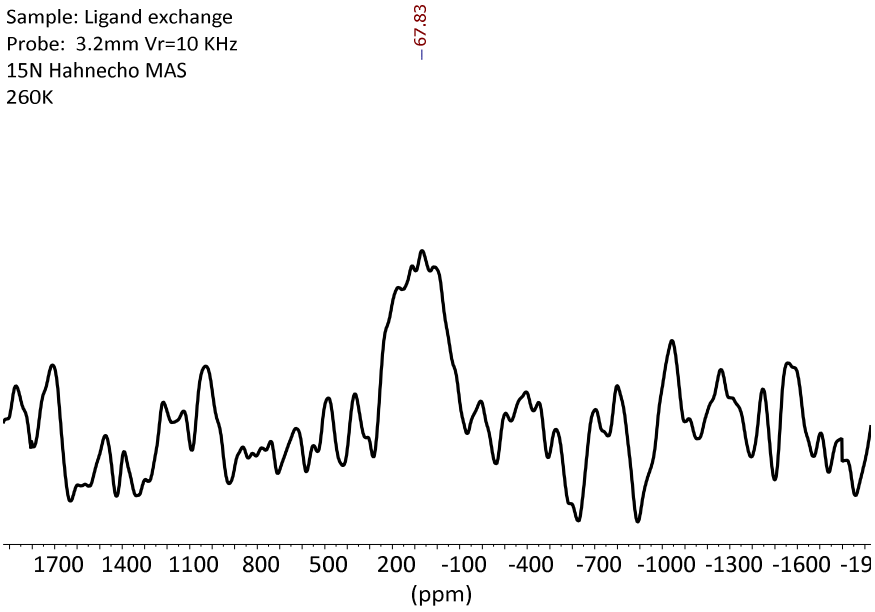


Fig. 3-20 ^{15}N Hahn echo solid state NMR of the complex recovered after the ligand exchange experiment

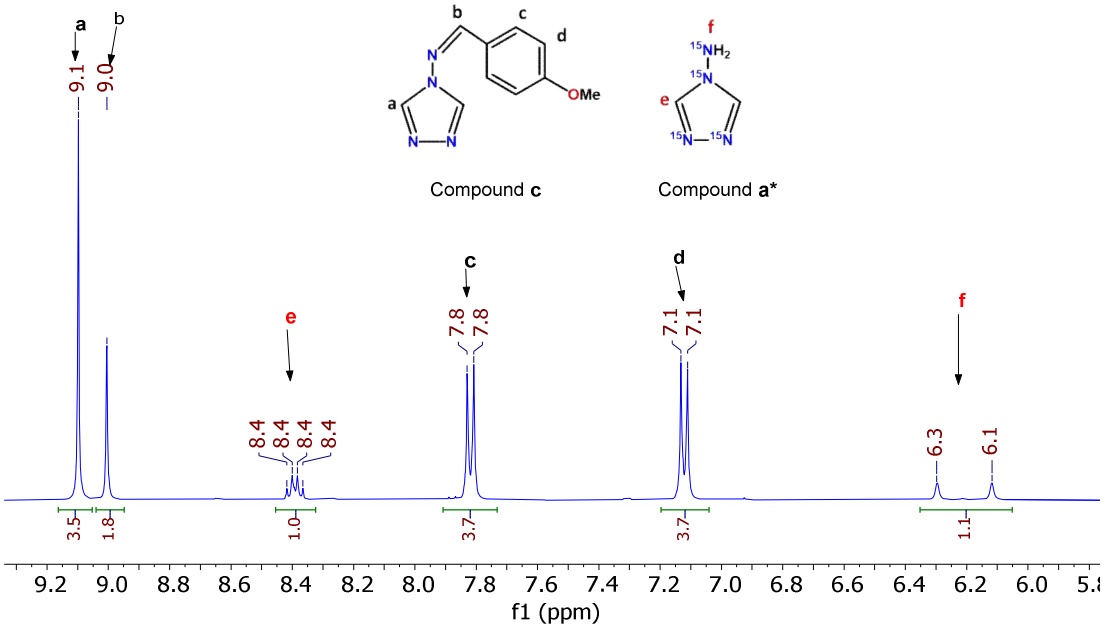


Fig. 3-21 ^{1}H NMR spectrum of the solution after PSM reaction on complex **2** with aminotriazole **a'**

On the other hand, the imine formed appears to correspond to imine **c**. If imine **c*** were predominantly formed, the CH signals of the triazole and imine groups would be expected to appear as multiplets due to the coupling between protons and ^{15}N (Fig. 3-21).[26, 27] Additionally, 2D ^{1}H/^{15}N NMR analyses (HMQC and HMBC) show little to no correlation between protons and nitrogen for the imine formed, while clear correlations are observed for aminotriazole **a*** (Fig. 3-22 and Fig. 3-23). These findings suggest that amine complex **1** is likely formed through a PSM reaction via ligand exchange.

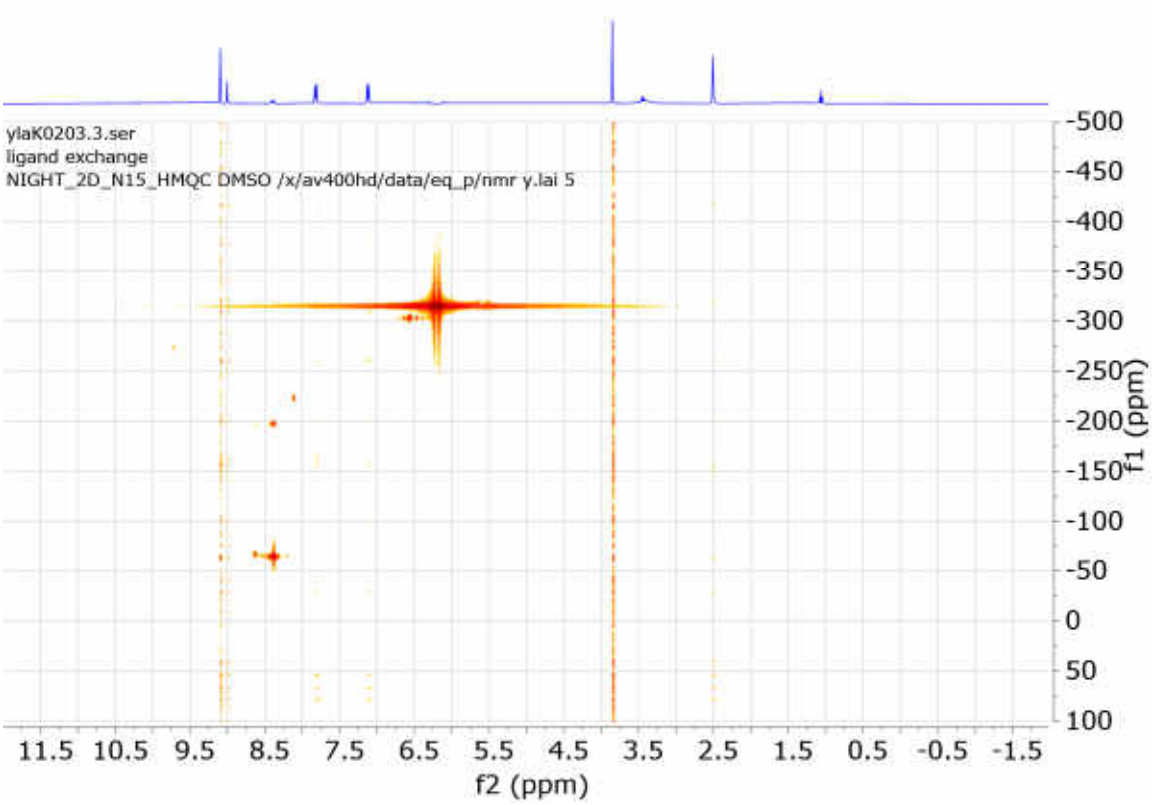


Fig. 3-22 ^{1}H-^{15}N HMQC (DMSO-d6) of the ligand exchange reaction.

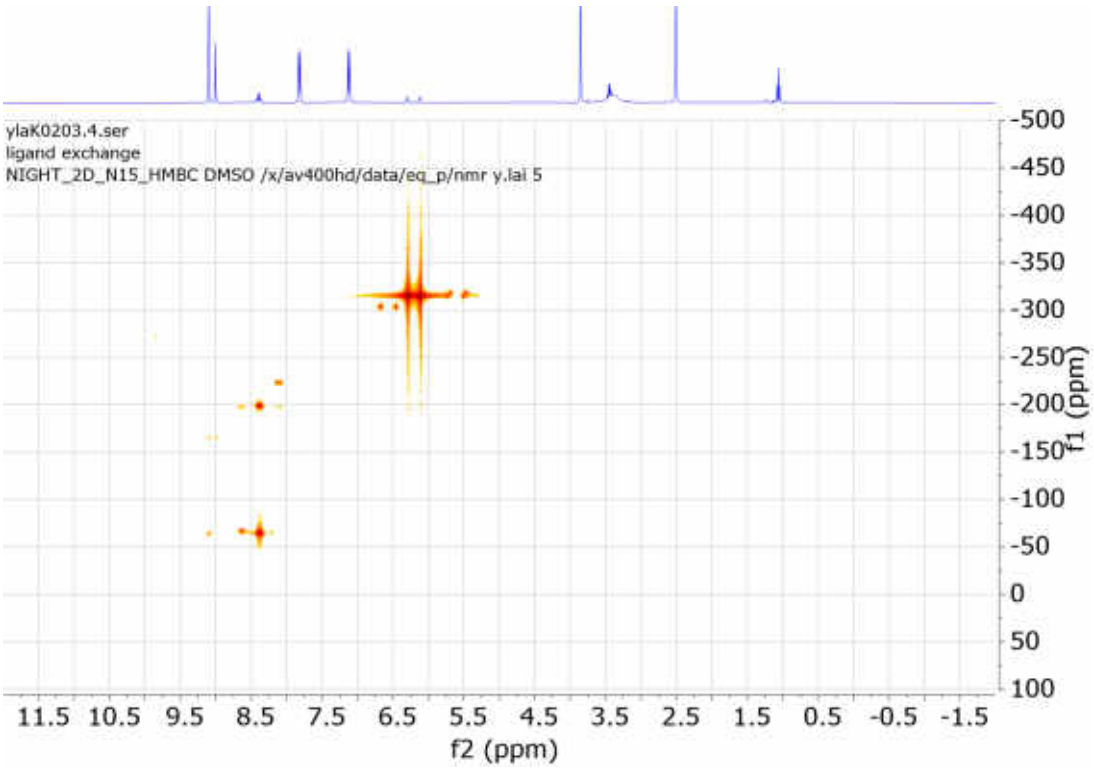


Fig. 3-23 ^{1}H-^{15}N HMBC (DMSO-d6) of the ligand exchange reaction

3.6 Mechanism study of the catalytic reaction

Finally, the potential mechanism of this catalytic reaction was considered. Based on the work described in the literature, it is possible that the iron complex acts as a Lewis acid.[23] The interaction of the iron complex with the aldehyde could increase the electrophilicity of the carbonyl group, thereby promoting the nucleophilic attack of the NH_2 group of aminotriazole **a**. If this mechanism is assumed, a stronger Lewis acid would facilitate the reaction more effectively. Given that iron(III) complexes are stronger Lewis acids than iron(II) complexes, the activity of the iron(III) complex would be expected to be greater than that of the iron(II) complex. However, the observation that this is not the case suggests that the mechanism may not be of the Lewis acid type. Moreover, even when a catalytic mechanism is well-established in the literature, it is essential to consider the reaction system as a whole, as the mechanism may depend heavily on the specific catalyst and/or catalytic substrates involved. This consideration is particularly important in this case, as aminotriazole **a** serves not only as a catalytic substrate but also as a strong ligand for iron, and the NH_2 group on the complex **1** can react with the aldehyde. As illustrated in Scheme 3-2, the transformation of imine complex **2** into amine complex **1** results in the formation of the desired imine compound **c**. This observation led to the hypothesis that the catalytic activity of the complex might be attributed to PSM reactions. If this hypothesis is true, and given that the complex constitutes only 2% of the aminotriazole **a**, a substantial number of PSM cycles would be necessary. However, when the imine complex and the imine compound generated during catalysis have the same substituent, it becomes challenging to determine whether the imine functions of the complex were originally present or were formed during the catalytic reaction. To address this challenge, we decided to study the catalytic reaction using an imine complex and an imine compound with different substituents. This approach will allow us to evaluate the occurrence of PSM cycles during the catalytic process.

3.6.1 Investigation of catalytic reactions when the substituent in the imine complex differs from that of the aldehyde that serves as the catalytic substrate.

3.6.1.1 Study of the reaction between aminotriazole a and vanillin d catalysed by the imine complex 2.

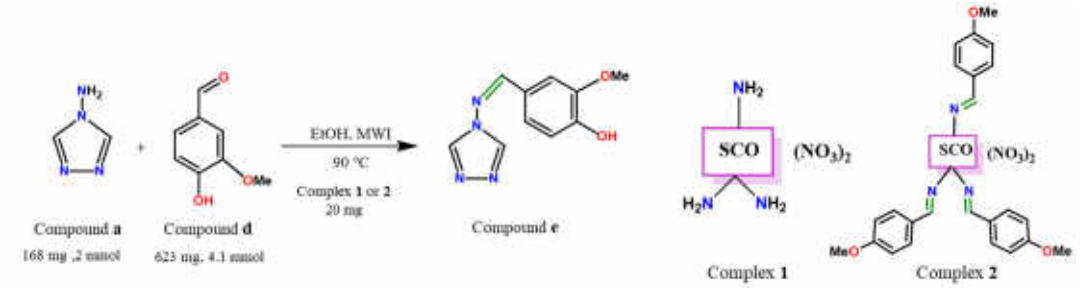
As mentioned above, when the imine complex and the imine compound produced during catalysis possess the same substituent, it becomes impossible to distinguish whether the imine functions of the complex were originally present or were generated during the catalytic reaction. This is why we decided to investigate the effect of introducing a catalytic amount of imine complex **2** in the reaction between aminotriazole **a** and vanillin **d**. Specifically, the composition of the recovered complex (percentages of amine function, imine function from the initial complex, and imine produced during the reaction) was analyzed after different reaction times.

With this in mind, we began by comparing the yields obtained after 10 minutes of reactions carried out in the absence of catalyst to those carried out in the presence of a catalytic amount of SCO complex (Table 3-6. This study confirms that our SCO complexes effectively catalyze this reaction, since in 10 minutes, in the presence of a catalytic amount of complex, yields of at least 68% are obtained, whereas in the absence of complex only 26% of imine is formed. Pre-

treatment of complex **1** brings the yield from 68% to quantitative. The reaction was also quantitative in 10 minutes when 20 mg of imine complex **2** was placed in the reaction medium. The complex recovered after catalysis in this final instance has a few amine functionalities but mainly imine functionalities (those derived from vanillin).

Kinetic studies of the catalysis demonstrate that when imine complex **2** is employed, the reaction is quantitative within 5 minutes (Fig. 3-24 (a)). The ^{1}H NMR spectrum of the solution shows the presence of imine **e** and traces of imine **c**, which results from the reaction between the imine complex **2** and aminotriazole **a** (Fig. 3-32).

Table 3-6 Yields of catalytic reaction between aminotriazole **a** and vanillin **d**



Entry	Solvent			Catalyst[a]	Conditions				Yield
	Suspension of complex	aldehyde	aminotriazole		Sonicate[b]	Heating[c]	Pre-treatment[d]	Reaction	
1	96% EtOH	EtOH	EtOH	complex **1**	10 min	-	-	10 min	68%
2	96% EtOH	EtOH	EtOH	complex **1**	10 min	-	10 min	10 min	100%
3	96% EtOH	EtOH	EtOH	complex **2**	10 min	-	-	10 min	97%
4	96% EtOH	EtOH	EtOH	-	-	-	-	10 min	26%

[a] 20 mg of the complex was suspended in 0.5 mL of solvent, two different solutions with a concentration of 4.1 mM of aldehyde (mixture 1) and 2 mM of aminotriazole (mixture 2) were prepared. [b] Sonicating only the suspension of the complex at room temperature. [c] Heating only the suspension of the complex at 90°C under MWI. [d] 1 mL of mixture 1 was added to the complex in suspension, and it was heated at 90 °C under MWI.

An analysis of the recovered complex's composition across reaction time yields important insights (Fig. 3-24b). Firstly, less than 3% of the imine functionalities from the initial complex remain during the first minute and throughout the catalytic reaction. After one minute of reaction, the recovered complex contains 78% of amine functionalities and 22% of imine functionalities resulting from the reaction of the amine groups on complex with vanillin **d**. From the first to the fourth minute, the percentage of imine functionalities formed from the reaction with vanillin **d** remains above 15%, then increases to over 80% by the fifth minute, at which point few aminotriazole **a** molecules remain in the medium, and imine complex **3** is recovered by the seventh minute. This suggests that aminotriazole **a** reacts very rapidly with imine complex **2**, resulting a complex that differs significantly from the initial one within less than a minute of the catalytic reaction. Furthermore, it was observed that within the first minute, a high percentage of imine functionalities from the reaction with vanillin **d** are present in the recovered complex. This result indicates that the complex also reacts very rapidly with catalytic substrate vanillin **d.**

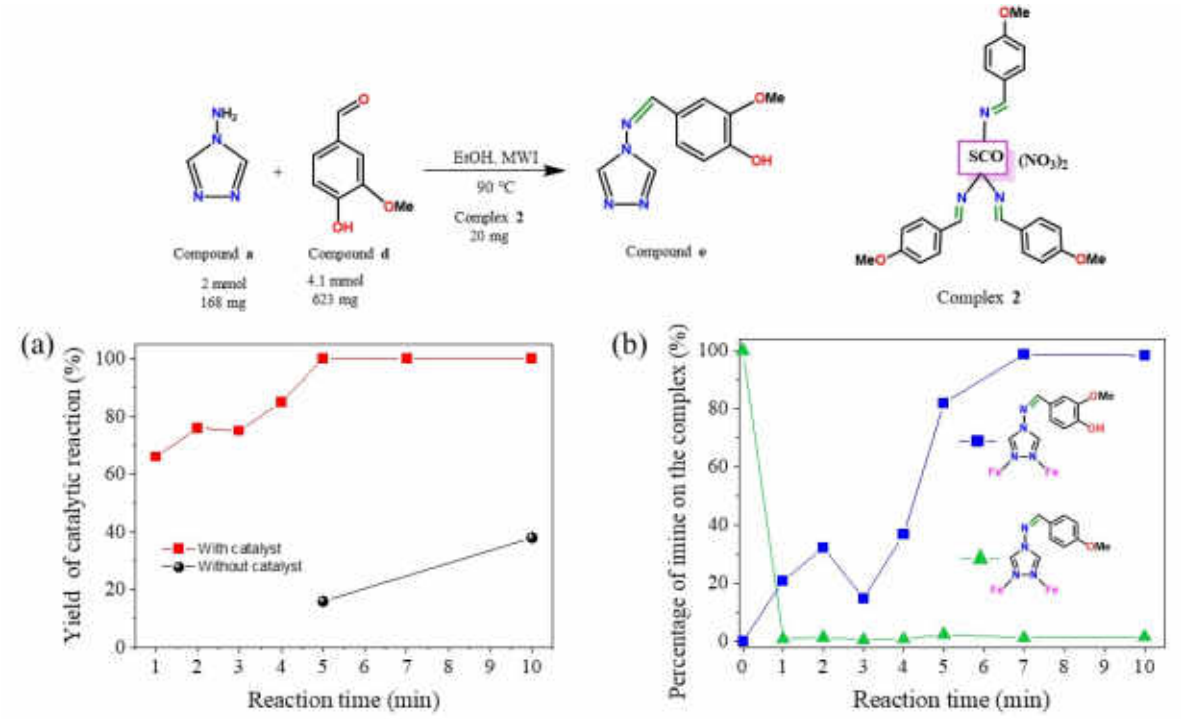


Fig. 3-24 Kinetic study of the catalysis reaction. a) yield of imine **e** as a function of reaction time; b) percentage of imine functionality on the complex recovered after catalysis as a function of reaction time.

3.6.1.2 Study of the presence of a catalytic amount of imine complex 4 in the reaction between aminotriazole a and p-anisaldehyde b

In parallel, we also wished to investigate the reaction between aminotriazole **a** and aldehyde **b**, which is catalyzed by the imine complex **4**. The imine complex **4** was synthesized via a PSM reaction between amine complex **1** and vanillin **d** (see experiment section 3.8.1.6). The catalytic efficiency of complex **4** was then evaluated in the reaction between aminotriazole **a** and *p*-anisaldehyde **b**. The kinetic study showed that the reaction did not progress between 5 and 10 minutes (around 60%), and in 15 minutes the yield was 86% (Fig. 3-25). An analysis of the composition of the complex recovered after various catalysis reaction times revealed that after just 2 minutes, only a small percentage of imine functions from complex **4** remained. In contrast to the previous experiment, all complexes recovered at different reaction times exhibited a very low percentage of imine. This suggests that the imine formed on the complex reacts immediately with aminotriazole **a**, resulting in the reaction medium containing predominantly the amine complex **1**. So, the complex in the reaction medium is almost exclusively the amine complex **1**, which as observed before needs longer reaction times, in agreement with what it is observed here.

These two investigations conclude that the entire initial complex was changed within the first two minutes. The complex could therefore go through many cycles of the two PSM reactions.

Table 3-7 Yields of catalytic reaction between aminotriazole **a** and *p*-anisaldehyde **b**

Entry	Reaction	Yield
1	2 min	34%
2	5 min	63%
3	7 min	61%
4	10 min	64%
5	12 min	76%
6	15 min	86%

Experimental conditions for catalysis reaction: 20 mg complex, 4.1 mmol aldehyde, 1.8 ml ethanol, 2 mmol aminotriazole, reaction carried out at 90°C under MWI irradiation. Before carrying out the catalytic reaction, the suspension of complex **4** in ethanol was sonicated for 10 minutes at room temperature.

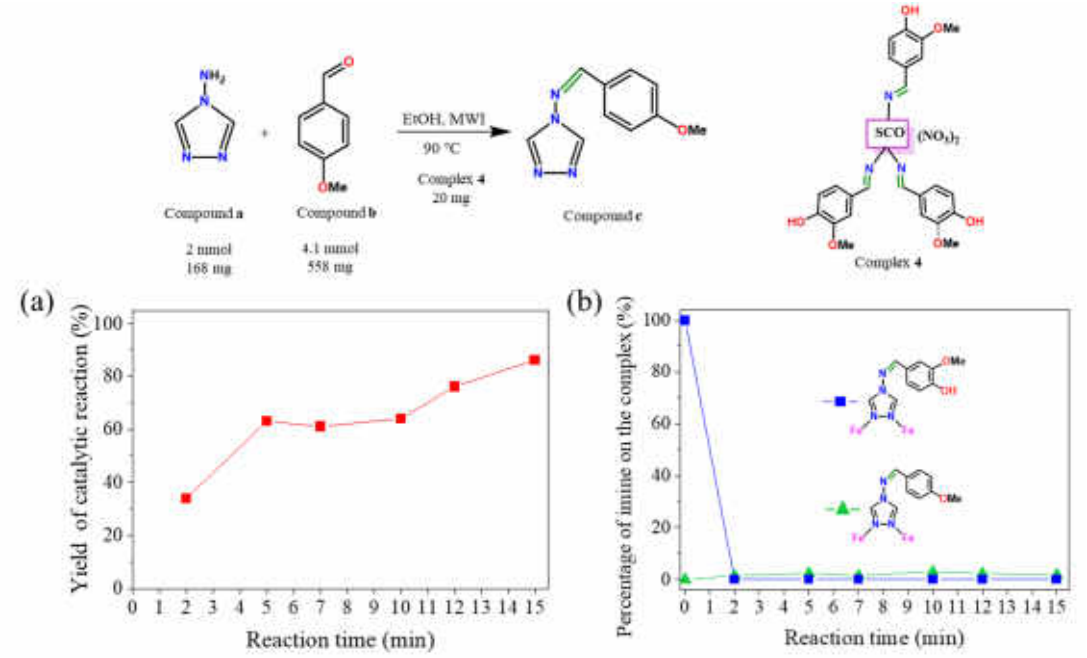


Fig. 3-25 Kinetic study of the catalysis reaction. a) yield of imine **c** as a function of reaction time; b) percentage of imine functionality, on the complex recovered after catalysis, as a function of reaction time.

3.6.2 Competitive reaction using aminotriazole, imine complex and aldehyde

3.6.2.1 Competitive reaction using aminotriazole a, imine complex 2 and vanillin d

Finally, we would like to determine whether aminotriazole exhibits a preferential reactivity toward complex **2** or vanillin **d**. For this reason, a competitive reaction was conducted under the conditions described in Fig. 3-26. This experiment was designed to evaluate whether PSM reactions are involved in the catalytic mechanism or are simply secondary reactions. If PSM reactions are involved in the mechanism, we would expect imine **c** to be formed preferentially from complex **2**. On the other hand, if complex **2**, as a Lewis acid (cationic) catalyst, is present in stoichiometric quantities, it should promote the formation of imine **e** even more than when it is present in catalytic quantities. In this case, the quantitative formation of imine **e** should be

observed within a few minutes.

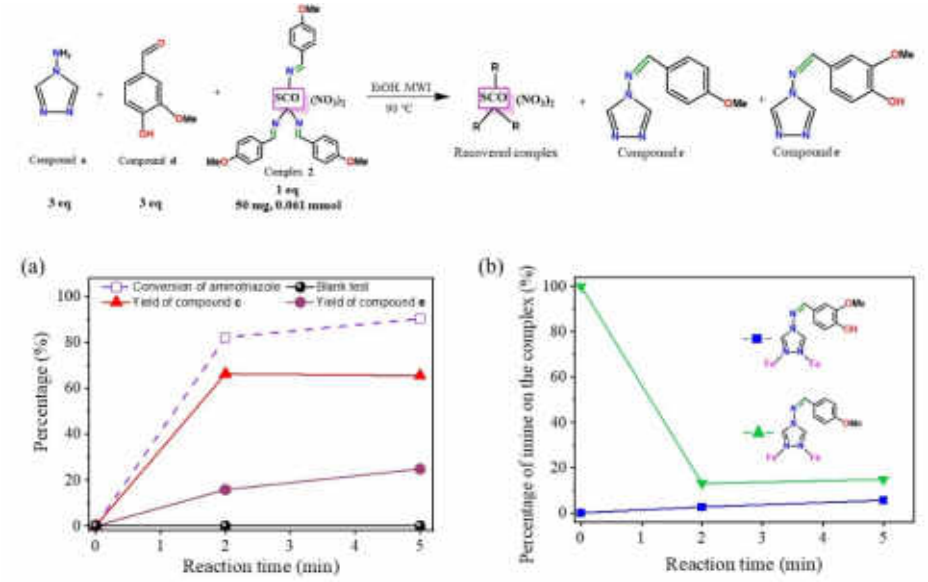


Fig. 3-26 Kinetic study of the competitive reaction. a) yields of imine **c** and **e** as a function of reaction time; b) percentage of imine functionality on the complex recovered after catalysis as a function of reaction time.

Within 5 minutes of reaction time, 90% of aminotriazole **a** is converted. It should be noted that the reaction is initially very rapid, as only around 20% of amine **a** remains after just 2 minutes (Fig. 3-26). Regardless of the reaction duration, imine **c** is predominantly formed. For instance, after 2 minutes of reaction, the quantity of imine **c** exceeds that of imine **e** by more than fourfold. The complexes recovered after the competitive reaction indicate that less than 20% of the original imine functions remain in complex **2**. As previously observed, aminotriazole **a** reacts very rapidly with complex **2**; however, between the second and fifth minute, the percentage of remaining imine remains relatively constant. Moreover, the recovered complex retains imine functions formed by the interaction of the NH_2 groups of the complex with vanillin **d**. Thus, the formation of imine **e** may result either from the reaction between aminotriazole **a** and vanillin **d**, or from the interaction of amine **a** with the imine functions present on the complex. These findings suggest that PSM reactions on the complex may, at least in part, contribute to its catalytic activity. In addition, we repeated the experiment to confirm its reproducibility. Fig. 3-27 shows consistent results for the competitive reaction of aminotriazole, vanillin and complex **2**, consistent with previous results.

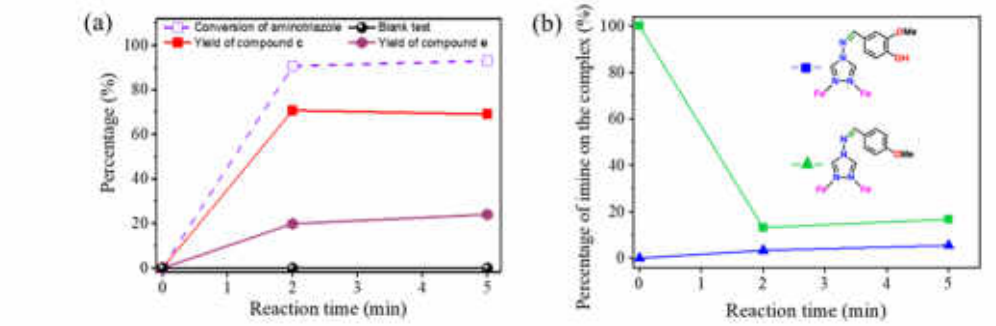


Fig. 3-27 Reproducible results of kinetic study of the competitive reaction. a) yields of imine **c** and **e** as a function of reaction time; b) percentage of imine functionality on the complex recovered after catalysis as a function of reaction time.

3.6.2.2 Competitive reaction using aminotriazole a, imine complex 2 and p-anisaldehyde b

In parallel, the competitive reaction involving aminotriazole **a**, imine complex **4**, and *p*-anisaldehyde **b** was tested (Fig. 3-28). The preferential attack of aminotriazole **a** on complex **4** was consistently observed, as imine **e** was formed in much greater quantities than imine **c**, regardless of the reaction time. This competitive reaction proceeds at a slower rate than the previous one, indicating that the attack of aminotriazole **a** on complex **4** is less favored compared to its reaction with complex **2**. One possible explanation for this difference in reactivity is the increased steric hindrance of the substituent on complex **4**, which could impede ligand exchange on the iron centre. The recovered complexes contain traces of imine formed by the interaction of the NH_2 groups of the complex with aldehyde **b**. The presence of approximately 30% of the imine functions from the initial complex may promote the formation of imine functions on the complex through reaction with aldehyde **b**. The rapid attack of aminotriazole **a** on these imine functions likely accounts for the low quantity of this type of imine function remaining on the complex. Consequently, the formation of imine **c** may result either from the reaction between amine **a** and aldehyde **b** or from ligand exchange on the iron complex.

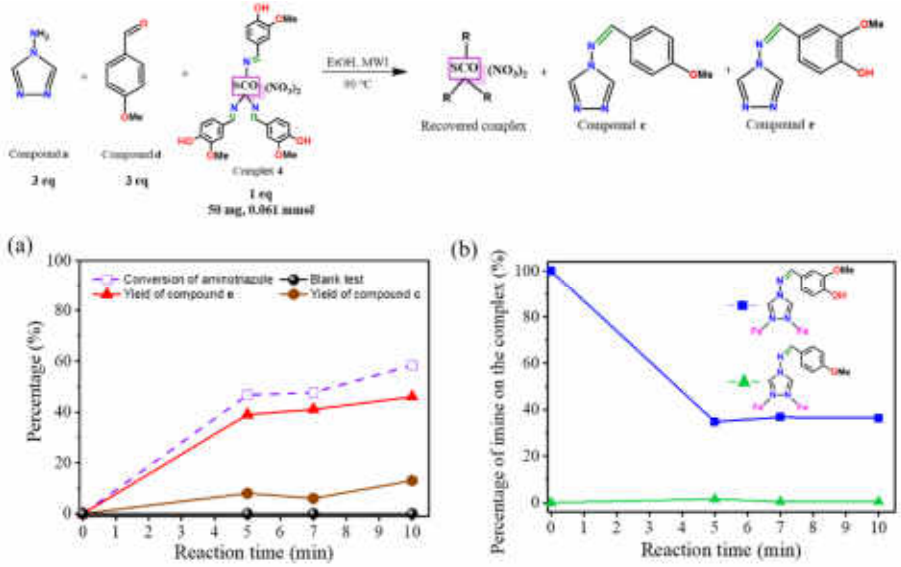


Fig. 3-28 Kinetic study of the competitive reaction. a) yields of imine **c** and **e** as a function of reaction time; b) percentage of imine functionality, on the complex recovered after catalysis, as a function of reaction time.

The competitive reaction of aminotriazole, *p*-anisaldehyde and complex **4** with a reaction time of 5 min also was repeated. Experimental results indicate the conversion of 43.8% aminotriazole and yields of imine **c** and imine **e** of 7.6% and 36.2% respectively. Moreover, the recovered complex also was analysed by digestion method, and the result shown the composition of the complex was 0.3% of imine ligand **c**, 46.5% of imine ligand **e** and 53.3% of aminotriazole. These results are consitent with previous results.

3.7 Conclusion

In conclusion, the reactivity of aminotriazole **a** toward aldehydes was compared with that of the NH_2 functional groups present in the $Fe(NH_2trz)_3(NO_3)_2$ complex **1**. Within 10 minutes of

reaction, the PSM reaction on complex **1** was quantitative, while under the same experimental conditions, only 10% of the imine was formed from aminotriazole. This result indicates that a reaction involving an insoluble reagent is not necessarily slower than one in which all reagents are in solution. Additionally, it illustrates how coordination with a metal can significantly alter the organic reactivity of the ligand. Therefore, combining the PSM method with a reaction, such as the digestion of the complex to de-coordinate the ligand from iron, presents an interesting approach for synthesizing new triazole-based organic molecules.

Subsequently, a competitive reaction was performed using a mixture containing stoichiometric amounts of complex **1**, aminotriazole **a**, and aldehyde **b**. The experimental results from this competitive reaction showed the quantitative formation of imine **c** in solution, while the recovered complex corresponded to amine complex **1**. The fact that the competitive reaction outcome was completely opposite to the results of the individual experiments led us to consider that the spin-crossover iron complex may catalyze the formation of imine from aminotriazole **a**. This is a significant finding because, to the best of our knowledge, it represents only the second example in the literature of the use of this family of complexes in catalysis.

Experimental studies of the catalytic reaction revealed that when amine complex **1** was pre-treated with aldehyde **b**, the catalytic reaction was quantitative in less than 10 minutes, with the amount of iron complex equivalent to 2.3% molar relative to aminotriazole **a**. Analysis of the iron complex recovered after the catalytic reaction provided several key insights. First, as expected, pre-treatment of the amine complex with aldehyde led to the formation of imine complex **2** via PSM reaction. While the presence of trace iron(III) complexes cannot be entirely ruled out, a significant proportion of the iron complex remained in the +2 oxidation state during both the pre-treatment and catalysis reactions. Furthermore, when the amine complex **1** was used without pre-treatment, and the catalytic reaction was complete with no remaining aminotriazole **a** in solution, the recovered complex corresponded to amine complex **1** with traces of imine functions. Interestingly, when amine complex **1** was pre-treated or imine complex **2** was used as a catalyst, the percentage of imine functions on the complex remained below 15% from the first minute until the catalytic reaction was complete. The formation of the amine complex can be attributed to the reaction of aminotriazole **a** with imine complex **2**. We proposed two possible mechanisms for this PSM reaction: trans-imination and/or ligand exchange at the iron center. Experiments using aminotriazole **a*** with ^{15}N suggest that the PSM reaction proceeds predominantly via ligand exchange. SEM charaterization revealed that while the complexes recovered, before the catalytic reaction was complete, exhibited molecular arrangement and spin-crossover properties similar to the starting amine complex **1**. The particles from the pre-treated amine complex or the imine complex were significantly different in size and shape from the original amine complex. Additionally, the conditions under which the PSM reaction of amine complex **1** with aldehyde was carried out had a significant effect on the morphology of the resulting imine complex **2** particles. Thus, performing a PSM reaction with an aldehyde followed by a PSM reaction with aminotriazole **a** on imine complex **2** enables the particle morphology of amine complex **1** to be modified without compromising its SCO properties. This finding is relevant not only for heterogeneous catalysis, where particle size and shape influence catalytic activity, but also for the integration of SCO compounds into devices.

The catalytic activity of the iron(III) imine complex was found to be comparable to that of the iron(II) imine complex. This is surprising, as iron(III) complexes are generally stronger Lewis acids than their iron(II) counterparts, and imine formation from aldehydes is typically catalyzed efficiently by Lewis acids. However, based on our results, we are confident that the iron(II) complex remains in this oxidation state during the catalytic reaction. Therefore, we conclude that the reaction mechanism is unlikely to be of the Lewis acid type and instead may involve PSM reactions. Two types of experiments were conducted to support this hypothesis. The first

set of experiments showed that after just one minute of catalysis, very few imine functions from the initial complex remained, while imine functions originating from the aldehyde used as a catalytic substrate were visible on the complex. This result suggests that the amine complex can rapidly undergo multiple catalytic cycles involving two PSM reactions, a crucial factor for the involvement of PSM reactions in the catalytic mechanism. The second type of experiment involved a competitive reaction in which the reaction mixture contained stoichiometric amounts of aminotriazole **a**, aldehyde, and imine complex **2**. The preferential attack of aminotriazole **a** on imine complex **2** rather than on the aldehyde supports a mechanism involving PSM reactions. In a Lewis acid mechanism, the presence of the complex in non-catalytic quantities would have greatly favored the attack of aminotriazole **a** on the aldehyde. This research, combined with our recent findings on the strong influence of spin state on the efficiency of the PSM method in this iron complex, suggests that spin-crossover complexes could be promising candidates for the development of switchable catalysis.

3.8 Experiment section

3.8.1 Materials synthesis

3.8.1.1 Synthesis of $[Fe(NH_2trz)_3](NO_3)_2$, complex 1

2.78 g (10 mmol) of $FeSO_4 \cdot 7H_2O$ and 1.5g of ascorbic acid were dissolved in 10 mL of deionised water in an Erlenmeyer flask. In a separate Erlenmeyer flask, 2.61 g (10 mmol) of $Ba(NO_3)_2$ were dissolved in 20 mL of deionised water. Both solutions were heated slowly until the reagents were completely dissolved. Then, the solution containing the iron sulfate was added to the solution of barium nitrate, which resulted in an immediate precipitation of barium sulfate. The suspension was left to cool down to room temperature and then centrifuged, resulting in 30 mL of a 0.333 M solution of $Fe(NO_3)_2$.

2.52 g (30 mmol) of 4-amino-1,2,4-triazole was added in 10 mL of EtOH in an Erlenmeyer flask, and then 30 mL of a freshly prepared 0.333 M solution of $Fe(NO_3)_2$ was added to it under vigorous stirring; the mixture was left stirring during 4 h resulting in a pink slurry. It was centrifuged and washed 3 times with 20 mL of ethanol and then 3 times with 20 mL of diethyl ether, after which it was dried in the oven at 70°C.

3.8.1.2 Synthesis of nanoparticles of complex 1

Two equivalent micellar solutions were prepared: 160 mL of cyclohexane, 72 mL of n-pentanol and 57 g of triton X-100 were vigorously mixed. To this mixture, 756 mg (9 mmol) of 4-amino-1,2,4-triazole dissolved in 20 mL of distilled water were added dropwise to obtain the first microemulsion, 20 mL of a 0.15 M $Fe(NO_3)_2$ solution was added dropwise to obtain the second microemulsion. These microemulsions were stirred at room temperature for about 15-20 minutes until a clear solution was observed, then the second microemulsion was added to the first one, and it was kept under vigorous stirring overnight. Then 500 mL of ethanol was added to destroy the microemulsion, the obtained nanoparticles were centrifuged and washed several times with ethanol to remove traces of the surfactant and then several times with diethyl ether, after which it was dried in the oven at 70°C.

3.8.1.3 Synthesis of [Fe(NH2-trz)3](SO4), complex 1b

5.45 g of 4-amino-1,2,4-triazole (60 mmol) were dissolved in 12 mL of deionised water in an

Erlenmeyer flask, 5.56 g of $Fe(SO_4)_2 \cdot 7H_2O$ (20 mmol) were dissolved in 12 mL of deionised water in a separate Erlenmeyer flask; the iron sulfate solution was added to the triazol solution and it was stirred like this for 40 h resulting in a pink slurry. It was centrifuged and washed 3 times with 20 mL of ethanol and then 3 times with 20 mL of diethyl ether, after which it was dried in the oven at 70°C.

3.8.1.4 Synthesis of imine complex 2 from complex 1

500 mg of the SCO complex 1, 3 mL of EtOH, and 500 µl of *p*-anisaldehyde were added to a vial, then it was immersed in a 90 °C oil bath for 1h. After the reaction was complete, it was then washed 3 times with diethyl ether, after which it was dried in the oven at 70°C.

3.8.1.5 Synthesis of Iron III complex (complex 3)

The Iron III complex was obtained in our previous study.[1] 500 mg of the SCO complex 1, 3 mL of Butanol, and 500 µl of p-anisaldehyde (for synthesis, Sigma-Aldrich, after distillation) were added to a vial, then it was immersed in a 90 °C oil bath for 3h. After the reaction was complete, it was then washed 3 times with diethyl ether, after which it was dried in the oven at 70°C.

3.8.1.6 Synthesis of imine complex 4 from complex 1

500 mg of the SCO complex **1**, 3 mL of EtOH, and 3 ml of a freshly prepared 0.004 **M** EtOH solution of Vanillin were added to a vial; then it was under the microwave indication at 90 °C for 10 min. After the reaction was complete, it was washed 3 times with EtOH and then washed 3 times with diethyl ether, after which it was dried in the oven at 70°C.

3.8.1.7 Synthesis of [$^{15}N_4$] 4-amino-1,2,4- triazole

500 mg (3.78 mmol) of ^{15}N2-hydrazine sulfate was suspended in 5 mL of distilled water and then it was added 100 ml (2.65 mmol) of formic acid was added to it and then under stirring, 770 mg (7.69 mmol) of potassium carbonate was added. The mixture was stirred like this at room temperature until there was no more bubbles coming from the reaction, then it was refluxed for about 18 h, and then in a drysyn bath it was heated to 200 °C for 6 h, during which the water was removed with the help of a Dean-Stark trap. After cooling, the remaining solid was suspended in ethanol and filtrated under vacuum, the solution was then left to crystallize, resulting in 35 mg (28%).

^{1}H-NMR (CD_3OD, 400 MHz): 8.43 ppm (m, 2H), 6.21 ppm (d, J=72 Hz, NH_2); ^{13}C-NMR (CD_3OD, 100 MHz): 145.8 ppm (dd, J=13.6, 2.2 Hz); ^{15}N-INEPT (CD_3OD, 40.5 MHz): -77.9 ppm (C=**N**, d, J=13.7 Hz), -197.1 ppm (C-**N**-NH_2, dd, J=13.0, 6.7 Hz), -319.5 ppm (**N**H_2).

3.8.1.8 Test for ligand exchange reaction with ^{15}N-aminotriazole

50 mg (0.061 mmol) of the complex **2** was suspended in 2 mL (17.5 mg, 0.178 mmol) of the previously prepared solution containing the ^{15}N-aminotriazole; then it was heated under MWI at 90 °C for 20 min. The mixture was then centrifuged, a sample of the solution was added to d_6-DMSO and the remaining solid was recovered and dried under vacuum.

3.8.2 The general procedure of the catalytic reaction

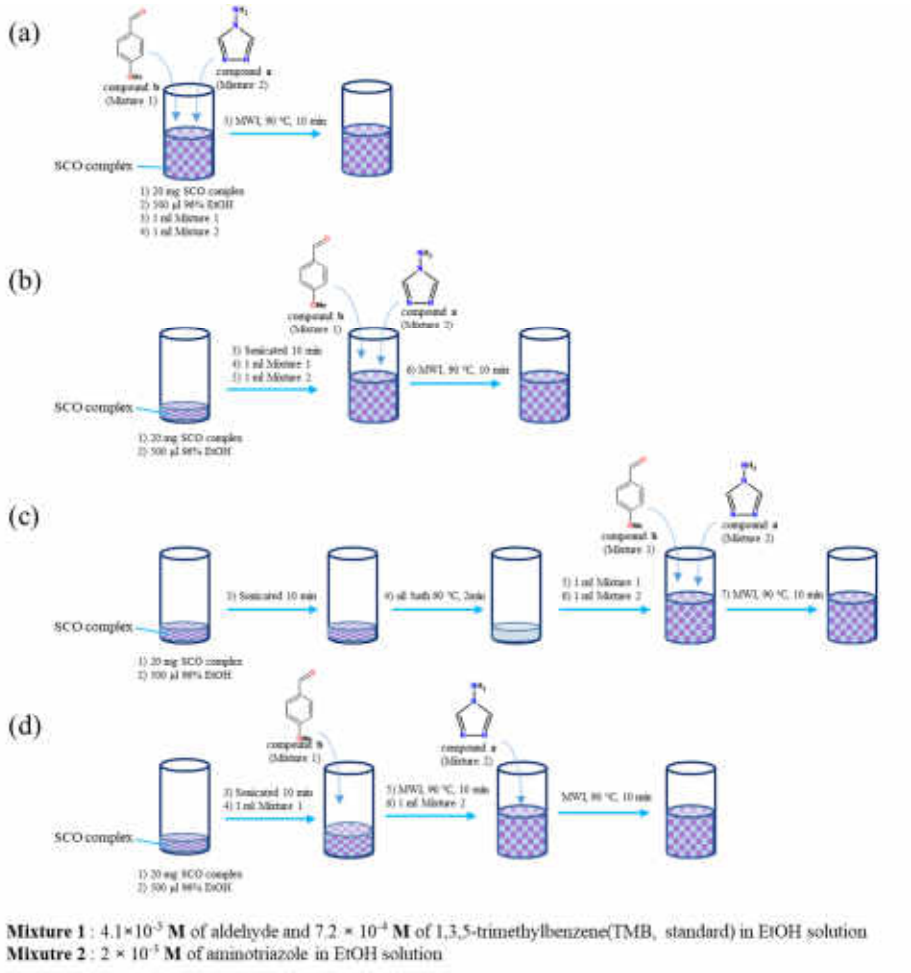


Fig. 3-29 Scheme of the experiment procedures (a)Without additional process. (b) With sonication. (c) With sonication and heating (d) With Pre-treatment.

Preparation of Mixtures

Two mixtures were prepared prior to the experiment. **Mixture 1** was prepared in a volumetric flask containing 4.1 × 10^{-3} **M** of aldehyde and 7.2 × 10^{-4} M of 1,3,5-trimethylbenzene (TMB, used as an internal standard) in absolute EtOH. **Mixture 2** was prepared in a separate volumetric flask containing 2 × 10^{-3} **M** of aminotriazole in absolute EtOH.

Typically, 96% EtOH was used as the solvent for suspending the complex, while absolute EtOH was used as the solvent for preparing **Mixture 1** and **Mixture 2**. If any specific solvent was used in the experiments, it will be highlighted in the text.

Procedure without additional processing :

For the catalytic reaction without additional process (Fig. 3-29 (a)), 20 mg of the complex was suspended in 0.5 ml of 96% EtOH. Then, 1 ml of **Mixture 1** and 1 ml of **Mixture 2** were added to the vial. The total reaction mixture consisted of 20 mg of complex, 4 mmol (558 mg) of aldehyde, 2 mmol (168mg) of aminotriazole, 100µl of TMB and 1.8 ml of EtOH. The vial was then sealed and subjected to microwave irradiation (MWI) for a specified period. Following the reaction, the mixture was centrifuged to separate the solid from the solution. The solution was

analyzed by ^{1}H NMR, and the recovered complex was washed once with absolute EtOH and twice with diethyl ether.

Procedure with sonication:

For the procedure with sonication (Fig. 3-29 (b)), 20 mg of the complex was suspended in 0.5 ml of 96% EtOH in a vial, which was then placed in a sonication bath for 10 minutes. Subsequently, 1 ml of **Mixture 1** and 1 ml of **Mixture 2** were added, and the vial was sealed and subjected to MWI for a specified period. The rest of the procedure followed the steps as previously described.

Procedure with Sonication and Heating:

For the procedure with sonication and heating (Fig. 3-29 (c)), 20 mg of the complex was suspended in 0.5 ml of 96% EtOH in a vial, which was then sonicated for 10 minutes. The vial was then subjected to MWI for 10 minutes. After cooling to room temperature, 1 ml of **Mixture 1** and 1 ml of **Mixture 2** were added, and the vial was sealed and subjected to MWI for the specified duration. The rest of the procedure followed the steps as previously described.

Procedure with Pre-treatment:

For the procedure with pre-treatment process (Fig. 3-29 (d)), 20 mg of the complex was suspended in 0.5 ml of 96% EtOH in a vial and sonicated for 10 minutes. Afterward, 1 ml of **Mixture 1** was added to the vial, which was then sealed and subjected to MWI for 10 minutes. After cooling to room temperature, 1 ml of **Mixture 2** was added, and the vial was sealed and subjected to MWI for the specified period. The rest of the procedure followed the steps as previously described.

3.8.3 Calculation of yield of catalytic reaction

To compare different experiments and ensure the amounts of reactants are added in all experiments, TMB is used as an internal standard. To determine the conversion and yield of the reaction, the ^{1}H-NMR is measured in DMSO-d6 after the reaction finishes. The spectra were recorded on either a Bruker Avance 300 or a Bruker Avance 400 spectrometer at 298 K.

$$n_{compound} = n_{TMB} \times \frac{I_{compound}}{I_{TMB}} \times \frac{\#H_{TMB}}{\#H_{compound}}$$

Where $I_{TMB}, I_{compound}$ corresponds to the integration of a specific peak, $\#H_{TMB}, \#H_{compound}$ to the number of hydrogens that corresponds to the integrated peak.

In all the spectra, we put the integration of the peak of TMB at 6.73 ppm to 3, which corresponds to 3 hydrogens. So, we can simplify the calculation

$$\boldsymbol{n_{compound}} = n_{TMB} \times \frac{I_{compound}}{\#H_{compound}}$$

The yield can be calculated.

$$\boldsymbol{Yield} = \frac{n_{imine\ compound}}{n_{aminotriazole} + n_{imine\ compound}} \times 100\%$$

3.8.4 The methodology used for the digestion and quantification of the percentage of imine functionality on the complex

We use the digestion method to quantify the percentage of imine functionality on the complex. Detailed information about the digestion method is already described in the experiment section of Chapter 2.

3.8.5 Calculation of conversion and yield (for competitive reaction)

To compare different experiments and ensure the amounts of reactants are added in all experiments, TMB is used as an internal standard. To determine the conversion and yield of the reaction, the ^{1}H-NMR is measured in DMSO-d6 after the reaction finishes. The spectra were recorded on either a Bruker Avance 300 or a Bruker Avance 400 spectrometer at 298 K.

$$n_{compound} = n_{TMB} \times \frac{I_{compound}}{I_{TMB}} \times \frac{\#H_{TMB}}{\#H_{compound}}$$

Where $I_{TMB}, I_{compound}$ corresponds to the integration of a specific peak, $\#H_{TMB}, \#H_{compound}$ to the number of hydrogens that corresponds to the integrated peak.

In all the spectra, we put the integration of the peak of TMB at 6.73 ppm to 3, which corresponds to 3 hydrogens. So, we can simplify the calculation

$$n_{compound} = n_{TMB} \times \frac{I_{compound}}{\#H_{compound}}$$

The conversion of aminotriazole and the yield can be cacultated.

$$\boldsymbol{Conversion}\ (aminotriazole) = \frac{n_{compound\ \boldsymbol{c}} + n_{compound\ \boldsymbol{e}}}{n_{compound\ \boldsymbol{a}} + n_{compound\ \boldsymbol{c}} + n_{compound\ \boldsymbol{e}}} \times 100\%$$

$$\boldsymbol{Yield}\ (compound\ \boldsymbol{c}) = \frac{n_{compound\ \boldsymbol{c}}}{n_{compound\ \boldsymbol{a}} + n_{compound\ \boldsymbol{c}} + n_{compound\ \boldsymbol{e}}} \times 100\%$$

$$\boldsymbol{Yield}\ (compound\ \boldsymbol{e}) = \frac{n_{compound\ \boldsymbol{e}}}{n_{compound\ \boldsymbol{a}} + n_{compound\ \boldsymbol{c}} + n_{compound\ \boldsymbol{e}}} \times 100\%$$

3.8.6 Selected NMR spectra

3.8.6.1 Selected NMR spectra of the catalytic reaction

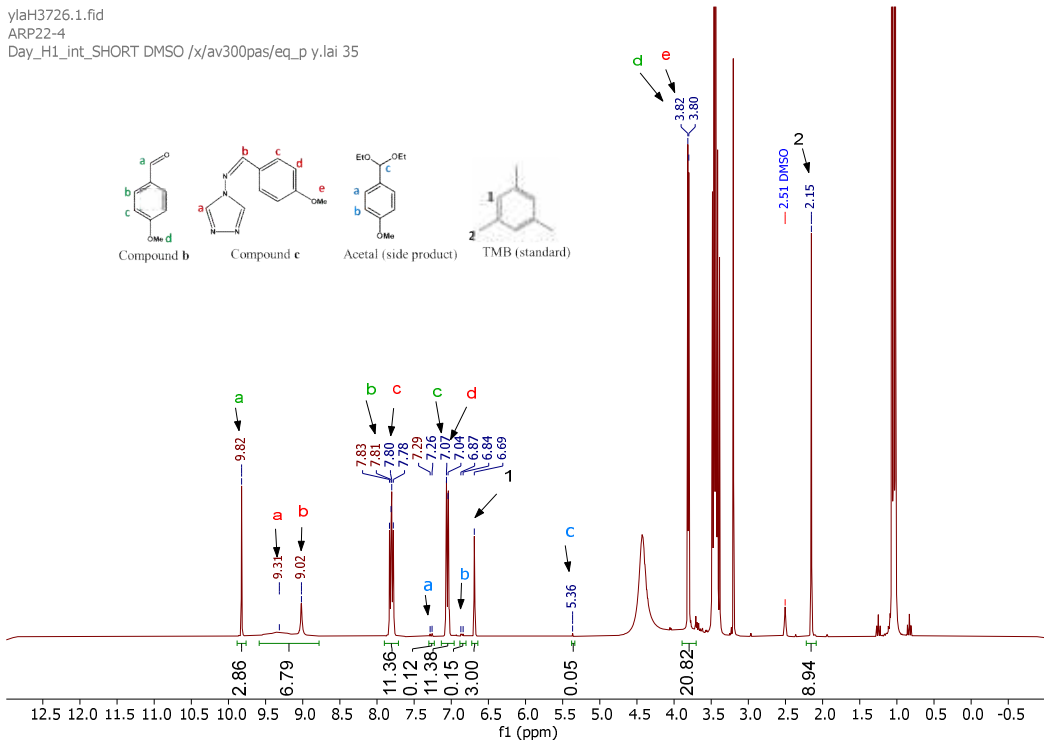


Fig. 3-30 ^{1}H NMR (DMSO-d6) of the mixture solution after 10 min reaction of *p*-anisaldehyde and aminotriazole using complex **1** (with pre-treatment) as the catalyst.

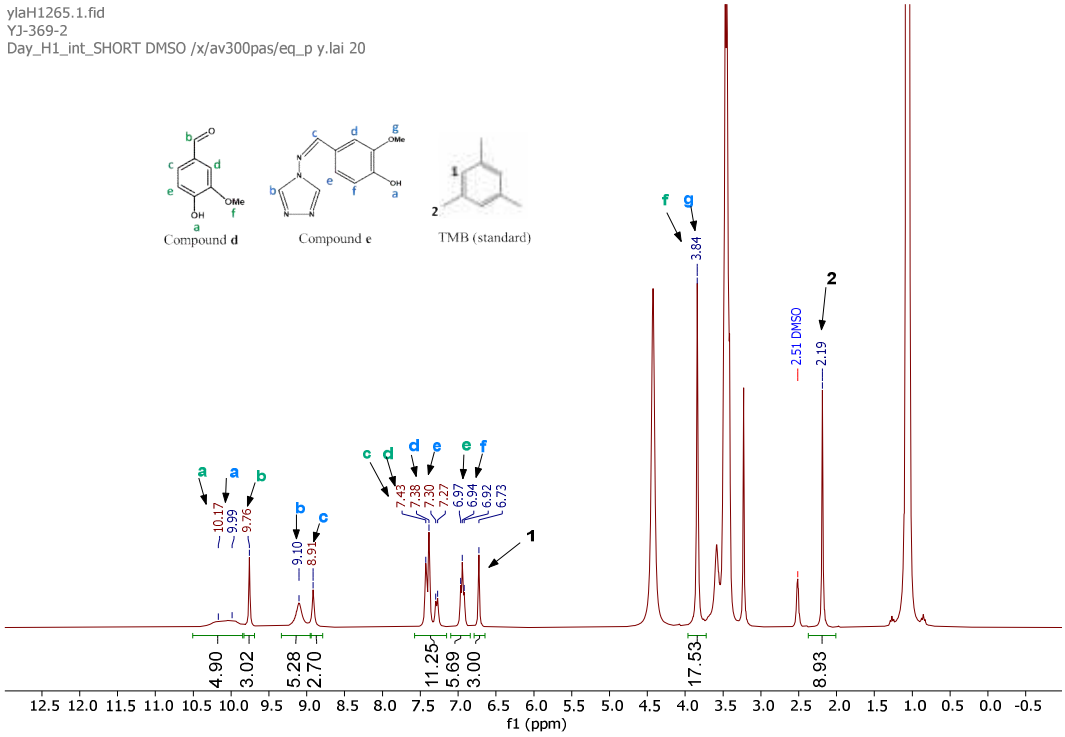


Fig. 3-31 ^{1}H NMR (DMSO-d_6) of the mixture solution after 10 min reaction of vanillin and aminotriazole using complex **1** (with pre-treatment) as the catalyst.

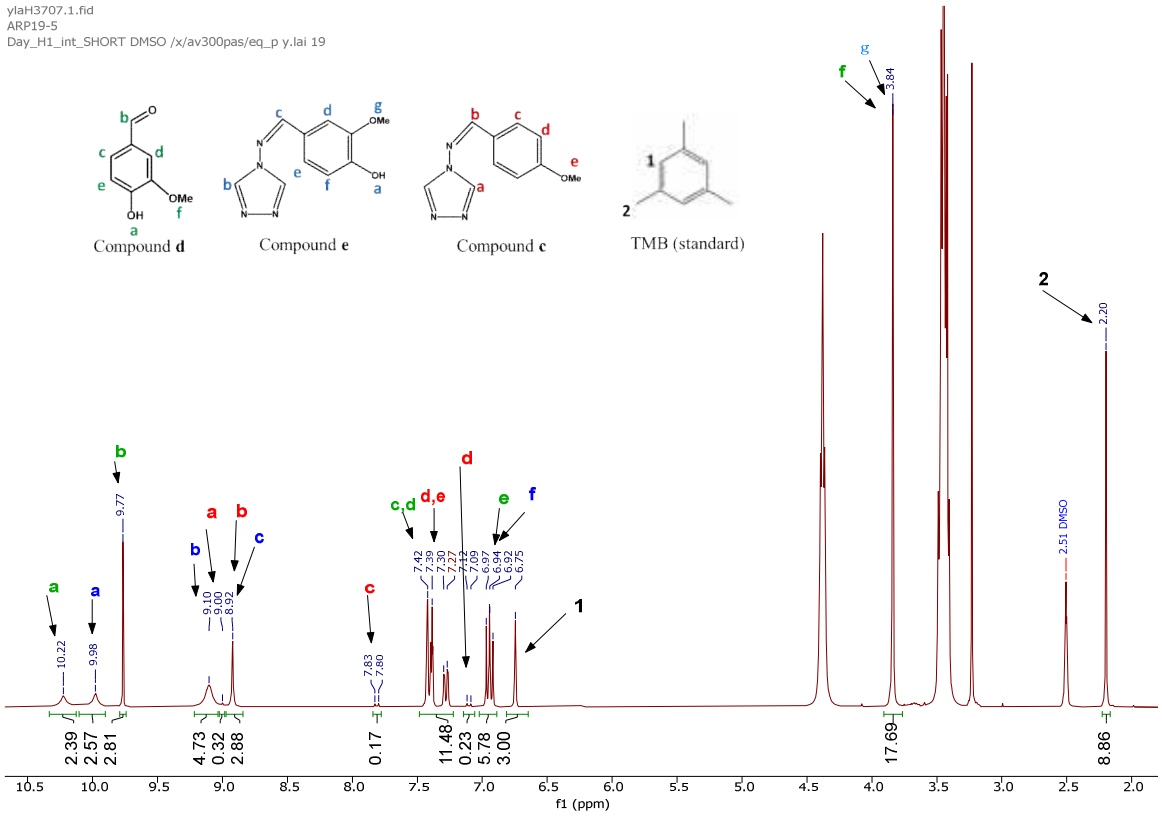


Fig. 3-32 ^{1}H NMR (DMSO-d6) of the mixture solution after 10 min reaction of vanillin **d** and aminotriazole **a** using complex **2** as the catalyst.

3.8.6.2 Selected NMR spectra of the digested samples

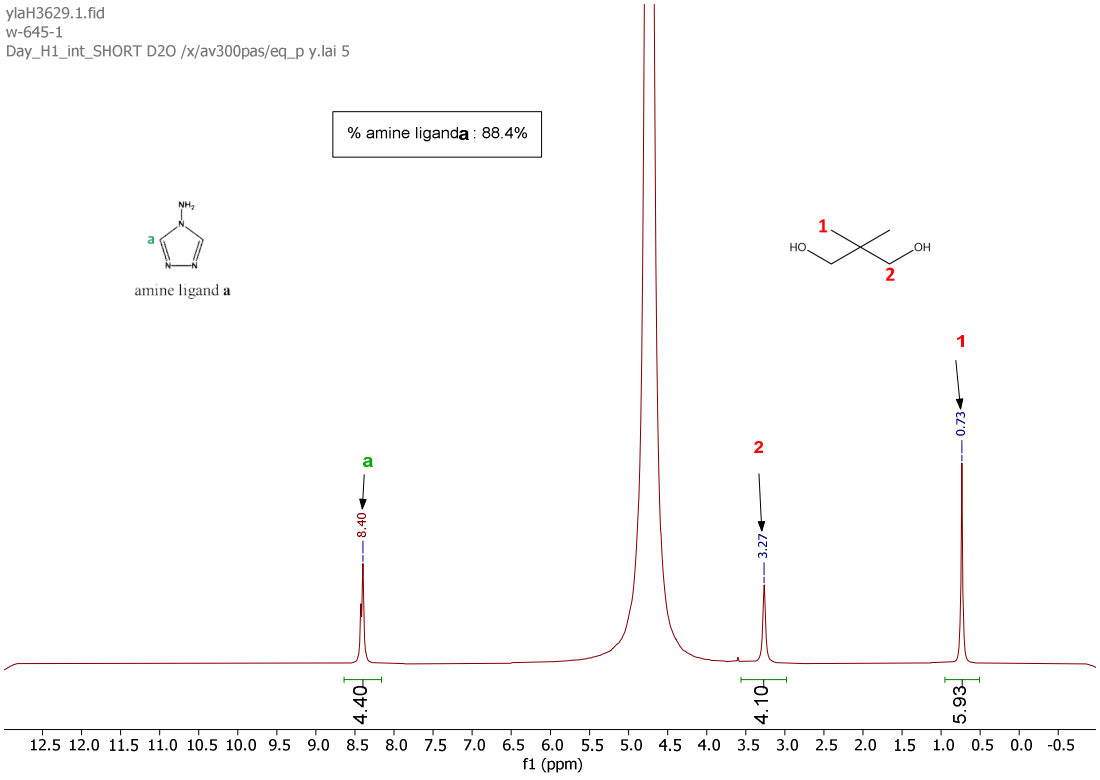


Fig. 3-33 ^{1}H NMR (D_2O) of the digestion of the complex recovered after 5 min of reaction of *p*-anisaldehyde and aminotriazole using complex **1** (with pre-treatment) as catalyst.

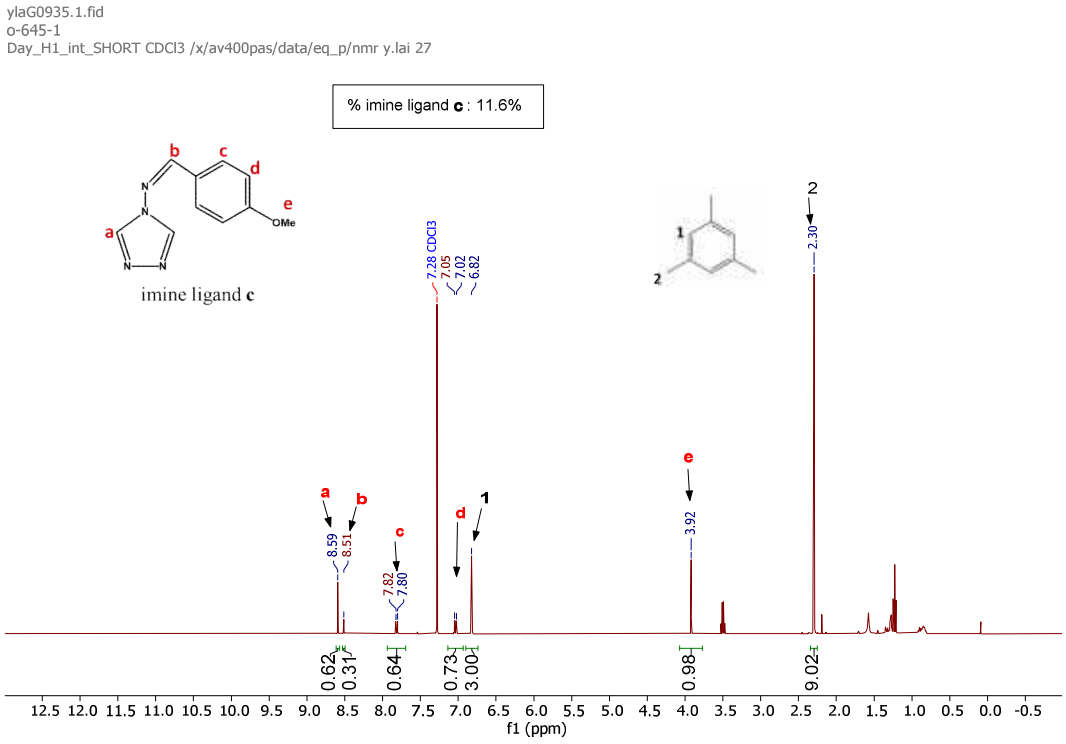


Fig. 3-34 ^{1}H NMR ($CDCl_3$) of the digestion of the complex recovered after 5 min of reaction of *p*-anisaldehyde and aminotriazole using complex **1** (with pre-treatment) as catalyst.

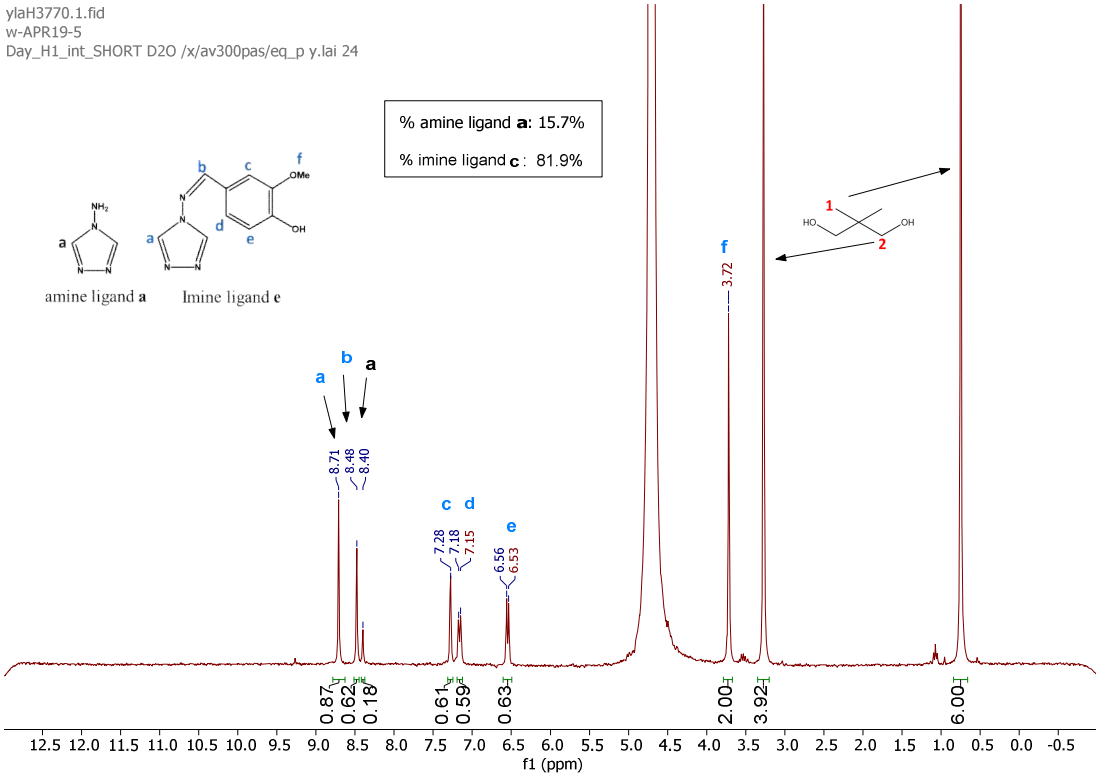


Fig. 3-35 ^{1}H NMR (D_2O) of the digestion of the complex recovered after 5 min of reaction of vanillin and aminotriazole using complex **2.**

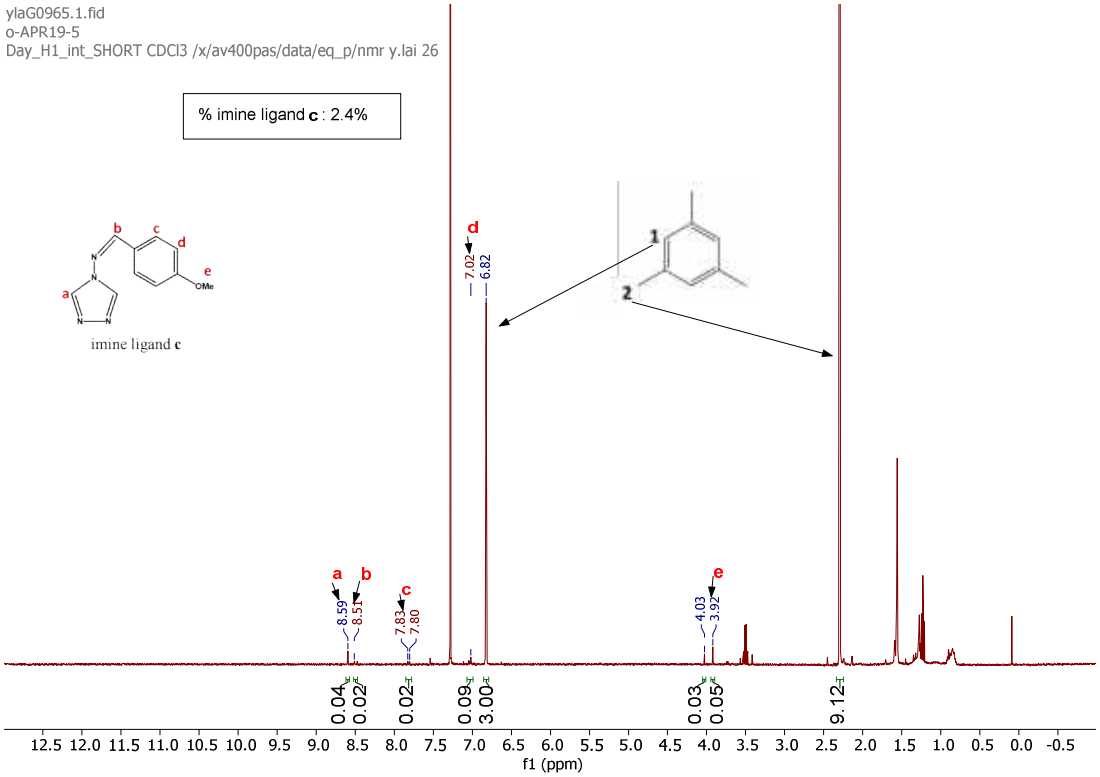


Fig. 3-36 ^{1}H NMR ($CDCl_3$) of the digestion of the complex recovered after 5 min of reaction of vanillin and aminotriazole using complex **2.**

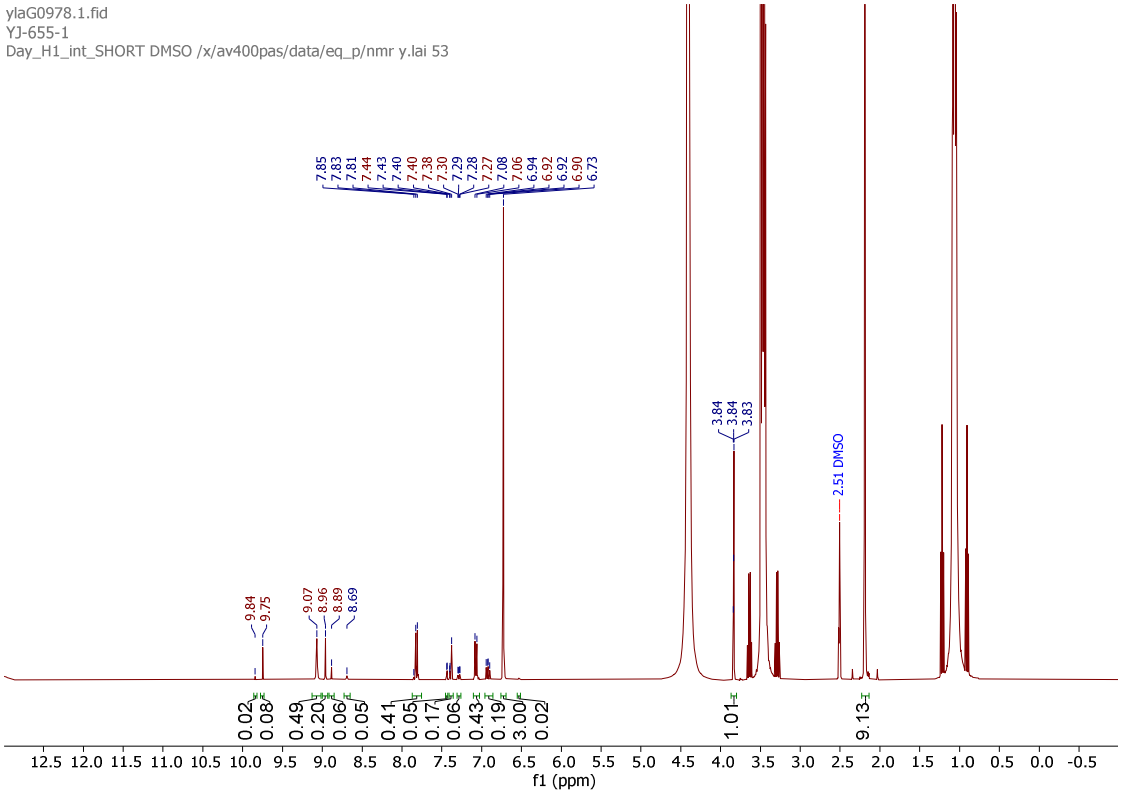


Fig. 3-37 ^{1}H NMR (DMSO-d6) of the mixture solution after 2 min reaction of vanillin and aminotriazole using complex 2 as the catalyst (competitive reaction).

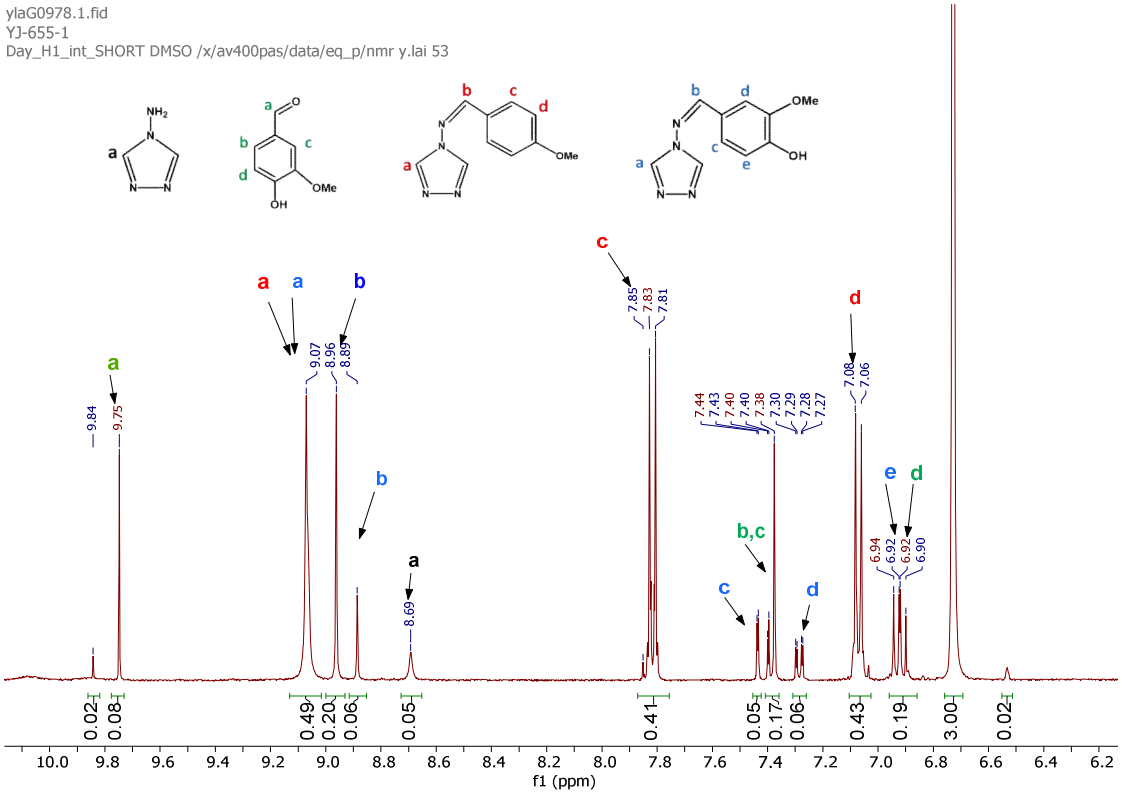


Fig. 3-38 The corresponding zoom-in spectrum of Fig. 3-37

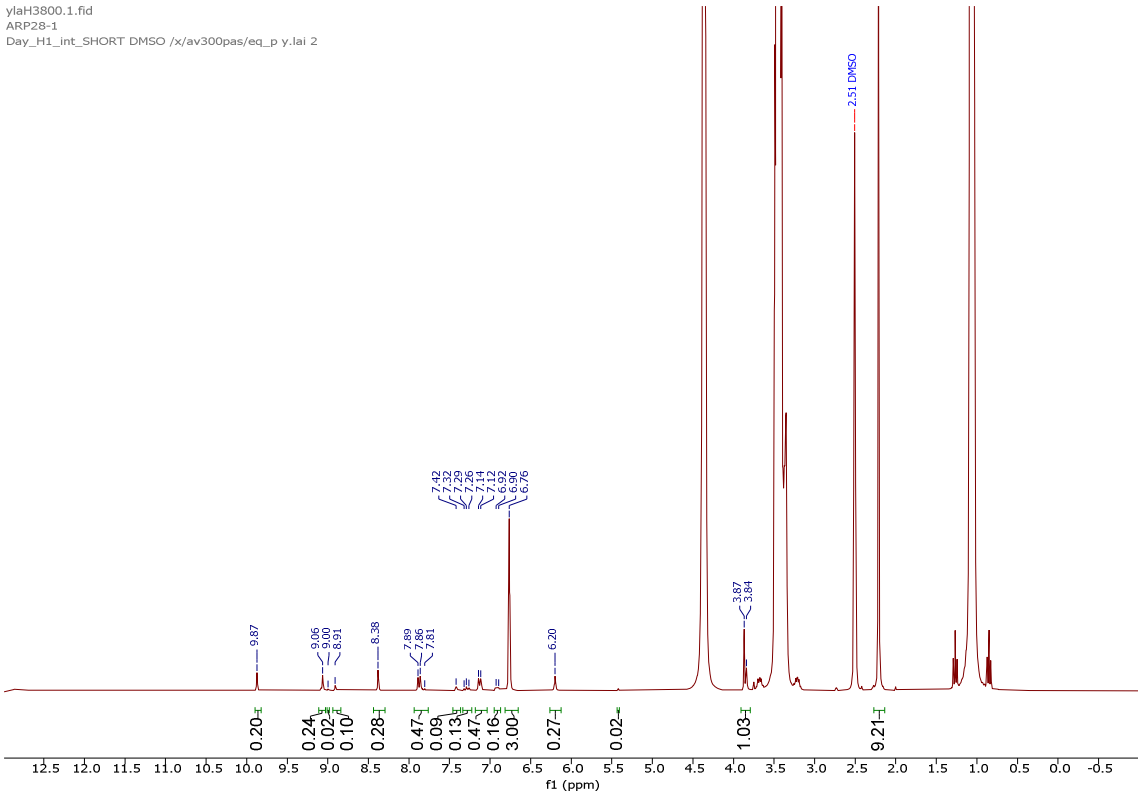


Fig. 3-39 ^{1}H NMR (DMSO-d6) of the mixture solution after 5 min reaction of *p*-anisaldehyde and aminotriazole using complex **3** as the catalyst. (competitive reaction)

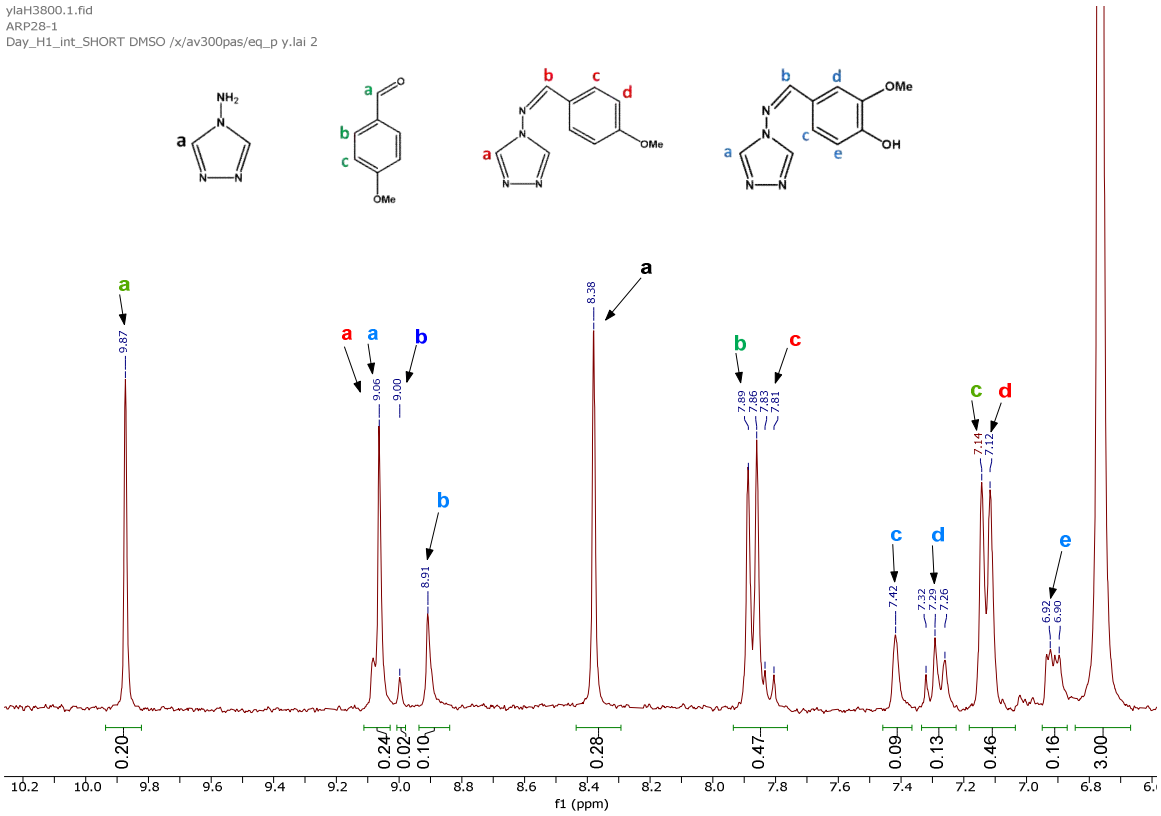


Fig. 3-40 The corresponding zoom-in spectrum of Fig. 3-39

3.9 References

[1] A. Enriquez-Cabrera, L. Getzner, L. Salmon, L. Routaboul, A. Bousseksou, Post-synthetic modification mechanism for 1D spin crossover coordination polymers, *New J. Chem.* **2022**, 46, 22004-22012.

[2] R. Tokala, S. Bale, I.P. Janrao, A. Vennela, N.P. Kumar, K.R. Senwar, C. Godugu, N. Shankaraiah, Synthesis of 1,2,4-triazole-linked urea/thiourea conjugates as cytotoxic and apoptosis inducing agents, *Bioorg. Med. Chem. Lett.* **2018**, 28, 1919-1924.

[3] Q. Zhang, X. Liu, W. Gan, J. Wu, H. Zhou, Z. Yang, Y. Zhang, M. Liao, P. Yuan, S. Xu, P. Zheng, W. Zhu, Discovery of Triazolo-pyridazine/-pyrimidine Derivatives Bearing Aromatic (Heterocycle)-Coupled Azole Units as Class II c-Met Inhibitors, *ACS Omega* **2020**, 5, 16482-16490.

[4] N. Thamban Chandrika, S.K. Shrestha, H.X. Ngo, O.V. Tsodikov, K.C. Howard, S. Garneau-Tsodikova, Alkylated Piperazines and Piperazine-Azole Hybrids as Antifungal Agents, *J. Med. Chem.* **2017**, 61, 158-173.

[5] A. Günther, Y. Deja, M. Kilic, K. Tran, P. Kotra, F. Renz, W. Kowalsky, B. Roth, Investigation of the molecular switching process between spin crossover states of triazole complexes as basis for optical sensing applications, *Scientific Reports* **2024**, 14.

[6] W.J. Wang, Z.H. Sun, S.C. Chen, J.F. Qian, M.Y. He, Q. Chen, Microwave‐assisted fabrication of a mixed‐ligand [Cu4(μ3‐OH)2]‐cluster‐based metal–organic framework with coordinatively unsaturated metal sites for carboxylation of terminal alkynes with carbon dioxide, *Appl. Organomet. Chem.* **2021**, 35.

[7] I.y.A. Gural'skiy, S.I. Shylin, V. Ksenofontov, W. Tremel, Spin‐State‐Dependent Redox‐Catalytic Activity of a Switchable Iron (II) Complex, *Eur. J. Inorg. Chem.* **2017**, 2017, 3125-3131.

[8] G.-Z. Huang, Y.-S. Xia, F. Yang, W.-J. Long, J.-J. Liu, J.-P. Liao, M. Zhang, J. Liu, Y.-Q. Lan, On–off switching of a photocatalytic overall reaction through dynamic spin-state transition in a Hofmann clathrate system, *J. Am. Chem. Soc.* **2023**, 145, 26863-26870.

[9] M. Isegawa, Mechanism of Photocatalytic CO2 Reduction by Iron Spin-Crossover Complex with Copper Photosensitizer, *Organometallics* **2022**, 41, 3568-3580.

[10] I. Prat, A. Company, T. Corona, T. Parella, X. Ribas, M. Costas, Assessing the impact of electronic and steric tuning of the ligand in the spin state and catalytic oxidation ability of the FeII (Pytacn) family of complexes, *Inorg. Chem.* **2013**, 52, 9229-9244.

[11] A. Bell-Taylor, J.D. Gorden, E.E. Hardy, C.R. Goldsmith, A spin-crossover Co (II) complex catalyzes the activation of sp3 C–H bonds by two-electron oxidants, *Inorg. Chim. Acta* **2018**, 482, 206-212.

[12] G. Arora, T. Sahni, S. Sharma, D. Verma, Green Tamarind Extract Catalyzed Synthesis of 4-Amino-1,2,4-Triazole Derivatives and Their In-vitro Antimicrobial Activity, *International Research Journal of Pure and Applied Chemistry* **2020**, 44-56.

[13] V. Shalabaeva, K. Ridier, S. Rat, M.D. Manrique-Juarez, L. Salmon, I. Séguy, A. Rotaru, G. Molnár, A. Bousseksou, Room temperature current modulation in large area electronic junctions of spin crossover thin films, *Appl. Phys. Lett.* **2018**, 112.

[14] A.-M. Li, E. Rentschler, 1,2,4-Triazole Schiff base directed synthesis of polynuclear iron complexes: Investigating the magnetic properties going from a dimer to a 1D chain to a 3D framework, *Polyhedron* **2018**, 154, 364-372.

[15] S.-H. Zhang, J.-M. Wang, H.-Y. Zhang, Y.-P. Fan, Y. Xiao, Highly efficient electrochemiluminescence based on 4-amino-1,2,4-triazole Schiff base two-dimensional Zn/Cd coordination polymers, *Dalton Trans.* **2017**, 46, 410-419.

[16] A.M. Li, T. Hochdörffer, J.A. Wolny, V. Schünemann, E. Rentschler, FeII Complexes with Triple N1,N2‐Triazole Bridge Schiff Base Ligand: Antiferromagnetic Dimer vs. Spin Conversion Trimer, *Eur. J. Inorg. Chem.* **2018**, 2018, 4190-4199.

[17] B.S. Creaven, M. Devereux, A. Foltyn, S. McClean, G. Rosair, V.R. Thangella, M. Walsh, Quinolin-2(1H)-one-triazole derived Schiff bases and their Cu(II) and Zn(II) complexes:

Possible new therapeutic agents, *Polyhedron* **2010**, 29, 813-822.
[18] S.-M. Zhang, H.-Y. Zhang, Q.-P. Qin, J.-W. Fei, S.-H. Zhang, Syntheses, crystal structures and biological evaluation of two new Cu(II) and Co(II) complexes based on (E)-2-(((4H-1,2,4-triazol-4-yl)imino)methyl)-6-methoxyphenol, *J. Inorg. Biochem.* **2019**, 193, 52-59.
[19] H. Nabipour, S. Rohani, Y. Hu, A bio-based vanillin ligand to remove silver ions from a waste stream and utilizing it to improve the fire safety of an epoxy thermoset and its thermal conductivity, *Journal of Environmental Chemical Engineering* **2024**, 12, 112121.
[20] H. Nabipour, H. Niu, X. Wang, S. Batool, Y. Hu, Fully bio-based epoxy resin derived from vanillin with flame retardancy and degradability, *Reactive and Functional Polymers* **2021**, 168, 105034.
[21] H. Eshghi, M. Bakavoli, J. Abedini-Torghabeh, M. Rahimizadeh, Efficient synthesis of novel 9H-xanthen-9-yl derivatives of bidentate heterocyclic nucleophiles by Fe(HSO4)3 as a catalyst, *Chin. Chem. Lett.* **2012**, 23, 1153-1156.
[22] A. Enríquez‐Cabrera, K. Ridier, L. Salmon, L. Routaboul, A. Bousseksou, Complete and versatile post‐synthetic modification on iron‐triazole spin crossover complexes: a relevant material elaboration method, *Eur. J. Inorg. Chem.* **2021**, 2021, 2000-2016.
[23] J.I. Padrón, V.S. Martín, Catalysis by means of Fe-based lewis acids, *Iron Catalysis: Fundamentals and Applications* **2011**, 1-26.
[24] D. Gajan, G. Lapadula, M. Schwarzwälder, C. Copéret, La RMN à l'état solide: Un outil clef pour la compréhension moléculaire des catalyseurs hétérogènes bien-définis, *L'Actualité chimique* **2012**, 2013, 82-89.
[25] F. HENOT, B. VIBERT, J. Boisbouvier, La RMN des protéines de haute masse moléculaire : importance du marquage isotopique, *L'Actualité chimique* **2024**, 491, 63-64.
[26] R.M. Claramunt, D. Sanz, S.H. Alarcón, M. Pérez Torralba, J. Elguero, C. Foces-Foces, M. Pietrzak, U. Langer, H.-H. Limbach, 6-Aminofulvene-1-aldimine: A Model Molecule for the Study of Intramolecular Hydrogen Bonds, *Angewandte Chemie International Edition* **2001**, 40, 420-423.
[27] D. Sanz, M. Pérez-Torralba, S.H. Alarcón, R.M. Claramunt, C. Foces-Foces, J. Elguero, Tautomerism in the solid state and in solution of a series of 6-aminofulvene-1-aldimines, *The Journal of Organic Chemistry* **2002**, 67, 1462-1471.

Chapter 4 Spin state effect on the catalytic activation of acetalization reaction

4.1 Introduction

We demonstrated in Chapter 2 that the PSM reaction with aldehyde performed from complex **1** ($[Fe(NH_2trz)_3](NO_3)_2$) at HS state led to higher yields than the reaction with complex **1** at LS state.[1] This study highlights the significant effect of the spin state on the organic reactivity of a functional group present in a metal complex. This result demonstrates that the spin state effect is not restricted to the atoms coordinated directly to the metal, and had an effect on the reactivity of the whole ligand. Next, we have shown that complex **1** catalyzes the formation of imine from aldehyde and aminotriazole.[2] We have evidence in support of a catalytic mechanism involving two PSM reactions. The first PSM reaction occurs between aldehyde and complex **1**, leading to imine complex **2**. The second PSM reaction is the attack of imine complex **2** by aminotriazole, leading to amine complex **1** and the release of the desired imine into the solution. In line with our work previously published in the literature,[3-6] the solvent also plays an important role in the catalytic activity of complex **1**. Indeed, we assume that solvents such as EtOH or MeOH enable better separation of the polymeric chains of complex **1**, allowing better contact between the catalytic substrate and the catalytic part of complex **1**.

These results suggest that manipulating the spin state can be a strategic approach to modulate the catalytic efficiency of SCO complexes. If this is possible, SCO complexes will become versatile tools for catalysis. In the upcoming chapter, we will further explore the impact of the spin state on catalysis, providing a comprehensive study of how modulating spin states can influence catalytic activation in various chemical reactions. Our aim is to offer a detailed understanding of the potential applications and benefits of using spin crossover complexes as switchable catalysts. This investigation will not only enhance our understanding of the spin crossover phenomenon but also pave the way for the development of innovative catalytic systems that can respond to external stimuli, thereby improving their effectiveness and efficiency in different chemical processes.

It is important to note that the team initiated this project before the start of my thesis. In particular, Livia Getzner carried out experiments on the catalytic use of this SCO complex during her Master's thesis. They obtained some of the results discussed in this chapter (sections 4.3, 4.4 and 4.6).

4.2 Presentation of our scientific approach

4.2.1 Criteria we considered when selecting the catalyst

We can foresee that in order to study the effect of the spin state on the catalytic efficiency of a SCO complex, the latter will have to satisfy a number of conditions. Firstly, the SCO complex will obviously have to possess catalytic activity. It is also evident that the temperature at which the catalytic reaction will take place must fall within the SCO temperature range of the complex. Therefore, for an initial study, it is preferable to choose a complex whose spin transition takes place above room temperature. On the other hand, the effect of the spin state on the catalytic properties of the complex will be easier to observe if the spin transition is abrupt. However, as the spin transition is induced by the application of a stimulus such as a change in temperature, it is impossible to determine whether the change in reactivity is due to the change in spin state

or to the change in reaction parameter. Ideally, therefore, the SCO complex should possess a large thermal hysteresis loop, as the catalytic efficiency of both spin states of the complex can be evaluated under strictly identical experimental conditions. The presence of a hysteresis cycle arises from strong cooperative effects between the molecules of the SCO complex, implying that the complex will have to remain in the solid state during the catalytic reaction. It should be noted that, in heterogeneous catalysis, efficient access to the catalytic site by the substrates is key to the activity of the complex. Complex **1** is an ideal candidate for this strategy. As discussed in previous chapters, complex **1** belongs to the iron-triazole family of compounds, which are characterised by 1D polymer chains with counter anions interspersed to maintain charge equilibrium. These compounds exhibit notable SCO properties, featuring a significant thermal hysteresis loop and a transition temperature above room temperature. Furthermore, the compound is insoluble in organic solvents, and even more importantly for us, particles of complex **1** suspended in EtOH exhibit SCO properties similar to those of pure complex **1** in the solid state (Fig. 4-1). This means the presence of abrupt spin transitions above room temperature and, above all, a considerable thermal hysteresis cycle of around 40 °C. As in Chapter 2, where we studied the effect of spin state on the efficiency of the PSM reaction on complex **1**, we will use the thermal hysteresis cycle to compare the catalytic performance of the two spin states of complex **1** under the same experimental conditions (reaction will be carried out at 55°C). Finally, the research work described in Chapter 3 has enabled us to demonstrate a catalytic activity for complex **1**.

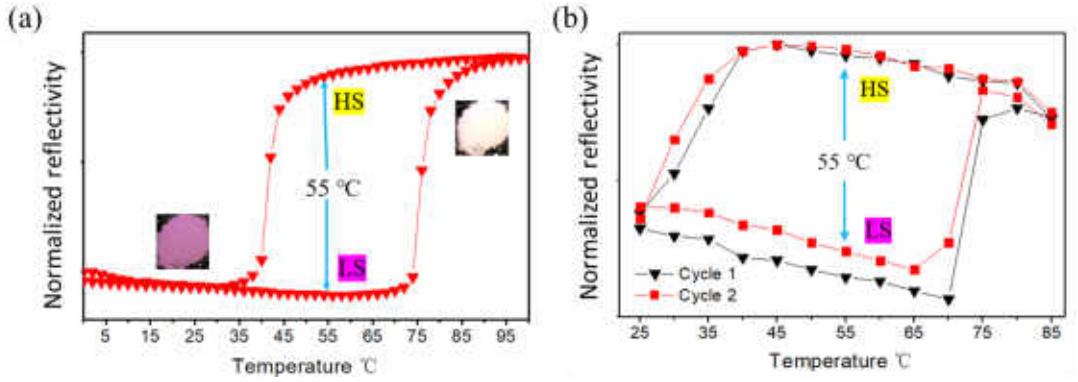


Fig. 4-1 Various temperature optical reflectivity experiments of complex **1** (a) in solid state (b) of particles of complex **1** in suspension in EtOH.

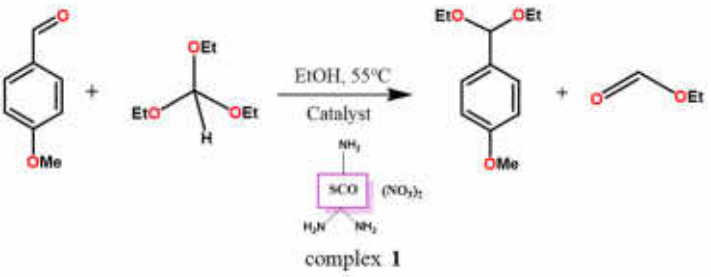
4.2.2 Criteria we considered when choosing the catalytic reaction

Several conditions must be met when selecting a catalytic reaction to study the spin state effect on catalytic activation. First, the reaction should be conducted within a temperature range of 40-75 °C. Second, neutral reaction conditions should be maintained, and the use of redox agents should be avoided to preserve the integrity of the SCO material. Furthermore, since complex **1** is used as a catalyst, it is very important that the reaction takes place in EtOH or MeOH. As mentioned in the previous chapters of this thesis, the use of EtOH leads to greater spacing of the polymeric chains,[3, 5] which is essential for effective contact between the catalytic site of the complex and the catalytic substrates. Finally, this study would be facilitated if the formation of the desired product in the reaction crude could be quantified using conventional analytical techniques such as liquid NMR or gas chromatography. From our previous research, we know that complex **1** is reactive towards aldehyde, and that this reactivity can be modulated by the spin state of the complex.[1] For this reason, we decided that one of the substrates for catalysis would be aldehyde. In the complex **1** catalyzed formation of imine from aminotriazole, we

observed the formation of a small amount of acetal.[2] We therefore decided to study the catalyzed formation of acetals. This reaction, which is very simple to set up and well documented, meets all the criteria mentioned in this paragraph.

4.3 Study of the effect of spin state on the catalytic activity of the $[Fe(NH_2trz)_3](NO_3)_2$).

The reaction involving *p*-anisaldehyde and the triethyl orthoformate ($CH(OEt)_3$), which leads to the synthesis of 1-(diethoxymethyl)-4-methoxybenzene, was chosen as a model of the catalytic reaction (Scheme 4-1). The experimental conditions used were inspired by the work of Mike Kotke and Peter R. Schreiner[7] and adapted to the use of complex **1** as a catalyst, in particular, the catalytic reaction carried out at 55°C.



Scheme 4-1 Reaction model selected to study the effect of spin state on the catalytic efficiency of complex **1**.

Before discussing the results in detail, it is important to explain how the experiments, using the two spin states of complex **1**, were carried out. Stabilization of the complex in its different spin states was carried out using the same strategy as that used to study the effect of spin state on the efficiency of the PSM reaction (Chapter 2). Preparing complex **1** in the LS state is straightforward. Complex **1**, which is in the LS state at room temperature, is suspended in EtOH, then this suspension is placed in the bath at 55°C (Fig. 4-2).

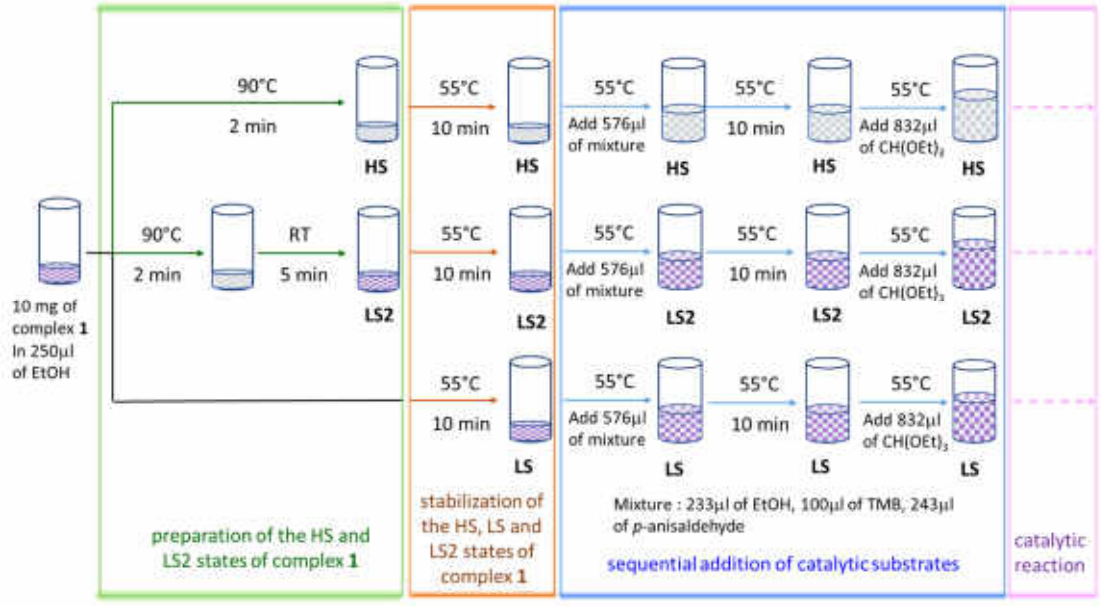
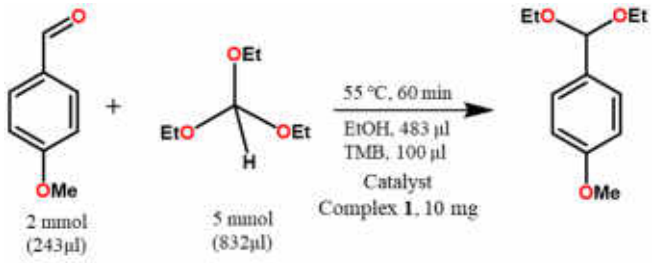


Fig. 4-2 Schematic representation of the catalytic reaction process.

The HS state was obtained by heating the suspension of complex **1** particles in EtOH at 90°C for 2 minutes (Fig. 4-2). The transition from the LS to the HS state is highlighted by the change in colour of the suspension (from pink to white). The suspension was then immediately transferred to a bath at 55°C, and the white colour of the suspension confirms that complex **1** remains in the HS state. It is important to mention that heating the suspension of complex **1** in EtOH to 90°C, which is necessary to obtain the HS state, may also have an impact on the molecular arrangement of complex **1**. To differentiate the effect of the spin state from that of possible molecular rearrangement, we also studied the complex in the LS2 state. The difference in catalytic activity between complex **1** in the HS state and that in the LS2 state will be attributed to the spin state of complex **1**, whereas the difference in catalytic activity between the complex in the LS state and that in the LS2 state will be attributed to a change in molecular arrangement induced by the heating to 90°C. Complex **1** in the LS2 state was prepared by heating the suspension of complex **1** in EtOH at 90°C for 2 minutes (as for the HS state, the suspension turns white), then the suspension was left at room temperature for 5 minutes (the pink colour of the suspension indicates that the complex **1** is in the low-spin state). Finally, the suspension is placed in the oil bath at 55°C (Fig. 4-2). It is very important to emphasize that the sequential addition of catalytic substrates begins after the suspensions of complex **1** in EtOH have been stabilized for 10 min at 55°C. In this way, the catalytic capacities of complex **1** in the different spin states are evaluated under strictly identical experimental conditions. So, after keeping the three suspensions at 55°C for 10 minutes, a preheated aldehyde solution was added to each suspension. After a further 10 minutes at 55°C, preheated triethyl orthoformate was added to each suspension, and it was immediately after this last addition that the catalytic time began.

As we had no information on the catalytic capacity of complex **1** in the acetalization reaction described in Table 4-1, we arbitrarily chose to start with a reaction time of one hour. We were very pleased with the results:

Table 4-1 The catalytic capacity of complex **1** in the acetalization reaction



Entry	Catalyst	Reaction time	Yield (%)			
			HS	LS2	LS	Δ (HS-LS2)
1	complex **1**	60 min	90%	87%	77%	3%
2	Without complex	60 min	No reaction			

1) First of all, as expected, the yield of the reaction can be easily and indisputably estimated by measuring the ^{1}H NMR of the reaction crude. As an example, the ^{1}H NMRs of crude reactions carried out under identical experimental conditions (Entry 1 in Table 4-1) using the different spin states of complex **1**, as well as in the absence of catalys (Entry 2 in Table 4-1). The ^{1}H NMR yields could be precisely determined by the presence of a known amount of mesitylene (TMB) in the reaction medium (as shown in Fig. 4-2, this is one of the constituents of the mixture which is added just after stabilization, at 55°C, of the spin states of complex **1**). To check that we were indeed considering the whole amount of aldehyde added, we systematically verified that the ratio $(n_{aldehyde} + n_{acetal})/n_{TMB}$ corresponded to the initial ratio

$n_{aldehyde}$ /n_{TMB}. It is also worth mentioning that, prior to NMR analysis, the reaction crude was filtered on celite. On the one hand, to avoid any traces of paramagnetic compounds, and on the other, to remove the complex **1** and thus prevent the catalysis reaction from continuing in the NMR tube.

2) In the absence of complex **1**, acetal formation is not observed, whereas in the presence of complex **1**, medium to high yields are obtained. Complex **1** thus catalyzes acetal formation. It should be noted that, although it will not be discussed hereafter, the blank was automatically run in parallel with the experiments with complex **1**. Systematically, under the experimental conditions studied, no acetal formation is observed in the absence of complex **1**.

3) More importantly, it appears that the spin state of complex **1** may have an effect on the catalytic capacity of complex **1**. The quasi-quantitative yield obtained for complex **1** in the HS state is not ideal for truly estimating the difference between the HS and LS2 states. The reaction time must therefore be less than one hour. In order to choose the best reaction time, we decided to carry out a kinetic study of the catalysis reaction.

The results of the kinetic study are shown in Fig. 4-3 (a). Before discussing the results obtained in greater detail, it is important to note that this kinetic study was not carried out by taking a sample of the same reaction medium at the desired time, but by carrying out independent reactions at the desired time. This applies to all the kinetic studies presented in this chapter. Furthermore, wherever possible, we preferred to carry out the entire kinetic study on the same day (in particular, using the same mixture for all experiments), but systematically, for each reaction time, studies of the catalytic efficiency of the different spin states of complex **1** were carried out in parallel.

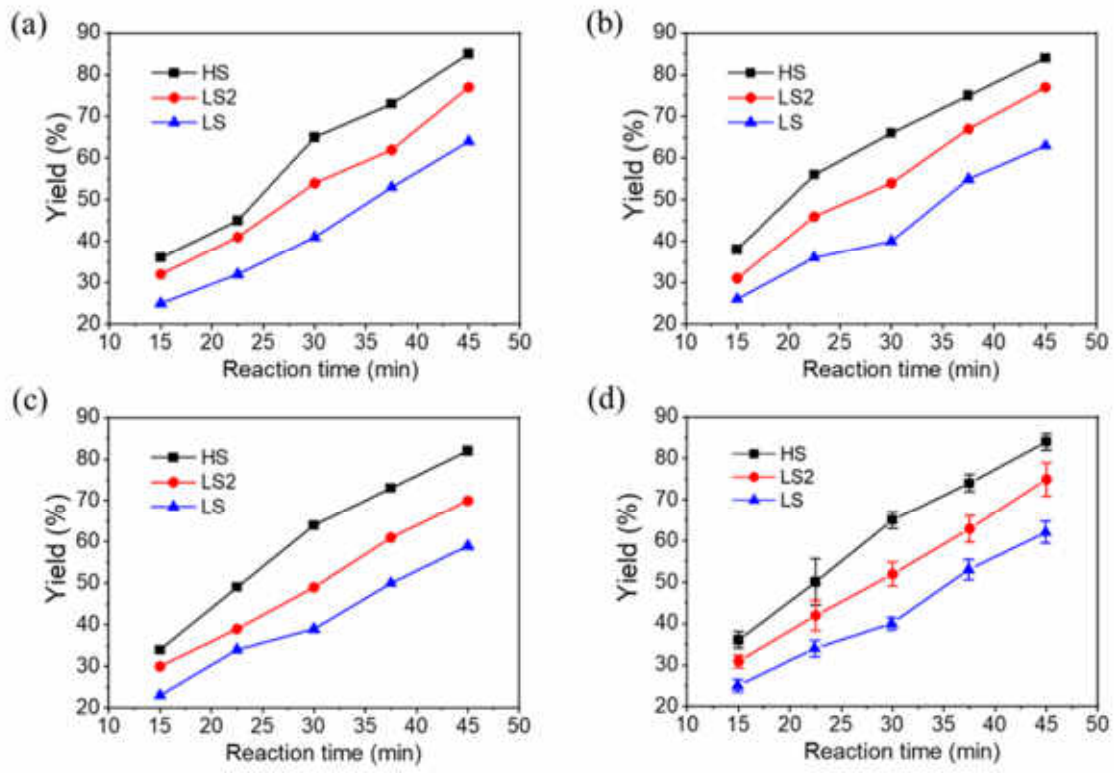


Fig. 4-3 (a)-(c) Yield of acetalisation reaction depending on the spin state (three repeated experiments). (d) Average yield of acetalisation reaction and error bars.

Table 4-2 The data corespond to Fig. 4-3, using complex **1** from batch A

Entry	Reaction time (min)	Correspond to Fig. 4-3	Yield (%)			
			HS	LS2	LS	Δ(HS-LS2)
1	15		36%	32%	25%	4%
2	22.5		45%	41%	32%	4%
3	30	Fig. 4-3 (a)	65%	54%	41%	11%
4	37.5		73%	62%	53%	11%
5	45		85%	77%	64%	8%
6	15		38%	31%	26%	7%
7	22.5		56%	46%	36%	10%
8	30	Fig. 4-3 (b)	66%	54%	40%	12%
9	37.5		75%	67%	55%	8%
10	45		84%	77%	63%	7%
11	15		34%	30%	23%	4%
12	22.5		49%	39%	34%	10%
13	30	Fig. 4-3 (c)	64%	49%	39%	15%
14	37.5		73%	61%	50%	12%
15	45		82%	70%	59%	12%
16	15		36%	31%	25%	5%
17	22.5		50%	42%	34%	8%
18	30	Fig. 4-3 (d)	65%	52%	40%	13%
19	37.5		74%	63%	53%	11%
20	45		84%	75%	62%	9%

* no reaction occurs (yield = 0) without a catalyst in 45 min

The kinetic study shows that, whatever the reaction time, the yields of reactions catalyzed by the HS complex are higher than those catalyzed by the LS2 state, which are themselves higher than those of reactions using complex **1** in the LS state. It would therefore appear that complex **1** in the HS state catalyzes the reaction more efficiently than complex **1** in the LS2 state. For this batch of complex **1** (Batch A), it would appear that the greatest difference in yield (around 12%) between reactions catalyzed by the HS and LS2 complex states is observed for reaction times of 30 and 37 minutes. We then repeated this kinetic study two times (Fig. 4-3 (b)-(c)). Similar results were obtained, with the same trend emerging each time. On average, for batch A, a reaction time of 30 minutes reveals a 12% difference between the yields obtained from the complex in the HS and LS2 spin states (Fig. 4-3 (d)). This means that for this reaction time, 1.25 times more acetal is formed when using complex **1** in the HS state than when the complex is in the LS2 state. We refer to a set of experiments as three reactions (one in the LS state, one in the LS2 state and one in the HS state) carried out under strictly identical experimental conditions (i.e. using the same batch of complex **1** and the same reaction time). Since each point in the kinetic studies represents an independent experiment, 16 sets of experiments have been carried out to date. All these sets of experiments indicate that the complex **1** in the HS state is more efficient than the complex in the LS2 state. This study also shows that the yields of LS samples are generally lower than those of LS2 samples. We attribute this difference in reactivity

to the fact that heating to 90°C may facilitate interactions between the complex **1** and EtOH, leading to significant separation of the polymeric chains of the complex. This would enable catalytic substrates to access the catalytic sites of the complex more easily, resulting in greater catalytic efficiency of the complex. Therefore, it is obvious that having also studied the catalytic efficiency of complex **1** in the LS2 state was a very good choice. Indeed, had we not done so, we would have significantly overestimated the effect of the spin state on the catalytic capacities of complex **1**.

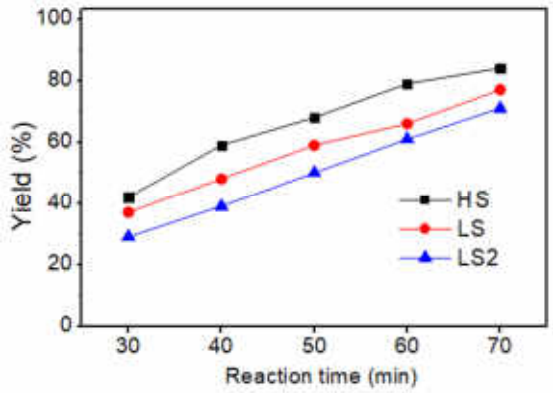
The difference in yield between the HS and LS2 samples, both subjected to the same heating process (90 °C, 2 minutes) under identical conditions, indicates that this difference in yield is due to the spin state effect. Two hypotheses are proposed to explain these results: 1) differences in electronic properties between the spin state,[8, 9] leading to increased yield in the HS state. 2) The transition causes a shift in polymer chains or changes in volume, creating more space between them and allowing easier access to solvent molecules.[10-15] This will be discussed further in the following section.

4.4 Study of the reproducibility of results

Initial results showed that complex **1** catalyzed acetal formation more efficiently in the HS state than in the LS2 state. And we also verified that from the same experimental conditions (identical reaction time and spin state), comparable results were obtained from complex **1** batch A. The next step was to verify that the effect of the spin state on the catalytic activity of the complex could be observed for other batches of complex **1**. Table 4-3 shows the acetal yields obtained as a function of the spin state and a batch of complex **1**. If we focus on the difference in yields between the HS and LS2 states, we notice that batches A, B and C are similar, while batch D is distinct. We speculated that the very small difference in catalytic activity of batch D could be explained by its low yields. We made this assumption on the basis of experience gained from studying the effect of spin state on the efficiency of the PSM reaction. Indeed, in Chapter 2, we showed that while for a given PSM percentage, the different batches of complex 1 had a similar difference in reactivity between the two spin states, the reaction time required to reach the desired PSM percentage was highly dependent on the batch of the complex. Acetal yields also varied from batch to batch (Table 4-3), with a particular difference of around 20% between batches A and D. It should also be noted that for a yield of 45% for the HS state of complex **1** batch A (Table 4-2, entry 2), a difference in yields between the HS and LS states of 4% is obtained. For these reasons, it is conceivable that extending the reaction time for complex **1** batch D would lead to an increase in the difference between the two spin states. Indeed, as shown in Fig. 4-4, a difference between the HS and LS2 states of 11% is obtained for a reaction time of 40 minutes.

Table 4-3 Acetal yields as a function of batch and spin state of complex **1**.

Entry	Batch of Complex **1**	Yield of acetal (%)			
		HS	LS2	LS	Δ(HS-LS2)
1	Batch A	65%	52%	40%	13%
2	Batch B	57%	44%	35%	13%
3	Batch C	54%	42%	38%	12%
4	Batch D	42%	37%	30%	5%



Reaction time	Yield of acetal			
	HS	LS2	LS	Δ(HS-LS2)
30 min	42%	37%	30%	5%
40 min	59%	48%	39%	11%
50 min	69%	59%	51%	10%
60 min	80%	67%	62%	13%
70 min	84%	78%	72%	6%

Fig. 4-4 The yield of the acetalisation reaction depends on the spin state using complex **1** (Batch D) as catalyst

This difference in catalytic performance between batches could be attributed to several factors: 1) The size of the particles depends on the batch. Complex **1** is an aggregate of several small particles, and the size of this aggregate depends on the precipitation rate during the synthesis process. Controlling this process is challenging, leading to differences in particle size and, consequently, catalytic performance across batches. 2) The water content in complex **1**. 3) The water content in the EtOH used in the experiments. These latter two factors are related to the water content. It is well known that water molecules can help separate the polymer chains of the iron triazole SCO complex, potentially altering the molecular arrangement and impacting the SCO properties and catalytic performance.

4.5 Optimization of experimental conditions

4.5.1 Study of the effect of using 96% EtOH instead of absolute EtOH

4.5.1.1 Study of the use of 96% EtOH as a solvent in catalytic reactions.

We have just mentioned that the presence of water in the reaction medium can modify the molecular arrangement of complex **1**, potentially leading to a change in its catalytic properties. We have previously shown that the presence of traces of water shortens the PSM reaction time[1, 3] of complex **1,** as well as the catalyzed formation of imine from aminotriazole. We therefore wondered whether the presence of a small amount of water would also accelerate acetal formation catalysed by complex **1**. As the volume of water that would have to be added to the medium is very small (a few microliters), it is easier to carry out this study by replacing part or all of the absolute EtOH with 96% EtOH.

As described in the experimental section and in Fig. 4-5, the experiment processes were divided into two steps. The first step involved preparing a suspension of complex **1** in EtOH in its HS, LS2, and LS states. In the second step, the reaction was initiated by adding the reagents.

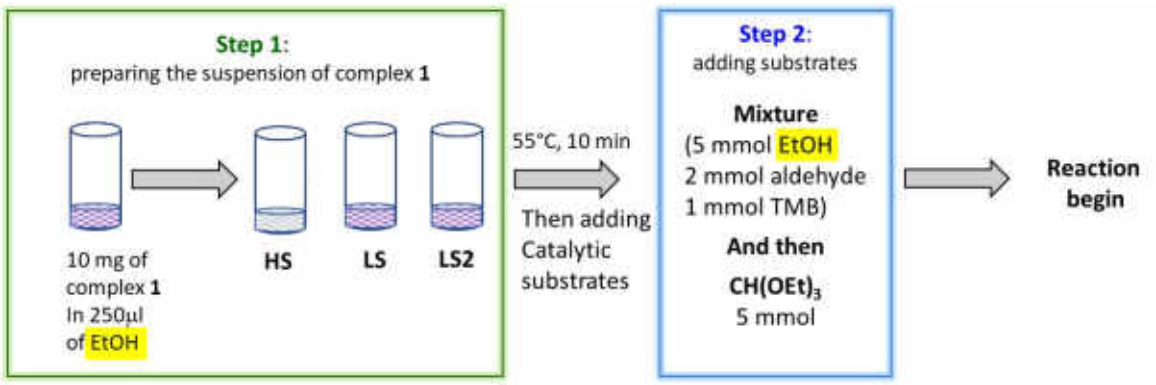


Fig. 4-5 Presence of EtOH in both steps of the process

EtOH was used in both steps, and we need to determine in which step it makes the most sense to use EtOH 96%. Table 4-4 indicates the quality of EtOH (absolute or 96%) used for each step in each type of condition (A, B, C and D). It is important to note that new bottles of each type of EtOH were opened for this study.

If the highest possible yield is desired, then it is preferable to use experimental conditions D, where 96% EtOH is used in both steps (Fig. 4-6). Using these conditions doubles the yields obtained when absolute EtOH is used for both steps (Conditions A). As we are interested in a difference in catalytic activity between the two spin states of complex **1**, it makes more sense to use 96% EtOH only in step 2 (Conditions C). Indeed, compared with condition A (absolute EtOH for both steps), using condition C greatly increases both yields and the difference in reactivity between the HS and LS2 states. On the other hand, it is a very bad idea to use 96% EtOH to produce the suspension of complex **1** (step 1), as in these cases no difference in activity is observed between the HS and LS2 states (Conditions B and D). Observation of the representative image of the experiments carried out under conditions B and D after the addition of $CH(OEt)_3$ enables us to quickly identify why, under these conditions, there is no difference in activity between the HS and LS2 states of complex **1**. (Fig. 4-7).

Complex **1** was insoluble in the solvent, and the colour of the suspension came from the complex. Fig. 4-7 (a) clearly shows that the LS sample was pink, which is expected as complex **1** is pink in the LS state. The HS sample was slightly yellow, which is normal as complex **1** is white in the HS state, and in the presence of aldehyde, the suspension can appear slightly yellow. Interestingly, the LS2 sample was also slightly yellow, similar to the HS sample, indicating that complex **1** in the LS2 sample was in the HS state rather than the LS state. This observation explains why the yields for the HS and LS2 samples were the same under conditions B and D, as complex **1** in the LS2 sample was actually in the HS state. Unlike the suspension of complex **1** in 96% EtOH, when complex **1** is suspended in absolute EtOH (condition C), the LS and LS2 samples remain in the low-spin state, while the HS sample remains in the HS state (Fig. 4-7 (b)). In addition, the results shown in Fig. 4-7 (a) suggest that when complex **1** is suspended in 96% EtOH, the LS2 sample has a transition temperature (LS → HS) that differs from that of the LS sample. It is therefore of interest to determine the spin transition temperatures of complex **1** when suspended in EtOH.

Table 4-4 The type of EtOH used in the experiment conditions A, B, C and D.

Experiment condition	EtOH used in the experiment		Reaction time
	Step 1	Step 2	
A	Absolute	Absolute	30 min
B	96%	Absolute	30 min
C	Absolute	96%	30 min
D	96%	96%	30 min

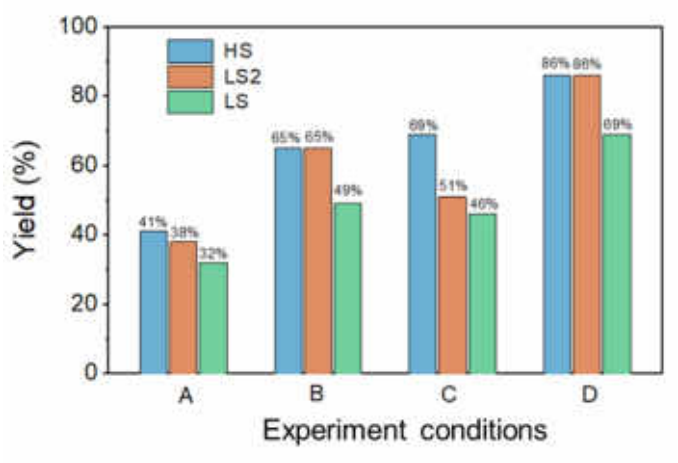


Fig. 4-6 Yields of acetal under serval experiment conditions A, B, C and D.

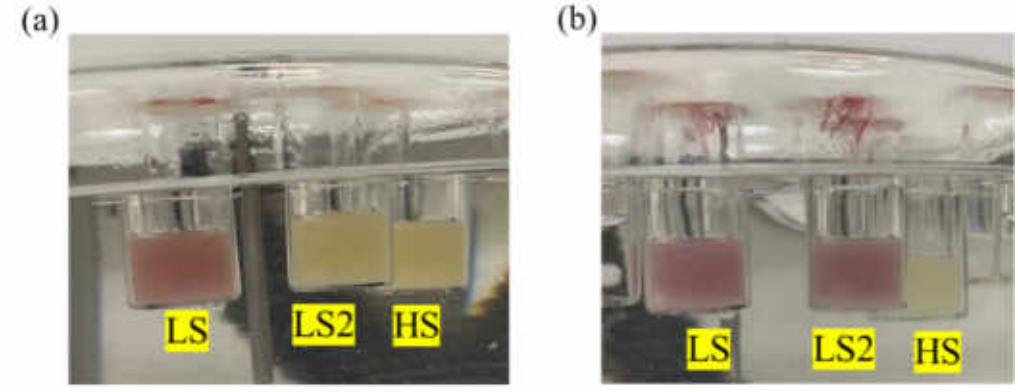


Fig. 4-7 Representative pictures of the experiment under (a) conditions B and D, (b) conditions A and C after adding the $CH(OEt)_3$

4.5.1.2 Study of the SCO transition of $[Fe(NH_2trz)_3](NO_3)_2$ suspended in absolute EtOH or 96% EtOH

In the above experiments, it is evident that the LS2 sample in 96% EtOH appears slightly yellow at 55°C, in contrast to the pink LS sample. This color suggests that complex **1** in the LS2 sample was actually in the HS state at 55°C in 96% EtOH. To confirm this observation and determine the exact transition temperature, four suspensions (LS and LS2 in absolute EtOH, and LS and LS2 in 96% EtOH) were immersed in an oil bath at various temperatures The experimental procedure is illustrated in Fig. 4-8 (a). As shown in Fig. 4-8 (b), all four samples were pink

initially at 50 °C, indicating they were in the LS state. When the temperature increased to 55 °C, the colour of sample 3 (LS2, 96% EtOH) changed, becoming noticeably less pink compared to the other three samples, suggesting that part of the complexes was in HS state and were at the transition temperature. At 60 °C, sample 3 was completely white, and sample 4 was nearly white, while samples 1 and 2 remained fully pink. When the temperature increased to 75 °C, all samples turned white. Table 4-5 summarises the experimental conditions for each sample and the transition temperatures (LS→HS). For samples 1 and 2 (absolute EtOH), the transition temperature ($T_{LS\rightarrow HS}$) was between 70-75 °C. For sample 3 (96% EtOH, LS), the $T_{LS\rightarrow HS}$ was between 60-65 °C. For sample 4 (96% EtOH, LS2), the $T_{LS\rightarrow HS}$ was between 50-60 °C. These results suggest that the presence of a small amount of water leads to a change in the transition temperature of complex **1**. This may be due to water molecules strongly interacting with the polymer chains of complex **1**, resulting in a change in molecular arrangement.

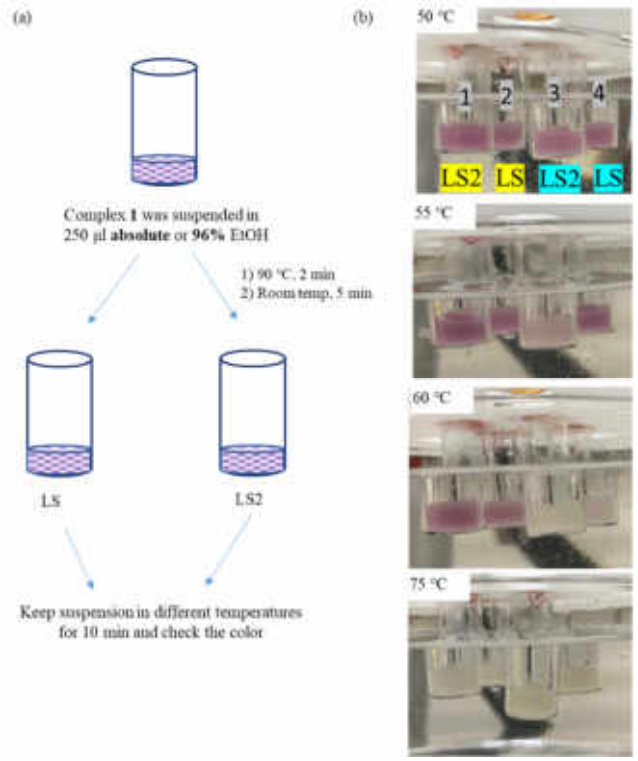


Fig. 4-8 (a) scheme of the experiment (b) the color of Sample 1, 2, 3 and 4 at 50 ℃, 55 ℃, 60 ℃ and 75 ℃.

Table 4-5 The transition temperature of Sample 1, 2, 3 and 4.

Entry	Conditions	Solvent	Transition temp (LS→HS)
Sample 1	LS	absolute EtOH	70-75 ℃
Sample 2	LS2	absolute EtOH	70-75 ℃
Sample 3	LS	96% EtOH	60-65℃
Sample 4	LS2	96% EtOH	50-60 ℃

Optical reflectivity measurements at varying temperatures were used to determine the SCO transition temperature of complex **1** suspended in absolute EtOH and 96% EtOH. For this measurement, 20 mg of complex **1** and 2 ml of absolute or 96% EtOH were introduced into a cuvette. The cuvette was then placed in a heating system equipped with a camera, which enabled the temperature to be monitored and photos of the suspension to be taken. The suspension was held at the desired temperature for 2 minutes before a photo was taken.

Fig. 4-9 shows the reflectivity results. At low temperatures, the suspension of complex **1** is pink (in its LS state), resulting in lower reflectivity compared to its HS state (white). In the absolute EtOH suspension (Fig. 4-9(a)), the $T\uparrow_{(LS\rightarrow HS)}$ was 70 °C, while the $T\downarrow_{(HS\rightarrow LS)}$ was around 35 °C, with a large hysteresis thermal loop of 35 °C. The first and second cycles were identical, indicating the stability of this suspension during the heating and cooling process.

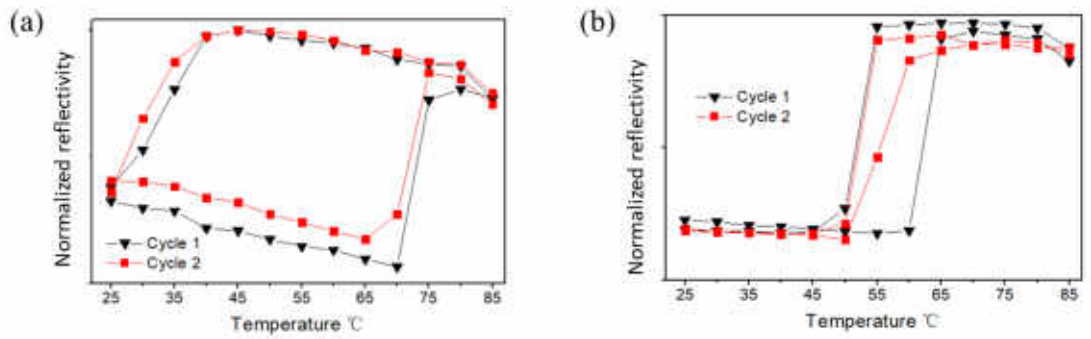


Fig. 4-9 Variable temperature optical reflectivity measurements of complex **1** in (a) absolute EtOH (b) 96% EtOH between 25 to 85 ℃

Fig. 4-9(b) shows the results of optical reflectivity measurements in a 96% EtOH suspension, which differed significantly from those in absolute EtOH. In the first cycle, the complex suspended in 96% EtOH exhibits a $T\uparrow_{(LS\rightarrow HS)}$ of 65 °C, and a $T\downarrow_{(HS\rightarrow LS)}$ of about 50 °C, with a thermal hysteresis loop of 15 °C, which is much smaller than the hysteresis loop of the complex suspended in absolute EtOH. Additionally, in 96% EtOH, the second cycle is different from the first one. Indeed, if we compare the two cycles, the temperature $T\uparrow_{(LS\rightarrow HS)}$ drops from 65 °C (1st cycle) to around 55 °C (2nd cycle) and the second major difference is that the 2nd cycle exhibits no hysteresis loop. This divergence in SCO properties could be due to changes in the molecular arrangement of the complex in the low-spin state. On the one hand, these results seem to confirm that in 96% EtOH complex **1** in the LS2 state has a significantly different molecular arrangement from that in the LS state, which could explain why the catalytic activity of complex **1** in the LS2 state is different from that in the LS state. On the other hand, this result is consistent with the observations of the catalytic reaction, where the LS2 sample prepared with 96% EtOH switched to the HS state during the reaction at 55 °C (Fig. 4-7 (a)).

Two hypotheses can be formulated to explain the change in the molecular arrangement of complex **1** in the low-spin state after the first cycle. The first hypothesis is that the change was induced by heating the suspension to 85 ℃. Indeed, more numerous and stronger interactions between water and the polymeric chains of complex **1** could take place at higher temperatures. The second hypothesis is that the change was induced by the transition of complex **1** to the HS state. Indeed, it is perfectly conceivable that the strength and number of interactions between complex **1** and water depend on the spin state of the iron complex. To find out which of these two hypotheses is correct, we need to compare, at the same temperature, the effect of adding a small amount of water on the HS and LS states of complex **1**. Thanks to the large thermal hysteresis cycle of complex **1** suspended in absolute EtOH, this study can be performed at 55 ℃.

In the experiment involving the addition of water to complex **1** in its HS state in suspension, 20 mg of complex **1** was suspended in 2 ml of absolute EtOH in a cuvette and then measured using variable temperature optical reflectivity. As shown in Fig. 4-10 (a), the first cycle was conducted under normal conditions, yielding the same results as before (Fig. 4-9(a)). In the second cycle, when the temperature cooled back to 55 °C (in HS state), 80 µl of H_2O (corresponding to 4% H_2O) was added to the suspension (Fig. 4-10 (b)). After 2 minutes, the

reflectivity of the suspension slightly decreased, suggesting that part of the complex had already transitioned back to the LS state at 55 °C. We then lowered the temperature and the complex **1** in this suspension completely reverted to the LS state at 45 °C (Fig. 4-10 (c)). Another cycle was measured, showing the temperature $T\uparrow_{(LS\rightarrow HS)}$ to be around 55 °C without a hysteresis loop, consistent with the previous result (Fig. 4-10 (d)). We can therefore conclude, at least from complex **1** in the HS state, that heating to 85 °C is not necessary to modify the molecular arrangement of the complex in the low-spin state.

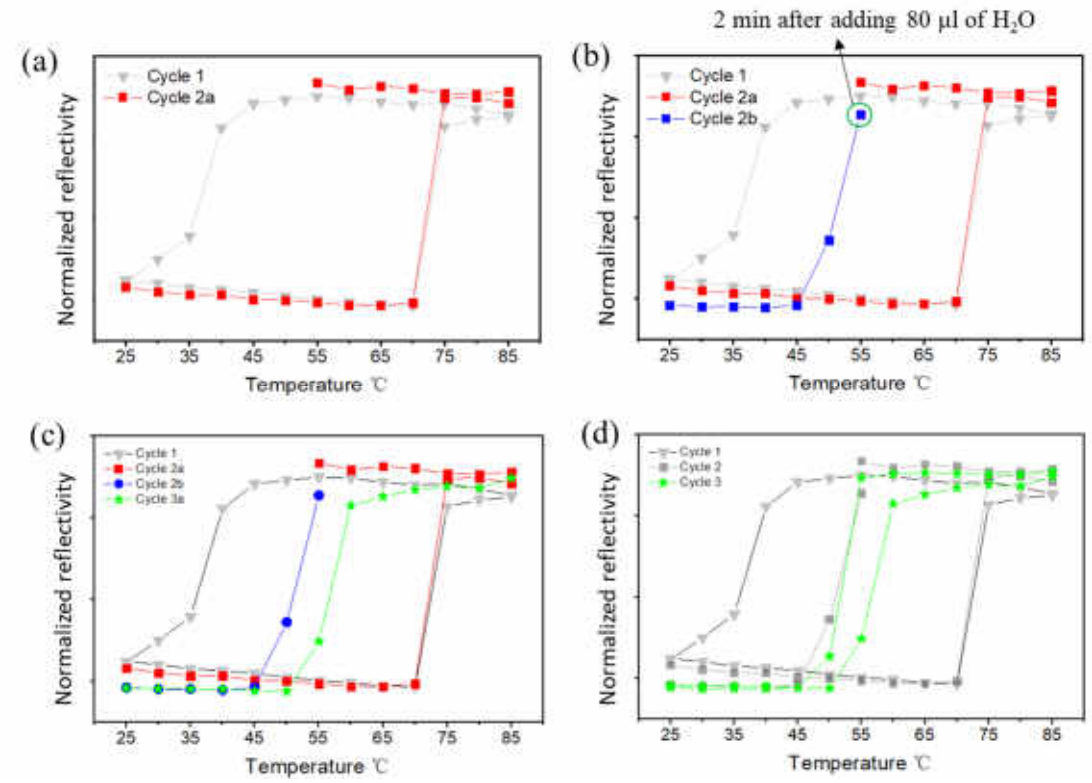


Fig. 4-10 Variable temperature optical reflectivity measurement of complex 1 in absolute EtOH, then 80 µl of water added to the **HS** complex at 55 °C. (a) the first cycle in the grey curve, the red curve in the second cycle stops at 55 °C during the cooling process. (b) After adding 80 µl of water, cool down to 25 °C. (c) the heating process of the third cycle. (d) the whole third cycle.

In the experiment involving the addition of water to Complex **1** in its LS state in suspension, 20 mg of Complex **1** was suspended in 2 ml of absolute EtOH in a cuvette and then measured using variable temperature optical reflectivity. As shown in Fig. 4-11 (a), the first two cycles were conducted under normal conditions, yielding the same results as before (Fig. 4-9(a)). In the third cycle, when the temperature was heated to 55 °C (in the LS state), 80 µl of H_2O (corresponding to 4% H_2O) was added to the suspension. After 2 minutes, the reflectivity of the suspension before and after adding the water remained nearly the same (Fig. 4-11 (b)). Then this third thermal cycle was completed, and we were able to note that the $T\uparrow_{(LS\rightarrow HS)}$ of Complex **1** was around 65 °C, and $T\downarrow_{(HS\rightarrow LS)}$ was around 50 °C (Fig. 4-11 (c)). The temperature $T\uparrow_{(LS\rightarrow HS)}$ indicates that the addition of water to the LS complex at 55°C did not change its molecular arrangement. The change in molecular arrangement therefore only occurs when water is added to the complex **1** in the HS state. This result confirms that, at the same temperature, the addition of water does not have the same effect on the crystal structure of complex **1** in the HS state as in the LS state. An additional thermal cycle was carried out, showing that complex 1 has a temperature $T\uparrow_{(LS\rightarrow HS)}$ of around 55°C, which differs from the third cycle but is consistent with

the previous result in the 96% EtOH suspension. (Fig. 4-11 (d) and Fig. 4-9(b)). Thus, the temperature observed during the 3rd thermal cycle corresponds to complex **1** LS, while that of the 4th thermal cycle 4 corresponds to complex **1** LS2.

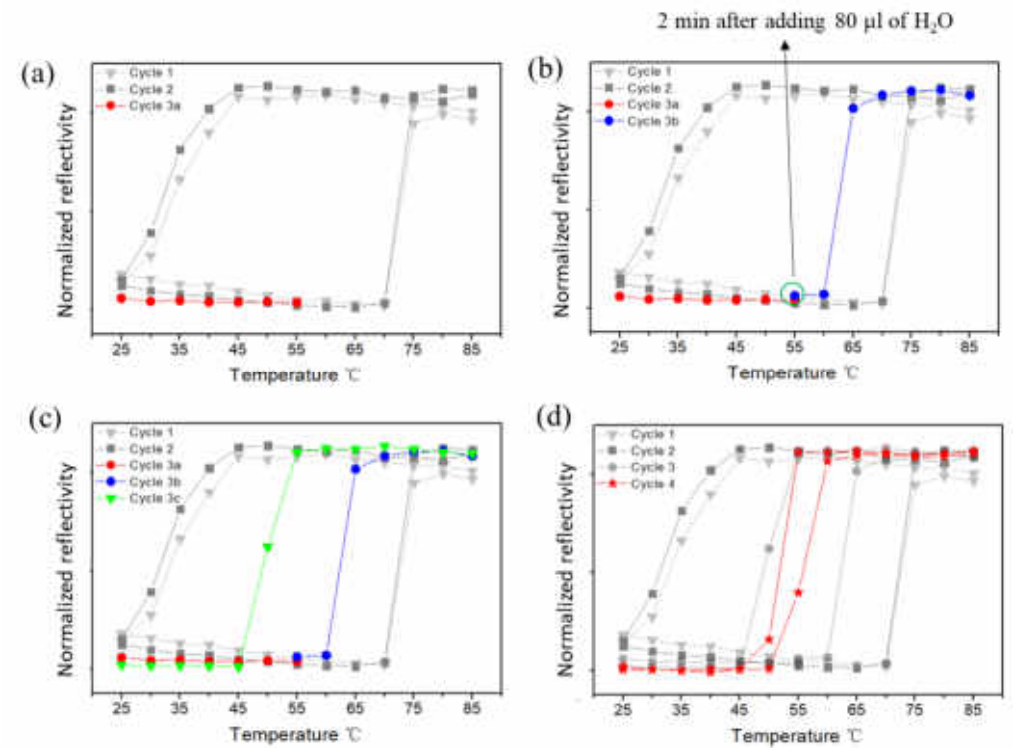


Fig. 4-11 Variable temperature optical reflectivity measurements of complex **1** in absolute EtOH, then 80 µl of water added to the **LS2** complex at 55 °C. (a) the first cycle in the grey curve, the red curve in the second cycle stops at 55 °C during the cooling process. (b) After adding 80 µl of water, and cool down to 25 °C. (c) the heating process of the third cycle. (d) the third cycle.

In conclusion, the interaction of water with complex **1** in the HS state is the key to modifying the molecular arrangement of the complex in the low-spin state. Furthermore, this study clearly demonstrates that under the same conditions, the addition of water does not have the same influence on the crystal structure of the complex in the high-spin state as in the low-spin state. As in heterogeneous catalysis, a change in molecular arrangement leads to a change in substrate access to catalytic sites, it becomes obvious that the presence of water in the medium will affect the catalytic activity of the HS state differently from that of the LS2 state.

4.5.1.3 Study of the reproducibility of the effect of 96% EtOH in the reaction medium on the catalytic activity of $[Fe(NH_2trz)_3](NO_3)_2$

This study is of interest to us because, on the one hand, it will enable us to assess the extent to which the presence of water in the medium will affect the catalytic activity of the HS and LS2 states differently. Secondly, it will enable us to confirm, on three other batches of complex **1**, the benefits of replacing absolute EtOH by 96% EtOH in the mixture introduced after stabilization of the spin states of complex **1** at 55°C. Fig. 4-12 shows the yield of acetal using these four batches of complex **1** (the three new batches plus batch E, which had been used for the study of the section 4.5.1.1) as the catalyst and a comparison of the results using mixtures with 96% EtOH and absolute EtOH. The results obtained in the presence of 96% EtOH are

similar whatever the batch of complex **1** used, and are also in line with what was observed in the study in Section 4.5.1.1. Using a mixture with 96% EtOH not only increases the yield but also significantly enhances the yield for the HS sample compared to the LS2 and LS samples, leading to a notable difference in yield between the HS and LS2 samples. Indeed, the yield for the HS sample using the mixture with 96% EtOH is nearly 30% higher than when using the mixture with absolute EtOH, while for the LS2 and LS samples, the difference is around 15%. By interacting more strongly with the complex in the HS state than in the LS2 state, water increases significantly the difference in catalytic activity between these two spin states of complex **1**.

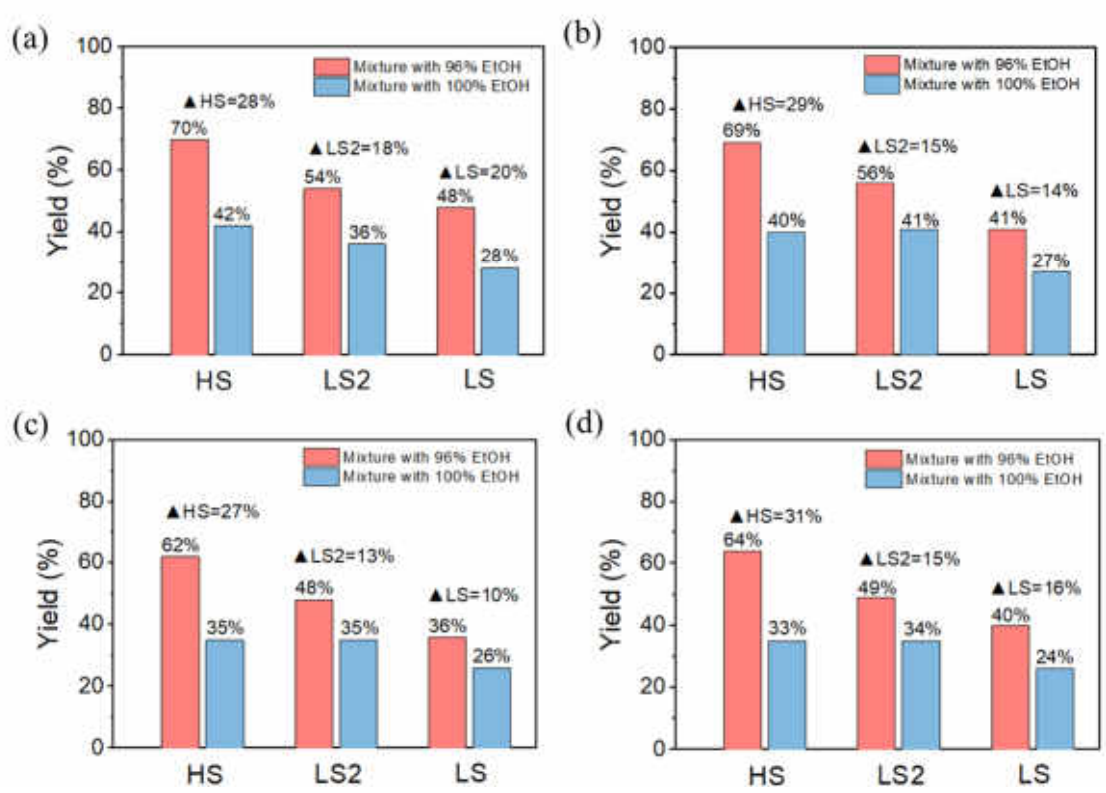


Fig. 4-12 Comparison of Mixture with 96% EtOH and absolute EtOH using the complex **1** of (a) Batch E. (b) Batch D. (c) Batch F. (d) Batch G. Reaction performed at 55 °C, 30 min

4.5.1.4 Comparative study of the kinetics of the catalytic reaction in the presence and absence of 96% EtOH

Whether or not 96% EtOH is present in the medium, and whatever the reaction time, the yields of reactions catalysed by complex **1** in the HS state are higher than those of reactions catalysed by the complex in the LS2 state (Fig. 4-13). The difference in yields of reactions catalysed by the HS and LS2 states of complex **1** can reach up to 21% in the presence of 96% EtOH and 14% in absolute EtOH. Reactions in 96% EtOH are faster than those in absolute EtOH. The greatest differences in yield between these two types of reaction medium are observed when the reactions are catalysed by complex **1** in the HS state. Indeed, it takes between 20 and 30 minutes for reactions catalysed by HS complex **1** in absolute EtOH to reach the same yield as those carried out in the presence of 96% EtOH. At approximate yields, the difference in catalytic activity between the HS and LS2 states of complex **1** is slightly greater in the presence of 96% EtOH. For example, for a reaction time of 30 minutes and in the presence of 96% EtOH, a difference in yield between the HS and LS2 states of 17% is observed, whereas for a reaction

time of 50 minutes in absolute EtOH the difference in activity of the HS and LS2 states is 14%.

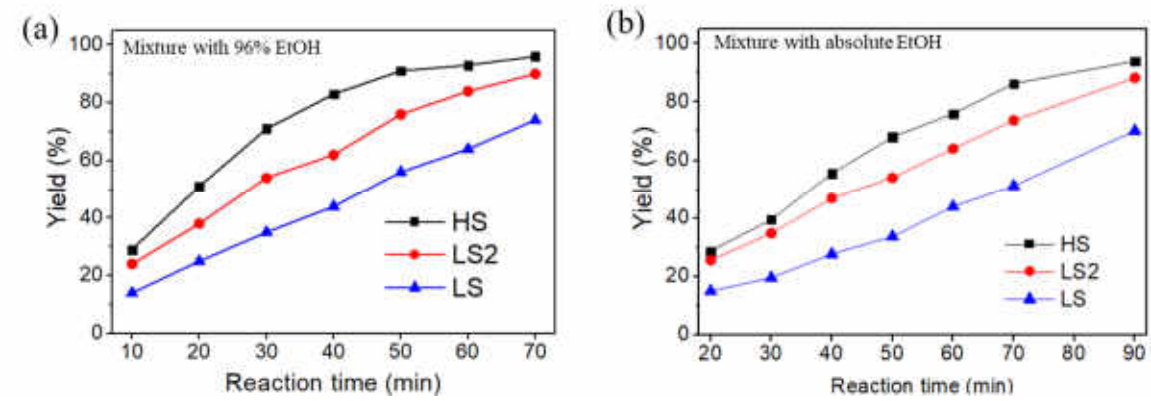


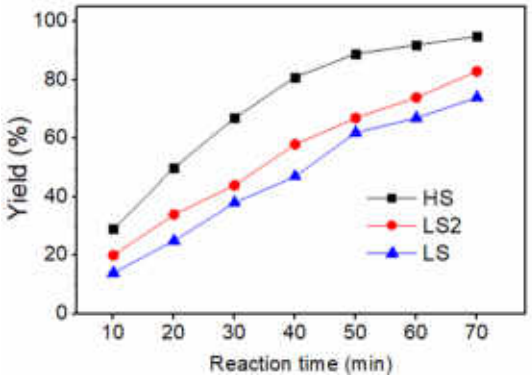
Fig. 4-13 Kinetic study of catalytic reactions carried out in absolute EtOH or in the presence of 96% EtOH. (Batch D)

Table 4-6 Kinetic study of catalytic reactions carried out in the presence of 96% EtOH (Batch D)

Reaction time	Yield of acetal (Mixture with 96% EtOH)			
	HS	LS2	LS	Δ(HS-LS2)
10 min	29%	24%	14%	5%
20 min	51%	38%	25%	13%
30 min	71%	54%	35%	17%
40 min	83%	62%	44%	21%
50 min	91%	76%	56%	15%
60 min	93%	84%	64%	9%
70 min	96%	90%	74%	6%

Table 4-7 Kinetic study of catalytic reactions carried out in absolute EtOH (Batch D)

Reaction time	Yield of acetal (Mixture with absolute EtOH)			
	HS	LS2	LS	Δ(HS-LS2)
20 min	29%	26%	15%	3%
30 min	40%	36%	20%	4%
40 min	56%	47%	28%	9%
50 min	68%	54%	34%	14%
60 min	76%	64%	44%	12%
70 min	86%	74%	51%	13%
90 min	94%	88%	70%	6%



Reaction time	Yield of acetal (Mixture with 96% EtOH)			
	HS	LS2	LS	Δ(HS-LS2)
10	29%	20%	14%	9%
20	50%	34%	25%	16%
30	66%	44%	38%	22%
40	81%	58%	47%	23%
50	89%	67%	62%	22%
60	91%	74%	66%	17%
70	94%	83%	73%	11%

Fig. 4-14 Kinetic study of catalytic reactions carried out in the presence of 96% EtOH (Batch D, Study of the reproducibility of the results)

After checking the reproducibility of the results obtained by batch D of complex **1** in 96% EtOH (Fig. 4-14), a kinetic study was also carried out using another batch of complex **1** (batch G). The results presented in Fig. 4-15 show the same trend as the previous results exhibit the same tendency as the previous results (Fig. 4-13). In general, catalytic reactions using complex **1** from batch G are slower than those from batch D. For example, it takes 50 minutes for the yield in the HS state to reach 72% with batch G, whereas it only takes 30 minutes for batch D. However, it is important to note that even though batch G takes longer than batch D to reach 72% yield, a 16% yield difference between reactions catalysed by the HS and LS2 states was observed, which is fully consistent with the result for batch D. The difference in activity between the D and G batches can perhaps be explained by a difference in particle size or agglomerate size in complex **1**. Indeed, larger particles have a smaller surface area, leading to less efficient catalysis

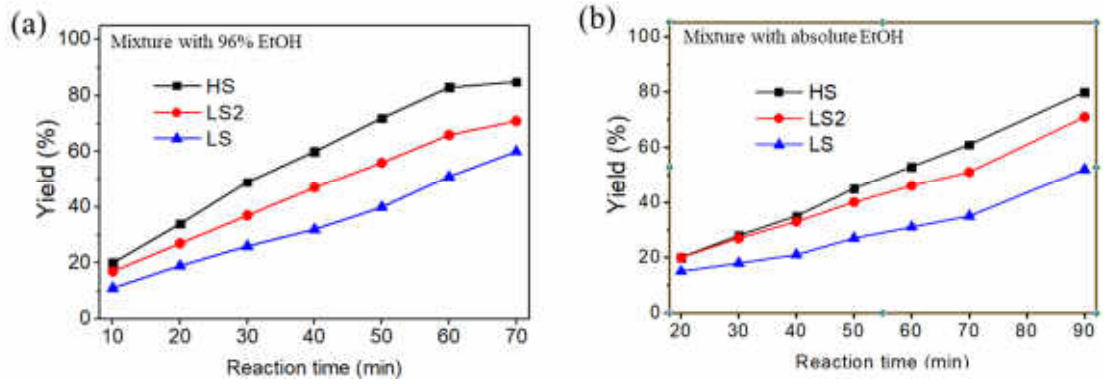


Fig. 4-15 Kinetic study of catalytic reactions carried out in absolute EtOH or in the presence of 96% EtOH. (Batch G)

4.5.1.5 Study of the effect of washing the complex with 96% EtOH on its catalytic activity

Until now, complex **1** was washed with absolute EtOH after formation. We therefore wondered whether washing the complex with 96% EtOH instead of absolute EtOH would increase the catalytic efficiency of complex **1**. To examine the effect of the washing process on complex **1**, a batch of complex **1** was synthesised and then equally divided into two batches (Batch F1 and Batch F2) at the end of the reaction. Batch F1 was washed with absolute EtOH, while Batch F2

was washed with 96% EtOH (Fig. 4-16 (a)). The results indicated in Fig. 4-16 show that reactions using complex **1** batch F1 as catalyst have identical yields to those using batch F2. This suggests that the catalytic capacity of complex **1** does not depend on This washing process. So there is no point in changing our washing procedure for complex **1**.

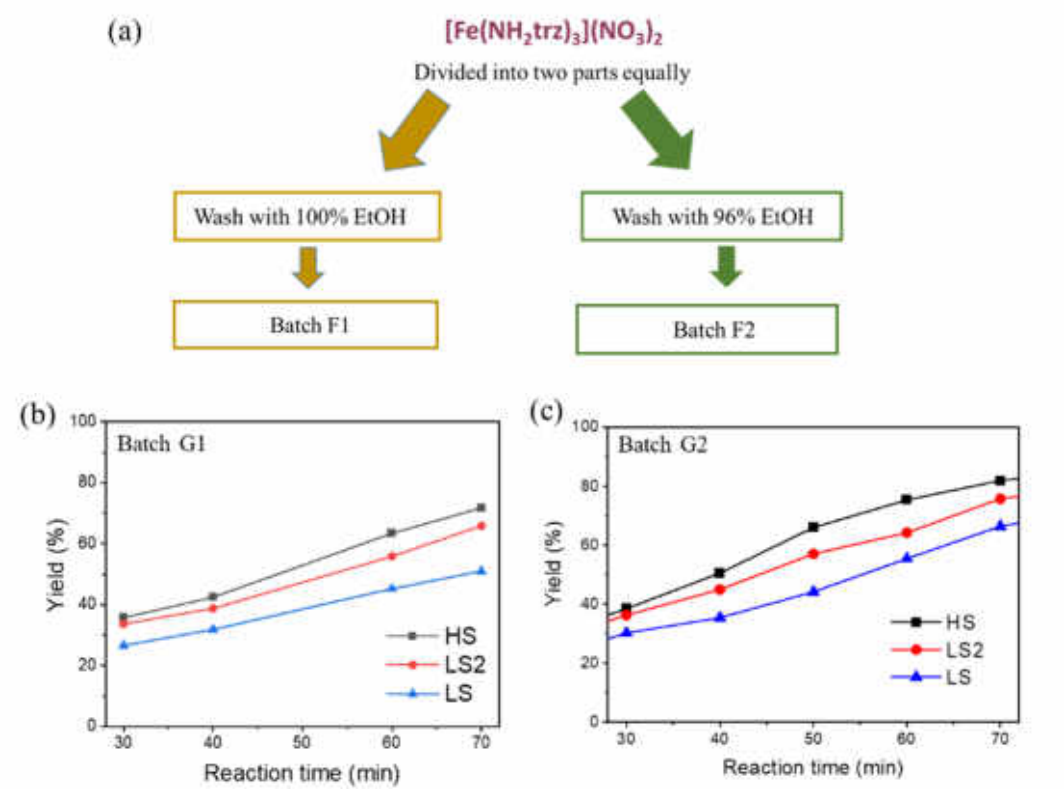


Fig. 4-16 (a) Figure showing the quality of the EtOH used to wash batches F1 and F2 of complex **1**. (b) and (c) Kinetic studies of reactions catalyzed by batches F1 and F2 of complex **1**

4.5.2 Effect of the ratio (catalyst/aldehyde)

At this stage, we knew that complex **1** efficiently catalyses the formation of acetal and that its catalytic activity depends, as expected, on the spin state of the iron complex. We then chose to optimize the mass percentage of the complex in respect of the aldehyde (R*). As we do not want to vary the concentration of reagents between experiments, each time we increase the amount of aldehyde and triethyl orthoformate, we'll also have to increase the amount of EtOH and TMB (Ratio 1, Eq. 4-1). On the one hand, we can expect that if we lower the R* ratio, then reaction yields might fall. But on the other hand, results described in the literature show that for some heterogeneous catalysts, decreasing the ratio 1 increases catalytic efficiency.[16, 17] This could be the case here. Indeed, complex **1** particles interact very strongly with each other, which leads, especially in concentrated suspensions, to a significant formation of agglomerates. This is not ideal, as these agglomerates, having a smaller contact surface than the more isolated particles, lead to a lower catalytic activity of complex **1**. It is therefore conceivable that lowering the ratio 1, by leading to better dispersion of the particles of our complex **1**, could increase its catalytic efficiency. The ideal R* ratio will therefore be large enough to ensure that catalysis remains effective, but also small enough to ensure good dispersion of the particles of complex **1**. It is conceivable that the value of the ratio R* will depend on the spin state of complex **1**, which could perhaps enable us to increase the difference in catalytic activity between the HS

and LS2 states of complex **1**. There are two approaches to decrease the ratio R*: reducing the catalyst mass or increasing the mass of the aldehyde. For our catalytic reaction, the catalyst mass used is 10 mg, making it impractical to weigh a smaller amount accurately. Therefore, increasing the amount of reagent and solvent is the preferable method. Table 4-8 below shows the volume of reagent and solvent used in the reaction under normal conditions and with progressively increased volumes, up to 10 times the normal amount.

$$Ratio\ \mathbf{1} = \frac{the\ mass\ of\ catalyst}{the\ mass\ of reagent\ and\ solvent} \qquad \text{(Eq. 4-1)}$$

Table 4-8 The volume of reagent and solvent used in the reaction and the R*

Entry	The volume of reagent and solvent (µl)					
	Normal	**Twice**	**4 times**	**6 times**	**8 times**	**10 times**
EtOH (Step 1)	250	500	1000	1500	2000	2500
Mixture (aldehyde)	576 (243)	1152 (486)	2304 (972)	3456 (1458)	4608 (1994)	5760 (2430)
$CH(OEt)_3$	832	1664	3328	4992	6656	8320
R*	3.68%	1.84%	0.92%	0.61%	0.46%	0.37%

$\boldsymbol{R^*} = \frac{m_{catalyst}}{m_{aldehyde}}$

Complex **1** from batch F1 was used as a catalyst under normal conditions and with up to ten times the amount of solvent and reagent. This experiment employed a mixture with absolute EtOH, and the reaction time was set to 60 minutes. The results shown in Fig. 4-17 indicate that a mass percentage of 0.46% complex to aldehyde mass is sufficient for effective catalysis. We were also very pleased to observe a clear increase in the difference in activity between the HS and LS2 states. Indeed, the difference in yields between the HS and LS2 samples increases from 3% to 21% by multiplying the quantity of solvents and reagents by 6. Catalysis remains effective even with an 8- or 10-fold increase in solvent and reagents. However, in the latter two cases, the suspension of complex **1** in LS turns yellow, which may suggest that some NH_2 functions in the complex have been converted to imine functions. Consequently, future studies will focus on conditions with up to 6 times the solvent and reagent.

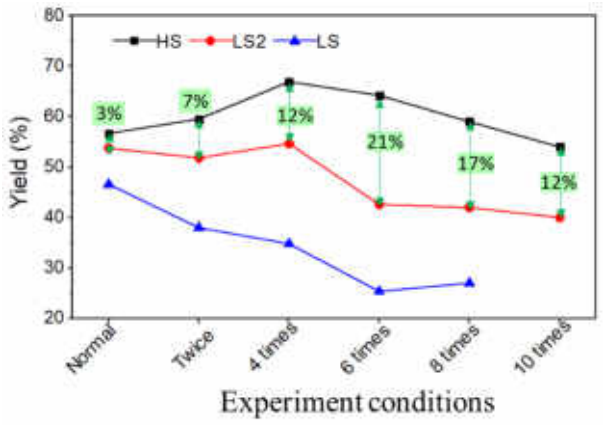


Fig. 4-17 Acetal yield as a function of the spin state of complex **1** and the number of times the aldehyde mass was multiplied relative to standard conditions. (Mixture with absolute EtOH, reaction time= 60 min, Batch F1)

After repeating this study a second time (Fig. 4-18 (a)) using batch F1, the effect of reducing the R* ratio on the catalytic efficiency of complex **1** was evaluated on 3 other batches of complex **1** (Fig. 4-18, Fig. 4-19, and Fig. 4-20). It should be noted that using batch D of complex **1**, we also carried out the same type of study twice, but using reaction media in which some of the absolute EtOH had been replaced by 96% EtOH. For these different trials, the reaction time was adjusted so that the yield of the reaction catalysed by the HS state of complex **1** was around 70%. In all cases, reducing the R* ratio leads to a significant increase in the difference in yield between the HS and LS2 samples. This increase can be explained by the fact that the catalytic activity remains of the same order of magnitude for all the R1 values studied, while that of the complex in the LS2 state decreases by around 12%. The yields obtained when the reaction is catalysed by the HS complex are up to 27% higher than those of reactions catalysed by the LS2 complex. In other words, up to 1.7 times more acetal is formed when the reaction is catalysed by the HS complex than when the reaction is catalysed by the LS2 complex. Studies carried out on batch D of complex **1** show that the substitution of 96% EtOH for part of the absolute EtOH leads to faster catalysis reactions and an increase in the difference in catalytic activity between the HS and LS2 states of complex **1**.

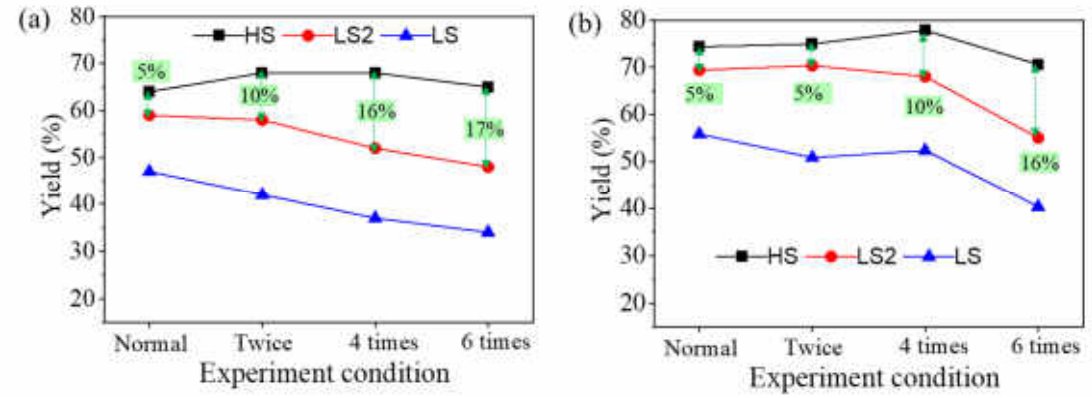


Fig. 4-18 Acetal yield as a function of the spin state of complex **1** and the number of times the aldehyde mass was multiplied relative to standard conditions. (a) Batch F1, Mixture with absolute EtOH, reaction time= 60 min. (b) Batch F2, Mixture with absolute EtOH, reaction time= 60 min.

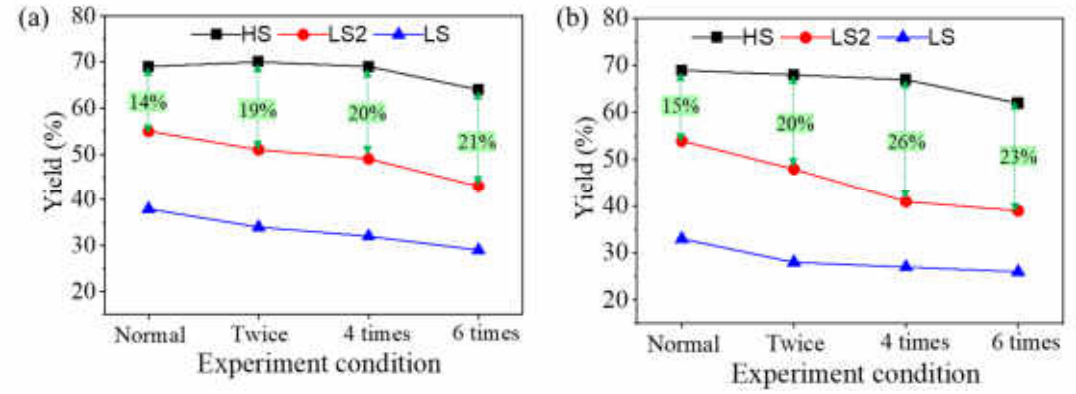


Fig. 4-19 Acetal yield as a function of the spin state of complex **1** and the number of times the aldehyde mass was multiplied relative to standard conditions. (a) Batch D, Mixture with absolute EtOH, reaction time= 50 min. (b) Batch D, Mixture with 96% EtOH, reaction time= 30 min.

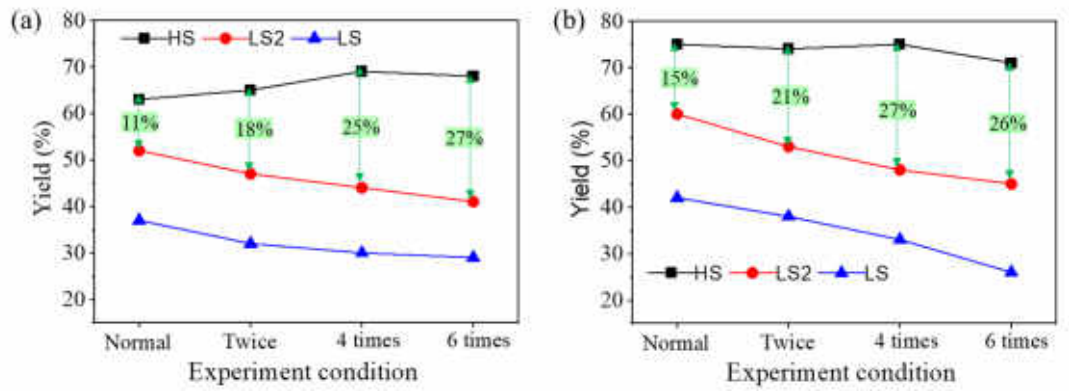


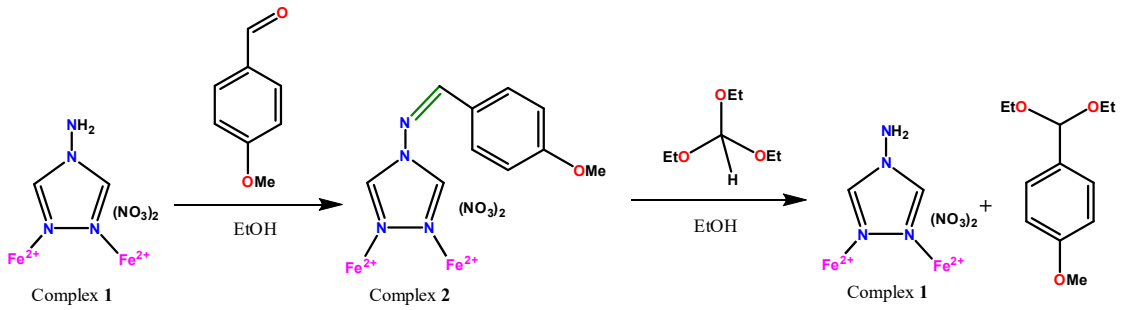
Fig. 4-20 Acetal yield as a function of the spin state of complex **1** and the number of times the aldehyde mass was multiplied relative to standard conditions. (a) Batch G, Mixture with absolute EtOH, reaction time= 70 min. (b) Batch G, Mixture with 96% EtOH, reaction time= 50 min.

4.6 Mechanistic study of the catalysis reaction

We then wished to investigate the mechanism by which complex **1** catalyses the formation of acetal. We envisaged three different types of mechanism: one in which PSM reactions would be involved, a second involving hydrogen bonds between the catalyst and the aldehyde, and the third in which the iron complex would be a Lewis acid.

4.6.1 Mechanism involving PSM reactions

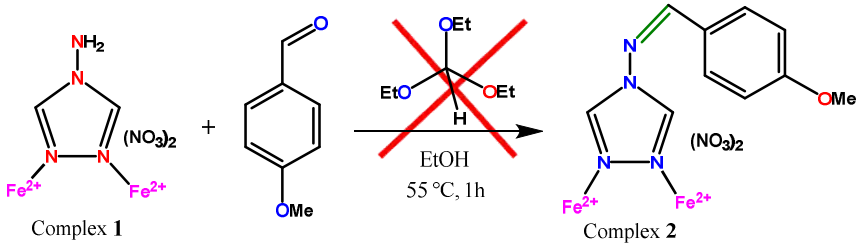
We have already demonstrated in Chapter 2 that complex **1** can catalyze the formation of imines from aminotriazole, and that the mechanism of this reaction involves post-synthetic modification (PSM) reactions. Consequently, we hypothesized that the mechanism of the acetalization reaction might also involve a PSM pathway. According to this hypothesis, the NH_2 groups present in complex **1** first react with the aldehyde to form an imine complex (complex **2**). Then, attack of the C=N bond by triethyl orthoformate or EtOH would release the acetal in solution and complex **1** would be reformed. Throughout these processes, the SCO complex **1** undergoes two PSM reactions (Scheme 4-2).



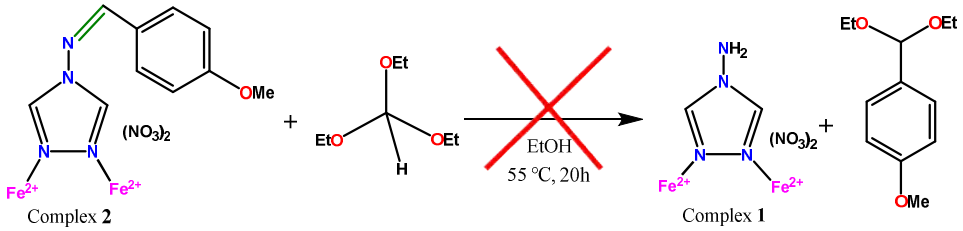
Scheme 4-2 Mechanism involving PSM reactions

To verify this hypothesis, the first step was examined to determine if the imine complex **2** could be obtained under the catalytic conditions of the acetalisation reaction. Experimental results showed that under the catalytic conditions, the imine complex was never observed after the catalytic reaction (Scheme 4-3). This result could indicate either that the imine complex **2** does not form under these experimental conditions, or that the attack on the imine function of the

complex is faster than the formation of complex **2**. We also studied the second step. For this purpose, the sample containing the suspension of the imine complex in EtOH and 130 equivalent of triethyl orthoformate was heated to 55°C for 20 h. Under these experimental conditions, acetal formation was not observed and the imine complex **2** remained unchanged (Scheme 4-4). In conclusion, as both steps were found to be unfavourable, the mechanism of acetalisation is unlikely to proceed through PSM reactions.



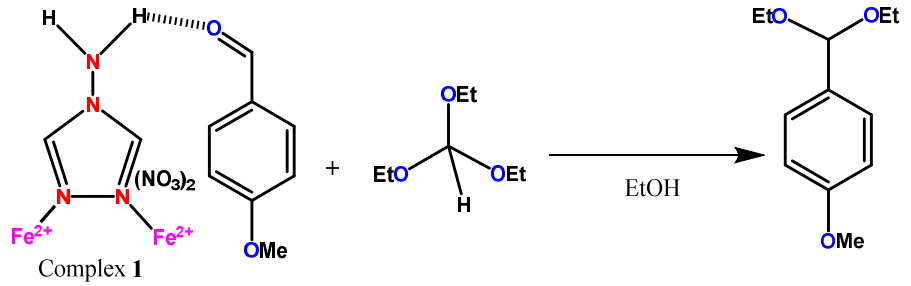
Scheme 4-3 Study of the formation of the imine complex **2** under the experimental conditions used for catalysis.



Scheme 4-4 Study of the attack of the imine function of complex **2** by EtOH or triethyl formate.

4.6.2 Mechanism involving hydrogen bonds

Results reported in the literature show that the presence of hydrogen bonds between the catalyst and the carbonyl oxygen increases the electrophilicity of the aldehyde carbon sufficiently to render it significantly more sensitive to attack by the alcohol.[7, 18-20]. As complex **1** presents an NH_2 functional group, which can form hydrogen bonds with aldehydes. (Scheme 4-5). If in our case the mechanism involves hydrogen bonding, the catalytic reactivity should depend on the amount of NH_2 functional groups present in complex **1**. The NH_2 groups in complex **1** can be transformed to C=N by reacting with *p*-anisaldehyde, and of course the pure imine complex **2** can also be synthesized. By controlling the time of the PSM reaction on the amine complex **1**, complexes with 6% and 30% imine functions were synthesized. The catalytic reactivity of these two complexes and that of the imine complex **2** have been investigated. (Table 4-9). If the mechanism involves hydrogen bonding, the best catalytic performance should be observed for the amine complex **1**. However, experimental results showed that an increase in imine substitution resulted in better catalytic reactivity. Even the imine complex without NH_2 functional groups exhibited excellent catalytic activity in the acetalisation reaction. Therefore, the results of this experiment suggest that, in our case, the mechanism is unlikely to proceed through hydrogen bonding.



Scheme 4-5 Catalytic reaction mechanism involving hydrogen bonds between the NH_2 functions of the complex and the aldehyde.

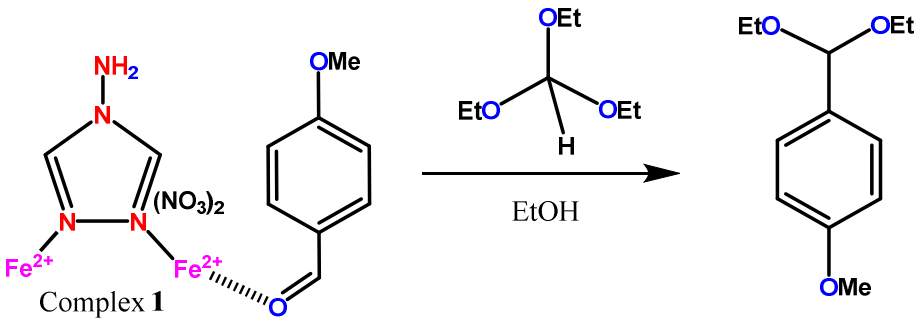
Table 4-9 The result of using complex with different imine substitutions (55 °C, 30 min)

Entry	Imine substitution (%)	Yield of acetal (%)	
		LS2	HS
1	0	20.9	26.8
2	6	29.2	37.2
3	30	94.0	93.0
4	100*	90.8	

* The imine complex is in HS state at 55°C

4.6.3 Mechanism involving the presence of a Lewis acid

A Lewis acid can effectively catalyse the acetalization of aldehydes by accepting an electron pair from the oxygen of the carbonyl function, thereby increasing the electrophilicity of the carbonyl function carbon and facilitating nucleophilic attack by orthoformate or EtOH. (Scheme 4-6).[21-27] Work described in the literature shows that iron complexes can be effective Lewis acids.[28-35] As shown in Scheme 4-6, we can therefore envisage complex **1** interacting with the aldehyde.



Scheme 4-6 Proposed mechanism if the complex **1** acts as a Lewis acid catalyst

It is also known that the Lewis acidity of cationic species is strongly influenced by the chemical structure of their counter ions. We decided to compare the catalytic efficiency of coordination polymers with the chemical formula $[Fe(NH_2trz)_3]X$, where X corresponds to the counter ion (nitrate, sulfate, tosylate, chloride) with that of iron II precursors.

The respective iron(II) salts ($FeCl_2 \cdot 4H_2O$, $Fe(OTs)_2 \cdot 6H_2O$, $Fe(BF_4)_2 \cdot 6H_2O$, and $FeSO_4 \cdot 7H_2O$) were also tested for their ability to catalyse the acetalisation reaction efficiently. It can be seen

that at identical concentrations of iron II, with the exception of iron sulfate, all the other iron precursors are significantly more efficient than complex **1**. This result is not very surprising if catalysis is due to the Lewis acidity of iron II. From the results described in Table 4-10, we can rank the iron II precursors in descending order of their catalytic efficiency in the acetalization reaction: $Fe(OTs)_2 > Fe(BF_4)_2 > FeCl_2 > FeSO_4$.

Table 4-10 Yield for acetalisation reaction using different iron salt as catalyst

Entry	Catalyst	c (µmol/ml)	Yield
1	$Fe(OTs)_2$	3.6	100%
2	$Fe(BF_4)_2$	3.6	100%
3	$FeCl_2$	3.6	100%
4	$FeSO_4$	3.6	44%
5	$Fe(OTs)_2$	0.9	100%
6	$Fe(BF_4)_2$	0.9	67%
7	$FeCl_2$	0.9	10%

In comparison, iron(II) triazole coordination compounds with different counter ions ($OTs^- BF_4^-$ SO_4^{2-}, and Cl^-) were also tested in the acetalization reaction (Table 4-11). Except for $[Fe(NH_2trz)_3]SO_4$, which afforded no yield, all other iron(II) triazole polymers demonstrated higher catalytic activity than $[Fe(NH_2trz)_3](NO_3)_2$. In addition, $[Fe(NH_2trz)_3](BF_4)_2$ and $[Fe(NH_2trz)_3](OTs)_2$ exhibited better catalytic performance than $[Fe(NH_2trz)_3]Cl_2$.

Thus, the efficiency ranking of iron coordination polymers is similar to the ranking of iron(II) precursors. This result is an element in favour of a mechanism involving Lewis acid iron(II) centres.

Table 4-11 Yield for acetalisation reactions (55 °C, 30 min) using different $[Fe(NH_2trz)_3](X)_2$ with X= $NO_3^-, OTs^-, BF_4^-, SO_4^{2-}$, and Cl^-

Entry	counter ion	Yield
1	NO_3^-	57%
2	SO_4^{2-}	0%
3	BF_4^-	100%
4	Cl^-	80%
5	OTs^-	100%

4.7 Investigation of the origin of the spin state effect on the catalytic activity of $[Fe(NH_2trz)_3](NO_3)_2$

We have demonstrated that complex **1** in the HS state is significantly more efficient in catalysis than complex **1** in the LS2 state. This greater activity of complex **1** in one of its spin states may be due either to differences in electronic properties between the spin states, or to a difference in substrate access to the catalytic site. As the catalyst is clearly more efficient in the HS than in the LS2 state, it is attempted to determine the kinetics of the reaction and calculate the

activation energy for both spin states. A change in activation energy could indicate a different pathway or transition state for LS2 and HS states, possibly stemming from a change in electron density at the catalytic site due to the spin transition.

The Arrhenius equation and the parameters within it, specifically the activation energy (E_a) and the Arrhenius factor (A_{rr}), provide significant insights into the dynamics of a chemical reaction (Eq 4-2).[36] Determining the E_a and A_{rr} of a chemical reaction involves understanding how the reaction rate varies with temperature.

$$K = A_{rr} e^{-\frac{Ea}{RT}} \qquad \text{(Eq. 4-2)}$$

Rearrange the equation to :

$$\ln(k) = -\frac{Ea}{R}\frac{1}{T} + \ln(A_{rr}) \qquad \text{(Eq. 4-3)}$$

where k is the rate constant, A_{rr} is the Arrhenius factor (frequency factor), Ea is the activation energy, R is the gas constant (8.314 J/(mol·K)), and T is the absolute temperature in Kelvin.

In order to determine the Ea and Arr, the first is to measure the reaction rate constant at different temperatures. Conduct experiments to measure the rate constant k of the reaction at various temperatures (T).

According to the first-order reaction:

$$ln[A]_t = ln[A]_{(t)0} - kt \qquad \text{(Eq. 4-4)}$$

Rearrange to solve for k:

$$k = \frac{\ln([A]_{(t)0}/[A]_t)}{t} \qquad \text{(Eq. 4-5)}$$

where: k is the rate constant, [A] is concentrations of the reactants, t is reaction time

Then the k can be obtained via the Graphical Method by plotting $\ln([A]_{(t)0}/[A]_t)$ (Fig. 4-21).

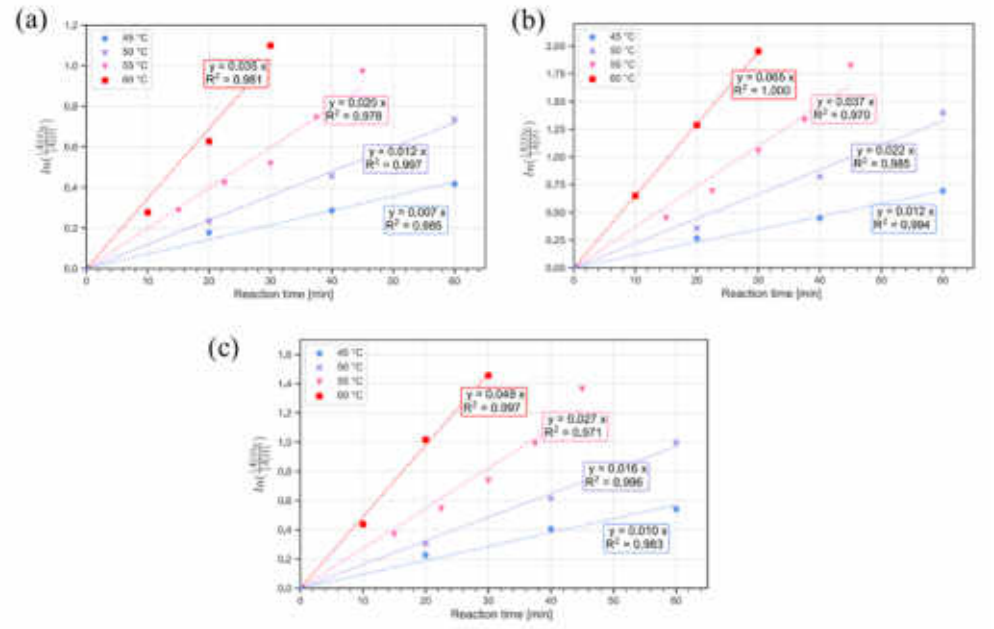


Fig. 4-21 Plotting $ln([A]_{(t)0}/[A]_t)$ versus the reaction time for all reactions carried out in (a) LS state. (b) HS state (c) LS2

Then the activation energy (E_a) and Arrhenius factor (A_{rr}) also can be obtained via the Graphical Method by plotting ln(k) vs. 1/T (Fig. 4-22).

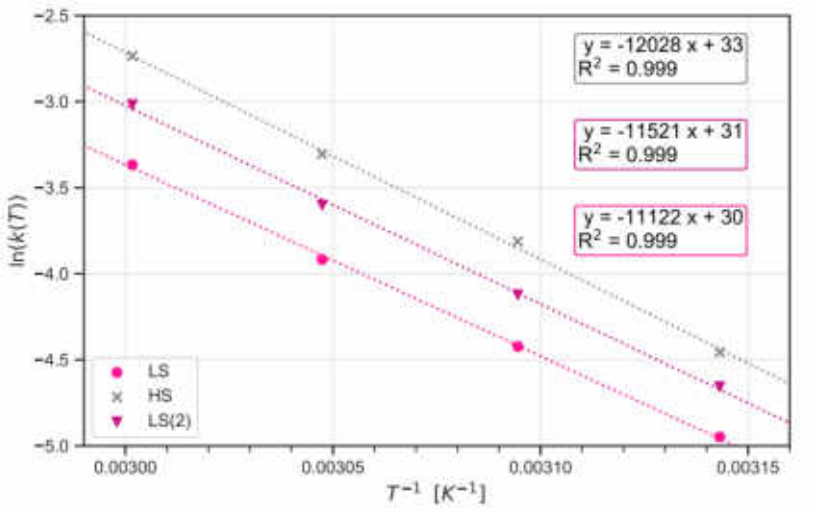


Fig. 4-22 The activation energy E_a for each spin state is proportional to the slope of the respective plot; the prefactor A_{arr} can be determined from the y-intercept.

As shown in Table 4-12, the activation energies for both spin states are in the range of 90-100 kJ mol^{-1}, with the HS state exhibiting the highest activation energy, followed by the LS2 and LS states.

Table 4-12 Activation energy E_a and prefactor A_{arr} for the LS, HS, and LS(2) states of the catalyst.

Entry	Spin state	E_a ($kJ\ mol^{-1}$)	A_{arr} (s^{-1})
1	LS	92.5	1.1×10^{13}
2	HS	100	3.1×10^{14}
3	LS2	95.8	5.0×10^{13}

The slight increase in activation energy from the LS to the HS state (+8.1%) is unexpected, as the reaction proceeds faster in the HS state than in the LS state. However, the Arrhenius prefactor A_{arr} which denotes the number of collisions per second that occur with the proper orientation to react, shows a significant difference, which could explain the difference in catalytic activity between the HS and LS states. The increase in the reaction rate constant for the HS state can be attributed to the almost 30-fold increase in properly oriented collisions. For the LS2 state, collisions occur five times more frequently than in the LS state.

Given that the differences in activation energy are small, this suggests that instead of a different electronic pathway, the higher catalytic activity of the HS state might be due to better access of the substrate to the active sites, which is a known important parameter for heterogeneous catalysis. In our case, two hypotheses can be put forward to explain why access to the catalytic site by the substrate is easier for the complex in the HS state. The first hypothesis implies that the HS complex has a larger molecular volume than the LS complex. This increase in molecular volume is explained by an increase in N-Fe bonds in the HS complex. Therefore, access to the Fe center could be easier for the complex in the HS state than in the LS state. The second hypothesis is based on the fact that the strength and number of interactions between the solvent

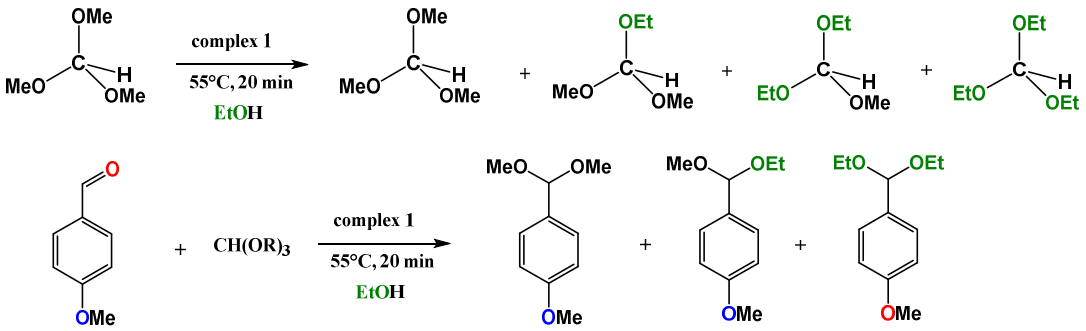
and the complex will necessarily depend on the spin state of the iron complex. These intermolecular interactions will modify the molecular arrangement of the complex and therefore access to the catalytic site by the substrates. We are more inclined to think that the difference in access is due to a change in molecular arrangement linked to interactions with the solvent. We think so because, firstly, although there is a systematic increase in molecular volume of the order of 12% when switching from the LS to the HS state, the magnitude of the change overall material is highly dependent on the SCO complex. In the case of complex **1** in the solid state, as reported in Chapter 2, the material expansion is only 1%. Furthermore, the difference in catalytic activity between the two spin states of complex **1** is dependent on the reaction solvent. This suggests that the solvent must also play a role in the difference in complex activity. Finally, the addition experiment at the same temperature with water on both complex states shows that water has stronger interactions with the complex in the HS state than with the LS state. This difference in interaction is sufficient for the arrangement of the complex in the LS state to be modified only after the complex has changed to the HS state.

4.8 Study of the catalytic efficiency of the $[Fe(NH_2trz)_3](NO_3)_2$ in other acetalisation reactions

We have demonstrated that complex **1** catalyzes the formation of acetal from *p*-anisaldehyde and, more importantly, that the catalytic efficiency of complex **1** is indeed dependent on the spin state of iron. We now wish to determine the scoop and limitations of using complex **1** in other acetalization reactions. First, we studied the acetalization reaction of *p*-anisaldehyde in the presence of trimethyl orthoformate instead of triethyl orthoformate. Then we studied the acetalization reaction from other aldehydes in the presence of triethyl orthoformate.

4.8.1 Study of the acetalization of *p*-anisaldehyde in the presence of trimethyl orthoformate

Firstly, it is preferable to use MeOH as solvent when the acetalization reaction is carried out in the presence of trimethyl orthoformate. Indeed, we have observed that complex **1** also catalyzes the attack of EtOH on trimethyl orthoformate, leading to the formation of 4 different trialkyl orthoformates and thus to the formation of three different acetals (Scheme 4-7).

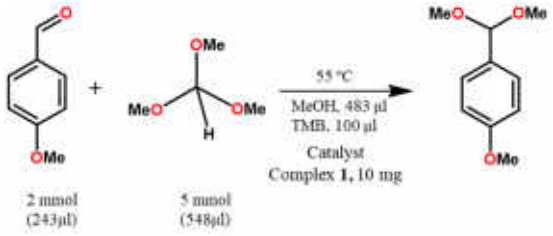


Scheme 4-7 Chemical structures of the acetals obtained when the reaction is carried out in the presence of triethyl orthoformate in EtOH.

Compared with our model reaction, the reaction described in Table 4-13 is much faster. Various hypotheses can be put forward to explain this greater reactivity. It is described in the literature that MeOH and trimethyl orthoformate are more reactive towards aldehyde than EtOH and triethyl orthoformate respectively. Other explanations more specific to our catalytic system can also be proposed: On the one hand, it is conceivable that trimethyl orthoformate, being a smaller molecule than triethyl orthoformate, can be inserted more easily between the polymeric chains of our complex. On the other hand, we have previously shown that the PSM reaction of complex **1** with *p*-anisaldehyde was faster in MeOH than in EtOH. We hypothesized that MeOH allows better separation of the polymeric chains of complex **1**, which facilitated the PSM reaction even more than in EtOH. It is conceivable that this explanation could also be applied to catalysis. The last hypothesis is that the reaction catalyst is no longer the amine complex **1**. We put forward this hypothesis because we observed that the color of the suspensions for complex **1** in the low-spin state (LS and LS2) were not pink as they should be, but yellow. We then suspected the significant formation of the imine complex, which was also compatible with the fact that the reaction was really very fast, even for the complex in the LS state, and that there was no difference in yield between the different spin states of complex **1**. To verify this, we recovered the complex from the catalytic reaction and analyzed it by IR. The bands at 1601 and 1512 cm^{-1} confirm the presence of a significant number of imine functions on the complex recovered after catalysis, whereas in the case of our model reaction, the recovered complex corresponds to complex **1**.

As complex **1** underwent a significant transformation of its NH_2 functions during catalysis, we decided not to pursue this study any further.

Table 4-13 The yield of acetal after 10 and 20 min using MeOH/$CH(OMe)_3$



Entry	Catalyst	Reaction time	Yield (%)		
			HS	LS2	LS
1	complex **1**	20 min	98%	98%	98%
2	complex **1**	10 min	98%	97%	97%

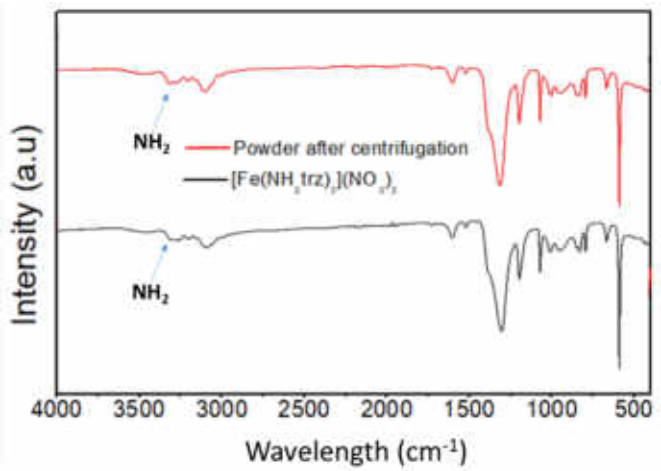


Fig. 4-23 FT-IR spectra of complex **1** before and after reaction with EtOH/$CH(OEt)_3$

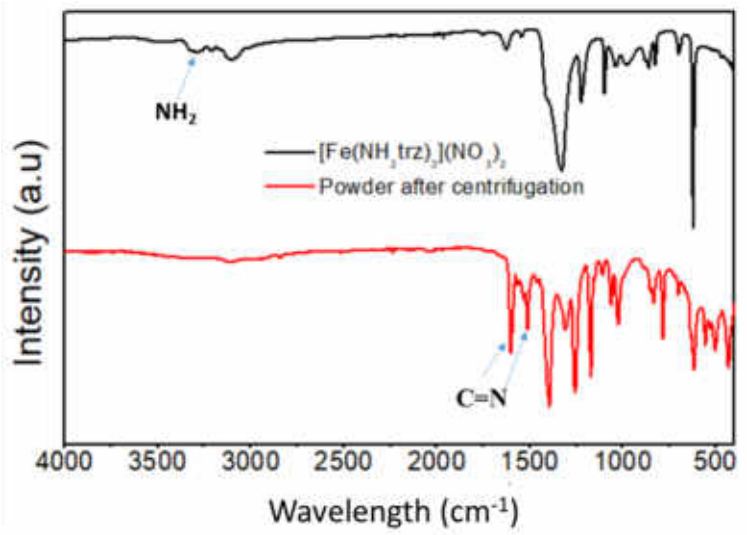


Fig. 4-24 FT-IR spectra of complex **1** before and after reaction with MeOH/$CH(OMe)_3$

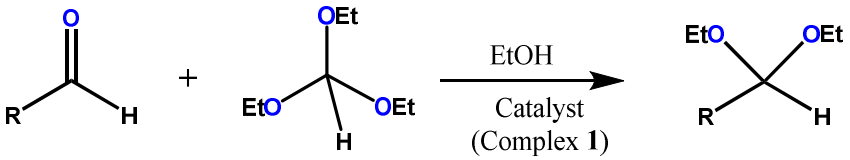
4.8.2 Acetalization reaction from other aldehydes

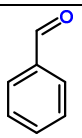
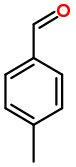
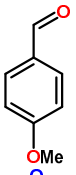
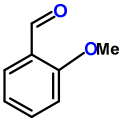
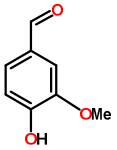
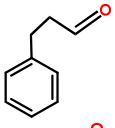
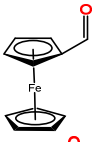
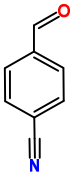
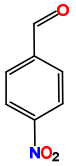
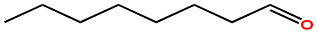
We then tested the catalytic efficiency of complex **1** in various acetalization reactions. We began with a pre-study in which the various acetalization reactions were carried out for 40 minutes at 55°C in the presence of complex **1** in the HS state. Firstly, in the case of aldehydes with electron-withdrawing groups (Table 4-14, entries 8 and 9), the results of the reactions carried out in the presence of complex **1** are identical to those of the reaction blanks, and hemiacetals are formed instead of acetals.

Furthermore, when the aldehyde is sterically highly hindered, such as ferrocene carboxaldehyde, complex **1** does not catalyze acetal formation (Table 4-14, entry 7). This result is not very surprising and can easily be explained by the inability of aldehyde to access the catalytic site due to the increased size of the molecule. On the other hand, the catalytic presence of the SCO complex enables acetals to be formed in good to excellent yields from benzaldehyde or aromatic aldehydes with electron-donating functional groups.

Complex **1** also effectively catalyzes acetal formation from alkyl aldehydes (Table 4-14, entry 10). These results suggest that the SCO complex could be used to selectively protect certain types of aldehydes. We then focused on acetalization reactions catalyzed by the SCO complex. We studied the effect of spin state on the catalytic efficiency of complex **1** in these reactions. We were pleased to see that in the case of benzaldehyde, *p*-tolualdehyde and octanal, a difference in the activity of the HS and LS2 states of complex **1** of over 15% was observed. Furthermore, a 10% difference in activity between the spin states of complex **1** was also observed in the acetalization of 3-phenylpropanal. For reactions with vanillin and *o*-anisaldehyde, no difference in activity was observed. In both cases, we believe that these results can be explained by the formation of imine complexes.

Table 4-14 aldehydes used for acetalization experiments and correspond yield



Entry	Aldehyde	Yield of acetal (%)				
		HS	LS2	LS	Δ (HS- LS2)	Without catalyst
1		61%	41%	30%	20%	0
2		60%	44%	27%	16%	0
3		70%	51%	37%	19%	0
4		99%	99%	94%	0%	3%
5		94%	91%	80%	3%	0
6		67%	57%	16%	10%	0
7		0	0	0	0	0
8*		0	0	0	0	0
9*		0	0	0	0	0
10		94%	78%	64%	16%	46%

*hemiacetal formed instead of acetal

4.9 Conclusion

The aim of this chapter was to determine whether the spin state of the iron could modulate the catalytic activity of the SCO coordination polymer. The acetalization of *p*-anisaldehyde, in EtOH, and in the presence of triethyl orthoformate was a very good reaction model for this purpose. In particular, this reaction had the advantage of being simple to set up and analyze. Moreover, the fact that the reaction did not take place under the conditions tested in the absence of a catalyst enabled us to demonstrate that iron complex **1** can effectively catalyze acetalization reactions.

Above all, we are very pleased with the results obtained, because under the right experimental conditions, the catalytic activity of complex **1** is indeed significantly modulated by the iron spin state. Complex **1** in the HS state is more efficient in this acetalization reaction than the complex in the LS2 state. Under the same experimental conditions, when the reaction was carried out using the HS-state complex up to 27% more acetal was formed compared with the reaction using the LS2-state complex. In other words, up to 1.3 times more acetal was observed in the HS complex sample than in the LS2 complex sample. The fact that over a hundred sets of experiments were carried out (a set corresponds to 3 experiments carried out under the same experimental conditions: one for the HS state, another for the LS2 state and the last for the LS state) and that 7 different batches of complex **1** were evaluated gives us confidence in the representativeness and reproducibility of the results. For each batch of complex, however, it is necessary to optimize the reaction time in order to obtain the desired percentage of acetal. This is because the synthesis method we use to form complex **1** does not allow us to control particle size (and particle agglomerates) and the amount of water contained in complex **1**.

In this study, we showed that the addition of a small amount of water at the right time greatly accelerated the reaction. As this acceleration is more significant in the presence of the complex in the HS state, it also increased the difference in yields between reactions carried out using complex **1** in the HS and LS2 states. On the other hand, we also noted that using the 3.68% mass percentage of complex **1** to aldehyde was not ideal for modulating the catalytic activity of the complex by its spin state. Perhaps surprisingly, the greatest differences in activity between the two spin states (HS and LS2) were observed at a complex mass percentage of 0.61%. This work illustrates perfectly that in heterogeneous catalysis, adding more catalyst does not automatically lead to better results.

In addition, we considered three types of catalytic mechanism for complex **1**: one involving PSM reactions, the other two involving the formation of hydrogen bonds between the complex and the aldehyde or the Lewis acidity of the iron atoms, respectively. The experiments carried out allow us to rule out the mechanism involving PSM reactions. The catalytic mechanism involving the Lewis acid sites of complex **1** seems the most likely of the three mechanisms considered.

Finally, in order to determine the origin of the spin state effect on catalytic efficiency, the activation energy for the reaction was determined. It is found to be similar for both spin states (90 kJ mol^{-1} for LS and 100 kJ mol^{-1} for HS state) which indicates that the difference in catalytic activity does not originate from electronic differences (allowing for a more stable transition state) but likely stems from an easier access to the catalytic active sties in HS state.

Being able to show the effect of the spin state of the metal on the reactivity of a spin-transition complex is a challenge. If we were able to do so in this study, it is because complex **1** was an excellent candidate. Indeed, the fact that suspending complex **1** in EtOH preserves the broad thermal hysteresis loop and transition temperatures of the pure complex was a major advantage.

The hysteresis cycle enabled us to test the catalytic efficiency of the spin states of complex **1** under the same experimental conditions, and thus to isolate the effect of the spin state from all other parameters that could modify the reactivity of the complex. The transition temperatures of complex **1** also had a serious advantage, as they corresponded well to the temperature range of many catalytic reactions.

In addition to its excellent SCO properties, the complex is also reactive. In this study, we confirmed that even though it remains in the solid state during the reaction, and its molecular arrangement is compact, under the right experimental conditions it can be highly reactive. Following on from the work described in Chapter 3, this study allows us to demonstrate for a second time that a complex synthesized and used for its spin transition properties can also be a good catalyst. Compared with the work described in the literature on the effect of spin state in catalysis, the use of SCO complexes such as complex **1** can have two advantages. Firstly, in the case of SCO complexes, we have both spin states of the same complex at our disposal, and this study demonstrates that starting from the HS or LS2 state will not necessarily lead to the same yield. Published results on the effect of spin state in catalysis are explained by different reaction paths depending on the spin state of the complex. In the case of a SCO complex, the spin state could affect catalytic activity via two very different mechanisms. As shown in this study, the spin state of the complex can affect the access of substrates to catalytic sites. This rather mechanical effect has the particular advantage of being able to be used, a priori, on many types of reactions. For example, here we have observed an effect of the spin state of the complex on a classical organic chemical reaction whose reaction mechanism is not dependent on a spin state. It is also conceivable that the spin state could modify the catalytic mechanism of a SCO complex. In future research, we hope to verify that the spin state of complex **1** can indeed modify the reaction pathway. However, the study described in this chapter already gives us grounds for optimism about the potential of SCO complexes in the field of switchable catalysis.

4.10 Experiment section

4.10.1 Acetalization reaction

The general experimental protocol for the catalytic tests is described below and can be separated into two steps (Fig. 4-25). The first step involves preparing the suspension of complex **1** in its HS, LS2, and LS states. The experiments are conducted by suspending 10.0 mg of complex **1** as the catalyst in ethanol (EtOH) in a closed 7 ml flask.

To prepare complex **1** in the HS state, the suspension is heated to 90 °C for 2 minutes to ensure a full transition, then immediately placed at the reaction temperature (55 °C) and stirred for 10 minutes.

To prepare complex **1** in the LS2 state, the suspension is heated to 90 °C for 2 minutes to ensure a full transition, then cooled back down to room temperature (returning to the LS state; second cycle), and then immediately placed at the reaction temperature (55 °C) and stirred for 10 minutes.

To prepare complex **1** in the LS state, the suspension is immediately placed at the reaction temperature (55 °C) and stirred for 10 minutes.

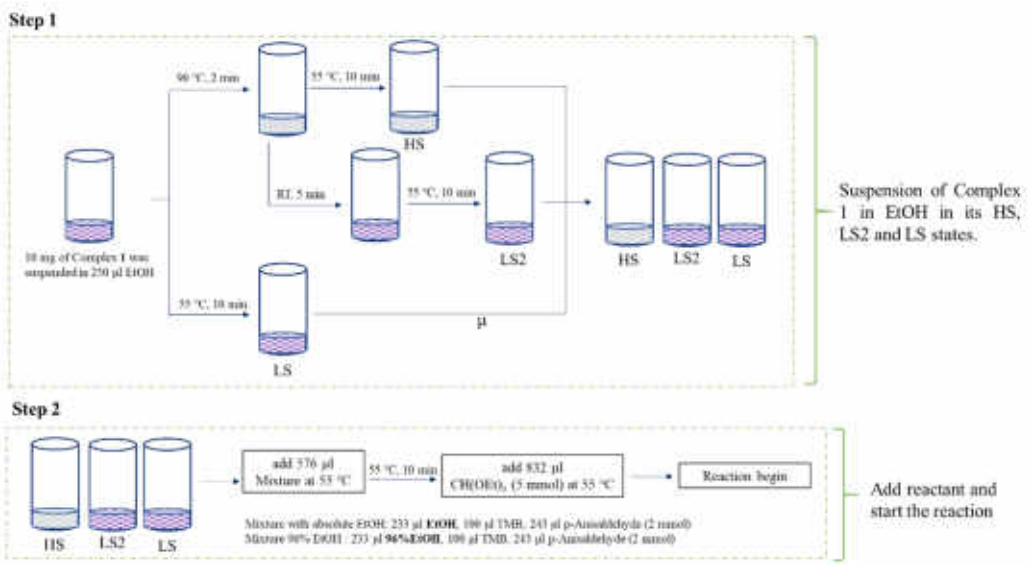


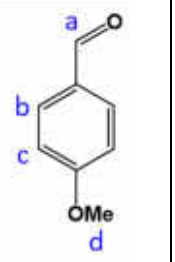
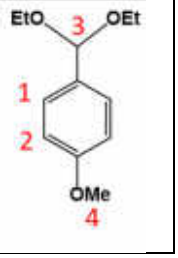
Fig. 4-25 General experimental procedures of acetalisation reaction

The second step involves adding the reagent and initiating the catalytic reaction. A mixture containing 2 mmol of the aldehyde, 233 µl of EtOH, and 100 µl of TMB, preheated to the reaction temperature, is added under stirring. After 10 minutes, 5 mmol of triethyl orthoformate, also preheated to the reaction temperature, is added to start the acetalisation reaction. After the designated reaction time, the mixture is immediately filtered through celite, and the yield of acetal is determined using ^{1}H-NMR measured in DMSO-d6. Each experiment is accompanied by a blank test without the catalyst.

4.10.2 Calculation of yield of the acetalisation reaction

To determine the yield of the reaction, the mixture is filtered through Celite after the reaction finishes, and the ^{1}H-NMR is measured in DMSO-d6. The spectra were recorded on either a Bruker Avance 300 or a Bruker Avance 400 spectrometer at 298 K.

Table 4-15 Chemical shift in ^{1}H NMR (DMSO d_6)

Signal	δ (ppm)	
Ha	9.88(s)	
Hb	7.87(d)	
Hc	7.13(d)	
Hd	3.87(s)	
H1	7.31(d)	
H2	6.91(d)	
H3	5.43(s)	
H4	3.75(s)	

The ratio of aldehyde to acetal is determined by comparing the peak areas of the relevant protons. The ^{1}H-NMR spectrum shows the four aromatic ring protons of 4-MeO-benzaldehyde at δ 7.87 ppm (d) and δ 7.13 ppm (d), and for the acetal at δ 7.31 ppm (d) and δ 6.91 ppm (d). The three protons from the methoxy groups are found at δ 3.87 ppm (s) and δ 3.75 ppm (s) for the aldehyde and acetal, respectively. The proton on the carbonyl group of the aldehyde is found at δ 9.88 ppm (s), while the respective proton for the acetal is at δ 5.42 ppm (Table 4-15 and Fig. 4-26).

In the case of the blank test, the ^{1}H-NMR corresponds to the mixture of aldehyde, TMB, EtOH, and triethyl orthoformate, indicating that no reaction is observed. Therefore, the formation of products when the catalyst is implemented is easily confirmed, and the yield of the reaction in the respective spin states can be determined.

To compare different experiments and ensure equal amounts of reactants are added in all experiments, TMB is used as an internal standard. It is important to note that, even if the blank test is not mentioned further in the following sections, it was systematically performed every time to ensure that the reaction only occurs when the catalyst is used.

The yield of acetal is calculated for each experiment (see Eq. 4-6).

$$Yield\ (acetal) = \frac{n_{acetal}}{n_{aldehyde}+n_{acetal}} \times 100\% \qquad \text{(Eq 4-6)}$$

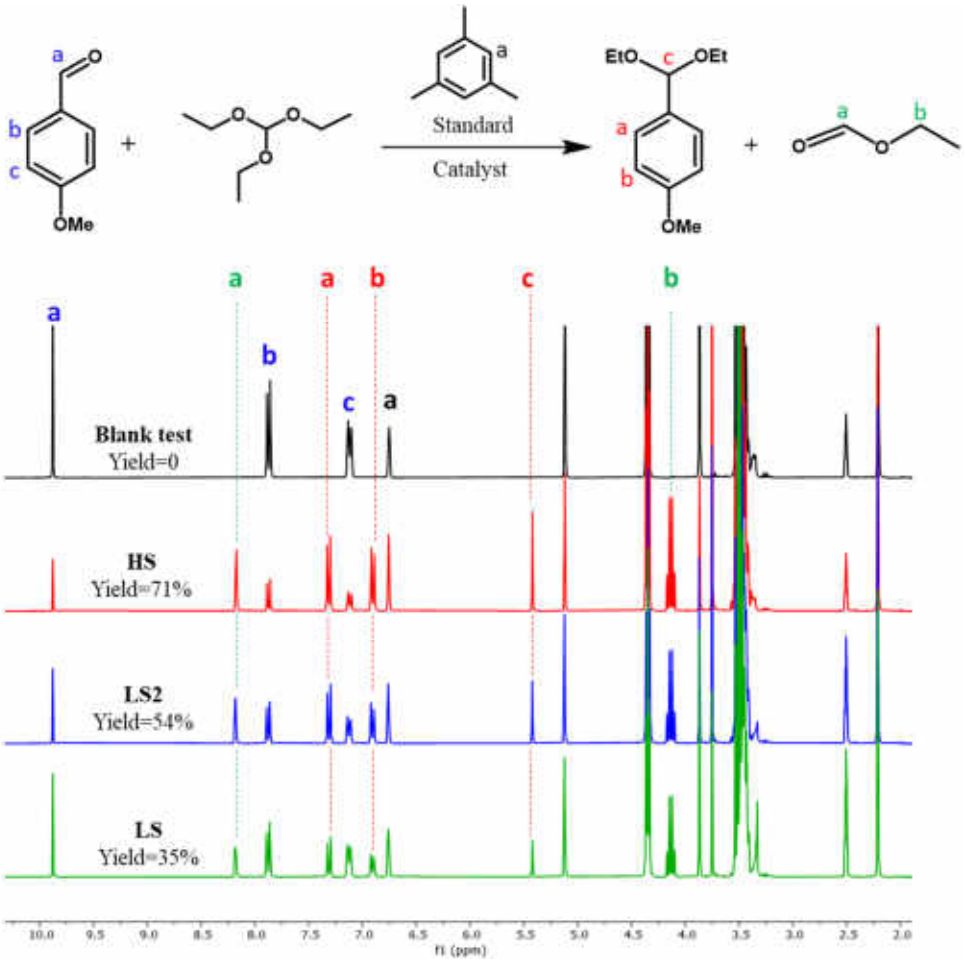
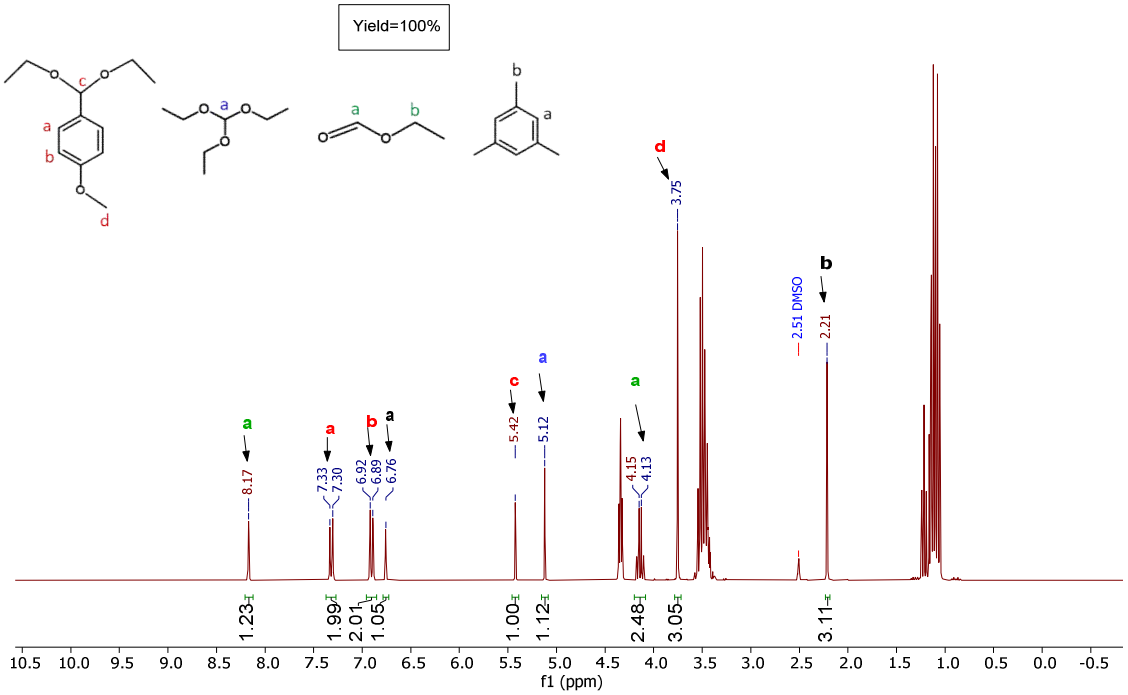


Fig. 4-26 The representative ^{1}H-NMR spectrum of the reaction mixture after the catalyst was removed by filtration on celite.

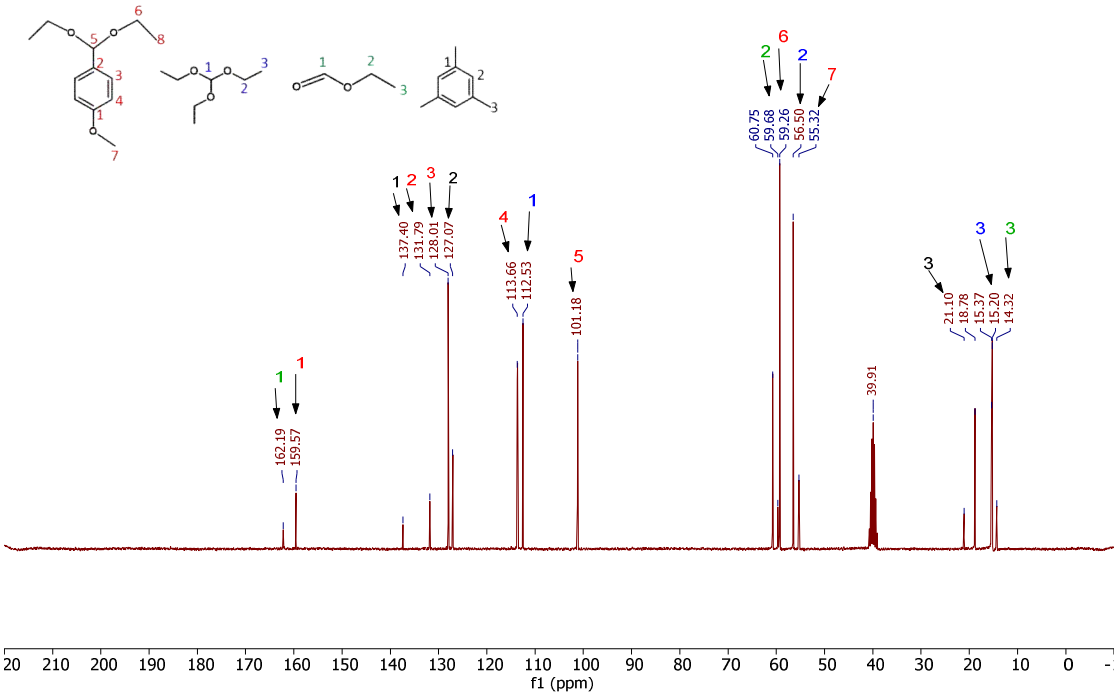
4.10.3 NMR spectra of the product

1-Diethoxymethyl-4-methoxybenzene

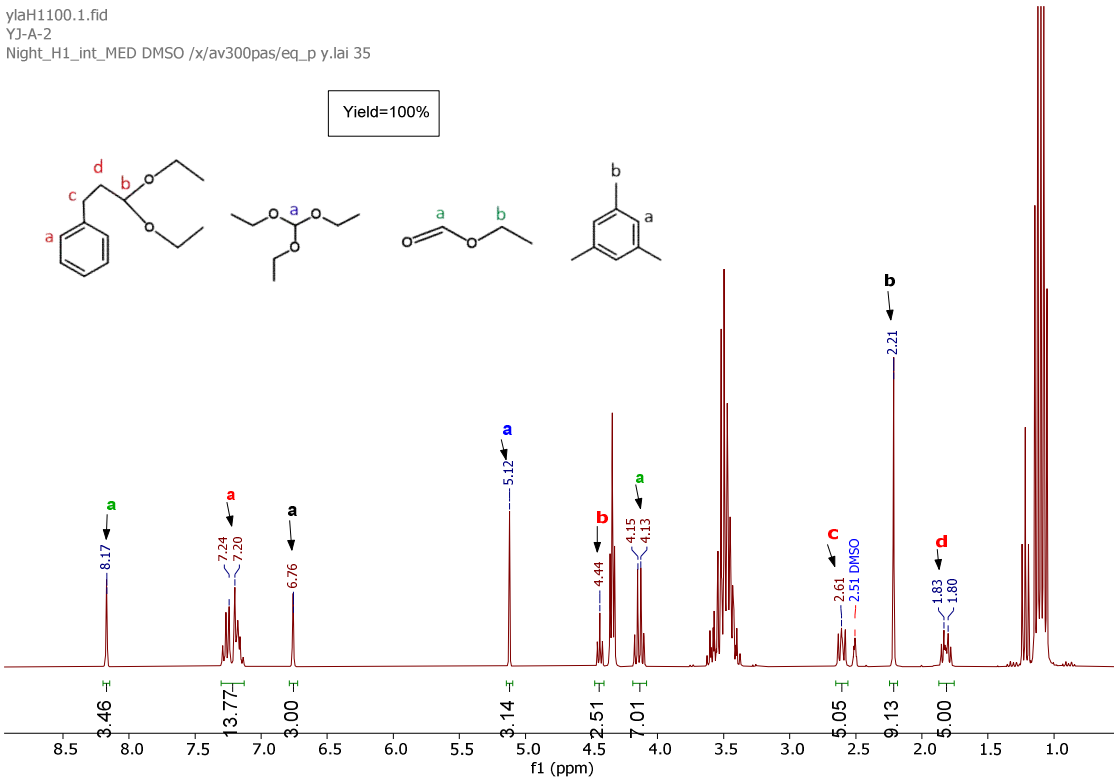
ylaH1099.1.fid
YJ-A-1
Night_H1_int_MED DMSO /x/av300pas/eq_p y.lai 34

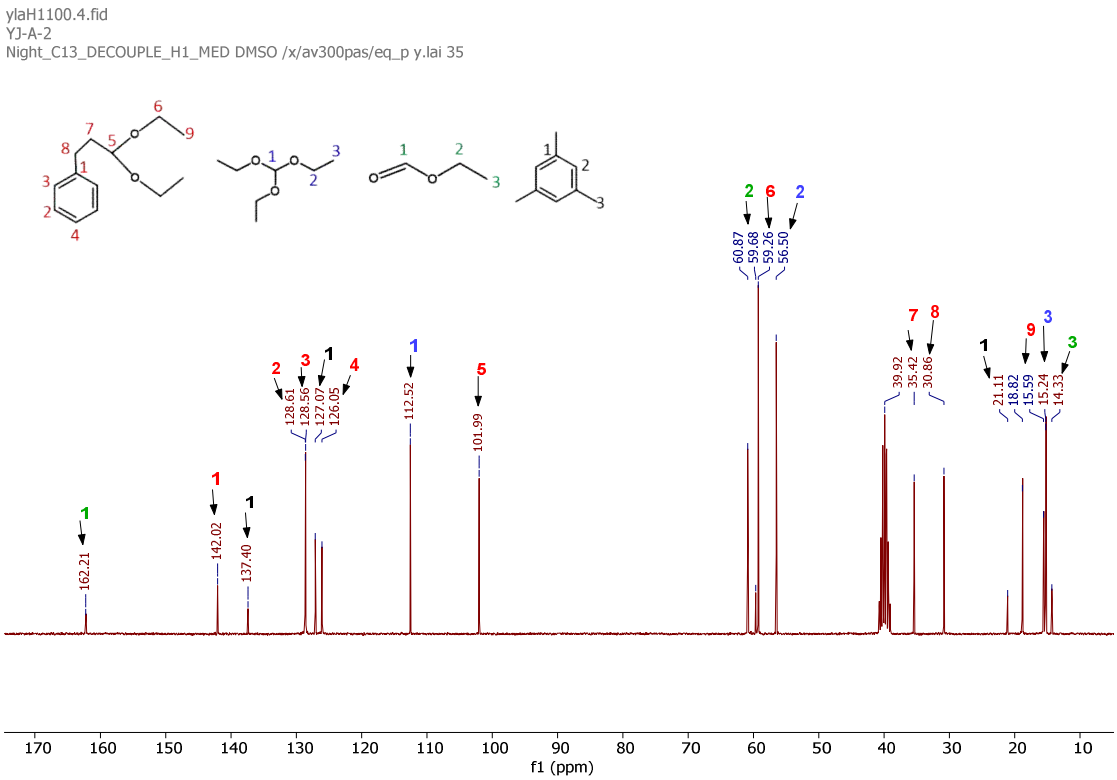


ylaH1099.4.fid
YJ-A-1
Night_C13_DECOUPLE_H1_MED DMSO /x/av300pas/eq_p y.lai 34

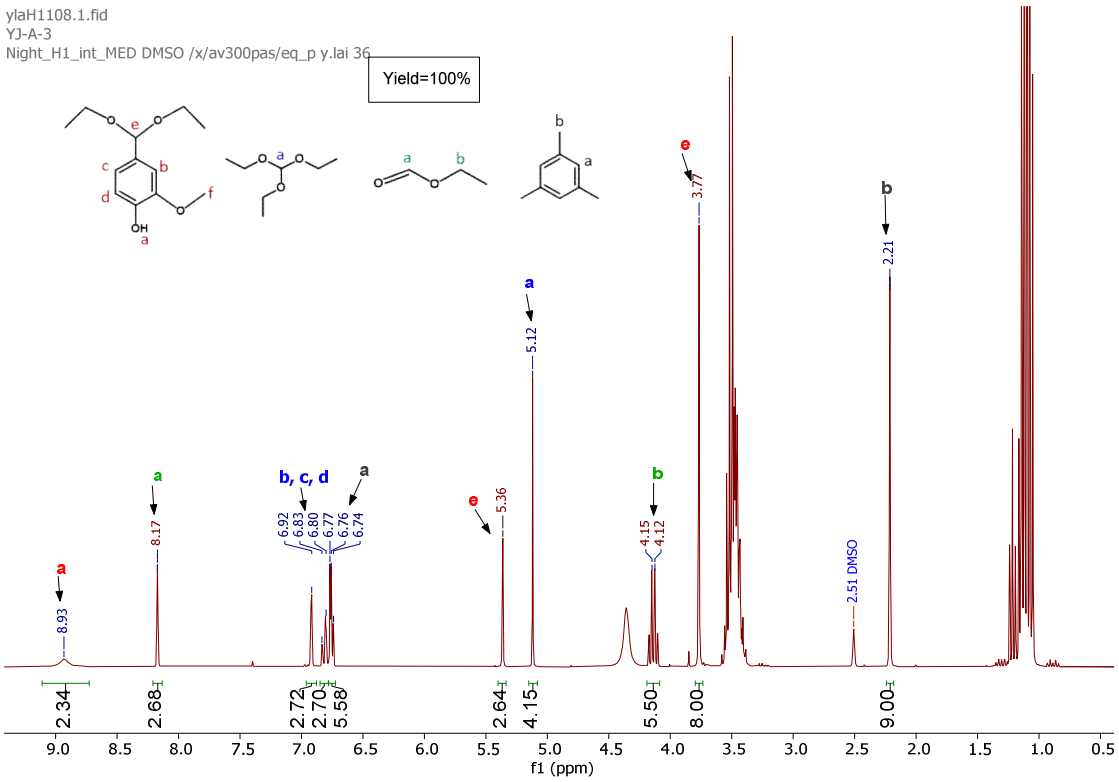


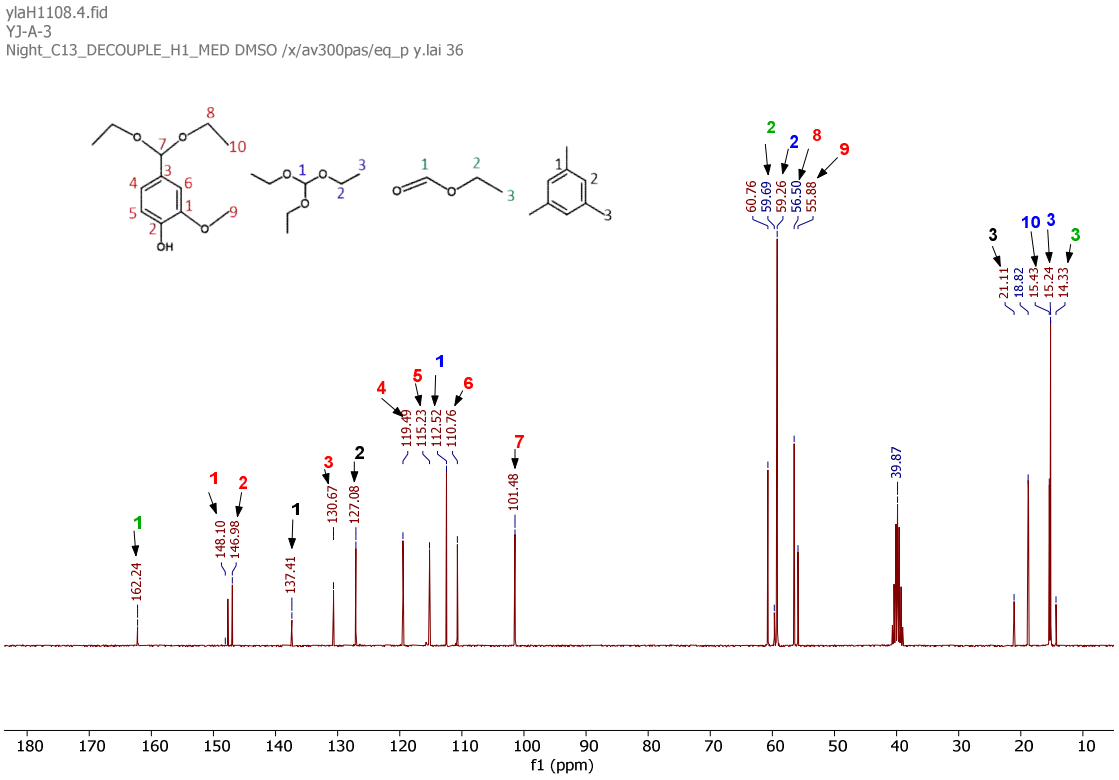
1-(3,3-diethoxypropyl)Benzene





4-Diethoxymethyl-2-methoxy-phenol

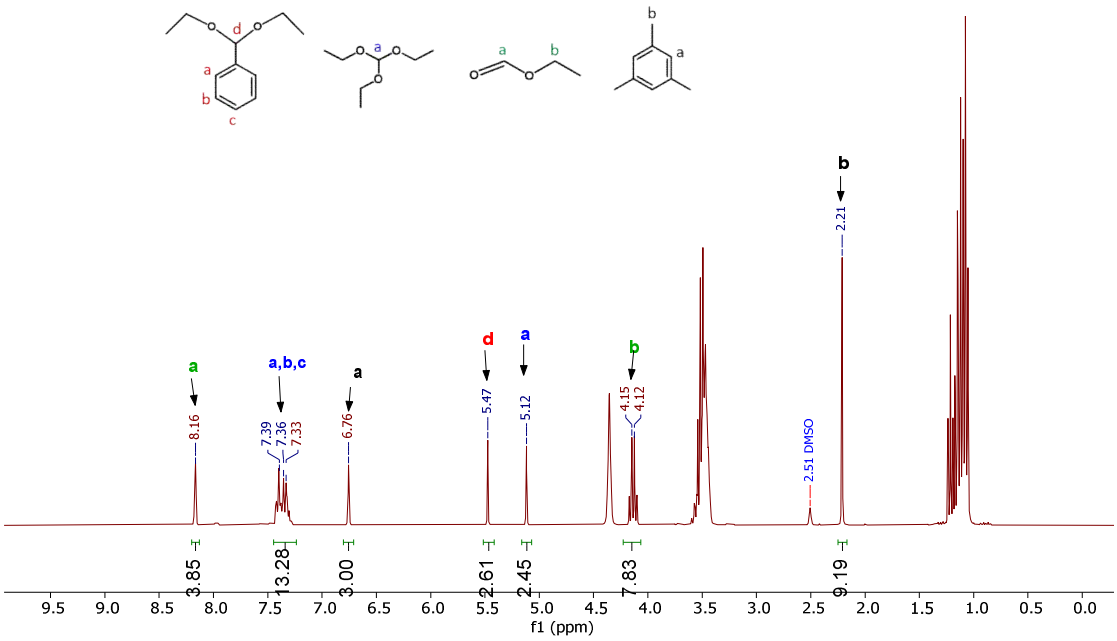




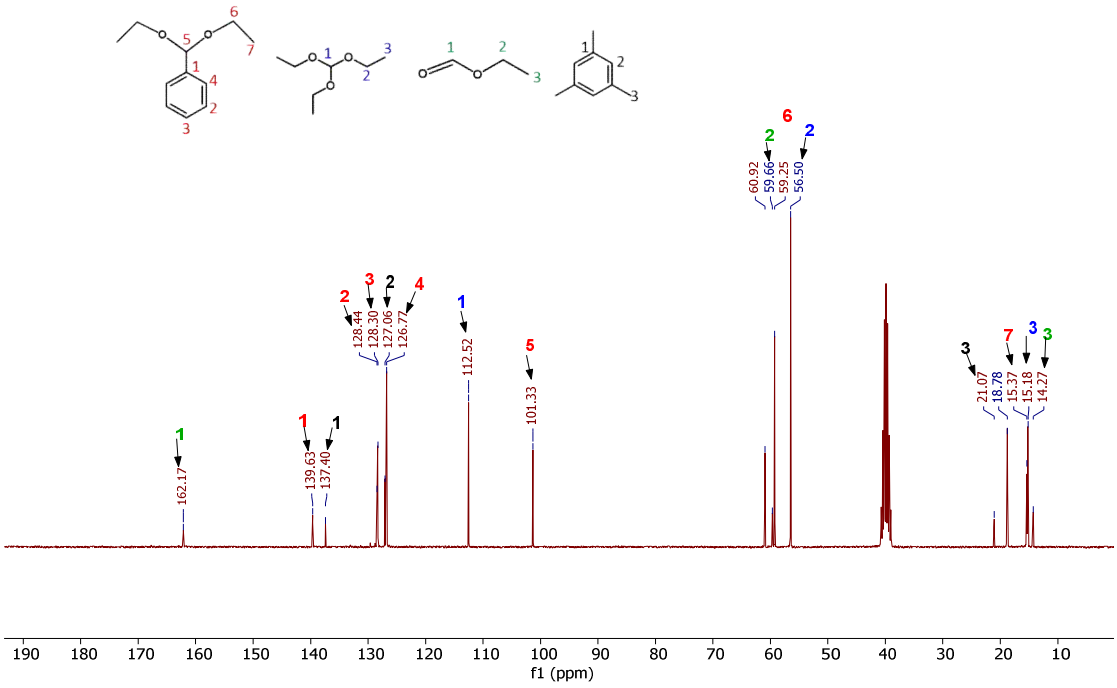
1,1-Diethoxymethylbenzene

ylaH1117.1.fid
YJ-A-55
Night_H1_int_MED DMSO /x/av300pas/eq_p y.lai 5

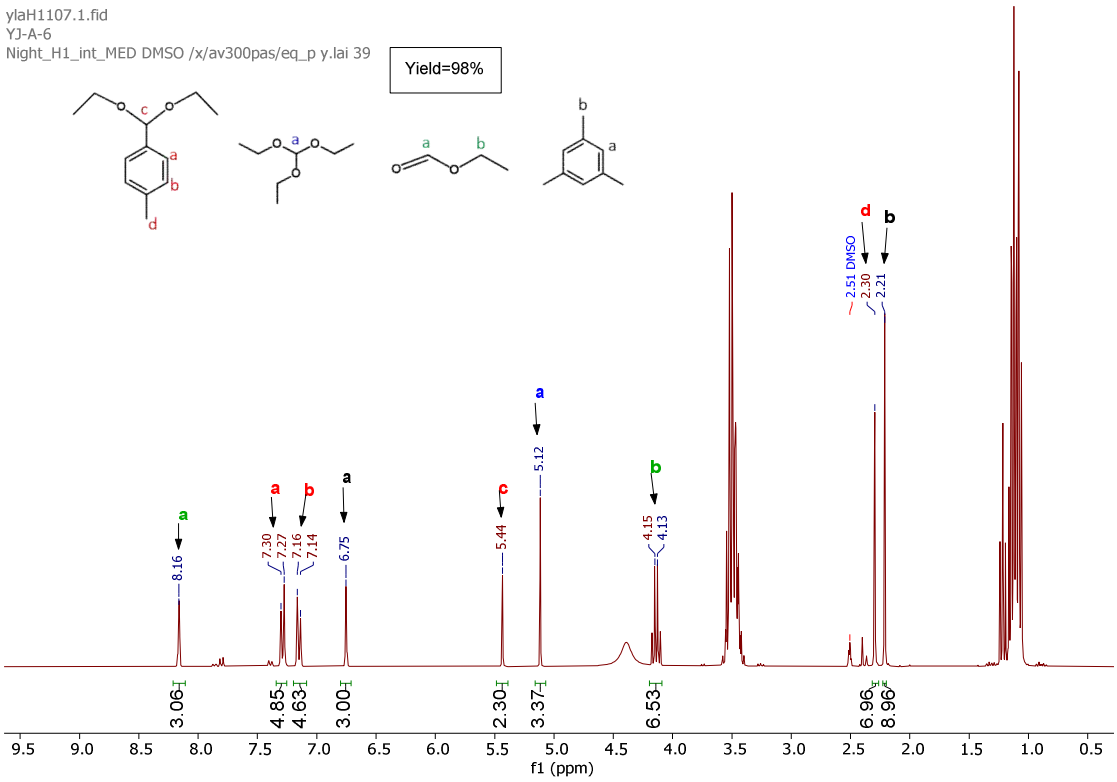
Yield=100%

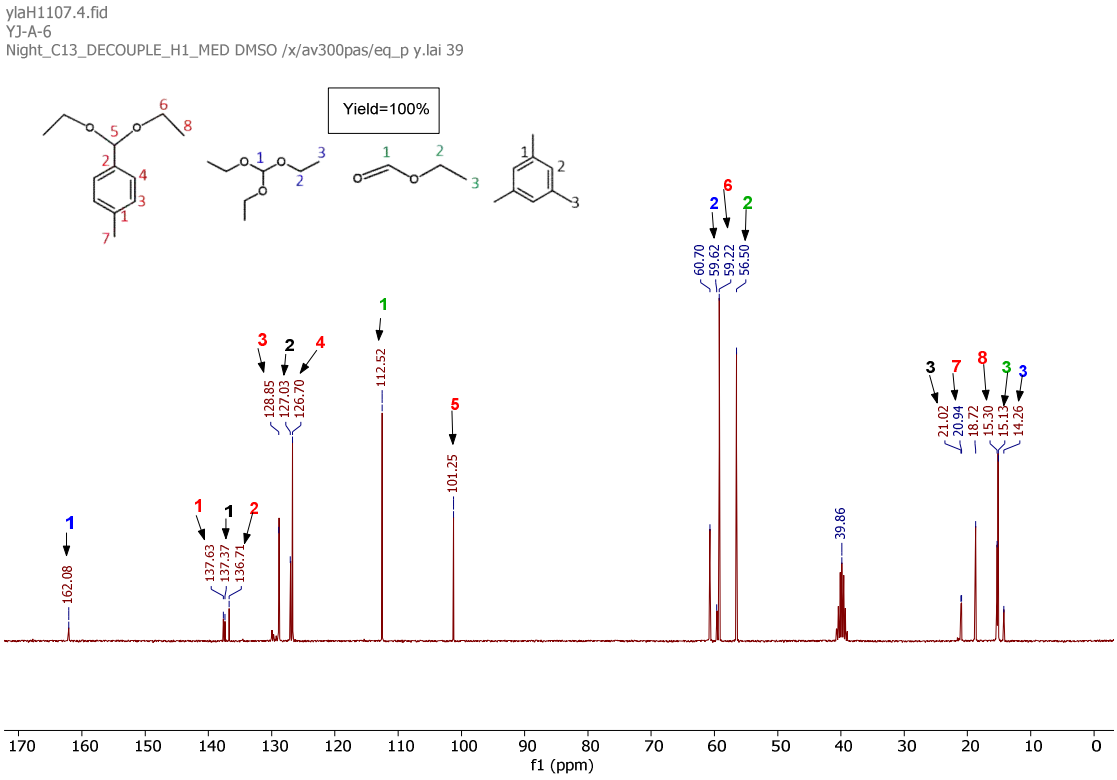


ylaH1117.2.fid
YJ-A-55
Night_C13_DECOUPLE_H1_MED DMSO /x/av300pas/eq_p y.lai 5

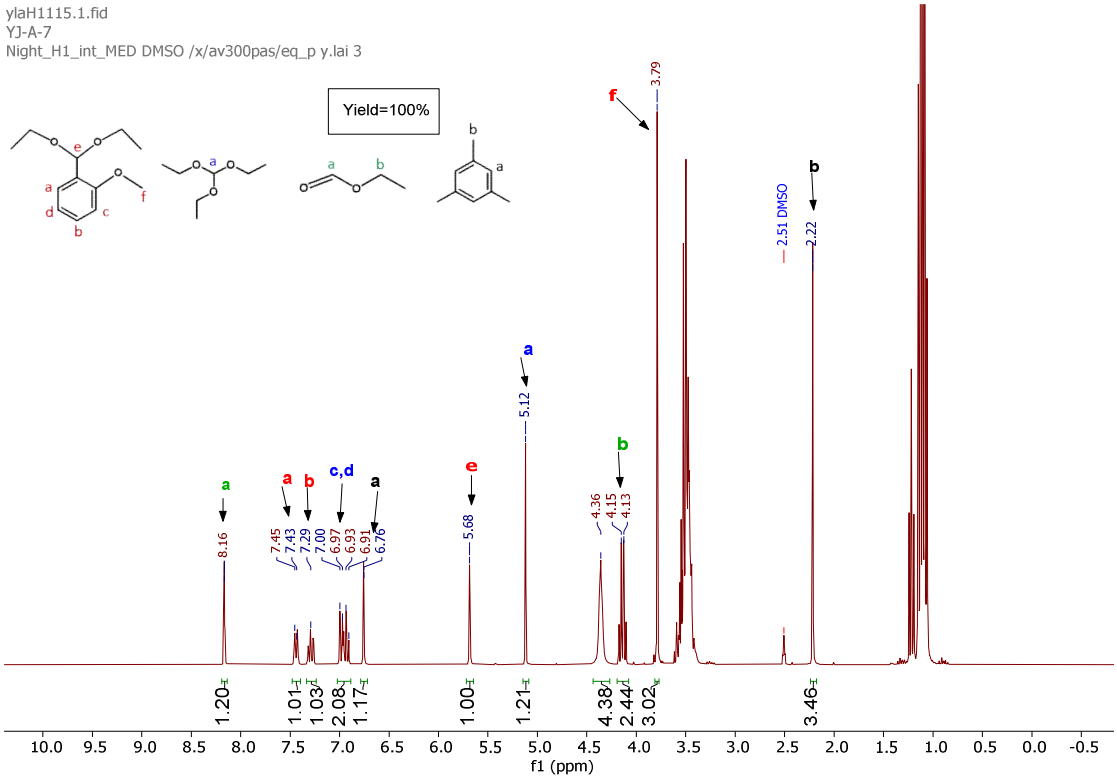


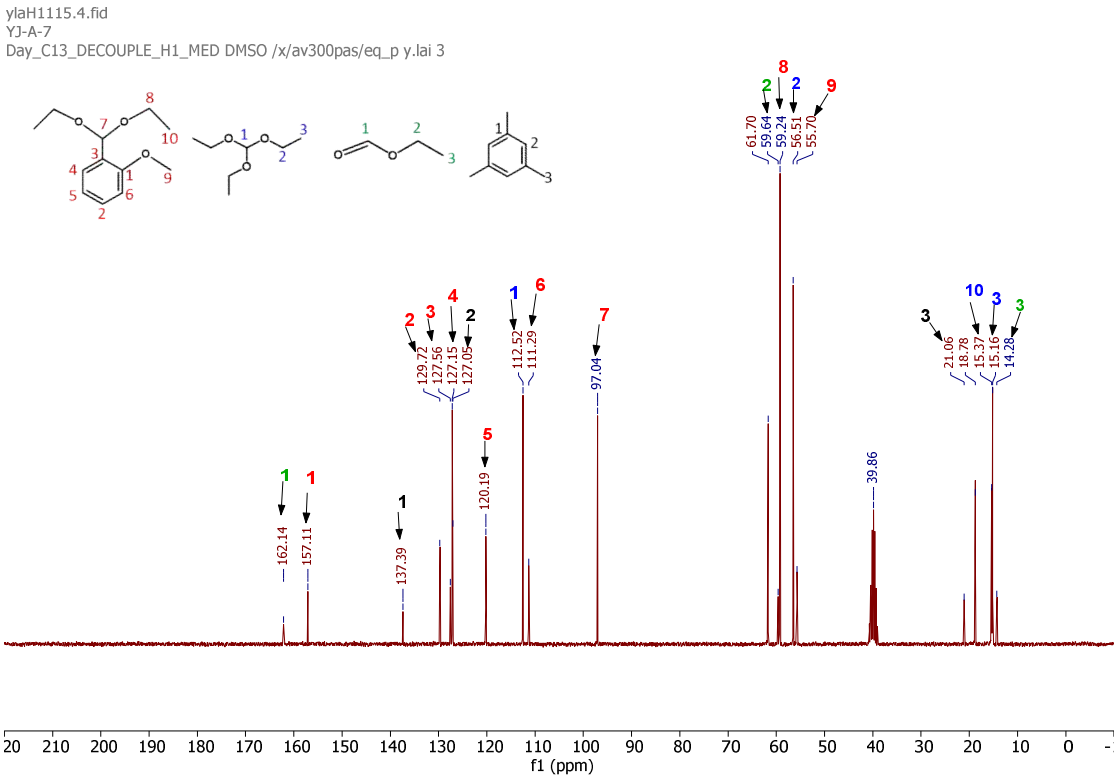
1-Diethoxymethyl-4-methylbenzene





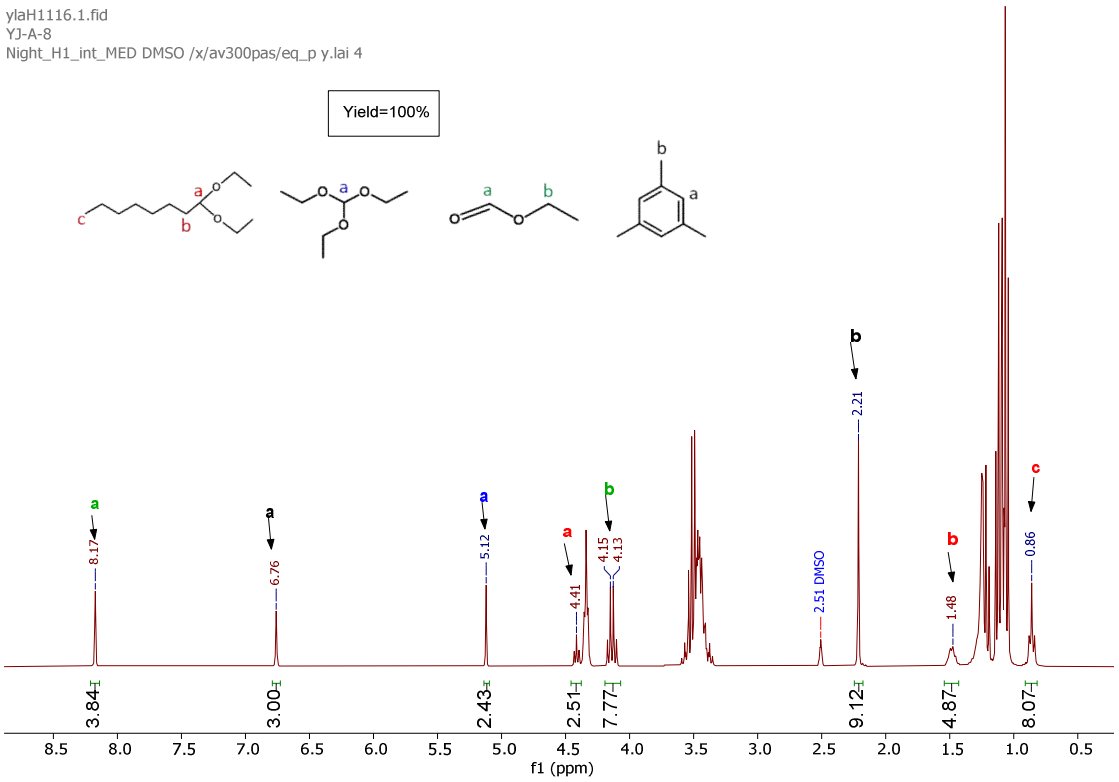
1-(Diethoxymethyl)-2-methoxybenzene



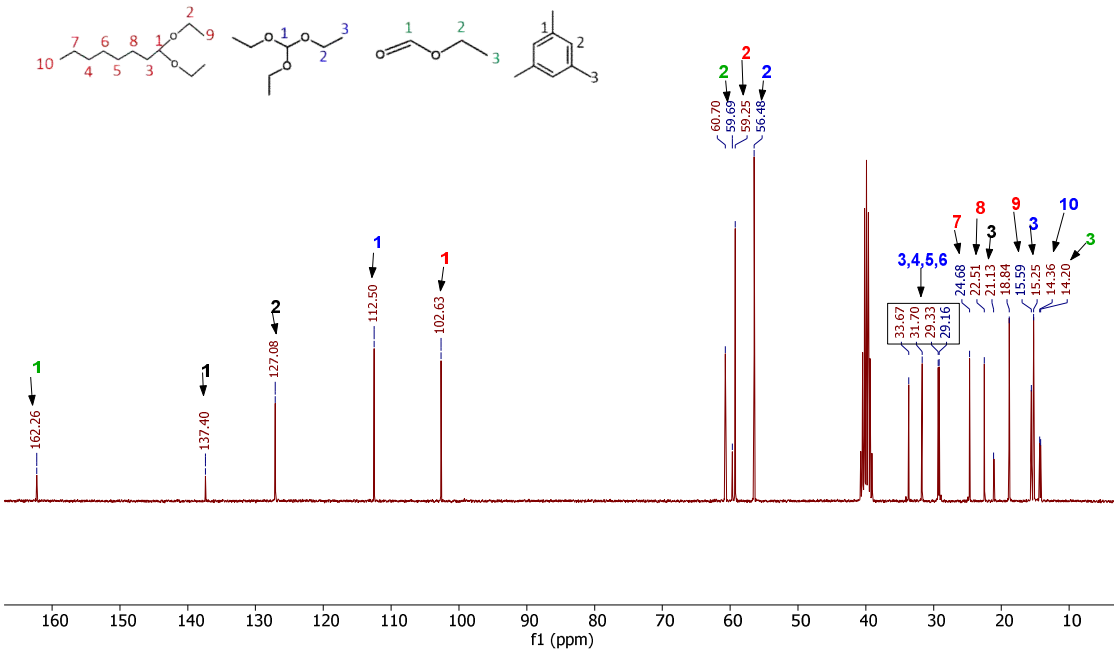


1,1-Diethoxy-octane

ylaH1116.1.fid
YJ-A-8
Night_H1_int_MED DMSO /x/av300pas/eq_p y.lai 4



ylaH1116.4.fid
YJ-A-8
Night_C13_DECOUPLE_H1_MED DMSO /x/av300pas/eq_p y.lai 4



4.11 References

[1] A. Enríquez-Cabrera, Y. Lai, L. Salmon, L. Routaboul, A. Bousseksou, Spin state effect on the efficiency of a post-synthetic modification reaction on a spin crossover complex, *submitted articles* **2024**.

[2] Y. Lai, A. Enríquez-Cabrera, L. Salmon, L. Routaboul, A. Bousseksou, When the study of the post-synthetic modification method on a 1D spin crossover coordination polymer highlights the catalytic activity of this iron complex, *submitted articles* **2024**.

[3] A. Enriquez-Cabrera, L. Getzner, L. Salmon, L. Routaboul, A. Bousseksou, Post-synthetic modification mechanism for 1D spin crossover coordination polymers, *New J. Chem.* **2022**, 46, 22004-22012.

[4] A. Enriquez-Cabrera, A. Rapakousiou, M.P. Bello, G. Molnár, L. Salmon, A. Bousseksou, Spin crossover polymer composites, polymers and related soft materials, *Coord. Chem. Rev.* **2020**, 419, 213396.

[5] A. Enríquez-Cabrera, K. Ridier, L. Salmon, L. Routaboul, A. Bousseksou, Complete and versatile post-synthetic modification on iron-triazole spin crossover complexes: a relevant material elaboration method, *Eur. J. Inorg. Chem.* **2021**, 2021, 2000-2016.

[6] A. Enríquez-Cabrera, L. Routaboul, L. Salmon, A. Bousseksou, Complete post-synthetic modification of a spin crossover complex, *Dalton Trans.* **2019**, 48, 16853-16856.

[7] M. Kotke, P.R. Schreiner, Acid-free, organocatalytic acetalization, *Tetrahedron* **2006**, 62, 434-439.

[8] W. Nicolazzi, A. Bousseksou, Thermodynamical aspects of the spin crossover phenomenon, *C. R. Chim.* **2018**, 21, 1060-1074.

[9] A. Bousseksou, G. Molnár, L. Salmon, W. Nicolazzi, Molecular spin crossover phenomenon: recent achievements and prospects, *Chem. Soc. Rev.* **2011**, 40, 3313-3335.

[10] A. Grosjean, P. Négrier, P. Bordet, C. Etrillard, D. Mondieig, S. Pechev, E. Lebraud, J.F. Létard, P. Guionneau, Crystal structures and spin crossover in the polymeric material [Fe (htrz) 2 (trz)](BF4) including coherent-domain size reduction effects, *Eur. J. Inorg. Chem.* **2013**, 2013, 796-802.

[11] A. Grosjean, N. Daro, S. Pechev, L. Moulet, C. Etrillard, G. Chastanet, P. Guionneau, The spin-crossover phenomenon at the coherent-domains scale in 1D polymeric powders: evidence for structural fatigability, *Eur. J. Inorg. Chem.* **2016**, 2016, 1961-1966.

[12] A. Grosjean, N. Daro, S. Pechev, C. Etrillard, G. Chastanet, P. Guionneau, Crystallinity and microstructural versatility in the spin-crossover polymeric material [Fe (Htrz) 2 (trz)](BF4), *Eur. J. Inorg. Chem.* **2018**, 2018, 429-434.

[13] A. Grosjean, Matériaux polymériques 1D à transition de spin: investigations structurales multi-échelles, Université de Bordeaux 1, 2013.

[14] X. Yang, A. Enriquez-Cabrera, K. Jacob, Y. Coppel, L. Salmon, A. Bousseksou, Room temperature spin crossover properties in a series of mixed-anion Fe (NH 2 trz) 3 (BF 4) 2− x (SiF 6) x/2 complexes, *Dalton Trans.* **2024**, 53, 6830-6838.

[15] D. Paliwoda, L. Vendier, L. Getzner, F. Alabarse, D. Comboni, B. Martin, S.E. Alavi, M.P. Bello, L. Salmon, W. Nicolazzi, Elastic Properties of the Iron (II)–Triazole Spin Crossover Complexes [Fe (Htrz) 2trz] BF4 and [Fe (NH2trz) 3] SO4, *Cryst. Growth Des.* **2023**, 23, 1903-1914.

[16] F. Zaera, Nanostructured materials for applications in heterogeneous catalysis, *Chem. Soc. Rev.* **2013**, 42, 2746-2762.

[17] C. Vogt, B.M. Weckhuysen, The concept of active site in heterogeneous catalysis, *Nature Reviews Chemistry* **2022**, 6, 89-111.

[18] M. Rumyantsev, N.S. Sitnikov, N.V. Somov, Hydrogen-bond-assisted organocatalytic acetalization of secondary alcohols: experimental and theoretical studies, *The Journal of Physical Chemistry A* **2015**, 119, 4108-4117.

[19] Y.-W. Zhu, W.-B. Yi, C. Cai, A recyclable fluorous hydrazine-1, 2-bis (carbothioate) with NCS as efficient catalysts for acetalization of aldehydes, *New J. Chem.* **2013**, 37, 890-892.

[20] M.X. Tan, L. Gu, N. Li, J.Y. Ying, Y. Zhang, Mesoporous poly-melamine-formaldehyde (mPMF)–a highly efficient catalyst for chemoselective acetalization of aldehydes, *Green Chem.* **2013**, 15, 1127-1132.
[21] A. Dhakshinamoorthy, M. Alvaro, H. Garcia, Metal organic frameworks as solid acid catalysts for acetalization of aldehydes with methanol, *Adv. Synth. Catal.* **2010**, 352, 3022-3030.
[22] Q. Bao, K. Qiao, D. Tomida, C. Yokoyama, Acetalization of carbonyl compounds catalyzed by GaCl3 immobilized on imidazolium-styrene copolymers, *Catal. Commun.* **2009**, 10, 1625-1628.
[23] Z. Duan, Y. Gu, Y. Deng, Green and moisture-stable Lewis acidic ionic liquids (choline chloride· xZnCl2) catalyzed protection of carbonyls at room temperature under solvent-free conditions, *Catal. Commun.* **2006**, 7, 651-656.
[24] D.B.G. Williams, M.C. Lawton, Highly atom efficient aluminium triflate catalysed acetal formation, *Green Chem.* **2008**, 10, 914-917.
[25] R.A. Ugarte, T.W. Hudnall, Antimony (V) catalyzed acetalisation of aldehydes: An efficient, solvent-free, and recyclable process, *Green Chem.* **2017**, 19, 1990-1998.
[26] B.T. Gregg, K.C. Golden, J.F. Quinn, Indium (III) trifluoromethanesulfonate as a mild, efficient catalyst for the formation of acetals and ketals in the presence of acid sensitive functional groups, *Tetrahedron* **2008**, 64, 3287-3295.
[27] S. Velusamy, T. Punniyamurthy, Cobalt (II)-catalyzed chemoselective synthesis of acetals from aldehydes, *Tetrahedron Lett.* **2004**, 45, 4917-4920.
[28] D. Lyons, R. Crocker, D. Enders, T. Nguyen, Tropylium salts as efficient organic Lewis acid catalysts for acetalization and transacetalization reactions in batch and flow, *Green Chem.* **2017**, 19, 3993-3996.
[29] J.I. Padrón, V.S. Martín, Catalysis by means of Fe-based lewis acids, *Iron Catalysis: Fundamentals and Applications* **2011**, 1-26.
[30] F. Zhang, J. Shi, Y. Jin, Y. Fu, Y. Zhong, W. Zhu, Facile synthesis of MIL-100 (Fe) under HF-free conditions and its application in the acetalization of aldehydes with diols, *Chem. Eng. J.* **2015**, 259, 183-190.
[31] E.M. Maya, E. Verde-Sesto, J.G. de la Campa, M. Iglesias, Polyiminopyridines based networks as supports to heterogenize iron (II) complexes. Application as efficient and selective ecofriendly catalysts, *ChemistrySelect* **2016**, 1, 396-402.
[32] G.K.B. Ferreira, C. Carvalho, S. Nakagaki, Studies of the catalytic activity of iron (III) porphyrins for the protection of carbonyl groups in homogeneous media, *Catalysts* **2019**, 9, 334.
[33] I. Karamé, M. Alamé, A. Kanj, G.N. Baydoun, H. Hazimeh, M. el Masri, L. Christ, Mild and efficient protection of diol and carbonyls as cyclic acetals catalysed by iron (III) chloride, *C. R. Chim.* **2011**, 14, 525-529.
[34] A. Dhakshinamoorthy, M. Alvaro, H. Chevreau, P. Horcajada, T. Devic, C. Serre, H. Garcia, Iron (III) metal–organic frameworks as solid Lewis acids for the isomerization of α-pinene oxide, *Catalysis Science & Technology* **2012**, 2, 324-330.
[35] A. Dhakshinamoorthy, M. Alvaro, P. Horcajada, E. Gibson, M. Vishnuvarthan, A. Vimont, J.-M. Grenèche, C. Serre, M. Daturi, H. Garcia, Comparison of porous iron trimesates basolite F300 and MIL-100 (Fe) as heterogeneous catalysts for lewis acid and oxidation reactions: roles of structural defects and stability, *Acs Catalysis* **2012**, 2, 2060-2065.
[36] M. Menzinger, R. Wolfgang, The meaning and use of the Arrhenius activation energy, *Angewandte Chemie International Edition in English* **1969**, 8, 438-444.

Chapter 5 Spin Crossover Composite Films as Catalysts for Acetalization Reactions

5.1 Introduction

In Chapter 4 we have demonstrated the effect of the spin state effect on the catalytic reactivity of a spin crossover complex in an acetalisation reaction. In particular, higher catalytic activity is observed in the HS state, which is not due to a different electronic pathway but rather to better access of the substrate to the active sites. As well known in heterogeneous catalysis, the accessibility of the catalytic sites is a critical factor in determining the overall efficiency.[1-3] Unlike homogeneous catalysis, where the catalyst and reactants are in the same phase, in heterogeneous catalysis the catalyst is in a different phase (often a solid) while the reactants are in a liquid or gas phase. Catalysis typically occurs at specific active sites where the reactants interact with the catalyst to form products. In some catalysis systems, the availability of catalytic sites can be affected by various factors such as the physical structure of the material[4] or external stimuli that alter the environment around the catalytic site.[5]

Access to catalytic sites is crucial not only in traditional heterogeneous catalysis but also in emerging switchable catalytic systems, as it directly affects the efficiency, selectivity and control of the catalytic process. Switchable catalysis refers to systems that can be reversibly activated or deactivated in response to external stimuli. [6-8] This switchable catalysis system represents a powerful approach to advancing dynamic, adaptive and efficient chemical processes. Recent studies have shown that controlling access to catalytic sites in switchable catalysis systems allows precise, on-demand regulation of catalytic activity, improving efficiency and adaptability.[9-11] We were particularly interested in two of these research studies since the movement of the catalyst components determines whether the reaction occurs. He and colleagues released the first of these in 2012. They created a hydrogel-based system that reacts to pH and temperature variations.[12] This hydrogel supports small tubular structures with catalyst-coated tips. When pH or temperature changes, the hydrogel swells or shrinks, causing the structures to move in and out of a reactant layer. This movement acts as a switch, controlling chemical reactions based on the catalyst used. The hydrogel can be composed of a polymer that swells when the pH is between 5 and 10, or one that responds to temperature (swelling below 32 °C and shrinking above it). When the hydrogel swells, the structures straighten, positioning the catalyst in contact with the reactants to initiate the reaction. As the hydrogel shrinks, the structures bend, retracting the catalyst and halting the reaction.

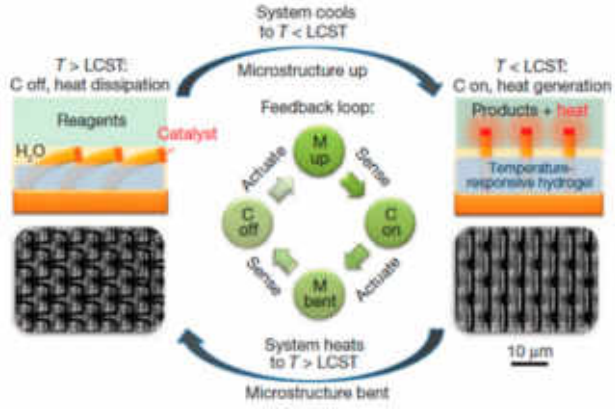


Fig.5-1 Homeostasis in SMARTS (Self-regulating Mechanically Actuated Responsive Triggered Systems) is achieved through self-regulated chemo-thermomechanical feedback loops.[12]

The authors also demonstrated that coupling a temperature-sensitive hydrogel with an exothermic reaction creates a self-regulating system (Fig.5-1). When the temperature is below the hydrogel's LCST (Lower Critical Solution Temperature), the structures straighten, triggering the reaction. As the temperature rises due to the reaction's heat, the hydrogel shrinks (T > LCST), stopping the reaction. When the temperature drops, the cycle repeats, creating continuous, self-regulated reaction cycles. This work is significant because it introduces a novel system that integrates smart materials with catalysis, utilizing mechanical actuation to precisely control chemical reactions. It opens new possibilities for responsive and adaptable catalytic systems in various applications.

In 2017, Mazur et al. introduced a system for mechanically controlled catalysis using a platinum (Pt) wire functionalized with a tightly packed self-assembled monolayer (SAM) of 1-naphthalene thiol.[13] In this system, switching between catalytically active and inactive states is achieved through the elastic deformation of the metal wire. Initially, the SAM-coated Pt wire is catalytically inactive toward hydrogen peroxide (H_2O_2) in the surrounding medium, as the SAM prevents direct contact between the catalyst surface and its substrate. However, when the wire is bent slightly, the SAM becomes less compact in the bent regions, allowing greater access of the reactants to the metal surface (Fig.5-2). This change facilitates the Pt-catalyzed decomposition of H_2O_2, producing oxygen bubbles. Once the compressive force is removed the wire returns to its original shape, restoring its protective layer and stopping the catalytic reaction.

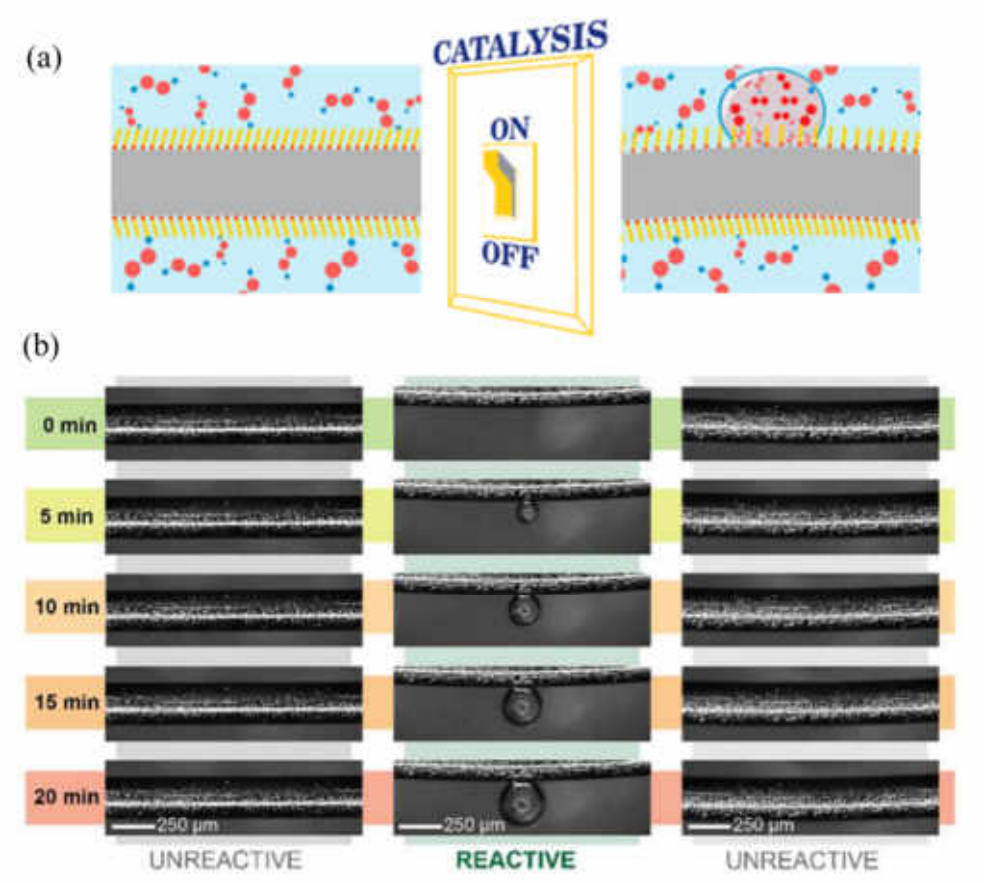


Fig.5-2 (a) Schematic representation of SAM (self-assembled monolayer) modification on the Pt wire following mechanical deformation. (b) Experimental images showing a Pt rod coated with a SAM of 1-naphthalenethiol, immersed in a H_2O_2 solution. In the initial state (left), the rod remains inactive. Upon bending (middle), the catalytic surface is exposed, initiating a reaction, as indicated by the formation of oxygen bubbles. Once the compressive force is removed (right), the rod returns to its original shape, and the catalytic reaction ceases.[13]

In recent years, our research team has demonstrated that spin crossover polymer composites, which combine SCO compounds with polymer matrices, have emerged as a powerful class of hybrid materials as functional, smart and switchable materials for mechanical actuators. These composites not only possess the switchable properties of SCO compounds but also benefit from the flexibility, processability and mechanical strength of polymers. For example, in 2022, Piedrahita-Bello et al. conducted a detailed investigation into SCO@P(VDF-TrFE)/Ag@P(VDF-TrFE) bimorph electrothermal actuators (P(VDF-TrFE) = poly(vinylidene fluoride-trifluoroethylene)). Their research demonstrated that the appropriate choice of SCO particle composition, concentration, and morphology can facilitate large bending movements in these actuators.[14] Following this work, they further presented in 2023 that these actuators exhibited excellent controllability, with high positioning accuracy and robustness in both open- and closed-loop configurations.[15] More recently, Zan et al.[16] demonstrated that the use of a soft polymer matrix, such as TPU (thermoplastic polyurethane), enables the reproducible construction of bending devices actuated by embedded SCO particles $[Fe(NH_2trz)_3](SO_4)$ (25 wt%). The soft matrix significantly enhances actuation strain and bending amplitude compared to similar devices utilizing a stiffer polymer matrix (Fig.5-3).

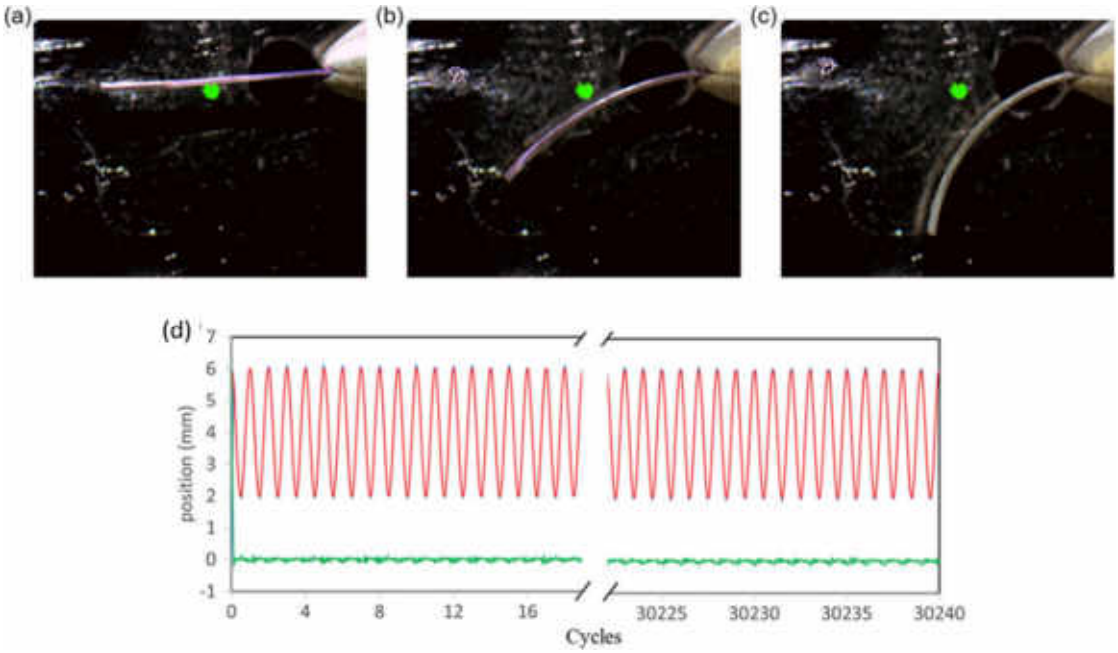


Fig.5-3 Movement of a rectangular bilayer strip upon the spin transition when heating from 20 to 100 °C. (a) Initial, (b) end of first cycle, and (c) end of second heating. (e) Closed-loop sinusoidal actuation of the device at the beginning and at the end of 30 240 cycles (7 days).[16]

Applications of spin-crossover materials have predominantly focused on the development of switchable devices.[17, 18] Extending their use to switchable catalytic systems is a novel and promising application of spin-crossover materials that has not been reported in the literature. As shown in Chapter 4, where the spin state modulates access to catalytic sites, the ability to regulate the spin state provides control over catalytic activity. This study highlights the potential of spin crossover complexes for the development of dynamic catalytic systems with tunable reactivity. Exploring the catalytic capabilities of spin crossover materials in this context offers a promising avenue for future research, with the potential to extend their applications in switchable catalysis beyond conventional applications.

In this chapter, we focus on the use of SCO@polymer composite films in catalysis. Switchable catalysis based on spin-crossover materials with mechanical movement is an innovative approach that may enable precise control of catalytic activity through mechanical movement. This concept uses bistable spin crossover materials that undergo reversible structural changes in response to external stimuli, altering their catalytic properties through mechanical movement to regulate catalytic reactions. To accomplish this long-term goal, we plan to create a bilayer material. One layer would have the SCO complex, which would serve as a catalyst, while the other layer would have another SCO complex, which would guarantee the composite material's movement. Recall that all SCO complexes have a 10% increase in molecular volume when they transition from the LS state to the HS state. This increase in molecular volume, however, causes a significant change in the volume of material for some SCO complexes. The entire polymeric layer lengthens when the SCO complex, which is responsible for ensuring movement, switches from the LS state to the HS state. Given that the two layers are connected, this volume change may cause the composite material to move and raise the porosity of the layer that contains the SCO complex, which would catalyze the reaction (Fig.5-4).

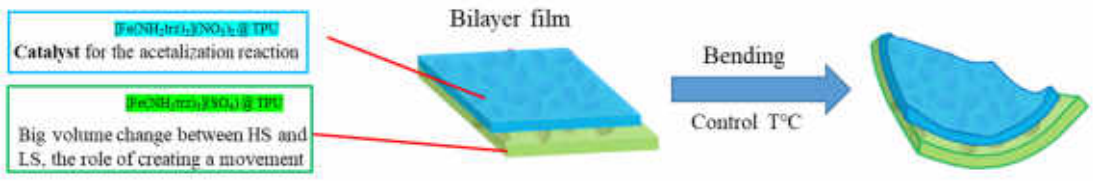


Fig.5-4 Sketch of the composite material we were planning to fabricate

By embedding the SCO material within a polymer matrix, these composite films offer a more practical application compared to powdered catalysts. In Chapter 4, we demonstrated that spin-crossover $Fe(NH_2trz)_3](NO_3)_2$ complex **1** serves as an effective catalyst for acetalization reactions. While the powdered form of the SCO complex permits catalyst recovery through methods such as filtration or centrifugation, these processes are often time-consuming and prone to catalyst loss, thereby reducing overall efficiency. It is anticipated that the thin film structure will make it easier to remove catalysts from reaction mixtures, doing away with the requirement for intricate recovery techniques. This strategy would greatly increase overall reuse while minimizing catalyst loss during recycling.

Indeed, polymer composite films have emerged as a promising solution to the challenge of catalyst recovery and reusability, which remains a significant hurdle in industrial applications.[19] Polymer composite films combine the unique properties of polymers-such as flexibility, durability, and chemical resistance-with the catalytic capabilities of embedded active species, like metals, metal oxides, complexes or enzymes. This integration creates a versatile platform for catalysis, where the active components are immobilized within the polymer matrix, reducing catalyst loss during reaction cycles. Additionally, the physical structure of these films allows for easy separation from reaction mixtures, enabling straightforward recovery and reuse. The potential of polymer composite films to enhance sustainability and reduce costs in catalytic technologies highlights their growing importance in both academic research and industrial practice. For example, In 2010, Hariprasad et al[20] presented a silver nanoparticle-embedded polymer thin film as a highly efficient and reusable catalyst. The silver nanoparticle-embedded poly(vinyl alcohol) (PVA) thin film, termed a “dip catalyst”, was designed for easy insertion into and removal from the reaction solution (Fig.5-5). After each reaction cycle, the catalyst film was carefully removed, washed with water and isopropyl alcohol to clean any residual reactants, and then dried under a vacuum. This simple cleaning process prepared the film for the next use. The catalyst was reused for over 30 cycles

in the reduction of 4-nitrophenol, maintaining excellent performance throughout. Each time, the catalytic activity was nearly the same as in previous runs, with only a marginal drop in efficiency after multiple cycles. This is partly attributed to the stability of the silver nanoparticles, which remained securely embedded in the polymer matrix, showing little leaching or degradation. This reusability, along with the negligible loss of catalytic activity, demonstrates the robustness and practicality of the system for sustainable catalysis applications.

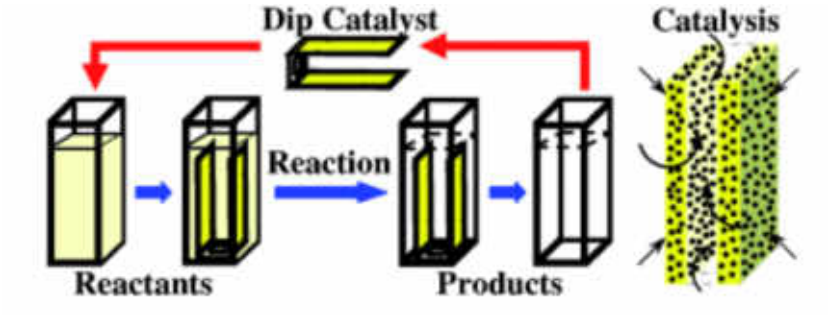
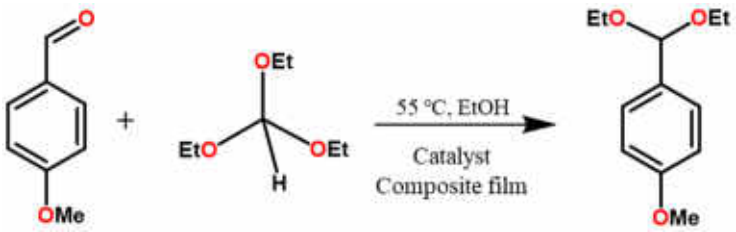


Fig.5-5 A reusable thin-film dip catalyst is utilised to reduce 4-nitrophenol using sodium borohydride.[20]

5.2 Our selections for spin crossover complex-based composite films used in catalysis.

5.2.1 Our selection of catalytic reaction

As in Chapter 4, we have demonstrated that the spin state of the iron could modulate the catalytic activity of the SCO coordination polymer. The acetalization of *p*-anisaldehyde in EtOH and in the presence of triethyl orthoformate was a very good reaction model. So, we will continue to focus on this model reaction to study using the SCO composite film as a catalyst.



Scheme 5-1 Acetalization of *p*-anisaldehyde with triethyl orthoformate using composite film as a catalyst.

5.2.2 Our selection of spin crossover complexes

Complex **1** ($[Fe(NH_2trz)_3](NO_3)_2$) is an ideal candidate for research on how the spin state affects its organic reactivity and catalytic capabilities, as we have demonstrated in earlier chapters. In this chapter, we will continue to employ it as the catalytic SCO complex.

To guarantee the composite material's movement, we have selected complex **1b** ($[Fe(NH_2trz)_3](SO_4)$). Complex **1b**, which is likewise a member of the 1D iron(II)-triazole coordination polymer family, has been used by our team to demonstrate the application of SCO bilayer composites as mechanical actuators. This complex **1b** displays a hysteresis loops above room temperature and undergoes significant volume changes of about 5%,[21] compared to the

$[Fe(NH_2trz)_3](NO_3)_2$ complex **1** (only about 1%).[22-25] It should be note that the complex **1b** cannot catalyze the acetalization reaction of *p*-anisaldehyde with triethyl orthoformate.

5.2.3 Our selection of Polymer

It is also crucial to select the appropriate polymer for this study project. Since ethanol is the solvent used in the catalytic reaction, the polymer must not dissolve in it. It must have enough porosity to let organic substrates reach the catalytic site, but not so much that the SCO complex particles are trapped inside the polymer. Apart from these catalytic reaction-related requirements, the polymer also needs to be soft and flexible enough to for the composite material to move. Our research team used Thermoplastic polyurethane (TPU) as a polymer to create complex SCO-based artificial muscles. More generally, TPU is a versatile material known for its excellent physical and chemical properties, which can be tailored through the control of its structure. It exhibits impressive mechanical strength, wear resistance, and a high dielectric constant, making it suitable for various applications. As illustrated in Fig.5-6, the hard segments of TPU consist of diisocyanates and chain extenders linked by hydrogen bonding and other intermolecular forces, providing rigidity and mechanical strength. The soft segments, typically composed of polyols, confer flexibility and elasticity, giving TPU its stretchable and adaptable nature. Due to these characteristics, TPU is a high-performance material with diverse potential applications, including energy harvesting, sensors, and actuators. [26-28] Given the team's expertise in the preparation of TPU-based composite materials and the fact that TPU is insoluble in ethanol, we decided to choose it as the polymer.

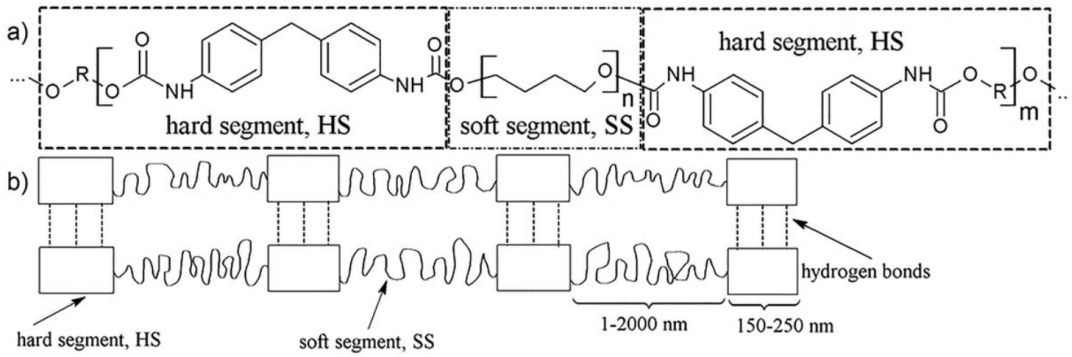


Fig.5-6 Schematic structure of the hard and soft segments of TPU. [27]

5.3 Fabrication and characterization of the SCO complexes@TPU films

As shown in Fig.5-7, we want to make composite films by embedding polymer particles in the TPU organic polymer.

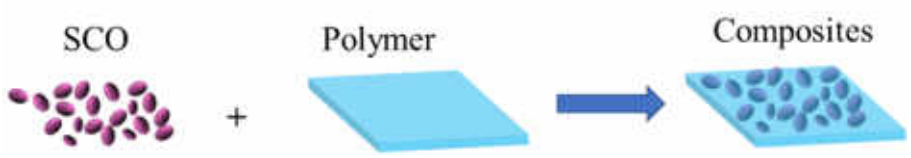


Fig.5-7 Schematic using the SCO complex, polymer and composite.

Bilayers are our primary focus for this project, but we have also created monolayers and trilayers (Fig.5-8). It is a little easier to fabricate and analyze monolayers. In particular, they were helpful for confirming that we could employ these composite materials as catalysts and for examining how the materials varied depending on the spin state of complex **1**. The complex **1b** monolayer was also created to check that this composite material could not catalyse the acetalisation reaction. The trilayer was of interest to us, to differentiate the effect of any increase in material porosity from the effect of movement of the composite material. In fact, the movement of the composite material is only observed for the bilayer. To verify the contribution of the layers containing the **1b** complex, the TPU-TPU/1-TPU complex trilayer was also tested. To achieve a still more robust catalytic film, the catalytic layer could potentially be shielded by the two extra layers.

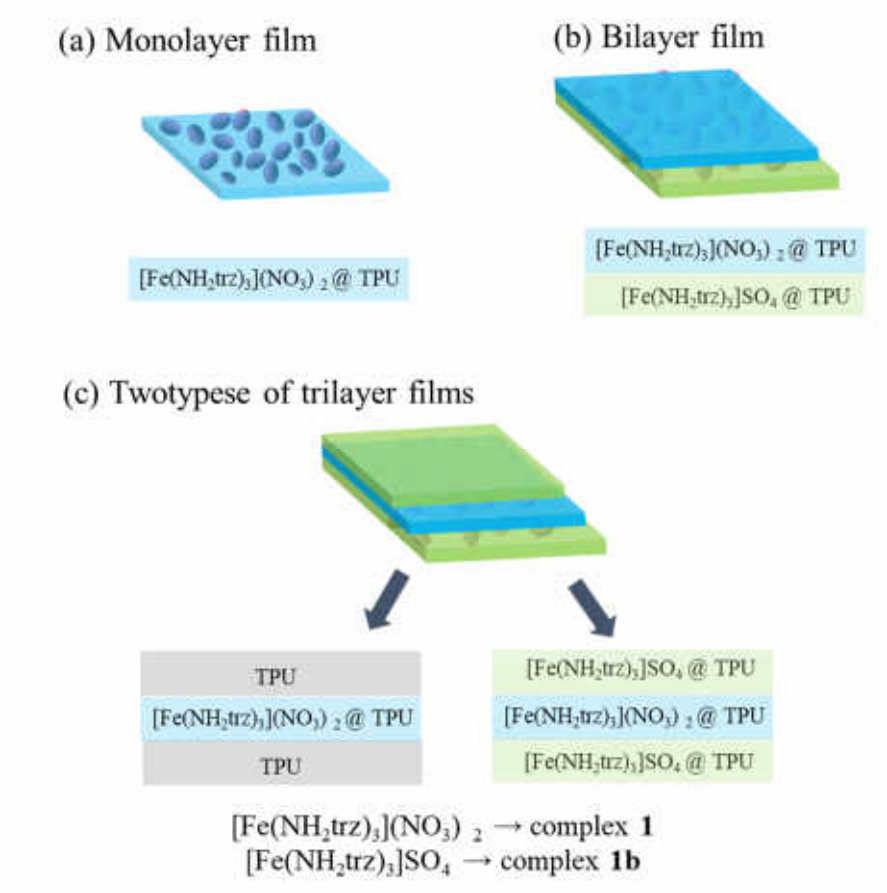


Fig.5-8 Schematic of the monolayer film, bilayer film and two types of three-layer film.

5.3.1 Monolayer film

The monolayer $[Fe(NH_2trz)_3](NO_3)_2$@TPU composite film was fabricated by a blade casting method. As shown in Fig.5-9, 200 mg of complex **1** was placed in a vial containing 3 ml of Tetrahydrofuran (THF), under stirring for 1 hour, to achieve a homogeneous dispersion and suspension of the complex. Then, 600 mg of TPU was added to the suspension, under stirring at 40 °C overnight. Blade casting was used for producing monolayer films on glass surfaces while regulating the substrate's temperature and the casting's blade height. The height of the blade cast was fixed at 0.5 mm. The obtained monolayer was kept at 40°C for 1 hour until the monolayer composite was completely dry. The obtained composite film consists of 25 wt% SCO filler.

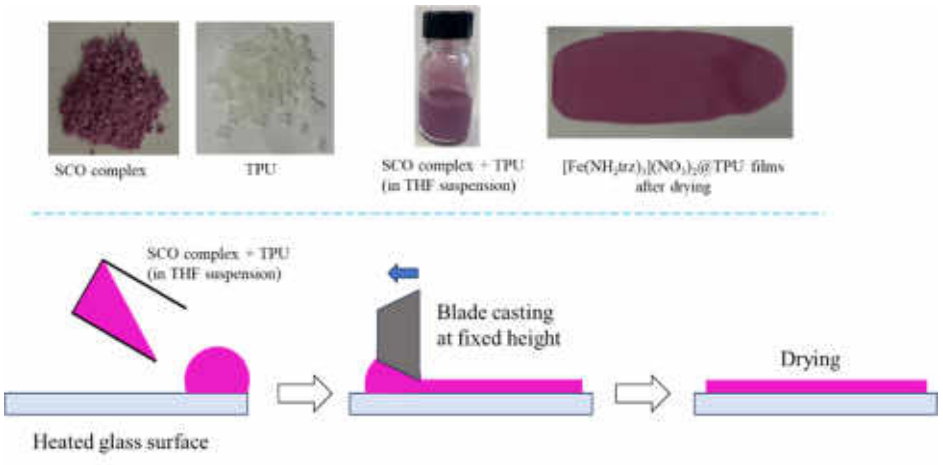


Fig.5-9 Schematic diagram of the blade casting method to fabricate the $[Fe(NH_2trz)_3](NO_3)_2$@TPU films

Several techniques can be employed to characterize the composite film. Infrared spectroscopy (IR) is useful for identifying functional groups in both the polymer and the filler. Variable temperature Optical reflectivity can be utilized to determine the transition temperature based on the colour change. Scanning Electron Microscopy (SEM) is an imaging technique widely used in material science, and it can provide us with the microscopy of composites.

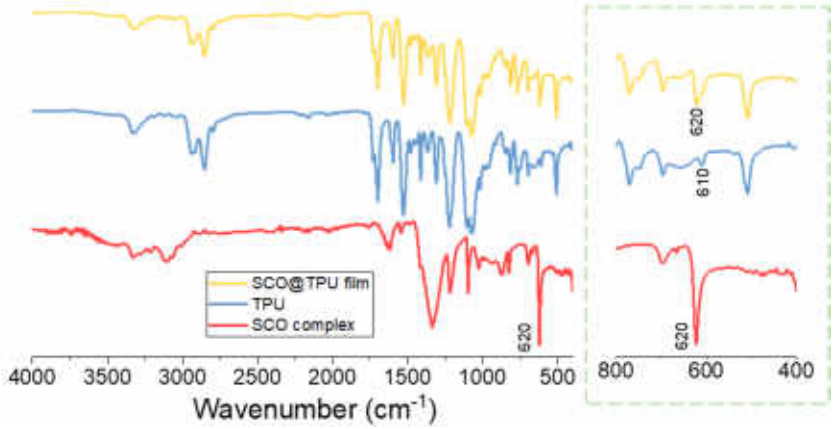


Fig.5-10 IR spectra of $[Fe(NH_2trz)_3](NO_3)_2$@TPU films, TPU and SCO complex.

Infrared spectroscopy is useful for identifying functional groups in a substance. The IR spectra of composite films, TPU, and SCO complexes are shown in Fig.5-10. When is in the composite, most of the bond for the complex is covered by TPU. Except the bands at 623 cm^{-1} appear in composite films related to the stretching vibration of C-H aminotriazole ligand in complex **1**, which is not observed in pure TPU.

It is well known that XRD can characterize crystal structure, giving information about chemical composition and physical properties. Grazing Incidence X-ray Diffraction (GIXRD) experiments were carried out in ambient conditions using a PANalytical X'Pert PRO MPD system using Cu Kα radiation and a parallel beam configuration to probe the crystallinity of the films. The result of XRD for the powder SCO complex **1**, complex **1**@TPU film and pure TPU film is shown in Fig.5-11.

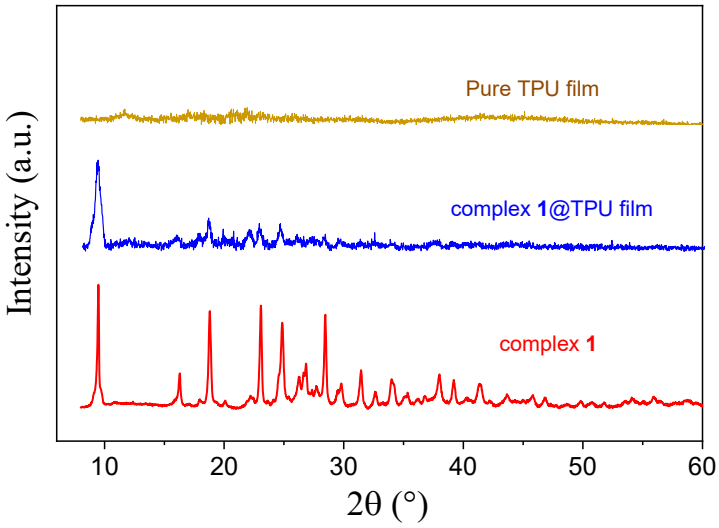


Fig.5-11 The result of XRD for the powder SCO complex **1**, complex **1**@TPU film and pure TPU film

The XRD pattern of complex **1** (Fig.5-11, bottom, red curve) exhibits several sharp, intense peaks between 8° and 30° (2θ), indicative of its highly crystalline structure. In contrast, the pure TPU film (Fig.5-11, top, yellow curve) displays a broad, featureless pattern, characteristic of an amorphous material. The XRD pattern of the complex **1**@TPU film (Fig.5-11, middle, blue curve) confirms the successful incorporation of complex **1** into the polymer matrix and clearly distinguishes it from the pure TPU film. However, the diffraction peaks corresponding to Complex **1** in the composite are significantly weaker and broader compared to those observed in the pure Complex **1** pattern. The most intense peak for the Complex **1**@TPU film is observed around 9.4° (2θ). This reduction in peak intensity and broadening is primarily attributed to the lower concentration of Complex **1** in the composite, which is present at only 25 wt%.

Scanning Electron Microscopy (SEM) is a widely utilized imaging technique in material science, offering high-resolution imaging capabilities. SEM images were obtained using a JEOL JSM 7800F Prime instrument, with all samples coated in platinum to enhance conductivity and image clarity. To prepare cross-sectional samples for SEM analysis, the composite film was rapidly cooled in liquid nitrogen and fractured at low temperatures to create a clean cross-section.

The cross-sectional SEM images reveal a uniform distribution of Complex **1** within the TPU matrix, as illustrated in Fig.5-12. This observation was further validated by Energy Dispersive X-ray (EDX) mapping, which confirmed the presence of nitrogen (N) and iron (Fe) elements. The monolayer film measured 68.8 μm in thickness, with the embedded aggregate particles measuring around 10 μm, consistent with the particle size observed in the powder form of Complex **1**. The surface SEM images (Fig.5-13) also show a uniform distribution of complex **1** on the surface of the TPU matrix, further confirmed by elemental mapping.

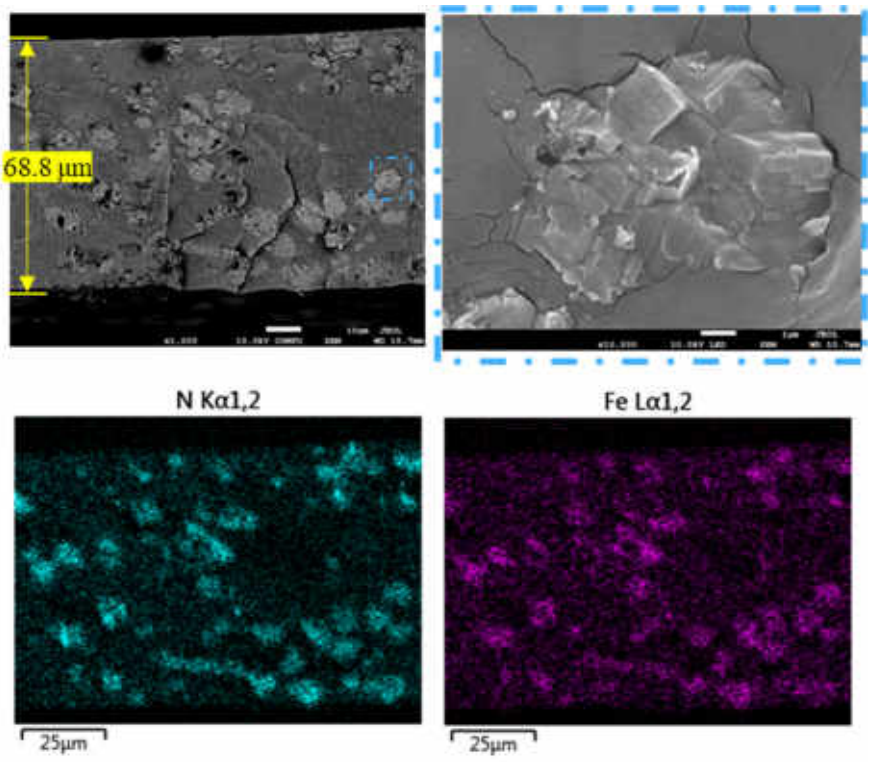


Fig.5-12 SEM image of the cross-section of $[Fe(NH_2trz)_3](NO_3)_2$@TPU films and EDX mapping.

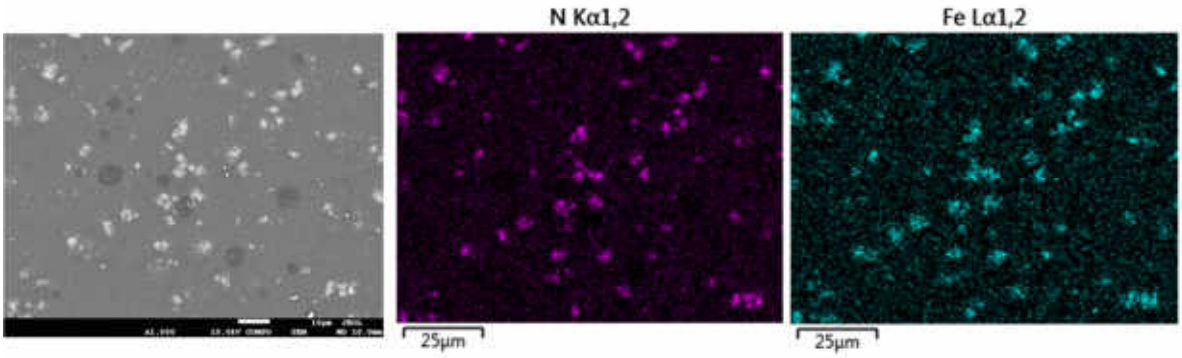


Fig.5-13 SEM image and EDX mapping of the surface of $[Fe(NH_2trz)_3](NO_3)_2$@TPU films.

The variable temperature optical reflectivity measurements were taken using a stereomicroscope equipped with a Moticam 1000 CCD camera. The temperature was controlled using a Linkam THMS600 liquid nitrogen cryostat at a temperature change rate of 2 ℃/min from 0 to 100 ℃. As shown in Fig.5-14, both the complex and composite films are measured in three cycles, with transition temperatures nearly the same. The transition temperatures are $T_{LS\rightarrow HS}$ = 73 ℃ and $T_{HS\rightarrow LS}$ = 38 ℃, exhibiting a large hysteresis loop (Δ=35 ℃). The result of optical reflectivity confirms that when complex **1** is distributed in the TPU matrix, it has the SCO property as the pure powder.

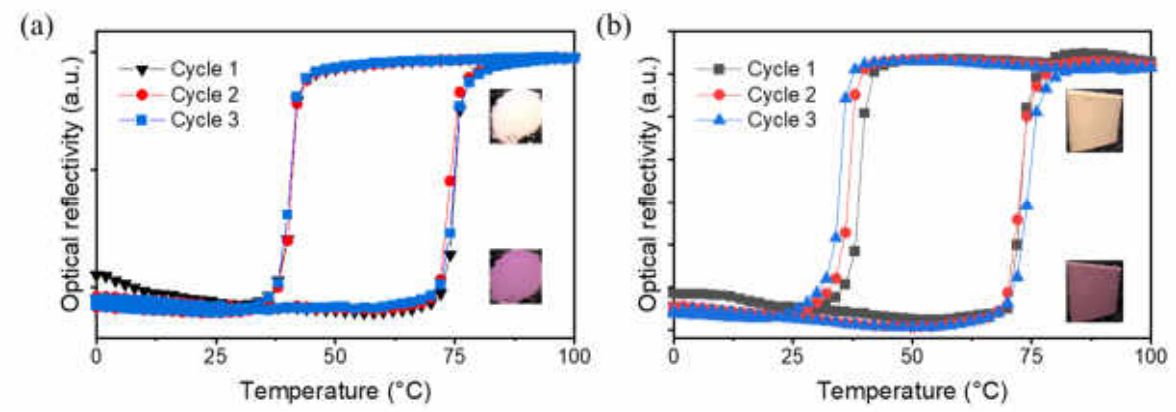


Fig.5-14 Variable temperature optical reflectivity of $[Fe(NH_2trz)_3](NO_3)_2$ complex (powder) and $[Fe(NH_2trz)_3](NO_3)_2$@TPU films.

5.3.2 Bilayer film

Fig.5-15 demonstrates a layer-by-layer method for fabricating a bilayer film on a glass surface using a blade-casting technique. The blade height and glass temperature can be adjusted to achieve the desired film. First, the $[Fe(NH_2trz)_3](NO_3)_2$@TPU layer (Nitrate layer) is cast, followed by the $[Fe(NH_2trz)_3](SO_4)$@TPU layer (Sulfate layer). The height of the blade cast was fixed at 0.5 mm. The obtained bilayer film was kept at 40°C for 1 hour until the monolayer composite was completely dry. In the bilayer film, each layer contains 25% of the SCO complex.

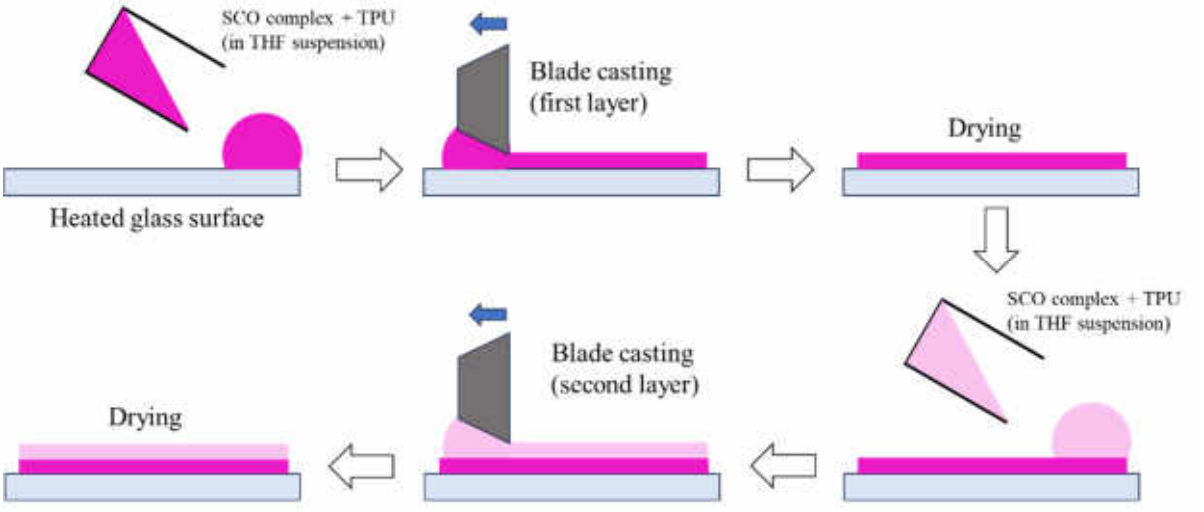


Fig.5-15 Schematic diagram of the blade casting method to fabricate the bilayer film. First, the $[Fe(NH_2trz)_3](NO_3)_2$@TPU layer is cast, followed by the $[Fe(NH_2trz)_3](SO_4)$@TPU layer.

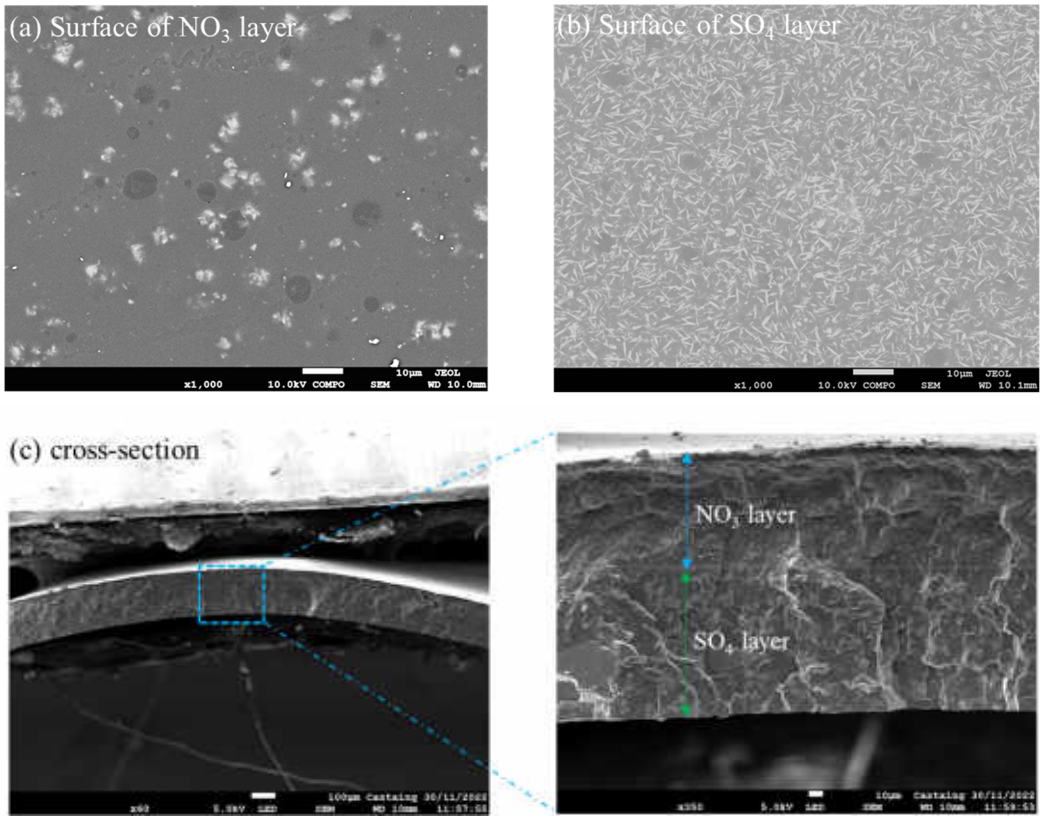


Fig.5-16 The SEM images of the cross-section of the bilayer film

Fig.5-16 shows the SEM images of the cross-section of the obtained bilayer film, clearly revealing the two layers: the nitrate layer and the sulfate layer. This bilayer film was also measured in variable temperature optical reflectivity. As shown in Fig.5-17, the transition temperatures observed from the sulfate layer side are $T_{LS\rightarrow HS} = 75°C$ and $T_{HS\rightarrow LS} = 63°C$, while from the nitrate layer side, the transition temperature from LS to HS state is around 75°C, while a two-step transition when cooling down the temperature. This occurs because, in the bilayer film, when measuring reflectivity from the side of the nitrate layer, the hysteresis loop for the sulfate complex is narrower than that of the nitrate complex. Thus, as the temperature decreases, the sulfate layer returns to pink (LS state) while the nitrate layer remains white (HS state), leading to a decrease in reflectivity intensity when measured from the nitrate layer side.

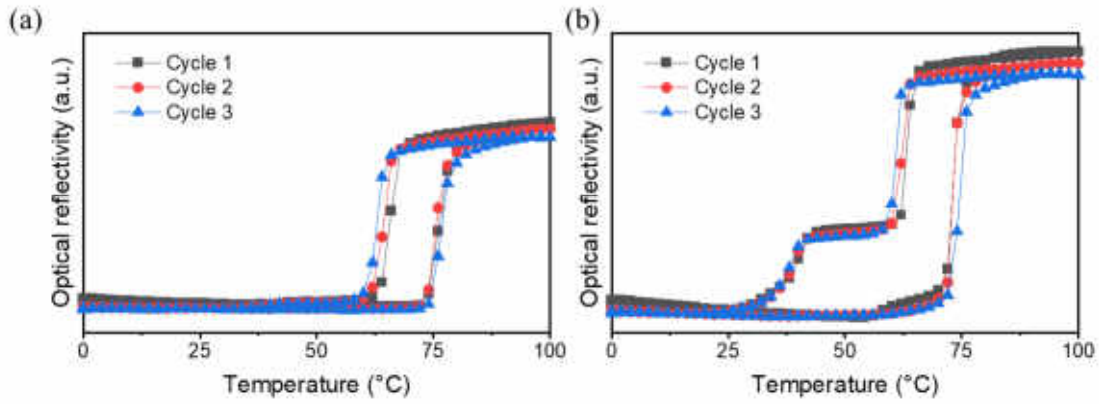


Fig.5-17 The Variable temperature optical reflectivity of bilayer film. (a) $[Fe(NH_2trz)_3](SO_4)$@TPU layer. (b) $[Fe(NH_2trz)_3](NO_3)_2$@TPU layer.

5.4 Three-layer film

Two types of three-layer films were also fabricated using the blade casting method, layer by layer, following a process similar to that of the bilayer film (as shown in Fig.5-15). For example, in the case of the TPU/Nitrate/TPU three-layer film, the first TPU layer was cast and allowed to dry. Once dry, the second layer (Nitrate) was cast, and after it dried, the final TPU layer was cast.

The SEM characterization confirms the successful fabrication of the three-layer structure (Fig.5-18 and Fig.5-19). For these two types of three-layer films, the cross-sectional SEM images demonstrated a clear sandwich-like structure, with well-defined boundaries between the outer layers and the central nitrate layer.

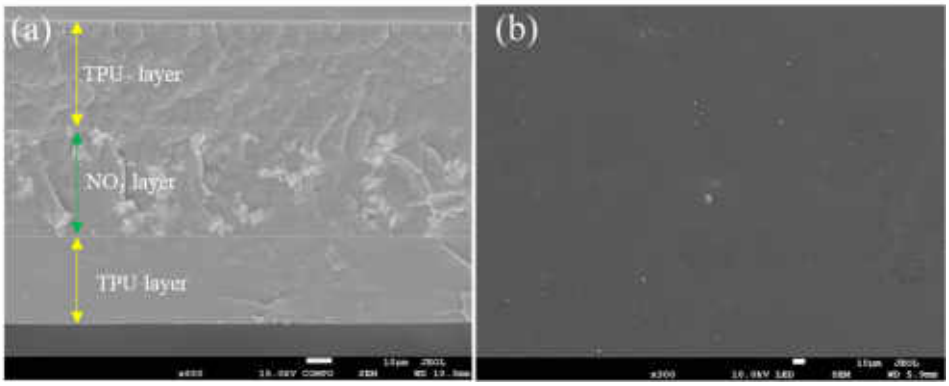


Fig.5-18 SEM images of TPU/Nitrate layer/TPU three layer film (a) cross-section and (b) surface

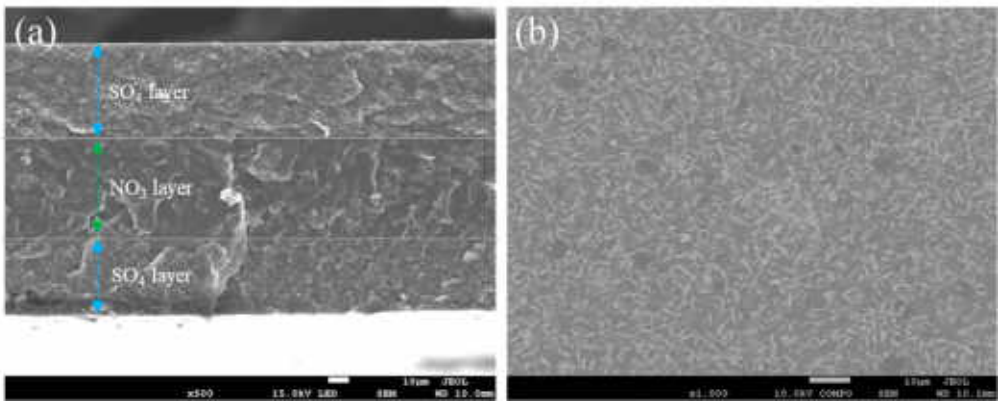


Fig.5-19 SEM images of Sulfate layer/Nitrate layer/TPU (a) cross-section and (b) surface

5.5 Study of the movement of bilayer film in EtOH

As shown in the previous section, the bilayer film was fabricated with one layer consisting of $Fe(NH_2trz)_3](SO_4)$ @TPU, which does not catalyse acetalisation but is expected to provide movement during heating and cooling. The second layer of the bilayer film, consisting of $Fe(NH_2trz)_3](NO_3)_2$@TPU, serves as the catalytic layer and is capable of catalysing acetalisation.

Some examples could be found in the literature that has presented the bending of bilayer films in response to external stimuli.[16, 29-31] To investigate whether our bilayer film exhibited similar

behaviour, we initially cut the film into small pieces and placed them in an oven at 70°C. As depicted in the figure, the bilayer film remained flat at room temperature and did not show significant changes upon heating to 70°C. However, when the bilayer film was immersed in EtOH, it began to exhibit bending even at room temperature. Specifically, the film started to bend from its edges, potentially due to the absorption of EtOH. Upon further heating to 70°C, the film changed colour from pink to white, and at the same time, it rolled into a tubular shape in the EtOH, exhibiting a self-rolling behaviour. Notably, the bilayer tube was retained after cooling to room temperature. This experiment was reproduced with serval bilayer films and several bilayer tubes were obtained through self-rolling in EtOH, as shown in Fig.5-20.

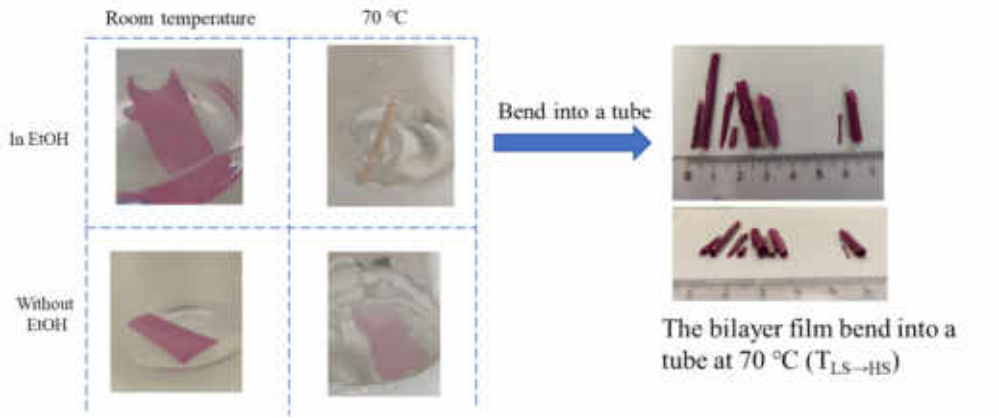


Fig.5-20 The picture of bilayer film in a vial with/without EtOH at room temperature and 70 °C

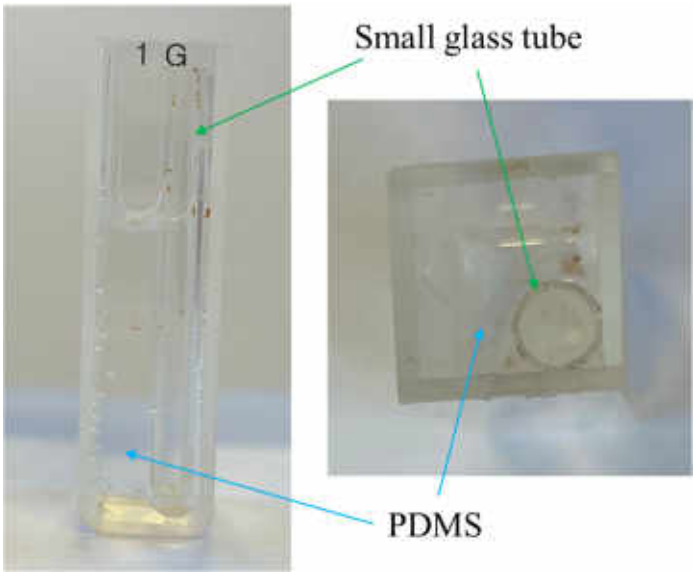


Fig.5-21 The images show the front and top view of a cuvette, which has a small fixed glass tube by PDMS

To characterize the self-rolling process, a small piece of the bilayer film (approximately 1.5 cm × 3 cm) was cut and placed in a small glass tube (d=5 mm) containing EtOH. This glass tube was already positioned in a cuvette (as shown in Fig.5-21; the small glass tube was fixed in the cuvette with PDMS) and equipped with a temperature control system and an optical microscope to capture images of the process. A top-view image of the bilayer film is shown in Fig.5-22. At room temperature, the bilayer remains in contact with the glass tube. The temperature was

gradually increased, and once stabilized, maintained for 5 minutes before recording the images. As depicted in Fig.5-22 (a)-(c), little changes were observed in the bilayer film when the temperature increased from 25°C to 65°C (below the transition temperature). However, as the temperature exceeded 70°C (the transition temperature), Fig.5-22 (d)-(h) reveal the self-rolling of the bilayer film, along with a colour change from pink to white. After rolling, the diameter of the hollow portion inside the bilayer tube decreased from 3.8 mm to 2.1 mm. Upon cooling back to 25°C (Fig.5-22 (i)), the rolled bilayer tube remained stable, forming a permanent structure. This indicates that the film has a tubular shape after being heated in ethanol, which it keeps even after being taken out of the system and dried in an oven. In contrast, the bilayer film was completely flat prior to heating in the presence of ethanol, and the glass tube was the only source of the original circular shape. Additionally, we confirmed that only the bilayer was able to produce this tubular shape. This self-rolling process occurs during the transition temperature as the complex changes from the low-spin to the high-spin state. This behaviour can be attributed to the non-uniformity of the bilayer film, which is composed of two distinct layers. In addition to the mechanical differences between the sulfate and nitrate layers (the sulfate complex undergoes a larger volume change during the spin transition compared to the nitrate complex), each layer absorbs ethanol (a solvent) differently. This phenomenon has already been described for other systems. [32-34]

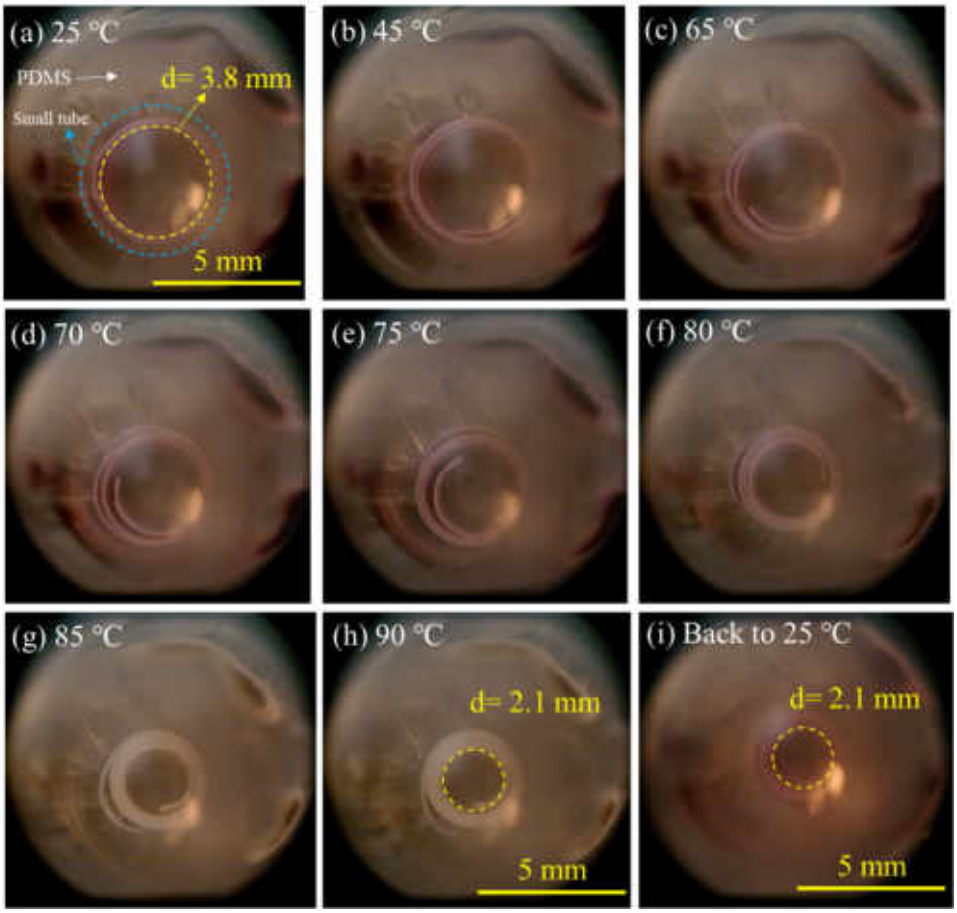


Fig.5-22 Various temperature optical picture of the self-rolling process of the bilayer film.

So, the self-rolling process of the bilayer film was clearly observed. Following this, the bilayer film was cut into a specific shape, as depicted in Fig.5-23. The cut film included small strips,

highlighted in the yellow circle in Fig.5-23 (a). This design aimed to examine whether the inner small tube would exhibit movement during the heating and cooling process, particularly around the transition temperature. Initially, these small strips bent into a small hollow tube, as shown in Fig.5-23 (b). Subsequently, a larger hollow tube formed, enclosing the smaller tube inside (Fig.5-23 (c)-(e)). The bilayer hollow tube was immersed in EtOH within a cuvette and characterized using a numeric microscope. Images captured from both top and side views revealed the presence of a small roll inside the tube (Fig.5-23 (d)-(e)). The cuvette was equipped with a temperature control system and a numeric microscope to monitor the process. The cuvette was heated from 45°C to 85°C to observe the movement of the bilayer tube at different temperatures.

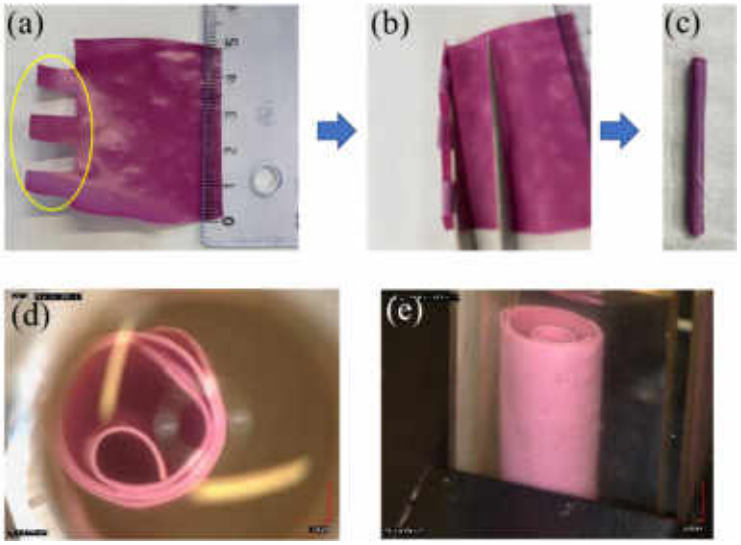


Fig.5-23 The shape of the bilayer film and the bending process. The bilayer tube in EtOH, from the top-view (d) and side view (e).

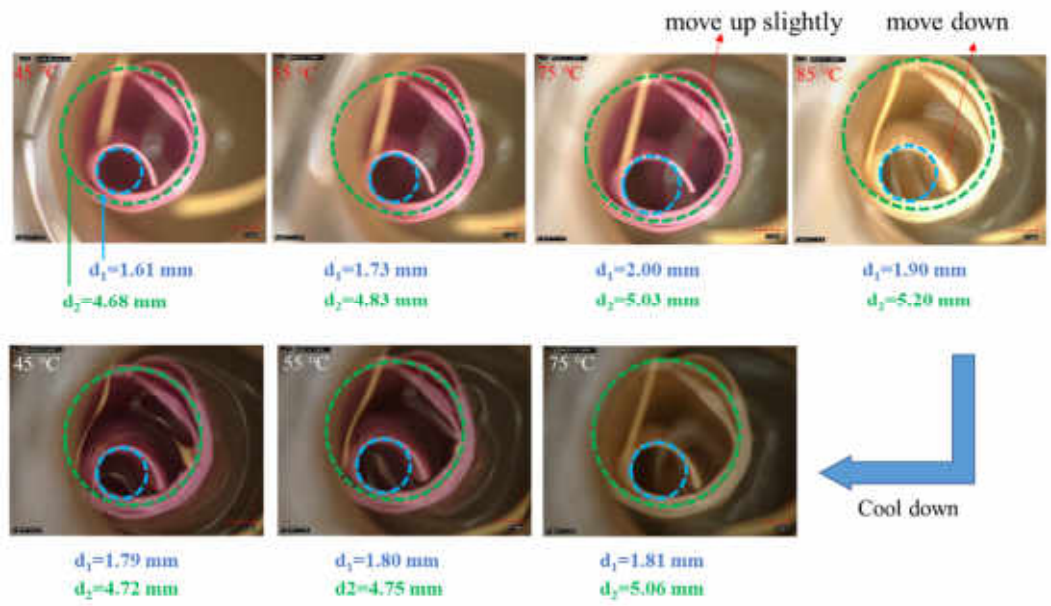


Fig.5-24 Images of the numeric microscope of bilayer tube at various temperatures

The top view of the bilayer tube is presented in Fig.5-24. During the heating process (from 45°C to 85°C), the diameter of the bilayer tube increased from 4.68 mm to 5.2 mm. Two

potential explanations for this expansion can be proposed. First, polymer swelling may occur as a result of heating. Second, the spin-crossover complex likely contributes to the expansion, particularly as $[Fe(NH_2trz)_3](SO_4)$ complex **1b** undergoes a significant volume change between its high-spin and low-spin states. Furthermore, during heating, the small roll inside the tube moved upward between 45°C and 75°C, followed by a downward movement from 75°C to 85°C. At the same time, the colour of the bilayer tube changed from pink to white, with the upward movement presumably caused by the volume change of complex **1b** during the spin transition. During the cooling process, from 90°C back to 45°C, the diameter of the bilayer tube decreased from 5.2 mm to 4.72 mm.

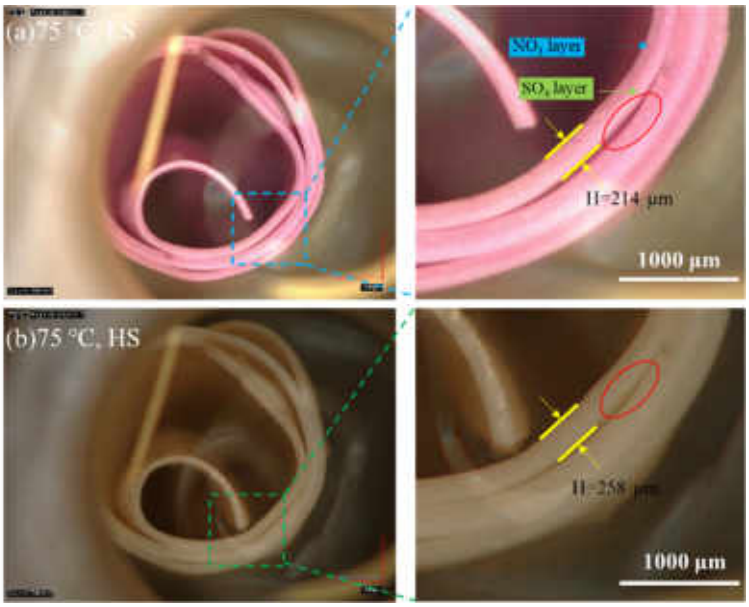


Fig.5-25 Images of the numeric microscope of bilayer tube at 75 °C

The bilayer tube can exist in both HS and LS states at the same temperature thank to the large hysteresis loop of the SCO complex. The complex remains in the HS state if heated to that state and then cooled to 75°C, or it retains the LS state if heated directly to 75°C from the LS state. Fig.5-25(a) illustrates the film in its LS state at 75°C, showing that it consists of two distinct layers with a total thickness of 214 μm. The dark pink layer represents the nitrate layer, while the light pink layer corresponds to the sulfate layer, both of which have approximately the same thickness. In Fig.5-23 (b), the bilayer film is in the HS state at 75°C. Since both layers appear white in the HS state, they cannot be distinguished through optical reflectivity. The thickness of the bilayer in the HS state at 75°C is 258 μm, which is greater than that in the LS state. Given that this change occurs at the same temperature, polymer swelling can be ruled out as a factor, and the increase in thickness is attributed to the spin state of the SCO complex, which occupies a larger molecular volume in the HS state compared to the LS state.

In the results discussed above, it was demonstrated that the bilayer film can form a tube through self-rolling. Additionally, a difference in the thickness of the bilayer film was observed, with the HS state exhibiting greater thickness compared to the LS state. The movement of the bilayer tube during the spin transition was also observed. In the following section, this bilayer tube, consisting of an inner layer of $Fe(NH_2trz)_3](NO_3)_2$@TPU as the catalytic layer and $Fe(NH_2trz)_3](SO_4)$@TPU as the layer responsible for controlling access between the catalytic layer and the reagent (Fig.5-26), will be employed to catalyze the acetalization reaction. This will be discussed in detail in the following section.

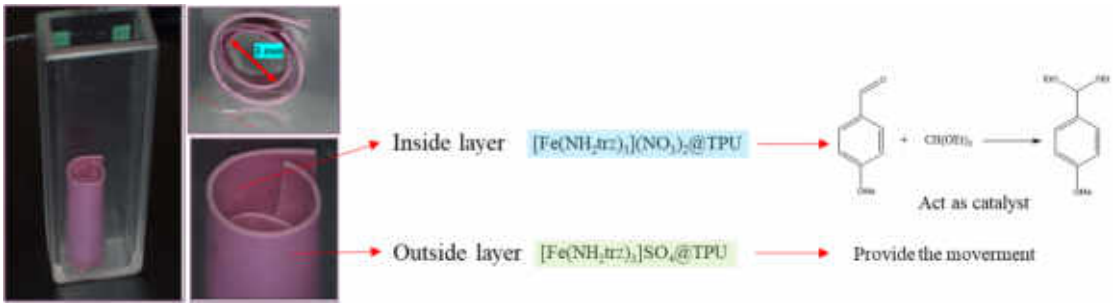


Fig.5-26 Pictures of bilayer tube obtained from numeric microscope.

5.6 Reaction of acetalization with SCO complexes@TPU films as the catalyst

5.6.1 Use of the monolayer film as a catalyst

5.6.1.1 Catalytic reaction under batch conditions

We have chosen the reaction of acetalisation of *p*-anisaldehyde with triethyl orthoformate in EtOH at 55 ℃ to study the catalytic performance of $[Fe(NH_2trz)_3](NO_3)_2$@TPU films and to evaluate the possibility of catalyst recycling and reuse under batch conditions. The composite films were cut into small pieces (15 mm × 10 mm), and the mass was thoroughly 13 mg. The substrates employed were EtOH, *p*-anisaldehyde, triethyl orthoformate (TEOF) and mesitylene (TMB, as the standard). After the reaction, the film was washed with EtOH and dried with paper. As shown in Fig.5-27, the SCO composite film can be used in the HS and LS states to evaluate the catalytic performance and spin effect on catalytic activation.

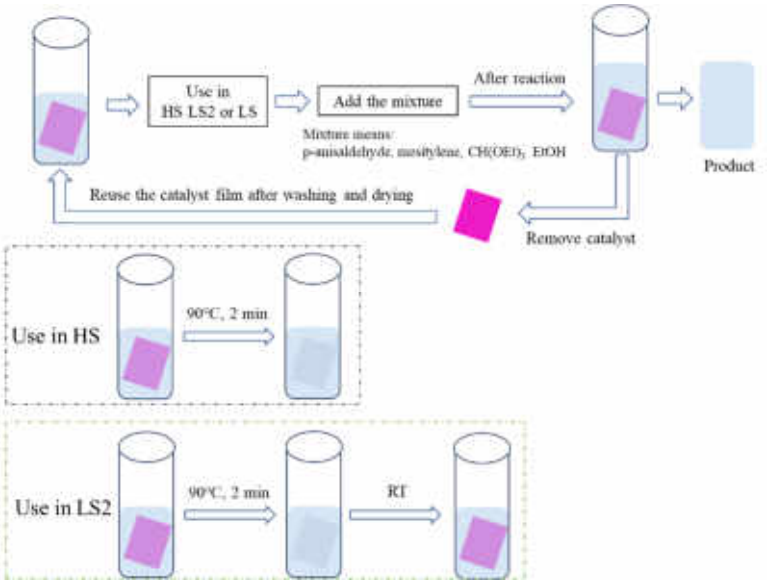


Fig.5-27 Schematic of the reuse route of the $[Fe(NH_2trz)_3](NO_3)_2$@TPU films as the catalyst

The yield of the composite film (**M1**) tested in the HS state as a catalyst for acetalisation is

shown in Fig.5-28. The results show that the composite film effectively catalyzes the reaction for up to 11 runs. It is important to note that the total mass of the film is 13 mg, with only 3.25 mg being the catalyst. Throughout these 11 runs, it produced a total of 4.02g of product with a TON (turnover number) of 3395 (Table 5-1). This indicates excellent catalytic capacity and reusability. Interestingly, the film appears pink when it contains the pink SCO complex filler in the TPU matrix, and the colour appears lighter when there is less SCO complex. The colour change of the composite film can indicate whether it is still effective as a catalyst, which is useful in determining whether the catalytic reaction is occurring efficiently if we reuse the film. For example, after the film has been used nine times, we can observe a slight pink, indicating that it can still be reused as an efficient catalyst for the reaction.

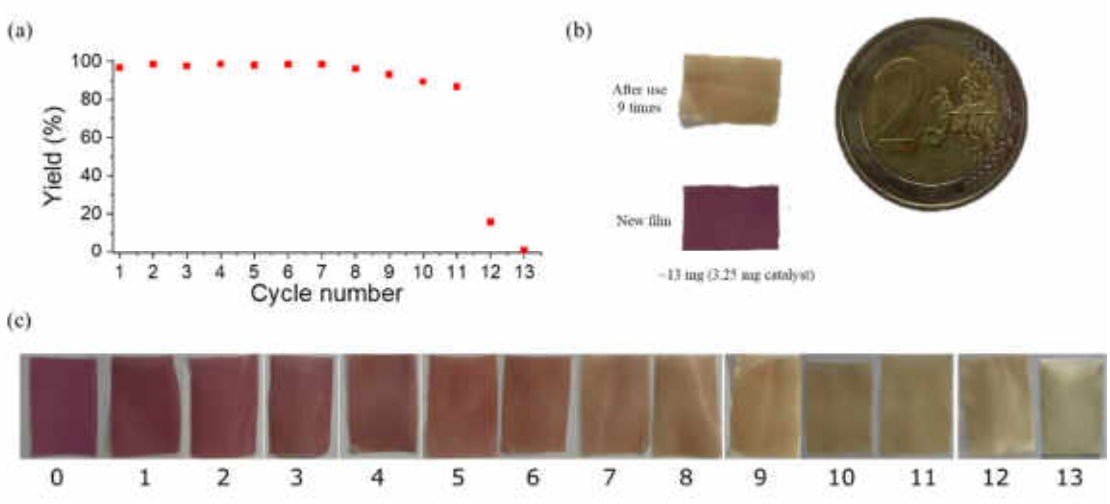


Fig.5-28 Reaction yield and repeated runs catalysed by the same $[Fe(NH_2trz)_3](NO_3)_2$@TPU films. (b) and (c) the pictures of the film after use.

Table 5-1 The detail data for the film M1 as catalyst in 11 runs.

Sample	Film	Catalyst	acetal (expected)	acetal (experimental)	Ratio 1	TON
M1	13 mg	3.25 mg	20 mmol	19.1 mmol (4.02 g)	1236	2539

$Ratio\ 1 = \frac{Mass\ of\ acetal}{Mass\ of\ catalyst}$

Comparison of the films used in HS and LS2 states. Two composite films**, M2** and **M3,** were prepared for this experiment and have the same shape and mass. One film (**M2**) will be used in the HS state, and another (**M3**) will be in the LS2 state. The result of the experiment shown in Fig.5-29 is that the yields of using **M2** and **M3** are higher than 90% at the first 4 tests, and the colour of the films is pink. After one month, the films were reused to catalyse the reaction. Both of them efficiently catalysed the reaction, with high yields (as shown in the blue background of Fig.5-29). The films were reused again the following day (as shown in the green background). Finally, these two films were used for 11 runs with yields higher than 90%, which is consistent with the previous result. As shown in Fig.5-29, in 13 runs, a total of 4.66g of acetal was obtained with a TON of 2951 for **M2**, and 4.44g of acetal was obtained with a TON of 2805 for **M3**. The film used in the HS state works better than in the LS2 state (Table 5-2).

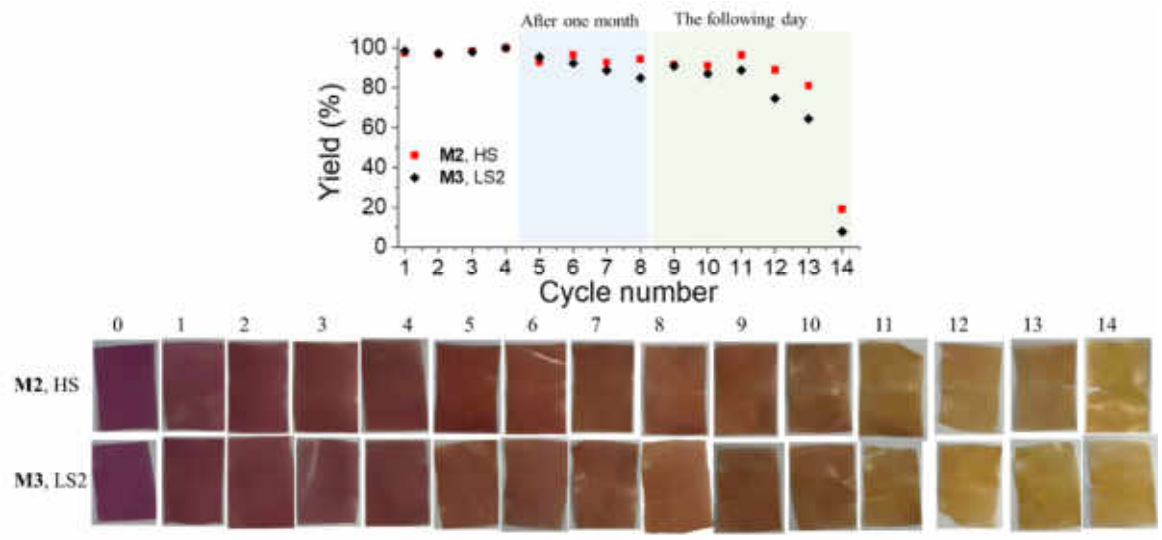


Fig.5-29 The yields and the colour of the composite films tested in HS and LS2.

Table 5-2 The detail data for film **M2** and **M3** as catalyst in 13 runs.

Sample	Film	Catalyst	acetal (expected)	acetal (experimental)	Ratio 1	TON
M2	13 mg	3.25 mg	23.6 mmol	22.2 mmol (4.66 g)	1434	2951
M3	13.1 mg	3.27 mg	23.6 mmol	21.1 mmol (4.44 g)	1358	2805

$$Ratio\ 1 = \frac{Mass\ of\ acetal}{Mass\ of\ catalyst}$$

The films **M2** and **M3**, used in HS and LS2 states, show excellent catalytic capacity and reusability(Fig.5-29). By simply checking the colour of the film, we can determine whether the reaction is occurring effectively or not if we use the composite film in HS and LS2. Next, we aimed to compare the films' recyclability in the LS, LS2, and HS states. Three composite films**, M4, M5,** and **M6,** were prepared for this experiment and have the same shape and mass. They will be used in the HS, LS2, and LS states to catalyse the reaction. The result of the experiment is shown in Fig.5-30. As expected, the films **M4** and **M5** efficiently catalysed the reaction and were reusable, with high yields(>90%), which was consistent with the previous experiment. The film containing the complex in the LS state (**M6**) catalyzes the reaction less efficiently than the other two films. Furthermore, the film **M6** is most effective for the 4th and 5th attempts. We find the same trend for the M6 film for the second use Fig.5-30(b). It seems necessary to be activated again before being effective which is not the case for **M4** and **M5** used in HS and LS2 states. Additionally, as shown in the pictures, the film used in the LS state seems to break into small pieces more easily, possibly due to stirring. However, this film destruction does not occur if it is used in its HS and LS2 states. This could be attributed to the films used in HS and LS2 being heated to 90°C, becoming more flexible.

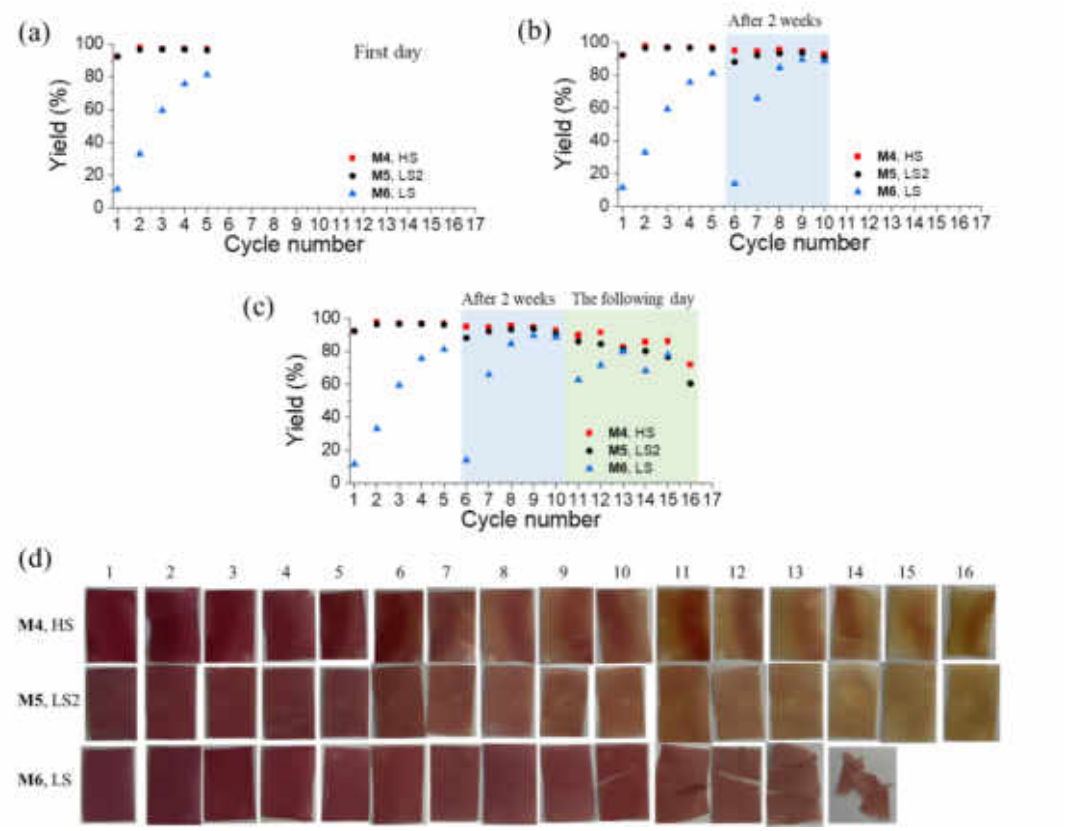


Fig.5-30 (a) Comparison of the $[Fe(NH_2trz)_3](NO_3)_2$@TPU films tested in HS, LS2 and LS states

Table 5-3 The detail data for film **M4, M5** as catalyst in 16 runs and **M6** in 15 runs.

Sample	Film	Catalyst	acetal (expected)	acetal (experimental)	Ratio 1	TON
M4	13.2 mg	3.3 mg	29.1 mmol	26.6 mmol (5.59 g)	1693	3536
M5	13.2 mg	3.3 mg	29.1 mmol	25.6 mmol (5.38 g)	1630	3403
M6	13.2 mg	3.3 mg	27.3 mmol	17.6 mmol (3.69 g)	1108	2339

$$Ratio\ 1 = \frac{Mass\ of\ acetal}{Mass\ of\ catalyst}$$

The above experiments show $[Fe(NH_2trz)_3](NO_3)_2$@TPU films can serve as catalysts in the acetalisation reaction. Furthermore, a noticeable colour change is observed after using the film, which can indicate whether the film can be reused or not. The colour change is attributed to the loss of the SCO complex in the composite. The question then arises as to whether the catalysis of the reaction really takes place inside the film or if it is catalyzed by the complex particles which have been released into solution. In order to verify this point, we collected the solution from the reaction and mixed it with a new mixture to determine whether the catalytic reaction occurred in the solution or inside the film. In parallel, we carried out a test where the solution resulting from the first catalytic reaction was filtered through Celite before being used in the second catalysis reaction. This filtration makes it possible to remove any particles of SCO complex. When we filtered the collected solution on the celite, there was no catalysis. However, when we did not filter the solution, the collected solution was able to catalyse the reaction from 32% to 41% in 15 minutes (Fig.5-31). Even while the complex particles in the solution had some catalytic potential, this is insufficient to account for the remarkable yields that were seen when the films were present. As a result, we think that the catalytic reaction mostly takes place

inside the film but also happens somewhat in the solution.

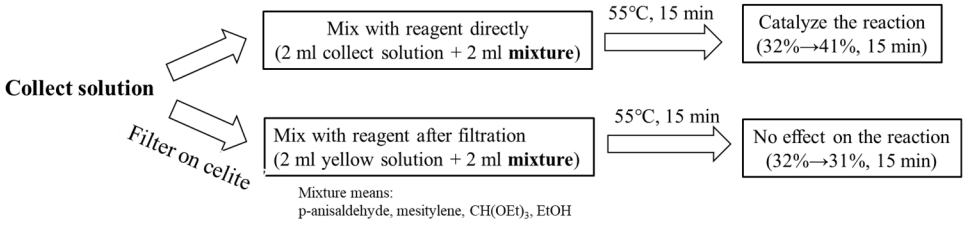


Fig.5-31 The scheme of checking the effect of the collected solution on the actualisation reaction

5.6.1.2 Catalytic reaction under continuous flow conditions

5.6.1.2.1 Presentation of our system inspired by continuous flow chemistry

The composite film shows excellent catalytic performance and reusability in batch conditions. However, studying the spin effect in the batch condition of the films used in HS and LS2 is difficult, as every run needed to be heated at 90 °C. So, we proceeded to use it in a continuous flow conditions catalytic system. As shown in Fig.5-32, our working system consists of an H tube and a mini pump to add the reagent.

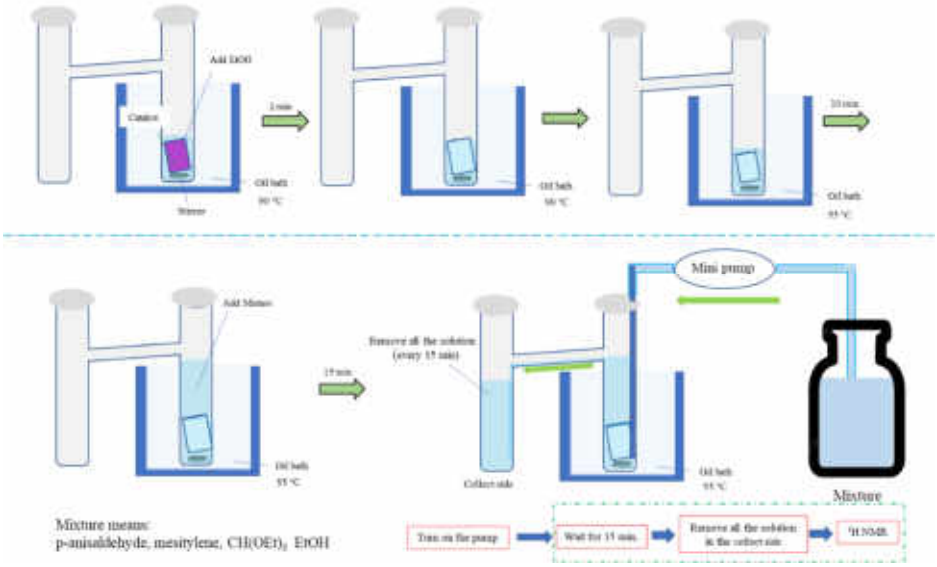


Fig.5-32 (a) The working system uses an H tube and a mini pump to add the reagent. The film used in HS state as an example.

If the composite film is used in its HS state (For the film used in LS2 and LS, see in the experiment section.), first place the composite film on the right side of the H tube and add 2 mL of EtOH. Then, put the H tube in a 90 °C preheated oil bath for 2 min. The colour of the film changes from pink to white. After 2 min, transfer the H tube to another 55°C preheated oil bath and wait for 10 minutes, and then add 2 ml of the mixture and connect to the minipump. The solution level is approximately reached by the bridge of the H tube. After 15 min, turn on the mini pump, and the mixture will be added automatically, and the solution will flow to the left side of the H tube (collect side). Every 15 minutes, the solutions on the collection side will be removed, and the yield will be measured using ^{1}H NMR.

5.6.1.2.2 Catalytic performance under flow condition

Fig.5-33 displays the catalytic performance of **M7** and **M8** used in HS and LS under a low adding speed of 3.2 ml per 15 minutes. The yields were approximately 90% high for both **M7** and **M8**, up to 25 runs. Throughout these 28 runs, it produced a total of 7.32g and 6.95g of product with a TON of 4626 and 4400 for **M7** and **M8**, respectively (Table 5-4). The experiments finished in two days, as indicated by the green dotted line and the first day involved 18 runs and 10 runs for the second day. Interestingly, when the yield began to decrease, the difference in yield between the film used in HS and LS2 was bigger, which means the film in HS state was more efficient than the film in LS2.

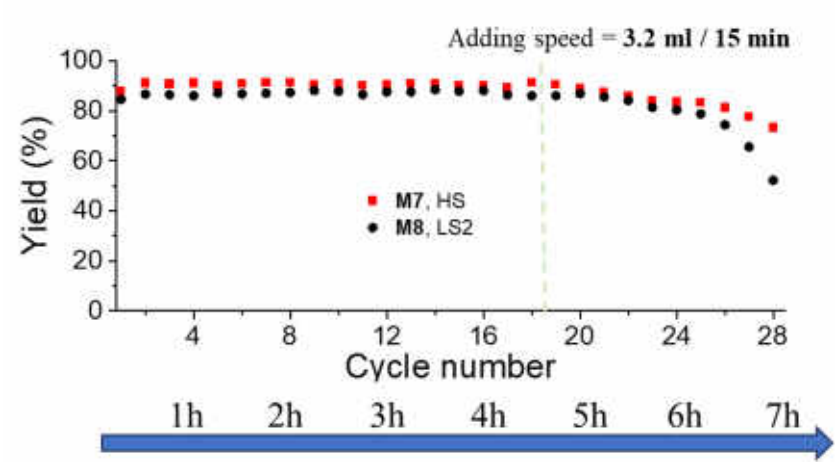


Fig.5-33 The catalytic performance of **M7** and **M8** used in the HS and LS2 states, and the adding speed was 3.2 ml per 15 minutes.

Table 5-4 The detailed data for film M7, M8 as catalyst under flow condition.

Sample	Film	Catalyst	acetal (expected)	acetal (experimental)	Ratio 1	TON
M7	13 mg	3.25 mg	39.5 mmol	34.8 mmol (7.32 g)	2252	4626
M8	13.1 mg	3.27 mg	39.5 mmol	33.1 mmol (6.95 g)	2125	4400

$$Ratio\ 1 = \frac{Mass\ of\ acetal}{Mass\ of\ catalyst}$$

To evaluate the effect of the released complex in the solution on the catalytic reaction, we took the collected solution from the reaction and mixed it with a new mixture. In parallel, we also carried out the experiment using the solution resulting from the catalysis which was filtered through celite. When we did not filter the solution, the collected solution was able to catalyse the reaction from 50% to 65% in 15 minutes (Fig.5-34). This result confirms that described in Fig.5-31. We can deduce again that the catalysis takes place mainly inside the composite material.

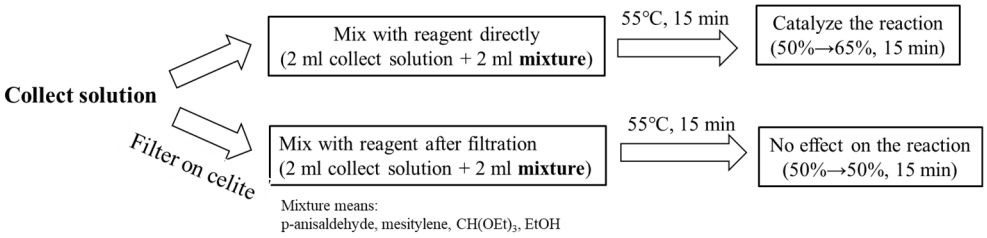


Fig.5-34 The scheme of checking the effect of the collected solution on the actualisation reaction.

5.6.1.2.3 Study of the effect of the spin state on the catalytic activation of complex 1.

Next, we wanted to investigate more closely how the spin state affected compound **1**'s catalytic activity in the composite material. We accelerated the rate at which the solution entered the H-tube. Our goal was to get a yield of between 70 and 80 percent, which is more suitable for examining how the spin state affects the complex's catalytic potential. Two composite films, **N1** and **N2**, were prepared for this experiment. These two films have almost the same shape and mass. The film **N1** and **N2** mass is 49.9 and 50.2, containing 12.5 and 12.6 mg of catalyst, respectively. These two films will be tested for 7 runs on the same day using the same mixture.

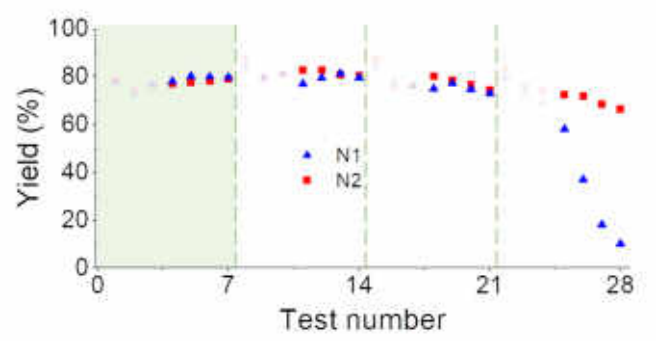


Fig.5-35 Catalytic performance of the composite film tested in HS and LS2, the adding speed is 7.5 ml per 15 minutes.

At the start of the experiment, as we used EtOH to prepare the film in the HS state and LS2 state, the concentration of the reagents was lower than in the mixture. So, the first 3 tests will not be considered (in the lighter colour in Fig.5-35); we will mainly consider the late 4 tests. To verify if these two are identical, both were tested in the HS state first, as shown in Fig.5-36 with a green background. Very similar yields are obtained when the two films are used as catalysts. The complex will be tested in the LS2 state using the film **N1** since it appears to be marginally more effective. According to chapter 4, we anticipate that the complex **1** in the HS state is more active than that in the LS2 state, and we don't want to overestimate this difference, thus we made this choice. Based on the result shown in Fig.5-36, it can be observed that the yield for **N2** (in HS state) is slightly higher than that of **N1** (in LS2 state) between 7 to 21 test cycles. However, after 21 test cycles, the difference in yield between **N1** and **N2** becomes large. This could be due to the film used in LS2 state releasing more complex into the solution than in HS state. As a result, after 21 tests, there were not enough complexes in **N1** to catalyse the reaction.

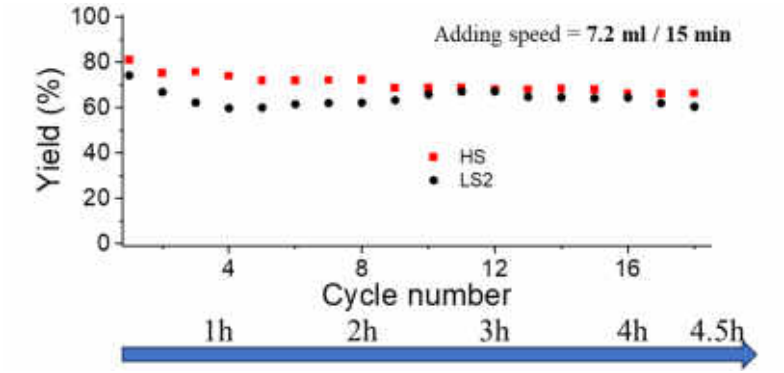


Fig.5-36 Catalytic performance of the composite film tested in HS state and LS state, the adding speed is 7.2 ml per 15 minutes

In order to test the reproducibility of the results, the catalytic capacity of two new monolayers was evaluated. Fig.5-36 shows that the film used in HS state works better than in LS state. Thus, it would appear that the monolayer with the complex in the HS state is slightly more efficient in catalysis than the monolayer containing the complex in the LS2 state.

5.6.2 Use of the bilayer films as a catalyst

5.6.2.1 Catalytic reaction under batch conditions

We also begin with the batch condition to check the catalytic performance of the bilayer film. Three vials were prepared for the experiment. **Vial 1** contained a bilayer film that could move with the stirrer bar in the vial. **Vial 2** had a bilayer hollow tube that was also free to move with the stirrer bar, but the catalytic layer was located inside this bilayer tube. In contrast, **Vial 3** had a bilayer film adhered to the inside of the vial using PDMS as an adhesive. This setup prevented the film from moving during the stirring process (Fig.5-37).

Three different bilayer films were tested in the HS state. Firstly, a certain amount of EtOH was added to the vial until it covered the bilayer film. Then, A mixture of 243 µl 4-methoxybenzaldehyde, 832 µl TEOF, and 100 µl TMB was added to the vial. The reaction was carried out at 55 ℃. In the first experiment, the reaction time was 60 minutes, and the yield was nearly 100%. The reaction time was reduced to 30 minutes in the second experiment, but the yield remained almost 100%. In the third experiment, the reaction time was further reduced to 15 minutes, yet the yield remained nearly 100%. The yield remained consistently high after ten tests with a 15-minute reaction time. All three **Vial** gave excellent results, with perhaps the best results obtained for the tube-shaped material (**Vial 2**).

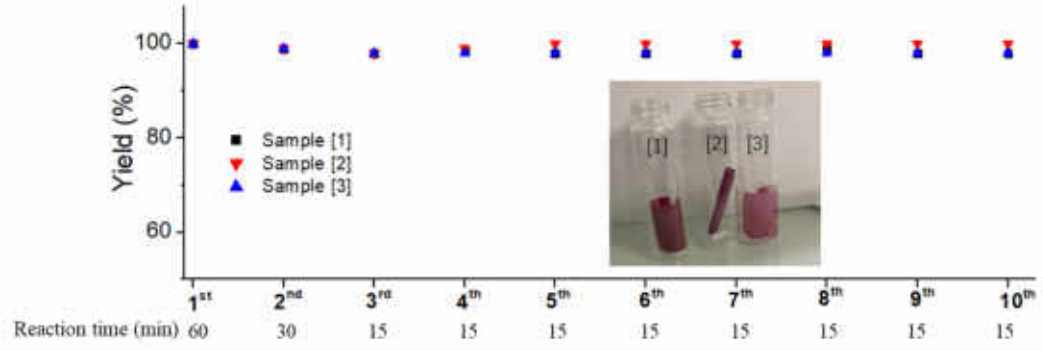


Fig.5-37 Catalytic performance of the bilayer films.

The tube-shaped bilayer film (**Vial 2**) was analysed by various methods after 10 time uses in catalysis. We began by measuring optical reflectivity at different temperatures. As a reminder, this technique highlights the spin transition due to the change in reflectivity intensity caused by the change in colour. When the complex is in the HS state, the colour is white, and the reflectivity is strong. On the other hand, when the complex is in the LS state, the colour is pink, and the reflectivity is considerably weaker. Fig.5-38 displays the optical reflectivity result of **Vial 2** after undergoing ten times use. The transition temperatures are similar to those of the film before use. However, there is a difference in the reflectivity intensity between the film in the HS and LS states compared to the film before use. This difference may be due to the release of a complex into the solution during the catalytic reaction. The difference in intensity between the film before and after catalysis is much important in the case of the nitrate complex **1** than

for the sulfate complex **1b**. So perhaps fewer particles of sulfate complex are released into solution than nitrate complex.

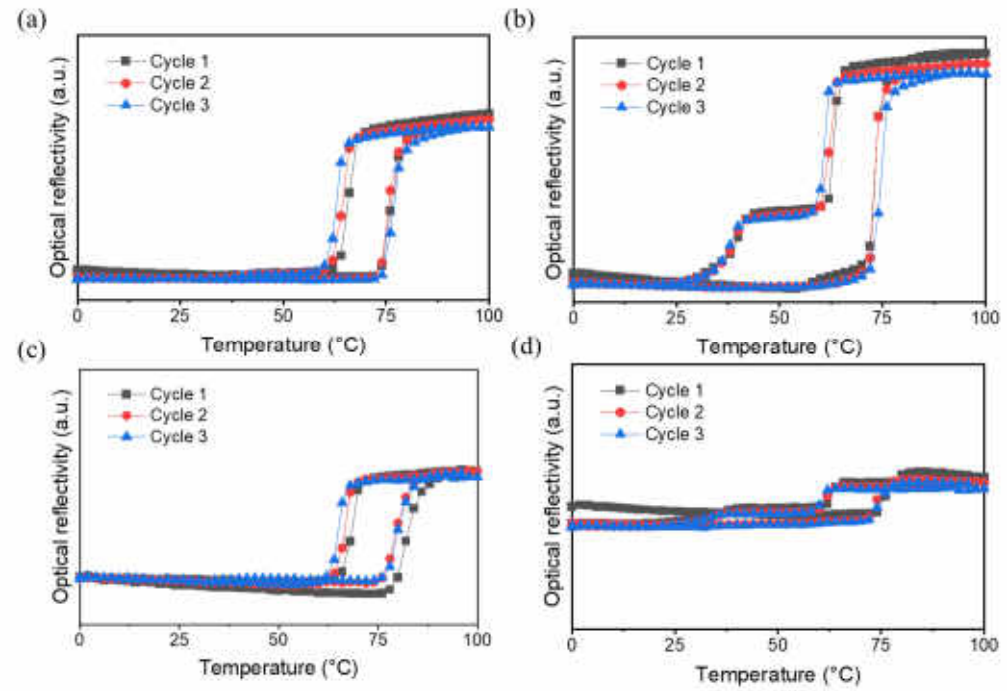


Fig.5-38 The variable temperature optical reflectivity of a new bilayer film, measured from (a) $[Fe(NH_2trz)_3](SO_4)$@TPU layer. (b) $[Fe(NH_2trz)_3](NO_3)_2$@TPU layer. And the bilayer film after use, measured from (c) $[Fe(NH_2trz)_3](SO_4)$@TPU layer. (d) $[Fe(NH_2trz)_3](NO_3)_2$@TPU layer.

The morphology of the bilayer film (**Vial 2**) was also analyzed using SEM. The resulting images in Fig.5-39 confirm that the film has two layers of similar thickness. The total thickness of the bilayer film remained nearly constant before and after use, indicating its stability in the reactant. In the Nitrate layer, SCO complexes were observed before use (some are indicated by red cycle), but the amount of SCO complex has decreased after use. The SCO complex is uniformly distributed in the polymer matrix in the Sulfate layer and remains consistent before and after use. This seems to confirm that fewer sulfate complex particles are released in solution than nitrate complex particles.

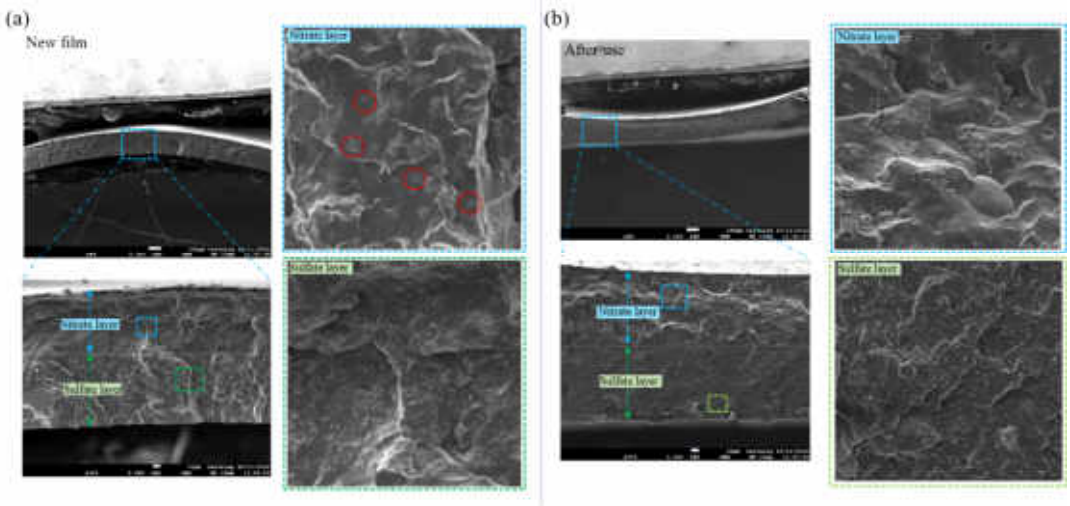


Fig.5-39 The SEM images of the cross-section of the bilayer film **Vial 2** (a) before use and (b) after use.

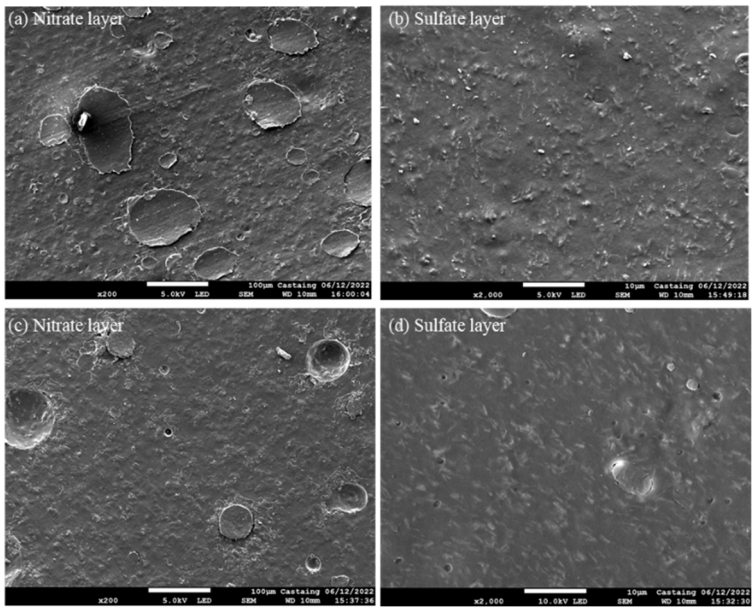


Fig.5-40 The SEM images of the surface of the bilayer film **Vial 2** (a)-(b) before use and (c)-(d) after use.

5.6.2.2 Acetalisation using an H tube system in flow condition

As shown in Fig.5-41, first, place the bilayer tube on the right side of the H tube and immerse it in EtOH. Then, put the H tube in a 90 ℃ preheated oil bath for 2 min. The colour of the film changes from pink to white. After 2 min, transfer the H tube to another 55℃ preheated oil bath, wait 10 minutes, and then add the mixture and connect to the minipump. The solution level is approximately reached by the bridge of the H tube. After 15 min, turn on the mini pump, and the mixture will be added automatically, and the solution will flow to the left side of the H tube (collect side). Every 20 minutes, the solutions on the collection side will be removed, and the yield will be measured using ^{1}H NMR.

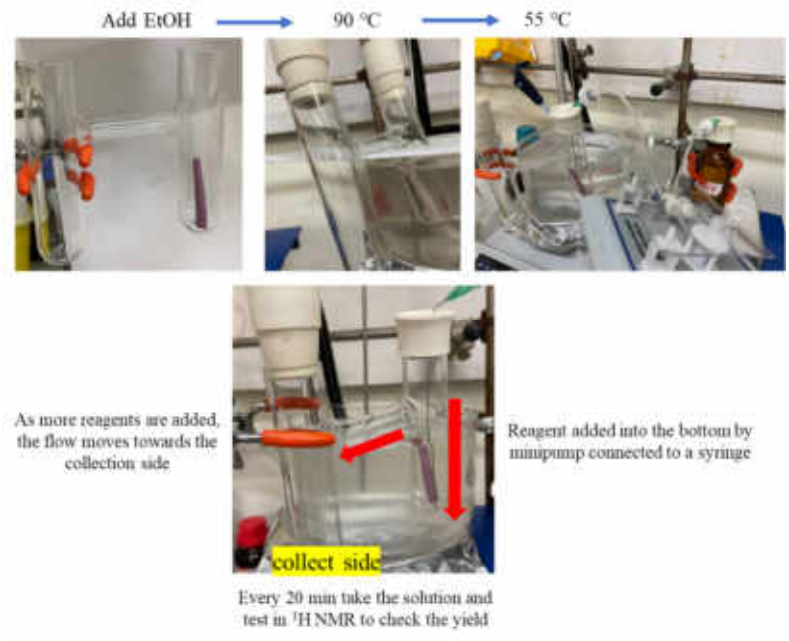


Fig.5-41 The pictures of the working system with an H tube and mini pump

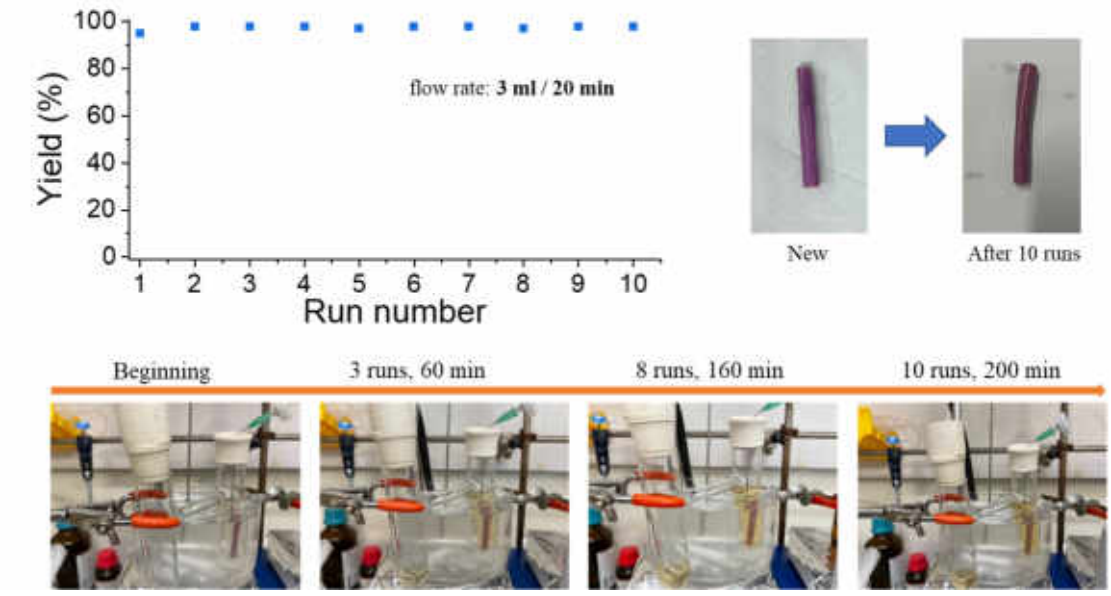


Fig.5-42 The Yields in 10 runs and the pictures of this experiment.

The bilayer tube **BF-1** was fabricated and used as a catalyst in the H-tube system, with a flow rate of 3 ml/20 min. It demonstrated excellent catalytic capacity, with yields exceeding 90% in 10 runs (Fig.5-42). Despite being in the reaction for a total of 200 minutes during these 10 runs, the **BF-1** remained similar to the new one, with only a slight colour change. The **BF-1** was then reused in the reaction, and the flow rate was increased to 5 ml/20 min. In 10 runs, the yields remained consistently higher than 90%. Furthermore, when the flow rate was further increased to 15 ml/20 min, and **BF-1** was reused again, the yield decreased to 84% after 5 runs (Fig.5-43). This suggests that the bilayer tube was robust, capable of efficiently catalysing the reaction, and reusable.

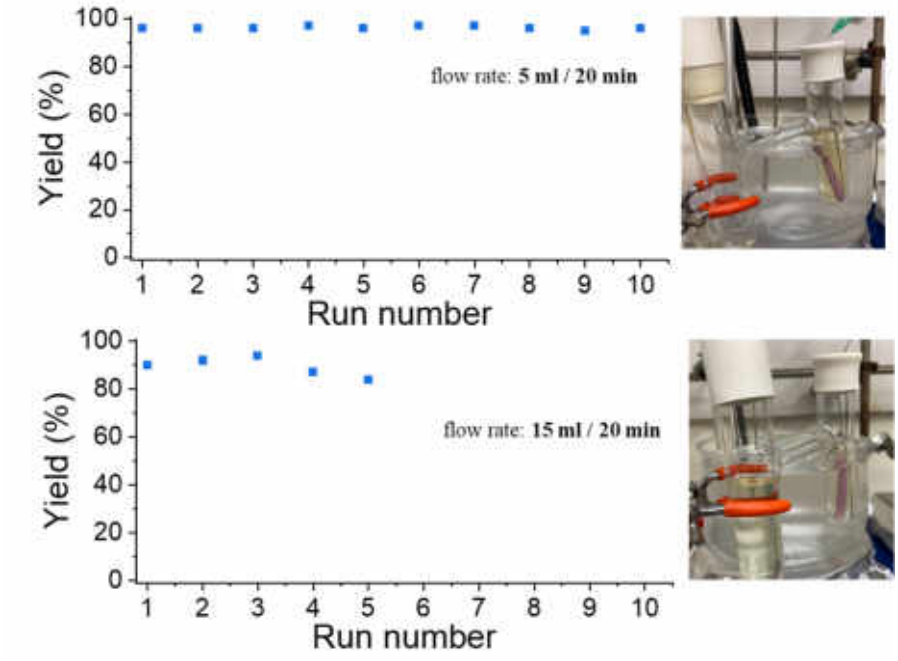


Fig.5-43 The yield of acetal, BT-1 is second-time reuse with a flow rate of 5ml/20 min, and the third-time reuse with the adding speed of 15 min/20 min.

We also try to use another polymer to fabricate the bilayer film, which is a copolymer that results from the combination of two monomers: polyvinylidene difluoride (PVDF) and trifluoroethylene (TrFE), called Poly(vinylidene fluoride-co-trifluoroethylene) P(VDF-TrFE). The P(VDF-TrFE) bilayer film is fabricated using a process similar to that of TPU, which involves 25 wt% SCO filler. The only difference is the solvent used to dissolve the polymer, 2-butanone (MEK) instead of THF. The obtained P(VDF-TrFE) bilayer film **BF-2** serves as a catalyst in the H-tube system with a 15 ml/20 min flow rate. Fig.5-44 shows that the yields range between 62% and 81% in 5 runs, which is lower than that of the TPU composite film.

Based on the above experiments, the bilayer film demonstrated excellent catalytic performance under flow conditions. Adjusting the flow speed of the reagent allowed for control over the yield of the catalytic system. Additionally, using TPU as the polymer matrix proved to be more effective compared to P(VDF-TrFE).

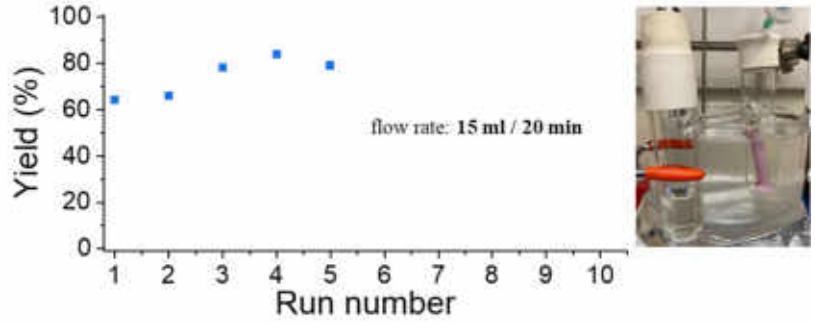


Fig.5-44 The yield of acetal using **BF-2** as a catalyst in the 15 ml/ 20 min flow rate.

5.6.2.3 Study of the spin state effect on catalytic activation.

The experiments above using the bilayer film have resulted in a highly effective catalyst for the acetalisation reaction, even at high flow rates. However, to study the spin effect on catalytic activation, it is necessary to maintain the yield at approximately 70%. The yield obtained in the previous experiment was too high, and we need to lower it. Usually, the yield decreases when the flow rate is higher, but we have already reached the maximum flow rate with the minipump. Therefore, we have decided to replace the H tube with a smaller one and reduce the size of the film used as the catalyst. In future experiments, all films will be cut into the shape shown in Fig.5-45 to ensure consistency.

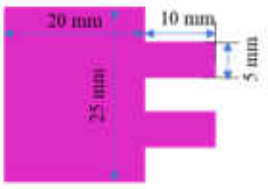


Fig.5-45 The shape of the cut in the film.

Two bilayer films, **BF-3** and **BF-4**, were prepared for use in this experiment. These films are almost identical, with the same mass of approximately 71 mg each. Before being used as catalysts in the acetalisation reaction, both films self-roll into a hollow tube when placed in EtOH at 90°C. It is worth noting that these two films will be tested for 7 runs each on the same day, using the same mixture. However, during the initial preparation of the films in the HS and

LS2 states using EtOH, the concentration of the reagents was lower than the mixture. Therefore, the first three tests will not be considered (shown in a lighter colour in Fig.5-46), and we will focus on the later four tests.

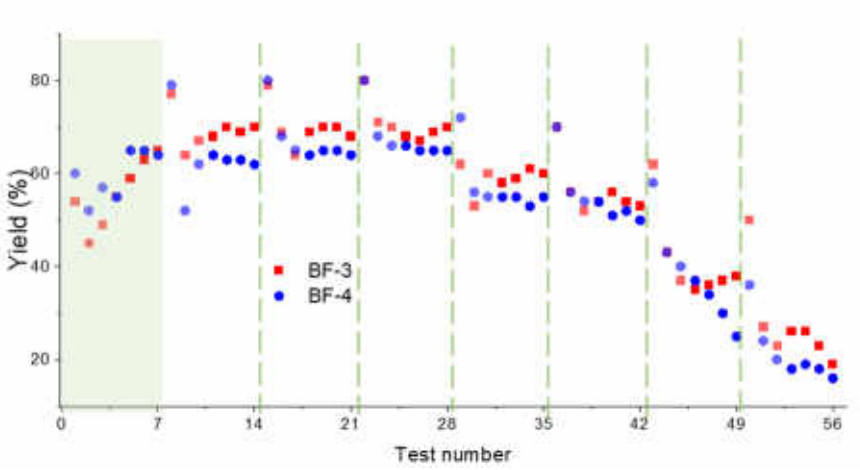


Fig.5-46 The yield of acetal using **BF-3** and **BF-4** as catalysts.

Note that the flow rate in this experiment is around 7.5 ml/ 15 min. To verify whether **BF-3** and **BF-4** are identical, they were tested in the HS state initially, as indicated by the green background in Fig.5-46. Both showed similar yields, with BF-4 having a slightly better yield. Subsequently, **BF-4** was tested in the LS2 state, while BF-3 was tested in the HS state in the following experiments. Based on the results shown in the figure, it can be observed that during the 56 tests, the yield of **BF-3** was slightly higher than that of **BF-4**. We find once again that the difference in catalytic activity of the films is much more marked in the latest tests.

To verify the reproducibility of the experiment, two additional bilayer films, **BF-5** and **BF-6**, were tested under the same conditions. Basically, the results indicated a similar trend to the previous experiment: the film used in the HS state performed better than in the LS state (Fig.5-47).

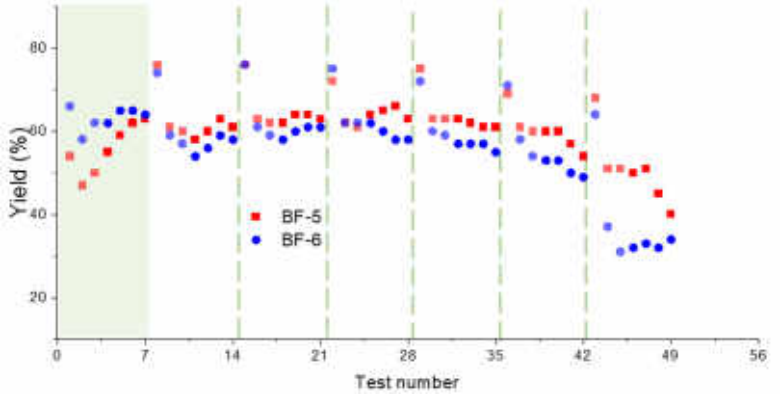


Fig.5-47 The yield of acetal using **BF-5** and **BF-6** as catalysts.

Fig.5-48 shows the morphology of a new bilayer film and the film after use in the catalytic reaction (**BF-5**). In the cross-sectional image, the two-layer structure is clearly visible. For the new film, the SCO complex is observable in both the cross-section and on the surface. However, after use in the reaction, significant changes are observed in the Nitrate layer. The complex appears to have been released into the solution, and numerous holes are visible on the surface

of the Nitrate layer. Only trace amounts of the complex are visible in the cross-section, which explains why **BF-5** is no longer able to catalyze the reaction efficiently. In contrast, the Sulfate layer shows no significant change before and after use.

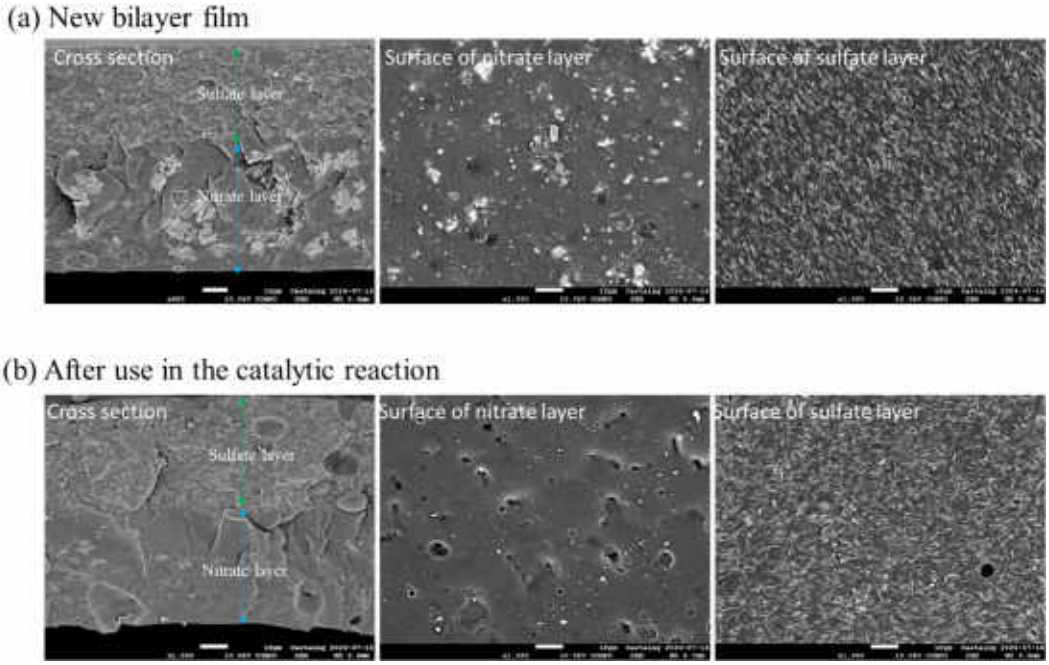


Fig.5-48 SEM image of the bilayer film before and after use in the catalytic reaction (**BF-5**)

A new bilayer film, **BF-7**, was prepared and used in the HS state in the following experiment. To better understand the stability of the bilayer film, which served as a catalyst in the acetalisation reaction, the number of runs will be increased until the yield significantly decreases. Fig.5-49 shows the yield of acetal using **BF-7** as a catalyst. The bilayer film **BF-7** has demonstrated exceptional catalytic performance in acetalisation reactions. At a flow rate of 7.5 ml / 15 min, the yields were over 70% over 36 runs, which amounts to a total of 9 h in the reaction. Even after 72 runs, which equals 18 hours in the reaction, the catalyst was still able to catalyse the reaction, although the yield decreased gradually. Therefore, the bilayer film can be utilised as a robust, reusable, and efficient catalyst for acetalisation reactions.

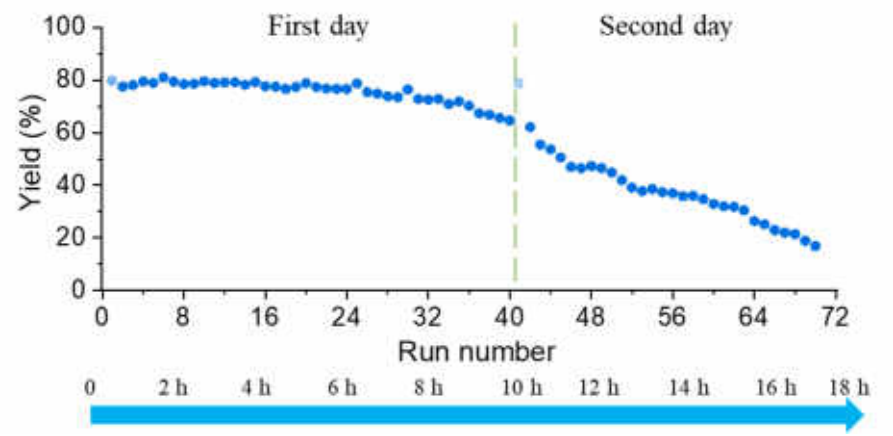


Fig.5-49 The yield of acetal using **BF-7** as catalyst.

5.6.2.4 Design and fabrication of microreactor

The bilayer film can self-roll and form a hollow tube in EtOH. This tube shows excellent catalytic capacity and stability. The Nitrate layer, which is the catalytic layer, is located inside the tube. The Sulfate layer is outside the tube and does not affect the acetalisation reaction. This arrangement allows the reactant inside the tube to access the catalyst easily. However, the motion caused by the spin transition is still relatively weak once the composite material is shaped like a tube. Then, we wondered whether this movement may not be enhanced if the tube were encircled by a more hard polymer that would stop it from moving outward. We reasoned that the movement inside the tube would be more noticeable if the outward movement was stopped. This is why we initially surrounded the bilayer film with Polydimethylsiloxane (PDMS). If this PDMS layer did not significantly increase the movement inside the tube, it gave us the idea of manufacturing a micro reactor. This micro-reactor would operate with a peristatic pump. In addition, the volume of the reactant inside the bilayer tube depends on the size of the tube. If the diameter of the tube increases, the inner volume of the tube also increases. Therefore, by controlling the tube size, we can change the access to the catalyst and control the yield and the rate. Fig.5-50 below illustrates the process of fabricating our micro reactor. I must point out that this micro-reactor was manufactured in particular by Romain Carrasco. The first step involves forming a self-rolling bilayer tube in EtOH at 90°C. Then, a cannula is inserted into the bilayer tube to prevent PDMS from entering the inner wall of the bilayer tube during the subsequent use of PDMS to cover the outside. PDMS is a versatile and soft silicone polymer with many applications.[35-37] Next, the outside of the bilayer tube is gradually covered with PDMS. Finally, a silicone tube connects to the bilayer tube, allowing reactants to pass through the inner portion of the bilayer tube.

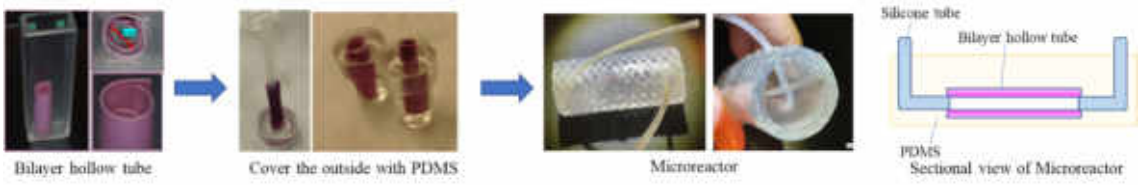


Fig.5-50 The fabrication process of microreactor

5.6.2.4.1 Acetalisation reaction using microreactor in flow condition

The obtained microreactor (**MR1**) was connected to a minipump. A mixture solution was prepared for this experiment, containing 3 ml EtOH, 0.3 ml TMB, 0.7 ml 4 methoxybenzaldehyde and 2.5 ml TEOF. The microreactor was placed in a preheated oil bath at 90 °C for 30 min. When in the oil bath at 90 °C, the colour of the bilayer tube changes from pink to white. Then, the microreactor is transferred to a 55 °C preheated oil bath, and the mixture will be added after 30 min. The colour of the outside of the bilayer tube layer is pink, and the inside layer is white at 55 °C. Then, the mixture was added, and the microreactor and the silicone tube by the minipup and the reaction star were kept flowing (Fig.5-51).

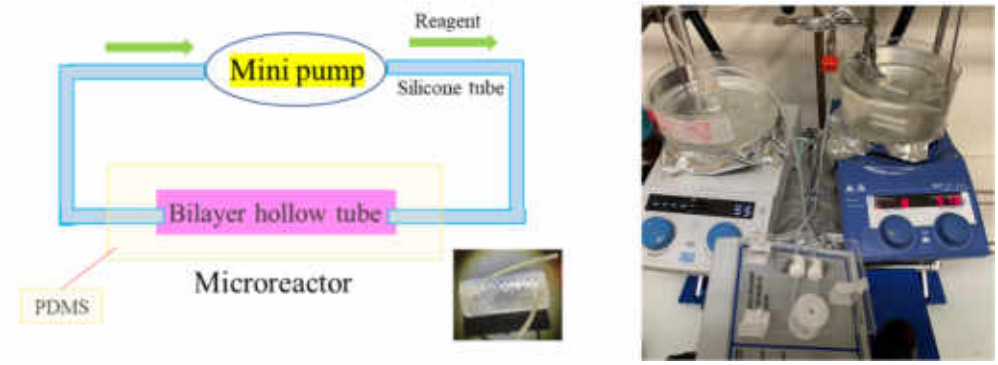


Fig.5-51 The working system for microreactor

After flowing for 3, 5 and 6 hours, the solution resulting from the cycle flow in the microreactor was analysed using ^{1}H NMR. It was observed that some acetal (product) had been formed, but the ratio between the reactant and TMB was different from that of the mixture solution used in the reaction (Fig.5-52). During the experiment, the TEOF, TMB, and side product Ethyl formate disappeared. The ratio of acetal/aldehyde also decreased, which may be due to the acetal disappearing or the acetal hydrolysing back to aldehyde. Also, the volume of the solution seems to decrease after the reaction. There are at least two possible explanations for this observation. One is leaks in the working system, and the other is that the mixture solution can diffuse into PDMS.

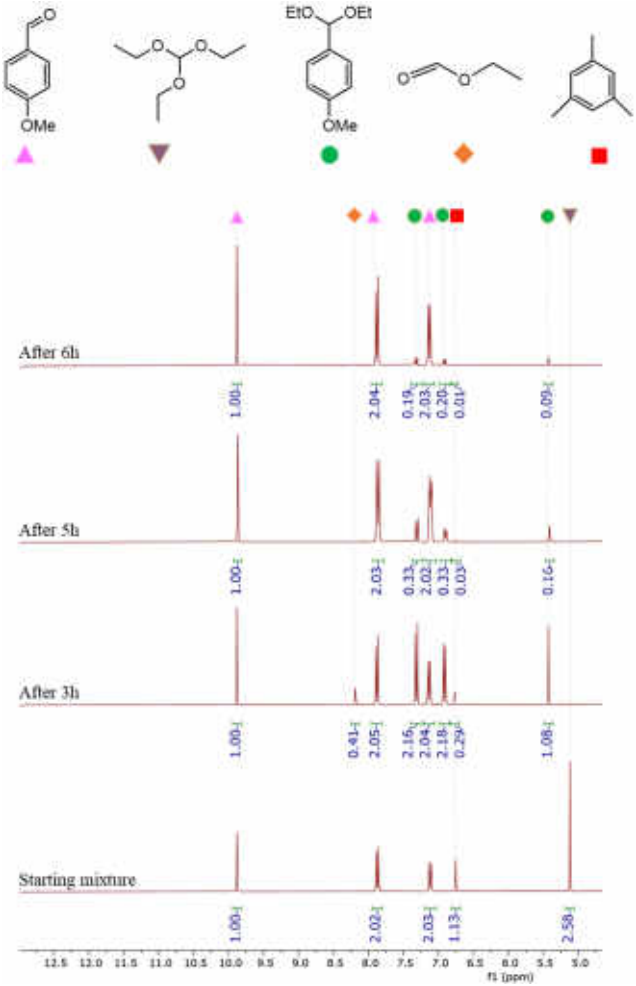


Fig.5-52 The NMR spectra of the experiment using the microreactor

To determine what caused a part of the mixture solution to disappear from the microreactor system, we used a dye called Bromocresol green (BCG), which has an intense colour and can help us locate any leaks or diffusion. We started by checking for leaks in the working system. We prepared a solution of pure Ethanol with BCG and added it to the microreactor system. This solution had a yellow colour. After circulating the solution with a minipump for 2 hours, we observed no leaks or diffusion, and the yellow solution was only visible inside the microreactor and silicone tube, as shown in Fig.5-53(a)-(c).

A solution with the same composition as the catalytic reaction, containing EtOH, 4-methoxybenzaldehyde, TMB, and TEOF, was prepared and added to the microreactor system along with BCG. Interestingly, no leaks were observed, but diffusion in the microreactor was visible. In the beginning, the yellow colour was only inside the tube. However, after the solution was circulated with a minipump for an hour, the yellow colour was also observed in the PDMS outside the tube, as shown in Fig.5-53(d)-(f). This confirms that 4-methoxybenzaldehyde, TMB, TEOF, and acetal, or at least one of them, can diffuse into the PDMS. Actually, PDMS is a widely used material for making microfluidic devices. Lee *et al*. conducted serval experiments to determine the compatibility of PDMS with various organic solvents.[38] They concluded that the solvents that caused the least amount of swelling in PDMS include water, nitromethane, dimethyl sulfoxide, ethylene glycol, perfluorotributylamine, perfluorodecalin, acetonitrile, and propylene carbonate. On the other hand, the solvents that caused the most swelling in PDMS were diisopropylamine, triethylamine, pentane, and xylenes. [38, 39] Thus, it is very likely that TMB, TEOF and ethyl formate can diffuse through PDMS

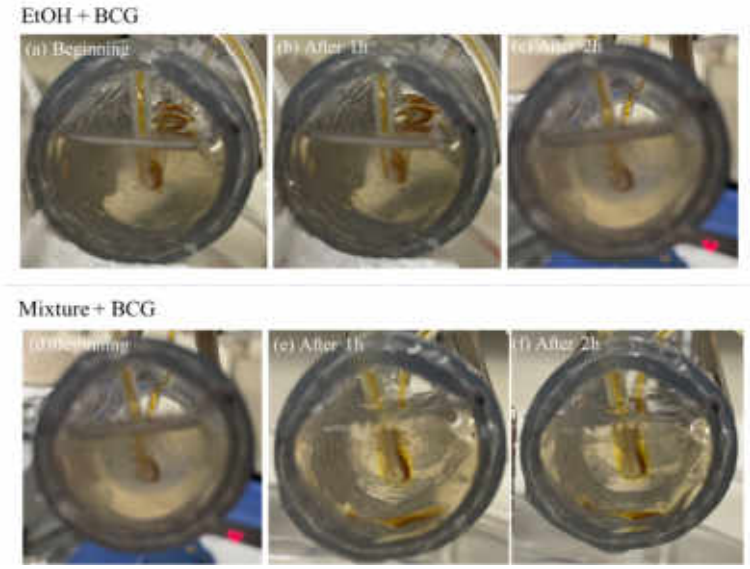


Fig.5-53 The experiment picture for the microreactor using BCG. (a)-(c) pure EtOH. (d)-(f) mixture.



Fig.5-54 The picture of the microreactor using two L-shaped tubes connected by PVC tube.

Table 5-5 The yield and ratio of reactant compared to TMB before and after reaction.

Sample	Y	R1	R2
Starting mixture	0%	2.76	7.23
After 2h	47%	3.26	7.92
After 4h	77%	3.75	7.02

$Y = \frac{n_{acetal}}{n_{acetal} + n_{aldehyde}} \times 100\%$ $R1 = \frac{n_{acetal} + n_{aldehyde}}{n_{TMB}}$ $R2 = \frac{n_{TEOF} + n_{Ethyl\ formate}}{n_{TMB}}$

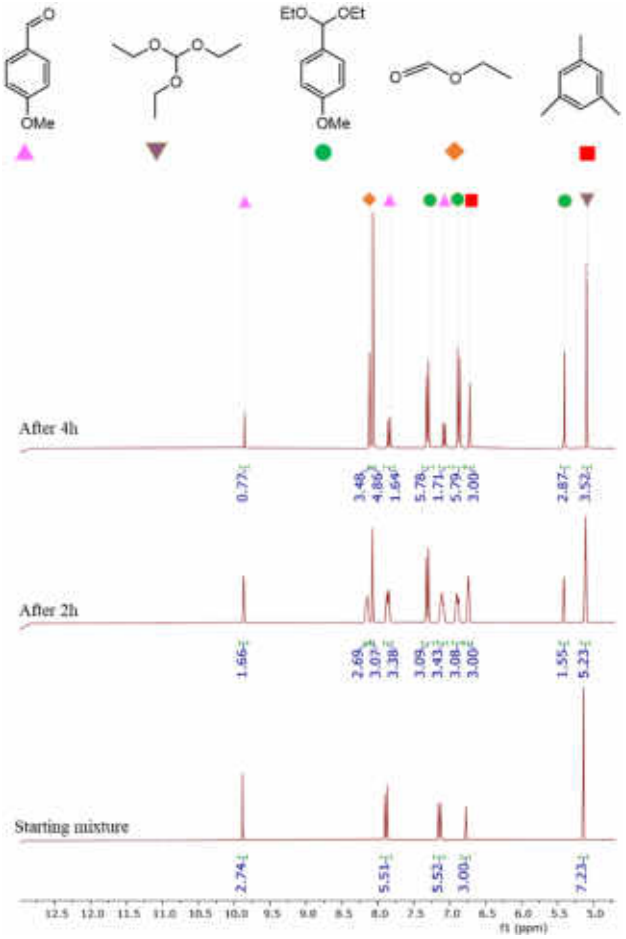


Fig.5-55 The ^{1}H NMR spectra of the experiment.

We decided to make a reactor that did not use PDMS since the organic solvents diffuse into PDMS. As shown in Fig. 5-3, we used Polyvinyl Chloride (PVC) and Polypropylene (PP) to create a microreactor. The bilayer tube was placed between two L-shaped tubes connected by a PVC tube. This **MR2** microreactor was used under the same conditions as **MR1**. The result is shown in Table 5-5 and Fig.5-55. We observed that compared to MR1, TEOF, TMB, and Ethyl formate did not disappear during the reaction, and another side product, which came from the PVC, was observed. The yield was 47% and 77% in 2 and 4 hours, respectively. However, if we compare the ratio of the compounds before and after the reaction, we can see that the ratio was different after the reaction. This indicates that some compounds diffused into the polymer, although it was less than in PDMS. Therefore, we discovered that it was preferable to minimize the amount of polymers present. Then we decided that glass would be preferable. This is where we envisioned the continuous flow chemistry-inspired H-tube system.

5.6.3 Use of the three layers film as a catalyst

Two three-layer films (TPU/Nitrate layer/TPU), **TL-1** and **TL-2**, were prepared for use in this experiment. It is worth noting that these two films will be tested for 7 runs each on the same day, using the same mixture. However, during the initial preparation of the films in the HS and LS2 states using EtOH, the concentration of the reagents was lower than the mixture. Therefore, the first three tests will not be considered (shown in a lighter colour in Fig.5-56), and we will focus on the later four tests.

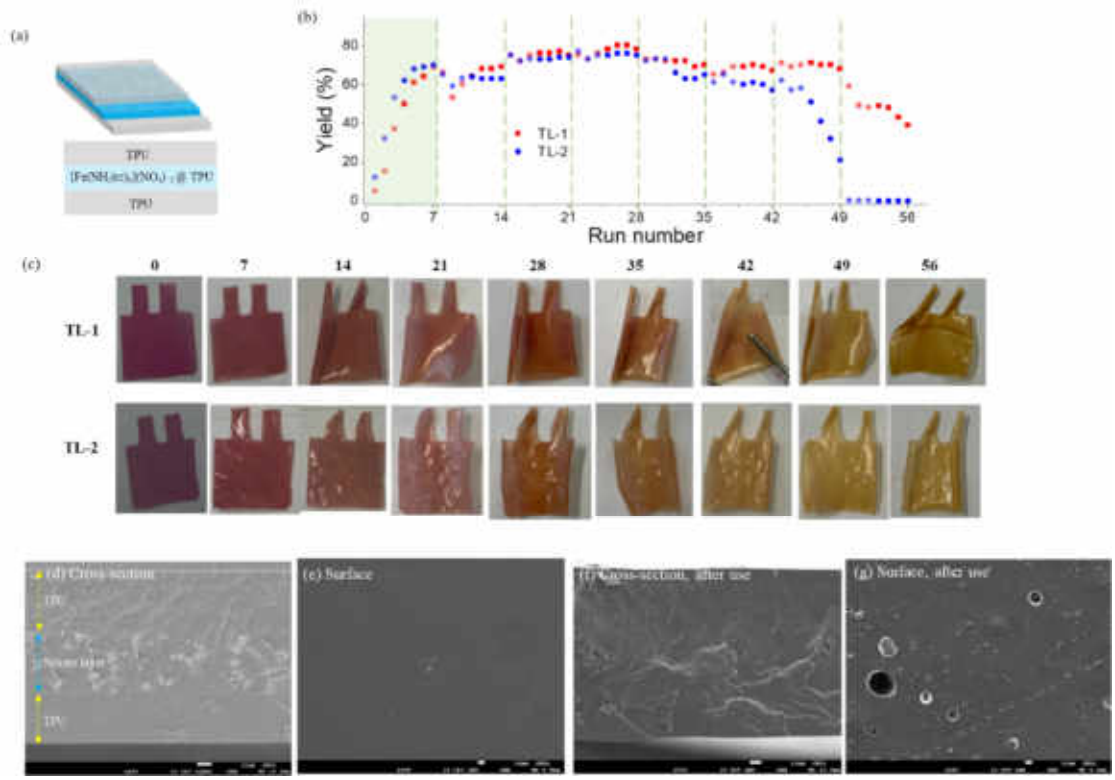


Fig.5-56 TPU/Nitrate layer/TPU three-layer film, (a) scheme of structure. (b) the yield of acetalisation reaction using TL-1 and TL-2 as catalysts. (c) the colour of TL-1 and TL-2 after use.(d)-(g) SEM image of TL-1 before and after use.

Note that the flow rate in this experiment is around 7.5 ml/ 15 min. To verify if these two are identical, both were tested in the HS state first, as shown in Fig.5-56 with a green background. Both yields are similar, and the yield of **TL-2** is even slightly better. Therefore, **TL-2** will be tested in the LS2 state, and **TL-1** will be tested in the HS state in the following experiments. Based on the result shown in the figure, it can be observed that the yield for **TL-1** is higher than that of **TL-2** during 56 tests.

The SEM image in the figure displays the cross-section and surface of **TL-1** before and after use. The image of the cross-section confirms the three-layer structure of **TL-1**. Before use, SCO complexes were distributed uniformly in the middle layer. However, after use, no complex was observed. The SEM image of the surface displays many holes after use, which could act as channels for reagents to penetrate the film and for the release of SCO complex from the film.

Two three-layer films (Sulfate layer/Nitrate layer/Sulfate layer), **TL-3** and **TL-4**, were prepared for use in this experiment. The experiment processes were the same as **TL-1** and **TL-2** in the

previous experiment. Basically, the **TL-3** that is used in the HS state work better than the TL-4 used in the LS2 state. In this case, the three layers are easier to break, as shown in Fig.5-57.

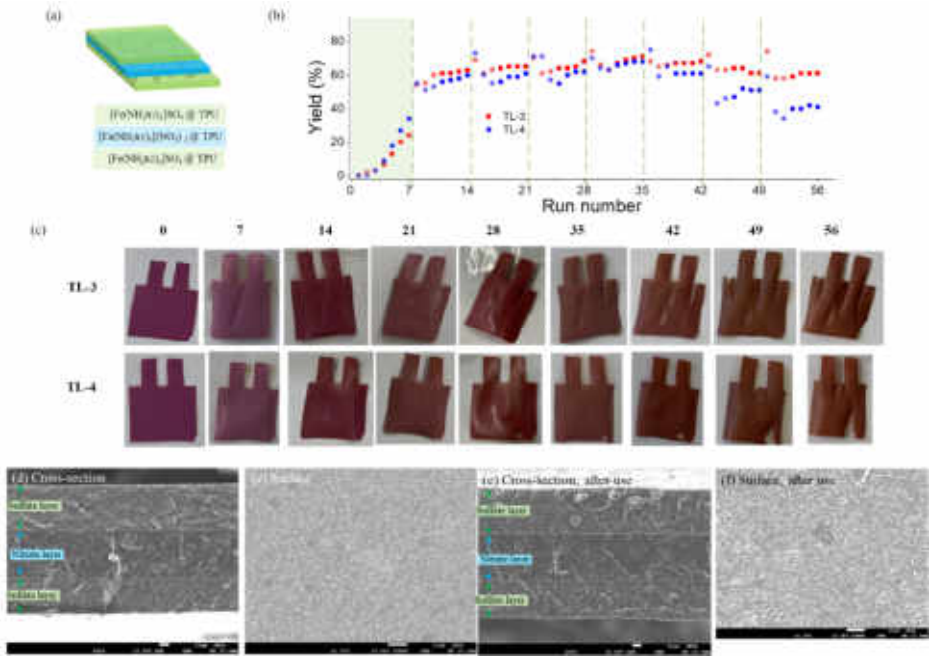


Fig.5-57 Sulfate layer/Nitrate layer/Sulfate layer, three-layer film, (a) scheme of structure. (b) the yield of acetalisation reaction using **TL-3** and **TL-4** as catalysts. (c) the colour of **TL-3** and **TL-4** after use.(d)-(g) SEM image of **TL-3** before and after use.

The SEM image displays the cross-section and surface of **TL-3** before and after use. It is evident that both before and after use, the sulfate complex remained uniformly distributed within the sulfate layer, with minimal leaching even after extended use. However, in the cross-section, significantly less nitrate complex was observed in the nitrate layer after prolonged use. Despite this, the three-layer film demonstrated a longer usable lifespan compared to the monolayer, owing to the two stable outer layers that protect the central catalytic layer.

5.7 Mechanism study of $[Fe(NH_2trz)_3](NO_3)_2$@TPU films as the catalyst

Films with complex **1** in the LS2 state have consistently shown lower effectiveness than those with the complex in the HS state in the latest tests. We therefore wondered what could be the reason for this difference in reactivity. To understand what is happening in the composite film during catalytic reactions, it is essential to study both the properties and morphology of the film. Instead of using bilayer or three-layer films, the monolayer film was selected for this investigation, as its single catalytic layer simplifies characterization and analysis. Twelve small pieces, each weighing approximately 13 mg, were cut from the same large film for use in four experiments (**A**, **B**, **C**, and **D**), consisting of 7, 14, 21, and 28 tests, respectively. Each experiment involved three films tested in HS, LS2, and LS states (Fig.5-58).

Following the reactions, all films were analyzed using XRD, IR, optical reflectivity, and SEM

techniques. The results of catalytic performance are presented in Fig.5-59, showing the outcomes of 7, 14, 21, and 28 test cycles. In general, the catalytic yield for the films used in the HS state was slightly higher than those in the LS2 state. When the films were used in the LS state, several activation cycles were required before the films could catalyze the reaction efficiently.

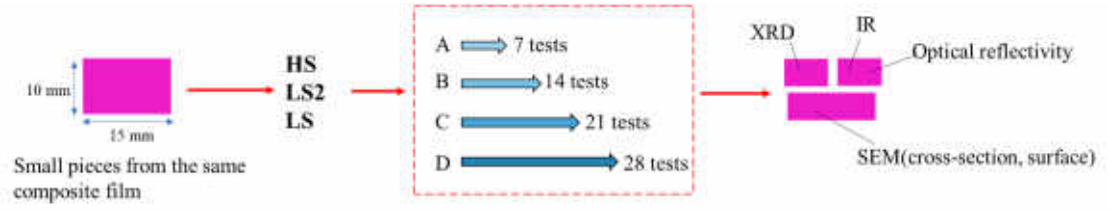


Fig.5-58 Scheme of experiments A, B, C, and D.

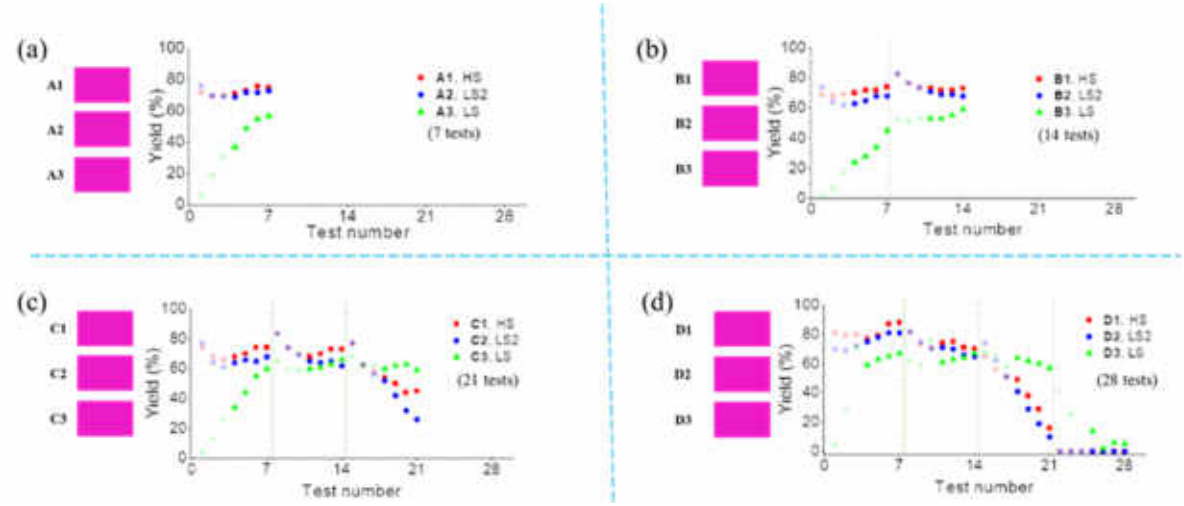


Fig.5-59 The yield of experiments A, B, C, D.

5.7.1 Characterisation of SCO composite film after use in catalytic reaction

5.7.1.1 Results of composite film from experiment A after 7 test cycles

Fig.5-60 presents the results of optical reflectivity, IR, and XRD measurements of the monolayer films from **experiment A** after 7 test cycles. The optical reflectivity results reveal that the intensity differences between the HS and LS states are 63, 37, and 32 for the new film and the films tested in the HS and LS2 states, respectively. This suggests that after seven test cycles, the films contain less SCO complex compared to the new film. Films **A1** (HS) and **A2** (LS2) exhibit similar results. In the IR spectra, a doublet at 620 cm^{-1} and 611 cm^{-1} was observed in **A1** (HS) and **A2** (LS2), while **A3** showed a single peak at 620 cm^{-1}, similar to the new film. This suggests that **A1** (HS) and **A2** (LS2) contain less SCO complex than **A3** (LS) and the new film, which is consistent with the optical reflectivity findings. The XRD results further confirm this, as films **A1** (HS) and **A2** (LS2) display less intense diffraction peaks compared to the new

film. These results are consistent with both the optical reflectivity and IR measurements, indicating that after seven test cycles, films **A1** (HS) and **A2** (LS2) contain less SCO complex than **A3** (LS) and the new film, which is released into the solution during the catalytic reaction.

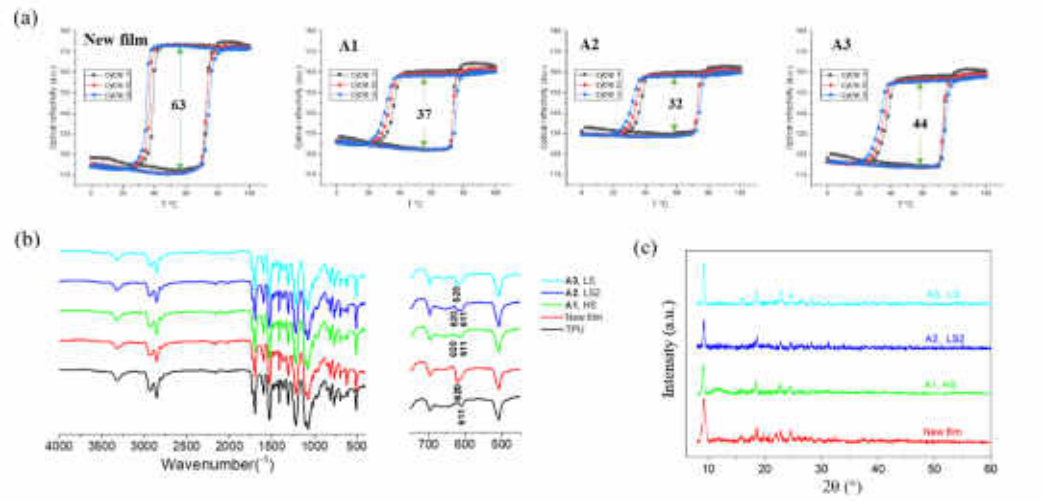


Fig.5-60 The result of monolayer film from **experiment A** after seven test cycles. (a) Variable temperature reflectivity measurement. (b) IR spectra and (c) XRD measurement

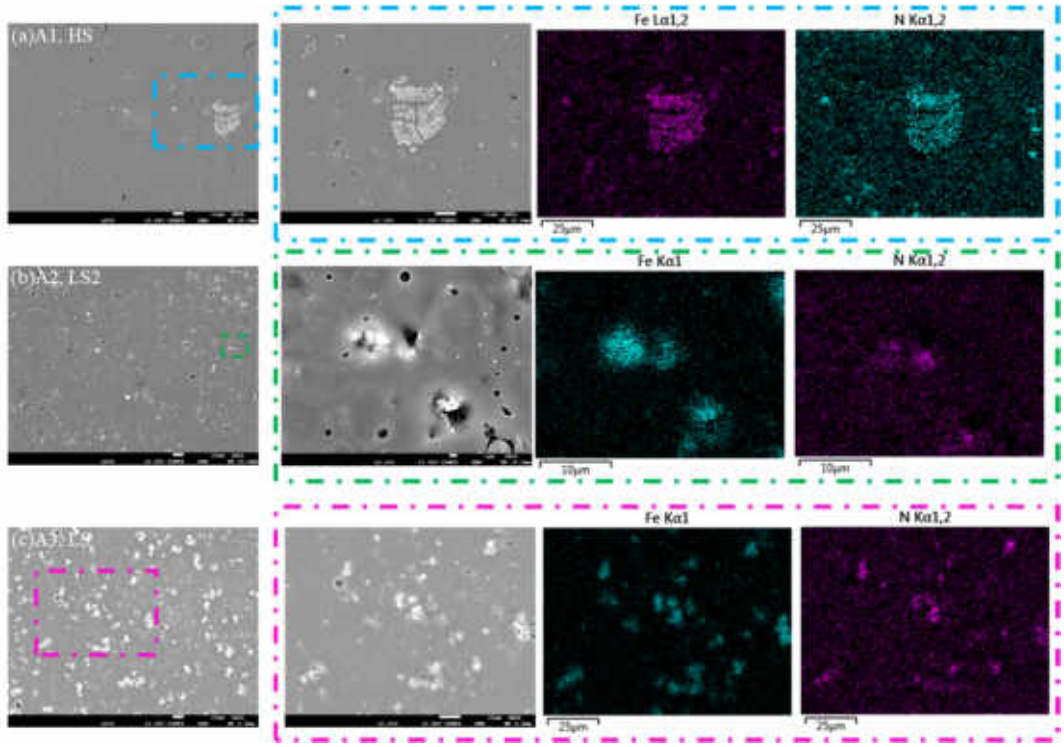


Fig.5-61 SEM images of the surface of monolayer film from **experiment A** after 7 test cycles and their images of corresponding EDX mapping. (a) **A1** (HS). (b) **A2** (LS2). (c) **A3** (LS).

Fig.5-61 and Fig.5-62 show SEM images of the surface and cross-section of monolayer film from **experiment A** after 7 test cycles. On the surface of films **A1** (HS) and **A2** (LS2), only a small amount of the SCO complex was observed, whereas the surface of film **A3** (LS) appeared

nearly identical to that of the new film, with a uniform distribution of the SCO complex. This suggests that, in films **A1** (HS) and **A2** (LS2), at least some of the SCO complexes located on the surface were released into the solution during the catalytic reaction.

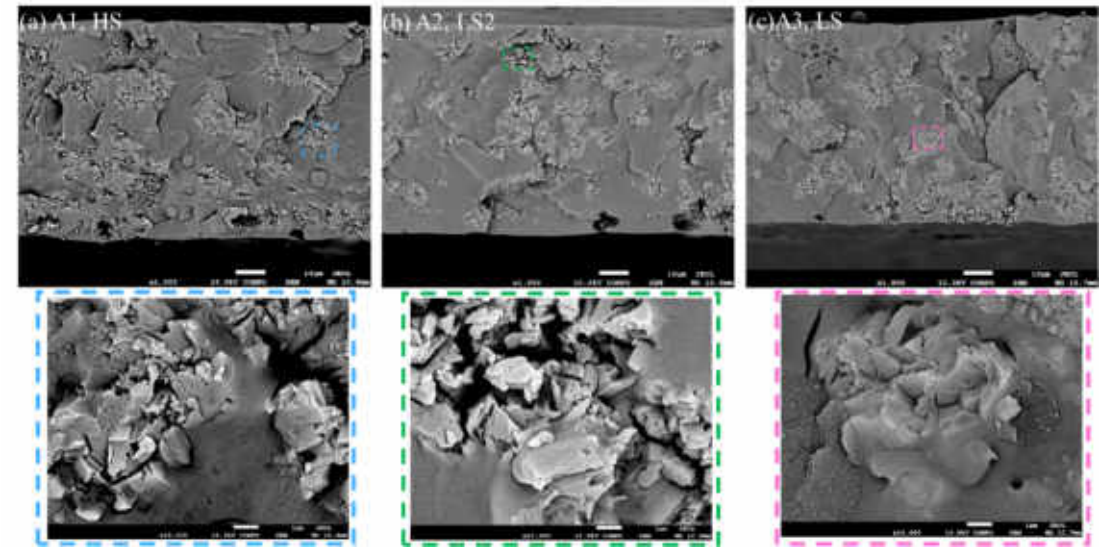


Fig.5-62 SEM images of the cross section of monolayer film from **experiment A** after seven test cycles and their images of corresponding EDX mapping. (a) **A1** (HS). (b) **A2** (LS2). (c) **A3** (LS).

The internal morphology of the composite film could be observed in the cross-sectional images. As shown in Fig.5-62, the SCO complex in the polymer matrix of the **A3** (LS) film remains in large, compact aggregates, similar to the structure observed in the new film. However, in samples **A1** (HS) and **A2** (LS2), the SCO complex appears more porous, with the particles separated and dispersed throughout the matrix. Additionally, many empty spaces and holes were observed in these two samples. This could be due to the separation of the complex, and the release of some of the SCO complex into the solution, leaving behind voids in the polymer matrix.

5.7.1.2 Results of composite film from experiment B after 14 test cycles

Fig.5-63 and Fig.5-63 presents the results of optical reflectivity, IR, and XRD measurements of the monolayer films from **experiment B** after 14 test cycles. The differences in optical reflectivity intensity between the films in the HS and LS states were 12, 9, and 35 for **B1** (HS), **B2** (LS2), and **B3** (LS), respectively, representing a significant decrease compared to the new film (62). This suggests that less SCO complex remains in the films, likely due to the release of some particles into the solution. Additionally, the IR spectra for **B1** (HS) and **B2** (LS2) did not exhibit the bond of the SCO complex, while **B3** (LS) exhibited a doublet at 620 cm^{-1} and 611 cm^{-1}. However, the XRD measurement still showed an intense peak around 10°, corresponding to the presence of the SCO complex. The discrepancy between the XRD and IR measurements arises because the IR analysis was performed using Attenuated Total Reflection (ATR) mode, which probes only a shallow layer of the film, typically just a few micrometres deep.[40] As the number of test cycles increased, more SCO complexes were released into the solution, leaving fewer complexes near the surface of films **B1** (HS) and **B2** (LS2). This explains why the SCO complex was undetectable in the IR spectra but still detectable in the XRD measurement.

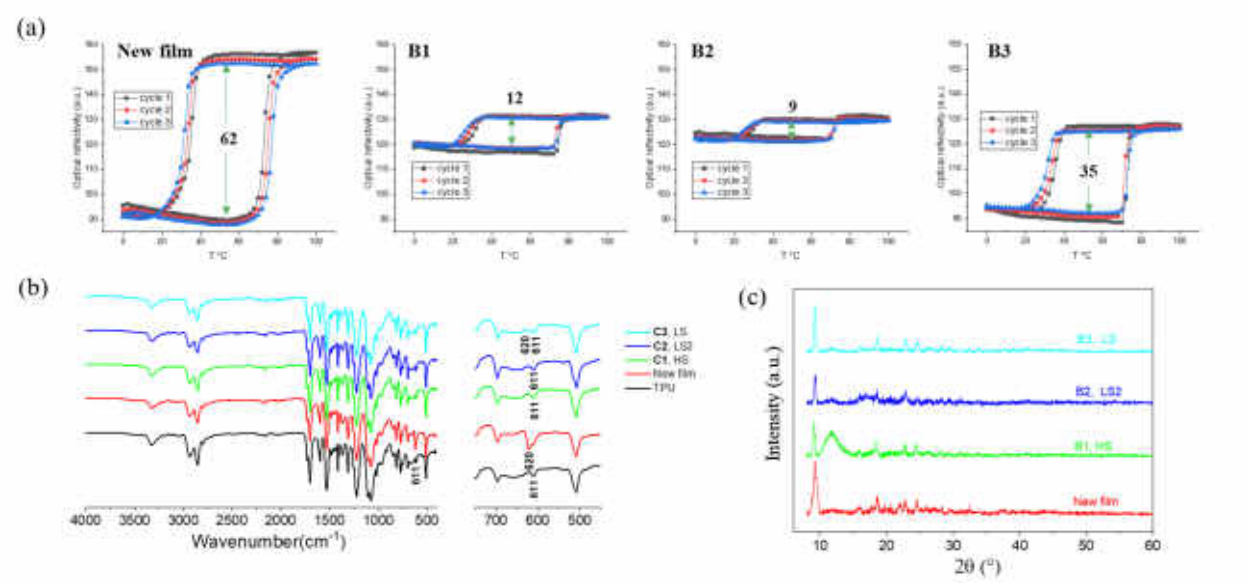


Fig.5-63 The result of monolayer film from **experiment B** after 14 test cycles. (a) Variable temperature reflectivity measurement. (b) IR spectra and (c) XRD measurement

Fig.5-64 and Fig.5-65 show the SEM images of the surface of the monolayer film from **experiment B** after 14 test cycles. Almost no SCO complex was observed on the surface of any of the three samples. Instead, numerous holes were visible, which may have provided channels for the SCO complex to move from the inner part of the film into the solution. The SEM images of the cross-section, also shown in Fig.5-65, support the results obtained from optical reflectivity and IR measurements. A significant decrease in the number of SCO complexes was observed in films **B1** (HS) and **B2** (LS2) after 14 tests, compared to the new film. Additionally, some holes were present, which may have originally been occupied by the SCO complex. These holes likely also serve as pathways for the SCO complex to be released into the solution. In contrast, the film used in the LS state (**B3**) still showed a uniform distribution of the SCO complex across the cross-section. Even after 14 tests for the sample of **B3** (LS), the SCO complex in the polymer matrix remained in large, compacted aggregates. However, for films **B1** (HS) and **B2** (LS2), the SCO complex appeared smaller, more dispersed, and more porous.

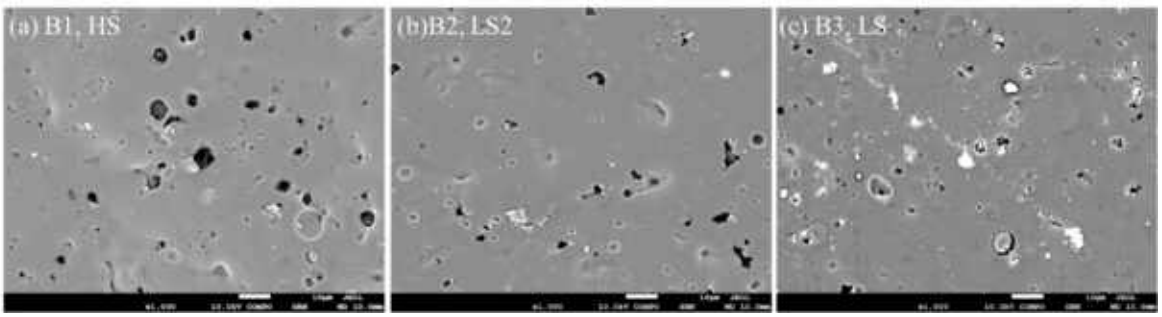


Fig.5-64 SEM images of the surface of composite film after 14 tests. (a) **B1**. (b) **B2**. (c) **B3**.

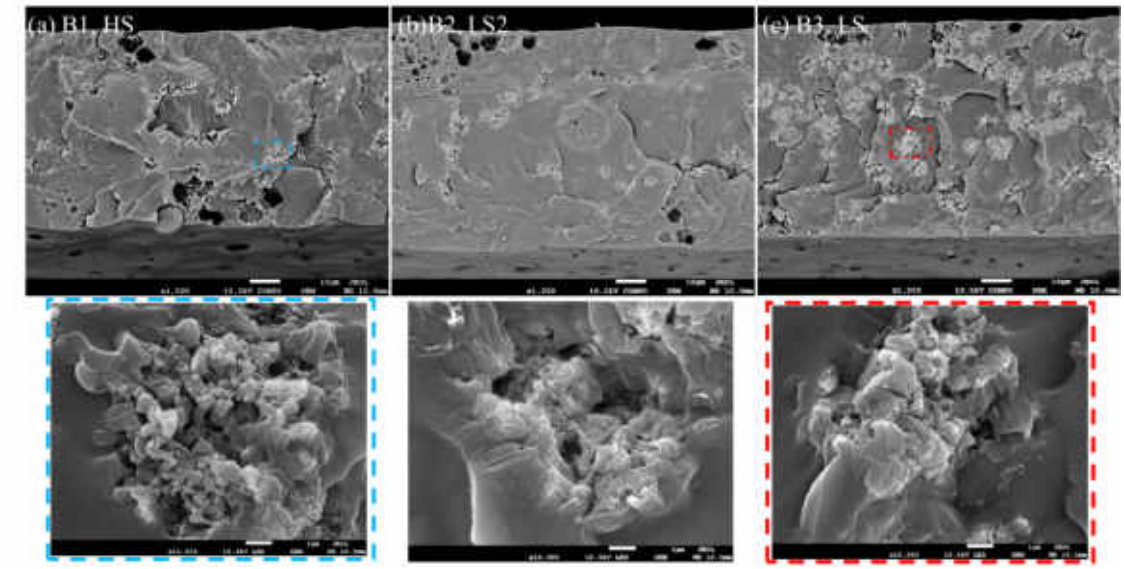


Fig.5-65 SEM images of the cross-section of the composite film after 14 tests. (a) **B1**. (b) **B2**.(c) **B3**

5.7.1.3 Results of composite film from experiment C after 21 test cycles

The figure presents the results of optical reflectivity, IR, and XRD measurements of the monolayer films from **experiment C** after 21 test cycles. As shown in Fig.5-59, there was a significant decrease in the yield for **C1** (HS) and **C2** (LS2), while the yield of **C3** (LS) remained higher. This result is normal, as the optical reflectivity test indicated no hysteresis loop for C1 and C2, suggesting no colour change during the reflectivity measurement. This implies that only a trace amount, or no SCO complex, remains in these two films. In contrast, film **C3** (LS) displayed a hysteresis loop, although the intensity difference HS and LS had significantly decreased to 17, compared to 61 in the new film. The IR and XRD results were consistent with the optical reflectivity measurements, showing that only film **C3** (LS) still contained the SCO complex after 21 test cycles.

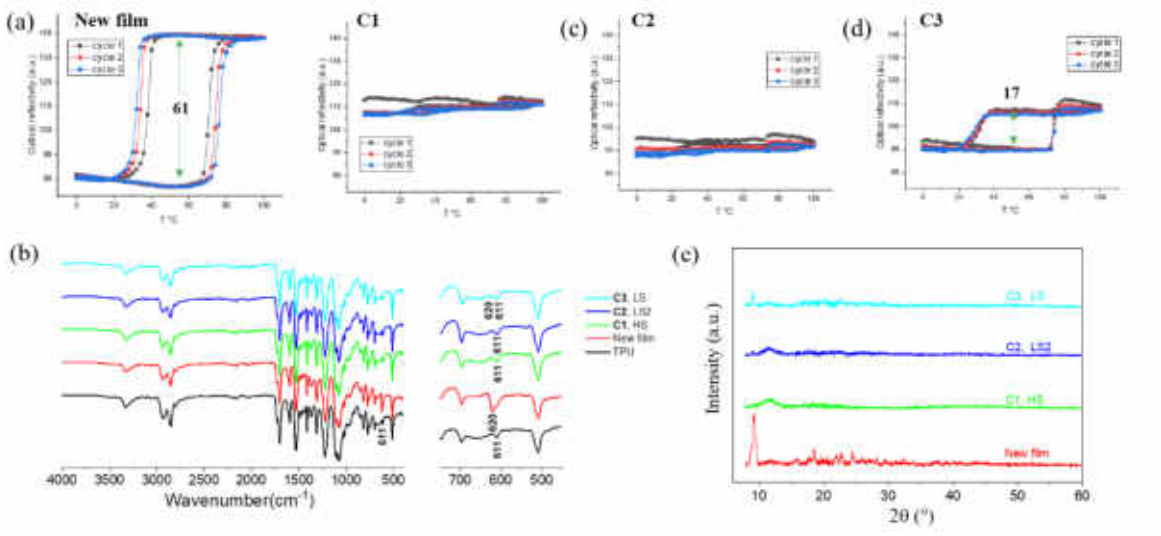


Fig.5-66 The result of monolayer film from **experiment C** after 21 test cycles. (a) Variable temperature reflectivity measurement. (b) IR spectra and (c) XRD measurement

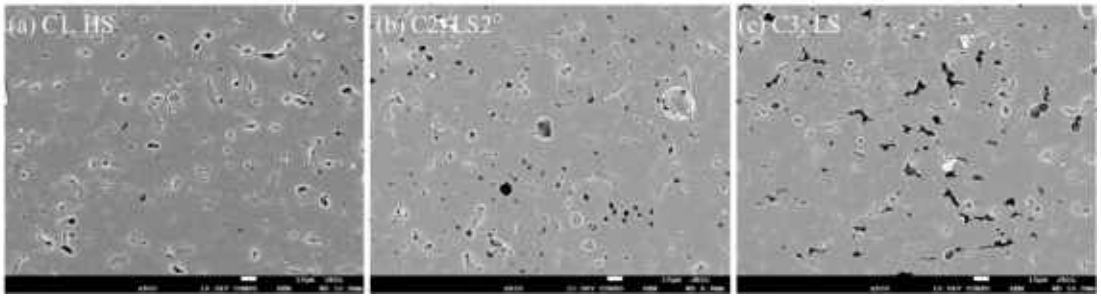


Fig.5-67 SEM images of the surface of composite film after 21 tests. (a) **C1**. (b) **C2**. (c) **C3**

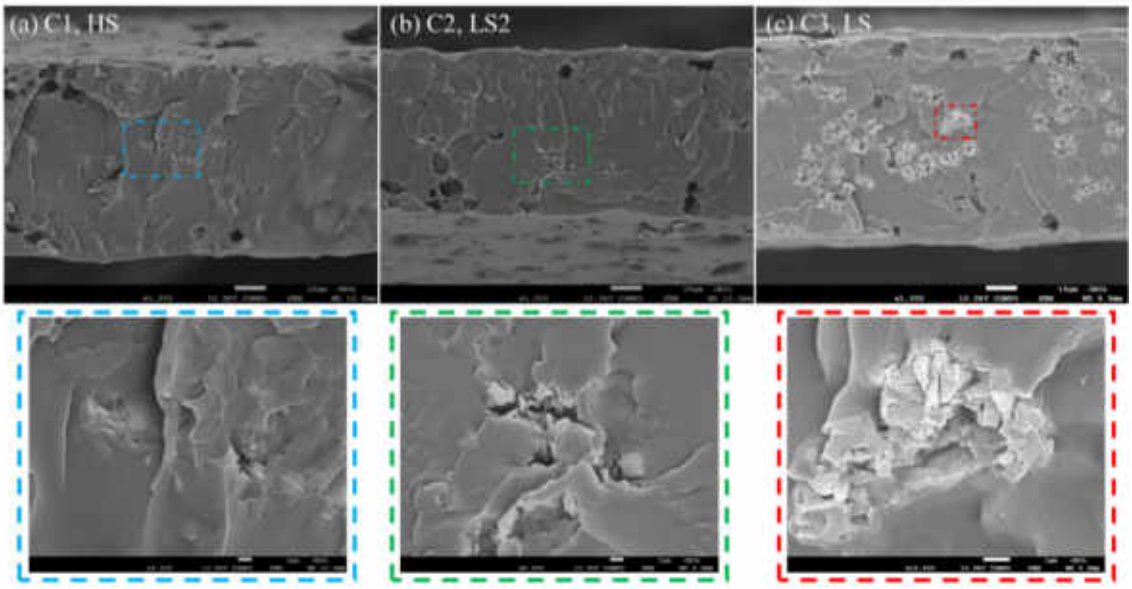


Fig.5-68 SEM images of the cross-section of the composite film after 21 tests. (a) **C1**. (b) **C2**. (c) **C3**

Fig.5-67 and Fig.5-68 show the SEM images of the surface of the monolayer films from **experiment C** after 21 test cycles. No SCO complex was observed on the surface of films **C1** (HS), **C2** (LS2), and **C3** (LS) but numerous holes were present, which may have acted as channels for the release of the complex from the film or were previously occupied by the complexes. In the cross-sectional images, only trace amounts of the complex were detected in films **C1** (HS) and **C2** (LS2), while a significant amount of the SCO complex was still present in film **C3** (LS). These results are consistent with the findings from the optical reflectivity, IR, and XRD measurements.

5.7.1.4 Results of composite film from experiment D after 28 test cycles

After 28 test cycles, the films could no longer catalyze the reaction efficiently. Based on the results from optical reflectivity, IR, XRD and SEM analyses, no SCO complex was detected in films **D1** (HS) and **D2** (LS2), while only trace amounts of the SCO complex were observed in film **D3** (LS).

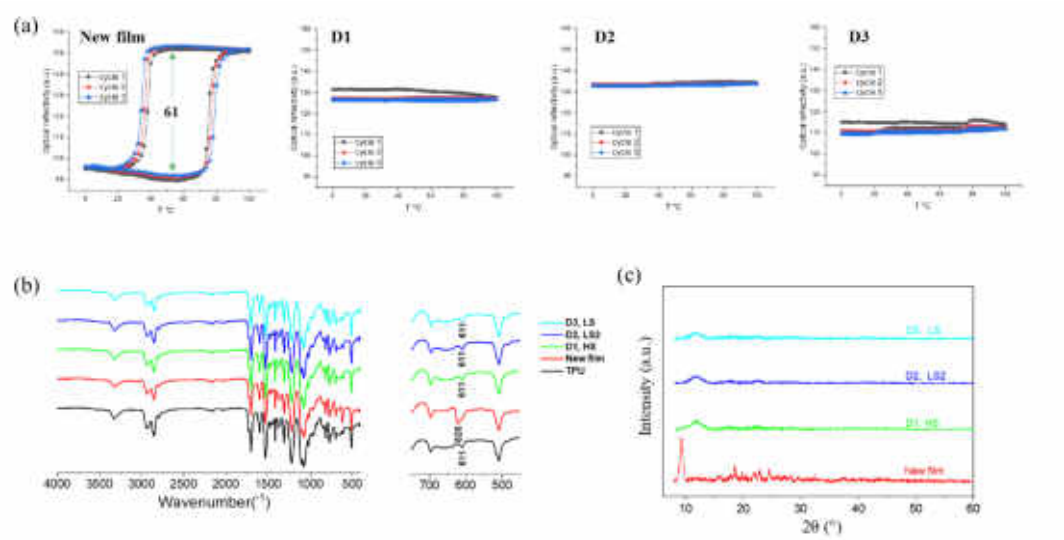


Fig.5-69 The result of monolayer film from **experiment D** after 28 test cycles. (a) Variable temperature reflectivity measurement. (b) IR spectra and (c) XRD measurement

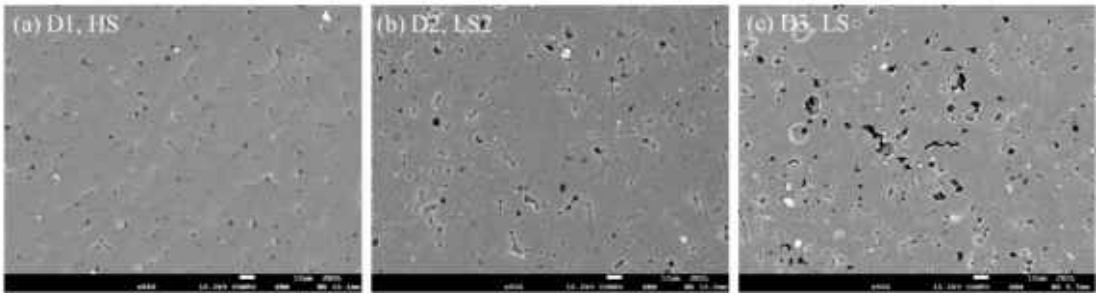


Fig.5-70 SEM images of the surface of composite film after 28 tests. (a) **D1**. (b) **D2**. (c) **D3**

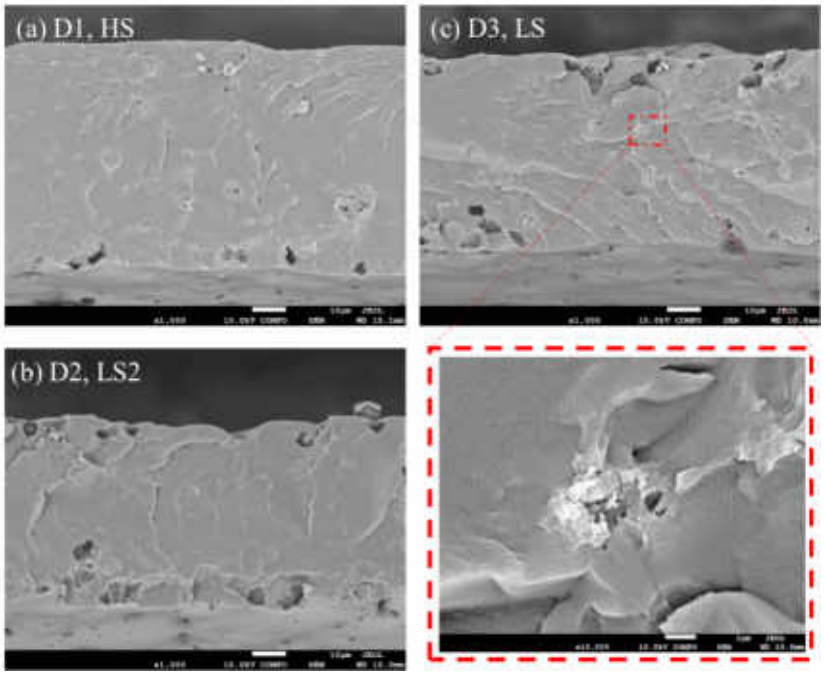


Fig.5-71 SEM images of the cross-section of composite film after 28 runs. (a) **D1**. (b) **D2**. (c) **D3**

5.7.2 The effect of solvent/reagent on SCO composite film

It is evident that the SCO complex is released from the film during the reaction, potentially due to the influence of the solvent or reagent used. A previous study[41] demonstrated that when the $Fe(NH_2trz)_3(NO_3)_2$ SCO complex is suspended in EtOH, the EtOH molecules interact with the polymer chains, leading to their separation. The EtOH molecules help disperse and separate large aggregates, suggesting that the solvent affects the size and morphology of the SCO complex.

Different mixtures were prepared, as illustrated in Fig.5-72, to investigate the impact of the solvent and reagent. The first mixture was used to study the catalytic reaction with EtOH, *p*-anisaldehyde, and TEOF. The second mixture excluded *p*-anisaldehyde, with the other components remaining the same as the first mixture. The final mixture consisted solely of pure EtOH. A total of 28 test cycles were conducted using these films in the HS, LS2, and LS states for the three mixtures.

The optical reflectivity measurement curves (Fig.5-72, Fig.5-73 and Fig.5-74) show that the films tested in the first mixture displayed no hysteresis loop after 28 tests, while a weak hysteresis loop was observed in the film tested with the second mixture. Compared to films with the complex **1** in the HS and LS2 states, the one with the complex in the LS2 state has a substantially higher number of complex particles. In contrast, the films tested in pure EtOH still exhibited a clear hysteresis loop, with intensity differences of 24, 22, and 31 for the films used in HS, LS2, and LS states, respectively. It is evident that all films, regardless of the mixture used, release SCO particles into the solution. The films tested in HS, LS2, and LS states exhibit the same general tendency. The films used in pure EtOH retain more SCO complex, whereas only trace amounts or none are observed in the films tested in the first mixture.

SEM images of the cross-section of the composite films after 28 tests confirm the optical reflectivity results. In the films tested in pure EtOH, the SCO complex remains distributed within the TPU matrix as large, compact aggregates. However, in the films used in the first and second mixtures, only trace amounts or no SCO complex were detected.

These results suggest that in the presence of EtOH, the solvent diffuses into the film and interacts with the SCO complex. This interaction helps disperse and separate the SCO complex from the polymer chains, facilitating the release of the SCO complex into the solution. Furthermore, the release of SCO particles is accelerated in the mixture of EtOH and TEOF. This may occur because TEOF forms hydrogen bonds with EtOH, which are then inserted into the polymer chains and separated more effectively. The larger hydrogen-bonded molecules formed by EtOH and TEOF lead to more efficient polymer chain separation compared to pure EtOH. Furthermore, NH_2 groups on compound **1** may react with the aldehyde to generate imine functions on the complex. Better polymer chain separation and maybe the loss of complex particles could result from this. It is also important to note that in the experiment using the second mixture (EtOH and TEOF), approximately 5% of TEOF was hydrolyzed in the presence of the composite film, compared to less than 1% in the blank test. This may be due to trace amounts of water in the reactant, and the composite film potentially catalyzes the hydrolysis of TEOF. Ethylfromate could perhaps react with NH_2 functions of complex **1** to form amide functions. Similar to imine functions, these amide functions could lead to greater separation of the polymer chains of the complex.

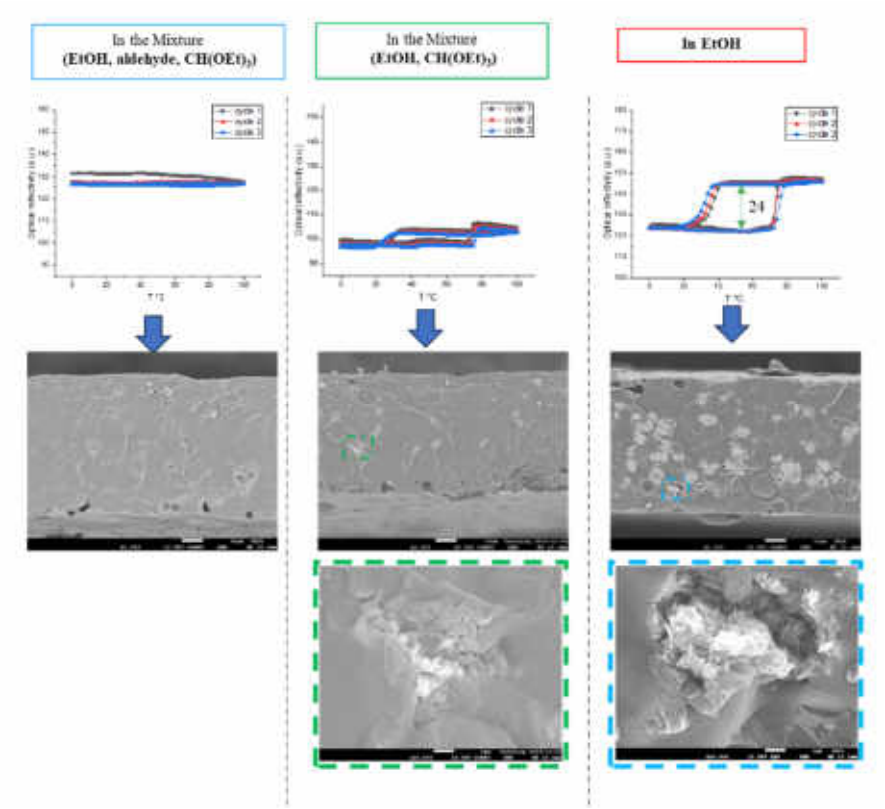


Fig.5-72 The optical reflectivity and SEM images of cross-section of composite film after 28 tests in HS state in different mixture

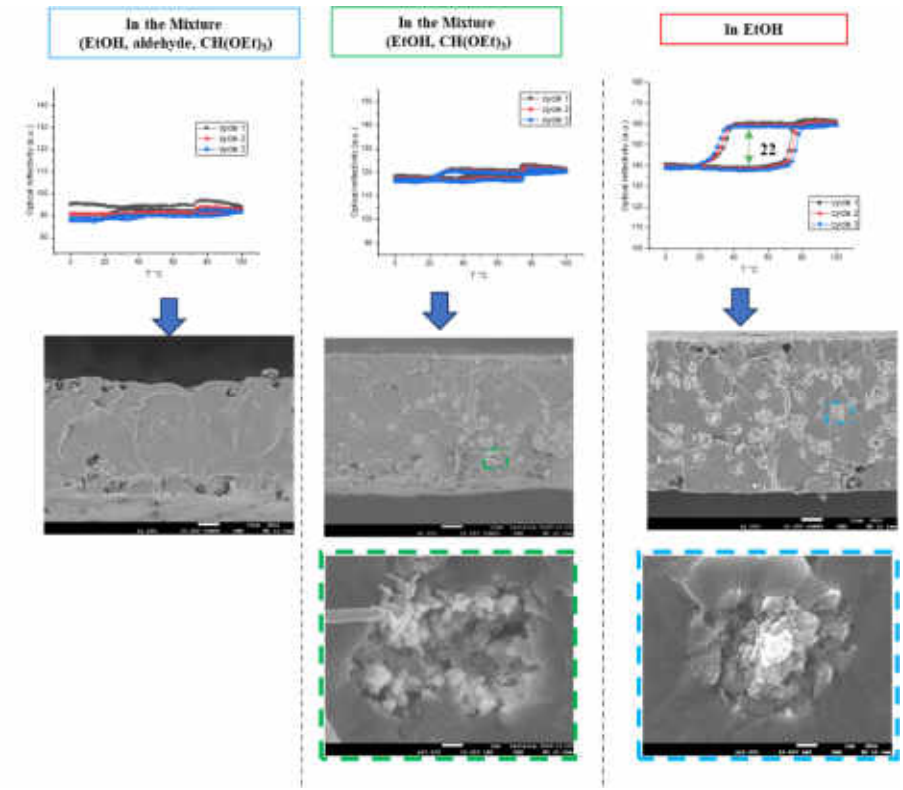


Fig.5-73 The optical reflectivity and SEM images of cross-section of composite film after 28 tests in LS2 state in different mixture

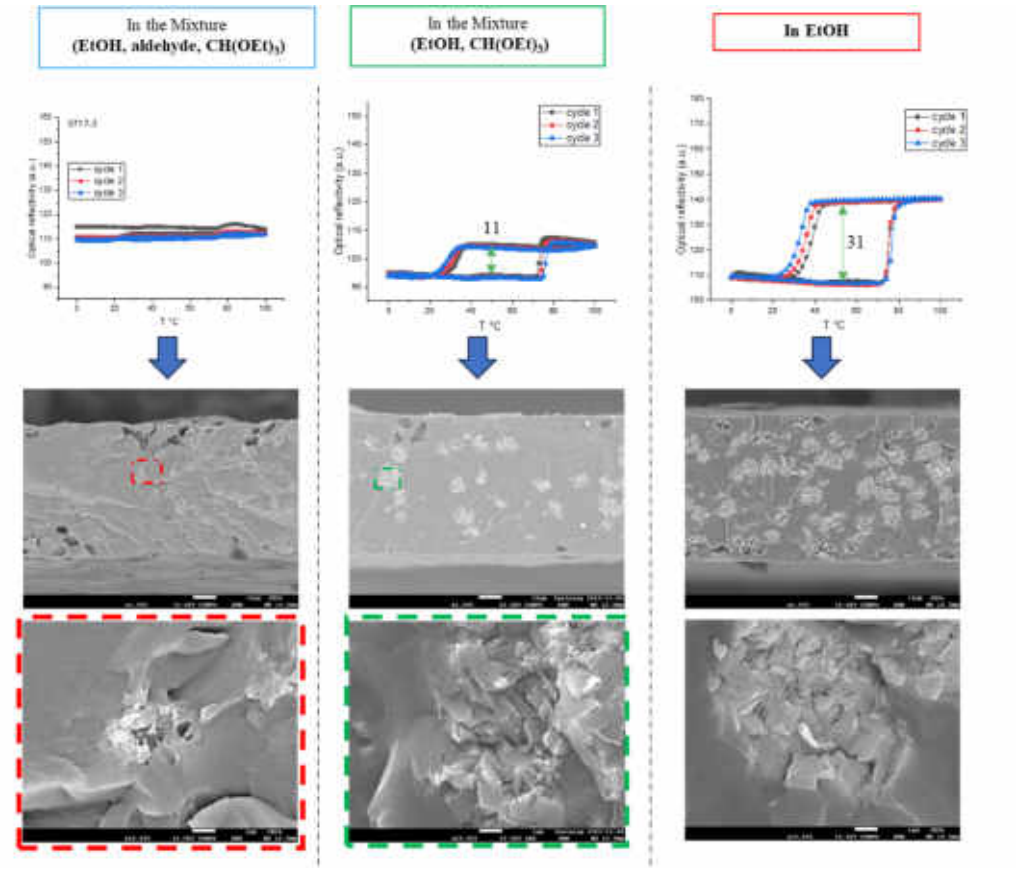


Fig.5-74 The optical reflectivity and SEM images of cross-section of composite film after 28 tests in LS state in different mixture

5.7.3 Study of a possible formation of imine complex in composite materials

The formation of imine functions on the complex may be one reason why complexes in the LS state release fewer particles than complexes in the HS and LS2 states. Therefore, we questioned whether the composite material would allow for this imine production. In this regard, we started by creating a composite material based on imine complex **2**. Fig.5-75 (a) and (b) show the morphology of the imine complex, which consists of uniform 1D rods. A composite film (Film **I1**) was fabricated using 25 wt% of the imine complex. Fig.5-75 reveals that we can clearly observe the rod-shaped particles of the imine complex in the composite material. As depicted in Fig.5-76, this film **I1** was used as a catalyst for the acetalization reaction. Interestingly, the yields obtained using film **I1** as a catalyst significantly decreased from the first test cycle, which is markedly different from the performance of the $[Fe(NH_2trz)_3](NO_3)_2$@TPU composite film. As shown in Fig.5-75 (d), no imine complex was observed on the surface of the composite after 7 tests. Instead, numerous holes were observed, which may have originally been occupied by the imine complex. These findings suggest that it would be relatively easy to distinguish the imine complex from the amine complex if it formed within the composite material. Moreover, the imine complex could potentially catalyze the acetalization reaction efficiently. However, according to the result shown in Fig.5-76, after 4 tests, there were not enough imine complexes remaining in the film to achieve high yields.

In a previous section 5.7, where the mechanism of using composite films in catalytic reactions was studied, no 1D rods that could represent the imine complex were observed in any of the

SEM characterizations. Additionally, IR analysis did not detect the presence of the imine complex.

To verify whether the imine complex could form within the film, a piece of $[Fe(NH_2trz)_3](NO_3)_2$@TPU film was placed in a vial containing 2 ml of EtOH and 200 µl of *p*-anisaldehyde and heated at 55°C overnight. The film remained fully pink the following morning. Tetrahydrofuran (THF) was then used to remove the TPU, and the SCO complex was analyzed by IR. As shown in the IR spectra (Fig.5-77), no band related to the imine bond was detected from the film after the overnight reaction. Therefore, no imine complex was found inside the film.

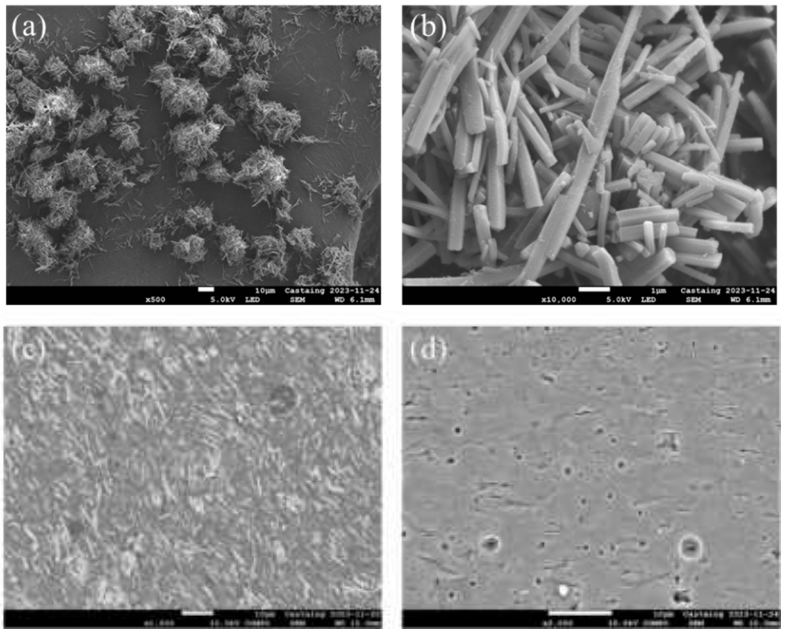


Fig.5-75 SEM images of (a) and (b) imine complex, (c) surface of imine complex@TPU film (d) surface of imine complex@TPU film after 7 tests.

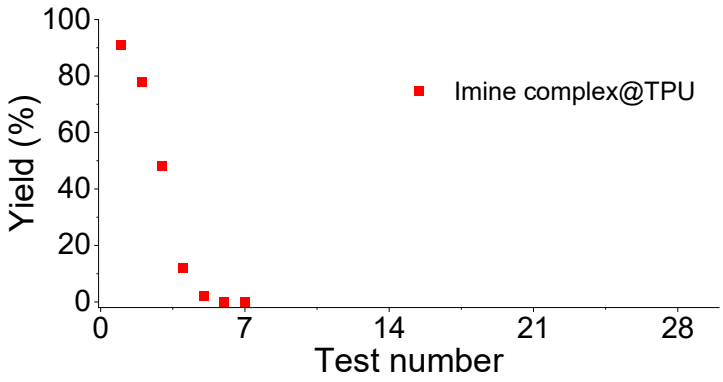


Fig.5-76 Catalytic performance of imine complex@TPU film

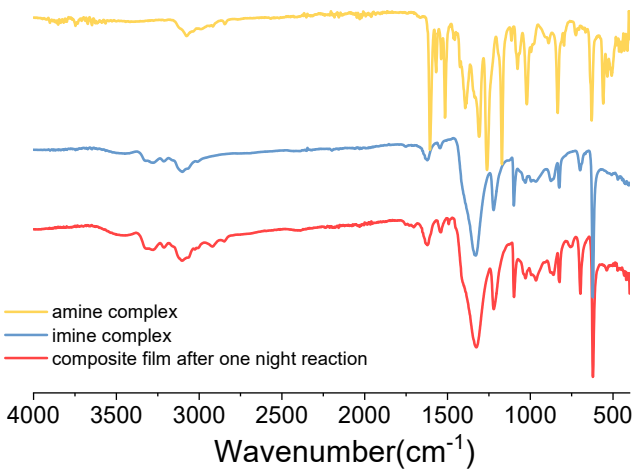


Fig.5-77 IR spectra of $[Fe(NH_2trz)_3](NO_3)_2$@TPU composite film after one night reaction

5.7.4 Study of the effect of the solvent and the aldehyde on the morphology of complex 1 particles

Another experiment was also performed to study the effect of the solvent/reagent on SCO complex powder. As shown in Table 5-6, 10 mg of the SCO complex were employed in different solvents/reagents under various conditions. After the reaction, take a few drops of the suspension, place it on aluminium foil, and remove the solvent under vacuum. Finally, characterise the sample using SEM (Fig.5-78).

Table 5-6 The summary of the experiment conditions to prepare the samples

Sample name	SCO complex	Solvent/ragent			Condition
		EtOH	96% EtOH	aldehyde	
S1	10 mg	2 ml	--	--	90°C 1h
S2		-	2 ml	--	90°C 1h
S3		2 ml	--	--	90°C 3min, 55 °C 1h
S4			2 ml	--	90°C 3min, 55 °C1 h
S5		2 ml	--	200 µl	90°C 1h
S6		--	2 ml	200 µl	90°C 1h
S7		2 ml	--	200 µl	90°C 3min, 55 °C 1h
S8		--	2 ml	200 µl	90°C 3min, 55 °C 1h

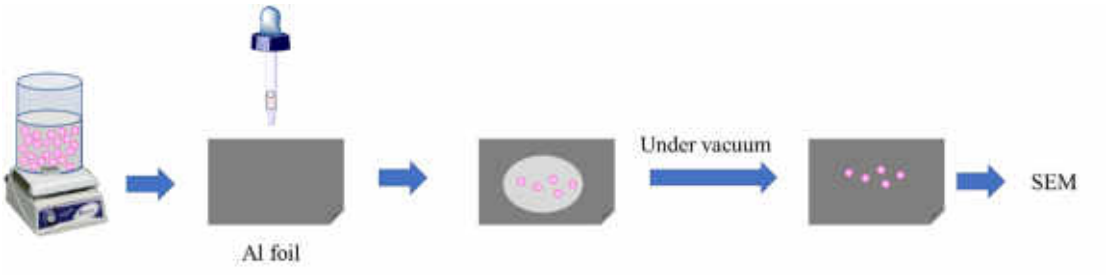


Fig.5-78 The process to prepare the sample for SEM characterisation

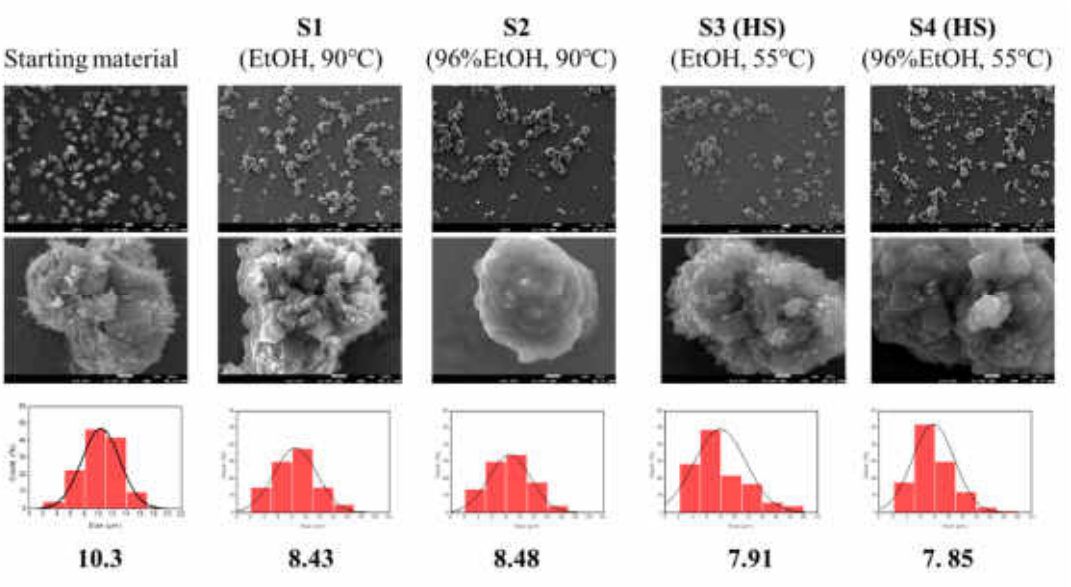


Fig.5-79 SEM image of samples **S1**, **S2**, **S3** and **S4.**

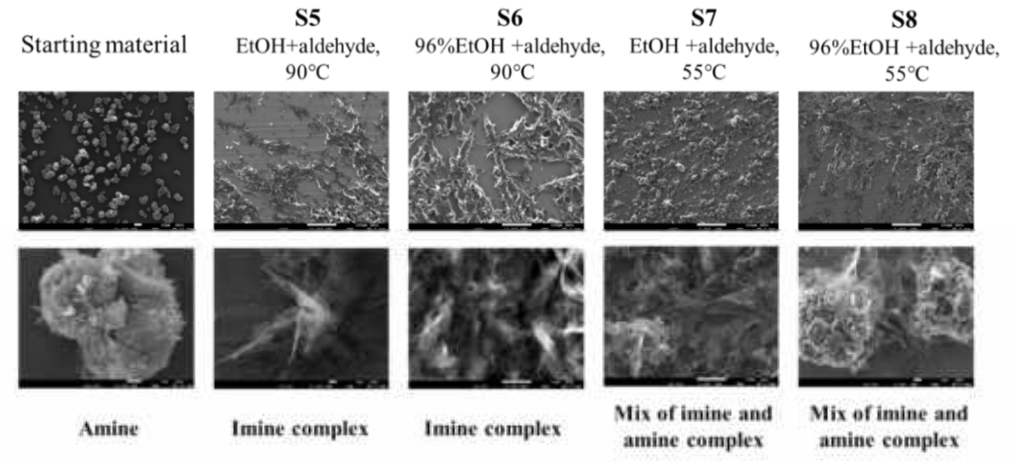


Fig.5-80 SEM image of samples **S5**, **S6**, **S7** and **S8**

First, we suspended complex **1** in pure absolute ethanol and 96% ethanol at 55°C and 90°C. As shown in Fig.5-79, the complex suspended in ethanol helped break down large aggregate particles, resulting in a decrease in particle size. Since ethanol can contain some water and water is formed during the catalytic reaction, we also investigated how 96% ethanol affected the shape of the complex particles. The presence of 96% ethanol drastically alters the particles' appearance. Compared to absolute ethanol, this is far more obvious. Interestingly, when the complex was suspended in 96% ethanol at 90°C, the smaller particles appeared to merge together (Fig.5-79, **S2**).

When complex **1** was suspended in ethanol and aldehyde at 55°C and 90°C, the imine complex was formed, leading to significant changes in the morphology of the complex (Fig.5-80). This observation is consistent with our previous study.[41]

Based on this study, it is clear that the solvent used in the reaction can affect the morphology of the complex, helping to separate large particle aggregates and reduce the size of the

aggregates. This reduction in size may facilitate the release of the complex from the composite film during the reaction.

5.7.5 Hydrolysis reaction of triethyl orthoformate

During the research in section 5.7.2, we observed that the film appeared to catalyze the hydrolysis of TEOF to produce ethylformate when the composite material was added to a mixture of ethanol, TEOF, and trace of water. This behavior could be useful for removing excess TEOF from the solution after the reaction and purifying the desired product. As an excess of TEOF used in the reaction, if the yield is 100%, the solution after the reaction contains acetal (product), TEOF, ethyl formate (side product) and EtOH, as shown in Fig.5-81. The boiling point of the side product ethyl formate is 54.5 ℃, which is easier to remove due to the lower boiling point compared to TEOF. Therefore, hydrolyzing TEOF to ethyl formate can aid in the purification of the acetal.

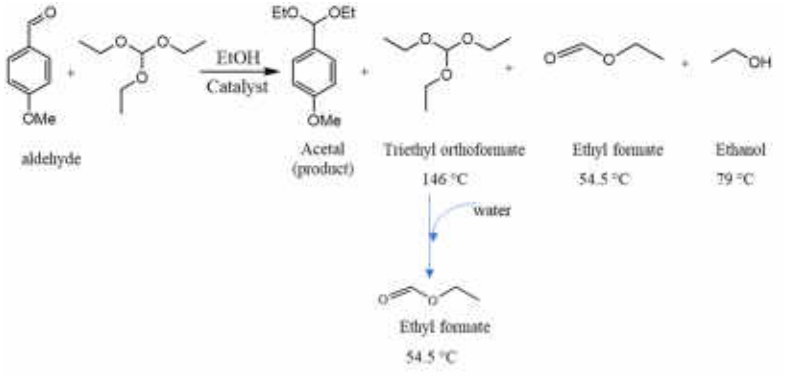


Fig.5-81 The compounds in the solution and their boiling point

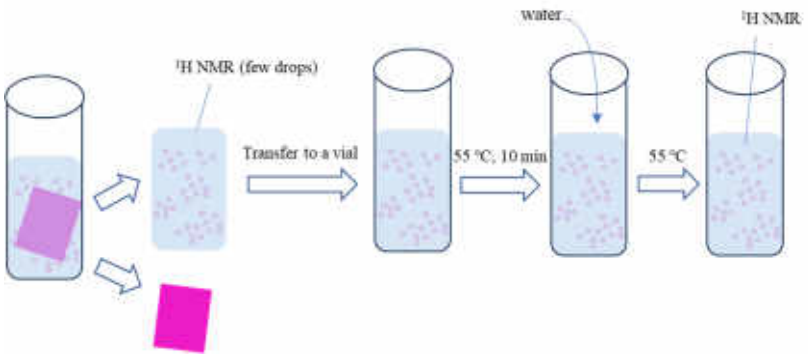


Fig.5-82 Scheme of the experiment process for hydrolysing the TEOF

Table 5-7 The yield and ratio before and after the reaction (without filtration)

Sample	Starting solution (Without filtration)		After adding water	
	Y	**R**	**Y***	**R***
1	100%	59%	17%	0%
2	100%	59%	19%	0%

$$Y = \frac{n_{acetal}}{n_{acetal}+n_{aldehyde}} \times 100\% \quad R = \frac{n_{TEOF\,(after\,reaction)}}{n_{TEOF\,(befor\,reaction)}} \times 100\%$$

Table 5-8 The yield and ratio before and after reaction (after filtration)

Sample	Starting solution (After filtration on celite)		After adding water	
	Y	**R**	**Y***	**R***
1	100%	64%	66%	38%
2	100%	64%	100%	64%

$$Y = \frac{n_{acetal}}{n_{acetal}+n_{aldehyde}} \times 100\% \quad R = \frac{n_{TEOF}}{n_{(TEOF+\text{ethyl formate})}} \times 100\%$$

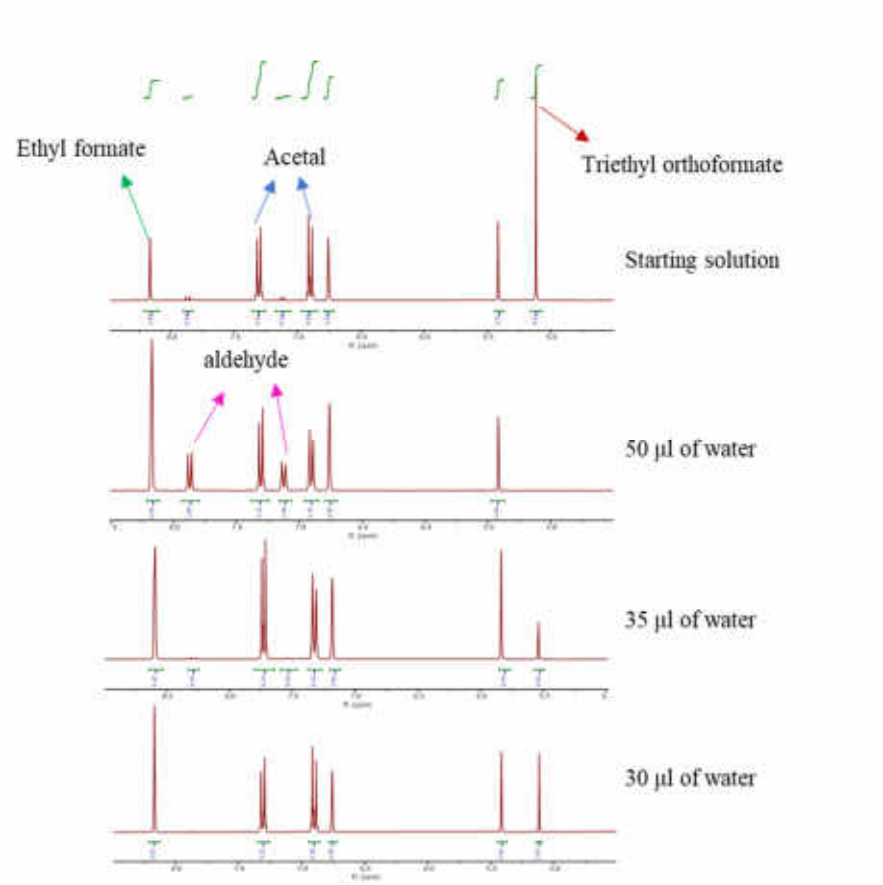


Fig.5-83 Represent NMR spectra before and after the reaction

First, we conducted a test to verify our hypothesis regarding the catalytic hydrolysis of TEOF to ethyl formate in the presence of a small amount of water. We prepared a vial under a 55°C oil bath containing a mixture of 3 mL EtOH and 600 µl TEOF. Then, 100 µl H2O was added, along with small pieces of the complex 1@TPU composite film. After 15 minutes of reaction time, the hydrolysis of TEOF was complete. In the blank test, only 3% of TEOF was hydrolyzed without the film. The hydrolysis of TEOF proceeded rapidly, with the reaction reaching completion in just 15 minutes. This suggests that the small amount of particles released from the film into the solution may be sufficient to catalyze the hydrolysis of TEOF. Based on the mechanism study, which showed that complexes are released from the film during the catalytic reaction, we hypothesize that these released complexes could be effectively utilized after acetalization by adding a small amount of water to remove excess TEOF. As shown in the figure, after the acetalization reaction, the composite film was removed, and a small amount of water was added to the vial. A few drops of this solution were then analyzed by NMR before

and after hydrolysis to monitor the reaction.

The main challenges in these experiments are determining the appropriate amount of water to add and optimizing the reaction time, as the amount of complex released from the composite film cannot be precisely controlled.

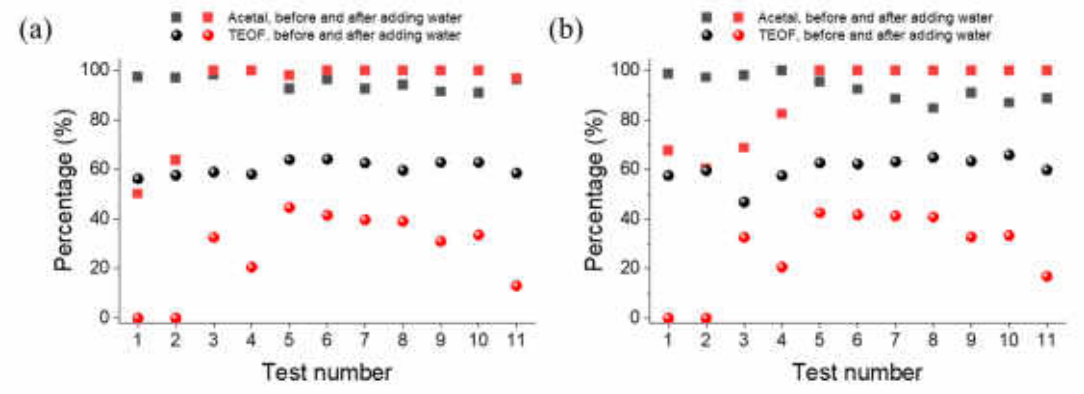


Fig.5-84 The percentage of remaining actal or TEOF before (black) and after (red) adding water. The starting solution from the experiment after remove composite film (a) **M2** and (b) **M3**.

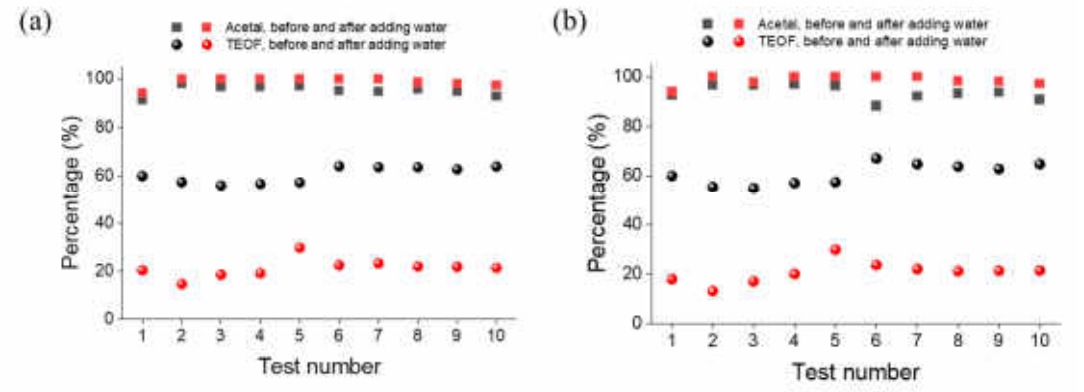


Fig.5-85 The percentage of remaining actal or TEOF before (black) and after (red) adding water. The starting solution from the experiment after remove composite film (a) **M4** and (b) **M5**.

We used the solution from the acetalization under batch conditions, and the composite films in both the HS and LS2 states achieved high acetal yields (>90%). To investigate the conditions for hydrolysing the TEOF, the solution obtained after acetalisation using the films **M1**, **M2**, **M3**, **M4**, and **M5** was utilised to study the hydrolysation of TEOF under serval conditions, as shown in Table 5-9, 0, Table 5-11, Table 5-12, Fig.5-84 and Fig.5-85. When the water added is too much (eg. 100 µl and 50 µl), all the TEOF was fully hydrolysed, and a part of acetal was also hydrolysed. The representative NMR spectra are shown in Fig.5-83. When the amount of water added was decreased to 30 µl, there was no observed hydrolysis of acetal, but the hydrolysis of TEOF was not complete. When 35 µl of water was added, a small amount of acetal was observed to be hydrolysed, but the hydrolysis of TEOF was still incomplete. So far, the best result has been achieved by adding 30 µl of water, which reduced the percentage of TEOS from approximately 68% to 20%.

The experimental results of hydrolysis using the solution from the composite film in the HS state were similar to those using the solution from the film in the LS2 state. Under these experimental conditions, the effect of the spin state on the hydrolysis of TEOF cannot be

accurately studied because the exact amount of complexes in solution is not known. Without having the same amount of complex in both HS and LS2 samples, it is impossible to make a reliable comparison between the results. In addition, it remains a challenge to determine the exact amount of water that should be added to hydrolyse TEOF without affecting the desired acetal product. However, these experiments have already demonstrated that TEOF can be hydrolysed by simply adding a small amount of water after the acetalisation reaction. As shown in Fig.5-85, the percentage of TEOF was reduced from around 60% to 20%, making it easier to purify the desired acetal product.

Table 5-9 The detailed information for hydrolysis of triethyl orthoformate. The starting solution from the experiment after remove composite film **M2** (this film was used in HS state).

Sample	Starting solution		H_2O (μl)	Reaction time (min)	After reaction	
	Y	R			Y*	R*
1	98%	59%	100	5	50%	0%
2	97%	58%	50	5	64%	0%
3	98%	61%	20	5	100%	37%
4	100%	59%	30	10	100%	21%
5	93%	65%	15	10	98%	45%
6	97%	64%	15	10	100%	43%
7	93%	62%	15	15	100%	41%
8	94%	60%	15	15	100%	41%
9	92%	63%	20	10	100%	32%
10	91%	62%	20	10	100%	35%
11	96%	62%	35	10	97%	14%

$$Y = \frac{n_{acetal}}{n_{acetal}+n_{aldehyde}} \times 100\% \quad R = \frac{n_{TEOF}}{n_{(TEOF+\text{ethyl formate})}} \times 100\%$$

Table 5-10 The details information for hydrolysis of triethyl orthoformate. The starting solution from the experiment after remove composites film **M3** (this film was used in LS2 state).

Sample	Starting solution		H_2O (μl)	Reaction time (min)	After reaction	
	Y	R			Y*	R*
1	99%	60%	100	5	68%	0%
2	97%	60%	50	5	60%	0%
3	98%	51%	20	5	69%	3%
4	100%	59%	30	10	83%	2%
5	96%	63%	15	10	100%	44%
6	92%	63%	15	10	100%	43%
7	89%	63%	15	15	100%	42%
8	85%	67%	15	15	100%	42%
9	91%	64%	20	10	100%	34%
10	87%	65%	20	10	100%	34%

11	89%	65%	35	10	100%	19%

$$Y = \frac{n_{acetal}}{n_{acetal}+n_{aldehyde}} \times 100\% \quad R = \frac{n_{TEOF}}{n_{(TEOF+\text{ethyl formate})}} \times 100\%$$

Table 5-11 The detailed information for hydrolysis of triethyl orthoformate. The starting solution from the experiment after remove composites film **M4** (this film was used in HS state).

Sample	**Starting solution**		**H_2O (μl)**	**Reaction time (**min**)**	**After reaction**	
	Y	**R**			**Y***	**R***
1	91%	64%	20	10	94%	22%
2	98%	61%	20	10	100%	17%
3	97%	60%	20	10	100%	20%
4	97%	61%	20	10	100%	21%
5	97%	61%	20	10	100%	32%
6	95%	66%	30	10	100%	24%
7	95%	65%	30	10	100%	25%
8	96%	65%	30	10	98%	23%
9	95%	65%	30	10	98%	24%
10	93%	65%	30	10	97%	23%

$$Y = \frac{n_{acetal}}{n_{acetal}+n_{aldehyde}} \times 100\% \quad R = \frac{n_{TEOF}}{n_{(TEOF+\text{ethyl formate})}} \times 100\%$$

Table 5-12 The detailed information for hydrolysis of triethyl orthoformate. The starting solution from the experiment after remove composites film **M5** (this film was used in LS2 state)..

Sample	**Starting solution**		**H_2O (μl)**	**Reaction time (**min**)**	**After reaction**	
	Y	**R**			**Y***	**R***
1	93%	65%	20	10	94%	20%
2	97%	61%	20	10	100%	15%
3	97%	61%	20	10	98%	19%
4	97%	61%	20	10	100%	23%
5	96%	62%	20	10	100%	33%
6	88%	68%	30	10	100%	25%
7	92%	67%	30	10	100%	24%
8	93%	65%	30	10	98%	23%
9	94%	65%	30	10	98%	24%
10	91%	66%	30	10	97%	23%

$$Y = \frac{n_{acetal}}{n_{acetal}+n_{aldehyde}} \times 100\% \quad R = \frac{n_{TEOF}}{n_{(TEOF+\text{ethyl formate})}} \times 100\%$$

5.8 Conclusion

This chapter presented a comprehensive study of spin crossover (SCO) polymer composite films used as catalysts in acetalization reactions. Various types of composite films, including monolayer, bilayer, and three-layer films, were fabricated using the blade-casting method. All of these films demonstrated high catalytic efficiency and remarkable reusability under both batch and continuous flow conditions, proving significantly more advantageous than traditional powdered catalysts. The composite films not only simplify the catalyst recovery process but also enhance the overall stability and longevity of the catalytic system.

The composite films in the high spin state consistently showed higher catalytic yields than those in the low spin state, with the differences becoming more pronounced over successive reaction cycles. In addition, the colour change of the monolayer films served as a useful indicator of catalytic activity. For example, after nine cycles of use, the film showed a slight pink colour, indicating that it could still be used as an effective catalyst for further reactions. This visual feedback provides a practical method of monitoring catalyst performance over time.

The bilayer composite films further demonstrated their versatility by exhibiting self-rolling behaviour in the presence of EtOH. This self-rolling property highlights the potential application of these materials not only in reusable catalysis but also in switchable catalysis, where external stimuli can modulate catalytic reactivity. The synergy between catalytic performance and mechanical movement in the bilayer films need to be further investigated. In addition, the three-layer films, incorporating two protective outer layers around the catalytic layer, exhibited greater robustness compared to the monolayer films, offering enhanced durability and improved catalytic performance.

The catalytic mechanism of the SCO composite films was studied in detail using monolayer films. According to the results of optical reflectivity, infrared spectroscopy (IR), X-ray diffraction (XRD), and scanning electron microscopy (SEM), some leaching of the SCO complex into the reaction solution was observed during the catalytic reaction. The formation of pores and voids within the polymer matrix, particularly after extended use. Moreover, the catalytic reaction mostly takes place inside the film but also happens somewhat in the solution. In conclusion, the composite films not only simplify catalyst recovery but also improve the stability and longevity of the catalytic system, making them highly promising for reusable and switchable catalysis systems.

5.9 Experiment section

5.9.1 The general procedure of testing the composite film in the batch condition

The general procedure began with the preparation of the reaction mixture, consisting of 0.83 mol/L of *p*-anisaldehyde, 2.31 mol/L of triethyl orthoformate (TEOF), and 0.33 mol/L of 1,3,5-trimethoxybenzene (TMB) in ethanol. This solution was pre-heated prior to the experiment. A composite film was placed in a small vial containing 2 mL of absolute ethanol, which was then immersed in a 90 °C preheated oil bath for 2 minutes to prepare the film in its high-spin (HS) state (the procedure for LS2 and LS samples are shown in the Fig.5-86). After heating at 90 °C, the vial was immediately transferred to a 55 °C preheated oil bath and stabilized for 10 minutes.

Subsequently, 2.16 mL of the pre-prepared reaction mixture was added to the vial to initiate the reaction. After 15 minutes, the reaction mixture was analyzed using ^{1}H-NMR spectroscopy to determine the product yield. The composite film was then removed from the solution, washed with ethanol, dried, and reused for subsequent catalytic cycle

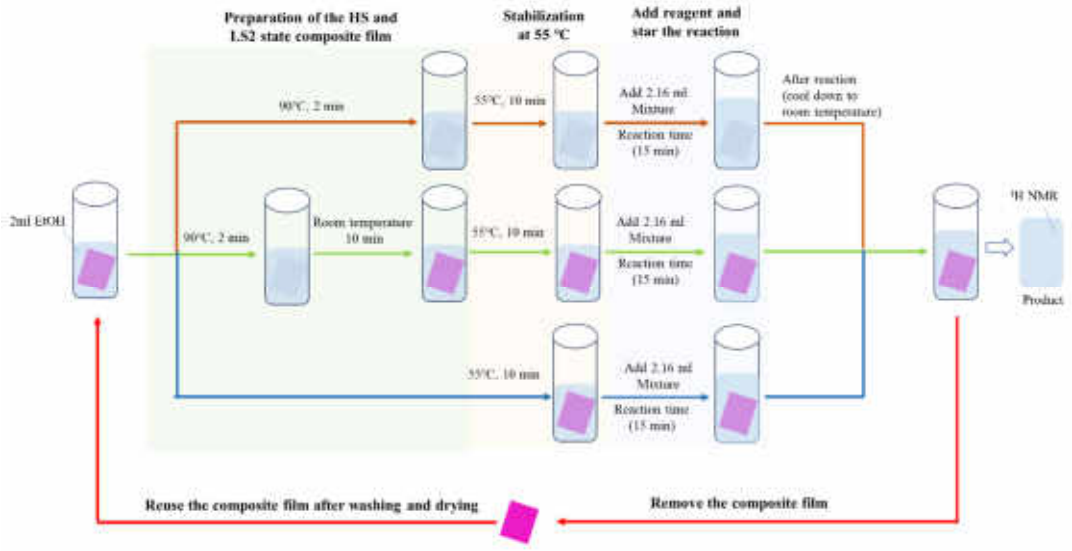


Fig.5-86 The general procedure of testing the composite film in the batch condition

5.9.2 The general procedure of testing the composite film in the H tube system

If the composite film is used in its HS state, first place the composite film on the right side of the H tube and add 2 mL of EtOH. Then, put the H tube in a 90 ℃ preheated oil bath for 2 min. The colour of the film changes from pink to white. After 2 min, transfer the H tube to another 55℃ preheated oil bath and wait for 10 minutes, and then add 2 ml of the mixture and connect to the minipump. The solution level is approximately reached by the bridge of the H tube. After 15 min, turn on the mini pump, and the mixture will be added automatically, and the solution will flow to the left side of the H tube (collect side). Every 15 minutes, the solutions on the collection side will be removed, and the yield will be measured using ^{1}H NMR.

If the composite film is used in its LS2 state, first place the composite film on the right side of the H tube and add 2 mL of EtOH. Then, put the H tube in a 90 ℃ preheated oil bath for 2 min. The colour of the film changes from pink to white. After 2 min, remove the H tube from the oil bath and let it in room temperature for 5 min, the coulour of the film change from whit to pink. Then, put the H tube into a preheated 55 ℃ oil bath. The rest procuduces are the same as above.

If the composite film is used in its LS state, first place the composite film on the right side of the H tube and add 2 mL of EtOH. Then, put the H tube into a preheated 55 ℃ oil bath. The rest procuduces are the same as above.

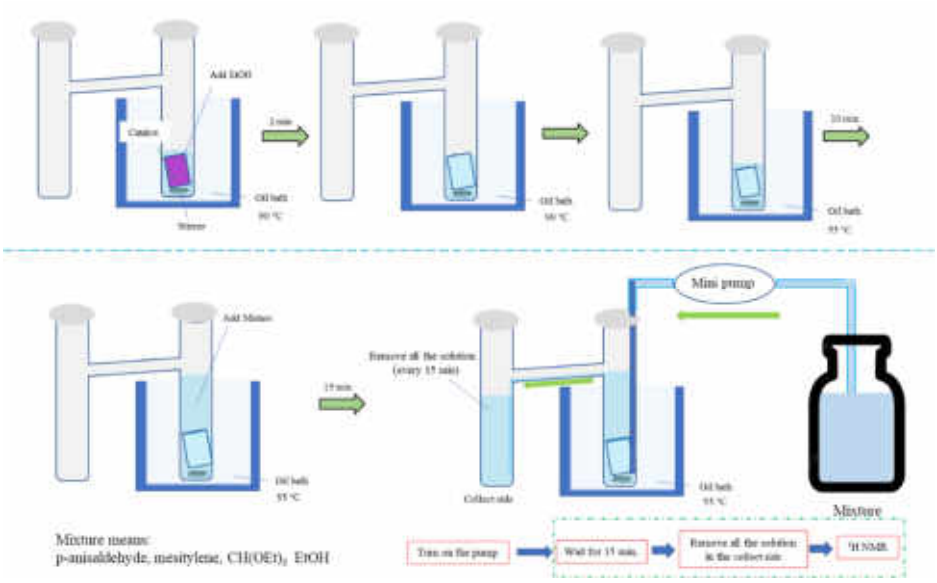


Fig.5-87 (a) The working system uses an H tube and a mini pump to add the reagent. The film used in HS state as an example.

5.10 References

[1] C. Vogt, B.M. Weckhuysen, The concept of active site in heterogeneous catalysis, *Nature Reviews Chemistry* **2022**, 6, 89-111.

[2] W. Guo, Z. Wang, X. Wang, Y. Wu, General design concept for single-atom catalysts toward heterogeneous catalysis, *Adv. Mater.* **2021**, 33, 2004287.

[3] A. Bavykina, N. Kolobov, I.S. Khan, J.A. Bau, A. Ramirez, J. Gascon, Metal–organic frameworks in heterogeneous catalysis: recent progress, new trends, and future perspectives, *Chem. Rev.* **2020**, 120, 8468-8535.

[4] J. Pérez-Ramírez, C.H. Christensen, K. Egeblad, C.H. Christensen, J.C. Groen, Hierarchical zeolites: enhanced utilisation of microporous crystals in catalysis by advances in materials design, *Chem. Soc. Rev.* **2008**, 37, 2530-2542.

[5] I. Vassalini, I. Alessandri, Switchable stimuli-responsive heterogeneous catalysis, *Catalysts* **2018**, 8, 569.

[6] A. Ghorbani-Choghamarani, Z. Taherinia, Recent advances utilized in artificial switchable catalysis, *RSC advances* **2022**, 12, 23595-23617.

[7] N. Das, C. Maity, Switchable aqueous catalytic systems for organic transformations, *Communications Chemistry* **2022**, 5, 115.

[8] G.C. Thaggard, J. Haimerl, R.A. Fischer, K.C. Park, N.B. Shustova, Traffic lights for catalysis: Stimuli - responsive molecular and extended catalytic systems, *Angewandte Chemie International Edition* **2023**, 62, e202302859.

[9] L. Pu, W. Wei, M. Zhu, S. Wu, X. Shen, S. Li, Artificial Reactor with Alterable Tandem Channeling for the Formation of Self-Screened Catalytic Ability, *Chem. Eng. Technol.* **2020**, 43, 317-328.

[10] J. Bacharouche, F. Badique, A. Fahs, M.V. Spanedda, A. Geissler, J.-P. Malval, M.-F. Vallat, K. Anselme, G. Francius, B. Frisch, Biomimetic cryptic site surfaces for reversible chemo-and cyto-mechanoresponsive substrates, *ACS Nano* **2013**, 7, 3457-3465.

[11] L. Zhang, Z. Liu, L.-Y. Liu, J.-L. Pan, F. Luo, C. Yang, R. Xie, X.-J. Ju, W. Wang, L.-Y. Chu, Nanostructured thermoresponsive surfaces engineered via stable immobilization of smart nanogels with assistance of polydopamine, *ACS Appl. Mater. Interfaces* **2018**, 10, 44092-44101.

[12] X. He, M. Aizenberg, O. Kuksenok, L.D. Zarzar, A. Shastri, A.C. Balazs, J. Aizenberg, Synthetic homeostatic materials with chemo-mechano-chemical self-regulation, *Nature* **2012**,

487, 214-218.
[13] T. Mazur, S. Lach, B.A. Grzybowski, Heterogeneous Catalysis “On Demand”: Mechanically Controlled Catalytic Activity of a Metal Surface, *ACS Appl. Mater. Interfaces* **2017**, 9, 44264-44269.
[14] M. Piedrahita-Bello, J.E. Angulo-Cervera, A. Enriquez-Cabrera, G. Molnár, B. Tondu, L. Salmon, A. Bousseksou, Colossal expansion and fast motion in spin-crossover@ polymer actuators, *Materials Horizons* **2021**, 8, 3055-3062.
[15] M. Piedrahita-Bello, X. Yang, S.E. Alavi, G. Molnár, L. Salmon, A. Bousseksou, Anisotropic spin-crossover composite actuators displaying pre-programmed movements, *Sensors and Actuators B: Chemical* **2023**, 393, 134147.
[16] Y. Zan, M. Piedrahita-Bello, S.E. Alavi, G. Molnár, B. Tondu, L. Salmon, A. Bousseksou, Soft Actuators Based on Spin - Crossover Particles Embedded in Thermoplastic Polyurethane, *Advanced Intelligent Systems* **2023**, 5, 2200432.
[17] G. Molnár, S. Rat, L. Salmon, W. Nicolazzi, A. Bousseksou, Spin crossover nanomaterials: from fundamental concepts to devices, *Adv. Mater.* **2018**, 30, 1703862.
[18] A. Bousseksou, G. Molnár, L. Salmon, W. Nicolazzi, Molecular spin crossover phenomenon: recent achievements and prospects, *Chem. Soc. Rev.* **2011**, 40, 3313-3335.
[19] Á. Molnár, A. Papp, Catalyst recycling—A survey of recent progress and current status, *Coord. Chem. Rev.* **2017**, 349, 1-65.
[20] E. Hariprasad, T. Radhakrishnan, A highly efficient and extensively reusable “dip catalyst” based on a silver-nanoparticle-embedded polymer thin film, *Chemistry–A European Journal* **2010**, 16, 14378-14384.
[21] D. Paliwoda, L. Vendier, L. Getzner, F. Alabarse, D. Comboni, B. Martin, S.E. Alavi, M.P. Bello, L. Salmon, W. Nicolazzi, Elastic Properties of the Iron (II)–Triazole Spin Crossover Complexes [Fe (Htrz) 2trz] BF4 and [Fe (NH2trz) 3] SO4, *Cryst. Growth Des.* **2023**, 23, 1903-1914.
[22] A. Grosjean, P. Négrier, P. Bordet, C. Etrillard, D. Mondieig, S. Pechev, E. Lebraud, J.F. Létard, P. Guionneau, Crystal structures and spin crossover in the polymeric material [Fe (htrz) 2 (trz)](BF4) including coherent-domain size reduction effects, *Eur. J. Inorg. Chem.* **2013**, 2013, 796-802.
[23] A. Grosjean, N. Daro, S. Pechev, C. Etrillard, G. Chastanet, P. Guionneau, Crystallinity and microstructural versatility in the spin-crossover polymeric material [Fe (Htrz) 2 (trz)](BF4), *Eur. J. Inorg. Chem.* **2018**, 2018, 429-434.
[24] A. Grosjean, N. Daro, S. Pechev, L. Moulet, C. Etrillard, G. Chastanet, P. Guionneau, The spin-crossover phenomenon at the coherent-domains scale in 1D polymeric powders: evidence for structural fatigability, *Eur. J. Inorg. Chem.* **2016**, 2016, 1961-1966.
[25] A. Grosjean, Matériaux polymériques 1D à transition de spin: investigations structurales multi-échelles, Université de Bordeaux 1, 2013.
[26] L. Lin, H. Quoc Pho, L. Zong, S. Li, N. Pourali, E. Rebrov, N. Nghiep Tran, K. Ostrikov, V. Hessel, Microfluidic plasmas: Novel technique for chemistry and chemical engineering, *Chem. Eng. J.* **2021**, 417, 129355.
[27] J. Datta, P. Kasprzyk, Thermoplastic polyurethanes derived from petrochemical or renewable resources: A comprehensive review, *Polym. Eng. Sci.* **2017**, 58.
[28] M. Fuensanta, J.M. Martín-Martínez, Structural and Viscoelastic Properties of Thermoplastic Polyurethanes Containing Mixed Soft Segments with Potential Application as Pressure Sensitive Adhesives, *Polymers* **2021**, 13, 3097.
[29] A. Enriquez-Cabrera, X. Yang, S.E. Alavi, L. Salmon, A. Bousseksou, Self-Healing Composite Polymers Based on Spin Crossover Materials for Multidirectional Preprogrammed Actuation, *ACS Applied Polymer Materials* **2024**, 6, 9364-9374.
[30] M. Piedrahita-Bello, Y. Zan, A. Enriquez-Cabrera, G. Molnár, B. Tondu, L. Salmon, A. Bousseksou, Effect of the spin crossover filler concentration on the performance of composite bilayer actuators, *Chem. Phys. Lett.* **2022**, 793, 139438.
[31] B. Tondu, M. Piedrahita-Bello, L. Salmon, G. Molnár, A. Bousseksou, Robust linear control of

a bending molecular artificial muscle based on spin crossover molecules, *Sensors and Actuators A: Physical* **2022**, 335, 113359.
[32] G. Stoychev, S. Zakharchenko, S. Turcaud, J.W. Dunlop, L. Ionov, Shape-programmed folding of stimuli-responsive polymer bilayers, *ACS Nano* **2012**, 6, 3925-3934.
[33] L. Ionov, Soft microorigami: self-folding polymer films, *Soft Matter* **2011**, 7, 6786-6791.
[34] V. Luchnikov, L. lonov, M. Stamm, Self‐rolled polymer tubes: Novel tools for microfluidics, microbiology, and drug‐delivery systems, *Macromol. Rapid Commun.* **2011**, 32, 1943-1952.
[35] S. Seethapathy, T. Gorecki, Applications of polydimethylsiloxane in analytical chemistry: A review, *Anal. Chim. Acta* **2012**, 750, 48-62.
[36] D. Zhu, S. Handschuh-Wang, X. Zhou, Recent progress in fabrication and application of polydimethylsiloxane sponges, *Journal of Materials Chemistry A* **2017**, 5, 16467-16497.
[37] A. Victor, J. Ribeiro, F.F. Araújo, Study of PDMS characterization and its applications in biomedicine: A review, *Journal of Mechanical Engineering and Biomechanics* **2019**, 4, 1-9.
[38] J.N. Lee, C. Park, G.M. Whitesides, Solvent compatibility of poly (dimethylsiloxane)-based microfluidic devices, *Anal. Chem.* **2003**, 75, 6544-6554.
[39] K. Ren, Y. Zhao, J. Su, D. Ryan, H. Wu, Convenient method for modifying poly (dimethylsiloxane) to be airtight and resistive against absorption of small molecules, *Anal. Chem.* **2010**, 82, 5965-5971.
[40] D.K. Singh, M. Pradhan, A. Materny, Modern Techniques of Spectroscopy, Springer2021.
[41] A. Enriquez-Cabrera, L. Getzner, L. Salmon, L. Routaboul, A. Bousseksou, Post-synthetic modification mechanism for 1D spin crossover coordination polymers, *New J. Chem.* **2022**, 46, 22004-22012.

General conclusions and perspectives

The impact of spin-state on chemical reactivity plays a crucial role in inorganic and organometallic chemistry, especially in reactions involving transition metal complexes, which can affect reaction pathways, activation energies, and selectivity. Despite the significance of these effects, very few studies have directly examined the reactivity of spin crossover (SCO) complexes. Exploring the reactivity of these SCO complexes could be promising in the development of switchable catalysis systems. Understanding how spin states affect the reactivity of spin crossover complexes and taking advantage of their unique properties in switchable catalysis were the goals of this thesis. We believed that the 1D iron(II)-triazole coordination polymer with formula $Fe(NH_2trz)_3(NO_3)_2$ (Complex **1**), was the most appropriate candidate for this investigation. This SCO complex has several benefits: 1) It exhibits a very large thermal hysteresis loop and abrupt spin transitions above room temperature; 2) It maintains its excellent SCO properties when suspended in organic solvents; and 3) Despite being a solid compound that is insoluble in solvents, it has been demonstrated to be reactive under appropriate conditions.

First, we wanted to know why a post-synthetic modification (PSM) on complex **1** was drastically more effective when the temperature was raised from 35°C to 90°C. This observation grabbed our interest since we anticipated that the iron spin state would have some role in this increase. Separating the effect of the spin state from other parameters that could explain an increase in reaction efficiency is a real challenge. We have succeeded in doing this by taking advantage of the excellent SCO properties of complex **1**, and more particularly its large thermal hysteresis loop above room temperature. We conducted 44 pairs of trials for this study, one of which included an experiment with the complex in the LS state and another with the complex in the HS state, both conducted under precisely the same experimental conditions. In these 44 pairs of experiments, which were conducted on 5 distinct batches of complex **1**, it was consistently found that the percentage of the PSM reaction was considerably higher (up to 22%) when complex **1** was used in the HS state as opposed to the LS state. Furthermore, we confirmed the precision and accuracy of the employed analytical technique. Even with an 8% variance in PSM reactions, the enormous number of trials conducted and the estimated error of the digesting method (±2%) demonstrate the significant difference in reactivity between the two spin states. On average, 1.37 times more imine is formed when complex **1** is in the HS state than in the LS2 state. Notably, this is the first reported case where the spin state influences the organic reactivity of a functional group within a metal complex. Remarkably, the spin state appears only to affect the kinetics of desired product formation, as complex **2** obtained at 35°C exhibits identical structural characteristics and SCO properties to that obtained at 90°C.

We initially connected the work in Chapter 2 to these findings because we wanted to conduct this investigation in order to gather further evidence supporting the formation of imine functionalities on the complex through a solid-state PSM reaction. If we have obtained this additional argument, serendipity finally led to one of the study's most significant findings. In fact, we discovered that by merely adding aminotriazole to the reaction, we may shift from a quantitative PSM reaction on complex **1** with an aldehyde to an effective utilization of this complex as a catalyst for the synthesis of imines under the right circumstances. Experimental studies of the catalytic reaction revealed that when amine complex **1** was pre-treated with *p*-anisaldehyde (heating to 90°C under microwave irradiation), the catalytic reaction was quantitative in less than 10 minutes, with the amount of iron complex equivalent to 2.3% molar relative to aminotriazole. Analysis of the iron complex recovered after the catalytic reaction provided several key insights. First, when amine complex **1** was used without pre-treatment, and the catalytic reaction was complete with no remaining aminotriazole in solution, the

recovered complex corresponded to amine complex **1** with traces of imine functions. Furthermore, as expected, pre-treatment of the amine complex with aldehyde led to the formation of imine complex **2** via PSM reaction. Interestingly, when amine complex **1** was pre-treated or imine complex **2** was used as a catalyst, the percentage of imine functions on the complex remained below 15% from the first minute until the catalytic reaction was complete. Two potential pathways for this PSM reaction, which proceeds from the imine complex **2** to the amine complex **1**, have been suggested by us. Experiments using aminotriazole with ^{15}N-labeled suggest that the PSM reaction proceeds predominantly via ligand exchange. Moreover, and. the result of scanning electron microscopy (SEM), X-ray diffraction (XRD), infrared spectroscopy (IR), and optical reflectivity measurements revealed that while the complexes recovered before the catalytic reaction was complete exhibited molecular arrangement and spin-crossover properties similar to the starting amine complex **1**, the particles from the pre-treated amine complex or the imine complex were significantly different in size and shape from the original amine complex. Additionally, the conditions under which the PSM reaction of amine complex **1** with aldehyde was carried out had a significant effect on the morphology of the resulting imine complex **2** particles. Thus, performing a PSM reaction with an aldehyde followed by a PSM reaction with aminotriazole on imine complex **2** enables the particle morphology of amine complex **1** to be modified without compromising its SCO properties. This finding is relevant not only for heterogeneous catalysis, where particle size and shape influence catalytic activity, but also for the integration of SCO compounds into devices. In addition, the catalytic activity of the iron(III) imine complex was found to be comparable to that of the iron(II) imine complex. This is surprising, as iron(III) complexes are generally stronger Lewis acids than their iron(II) counterparts, and imine formation from aldehydes is typically catalyzed efficiently by Lewis acids. However, based on our results, we are confident that the iron(II) complex remains in this oxidation state during the catalytic reaction. Therefore, we conclude that the reaction mechanism is unlikely to be of the Lewis acid type and instead may involve PSM reactions. This research, combined with our recent findings on the strong influence of spin state on the efficiency of the PSM method in this iron complex, suggests that spin-crossover complexes could be promising candidates for the development of switchable catalysis.

As discussed above, we have demonstrated that the 1D polymeric iron-triazole complex can be used as a catalyst in chemical reactions. In the following study, we aimed to determine whether the spin state of the iron in the SCO coordination polymer could modulate its catalytic activity. To investigate this, we chose the acetalisation of *p*-anisaldehyde in ethanol with triethyl orthoformate as a model reaction. We then investigated the effect of the spin state of complex **1** on its catalytic reactivity in this reaction. Under identical experimental conditions, the reaction using the complex in the HS state produced up to 27% more acetal compared to the complex in the LS2 state. Over a hundred sets of experiments were conducted, and seven different batches of Complex **1** were evaluated, ensuring the reproducibility and representativeness of the results. Additionally, we discovered that a tiny amount of water added at the ideal moment greatly sped up the reaction. When the complex was in the HS state, this acceleration was more noticeable, which increased the yield gap between the LS2 and HS states. Interestingly, while using 3.68% mass of complex **1** relative to the aldehyde was not ideal for modulating catalytic activity by spin state, the most significant differences between the HS and LS2 states were observed at a mass percentage of 0.61%. This discovery emphasizes an important principle in heterogeneous catalysis: better outcomes are not necessarily achieved by using more catalysts. Three potential catalytic mechanisms for complex **1** were examined: one involved PSM reactions and the other two involved the Lewis acidity of the iron atoms or the creation of hydrogen bonds between the complex and the aldehyde. Based on the experimental results, we were able to rule out the PSM mechanism and determine that the Lewis acid mechanism was the most likely. To figure out how the spin state affects catalytic efficiency, we

compared the activation energies of the acetalization reactions catalyzed by different spin states of complex **1**. The activation energy of the reaction catalyzed by the complex in the LS state was 90 kJ mol^{-1}, while in the HS state, the activation energy was 100 kJ mol^{-1}. Given that these values are similar, it is likely that the variation in catalytic activity results from easier access to catalytic active sites in the HS state rather than from electronic factors stabilizing the transition state. Overall, this study demonstrates that the spin state of iron can modulate the catalytic activity of the SCO coordination polymer, highlighting the potential of SCO complexes in developing switchable catalysis systems.

Despite having strong catalytic activity, the powdered SCO complex **1** is difficult to recycle. For example, while the powdered form of the SCO complex allows catalyst recovery by methods such as filtration or centrifugation, these processes are often time-consuming and prone to catalyst loss, reducing overall efficiency. In recent years, polymer composite films have emerged as a promising solution to improve catalyst recovery and reusability, making them more suitable for industrial applications, particularly in continuous processes where reusability is critical. In addition, SCO@polymer composite films have shown significant potential in mechanical actuators. The spin transition of the iron complex guarantees the material's controlled motion. Indeed, the spin transition for certain SCO complexes is accompanied by an important change in the volume of material. In this context, we decided to integrate these SCO complexes into polymer matrices to fabricate composite films and use them in catalytic systems. The formation of these composite materials should therefore enable us to recycle the catalyst more easily while offering a fascinating opportunity to investigate a possible synergy between the motion of composite material and its catalytic activity. We hypothesised that the shape of the composite material would also influence access to the catalyst. The movement imposed by the spin transition can modulate the shape of the material. So this motion could allow us to increase the difference in yields between the acetalisation reactions catalysed by the different spin states of complex **1**. Subsequently, we present a detailed study of spin crossover polymer composite films used as catalysts in acetalisation reactions. Different types of films, including monolayer, bilayer and three-layer films, were prepared using the blade casting method. These films exhibited high catalytic efficiency and excellent reusability under both batch and continuous flow conditions, offering advantages over conventional powder catalysts. The films in the high spin state consistently exhibited slightly higher catalytic yields than those in the low spin state, with the differences becoming more pronounced over successive reaction cycles. The bilayer composite films further demonstrated their versatility by exhibiting self-rolling behaviour in the presence of EtOH. This self-rolling property highlights the potential application of these materials not only in reusable catalysis but also in switchable catalysis, where external stimuli can modulate catalytic reactivity. In addition, the three-layer films, incorporating two protective outer layers around the catalytic layer, exhibited greater robustness compared to the monolayer films, offering enhanced durability and improved catalytic performance. Furthermore, we investigated the evolution of the composite film after its use in catalytic reactions, with a particular focus on the properties and morphology of the spin-crossover particles within the film. For this study, we selected the monolayer film and analyzed its characteristics using optical reflectivity, infrared spectroscopy (IR), X-ray diffraction (XRD), and scanning electron microscopy (SEM). These analyses revealed the dispersion of the SCO complex within the polymer matrix, along with some leaching of the SCO complex into the reaction solution during the catalytic process. Additionally, the formation of pores and voids within the polymer matrix was observed, particularly after extended use. Overall, the composite films not only facilitate catalyst recovery but also enhance the stability and longevity of the catalytic system, making them highly promising for reusable and switchable catalytic applications.

In summary, this thesis focuses on 1D polymeric iron(II)-triazole spin crossover (SCO) complexes with the aim of understanding the effect of spin states on reactivity and exploring their potential for use in switchable catalytic systems. Firstly, we demonstrated the effect of spin states on the efficiency of post-synthetic modification reactions in a SCO complex. Following this work, we found that the spin crossover complex could act as a catalyst in organic reactions under appropriate conditions. In addition, we demonstrated that the spin state can modulate the catalytic activity of the SCO complex using acetalisation as a model reaction. Finally, we successfully fabricated spin-crossover polymer composite films that exhibited excellent catalytic performance. The results of this thesis indicate that SCO complexes can be effectively used in catalytic systems, with the spin state playing a crucial role in modulating the catalytic activity, highlighting their potential for the development of switchable catalytic systems based on the SCO phenomenon. To further develop switchable catalytic systems using spin crossover complexes, future work would focus on improving the catalytic system, exploring the synergy between catalytic performance and mechanical motion in bilayer films, and investigating the use of these SCO complexes in a variety of catalytic reactions.

Abstracts in English and French

Title: Switchable catalysis using spin crossover complexes

Keywords: spin crossover complexes, spin state effect, post-synthetic modification, (switchable) catalysis, composite film

Abstract: This thesis discusses the influence of the spin state of iron on the chemical reactivity and catalytic capabilities of spin crossover (SCO) 1D iron(II)-triazole coordination polymers. Our long-term objective is to fully explore the potential of SCO complexes in the field of switchable catalysis. We first studied the impact of spin states on the efficiency of the post-synthetic modification (PSM) reaction on the complex of formula $[Fe(NH_2trz)_3](NO_3)_2$ (Complex **1**). It should be noted that a considerable 22% improvement in PSM efficiency was observed when complex **1** was in its high spin (HS) state compared to its low spin (LS) state. To the best of our knowledge, this is the first example of the influence of the metal spin state on the organic reactivity of a functional group within a metal complex. Secondly, we have demonstrated that, under appropriate conditions, a simple addition of aminotriazole to the reaction medium allows us to switch from a quantitative PSM reaction on complex **1** with an aldehyde to the use of the SCO complex as a catalyst for the formation of imines from aminotriazole. Analysis of the complexes recovered after catalysis enabled us to envisage that PSM reactions might be involved in the catalytic mechanism of this SCO complex. While this is the second example of the catalytic use of a 1D iron(II)-triazole coordination polymer, it is the first example in which the active species is actually the SCO complex. We also studied the influence of the spin state on the catalytic activity of complex **1** in the acetalisation of *p*-anisaldehyde in the presence of triethyl orthoformate. Under strictly identical experimental conditions, the reaction carried out in the presence of the HS complex yielded up to 27% more acetal than when the reaction was carried out with the LS complex. This means that the HS complex is much more effective at catalysing the acetalisation reaction than the LS complex. The wide number of comparative tests carried out means that we can be confident about the generality and reproducibility of these results. Studies carried out to understand the origin of the spin state effect on the catalytic activity of the SCO complex suggest that the observed difference in activity is due to a change in substrate access to the catalytic site. Finally, we fabricated SCO polymer composite films. These were used as catalysts in acetalisation reactions. The composite films demonstrated high catalytic efficiency and excellent reusability under batch and continuous flow conditions. These composite films not only simplify catalyst recycling, but also improve the stability and longevity of the catalytic system. This thesis highlights the influence of the metal spin state on the organic reactivity of SCO complexes and demonstrates the potential of this family of complexes for the development of switchable catalytic systems.

Titre: Catalyse commutable utilisant des complexes à transition de spin

Mots-clés : complexes à transition de spin, effet de l'état de spin, modification post-synthétique, catalyse (commutable), film composite

Résumé : Cette thèse discute de l'influence de l'état de spin du fer sur la réactivité chimique ainsi que sur les capacités catalytiques des polymères de coordination 1D de fer(II)-triazole à transition de spin (TS). Notre objectif à long terme est d'explorer pleinement le potentiel des complexes à transition de spin dans le domaine de la catalyse commutable. Nous avons, tout d'abord, étudié l'impact de l'état de spin du fer sur l'efficacité de la réaction de modification post-synthétique (PSM) sur le complexe de formule $[Fe(NH_2trz)_3](NO_3)_2$ (Complexe **1**). Il convient de noter qu'une amélioration considérable de 22% de l'efficacité de la PSM a été observée lorsque le complexe **1** était à l'état haut spin (HS) par rapport à son état bas spin (BS). A notre connaissance, il s'agit du premier exemple de l'influence de l'état de spin du métal sur la réactivité organique d'un groupement fonctionnel au sein d'un complexe métallique. Ensuite, nous avons démontré que, dans des conditions appropriées, un simple ajout d'aminotriazole dans le milieu réactionnel permet de passer d'une réaction PSM quantitative sur le complexe **1** avec un aldéhyde à l'utilisation du complexe à TS comme catalyseur pour la formation d'imines à partir d'aminotriazole. L'analyse des complexes récupérés après catalyse nous a permis d'envisager que des réactions PSM puissent intervenir dans le mécanisme catalytique de ce complexe à TS. Si c'est le deuxième exemple d'utilisation, en catalyse, d'un polymère de coordination 1D de fer(II)-triazole, c'est le premier exemple dans lequel l'espèce active est réellement le complexe à TS. Nous avons aussi étudié l'influence de l'état de spin sur l'activité catalytique du complexe **1** dans l'acétalisation du *p*-anisaldéhyde en présence de triéthyle orthoformate. Dans des conditions expérimentales strictement identiques, la réaction réalisée en présence du complexe à l'état HS permet d'obtenir jusqu'à 27 % d'acétal en plus que lorsque la réaction est réalisée avec le complexe à l'état BS. Ainsi le complexe à l'état HS est bien plus efficace pour catalyser la réaction d'acétalisation que le complexe à l'état BS. Le nombre important de tests comparatifs réalisés permet d'être confiant sur la généralité et la reproductibilité de ces résultats. Les études réalisées pour comprendre l'origine de l'effet de l'état de spin sur l'activité catalytique du complexe à TS semblent indiquer que la différence d'activité observée serait due à une modification d'accès des substrats au site catalytique. Enfin, nous avons fabriqué des films composites polymères à TS. Ces derniers ont été utilisés comme catalyseurs dans des réactions d'acétalisation. Les films composites ont fait preuve d'une grande efficacité catalytique et d'une excellente réutilisation dans des conditions de flux discontinu et continu. Ces films composites simplifient non seulement le recyclage du catalyseur, mais améliorent également la stabilité et la longévité du système catalytique. Cette thèse met en lumière, l'influence de l'état de spin du métal sur la réactivité organique des complexes à TS et démontre le potentiel de cette famille de complexes pour le développement de systèmes catalytiques commutables.

Résumé de la thèse en français

Catalyse commutable utilisant des complexes à transition de spin

Les travaux de recherches effectués lors de ma thèse avaient pour objectif principal d'étudier l'effet de l'état de spin du fer sur la réactivité chimique d'un complexe à transition de spin. Après une introduction bibliographique sur les complexes à transition de spin ainsi que sur l'effet de l'état de spin du métal sur les capacités catalytiques de complexes organométalliques, les résultats clés acquis au cours de ma thèse sont présentés. Le chapitre 2 résume l'étude réalisée afin de déterminer l'effet de l'état de spin du fer sur l'efficacité d'une réaction de modification post-synthétique sur un polymère de coordination à transition de spin (TS). Le chapitre 3 présente comment, par sérendipité, nous sommes passés de l'étude d'une réaction PSM sur le polymère de coordination à l'utilisation du complexe à TS comme catalyseur pour la formation d'imine. Le chapitre 4 regroupe les résultats concernant l'étude de l'effet de l'état de spin du fer sur les capacités catalytiques du complexe à TS dans une réaction d'acétalisation. Enfin, la formation de matériaux composites à base de complexes à TS ainsi que leurs utilisations comme catalyseurs de la réaction d'acétalisation sont décrites dans le chapitre 5.

Chapitre 1 : Introduction bibliographique sur le phénomène de transition de spin ainsi que sur l'influence des états de spin du métal sur la réactivité chimique d'un complexe.

Le phénomène de transition de spin (TS) est une transition réversible entre les états haut spin et bas spin de métaux de transition de configurations électroniques d^4-d^7 (Fig.1).[1] Cette transition de spin est déclenchée par des stimuli externes tels que la température, la pression, la lumière et les champs magnétiques. La transition de spin conduit à une modification importante des propriétés du complexe à TS (changement de propriétés magnétiques, de volume moléculaire, de couleur du composé…). Cette modulation réversible des propriétés, fait que les matériaux à TS suscitent un vif intérêt de la communauté scientifique et trouvent des applications dans des domaines très variés. Par exemple, ils peuvent être utilisés comme capteur ou actionneurs mécaniques et on les retrouve aussi dans des dispositifs photoniques et électroniques.[2-4]

Selon la théorie du champ cristallin, l'interaction entre l'ion central d'un composé de coordination et ses ligands peut être considérée comme une force purement électrostatique. L'ion central chargé positivement est situé dans un champ cristallin créé par les ligands chargés négativement. Lorsqu'un métal de transition est exposé à l'influence électrostatique de ces ligands, les orbitales d dégénérées de l'ion métallique se divisent en différents niveaux d'énergie. Dans les complexes octaédriques (Fig.2),[5] les cinq orbitales d sont divisées en deux niveaux d'énergie : les orbitales e_g (orbitales d_{z^2} et $d_{x^2-y^2}$) et les orbitales t_{2g} (orbitales d_{xy}, d_{xz}et d_{yz}), les orbitales e_g étant plus énergétiques que les orbitales t_{2g}. Cette différence d'énergie entre les orbitales d notée Δ ou le plus souvent 10Dq correspond à l'énergie de stabilisation du champ cristallin. Comme le montre la Fig.2, la distribution des électrons dans ces orbitales d respecte les principes de l'énergie minimale et la règle de Hund. Lorsque l'énergie Δ dépasse l'énergie d'appariement des électrons (P), les électrons s'apparient dans les orbitales de plus

faible énergie t_{2g} avant d'occuper les orbitales e_g d'énergie plus élevée. Dans ce cas-là, l'ion central est à l'état bas spin. En revanche, si Δ est inférieur à P, les électrons occuperont le nombre maximal d'orbitales conformément à la règle de Hund. Dans ce dernier cas, l'ion métallique sera à l'état haut spin.

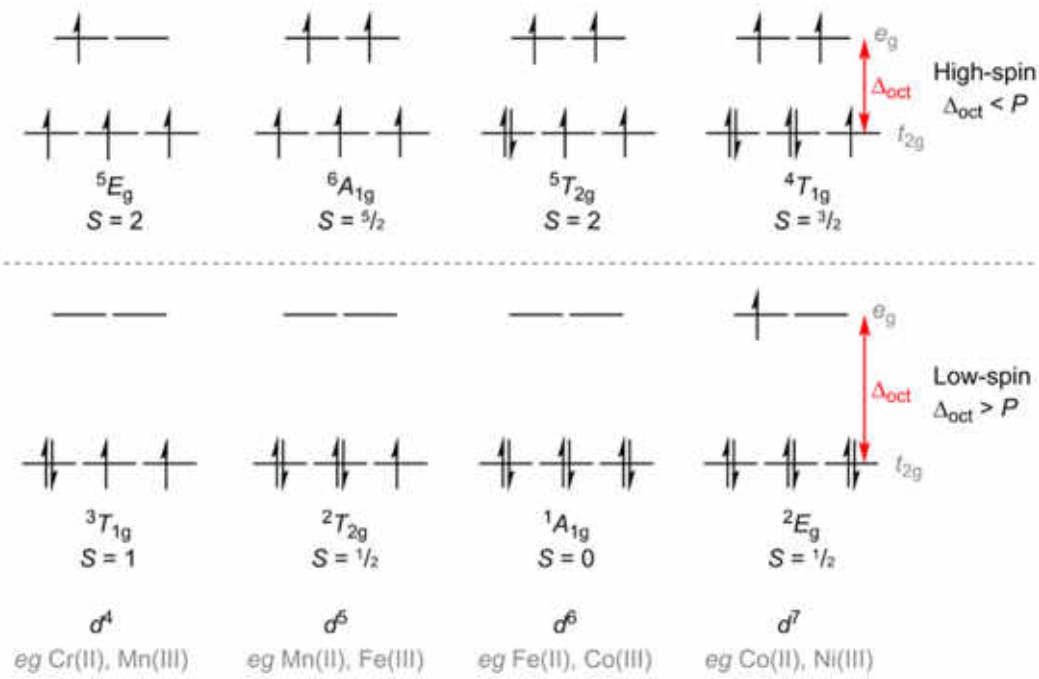


Fig.1 Dans un champ de ligands octaédriques, les ions métalliques de transition d^4-d^7 peuvent présenter des configurations électroniques à spin élevé ou à spin faible.[1]

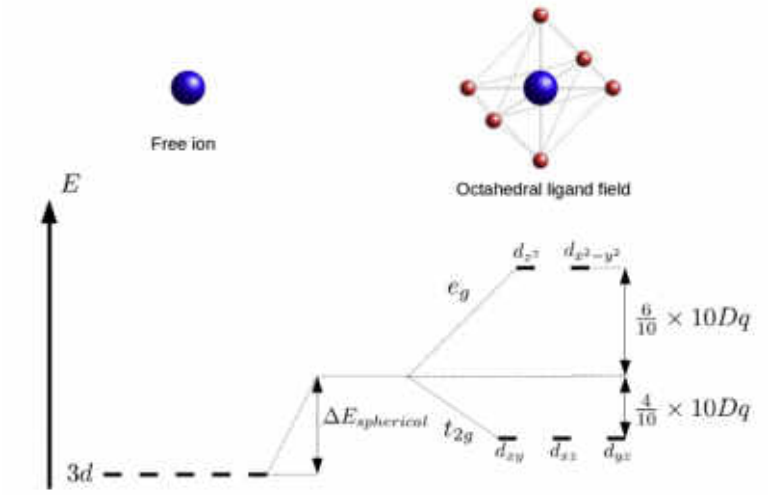


Fig.2 Représentation schématique du fractionnement de la dégénérescence partielle des orbitales 3d dû à la présence du champ du ligand octaédrique.[5]

Lorsque l'énergie Δ est comparable à l'énergie d'appariement des électrons (P) et que la différence d'énergie entre l'état fondamental à haut spin et l'état fondamental à bas spin est du même ordre de grandeur que kT (où k est la constante de Boltzmann et T la température), les états de spin peuvent être intervertis par des facteurs externes tels que la température, la lumière ou la pression. Ce phénomène est connu sous le nom de "transition de spin".

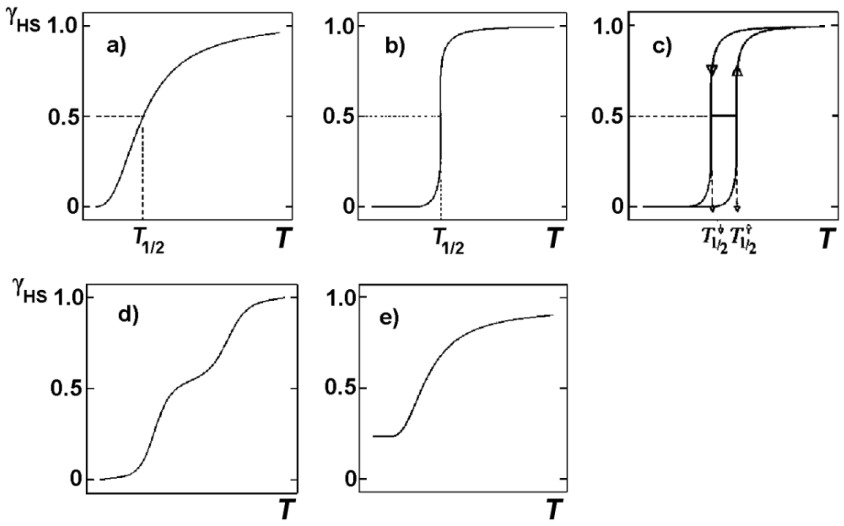


Fig.3 Représentation schématique de cinq types de courbes de transition de spin. (a) graduelle ; (b) abrupt; (c) abrupte avec cycle d'hystérésis thermique ; (d) transition en deux étapes ; (e) transition incomplète.[1, 6]

Comme déjà mentionné, le phénomène de transition de spin peut être induit par divers stimuli externes.[2, 3] La température est probablement le stimulus le plus utilisé pour induire la transition de spin des complexes métalliques. Lorsque la température change, la population de molécules dans l'état haut spin ou dans l'état bas spin s'ajuste en conséquence. L'allure de la courbe de susceptibilité magnétique en fonction de la température (γHS vs. T) d'un complexe permet notamment de déterminer si la transition est graduelle (Fig.3a) ou abrupte (Fig.3b), la présence d'un cycle d'hystérésis thermique (Fig.3c), si la transition se fait en deux étapes (Fig. 2d) ou si elle est incomplète (Fig.3e).[1, 6]

Par ailleurs, l'état de spin du métal joue également un rôle essentiel dans la synthèse de certains composés, car il affecte, en particulier, la réactivité chimique des complexes de métaux de transition.[7-9] En effet, l'état de spin du complexe influence considérablement les énergies d'activation des réactions, les chemins réactionnels ainsi que les sélectivités. L'étude de l'effet de l'état de spin sur la réactivité chimique revêt un grand intérêt pour divers domaines scientifiques comme la biochimie, la chimie organométallique et la catalyse. [10-19]

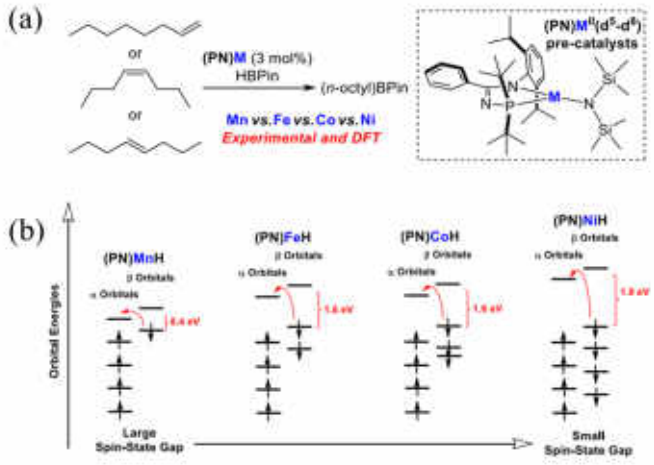


Fig.4 (a) Isomérisation-hydroboration de l'alcène catalysée par des complexes N-Phosphinoamidinate de Mn, Fe, Co et Ni. (b) Changements idéalisés de l'occupation de l'orbitale d de l'état bas spin à l'état haut spin.[20]

Dans les systèmes catalytiques, la transition de spin peut influencer de manière significative la réactivité et l'efficacité du processus. La sphère de coordination du métal, les énergies d'activation et les chemins réactionnels peuvent être affectés par des modifications de l'état de spin du métal. Ce phénomène peut être observé dans divers systèmes catalytiques, où la transition entre les états haut spin et bas spin joue un rôle crucial dans la détermination de l'activité catalytique et des sélectivités réactionnels. Ainsi, il est essentiel de comprendre la dynamique de la transition de spin pour optimiser les performances des catalyseurs et concevoir des procédés catalytiques plus efficaces. Par exemple, en 2018, Macaulay et al.[20] ont étudié la réactivité de précatalyseurs métalliques (N-phosphinoamidinate) ($N(SiMe_3)_2$) ((PN)M ; où M = Mn^{2+}, Fe^{2+}, Co^{2+}, et Ni^{2+} ; d^5-d^8) dans l'isomérisation-hydroboration du 1-octène, du cis-4-octène et du trans-4-octène avec le pinacolborane (HBPin) (Fig.4). Leur étude a révélé une différence de réactivité et de sélectivité catalytiques entre les complexes de la série (PN)M. Alors que les complexes (PN)Mn et (PN)Ni présentaient de faibles rendements d'hydroboration, les complexes (PN)Fe et (PN)Co atteignaient des taux de conversion et une sélectivité élevés en 1-octyboronate. Les calculs DFT ont révélés que les divergences de réactivité entre ces pré-catalyseurs sont étroitement liées à leurs écarts d'énergie de l'état de spin. Dans la réaction impliquant le (PN)MnH et le trans-4-octène, l'absence de transition de spin conduit à une insertion migratoire lente et donc à de faibles rendements de réaction. En revanche, la barrière d'énergie d'activation pour le complexe (PN)FeH est plus faible du fait de la transition de spin, et la barrière d'énergie pour l'insertion migratoire est très faible pour le complexe (PN)CoH à l'état bas spin. Cette étude permet de mieux comprendre les voies mécanistiques et les performances catalytiques relatives de la série de pré-catalyseurs (PN)M, en soulignant le rôle crucial de l'état de spin dans l'accélération des réactions catalytiques.

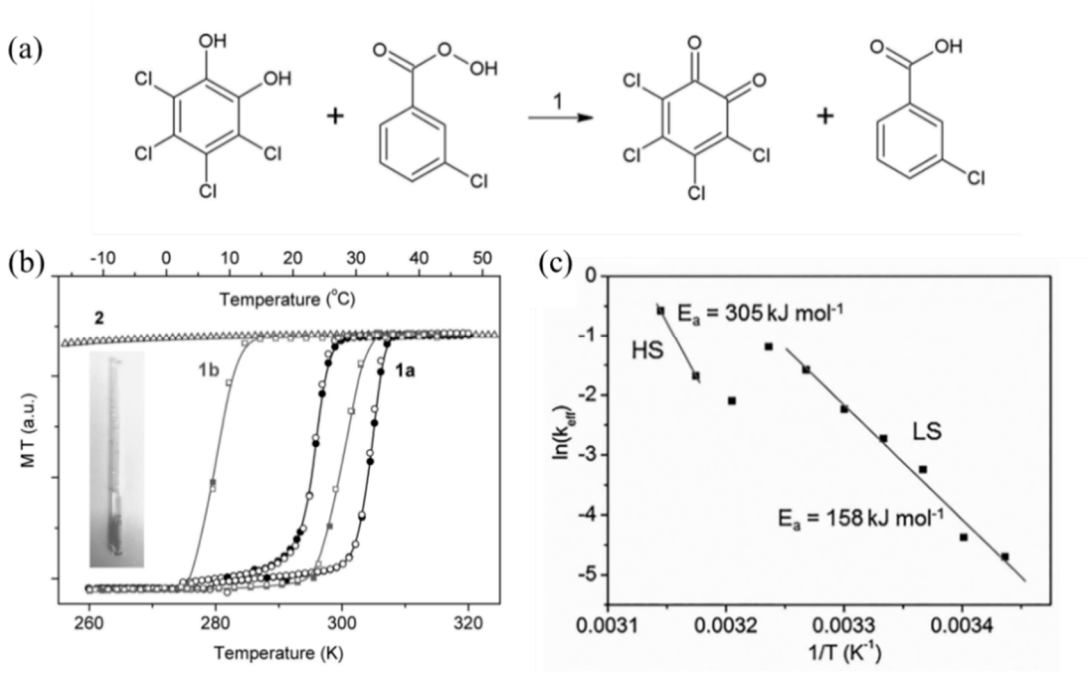


Fig.5 (a) Oxydation du 3,4,5,6-tétrachlorocatéchol en sa quinone correspondante en présence d'acide 3-chloroperbenzoïque. (b) Propriétés magnétiques de $[Fe(NH_2trz)_3]Br_2$. (c) Tracé d'Arrhenius illustrant la présence de deux régimes cinétiques correspondant à HS et BS.[21]

Enfin, l'utilisation directe de complexes à transition de spin en tant que catalyseurs peut

constituer une approche prometteuse pour améliorer les processus catalytiques. A notre connaissance il existe seulement cinq exemples, décrits dans la littérature, d'utilisation en catalyse de complexes développés pour leurs propriétés à transition de spin.[21-25] Les travaux de recherches les plus proches de notre objectif ont été décrits par Gural'skiy et al. en 2017.[21] Ils ont rapporté pour la première fois l'utilisation de complexes polymériques 1D à TS (plus précisément le complexe $[Fe(NH_2trz)_3]Br_2$ (où NH_2trz = 4-amino-1,2,4-triazole)), dans l'oxydation du 3,4,5,6-tétrachlorocatéchol (TCC) en présence de l'acide 3-chloroperbenzoïque (CPBA)(Fig.5). Leurs conclusions ont révélé que les espèces à l'état BS présentaient des vitesses de réaction plus élevées et des énergies d'activation plus faibles que leurs analogues à l'état HS. En outre, leur étude a également démontré que l'espèce active dans ce processus catalytique est le complexe SCO oxydé, qui se forme par oxydation avec le CPBA. Une fois oxydé, ce complexe est ensuite réduit par le TCC, régénérant ainsi le complexe SCO initial. Ainsi, le véritable catalyseur actif dans ce système n'est pas le complexe Fe(II) lui-même, mais sa forme oxydée. L'activité catalytique plus élevée observée pour les espèces BS a été attribuée au fait que l'étape déterminant la vitesse de réaction (l'oxydation du complexe SCO) se produit plus facilement dans l'état BS que dans l'état HS.

En conclusion dans cette première partie nous avons souligné que les complexes à TS sont utilisés dans de nombreux domaines. L'intérêt porté à cette catégorie de complexes découle de leur capacité à changer, de façon réversible et à la demande, de propriétés physiques. Nous souhaitons maintenant démontrer que ces complexes peuvent être aussi de bon catalyseurs. Et plus précisément notre objectif à long terme, est de démontrer que ce sont d'excellents catalyseurs commutables. Si l'état de spin d'un métal est connu pour influencer l'activité catalytique de complexes métalliques, de façon paradoxale très peu de résultats sur l'utilisation de complexes à TS en catalyse ont été décrits dans la littérature. Ainsi, dans ce contexte, les travaux de recherche décrits dans ce manuscrit avaient pour but d'étudier l'effet de l'état de spin du fer sur la réactivité et l'activité catalytique d'un complexe à transition de spin.

Chapitre 2 : Effet de l'état de spin sur l'efficacité d'une réaction de modification post-synthétique sur un complexe à transition de spin

Les complexes à TS sont des matériaux fascinants qui présentent une transition réversible entre différents états de spin en réponse à des facteurs externes. Les complexes fer(II)-triazole se distinguent par leurs transitions de spin abruptes ainsi que par la possibilité de moduler leurs propriétés à TS. Ces complexes suivent généralement la formule $[Fe(NH_2trz)_3]Anion\text{-}xH_2O$, où l'anion représente un contre-ion mono- ou divalent (Fig.6a). Les transitions de spin de ce polymère de coordination 1D de fer(II) sont abruptes et ont lieu au-dessus de la température ambiante. Par ailleurs, ce complexe possède une large boucle d'hystérésis thermique (Fig.6b). Les excellentes propriétés de TS des complexes fer-triazole les rendent très attractifs pour diverses applications technologiques, y compris les capteurs, les dispositifs électroniques et les actionneurs mécaniques. C'est pourquoi nous voulions synthétiser une grande diversité de complexes à partir du même complexe parent (le complexe **1**). Cet objectif pouvait être atteint en utilisant la méthode de modifications post-synthétiques (PSM) (Fig.7). [26-37]

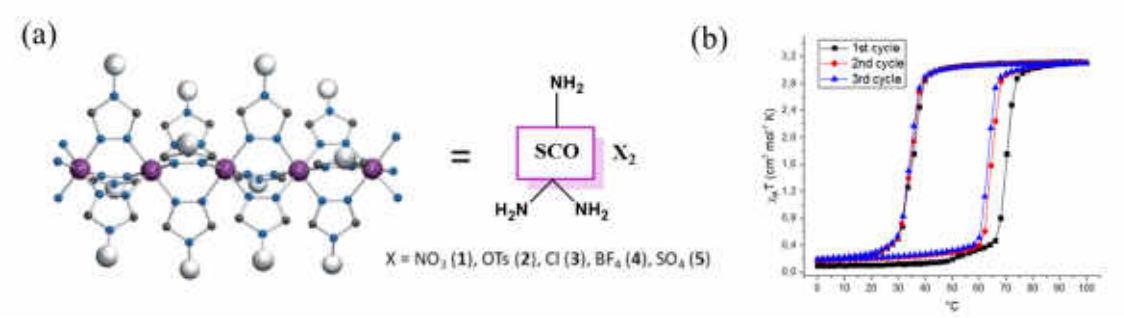


Fig.6 (a) Schéma de l'anion $[Fe(NH_2trz)_3]$-xH_2O et (b) propriété magnétique du complexe lorsque l'anion est le nitrate.

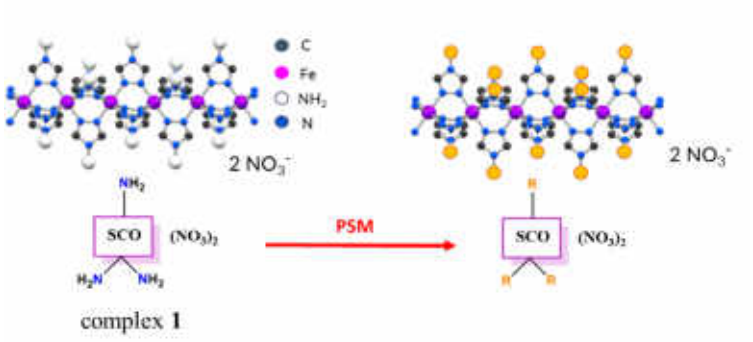


Fig.7 General scheme of synthesis new complex by PSM reaction from complex **1**

Comme illustré ci-dessous, la méthode de modification post-synthétique commence par la synthèse des matériaux. Les groupements fonctionnels présents sur ces matériaux sont ensuite modifiés par réactions chimiques, ce qui permet d'obtenir les composés souhaités. Les mêmes matériaux peuvent également être obtenus par la méthode traditionnelle de synthèse directe (DS), qui implique d'abord la synthèse du ligand souhaité puis la coordination de ce dernier à l'ion métallique. L'utilisation de la méthode PSM présente plusieurs avantages par rapport aux méthodes traditionnelles de synthèse directe : 1) La méthode PSM permet de synthétiser une grande libraire de composés à partir d'un même composé parent. 2) Dans certains cas, la méthode PSM permet d'accéder à des complexes difficiles ou impossibles à synthétiser par d'autres méthodes de synthèse. 3) La méthode PSM permet parfois un meilleur contrôle de la structure chimique du matériau produit.

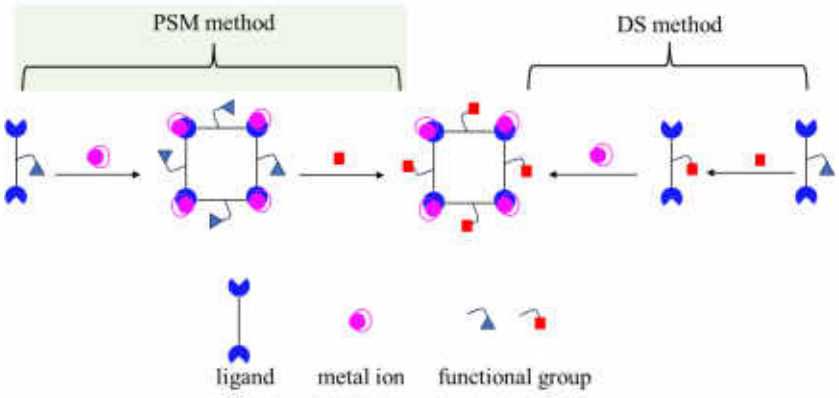


Fig.8 Représentation schématique des méthodes de modification post-synthétique et de synthèse directe

Avant le début de ma thèse, l'équipe avait déjà commencé à étudier les réactions PSM sur le complexe parent **1**. Tout d'abord, ces études ont permis de démontrer que les propriétés à TS

du matériau dépendent aussi de la méthode utilisée pour synthétiser le complexe.[34] En effet, il a été notamment observé qu'un matériau obtenu par méthode PSM a des propriétés de TS alors que le même composé synthétisé par la méthode directe n'a pas de propriétés de TS. Par la suite, l'équipe a aussi démontré qu'une large librairie de complexes a pu être crée par réactions PSM à partir du complexe **1**.[36] Ces travaux ont notamment confirmé la faisabilité d'effectuer des réactions PSM quantitatives à partir du complexe parent **1**. Enfin, l'équipe a aussi démontré que la nature du solvant réactionnel influence très fortement l'efficacité de la réaction PSM sur le complexe **1**. Mes premiers travaux de recherches ont commencé par la constatation que le même complexe imine pouvait être obtenu quantitativement soit en effectuant la réaction de PSM à 35°C pendant 72h, soit à 90°C pendant 10 minutes (Fig.9). Cette différence dans les temps de réaction soulève une question importante : l'état de spin du complexe à TS joue-t-il un rôle dans l'amélioration de la réactivité ?

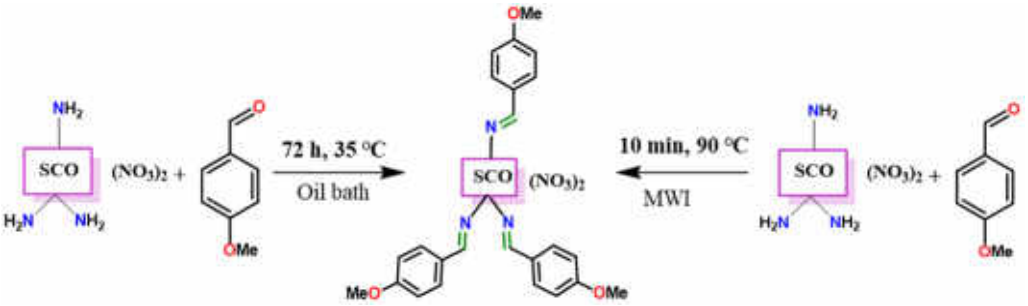


Fig.9 Un complexe imine a été synthétisé par une réaction post-synthétique, une réaction étant effectuée à basse et à haute température.[34, 36]

Isoler l'effet de l'état de spin des autres facteurs contributifs est un réel défi. En effet, le phénomène de la TS est déclenché par un stimulus, mais ce dernier a souvent un effet sur l'activité réactionnel du composé. Dans notre cas, la meilleure efficacité de la réaction PSM à plus haute température pourrait être attribuée à une combinaison de trois facteurs : (1) l'activation thermique, (2) les effets structurels induits par les changements de température, et (3) l'état de spin du complexe.

4) **Activation thermique** : En effet, des températures plus élevées peuvent fournir l'énergie nécessaire pour surmonter les barrières d'activation de la formation de groupement fonctionnel, facilitant ainsi la synthèse du produit. En règle générale, des températures plus élevées conduisent à des rendements plus élevés, et lorsqu'un produit souhaité n'est pas obtenu ou que les vitesses de réaction sont faibles, des températures plus élevées sont souvent envisagées comme solution.

5) **Effet structurel** : Une augmentation de la température peut faciliter les interactions entre les réactifs, ainsi qu'entre les réactifs et le solvant. Il s'agit d'un paramètre important, car la vitesse d'une réaction dans laquelle l'un des réactifs est à l'état solide dépend fortement du contact entre les réactifs. En effet, un changement dans les interactions moléculaires entraînera un changement dans l'arrangement moléculaire du composé solide, conduisant à un accès différent aux groupes fonctionnels. Ce paramètre ne doit pas être négligé, car l'équipe a précédemment démontré que l'éthanol permet une meilleure séparation des chaînes de polymères du complexe **1**, conduisant à une réaction PSM quantitative.

6) **Effet d'état de spin** : Le complexe **1** est dans l'état BS à basse température (35 °C) mais à l'état HS à haute température (90 °C). Comme la réactivité du complexe de fer dépend également de l'état de spin de son métal, il est alors concevable que l'état de spin ait une influence sur l'efficacité de la réaction PSM.

Diverses expériences ont été menées pour définir comment l'activation thermique, les effets structurels et les changements d'état de spin contribuent à l'amélioration de l'efficacité de la méthode de modification post-synthétique (PSM). Nous avons tout d'abord comparé l'impact de la hausse de température sur la réaction PSM sur le complexe **1** avec le *p*-anisaldéhyde à celui sur la réaction entre 4-amino-1,2,4-triazole (le ligand libre) et le *p*-anisaldéhyde (Fig.10). Cette étude a été réalisée afin de déterminer si l'augmentation de l'efficacité de la réaction PSM était principalement liée au dépassement de la barrière de l'énergie d'activation,

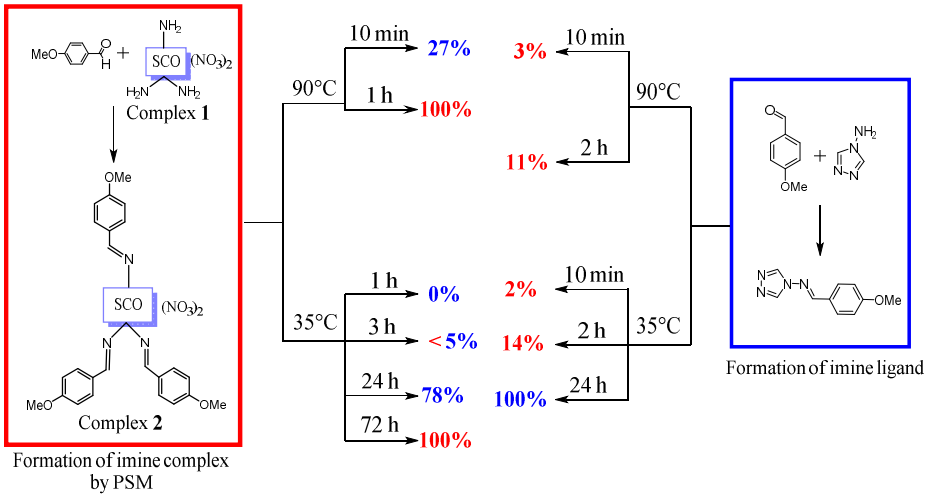


Fig.10 Conditions expérimentales et rendements pour la synthèse du complexe correspondant 2 (à gauche) et du ligand imine (à droite)

Le fait que l'augmentation de la température de 35°C à 90°C n'a absolument pas influencé le rendement en imine à partir du ligand libre, suggère que l'activation thermique n'est pas la raison principale de l'augmentation de l'efficacité observée pour la réaction PSM sur le complexe **1**. Ce résultat suggère également que l'augmentation de réactivité est liée spécifiquement au complexe **1**. Cette information, nous pousse à envisager que l'augmentation d'efficacité puisse principalement résulter d'un changement structurel et/ou d'une influence de l'état de spin du métal. Nous avons alors, souhaité déterminer plus précisément à quelle(s) température(s) l'augmentation de l'efficacité de la réaction PSM était la plus significative. Si comme on l'espérait cette augmentation d'efficacité est bien due à une influence de l'état de spin on devrait noter une différence d'efficacité plus significative aux abords des températures de la transition de spin du complexe **1**. Pour mener à bien cette étude, nous avons déterminé les rendements, de la réaction PSM sur le complexe **1**, obtenus en une heure et à diverses températures. La principale conclusion de cette étude, est que la courbe générée à partir des rendements PSM en fonction de la température coïncide avec la courbe de transition de spin de la suspension du complexe **1** dans l'éthanol (Fig.11). Cette étude semble donc suggérer que l'état de spin puisse contribuer à l'amélioration de l'efficacité de la réaction PSM. Par contre, cette étude ne permet pas de séparer l'effet de l'état de spin de celui d'un réarrangement structurel induit par une hausse de température. En effet, cette hausse de température pourrait conduire à des interactions plus favorables entre l'EtOH et les chaînes de polymères du complexe **1** (effet solvothermique). Dans ce cas, les chaines polymériques du complexes **1** seraient mieux séparées ce qui faciliterait la réaction PSM.

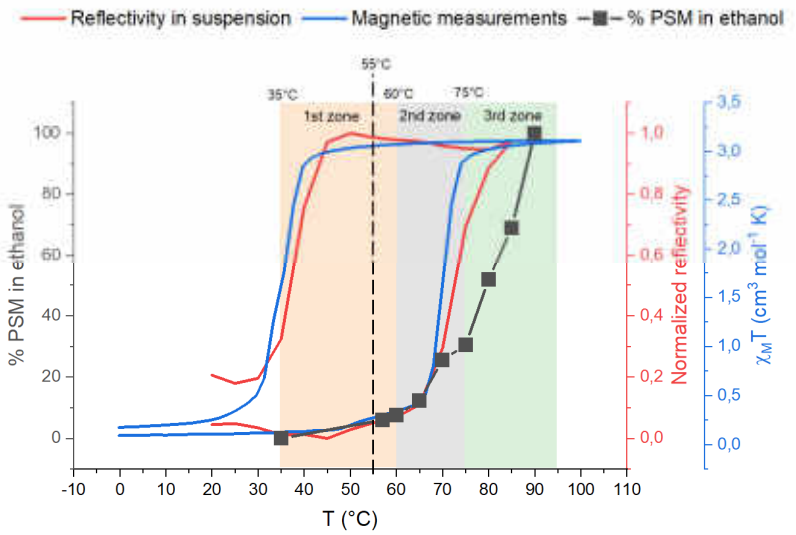


Fig.11 Mesures magnétiques à température variable (courbe bleue) ; mesures de réflectivité à température variable du complexe **1** dans une suspension d'éthanol (courbe rouge) ; rendements de PSM en fonction de la température de réaction (courbe noire).

Ainsi pour pouvoir séparer l'effet de l'état de spin d'un effet solvothermique, il faut obligatoirement comparer la réactivité des deux états de spin du complexe **1** à la même température. Pour la plupart des composés à TS cette étude comparative est infaisable. Mais dans notre cas, c'est possible en mettant à profit le large cycle d'hystérésis thermique du complexe **1**. Cette étude a donc été effectuée à 55°C, car cette température se situe au centre du cycle d'hystérésis du complexe 1 en suspension dans l'éthanol. Avant de discuter des résultats, il est important de mentionner que les réactions à partir des différents états de spin du complexe **1** ont été réalisées dans des conditions expérimentales strictement identiques. En particulier l'aldéhyde a été rajouté à la suspension après que les états de spin du complexe **1** aient été stabilisés pendant 10 minutes à 55°C (Fig.12).

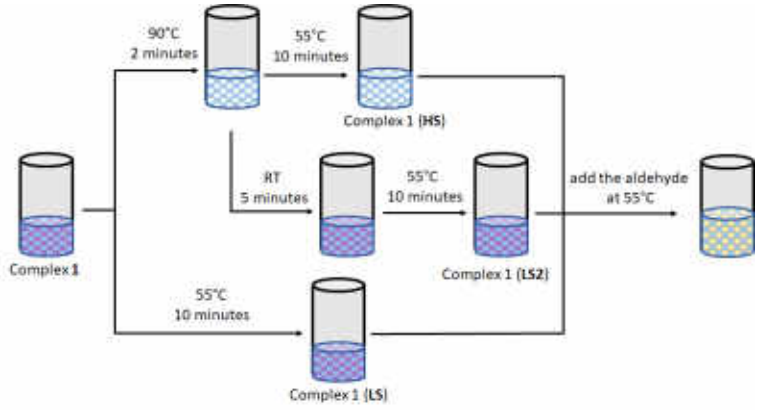


Fig.12 Représentation schématique de la préparation du complexe **1** dans les états HS, BS et BS2

Les résultats ont révélé que les réactions réalisées à partir du complexe **1** à l'état HS présentaient des rendements en PSM significativement supérieurs à celles des réactions réalisées à partir du complexe **1** aux états BS et BS2 (Table 1). Nous sommes particulièrement satisfaits d'observer,

pour un temps de réaction de 4 heures, une différence d'environ 20 pourcents de rendements entre la réaction effectuée à partir du complexe à l'état HS et celle effectuée à partir de l'état BS2.

Table 1 Rendements de la réaction PSM en fonction du temps de réaction et de l'état de spin du complexe

	PSM as function of the spin state(%)			difference in the efficiency of the PSM (%)		
time (hour)	LS	HS	LS2	Δ_{HS-LS2}	Δ_{HS-LS}	Δ_{LS2-LS}
1	6	8	/	/	2	/
3	29	41	33	8	12	4
4	50	72	51	21	22	1

Ainsi le complexe **1** à l'état HS semble bien plus réactif vis-à-vis de l'aldéhyde que le complexe à l'état LS2. Cette différence de réactivité entre les deux états de spin du complexe **1** pourrait provenir d'effet électroniques et/ou d'effets stériques. D'une part, l'état de spin du fer peut affecter la densité électronique au niveau de la fonction NH_2, ce qui va changer la nucléophilicité de l'atome d'azote. D'autre part, nous pensons que l'état de spin du fer puisse affecter les interactions entre les chaines polymériques du complexe **1** et l'éthanol. Le nombre et la force de ces interactions vont moduler l'arrangement moléculaire du complexe ce qui pourrait conduire à une différence de contact entre les fonctions NH_2 du complexe et l'aldéhyde. A notre connaissance, c'est la première fois que l'on constate l'effet de l'état de spin sur la réactivité organique d'un groupement fonctionnel présent sur un complexe métallique.

Enfin nous avons souhaité contôler la reproductibilité et la généralité de ce résultat remarquable. Ainsi plus de 44 paires d'expériences ont été menées et 5 lots distincts de complexe **1** ont été testés. Chaque paire d'expériences comprend une réaction PSM effectuée à partir du complexe **1** à l'état HS et une réaction effectuée à partir du complexe à l'état BS2. On a mené ces deux réactions en parallèle dans le même bain d'huile et en utilisant des conditions expérimentales parfaitement identiques (les mêmes bouteilles d'éthanol et d'aldéhyde, même temps de réaction, même lot de complexe). Par ailleurs, chaque expérience a été analysée deux fois de façon indépendante. On a regroupé les résultats de la première analyse des expériences dans la série 1, tandis que la série 2 regroupe tous les résultats de la deuxième analyse. A titre d'exemple, la Fig.13 indique les résultats de 18 paires d'expériences effectuées à partir du lot 5 de complexe **1**. Ces résultats sont représentatifs et illustrent les conclusions tirées de la mise en oeuvre des 44 paires d'expériences. Systématiquement le complexe **1** à l'état HS était plus réactif vis-à-vis de l'aldéhyde que le complexe **1** à l'état BS. En effet, lorsque la réaction PSM était effectuée à partir du complexe **1** à l'état HS, nous avons constaté jusqu'à 22 % de rendement supplémentaire par rapport à la réaction réalisée à partir du complexe **1** en condition BS2. Par ailleurs, cette différence de réactivité est bien significative car nous avons montré que la marge d'erreurs de notre méthode d'analyse est de ±2%. La cohérence des résultats obtenus sur plusieurs lots de complexe **1** ainsi que la variété de conditions expérimentales testées confirment la validité et la généralité de ce résultat.

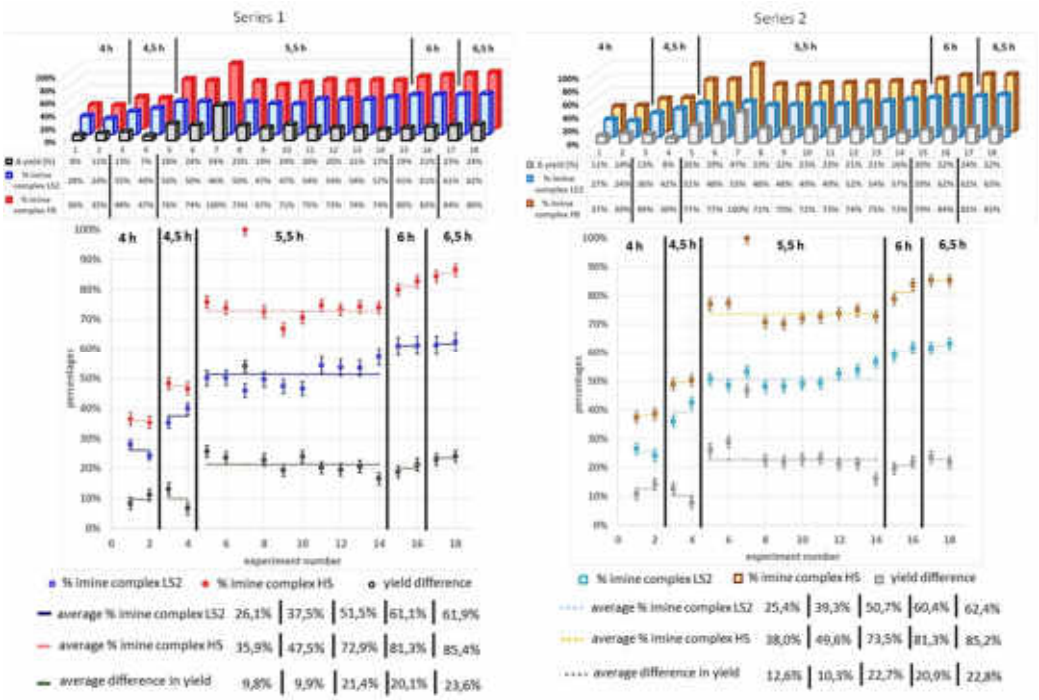


Fig.13 Rendements en imine obtenus pour le lot 5 (séries 1 et 2) après 4, 4,5, 5,5, 6 et 6,5h de réaction (conditions normales), pour le HS et le BS2 et la différence entre les deux états de spin.

Le nombre important d'expériences effectuée nous a permis de réalisée une analyse statistique des résultats obtenus. Cette dernière nous a permis de quantifier la différence de réactivité entre les états HS et BS2 du complexe **1**. Le rapport entre le rendement PSM obtenu lorsque la réaction était réalisée à partir du complexe **1** à l'état HS et celui obtenu pour la réaction à partir de l'état BS2 a été calculé pour toutes les expériences (Fig.14). En moyenne, à partir du complexe à l'état HS, 1,34 fois plus d'imine est obtenue qu'à partir du complexe à l'état BS2. Le fait que l'écart-type des résultats (σ=0.11) est relativement faible, met en évidence la cohérence des résultats.

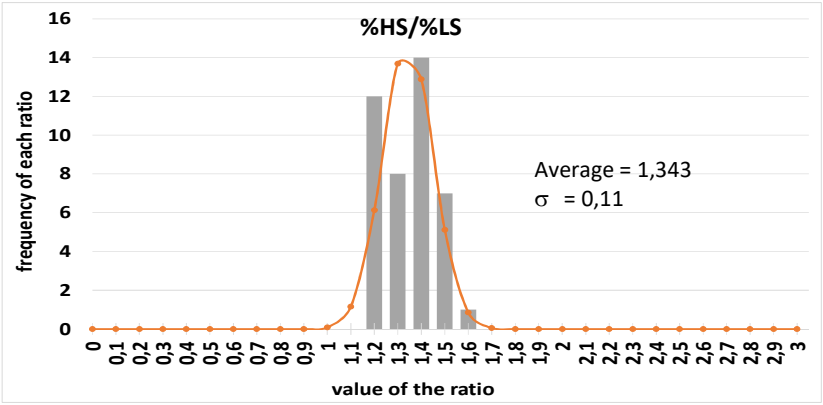


Fig.14 Fréquence du rapport %HS/%LS2 valeur et écart-type

Pour conclure, sur 44 paires d'expériences menées sur 5 lots distincts de complexe **1**, on a systématiquement observé que le pourcentage d'imine dans l'échantillon HS depassait celui de l'échantillon BS2. L'efficacité de la réaction PSM s'est considérablement améliorée, atteignant

jusqu'à 22%, lorsque le complexe **1** était à l'état HS en comparaison de l'état BS2 du complexe **1**. La multitude d'expériences et l'estimation de l'erreur de la méthode de digestion (± 2 %) confirment la différence significative de réactivité entre les deux états de spin du complexe **1**. En moyenne, 1,37 fois plus d'imine est formée lorsque le complexe **1** est dans l'état HS par rapport à l'état BS2. Ces travaux de recherche illustrent pour la première fois l'effet de l'état de spin sur la modification post-synthétique d'un polymère de coordination 1D à transition de spin. Il s'agit aussi du premier exemple de l'effet de l'état de spin sur la réactivité organique d'un groupement fonctionnel au sein d'un complexe métallique.

Chapitre 3 : Étude de l'activité catalytique du polymère de coordination $[Fe(NH_2trz)_3](NO_3)_2$ à transition de spin pour la formation d'imine à partir de 4-amino-1,2,4-triazole

Les résultats décrits dans la Fig.10 ont été le point de départ des travaux de recherche du chapitre 3 de ma thèse. Ces résultats nous intéressaient car ils nous permettaient d'avoir un argument supplémentaire de la formation du complexe imine par réaction PSM sur le complexe **1**. Dans ce contexte, la réactivité de l'aminotriazole **a** vis-à-vis des aldéhydes a été comparée à celle des groupements NH_2 présents sur le complexe **1**. En 10 minutes à 90°C sous irradiation micro-onde, la réaction PSM sur le complexe **1** était quantitative, alors que dans les mêmes conditions expérimentales, seulement 10% de l'imine était formée à partir de l'aminotriazole (Fig. 3-2). Ce résultat indique qu'une réaction impliquant un réactif insoluble n'est pas nécessairement plus lente qu'une réaction dans laquelle tous les réactifs sont en solution. Par ailleurs, ce résultat illustre comment la coordination sur un métal peut modifier de manière significative la réactivité organique du ligand. Par conséquent, la combinaison de la méthode PSM avec une réaction, telle que la digestion du complexe pour décoordiner le ligand du fer, présente une approche intéressante pour synthétiser de nouvelles molécules organiques à base de triazole.

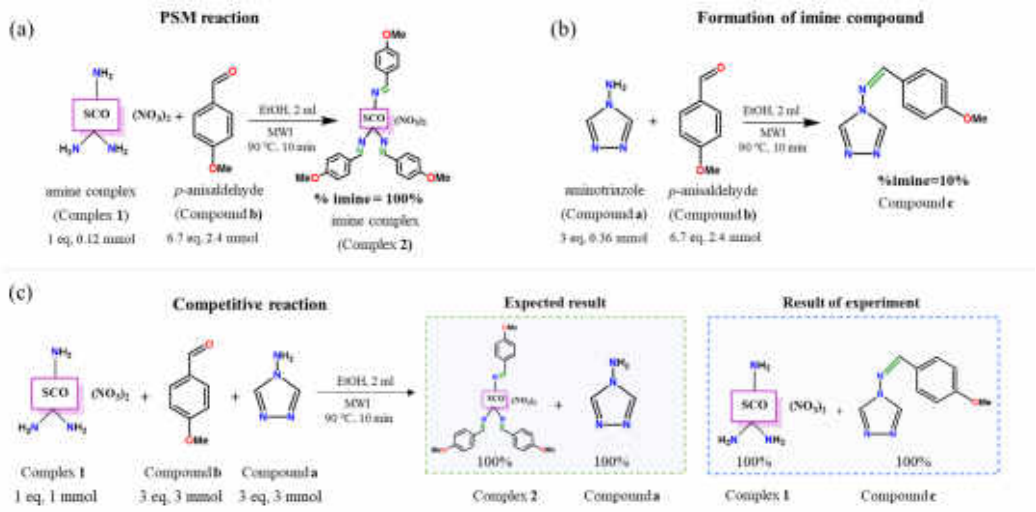
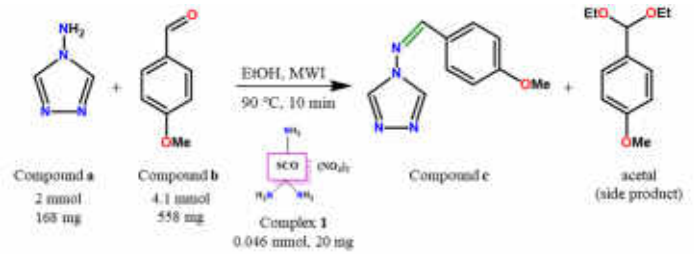


Fig.15 Réactions effectuées sous irradiation micro-ondes à 90°C pendant 10 minutes. (a) Réaction PSM sur le complexe **1** avec l'aldéhyde **b**. (b) Formation d'un composé imine entre l'aminotriazole **a** et l'aldéhyde **b**. (c) Réaction compétitive en présence du complexe **1**, de l'amine **a** et de l'aldéhyde **b**.

Par la suite, une réaction compétitive a été réalisée en utilisant un mélange contenant des quantités stœchiométriques du complexe **1**, de l'aminotriazole **a** et de l'aldéhyde **b.** Les résultats expérimentaux de cette réaction compétitive ont montré la formation quantitative de l'imine **c** en solution, alors que le complexe récupéré correspondait au complexe amine **1**. Le fait que le résultat de la réaction compétitive soit complètement opposé aux résultats des expériences individuelles nous a amené à considérer que le complexe de fer à TS puisse catalyser la formation de l'imine à partir de l'aminotriazole **a**. Cette découverte est importante car, à notre connaissance, elle représente le deuxième exemple de l'utilisation de cette famille de complexes en catalyse. De plus, il s'agit du premier exemple dans lequel l'espèce catalytiquement active est le complexe à transition de spin.

Tableau 2 Formation de l'imine **c** catalysée par le complexe de fer **1**.



Entrée	Catalyseur[a]	Conditions				Rendement (imine)	Rendement (acétal)
		Sonicate[b]	Chauffage[c]	Prétraitement[d]	Réaction		
1	Complexe **1**	-	-	-	10 min	40%	2%
2	-	-	-	-		10%	2%
3	Complexe **1**	10 min	-	-		54%	2%
4	Complexe **1**	10 min	10 min	-		58%	2%
5	Complexe **1**	10 min	-	10 min		>98%	1%

[a] 20 mg du complexe ont été suspendus dans 0,5 ml d'éthanol, deux solutions différentes avec une concentration de 4,1 mM d'aldéhyde (mélange 1) et 2 mM d'aminotriazole (mélange 2) ont été préparées. [b] Sonication uniquement de la suspension du complexe à température ambiante. [c] Chauffer uniquement la suspension du complexe à 90°C sous MWI. [d] 1 mL du mélange 1 a été ajouté au complexe en suspension, et il a été chauffé à 90 °C sous MWI.

Afin de vérifier notre hypothèse, nous avons étudié la formation de l'imine **c** en présence d'une quantité catalytique du complexe **1**. Tout d'abord, le complexe **1** catalyse bien la réaction car en sa présence catalytique (2,3 % molaire par rapport à l'aminotriazole **a**), un rendement de 40% est obtenu alors qu'en son absence un rendement de 10% est obtenu (entrées 1 et 2, Tableau 2). La sonication de la suspension des particules de complexe **1** dans l'éthanol pendant 5 minutes avant la réaction catalytique a encore amélioré le rendement, qui est passé à 54 % (entrée 3, Tableau 2). Cette augmentation du rendement peut être attribuée à un meilleur accès au site catalytique, car le complexe **1** est insoluble dans l'éthanol, et il est bien connu que l'augmentation de la surface de contact d'un catalyseur hétérogène améliore son activité catalytique. Bien que les conditions de sonication utilisées pour la suspension du complexe **1** dans l'éthanol ne réduisent pas la taille des particules du complexe **1**, elles sont suffisantes pour réduire la taille des agglomérats. Le rendement a pu être légèrement augmenté en appliquant une irradiation par micro-ondes à 90°C pendant 10 minutes à la suspension préalablement soniquée du complexe **1** dans l'éthanol (entrée 4, Tableau 2). Ce chauffage facilite probablement l'interaction entre l'éthanol et le complexe **1**, permettant une plus grande diffusion du solvant dans le solide et conduisant à une meilleure séparation des chaînes polymériques

dans le complexe **1**. Comme nous l'avons observé dans notre étude précédente de la méthode PSM, cette meilleure séparation des chaînes polymériques peut entraîner des rendements plus élevés. Enfin, lorsque le complexe amine **1** est prétraité avec l'aldéhyde **b**, la réaction est quantitative en moins de 10 minutes (Entrée 4, Tableau 2).

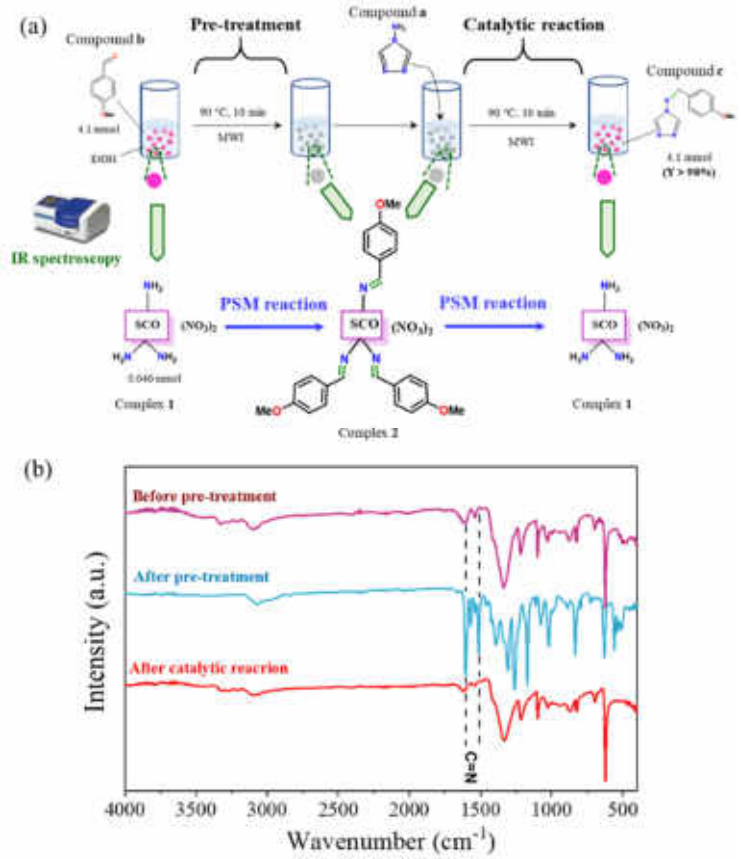


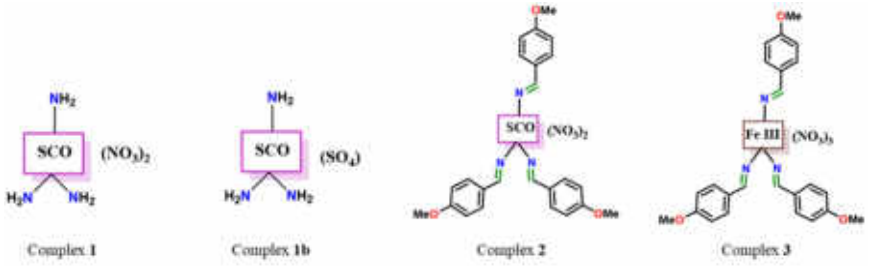
Fig.16 Prétraitement du complexe **1** avant son utilisation en catalyse. a) Représentation schématique de la procédure suivie. b) Spectres IR du complexe obtenu après prétraitement.

Comme le montre la Fig.16 (b), les spectres IR du complexe récupéré après le prétraitement ont révélé l'apparition de bandes caractéristiques de la liaison C=N, confirmant que le complexe **1** a été transformé en complexe **2** au cours du prétraitement. Après la réaction catalytique et le refroidissement ultérieur à température ambiante, le complexe récupéré reprend sa couleur rose. L'analyse IR confirme que le complexe récupéré après catalyse ne présente plus les bandes caractéristiques de la fonctionnalité C=N, mais correspond à celle du complexe aminé **1**. Ainsi, le complexe amine **1** subit deux réactions PSM au cours des réactions de prétraitement et de catalyse. La première réaction PSM se produit lorsque le complexe amine **1** réagit avec l'aldéhyde **b**, entraînant la formation du complexe imine **2** correspondant. Une deuxième réaction PSM n'a lieu que si l'aminotriazole **a** est présent en solution, où il réagit avec le complexe imine **2** pour régénérer le complexe de départ **1**. Au cours de cette deuxième réaction PSM, l'imine **c** est relargée en solution.

Ensuite, nous avons testé l'influence de la nature du catalyseur sur le rendement de la formation de l'imine **c** (Table 3). Les deux points les plus importants de cette étude sont : 1) comme attendu le complexe imine **2** catalyse quantitativement la formation de l'imine c en moins de 10 minutes; 2) de façon surprenante l'activité catalytique du complexe imine de fer (III) (complexe **3**) semble du même ordre de grandeur que celle du complexe imine **2** dont le fer est au degré d'oxydation +II.

Table 3 Effet de la nature du catalyseur sur l'efficacité de la réaction catalytique

Entry	Solvent			Catalyst[a]	Conditions				Yield
	Suspension of complex	aldehyde	aminotriazole		Sonicate[b]	Heating[c]	Pre-treatment[d]	Reaction	
1	96% EtOH	EtOH	EtOH	nanoparticles of complex **1**	-	-	-	10 min	76%
2	96% EtOH	EtOH	EtOH		10 min	-	-	10 min	81%
3	96% EtOH	EtOH	EtOH		10 min	-	10 min	10 min	100%
4	96% EtOH	EtOH	EtOH	complex **1b**	10 min	-	-	10 min	20%
5	96% EtOH	EtOH	EtOH		10 min	-	10 min	10 min	22%
6	96% EtOH	EtOH	EtOH	complex **3**	10 min	-	-	2 min	69%
7	96% EtOH	EtOH	EtOH		10 min	-	-	5 min	80%
8	96% EtOH	EtOH	EtOH		10 min	-	-	7min	100%
9	96% EtOH	EtOH	EtOH	complex **2**	10 min	-	-	5 min	100%
10	96% EtOH	EtOH	EtOH		10 min	-	-	10 min	100%
11	EtOH	EtOH	EtOH		10 min	-	-	10 min	100%
12	Toluene	Toluene	EtOH		10 min			10 min	74%



[a] 20 mg of the complex was suspended in 0.5 mL of solvent, two different solutions with a concentration of 4.1 mM of aldehyde (mixture 1) and 2 mM of aminotriazole (mixture 2) were prepared. [b] Sonicating only the suspension of the complex at room temperature. [c] Heating only the suspension of the complex at 90°C under MWI. [d] 1 mL of mixture 1 was added to the complex in suspension, and it was heated at 90 °C under MWI..

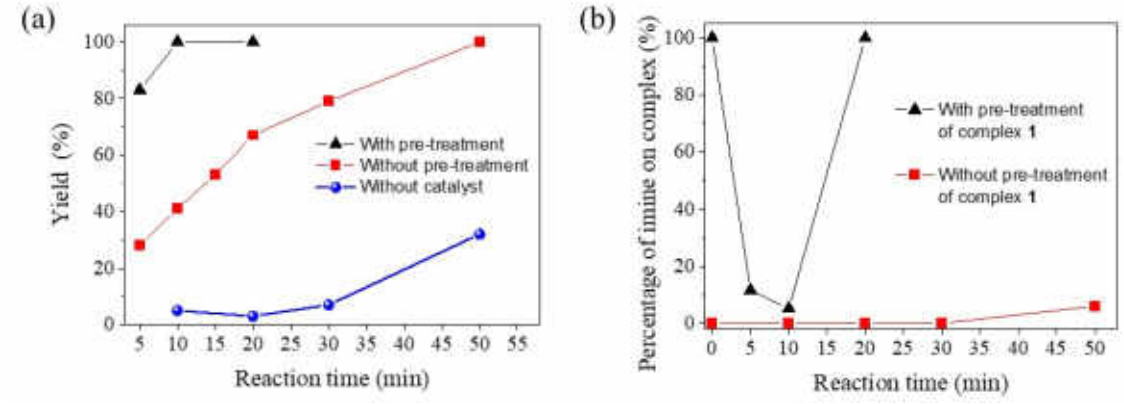


Fig.17 Étude cinétique de la réaction de catalyse. a) rendement de l'imine **c** en fonction du temps de réaction ; b) pourcentage de la fonctionnalité imine, sur le complexe récupéré après la catalyse, en fonction du temps de réaction.

Par la suite nous avons effectué un suivi cinétique de la formation catalysée de l'imine **c**. Lors de cette étude nous avons aussi récupéré et analysé les complexes issus de la réaction de catalyse. Il est intéressant de noter que lorsque le complexe amine **1** a été prétraité ou que le complexe imine **2** a été utilisé comme catalyseur, le pourcentage de fonctions imine sur le complexe est resté inférieur à 15 % de la première minute jusqu'à la fin de la réaction catalytique

(Fig.17). La formation du complexe amine peut être attribuée à la réaction de l'aminotriazole **a** avec le complexe imine **2**. Par ailleurs, lorsque le complexe amine **1** a été utilisé sans prétraitement et que la réaction catalytique est terminée, le complexe récupéré correspondait au complexe amine **1** avec des traces de fonctions imine. Les complexes récupérés avant la fin de la réaction catalytique, correspondent parfaitement au complexe amine **1** (mêmes spectres IR et XRD et propriétés de transition de spin similaires).

L'analyse par MEB a révélé que lorsque le complexe amine était prétraité ou que le complexe imine **2** était utilisé comme catalyseur, les particules des complexes amines récupérés suite à la réaction de catalyse présentent des tailles et des formes significativement différentes de celles du complexe amine **1** (Fig.18). Ainsi, la réalisation d'une réaction PSM avec un aldéhyde suivie d'une réaction PSM sur le complexe d'imine **2** avec l'aminotriazole **a** permet de modifier la morphologie des particules du complexe d'amine **1** sans compromettre ses propriétés à transition de spin. Cette découverte est importante non seulement pour la catalyse hétérogène, où la taille et la forme des particules influencent l'activité catalytique, mais aussi pour l'intégration des composés à TS dans des dispositifs.

A noter que lorsque le complexe imine de fer III est utilisé comme catalyseur, à la fin de réaction de catalyse le complexe récupéré ne correspond pas au complexe amine **1**. Ce résultat montre que, si la présence de traces de complexes de fer(III) ne puisse être totalement exclue, dans leurs quasi intégralités le complexe amine **1** prétraité ainsi que le complexe imine **2** sont restés à l'état d'oxydation +II pendant les réactions de prétraitement et de catalyse.

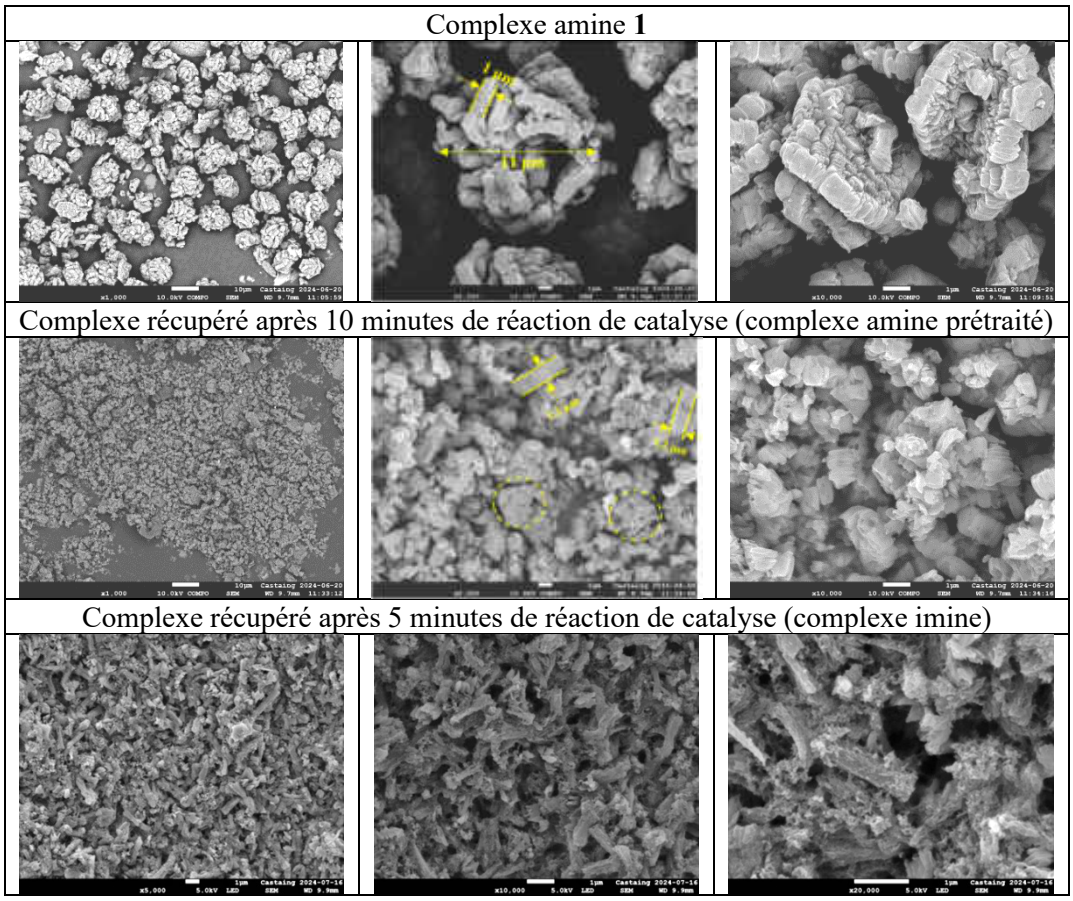


Fig.18 Images MEB du complexe **1**et des complexes récupérés après la catalyse

Nous sommes alors intéressé à la formation du complexe amine **1** par réaction PSM sur le complexe imine **2** avec l'aminotriazole **a**. Nous avons proposé deux mécanismes possibles pour cette réaction PSM : la trans-imination et l'échange de ligands au niveau du centre ferreux. Des expériences utilisant l'aminotriazole **a*** avec ^{15}N suggèrent que la réaction PSM se déroule principalement par échange de ligand (Fig.19).

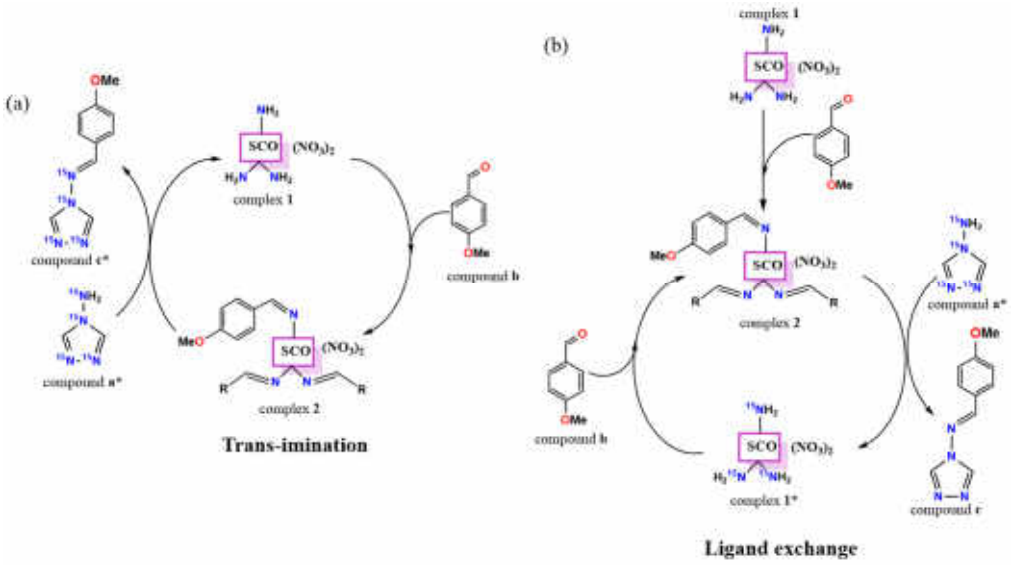


Fig.19 Mécanismes envisagés pour la formation du complexe **1** à partir du complexe **2**

Finalement nous nous sommes interrogé sur le mécanisme de l'activité catalytique du complexe à transition de spin dans cette réaction. Il est connu que la formation d'imines à partir d'aldéhydes est catalysée efficacement par des acides de Lewis et que les complexes de fer peuvent jouer le rôle d'un acide de Lewis. L'activité catalytique du complexe d'imine de fer(III) s'est avérée comparable à celle du complexe d'imine de fer(II). Ceci est surprenant, car les complexes de fer(III) sont généralement des acides de Lewis plus puissants que leurs homologues de fer (II). Par conséquence, nous pensons qu'il est peu probable que le mécanisme de réaction soit de type acide de Lewis. Nous imaginons que le mécanisme pourrait impliquer les deux types de réactions PSM décrites dans ce chapitre (Fig.20).

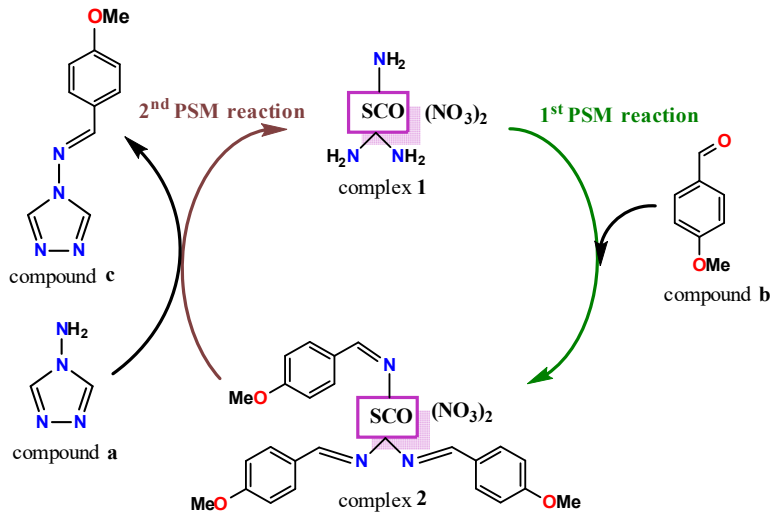


Fig.20 Le mécanisme de catalyse pourrait impliquer les deux types de réactions PSM suivants

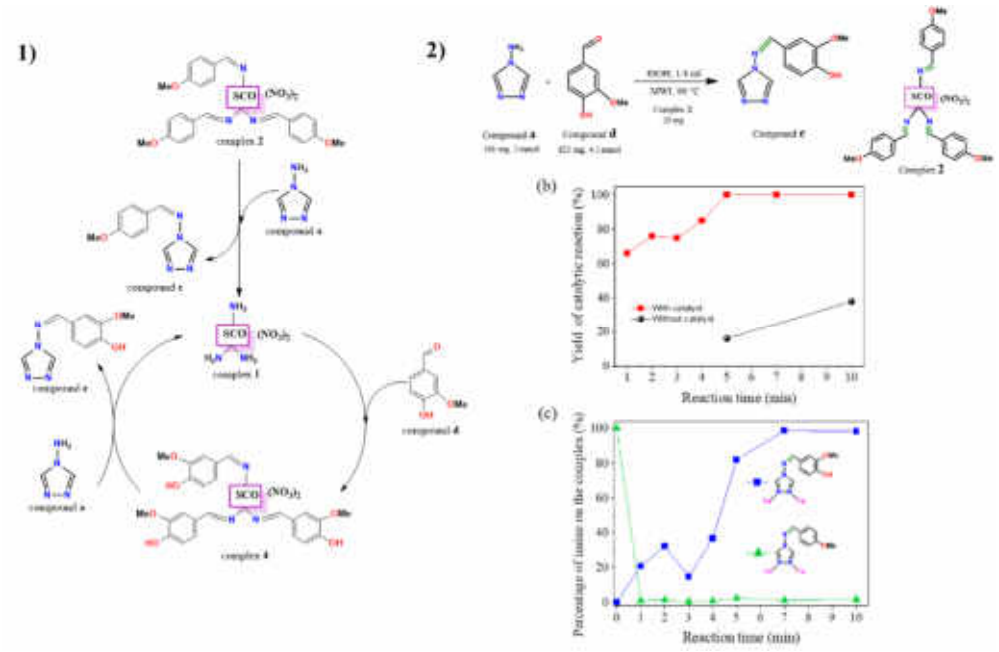


Fig.21 1) Mécanismes proposés pour la formation du complexe **4** à partir du complexe **2**, 2) Étude cinétique de la réaction catalytique entre la vanilline et l'aminotriazole, où le complexe 2 est utilisé comme catalyseur. a) Rendement de l'imine e en fonction du temps de réaction (avec et sans catalyseur) ; b) pourcentage des fonctions imine sur le complexe (à partir de la vanilline en bleu, et du p-anisaldéhyde en vert) en fonction du temps de réaction.

Deux types d'expériences ont été réalisés pour vérifier cette hypothèse. La première série d'expériences a montré qu'après seulement une minute de catalyse, très peu de fonctions imine du complexe **2** initial subsistaient, alors que des fonctions imine provenant de l'aldéhyde **d** utilisé comme substrat catalytique étaient visibles sur le complexe (Fig.21). Ce résultat suggère que le complexe amine peut rapidement subir de multiples cycles catalytiques impliquant deux réactions PSM, un facteur crucial pour l'implication des réactions PSM dans le mécanisme catalytique.

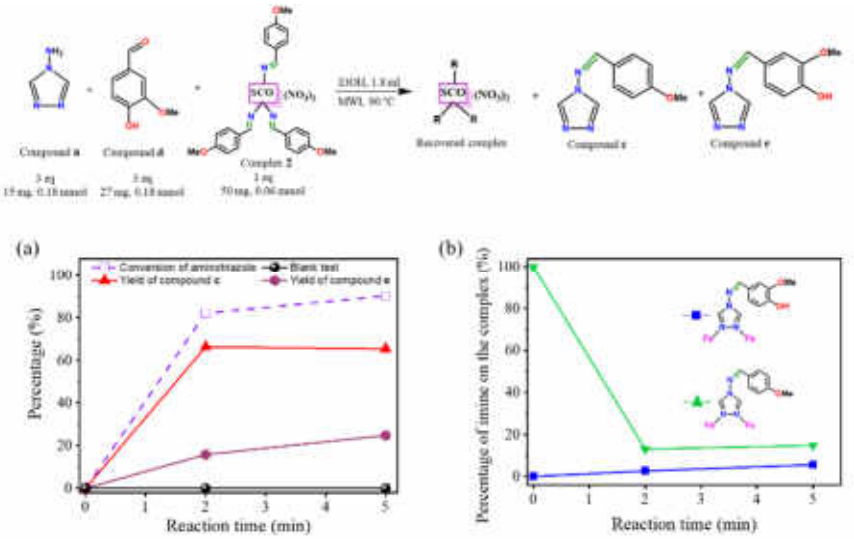


Fig.22 Étude cinétique de la réaction compétitive de l'aminotriazole a entre la vanilline d et le complexe **2**. a) Rendements des imines **c** (rouge) et **e** (violet) en fonction du temps de réaction ; b) pourcentage des fonctions imines sur le complexe (de la vanilline en bleu, et du *p*-anisaldéhyde en vert) en fonction du temps de réaction.

Le deuxième type d'expérience implique une réaction compétitive dans laquelle le mélange réactionnel contient des quantités stœchiométriques d'aminotriazole **a**, d'aldéhyde et de complexe d'imine **2** (Fig.22). L'attaque préférentielle de l'aminotriazole **a** sur le complexe imine **2** plutôt que sur l'aldéhyde est en faveur du mécanisme impliquant des réactions PSM. En effet, selon un mécanisme de type acide de Lewis, la présence du complexe en quantités non catalytiques aurait fortement favorisé l'attaque de l'aminotriazole **a** sur l'aldéhyde et nous aurions ainsi obtenu principalement l'imine **e**.

En conclusion nous avons démontré que dans des conditions appropriées, il est possible de passer d'une réaction PSM quantitative sur le complexe $Fe(NH_2trz)_3(NO_3)_2$ avec un aldéhyde, à l'utilisation efficace de ce complexe comme catalyseur pour la formation d'imine en ajoutant simplement de l'aminotriazole à la réaction. De plus, il s'agit du premier exemple dans lequel l'espèce catalytiquement active est le complexe à transition de spin. Par ailleurs, nous avons observé que la réalisation de deux réactions PSM, permettait de moduler la taille et la forme des particules du complexe amine **1**. Enfin, ces résultats illustrent que même si un mécanisme d'une réaction est bien connu dans la littérature, il est important de réfléchir à la réaction dans sa globalité car le mécanisme peut fortement dépendre des substrats de catalyse ainsi que du catalyseur. Cette recherche, combinée aux résultats décrits dans le chapitre 2 sur la forte influence de l'état de spin sur l'efficacité de la méthode PSM sur ce complexe de fer, suggère que les complexes à transition de spin pourraient être des candidats prometteurs pour le développement de la catalyse commutable.

Chapitre 4 : Effet de l'état de spin sur l'activation catalytique de la réaction d'acétalisation

Les travaux de recherche décrits dans ce chapitre avaient pour objectif de déterminer la capacité de l'état de spin du fer à moduler l'activité catalytique du complexe à TS de formule $[Fe(NH_2trz)_3](NO_3)_2$. Nous avions anticipé que la réaction de catalyse devait remplir différentes conditions : 1) la possibilité de réaliser la réaction dans l'éthanol. Ce solvant facilite la séparation des chaines polymériques du complexe **1**, ce qui permet que le complexe soit réactif. ; 2) qu'elle puisse être effectuée à 55°C. Cette température se situe au milieu du cycle d'hystérésis des particules de complexe **1** en suspension dans l'éthanol. Ainsi on pourra tester les deux états de spin du complexe **1** dans les mêmes conditions expérimentales. ; 3) qu'un des réactifs soit l'aldéhyde. En effet, dans les chapitres précédents nous avons vu que le complexe **1** est réactif vis-à-vis des aldéhydes aromatiques; 4) il serait préférable que cette réaction soit facilement mise en œuvre et qu'on puisse déterminer le rendement de la réaction sans avoir à isoler le produit formé. Pour toutes ces raisons, l'acétalisation du *p*-anisaldéhyde dans l'ethanol, en présence de triéthylorthoformate, a été choisie comme modèle de réaction.



Fig.23 Modèle de réaction choisi pour étudier l'effet de l'état de spin sur l'efficacité catalytique du complexe

Il est important de préciser que tous les résultats présentés dans cette partie ont été reproduits plusieurs fois et ils sont représentatifs de tous les lots de complexe **1** examinés. Par ailleurs, les réactions sans complexe, effectuées systématiquement en parallèle des réactions catalytiques, ne permettent pas la formation du produit souhaité. Ainsi le complexe **1** catalyse bien la réaction d'acétalisation. Enfin, les suivis cinétiques ont été effectués en conduisant des réactions distinctes pendant le temps nécessaire, plutôt qu'en prélevant un échantillon identique du même milieu réactionnel à plusieurs reprises.

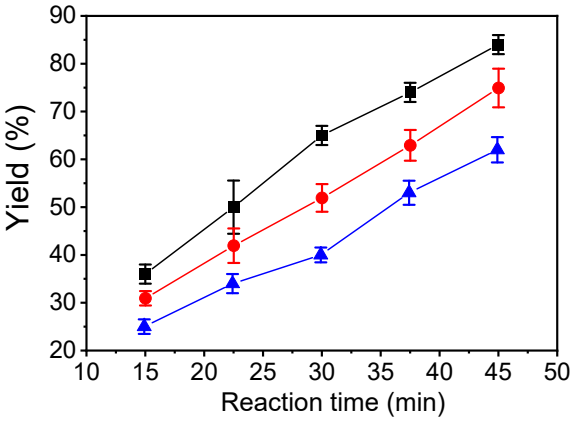


Fig.24 Rendement moyen de la réaction d'acétalisation, les barres d'erreur signifient l'écart-type calculé à partir de trois séries d'expériences ; spécificités de la réaction : 10 mg de complexe, 2 mmol de *p*-anisaldéhyde, 5 mmol de $CH(OEt)_3$ et 483 µl d'EtOH ; temps de réaction = 15, 22, 30, 37 et 45 min, température de réaction = 55 °C.

Une première étude cinétique a été réalisée trois fois, et les courbes de la Fig.24 représentent la moyenne des valeurs obtenues lors de ces suivis. Quel que soit le temps, les rendements des réactions catalysées par le complexe **1** dans l'état HS sont plus élevés que ceux des réactions catalysées par le complexe dans l'état BS2. Nous observons que la différence de rendements, entre les expériences réalisées à partir du complexe **1** à l'état HS et celles réalisées à partir de l'état BS2, peut atteindre une dizaine de pourcents.

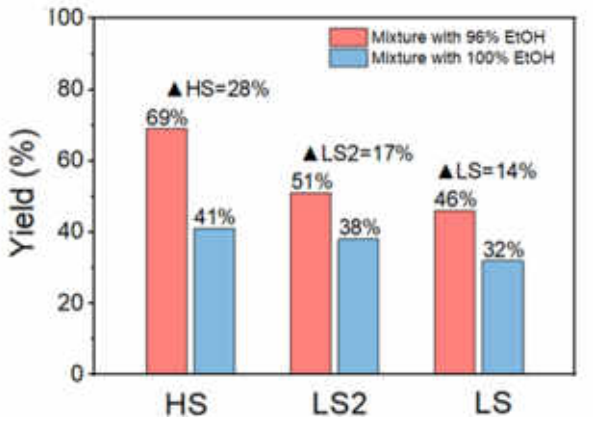


Fig.25 Comparaison du mélange avec 96% d'EtOH et l'EtOH absolu en utilisant le complexe **1**. Réaction effectuée à 55 °C, 30 min.

Par ailleurs, nous avons constaté que l'ajout d'une petite quantité d'eau au bon moment accélérait considérablement la réaction. C'est d'autant plus intéressant que cette accélération est plus

marquée pour le complexe **1** à l'état HS que pour les états bas spin (Fig. 4-12). Ainsi la présence de cette faible quantité d'eau dans le milieu réaction permet d'accroitre la différence d'activité catalytique entre les états de spin du complexe. Nous pensons que cette augmentation de différence d'activités catalytiques entre les états de spin du complexe **1** en présence de l'eau pourrait résulter d'une différence d'interaction entre l'eau et les chaînes polymérique du complexe **1**. En effet, nous pensons que l'eau interagisse plus fortement avec le complexe à l'état HS qu'avec le complexe à l'état BS2. L'eau étant encore plus efficace que l'éthanol pour séparer les chaînes polymériques, l'accès aux sites catalytique par l'aldéhyde devrait ainsi être favorisée si le complexe **1** est à l'état HS.

Les suivis cinétiques montre que la différence de rendement des réactions catalysées par les états HS et BS2 du complexe **1** peut atteindre jusqu'à 21% en présence d'EtOH à 96% et 14% dans l'EtOH absolu (Fig. 4-13). Les réactions en présence d'EtOH à 96% sont plus rapides que celles dans l'EtOH absolu. Les plus grandes différences de rendement entre ces deux types de milieu réactionnel sont observées lorsque les réactions sont catalysées par le complexe **1** à l'état HS. En effet, les réactions catalysées par le complexe HS **1** dans l'EtOH absolu nécessitent une durée supplémentaire d'environ 20 à 30 minutes pour obtenir un rendement identique à celui observé en présence d'EtOH à 96%. Par ailleurs pour des rendements comparables des réactions à partir du complexe **1** à l'état HS, la différence d'activité catalytique entre les états HS et BS2 est légèrement supérieure en présence d'EtOH à 96%. Par exemple, pour un temps de réaction de 30 minutes et en présence de d'EtOH à 96%, une différence de rendement entre les états HS et BS2 de 17% est observée, alors que pour un temps de réaction de 50 minutes dans l'EtOH absolu, la différence d'activité des états HS et BS2 est de 14%.

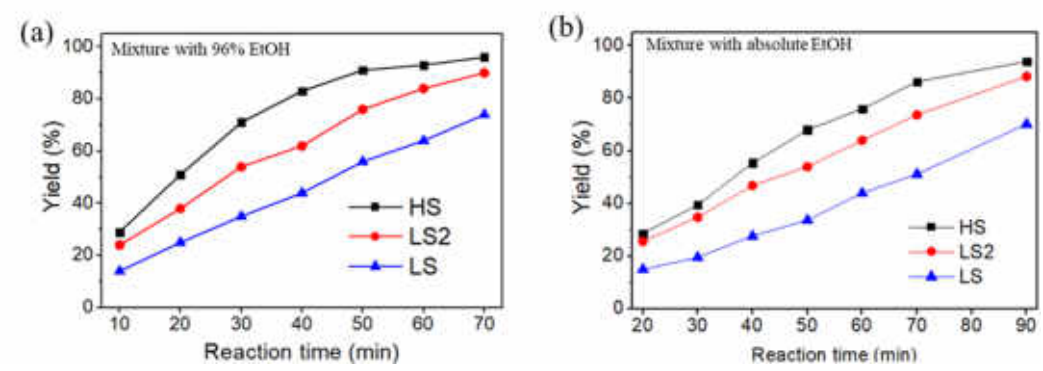


Fig.26 Étude cinétique des réactions catalytiques réalisées dans l'EtOH absolu ou en présence d'EtOH à 96%.

Par la suite nous avons cherché à déterminer si nous pouvions réduire le rapport entre la masse du catalyseur et celle de l'aldéhyde. Ainsi nous avons maintenu la même masse de catalyseur tout en augmentant graduellement la quantité d'aldéhyde dans le milieu. Pour conserver une concentration en aldéhyde constante nous avons aussi augmenté la quantité de l'éthanol et des autres réactifs. Cette étude avait deux objectifs principaux : 1) déterminer le pourcentage molaire minimum requis en catalyseur pour assurer une réaction d'acétalisation efficace. 2) tenter d'accroitre la différences d'activité catalytique entre les deux états de spin du complexe 1. L'augmentation de la dispersion des particules d'un catalyseur hétérogène contribue parfois à son efficacité catalytique. Cependant, une réduction de la quantité du catalyseur par rapport à l'aldéhyde pourrait entraîner une diminution des rendements. Ainsi la masse optimale de catalyseur sera donc un équilibre entre ces deux critères. Nous espérions que la masse idéale de complexe **1** dépende aussi de l'état de spin du fer. Nous sommes ravis de constater que, selon les graphes de la Fig. 4-20, dans des conditions expérimentales similaires, l'utilisation du

complexe **1** à l'état HS a permis de produire jusqu'à 27 % d'acétal supplémentaire en comparaison du complexe à l'état BS2.

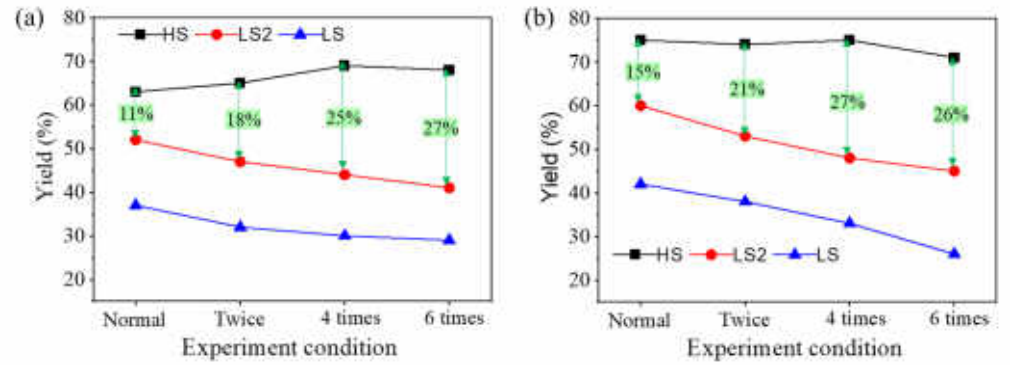
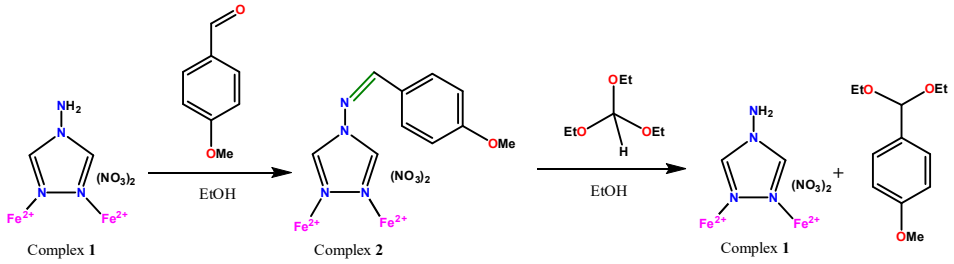


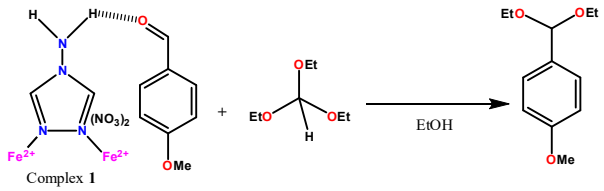
Fig.27 Rendement en acétal en fonction de l'état de spin du complexe **1** et du nombre de fois que la masse d'aldéhyde a été multipliée par rapport aux conditions standard. (a) Lot G, mélange avec EtOH absolu, temps de réaction = 70 min. (b) Lot D, mélange avec EtOH 96%, temps de réaction = 50 min.

Ensuite nous nous sommes intéressés au mécanisme catalytique (Fig.28). Trois mécanismes catalytiques possibles ont été envisagés pour le complexe **1** : un impliquant des réactions PSM, et deux impliquant soit la formation de liaisons hydrogène avec l'aldéhyde, soit l'acidité de Lewis des atomes de fer. Les expériences que nous avons réalisé ont permis d'écarter le mécanisme PSM. Nous pensons que le mécanisme le plus probable est celui qui implique l'acidité de Lewis des atomes de fer (II).

(a) Mechanism involving PSM reactions



(b) Mechanism involving hydrogen bonds



(c) Mechanism if the complex 1 acts as a Lewis acid catalyst

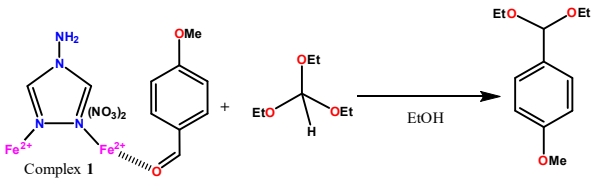


Fig.28 Mécanisme de réaction catalytique proposé, (a) impliquant des réactions PSM, (b) impliquant des liaisons hydrogène, (c) si le complexe **1** agit comme un catalyseur acide de Lewis

Enfin, pour comprendre l'origine de l'effet de l'état de spin sur l'efficacité catalytique, nous avons déterminé l'énergie d'activation de la réaction. La similarité des énergies d'activation pour les deux états de spin (Table 4-12), suggère que les divergences d'activité catalytique ne résultent pas de facteurs électroniques qui stabilisent l'état de transition. Nous pensons que la plus grande efficacité du complexe à l'état HS résulte probablement d'un accès plus aisé à ses sites actifs catalytiques.

Table 4 Énergie d'activation E_a et le préfacteur A_{arr} pour les états BS, HS et BS(2) du catalyseur.

Entrée	État de spin	E_a ($kJ\ mol^{-1}$)	A_{arr} (s^{-1})
1	BS	92.5	1.1×10^{13}
2	HS	100	3.1×10^{14}
3	BS2	95.8	5.0×10^{13}

Pour conclure, les résultats présentés dans cette étude sont très prometteurs, puisque l'état de spin du fer affecte considérablement l'activité catalytique du complexe **1**. Sur l'ensemble des lots testés, l'état HS s'avère systématiquement le plus efficace, et le rendement en acétal a été multiplié par 1,7 par rapport à l'état LS2. Nous sommes convaincus de la représentativité et de la reproductibilité des résultats car plus d'une centaine de séries d'expériences ont été réalisées (une série consiste en trois expériences menées dans les mêmes conditions expérimentales : une pour l'état HS, une pour l'état LS2 et une pour l'état LS) et sept lots du complexe **1** ont été évalués. En ajoutant une petite quantité d'eau au moment opportun, la vitesse de réaction est considérablement accrue, ce qui affecte d'avantage l'état HS que l'état BS2. Il est peut-être surprenant de constater que la différence d'activité catalytique du complexe **1** entre l'état HS et l'état BS2 s'est également accentuée lorsque la fraction massique du complexe **1** par rapport à l'aldéhyde a été ramenée de 3,68 % à 0,61 %. C'est un exemple parfait pour illustrer que l'ajout d'une plus grande quantité de catalyseur ne garantit pas nécessairement des rendements supérieurs en catalyse hétérogène. Cette étude démontre pour la deuxième fois qu'un composé synthétisé et utilisé pour ses propriétés de transition de spin peut aussi être un catalyseur efficace. Cette étude constitue une avancée considérable par rapport aux travaux antérieurs sur l'effet de l'état de spin en catalyse, puisque les composés à transition de spin permettent d'accéder aux deux états de spin en utilisant le même complexe. Les données recueillies lors de cette étude paraissent suggérer que la plus grande activité catalytique de l'état HS serait due à un accès plus efficace de l'aldéhyde aux sites catalytiques du complexe de fer. L'un des atouts majeurs, est l'opportunité d'appliquer cet effet principalement mécanique à une diversité de réactions. De plus, des recherches ultérieures seront dédiées aux réactions catalytiques susceptibles d'être davantage affectées par une modification électronique provoquée par la transition de spin du complexe **1**. Ce concept consisterait à modifier le chemin réactionnel de la catalyse en jouant sur l'état de spin du complexe. Ces travaux de recherches démontrent que nous pouvons avoir confiance quant au potentiel considérable des complexes à transition de spin dans le domaine de la catalyse commutable.

Chapitre 5 : Utilisation de films composites à base de complexe à transition de spin comme catalyseurs pour les réactions d'acétalisation

Dans ce chapitre, nous nous concentrons sur l'utilisation de films composites à TS @polymère dans les réactions d'acétalisation (Fig.29). L'intégration du complexe **1** dans une matrice polymère facilite et optimise le recyclage du catalyseur à TS.

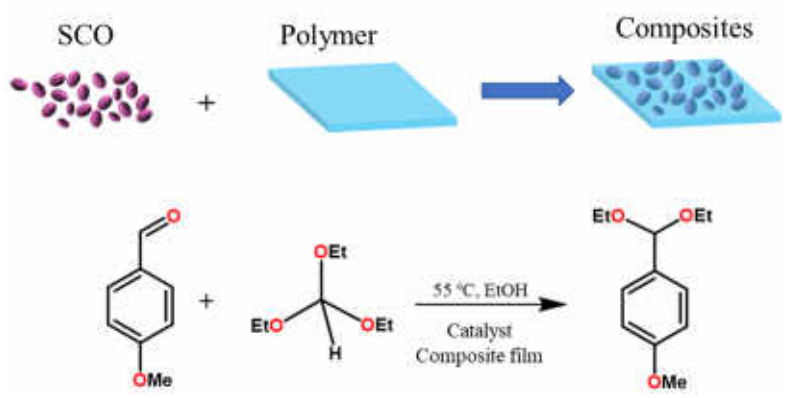


Fig.29 Acétalisation du *p-anisaldéhyde* avec l'orthoformate de triéthyle en utilisant un film composite comme catalyseur.

En effet, les films composites polymères sont apparus comme une solution prometteuse pour relever le défi de la récupération et de la réutilisation des catalyseurs, qui reste un obstacle important dans les applications industrielles. Les films composites polymères combinent les propriétés uniques des polymères- telles que la flexibilité, la durabilité et la résistance chimique - avec les capacités catalytiques des espèces actives intégrées, telles que les métaux, les oxydes métalliques, les complexes ou les enzymes. Cette intégration crée une plateforme polyvalente pour la catalyse, où les composants actifs sont immobilisés dans la matrice polymère, ce qui réduit la perte de catalyseur au cours des cycles de réaction. Par ailleurs, la structure physique de ces films permet de les séparer facilement des mélanges réactionnels, ce qui facilite leur récupération et leur réutilisation. Le potentiel des films composites polymères pour améliorer la durabilité et réduire les coûts des technologies catalytiques souligne leur importance croissante dans la recherche universitaire et la pratique industrielle.

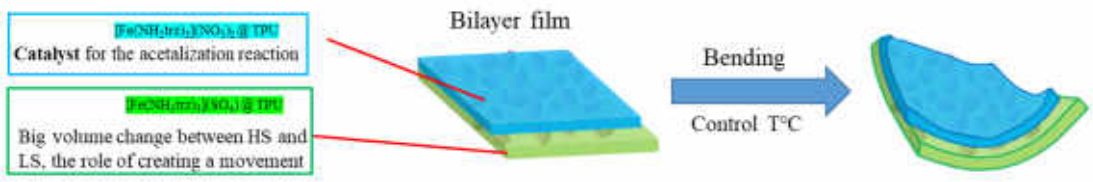


Fig.30 Croquis du matériau composite que nous envisagions de fabriquer

Par ailleurs, des études récentes ont montré que le contrôle de l'accès des substrats aux sites catalytiques des systèmes commutables permet une régulation précise et à la demande de l'activité catalytique. La catalyse commutable basée sur des matériaux à transition de spin est une approche innovante. Dans ce chapitre nous souhaitons étudier si le mouvement des films composites à TS@polymère pourrait augmenter la différence d'activité catalytique entre les deux états de spin du complexe **1**. Pour atteindre cet objectif à long terme, nous prévoyons de créer un matériau de type bicouche. Une couche contiendrait le complexe **1**, qui servirait de catalyseur, tandis que l'autre couche contiendrait un autre complexe à TS, qui garantirait le mouvement du matériau composite. Rappelons que tous les complexes à TS présentent une augmentation de 10 % de leur volume moléculaire lorsqu'ils passent de l'état BS à l'état HS. Cette augmentation du volume moléculaire entraîne toutefois une modification significative du volume de matériau que pour certains complexes à TS. L'ensemble de la couche polymérique s'allonge lorsque le complexe à TS, chargé d'assurer le mouvement, passe de l'état BS à l'état HS. Étant donné que les deux couches sont connectées, ce changement de volume peut entraîner

une modification de la forme du matériau composite et augmenter la porosité de la couche contenant le complexe à TS, ce qui favoriserait la catalyse de la réaction (Fig.30)

Différents types de films composites, y compris des films monocouches, bicouches et tricouches, ont été fabriqués à l'aide de la méthode de coulée de lames (Fig.31 et Fig.32).

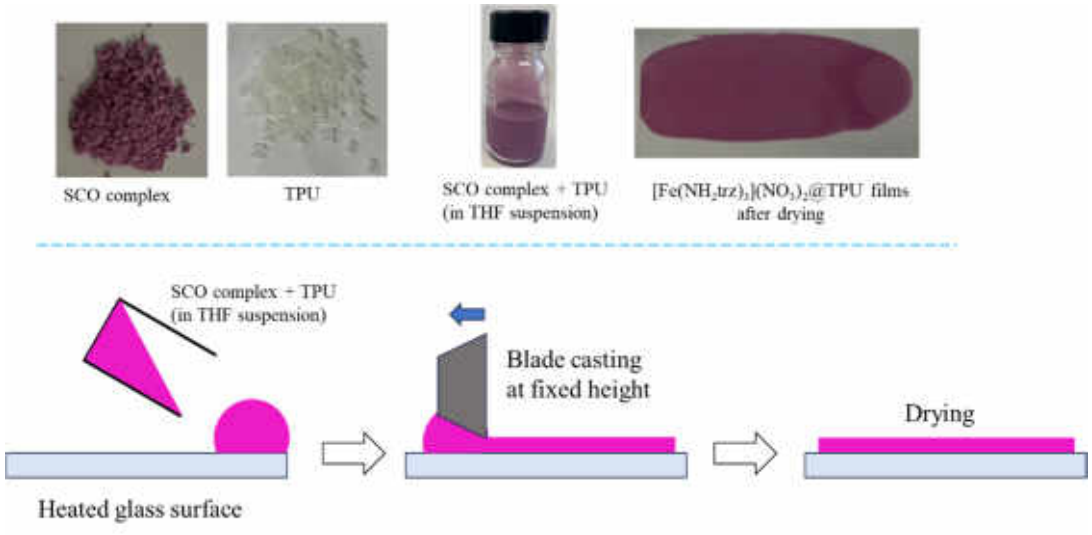


Fig.31 Schéma de la méthode de moulage des lames pour fabriquer le film composite

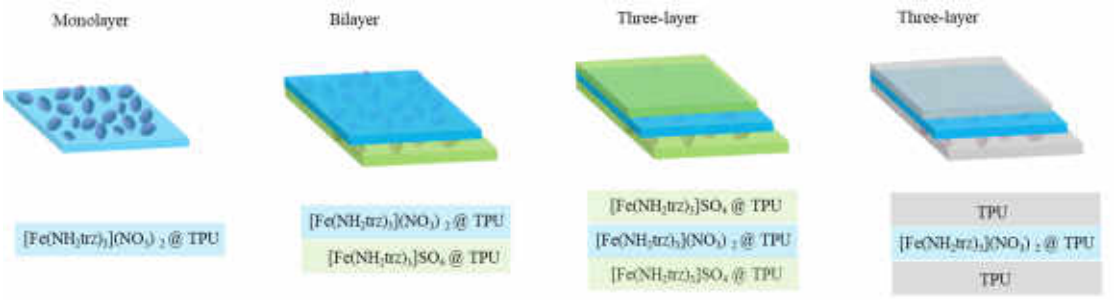


Fig.32 Présentation schématique des films composites monocouche, bicouche et tricouche.

Suite à la fabrication de ces matériaux composites nous avons notamment souhaité déterminer si la transition de spin pourrait engendrer un mouvement du matériau. Nous avons constaté que le film bicouche demeurait plat à température ambiante et qu'il ne changeait pas de forme une fois chauffé à 70°C. Cependant, lorsque le film bicouche a été immergé dans de l'EtOH, il a commencé à se plier même à température ambiante (Fig.33). Plus précisément, le film a commencé à se plier à partir de ses bords, potentiellement en raison de l'absorption d'EtOH. Après avoir été chauffé à 70°C, le film a changé de couleur, passant du rose au blanc, et s'est simultanément enroulé en forme de tube dans l'alcool éthylique, montrant ainsi un comportement d'auto-enroulement. Le film conserve sa forme tubulaire même à température ambiante ou après son séchage à l'étuve.

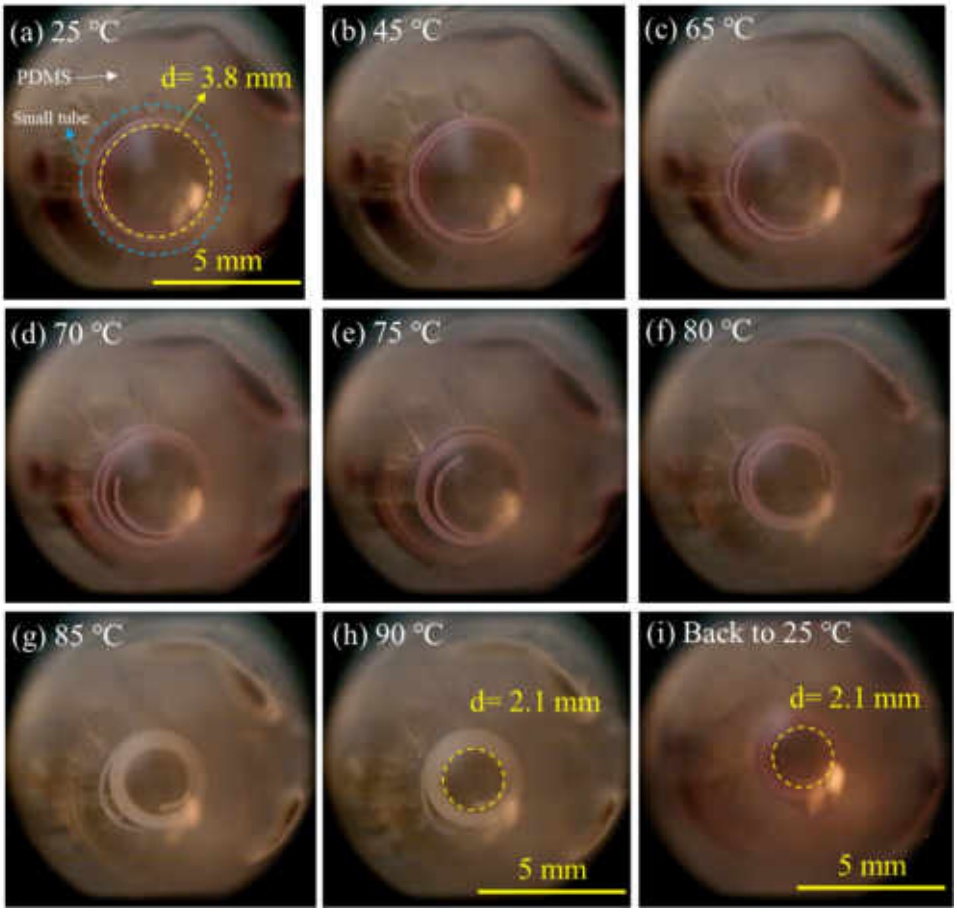


Fig.33 Image optique à différentes températures du processus d'auto-laminage du film bicouche.

Nous avons d'abord testé l'efficacité catalytique du film monocouche $[Fe(NH_2trz)_3](NO_3)_2$ @TPU dans la réaction d'acétalisation du *p*-anisaldéhyde en présence de triéthylorthoformate dans l'EtOH à 55 °C. Après la réaction, le film a été lavé avec de l'EtOH et séché avec du papier, puis réutilisé comme indiqué dans la Fig.5-27.

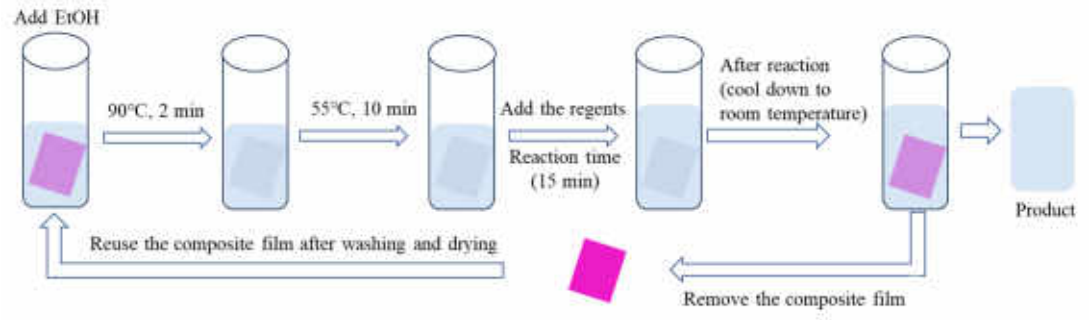


Fig.34 Schéma de la voie de réutilisation des films $[Fe(NH_2\ trz)_3](NO_3)_2$ @TPU comme catalyseur

Comme le montre la Fig.35, l'utilisation du film permet d'obtenir des rendements en acétal supérieur à 90% en 15 minutes. Par ailleurs, le film peut être réutilisé 11 fois sans perte significative d'efficacité catalytique. Il est important de noter que la masse totale du film est de 13 mg, dont seulement 3,25 mg de catalyseur. Au cours de ces 11 essais, le film a conduit à la production de 4,02 g d'acétal. Cela indique une capacité catalytique et une réutilisation

excellentes. Il convient de souligner que le film apparaît rose lorsque la matrice TPU renferme une quantité significative du complexe à TS, tandis que cette teinte se révèle plus claire lorsqu'il y a moins de complexe à TS présent dans le matériau. De ce fait, la modification de couleur du film composite donne un indice sur son efficacité catalytique. Ceci est notamment bénéfique pour identifier si la réaction demeurera efficacement catalysée si le nous réutilisons le film. Par exemple, le film utilisé neuf fois à une légère teinte rose, ce qui indique qu'il peut encore être réutilisé pour catalyser efficacement la réaction.

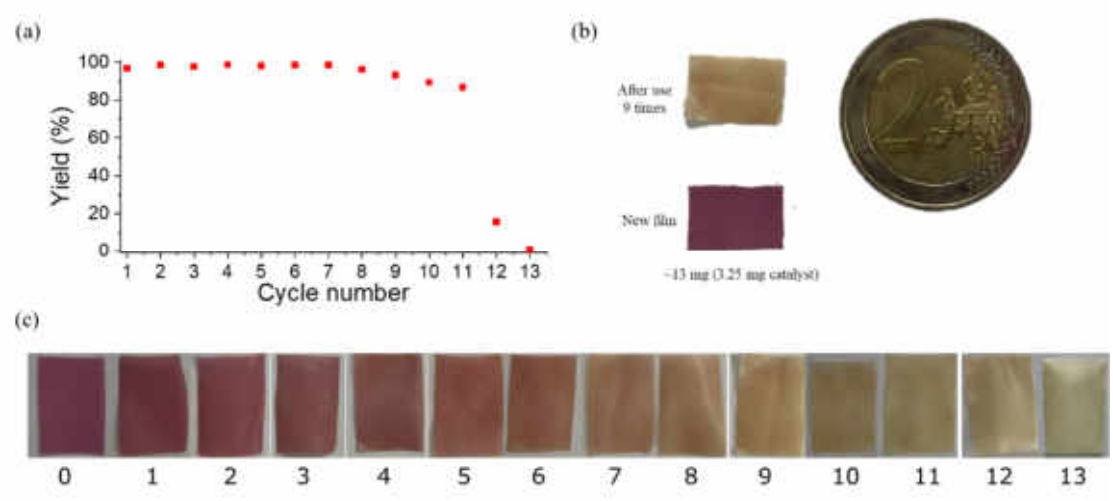


Fig.35 Rendement de la réaction et répétitions catalysées par les films **M1**. (b) et (c) les photos du film après utilisation.

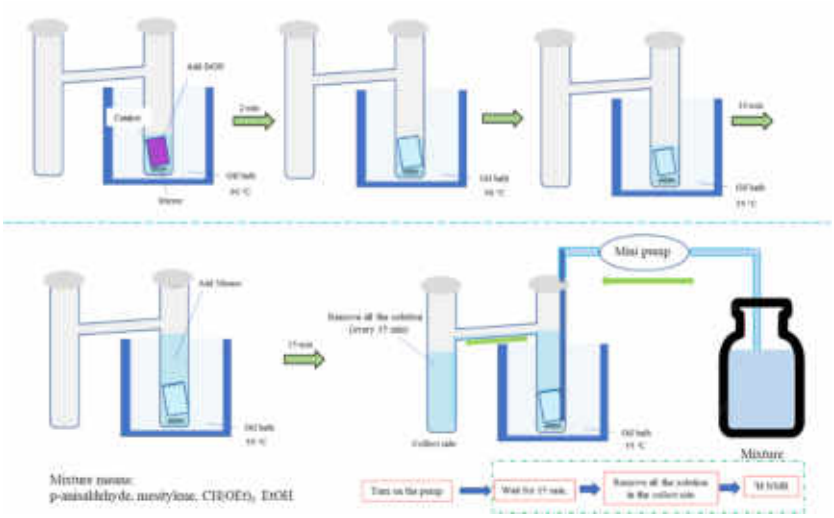


Fig.36 Le système de travail utilise un tube H et une mini-pompe pour ajouter le réactif. Le film utilisé dans l'état HS est un exemple.

Nous avons bien évidemment commencé à examiner l'effet de l'état de spin du fer sur l'activité catalytique des particules de complexe **1** intégrées dans la matrice polymérique. Cette étude n'était pas possible en utilisant le système illustré dans la Fig.5-27. Ainsi, nous nous sommes inspiré de la chimie en flux continu pour concevoir un montage qui nous permettrait de faire l'étude souhaitée tout en exploitant le matériel disponible dans notre laboratoire. Comme le montre la Fig.36 notre système de travail se compose d'un tube en H et d'une mini-pompe pour

ajouter le réactif. Il faut d'abord placez d'abord le film composite sur le côté droit du tube en H et ajoutez 2 mL d'EtOH. Ensuite, placer le tube H dans un bain d'huile préchauffé à 90 ℃ pendant 2 minutes (étape nécessaire que pour les états HS et BS2). La couleur du film passe du rose au blanc. Après 2 minutes, transférer le tube en H dans un autre bain d'huile préchauffé à et attendre 10 minutes, puis ajouter 2 ml du mélange et connecter le tube en H à la mini-pompe. Le niveau de la solution est approximativement atteint par le pont du tube H. Après 15 minutes, mettre la mini-pompe en marche, le mélange est ajouté automatiquement et la solution s'écoule vers le côté gauche du tube en H (côté collecteur). Toutes les 15 minutes, les solutions sur le côté de collecte seront enlevées, et le rendement sera mesuré en utilisant ^{1}H NMR.

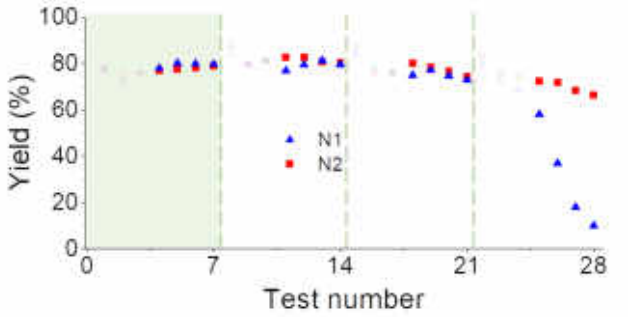


Fig.37 Performance catalytique du film composite testé en HS et BS2, la vitesse d'ajout est de 7,5 ml par 15 minutes.

Deux films composites, **N1** et **N2**, ont été préparés pour cette expérience. Ces deux films ont pratiquement la même forme et la même masse. La masse des films **N1** et **N2** est de 49,9 et 50,2, contenant respectivement 12,5 et 12,6 mg de catalyseur. Ces deux films ont été testés pendant 7 essais le même jour en utilisant le même mélange. Au début de l'expérience, comme nous avons utilisé de l'EtOH pour préparer le film à l'état HS et à l'état BS2, la concentration des réactifs était inférieure à celle du mélange. Par conséquent, les 3 premiers essais ne seront pas pris en compte (en couleur plus claire dans la Fig.5-35). Pour vérifier que ces deux films ont des propriétés catalytiques similaires, ils ont d'abord été testés tous les deux à l'état HS (Fig.5-35, fond vert). D'après les résultats de la Fig.5-35, on peut observer que le rendement de **N2** (à l'état HS) est très légèrement supérieur à celui de **N1** (à l'état BS2) entre 7 et 21 cycles d'essai. Cependant, après 21 cycles d'essai, la différence de rendement entre **N1** et **N2** devient importante. Cela pourrait être attribué au fait que le film utilisé dans l'état BS2 libère plus de complexe dans la solution que dans l'état HS. Par conséquent, après 21 tests, il n'y a plus assez de complexe à TS dans **N1** pour catalyser la réaction.

En outre, nous avons également testé les performances catalytiques de films bicouches et tricouches. Tous ces films ont fait preuve d'une grande efficacité catalytique et d'une remarquable réutilisabilité dans des conditions de flux continu et discontinu.

Il nous a semblé essentiel d'étudier à la fois les propriétés et la morphologie des particules du complexe inclus dans la matrice polymérique. Au lieu d'utiliser des films bicouches ou tricouches, le film monocouche a été choisi pour cette étude, car son unique couche catalytique simplifie la caractérisation et l'analyse. Douze petits morceaux, pesant chacun environ 13 mg, ont été découpés dans le même grand film pour être utilisés dans quatre expériences (A, B, C et D), comprenant respectivement 7, 14, 21 et 28 essais (Fig.38). Chaque expérience comprenait trois films testés dans les états HS, BS2 et BS.

Après leurs utilisations comme catalyseurs, les films ont été analysés à l'aide des techniques XRD, IR, réflectivité optique et MEB. En général, l'activité catalytique des films utilisés dans l'état HS était légèrement supérieure à celle des films utilisés dans l'état BS2. Lorsque les films ont été utilisés dans l'état BS, plusieurs cycles d'activation ont été nécessaires avant que les films puissent catalyser la réaction de manière efficace (Fig.38).

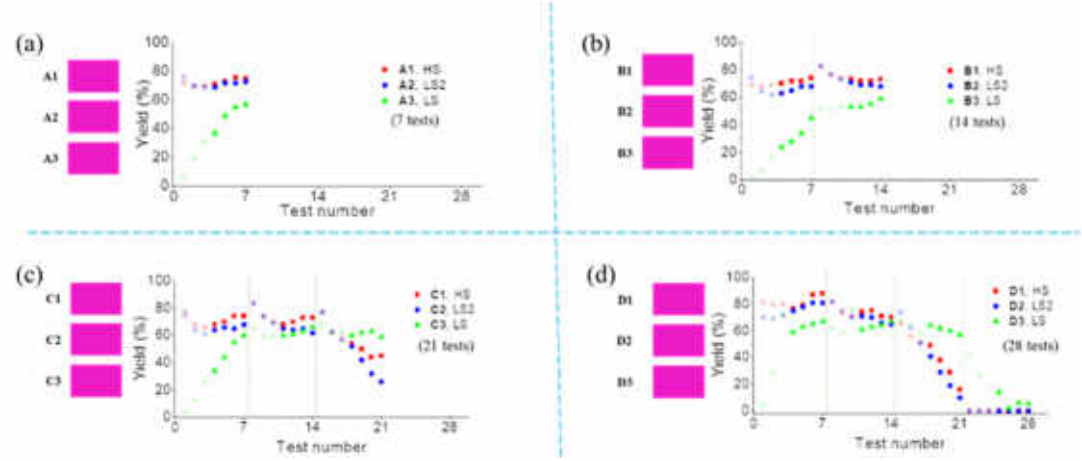


Fig.38 Le résultat des rendements des expériences A, B, C, D.

D'après les résultats de la réflectivité optique, de la spectroscopie infrarouge (IR), de la diffraction des rayons X (XRD) et de la microscopie électronique à balayage (MEB), semble indiquer un relargage progressif des particules de complexes en solution. Fig.39 et Fig.40 montrent la morphologie de la section transversale des films monocouches avant et après utilisation. La formation de pores et de vides dans la matrice polymère, en particulier après une utilisation prolongée est observée. Par ailleurs, il convient de souligner que la réaction catalytique se produit principalement dans le film bien que les particules de complexes en solution puissent également catalyser le processus.

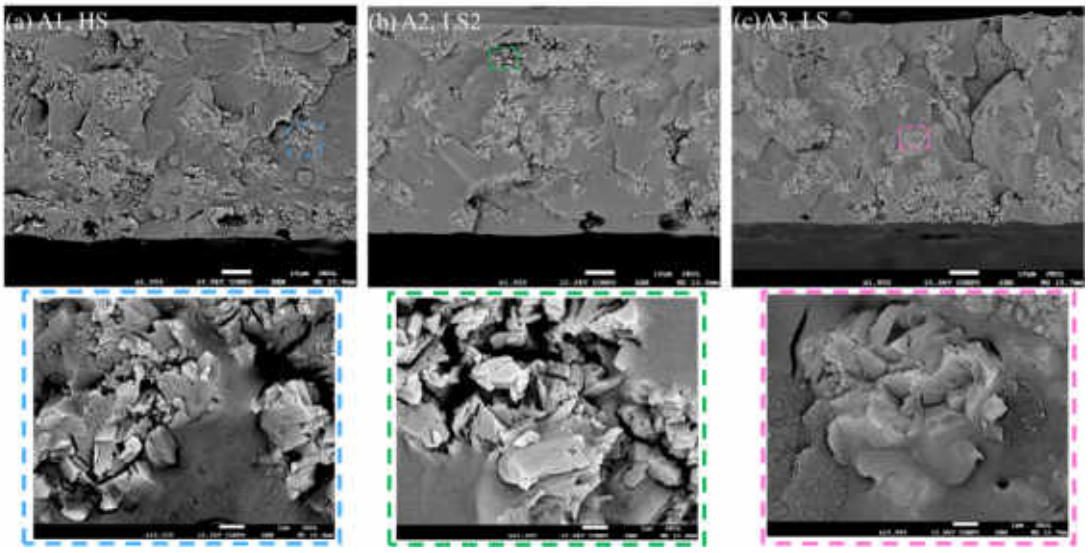


Fig.39 Images MEB de la section transversale du film monocouche de l'expérience A après sept cycles de test et images de la cartographie EDX correspondante. (a) **A1** (HS). (b) **A2** (BS2). (c) **A3** (BS).

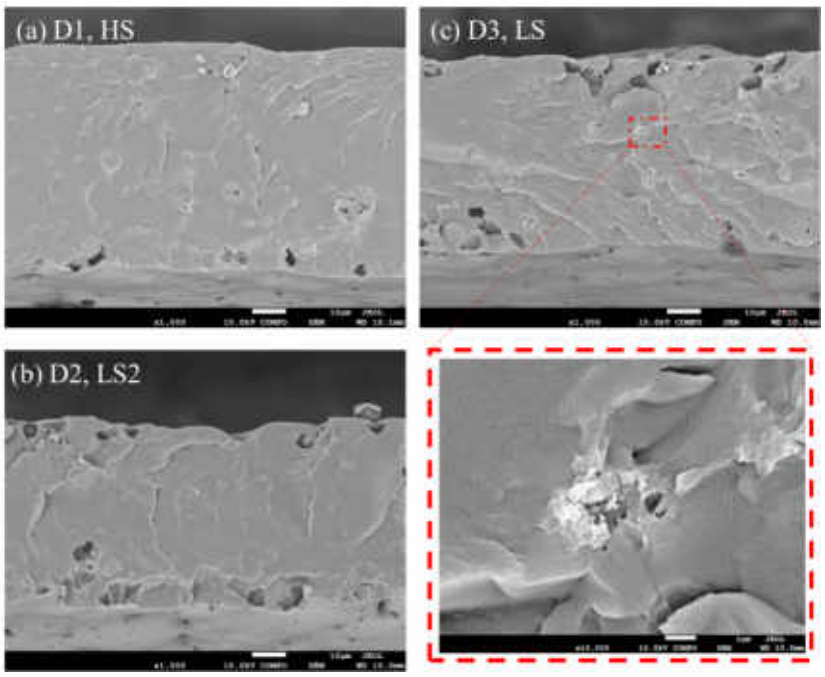


Fig.40 Images SEM de la section transversale du film composite après 28 passages. (a) **D1**. (b) **D2**. (c) **D3**

En conclusion, ce chapitre a présenté la fabrication de matériaux composites à base de complexes à transition de spin ainsi que leurs utilisations comme catalyseurs d'une réaction d'acétalisation. Ces films composites ont fait preuve d'une grande efficacité catalytique et d'une réutilisation exceptionnelle dans des conditions de flux continu et discontinu. Le complexe à l'état HS contenu dans ces films a systématiquement conduit à des rendements catalytiques légèrement plus élevés que ceux à l'état bas spin. Par ailleurs, les films composites bicouches ont présenté un comportement d'auto-enroulement en présence d'éthanol.

Conclusions générales et perspectives.

Cette thèse étudie l'impact des états de spin du fer sur la réactivité chimique et catalytique du complexe à transition spin de coordination (SCO) fer(II)-triazole, $[Fe(NH_2trz)_3](NO_3)_2$ (complexe **1**), dans le but d'utiliser les complexes SCO pour des applications en catalyse commutable. Tout d'abord, nous avons démontré l'effet des états de spin sur l'efficacité de la modification post-synthétique (PSM) sur le complexe **1**, révélant une amélioration significative de 22% de l'efficacité de la PSM dans l'état de spin bas (BS) par rapport à l'état de spin haut (HS). À notre connaissance, il s'agit du premier cas documenté dans lequel l'état de spin d'un métal influence directement la réactivité organique d'un groupe fonctionnel au sein d'un complexe métallique.

Par la suite, nous avons démontré que, dans des conditions appropriées, une simple addition d'aminotriazole au milieu réactionnel permet de passer d'une réaction PSM quantitative sur le complexe **1** avec un aldéhyde à l'utilisation du complexe SCO comme catalyseur pour la formation d'imines à partir de l'aminotriazole. L'analyse des complexes post-catalytiques a indiqué que les réactions PSM peuvent jouer un rôle dans le mécanisme catalytique du complexe SCO. Cette étude présente le premier cas où l'espèce catalytique active est le complexe SCO lui-même dans un complexe SCO 1D fer(II)-triazole.

Nous étudions ensuite comment les états de spin modulent l'activité catalytique dans

l'acétalisation du *p*-anisaldéhyde avec l'orthoformate de triéthyle. Dans des conditions expérimentales strictement identiques, la réaction effectuée en présence du complexe HS a donné jusqu'à 27 % d'acétal en plus que lorsque la réaction a été effectuée avec le complexe LS. Cela signifie que le complexe HS est beaucoup plus efficace pour catalyser la réaction d'acétalisation que le complexe LS. Les études menées pour comprendre l'origine de l'effet de l'état de spin sur l'activité catalytique du complexe SCO suggèrent que la différence d'activité observée est due à un changement dans l'accès du substrat au site catalytique.

Enfin, nous avons fabriqué des films composites en polymère SCO, qui ont été utilisés comme catalyseurs d'acétalisation. Ces films ont démontré une efficacité catalytique élevée et une réutilisation dans des conditions de traitement par lots et de flux continu. En particulier, les films composites bicouches ont présenté un comportement d'auto-enroulement en présence d'EtOH, ce qui a démontré leur polyvalence. Dans l'ensemble, les films composites facilitent la récupération du catalyseur et améliorent la stabilité et la longévité du système catalytique, ce qui les rend très prometteurs pour les applications catalytiques réutilisables et commutables.

Les résultats de cette thèse indiquent que les complexes SCO peuvent être utilisés efficacement dans les systèmes catalytiques, l'état de spin jouant un rôle crucial dans la modulation de l'activité catalytique, soulignant leur potentiel pour le développement de systèmes catalytiques commutables basés sur le phénomène SCO. Pour continuer à développer des systèmes catalytiques commutables utilisant des complexes à spin croisé, les travaux futurs devraient se concentrer sur l'amélioration du système catalytique, l'exploration de la synergie entre la performance catalytique et le mouvement mécanique dans les films bicouches, et l'étude de l'utilisation de ces complexes SCO dans une variété de réactions catalytiques.

Références

[1] M.A. Halcrow, The effect of ligand design on metal ion spin state—lessons from spin crossover complexes, *Crystals* **2016**, 6, 58.

[2] A. Bousseksou, G. Molnár, L. Salmon, W. Nicolazzi, Molecular spin crossover phenomenon: recent achievements and prospects, *Chem. Soc. Rev.* **2011**, 40, 3313-3335.

[3] G. Molnár, S. Rat, L. Salmon, W. Nicolazzi, A. Bousseksou, Spin crossover nanomaterials: from fundamental concepts to devices, *Adv. Mater.* **2018**, 30, 1703862.

[4] A. Enriquez-Cabrera, A. Rapakousiou, M.P. Bello, G. Molnár, L. Salmon, A. Bousseksou, Spin crossover polymer composites, polymers and related soft materials, *Coord. Chem. Rev.* **2020**, 419, 213396.

[5] W. Nicolazzi, A. Bousseksou, Thermodynamical aspects of the spin crossover phenomenon, *C. R. Chim.* **2018**, 21, 1060-1074.

[6] C.J. O'Connor, Magnetochemistry—advances in theory and experimentation, *Prog. Inorg. Chem.* **1982**, 203-283.

[7] J.N. Harvey, R. Poli, K.M. Smith, Understanding the reactivity of transition metal complexes involving multiple spin states, *Coord. Chem. Rev.* **2003**, 238, 347-361.

[8] D. Schröder, S. Shaik, H. Schwarz, Two-state reactivity as a new concept in organometallic chemistry §, *Acc. Chem. Res.* **2000**, 33, 139-145.

[9] J.P. Lomont, S.C. Nguyen, C.B. Harris, Ultrafast infrared studies of the role of spin states in organometallic reaction dynamics, *Acc. Chem. Res.* **2014**, 47, 1634-1642.

[10] S. Shaik, D. Kumar, S.P. de Visser, A. Altun, W. Thiel, Theoretical perspective on the structure and mechanism of cytochrome P450 enzymes, *Chem. Rev.* **2005**, 105, 2279-2328.

[11] I.G. Denisov, T.M. Makris, S.G. Sligar, I. Schlichting, Structure and chemistry of cytochrome P450, *Chem. Rev.* **2005**, 105, 2253-2278.

[12] M.L. Merlini, G.J. Britovsek, M. Swart, P. Belanzoni, Understanding the catalase-like activity of a bioinspired manganese (II) complex with a pentadentate NSNSN ligand framework. A

computational insight into the mechanism, *ACS Catalysis* **2018**, 8, 2944-2958.
[13] M.H. Al-Afyouni, E. Suturina, S. Pathak, M. Atanasov, E. Bill, D.E. DeRosha, W.W. Brennessel, F. Neese, P.L. Holland, Spin Isomers and Ligand Isomerization in a Three-Coordinate Cobalt (I) Carbonyl Complex, *J. Am. Chem. Soc.* **2015**, 137, 10689-10699.
[14] L.V. Liu, S. Hong, J. Cho, W. Nam, E.I. Solomon, Comparison of high-spin and low-spin nonheme FeIII–OOH complexes in O–O bond homolysis and H-atom abstraction reactivities, *J. Am. Chem. Soc.* **2013**, 135, 3286-3299.
[15] P. Pérez, J. Andrés, V. Safont, O. Tapia, R. Contreras, Spin-philicity and spin-donicity as auxiliary concepts to quantify spin-catalysis phenomena, *The Journal of Physical Chemistry A* **2002**, 106, 5353-5357.
[16] C. Chen, T.R. Dugan, W.W. Brennessel, D.J. Weix, P.L. Holland, Z-selective alkene isomerization by high-spin cobalt (II) complexes, *J. Am. Chem. Soc.* **2014**, 136, 945-955.
[17] E.A. Glascoe, K.R. Sawyer, J.E. Shanoski, C.B. Harris, The influence of the metal spin state in the iron-catalyzed alkene isomerization reaction studied with ultrafast infrared spectroscopy, *The Journal of Physical Chemistry C* **2007**, 111, 8789-8795.
[18] K.R. Sawyer, E.A. Glascoe, J.F. Cahoon, J.P. Schlegel, C.B. Harris, Mechanism for Iron-Catalyzed Alkene Isomerization in Solution, *Organometallics* **2008**, 27, 4370-4379.
[19] S.A. Lutz, A.K. Hickey, Y. Gao, C.-H. Chen, J.M. Smith, Two-state reactivity in iron-catalyzed alkene isomerization confers σ-base resistance, *J. Am. Chem. Soc.* **2020**, 142, 15527-15535.
[20] C.M. Macaulay, S.J. Gustafson, J.T. Fuller III, D.-H. Kwon, T. Ogawa, M.J. Ferguson, R. McDonald, M.D. Lumsden, S.M. Bischof, O.L. Sydora, Alkene isomerization–hydroboration catalyzed by first-row transition-metal (Mn, Fe, Co, and Ni) N-phosphinoamidinate complexes: origin of reactivity and selectivity, *ACS Catalysis* **2018**, 8, 9907-9925.
[21] I.y.A. Gural'skiy, S.I. Shylin, V. Ksenofontov, W. Tremel, Spin-State-Dependent Redox-Catalytic Activity of a Switchable Iron (II) Complex, *Eur. J. Inorg. Chem.* **2017**, 2017, 3125-3131.
[22] I. Prat, A. Company, T. Corona, T. Parella, X. Ribas, M. Costas, Assessing the impact of electronic and steric tuning of the ligand in the spin state and catalytic oxidation ability of the FeII (Pytacn) family of complexes, *Inorg. Chem.* **2013**, 52, 9229-9244.
[23] A. Bell-Taylor, J.D. Gorden, E.E. Hardy, C.R. Goldsmith, A spin-crossover Co (II) complex catalyzes the activation of sp3 C–H bonds by two-electron oxidants, *Inorg. Chim. Acta* **2018**, 482, 206-212.
[24] M. Isegawa, Mechanism of Photocatalytic CO2 Reduction by Iron Spin-Crossover Complex with Copper Photosensitizer, *Organometallics* **2022**, 41, 3568-3580.
[25] G.-Z. Huang, Y.-S. Xia, F. Yang, W.-J. Long, J.-J. Liu, J.-P. Liao, M. Zhang, J. Liu, Y.-Q. Lan, On–off switching of a photocatalytic overall reaction through dynamic spin-state transition in a Hofmann clathrate system, *J. Am. Chem. Soc.* **2023**, 145, 26863-26870.
[26] S. Mandal, S. Natarajan, P. Mani, A. Pankajakshan, Post-synthetic modification of metal–organic frameworks toward applications, *Adv. Funct. Mater.* **2021**, 31, 2006291.
[27] J.L. Segura, S. Royuela, M.M. Ramos, Post-synthetic modification of covalent organic frameworks, *Chem. Soc. Rev.* **2019**, 48, 3903-3945.
[28] C.F. Wang, R.F. Li, X.Y. Chen, R.J. Wei, L.S. Zheng, J. Tao, Synergetic Spin Crossover and Fluorescence in One-Dimensional Hybrid Complexes, *Angew. Chem.* **2015**, 127, 1594-1597.
[29] A.D. Burrows, C.G. Frost, M.F. Mahon, C. Richardson, Post-Synthetic Modification of Tagged Metal–Organic Frameworks, *Angew. Chem.* **2008**, 120, 8610-8614.
[30] V. Valtchev, G. Majano, S. Mintova, J. Pérez-Ramírez, Tailored crystalline microporous materials by post-synthesis modification, *Chem. Soc. Rev.* **2013**, 42, 263-290.
[31] Y. Goto, H. Sato, S. Shinkai, K. Sada, "Clickable" metal− organic framework, *J. Am. Chem. Soc.* **2008**, 130, 14354-14355.
[32] J.H. Askew, H.J. Shepherd, Post-synthetic anion exchange in iron (II) 1, 2, 4-triazole based spin crossover materials via mechanochemistry, *Dalton Trans.* **2020**, 49, 2966-2971.
[33] C.F. Wang, G.Y. Yang, Z.S. Yao, J. Tao, Monitoring the Spin States of Ferrous Ions by

Fluorescence Spectroscopy in Spin‐Crossover–Fluorescent Hybrid Materials, *Chemistry–A European Journal* **2018**, 24, 3218-3224.
[34] A. Enríquez-Cabrera, L. Routaboul, L. Salmon, A. Bousseksou, Complete post-synthetic modification of a spin crossover complex, *Dalton Trans.* **2019**, 48, 16853-16856.
[35] E. Resines-Urien, L. Piñeiro-López, E. Fernandez-Bartolome, A. Gamonal, M. Garcia-Hernandez, J.S. Costa, Covalent post-synthetic modification of switchable iron-based coordination polymers by volatile organic compounds: a versatile strategy for selective sensor development, *Dalton Trans.* **2020**, 49, 7315-7318.
[36] A. Enríquez‐Cabrera, K. Ridier, L. Salmon, L. Routaboul, A. Bousseksou, Complete and versatile post‐synthetic modification on iron‐triazole spin crossover complexes: a relevant material elaboration method, *Eur. J. Inorg. Chem.* **2021**, 2021, 2000-2016.
[37] A. Enriquez-Cabrera, L. Getzner, L. Salmon, L. Routaboul, A. Bousseksou, Post-synthetic modification mechanism for 1D spin crossover coordination polymers, *New J. Chem.* **2022**, 46, 22004-22012.

Titre : Catalyse commutable utilisant des complexes à transition de spin

Mots clés : complexes à transition de spin, effet de l'état de spin, modification post-synthétique, catalyse (commutable), film composite

Résumé : Cette thèse discute de l'influence de l'état de spin du fer sur la réactivité chimique ainsi que sur les capacités catalytiques des polymères de coordination 1D de fer(II)-triazole à transition de spin (TS). Notre objectif à long terme est d'explorer pleinement le potentiel des complexes à transition de spin dans le domaine de la catalyse commutable. Nous avons, tout d'abord, étudié l'impact de l'état de spin du fer sur l'efficacité de la réaction de modification post-synthétique (PSM) sur le complexe de formule [Fe(NH2trz)3](NO3)2 (Complexe 1). Il convient de noter qu'une amélioration considérable de 22% de l'efficacité de la PSM a été observée lorsque le complexe 1 était à l'état haut spin (HS) par rapport à son état bas spin (BS). A notre connaissance, il s'agit du premier exemple de l'influence de l'état de spin du métal sur la réactivité organique d'un groupement fonctionnel au sein d'un complexe métallique. Ensuite, nous avons démontré que, dans des conditions appropriées, un simple ajout d'aminotriazole dans le milieu réactionnel permet de passer d'une réaction PSM quantitative sur le complexe 1 avec un aldéhyde à l'utilisation du complexe à TS comme catalyseur pour la formation d'imines à partir d'aminotriazole. L'analyse des complexes récupérés après catalyse nous a permis d'envisager que des réactions PSM puissent intervenir dans le mécanisme catalytique de ce complexe à TS. Si c'est le deuxième exemple d'utilisation, en catalyse, d'un polymère de coordination 1D de fer(II)-triazole, c'est le premier exemple dans lequel l'espèce active est réellement le complexe à TS. Nous avons aussi étudié l'influence de l'état de spin sur l'activité catalytique du complexe 1 dans l'acétalisation du p-anisaldéhyde en présence de triéthyle orthoformate. Dans des conditions expérimentales strictement identiques, la réaction réalisée en présence du complexe à l'état HS permet d'obtenir jusqu'à 27 % d'acétal en plus que lorsque la réaction est réalisée avec le complexe à l'état BS. Ainsi le complexe à l'état HS est bien plus efficace pour catalyser la réaction d'acétalisation que le complexe à l'état BS. Le nombre important de tests comparatifs réalisés permet d'être confiant sur la généralité et la reproductibilité de ces résultats. Les études réalisées pour comprendre l'origine de l'effet de l'état de spin sur l'activité catalytique du complexe à TS semblent indiquer que la différence d'activité observée serait due à une modification d'accès des substrats au site catalytique. Enfin, nous avons fabriqué des films composites polymères à TS. Ces derniers ont été utilisés comme catalyseurs dans des réactions d'acétalisation. Les films composites ont fait preuve d'une grande efficacité catalytique et d'une excellente réutilisation dans des conditions de flux discontinu et continu. Ces films composites simplifient non seulement le recyclage du catalyseur, mais améliorent également la stabilité et la longévité du système catalytique. Cette thèse met en lumière, l'influence de l'état de spin du métal sur la réactivité organique des complexes à TS et démontre le potentiel de cette famille de complexes pour le développement de systèmes catalytiques commutables.

Title: Switchable catalysis using spin crossover complexes

Key words: spin crossover complexes, spin state effect, post-synthetic modification, (switchable) catalysis, composite film

Abstract: This thesis discusses the influence of the spin state of iron on the chemical reactivity and catalytic capabilities of spin crossover (SCO) 1D iron(II)-triazole coordination polymers. Our long-term objective is to fully explore the potential of SCO complexes in the field of switchable catalysis. We first studied the impact of spin states on the efficiency of the post-synthetic modification (PSM) reaction on the complex of formula [Fe(NH2trz)3](NO3)2 (Complex 1). It should be noted that a considerable 22% improvement in PSM efficiency was observed when complex 1 was in its high spin (HS) state compared to its low spin (LS) state. To the best of our knowledge, this is the first example of the influence of the metal spin state on the organic reactivity of a functional group within a metal complex. Secondly, we have demonstrated that, under appropriate conditions, a simple addition of aminotriazole to the reaction medium allows us to switch from a quantitative PSM reaction on complex 1 with an aldehyde to the use of the SCO complex as a catalyst for the formation of imines from aminotriazole. Analysis of the complexes recovered after catalysis enabled us to envisage that PSM reactions might be involved in the catalytic mechanism of this SCO complex. While this is the second example of the catalytic use of a 1D iron(II)-triazole coordination polymer, it is the first example in which the active species is actually the SCO complex. We also studied the influence of the spin state on the catalytic activity of complex 1 in the acetalisation of p-anisaldehyde in the presence of triethyl orthoformate. Under strictly identical experimental conditions, the reaction carried out in the presence of the HS complex yielded up to 27% more acetal than when the reaction was carried out with the LS complex. This means that the HS complex is much more effective at catalysing the acetalisation reaction than the LS complex. The wide number of comparative tests carried out means that we can be confident about the generality and reproducibility of these results. Studies carried out to understand the origin of the spin state effect on the catalytic activity of the SCO complex suggest that the observed difference in activity is due to a change in substrate access to the catalytic site. Finally, we fabricated SCO polymer composite films. These were used as catalysts in acetalisation reactions. The composite films demonstrated high catalytic efficiency and excellent reusability under batch and continuous flow conditions. These composite films not only simplify catalyst recycling, but also improve the stability and longevity of the catalytic system. This thesis highlights the influence of the metal spin state on the organic reactivity of SCO complexes and demonstrates the potential of this family of complexes for the development of switchable catalytic systems.